

https://dspace.org/

The Tsumeb ore body, Namibia, and related dolostone-hosted base metal ore deposits of Central Africa

Hughes, Martin James

2013-08-16
http://hdl.handle.net/10539/13037

Downloaded from a DSpace repository. https://dspace.org/

The copyright of the above-mentioned described thesis rests with the author or the University to which it was submitted. No portion of the text derived from it may be published without the prior written consent of the author or University (as may be appropriate). *Short quotations may be included in the text of a thesis* or dissertation for purposes of illustration, comment or criticism, provided full acknowledgement is made of the source, author and University.

THE TSUMEB ORE BODY, NAMIBIA, AND RELATED DOLOSTONE-HOSTED BASE METAL ORE DEPOSITS OF CENTRAL AFRICA

Martin James Hughes

A Thesis submitted to the Faculty of Science,
University of the Witwatersrand, Johannesburg,
for the degree of Doctor of Philosophy.

Johannesburg 1987

I declare that "The Tsumeb ore body, Namibia, and related dolostone-hosted base metal ore deposits of central Africa" is my own work and that all sources that I have used or quoted have been indicated and acknowledged by means of complete references. Neither the substance of this work or any part of it has been submitted in the past or is being or is to be submitted for a degree at any other university.



M.J Hughes

We may reasonably infer that water, in its passage through the earth to the principal fissures, imbibes, together with the natural salts and acids, the mineral and metallic particles with which the strata are impregnated ... to form different ores more or less homogeneous, and more or less rich according to the different mixtures which the acid had held dissolved, and the voids in which it is deposited.

- Pryce (1778)

ABSTRACT

The Tsumeb ore body is a steeply plunging breccia pipe within sedimentary carbonate rocks of Late Proterozic age. "Pseudo-aplite", a rock which occurs within the ore body, has been variously interpreted by previous workers as either a sedimentary rock or an igneous rock. The ore is mineralogically complex and consists of massive lead-copper-zinc sulphide and sulphosalt minerals, which include rare germanium and gallium species. The ore body is therefore difficult to classify genetically, and magmatic, tectonic and karstic origins have been proposed by previous workers.

The aim of the study was to identify as many variables as possible relevant to the origin of the Tsumeb ore body and related ore bodies of central Africa. These include: (1) the origin of the ore loci and their deformational history, (2) the physicochemical conditions of ore deposition (including the controls on mineralogical zoning in the Tsumeb ore body and the reasons for the unique composition of the ore), (3) the nature of the ore fluids and their migration paths, (4) the sources of metal and sulphur in the ore bodies, and (5) the reasons for the apparent time-dependence of mineralization of Tsumeb type throughout central Africa.

The ore bodies were investigated using petrographic, mineralogical and geochemical methods. Some fluid inclusion data were available from previous studies, so stable isotope and radiogenic isotope techniques were selected to provide further information about ore forming processes. A reaction line was constructed for the preparation of sulphur isotope samples, and existing facilities were used for lead, carbon and oxygen isotope studies.

Geological, geochemical and isotopic data indicate that the "pseudo-aplite" is a sedimentary rock, and that the Tsumeb pipe and similar structures in central Africa formed during subaerial karsting on a regional scale. These structures were mineralized at approximately 600 m.y., prior to deformation of the enclosing rocks or during the early stages of such deformation. The Tsumeb ore body formed from an ore fluid with a large Cu:Fe ratio, an intermediate

oxygen fugacity and a large sulphur fugacity. Vertical zoning of rock alteration in the Tsumeb pipe was caused by the mixing of fluids of different chemical composition, and vertical zoning of minerals of the Cu-Fe-As-S system was controlled mostly by variations in the sulphur fugacity of the ore fluid. The Tsumeb ore body and other ore bodies of central Africa contain sulphur of crustal, probably evaporitic, origin. An evaporite horizon in the upper part of the Tsumeb ore body influenced the sulphur concentration (and sulphur fugacity) of the ore fluid. This controlled the above zoning and was the dominant cause of ore deposition. The unique mineralogical and chemical composition of ore of Tsumeb type resulted from a high concentration of both copper and unusual trace elements in the ore fluids.

Lead isotope data indicate a genetic relationship between Tsumeb-type mineralization, Berg Aukas-type mineralization (karst-filling lead-zinc mineralization) and Tschudi-type mineralization (stratiform copper mineralization in sandstone). The data are most consistent with a model in which the ore fluids which formed each of the above members of the Owambo basin-type ore association were evolved connate brines, which were expelled from evaporite deposits in a graben to the south of the present Otavi Mountain Land. The ore fluids which formed each type of mineralization migrated through separate aquifers at approximately the same time. The fluids were derived from a large area of the graben and migrated more than 60 km up-dip, penetrating sedimentary sequences more than 1000 m thick, to form mineral districts at least 5000 sq. km in area. Metals, including lead (as indicated by the lead isotope data), were added to the fluids en route. The time dependence of mineral districts which contain the Owambo basin-type ore association resulted from time-dependent rifting, continental break-up, and the formation of salt basins (which supplied the ore-forming brines).

ACKNOWLEDGEMENTS

I wish to express my gratitude to:

The late Prof. H. L. Allsopp, Dr. H. J. Welke, Prof. B.T. Verhagen, Dr. G.N. Phillips, and my supervisor, Prof. S. Maske, for useful discussions and their encouragement and guidance. Also, other staff of the University of the Witwatersand and the many overseas workers with whom I corresponded.

Dr. M.L. Coleman, for advice on design of the sulphur isotope line, and Mr. M. Miles for assistance in its construction.

The late Prof. L. Cahen, Dr. G.Scolari, and other workers who supplied samples from central Africa.

Dr. E.Cable and other analysts acknowledged in the text.

The management and staff of Tsumeb Corporation Limited for logistical, financial and other support.

Mrs. A. Robins (Johannesburg) and the staff of G.Mould and Associates (Melbourne) for typing the manuscript.

My wife, Carol, for drafting the figures and for her infinite patience and continuous encouragement and help.

CONTENTS

	PAGE NO.
CHAPTER ONE: INTRODUCTION	1
1.1 BACKGROUND TO THE STUDY	1
1.2 METHOD OF STUDY	4
CHAPTER TWO: GEOLOGICAL SETTING OF THE TSUMEB ORE BODY	6
2.1 GEOLOGY OF THE OWAMBO BASIN	6
2.2 THE DAMARA SEQUENCE IN THE OTAVI MOUNTAIN LAND	11
2.2.1 Abenab Subgroup	11
2.2.2 Chuos Formation	15
2.2.3 Tsumeb Subgroup	15
2.2.4 Mulden Group	18
2.3 PETROLOGICAL STUDIES	19
2.3.1 Otavi Group dolostone and chert	19
2.3.2 Otavi Group breccia	25
2.3.3 Phosphatic rocks of the Hüttenberg Formation	27
2.3.4 Hüttenberg Formation evaporites	29
2.3.5 Other Otavi Group evaporites	33
2.3.6 Mulden Group sedimentary rocks	35
CHAPTER THREE: TSUMEB ORE BODY	40
3.1 DESCRIPTION	44
3.2 PREVIOUS STUDIES OF THE TSUMEB ORE BODY	47
3.3 TSUMEB PIPE AND ITS SEDIMENTARY INFILL	51
3.3.1 Petrology of the dolostone breccia core	52
3.3.2 Other types of dolostone breccia	58
3.3.3 Petrology of sandstone ("pseudo-aplite") and sandstone breccia bodies	59
3.3.4 Spatial relationships between breccia bodies of the pipe core	62
3.3.5 Temporal relationships between dolostone breccia, sandstone and sandstone breccia	66

3.3.6 Relationships between different sandstone and sandstone breccia bodies 67
3.3.7 Strata-bound sandstone of zone T6 69
3.4 ZONES OF ROCK ALTERATION 72
3.4.1 Alteration of the dolostone breccia 72
3.4.2 Calcitization in the Tsumeb pipe 73
3.4.3 Silicification in the Tsumeb pipe 80
3.4.4 Rock alteration in the North Break zone 84
3.4.5 Carbon in the Tsumeb pipe 89
3.4.6 Alteration of the pipe sandstone 92
3.4.7 Summary 94
3.5 STRUCTURAL AND STRATIGRAPHIC CONTROLS OF MINERALIZATION . 95
3.5.1 Steeply dipping massive sulphide bodies 96
3.5.2 Mantos 99
3.5.3 E49 manto near 28 level 101
3.5.4 S110 and North Break ore bodies 105
3.5.5 Disseminated mineralization 106
3.6 ORE CHEMISTRY AND MINERALOGY 107
3.6.1 Mineralogy of the hypogene ore 107
3.6.2 Chemistry of the hypogene ore minerals 110
3.6.3 Supergene sulphide enrichment and oxidation 114
3.6.4 Contrasting metal ratios in disseminated and massive ore 119
3.6.5 Mineralogical and chemical zoning in the pipe core 120
3.6.6 Chemical zoning in massive sulphide ore 125
3.6.7 Mineralogical classification of massive ore types . 127
3.6.8 Distribution of massive ore types 134
3.6.9 Zoning of gangue minerals 137
3.6.10 Previous paragenetic studies and present approach
3.6.11 Paragenesis of massive sulphide ore 139
3.6.12 Paragenesis of disseminated ore 143
3.6.13 Paragenesis of trace minerals 144
3.6.14 Paragenesis of gangue minerals 145
3.6.15 Summary 146
3.7 DEFORMATION OF THE TSUMEB ORE BODY 148
3.7.1 S_1 cleavage in the Tsumeb pipe 149
3.7.2 Contrasting deformation mechanisms during F_1 folding 156
3.7.3 Deformation of sulphide ore 162

3.7.4 Minor folds associated with the Tsumeb pipe 168
3.7.5 Origin of the marginal fracture zone and minor folds 170
3.7.6 Strain across the Tsumeb pipe caused by F_1 folding 173
3.7.7 Thrusting in zone T5 174
3.7.8 Thrusting in zone T7 176
3.7.9 Relationship between the E2200 and Old Compound breccia bodies 180
3.7.10 Other deformation 180
3.7.11 Metamorphism of Otavi Group and Mulden Group rocks 183
3.7.12 Timing of mineralization, deformation and metamorphism 185
3.7.13 Conclusions 186

CHAPTER FOUR: MINERALIZATION IN THE OTAVI MOUNTAIN LAND..... 189

4.1 PREVIOUS STUDIES 189
4.2 TYPES OF MINERALIZATION 192
4.3 DISTRIBUTION OF MINERALIZATION 195
4.4 DESCRIPTIONS OF INDIVIDUAL AREAS 197
4.4.1 Tsumeb area 197
4.4.2 Ore controls in the Otavi Valley area 201
4.4.3 Mineralogy of the Kombat ore bodies 203
4.4.4 Deformation of the Kombat ore bodies 207
4.4.5 Mineralization in the Kombat Formation 213
4.4.6 Harasib area 214
4.4.7 Strata-bound breccia of the Elandshoek Formation . 215
4.4.8 Mineralization in the Auros Formation 217
4.4.9 Mineralization in the Gauss Formation 218
4.5. SUMMARY OF MINERALIZATION IN THE OTAVI MOUNTAIN LAND ... 219
4.6 COMPARISONS WITH AREAS OUTSIDE THE OTAVI MOUNTAIN LAND .. 221
4.6.1 Tsumeb-type mineralization of central Africa : stratigraphic position 222
4.6.2 Tsumeb-type mineralization of central Africa: ore loci 228
4.6.3 Tsumeb-type mineralization of central Africa: mineralogy 229
4.6.4 Tsumeb-type mineralization of central Africa: timing and conclusions..... 231
4.6.5 Mineralogically similar occurrences outside central Africa 232

4.6.6 Other similarities between ore deposits of sedimentary basins 236
4.6.7 Epigenetic veins in basement rocks and their relationships to basin-hosted ore deposits 240

CHAPTER FIVE: ISOTOPE STUDIES..... 243

5.1 SULPHUR ISOTOPES 243
5.1.1 Anhydrite, gypsum and native sulphur, Tsumeb Subgroup 243
5.1.2 Tsumeb-type mineralization, Otavi Mountain Land .. 246
5.1.3 Tsumeb-type mineralization elsewhere in central Africa 250
5.1.4 Berg Aukas-type mineralization 251
5.1.5 Summary 253
5.2 CARBON AND OXYGEN ISOTOPES 253
5.2.1 Sedimentary carbonate rocks of the Otavi Group ... 254
5.2.2 Alteration zone and gangue minerals 257
5.2.3 Controls on oxygen isotopic ratios 258
5.2.4 Carbon source, and controls on carbon isotopic ratios 260
5.2.5 Calcite of supergene origin 261
5.2.6 Other carbonate minerals 263
5.3 LEAD ISOTOPES 264
5.3.1 Inherent error in lead isotope ratio measurements. 264
5.3.2 Galena from the Otavi Mountain Land 266
5.3.3 Geographic and stratigraphic variations in lead isotope ratios 274
5.3.4 The linear lead isotope trends as isochrons 278
5.3.5 A mixing origin for lead of the Otavi Mountain Land 282
5.3.6 Dolostone isochrons, Otavi Group 286
5.3.7 Source of the ore lead 288
5.3.8 Conclusions from the Otavi Mountain Land data ... 294
5.3.9 U-Pb zircon studies 297
5.3.10 Galena from central Africa 298
5.3.11 Comparisons with lead isotope data from ore deposits of related types 301
5.3.12 Mississippi Valley-type ore deposits 302
5.3.13 Sedex deposits 304
5.3.14 Sandstone lead deposits 306

5.3.15 Stratiform copper deposits and the Saxonic vein association 308
5.3.16 Conclusions 311

CHAPTER SIX: GENESIS OF THE OWAMBO BASIN-TYPE ORE ASSOCIATION 313

6.1 FORMATION OF THE ORE LOCUS 313
6.1.1 Source of the sedimentary infill of the Tsumeb pipe ... 313
6.1.2 Controls on karsting and syn-sedimentary faulting. 315
6.1.3 A model for formation of the Tsumeb pipe 317
6.1.4 Ore loci elsewhere in the Owambo Basin 320
6.1.5 Comparisons with modern solution collapse and karst structures 321
6.1.6 Mineralized karst and solution collapse features elsewhere in the world 325
6.2 PHYSICO-CHEMICAL CONDITIONS DURING ORE DEPOSITION, AND THE SOURCE OF SULPHUR 327
6.2.1 Oxygen fugacity, sulphur fugacity, pH and sulphur concentration of the Tsumeb ore fluid 329
6.2.2 Zoning of rock alteration 337
6.2.3 Sulphide mineral zoning and chemical controls of ore deposition 340
6.2.4 Controls of ore composition in the Owambo basin-type ore association 343
6.2.5 The importance of sedimentary sources of sulphur.. 345
6.3 FLUID SOURCE 350
6.3.1 Fluid flow and temperatures in sedimentary basins. 350
6.3.2 The origin of brines in sedimentary basins 353
6.3.3 The compositions of contemporary, mineralized basin fluids 359
6.3.4. The tectonic setting and origin of contemporary, mineralized brine..... 362
6.3.5 Comparison with ore fluids which form basin-related ore deposits 367
6.3.6 The importance of major salt basins 373
6.3.7 Source of the Owambo basin-type ore fluids 378
6.4 METAL SOURCE AND FLUID CHANNELWAYS 383

6.4.1 Minor elements in rocks of sedimentary basins 383
6.4.2 Metal sources and fluid channelways in the Otavi Mountain Land 385
6.5 THE TIME DEPENDENCE OF TSUMEB-TYPE ORE DEPOSITS 388

CHAPTER SEVEN: CONCLUSIONS..... 394

REFERENCES 398

APPENDICES 425

1 **CHEMICAL ANALYSES**..... 425
1.1 Total rock analyses 425
1.2 Analyses of sulphide and sulphosalt minerals 427
1.3 Other chemical analyses 427
2 **ISOTOPE ANALYSES** 427
2.1 Sulphur isotopes 427
2.2 Carbon and oxygen isotopes 434
2.3 Lead isotopes 437

3 **FLUID INCLUSION DATA**..... 445

CHAPTER ONE

INTRODUCTION

1.1 BACKGROUND TO THE STUDY

The Tsumeb ore body of the Tsumeb Corporation Limited is situated in the town of Tsumeb, approximately 400 km north of Windhoek (Figs. 1,3). The ore body occurs in Late Proterozoic carbonate rocks of the central African copper province. It displays a number of features not seen in other pipe-like base metal bodies. The ore locus is a steeply plunging breccia pipe, in an area dominated by sedimentary carbonate rocks (Fig. 20). There is an apparent lack of felsic intrusive rocks in the area, such as are commonly associated with mineralized pipes, although the possible presence of such rocks has been debated. The ore consists of mineralogically complex, massive lead-copper-zinc sulphide and sulpho-salt minerals, which include rare germanium- and gallium-bearing minerals. The ore body is, therefore, difficult to classify genetically, and its relationship to other types of mineralization is not obvious.

Origins which have been proposed for the Tsumeb breccia pipe are magmatic hydrothermal (including carbonatitic), tectonic and karstic. The quartzo-feldspathic "pseudo-aplite" of the pipe has been interpreted as either a magmatic or a sedimentary rock. Sedimentary origins proposed include *in situ* sedimentation, and re-mobilization of sediment. The ore has been variously thought to pre-date, post-date, or to be synchronous with deformation. These origins are reviewed in Chapter 3.2.

A number of factors are involved in the formation of a hydrothermal ore body (Skinner 1979). An aqueous fluid is required, which must be capable of transporting significant quantities of ore constituents. This fluid may contain: (1) meteoric, (2) sea or connate, (3) metamorphic, or (4) magmatic

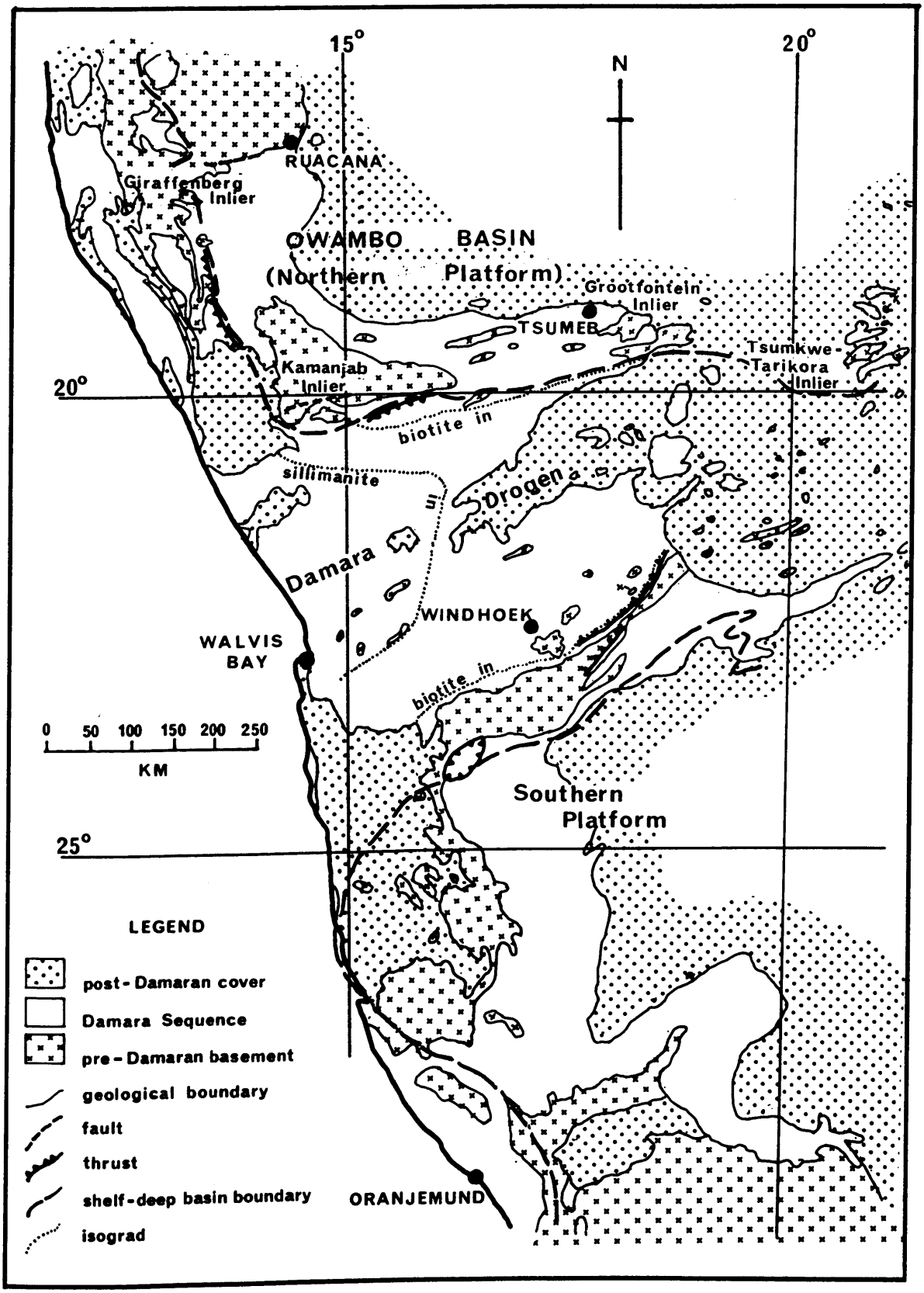

Fig. 1
Damara Sequence of S.W.A./Namibia and adjoining areas. Compiled from South Africa Geological Survey, 1963; Clifford, 1967; Hedberg, 1979.

water. The fluid must migrate from its source to the site of ore deposition via channel ways. The dissolved constituents of the ore fluid may be present at the source, or derived en route. Special physicochemical conditions and permeability characteristics must exist at the site of mineral deposition if an ore deposit is to result.

This study attempts to identify as many of the above variables involved in the formation of the Tsumeb ore body as possible, especially the major controls on ore deposition. A number of problems are investigated in detail. The first is the origin of the Tsumeb pipe and similar mineralized bodies of the surrounding area. Most pipe-like breccia bodies elsewhere in the world are closely associated with magmatic activity, or with hydraulic brecciation caused by boiling or other overpressuring. However, karst pipes and other types of solution pipe are known. The second problem investigated is the deformational history of the Tsumeb pipe and its sulphide ore. Thirdly, mineralogical zoning occurs within the pipe over a depth interval of 1500 m. This might result from a pressure drop with resultant boiling, or a temperature decrease, at shallow depths. Alternatively, it might result from mixing of different fluids within the pipe, or from progressive temporal or spatial changes in the composition of fluids traversing the pipe. Finally, the mineralogical complexity of the ore may be a function of unusual fluid composition or metal sources, physicochemical parameters at the site of deposition, or a combination of these.

The relationship, if any, between the Tsumeb ore body and other ore bodies and ore associations is investigated, with particular reference to the central African mineral province. This is relevant to mineral exploration, but also to more fundamental problems of ore genesis. The first is the possible need for major sources of sulphur at sites of ore deposition. Reduced sulphur must either be transported with metals in the same solution or be provided at the site of deposition, if a sulphide ore deposit is to form. Some metals can be transported as thio-complexes, and metals and reduced sulphur could be transported

together in this way. However, the solubility of other metals is far higher in chloride solutions which lack reduced sulphur (Barnes, 1979). Metal-rich basin fluids sampled from some petroleum and geothermal wells are sulphur-deficient, indicating that an independent sulphur source is required if these fluids are to precipitate sulphide ores. This conclusion is supported by the presence of sedimentary sulphate minerals, sometimes replaced by ore sulphides, in the immediate vicinity of many ore bodies (Chapter 6.2.5).

The second problem is the importance of ore concentration processes, relative to long-lived geochemical anomalies in limited volumes of crust, in determining the position of mineral provinces. Process-dependent factors include the efficiency of hydrothermal circulation and the compositions of the fluids. The geochemical anomalies correspond to the "metal domains" of Routhier (1983), which have been acted upon by these processes to produce ore deposits.

The third problem relates to the observation that some types of ore deposit formed most frequently within restricted periods of time in earth history (Meyer, 1981). This time-dependence may reflect important steps in the tectonic evolution of the earth. An example is komatiite-hosted nickel deposits, the metallic ore constituents of which were introduced directly from the mantle. Other ore deposits, such as mid-Proterozoic iron and uranium ores, may owe their time-dependence to chemical evolution at the earth's surface (Meyer, 1981). The reason for the time-dependence of some ores, such as stratiform copper and carbonate-hosted base metal ores (including the Tsumeb ore body) is less obvious. It may primarily be a function of chemical evolution at the earth's surface, or alternatively it may result from fluid circulation at shallow depths, and re-concentration of metals, as a response to tectonic evolution (e.g. rifting and continental break-up). Alternatively, it may be more directly related to mantle evolution.

1.2 METHOD OF STUDY

The Tsumeb ore body was subjected to petrographic, mineralogical

and minor geochemical studies. Limited fluid inclusion data were available from a previous study, and these indicated that most primary inclusions had been destroyed by deformation (Ypma, 1973a, b). Detailed geochemical studies were limited by a lack of microprobe facilities. It was, therefore, decided that stable and radiogenic isotope studies would provide the most information on ore forming processes. These studies were conducted at the University of the Witwatersrand. A reaction line was constructed in the Geology Department by the writer for the preparation of sulphur isotope samples. Existing facilities at the Nuclear Physics Research Unit (N.P.R.U.) were used for carbon and oxygen isotope analyses. Prof. H.L. Allsopp and Dr. H.J. Welke of the Bernard Price Institute of Geophysics (B.P.I) had already commenced a lead isotope study of the Tsumeb ore. This was continued as a co-operative project, and was extended to include rocks and ores from throughout the Otavi Mountain Land and central Africa.

The staff of Tsumeb Corporation Limited conducted extensive geological mapping of the Tsumeb mine (mainly at 1:250 scale) during development and exploitation of the ore body. A geological base was therefore available when this study commenced. However, negligible diamond drill core was available from above 35 level (Fig. 19), so core could not be used to re-interpret this earlier mapping in areas which were by then inaccessible. Geological mapping during the present study was confined to accessible mine openings below 26 level. Many exposures above 32 level were confined to pillars. These were limited in extent, dirty and only briefly accessible. Numerous stopes were accessible between 32 and 35 levels, and a brief examination was made of newly-opened stopes on 38 level in mid-1979. Diamond drill core was available from 35 level to below the lowest (44) level. Geological information was extrapolated upwards from below 26 level, using existing geological mapping, reports, and the rock and mineral collection of Tsumeb Corporation Limited.

Minor field studies were undertaken in surrounding areas of the Otavi Mountain Land to establish the regional setting of mineralization. These were limited by the security situation, and some important areas (e.g. Abenab West, and north of the Otavi Valley) could not be revisited.

CHAPTER TWO

GEOLOGICAL SETTING OF THE TSUMEB ORE BODY

2.1 GEOLOGY OF THE OWAMBO BASIN

The Tsumeb ore body is hosted by sedimentary carbonate rocks of the Damara Sequence, of Late Precambrian age, in the south-eastern part of the Owambo basin (Figs. 1, 3). The following discussion of Owambo basin geology is summarized from Hedberg (1979), modified to conform to SACS (1980), except where otherwise stated. Precambrian outcrops are confined to the western and southern borders of the Owambo basin, but the geology of the south-western part of the central basin can be interpreted from seismic and drilling information. A reconnaissance aeromagnetic survey in the eastern basin indicated that sediment thicknesses comparable to those exposed in the west continue east-north-eastwards beyond South West Africa/Namibia into Angola and Botswana.

The Owambo basin is separated both from the coastal branch, and from the central zone, of the intra-continental branch of the Damaran fold belt by basement ridges. These are present along the western and southern boundaries of the basin, respectively. They include the Giraffenberg inlier, Kamanjab inlier, Grootfontein inlier and Tsumkwe-Tarikora inlier (Fig. 1). The boundary between the miogeosynclinal or platform facies, and the eugeosynclinal or deep water facies of Damaran sedimentation, lies slightly outside these limits (e.g. to the west and south of the Kamanjab inlier). This is shown as the "shelf-deep basin boundary" of Figure 1.

The basement rocks include the Epupa and Huab Complexes and the Kunene Basic Complex. The granitoid Fransfontein Suite of the Kamanjab inlier intruded these previously deformed and metamorphosed basement rocks. Burger et al. (1976) obtained zircon U-Pb ages of 1730 $\pm$ 30 Ma and 1870 $\pm$ 30 Ma from these granitoids. A regional

angular unconformity exists between these rocks and the overlying Khoabendus Group. This group was deformed and eroded prior to the development of the Damara geosyncline. The gneissic, granitoid and metasedimentary rocks of the Grootfontein Complex, of the Grootfontein inlier, pre-date the Damara Sequence but their age is unknown.

The axis of maximum deposition of units which post-date basement rocks in the Owambo basin trends north-east from between the Giraffenberg and Kamanjab inliers (Fig. 1). The basement displays a regional north-west dip to the south of this axis, but probably rises further to the north-west to crop out along the east-north-east trending basement exposures which pass through Ruacana. The basin is filled with up to 7000 m of Late Precambrian sediments (e.g. Oshakati area), which thin to about 4000 m along the southern and western basement highs. Laterally equivalent accumulations in the eugeosyncline attain a thickness of about 15 000 m.

Hedberg (1979) divided the Damara Sequence of the Owambo basin into a basal arenaceous unit (Nosib Group), a middle carbonate unit (Otavi Group) and a late orogenic clastic unit (Mulden Group). The earliest deposits consist of fluviatile conglomerate, sandstone, quartzite, lava and pyroclastic rock of the Nosib Group (Fig. 2). A slight angular unconformity occurs at the top of the Nosib Group in the Otavi Mountain Land. However, to the west of the Giraffenberg and Kamanjab inliers the Nosib Group was affected by folding and amphibolite facies metamorphism before deposition of the Otavi Group (Guj, 1970). Syenite and carbonatite intrusion, uplift and erosion affected the Nosib Group to the south of the Kamanjab inlier, prior to further sedimentation (Frets, 1969). Miller and Burger (1983a) obtained a U-Pb zircon age of 728 $\pm$ 40 m.y. from volcanic rocks of the Nosib Group.

The Otavi Group commences with carbonate rocks of the Abenab Subgroup, which are overlain by mixtites and other sedimentary rocks of the Chuos Formation. The base of the Chuos Formation is an unconformity throughout most of the western Owambo basin, but is a mild disconformity in the Otavi Mountain Land (south of Tsumeb and west of

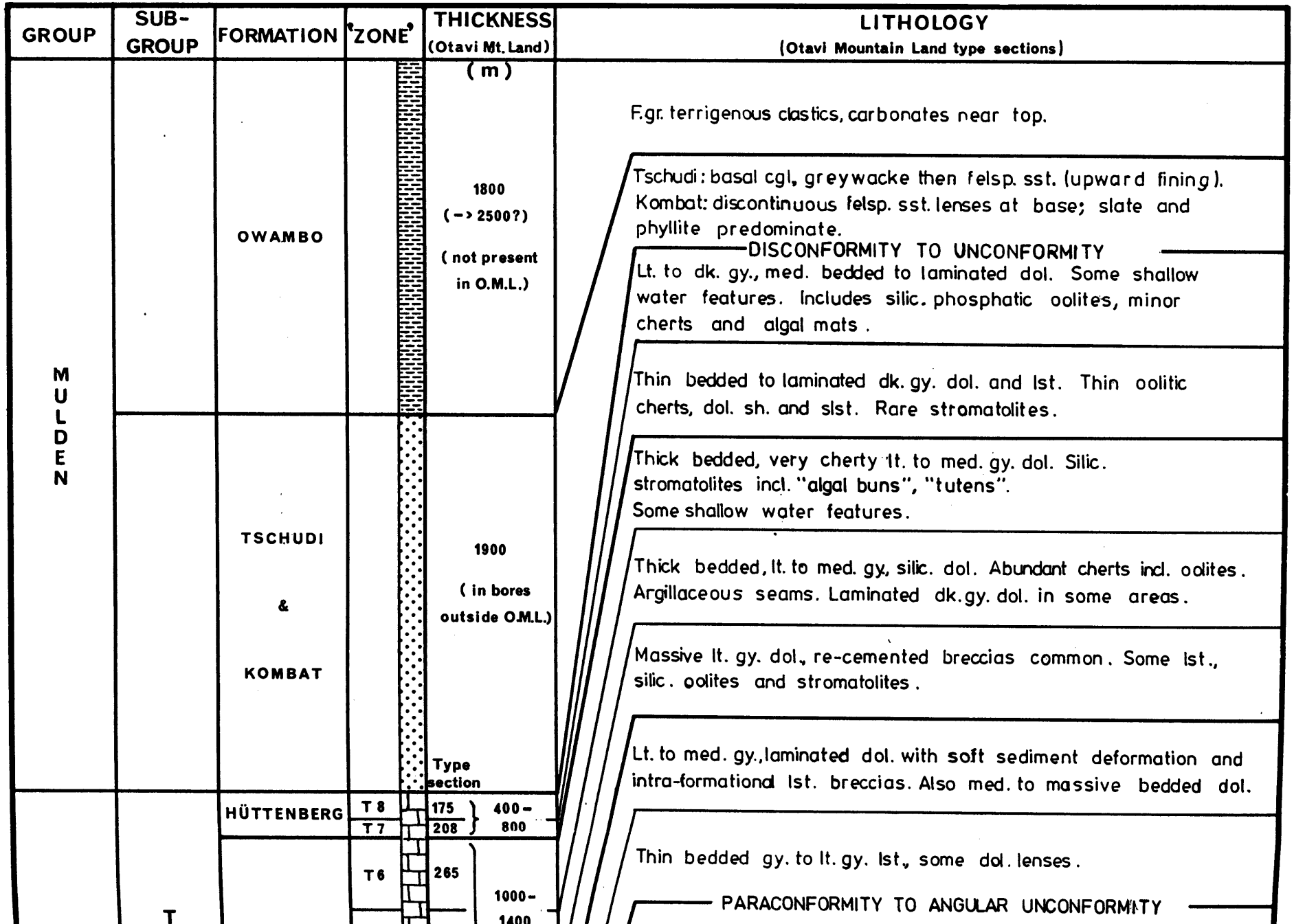
GROUP
SUB-GROUP
FORMATION
'ZONE'
THICKNESS (Otavi Mt. Land)
(m)
LITHOLOGY
(Otavi Mountain Land type sections)
MULDEN
OWAMBO
1800
(-> 2500?)
(not present in O.M.L.)
F.gr. terrigenous clastics, carbonates near top.
Tschudi: basal cgl, greywacke then felsp. sst. (upward fining).
Kombat: discontinuous felsp. sst. lenses at base; slate and phyllite predominate.
DISCONFORMITY TO UNCONFORMITY
TSCHUDI & KOMBAT
1900
(in bores outside O.M.L.)
Type section
Lt. to dk. gy., med. bedded to laminated dol. Some shallow water features. Includes silic. phosphatic oolites, minor cherts and algal mats.
Thin bedded to laminated dk. gy. dol. and lst. Thin oolitic cherts, dol. sh. and slst. Rare stromatolites.
Thick bedded, very cherty lt. to med. gy. dol. Silic. stromatolites incl. "algal buns", "tutens". Some shallow water features.
Thick bedded, lt. to med. gy, silic. dol. Abundant cherts incl. oolites. Argillaceous seams. Laminated dk.gy. dol. in some areas.
Massive lt. gy. dol., re-cemented breccias common. Some lst., silic. oolites and stromatolites.
Lt. to med. gy., laminated dol. with soft sediment deformation and intra-formational lst. breccias. Also med. to massive bedded dol.
HÜTTENBERG
T 8
T 7
175
208
400-800
T 6
265
1000-1400
Thin bedded gy. to lt. gy. lst., some dol. lenses.
PARACONFORMITY TO ANGULAR UNCONFORMITY

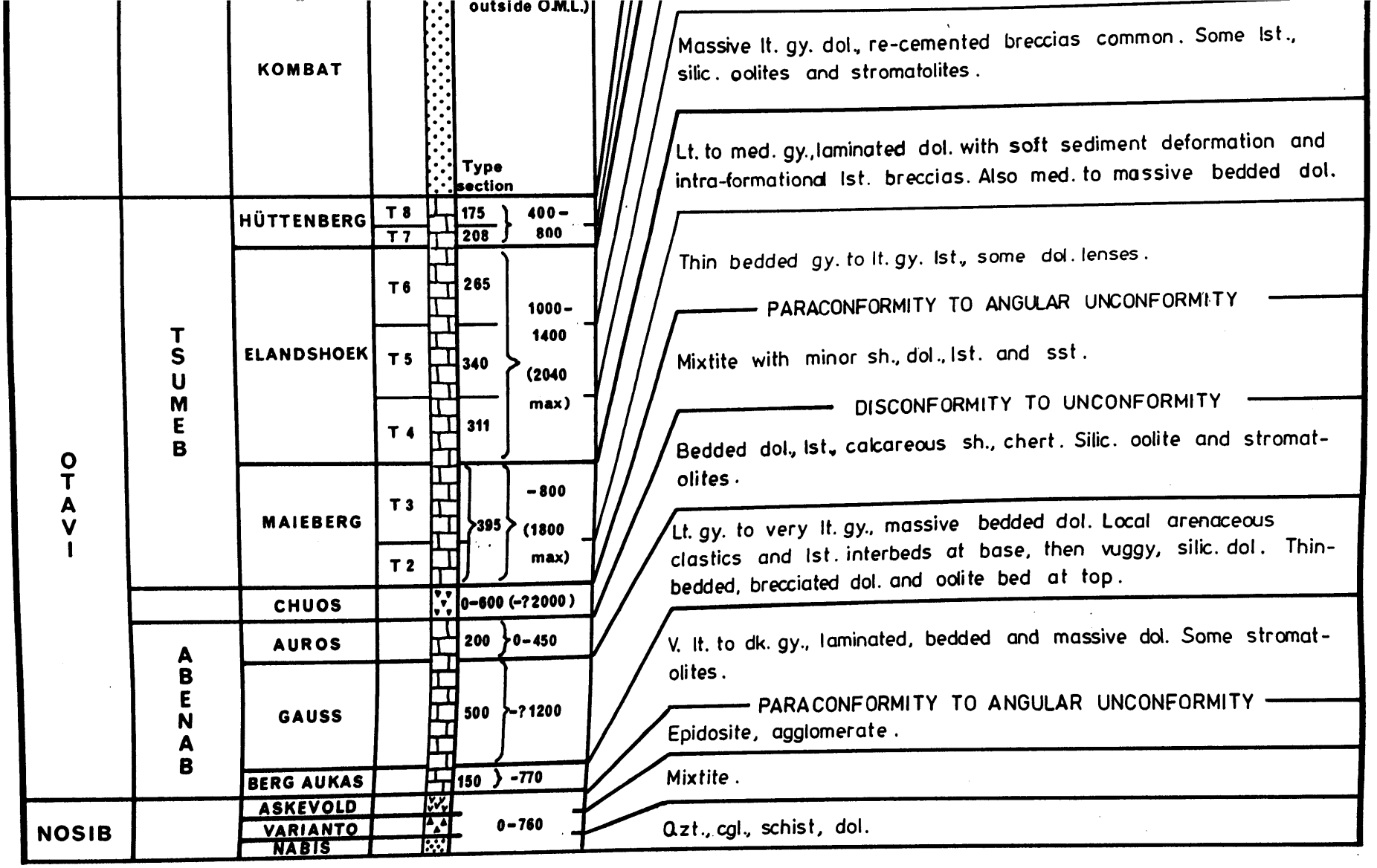

Fig. 2

Damara Sequence of the Owambo Basin. Modified from Sohnge, 1957, and Hedberg, 1979. Abbreviations: *incl. = including; qzt. = quartzite; v.,gy = very, grey; cgl. = conglomerate; lt, med., dk = light, medium, dark; sst. = sandstone; f.gr. = fine grained; dol. = dolostone; silic. = silicified; lst. = limestone; felsp. = feldspathic; sh. = shale; slst. = siltstone.*

the Grootfontein inlier; Fig. 3). The Chuos Formation is absent along most of the length of a broad, east-north-east trending zone which extends from the Kamanjab inlier to the central Otavi Mountain Land. This may be because this zone was a source area for the Chuos Formation. Alternatively, the formation might have been removed by subsequent erosion. Tsumeb Subgroup carbonate rocks conformably overlie the Chuos Formation in the Otavi Mountain Land, and paraconformably to unconformably overlie older units where the formation is absent. This contact becomes an angular unconformity to the south as the deeper part of the basin is approached.

The east-north-east trending ridge existed between the Kamanjab inlier and Tsumeb throughout the period of deposition of the Tsumeb Subgroup. This is indicated by the reduced thickness of sedimentation in the vicinity of the ridge. Shallow water indicators such as oolites, stromatolites, ripple-marks, cross-bedding and desiccation features occur at the top of the Tsumeb Subgroup throughout the basin. Hedberg (1979) considered that the Nosib and Otavi Groups represent a transgressive cycle, the formations of which are mappable from the Otavi Mountain Land to Ruacana. Maximum marine transgression probably occurred during deposition of the Tsumeb Subgroup. The probable equivalent of the Tsumeb Subgroup in the zone transitional to the deep basin (i.e. to the south of the Kamanjab Inlier; Fig. 1) is the Khomas Subgroup. The Khomas Subgroup was folded and metamorphosed prior to the deposition of the Mulden Group (Frets, 1969). The upper formation of the Tsumeb Subgroup was removed prior to sedimentation of the Mulden Group in the Baynes Mountains, west of Ruacana. A paraconformable relationship exists between these groups within the Owambo basin proper.

Hedberg (1979) considered that the Mulden Group probably consists of continental deposits. These deposits were produced as a result of uplift of the adjoining areas during the preceding phase of the Damaran Orogeny, and were subsequently folded by a later phase of this orogeny. He concluded that the Mulden Group represents a progressively finer regressive cycle ("molasse"). The "Lower Mulden" of Hedberg (1979) is variable in lithology and includes shale and conglomerate, and is overlain by sandstone of the Tschudi Formation

("Upper Mulden"). The sandstone is overlain with apparent conformity by the Owambo Formation, which consists of fine-grained terrigenous clastic sediments with carbonate rocks in the uppermost beds. Hedberg (1979) suggested that the lower Mulden Group of the south-western Owambo basin was initially derived from an Otavi Formation source, then from the Khoabendus Formation and Nosib Group, and finally from the Fransfontein Suite. He considered that this was in response to the continued uplift of the basement ridge along the southern boundary of the basin. The finer clastic sediments of the Owambo Formation were thought to result from the reduced relief of the source area, and an attendant reduced rate of erosion. Alternatively, these sediments could have been derived from a more distant source, such as the eugeosynclinal regions to the south and west.

Folds in the Damara Sequence to the north and east of the basement ridges are typically open and of flexural-slip type. A regular decrease in amplitude, and an increase in wavelength, occurs north-north-eastwards towards the Angola-Congo craton (outside Fig. 1, to the north). The axial surfaces trend north to north-west in the western part of the basin and east to east-north-east in the south. This is parallel to the more intense folding of the adjacent coastal and central intra-continental branches of the Damaran belt, respectively. South of the basement ridges the axial surfaces dip south, but folds are more symmetrical north of the ridges. Later north-east trending cross-folds are present on the southern flank of the Kamanjab inlier. These are possibly related to north-east trending cross-folds of unknown age which occur to the north and north-east of the inlier. Major faulting, including some thrusting, is associated with the southern margin of the east-north-east trending basement ridge which forms the southern boundary of the Owambo basin. Mulden Group sediments are locally involved in thrusting and are over-ridden by nappes outside the western boundary of the basin (Guj, 1970).

The Mulden Group of the Owambo basin has undergone only low to very low grade metamorphism. Clauer and Kröner (1979) proposed two metamorphic events in the central Owambo basin, at 535 m.y. and 455 m.y. (Chapter 3.7.11). Stilpnomelane is present, clay has been

isotopically re-set, but biotite has not formed. The biotite isograd is reached immediately outside of the southern and western boundaries of the basin (Fig. 1). Syn- and post-tectonic granitoid intrusions are unknown within the basin, but at least some of the granites of the Salem Suite, to the south of the Owambo basin, post-date the Mulden Group (Miller, 1980). Haack et al. (1980) obtained Rb/Sr whole rock isochrons of 465-553 Ma from granites of this suite (e.g. 553 $\pm$ 22 m.y. for the Okambahe granodiorite).

2.2 THE DAMARA SEQUENCE IN THE OTAVI MOUNTAIN LAND

The Otavi Mountain Land is an area of low but rugged relief on the southern margin of the Owambo basin, immediately to the west of the Grootfontein basement inlier (Figs. 1, 3, 4). All economically important base metal mineralization in the Owambo basin is confined to this area. Mineralization of the type studied is restricted to the Abenab Subgroup, Chuos Formation and Tsumeb Subgroup of the Otavi Group, and to the Mulden Group (Fig. 2). The Nosib Group is therefore not discussed.

The following description is summarized from Söhnge (1957) and Hedberg (1979), except where otherwise stated. The type section of Hedberg (1979) on Elandshoek farm is 10 km south of Tsumeb.

2.2.1 Abenab Subgroup

The Abenab Subgroup overlies the Nosib Group with angular unconformity in parts of the Otavi Mountain Land, such as the type section on Elandshoek farm. However, their contact is paraconformable in other areas. The Berg Aukas, Gauss and Auros Formations constitute the subgroup. These formations consist almost entirely of carbonate rocks.

The basal Berg Aukas Formation (Fig. 2) consists of 206 m of light to dark grey, laminated dolostone with minor stromatolites in the type section on Elandshoek farm. In other areas, arenaceous clastic rocks (derived from Nosib Group or basement rocks), shale, and dark and

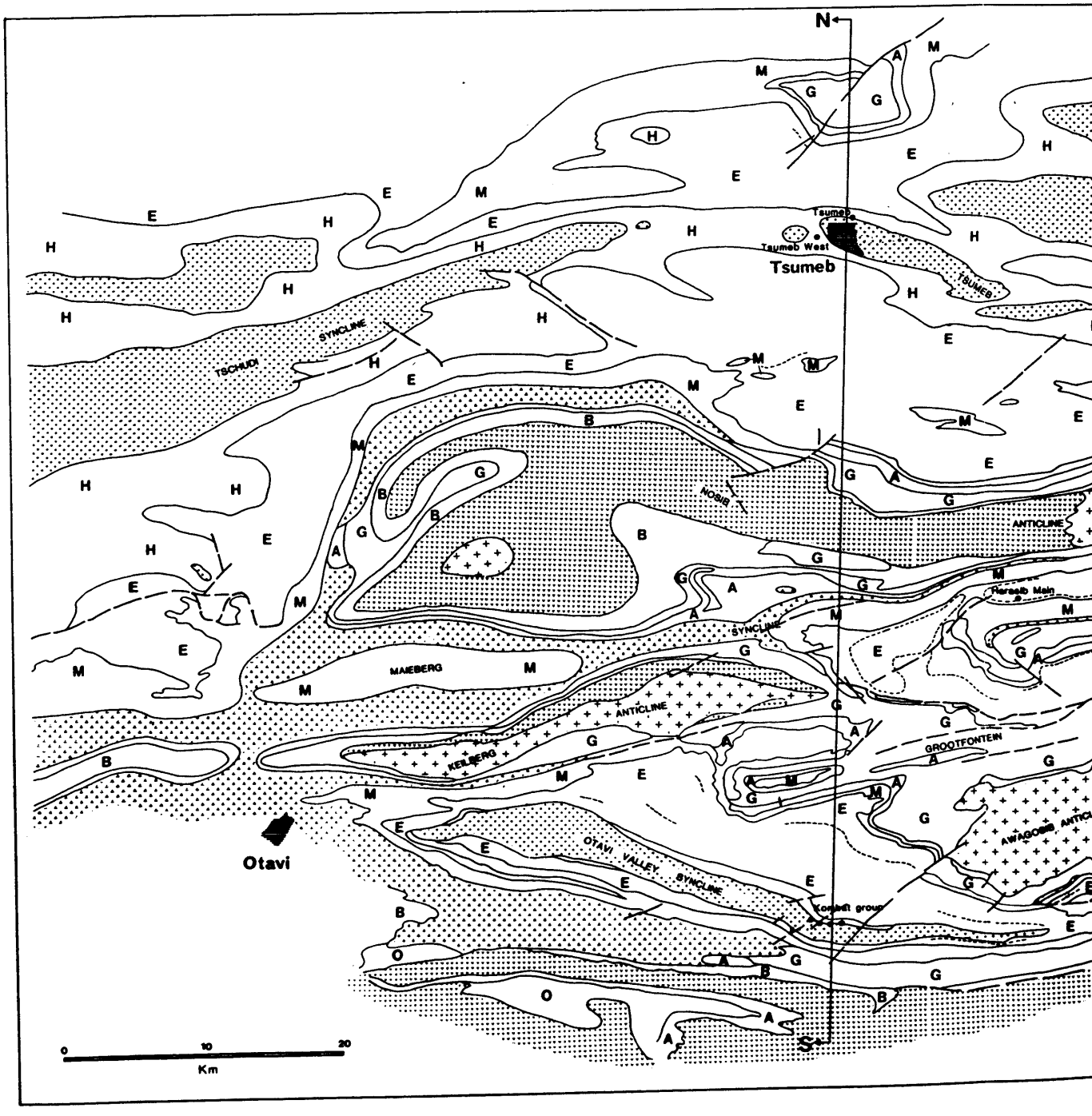

Fig. 3
Geological map of the Otavi Mountain Land. Modified from mapping by
Hedberg, 1979. See Figure 4 for location of section line N-S.

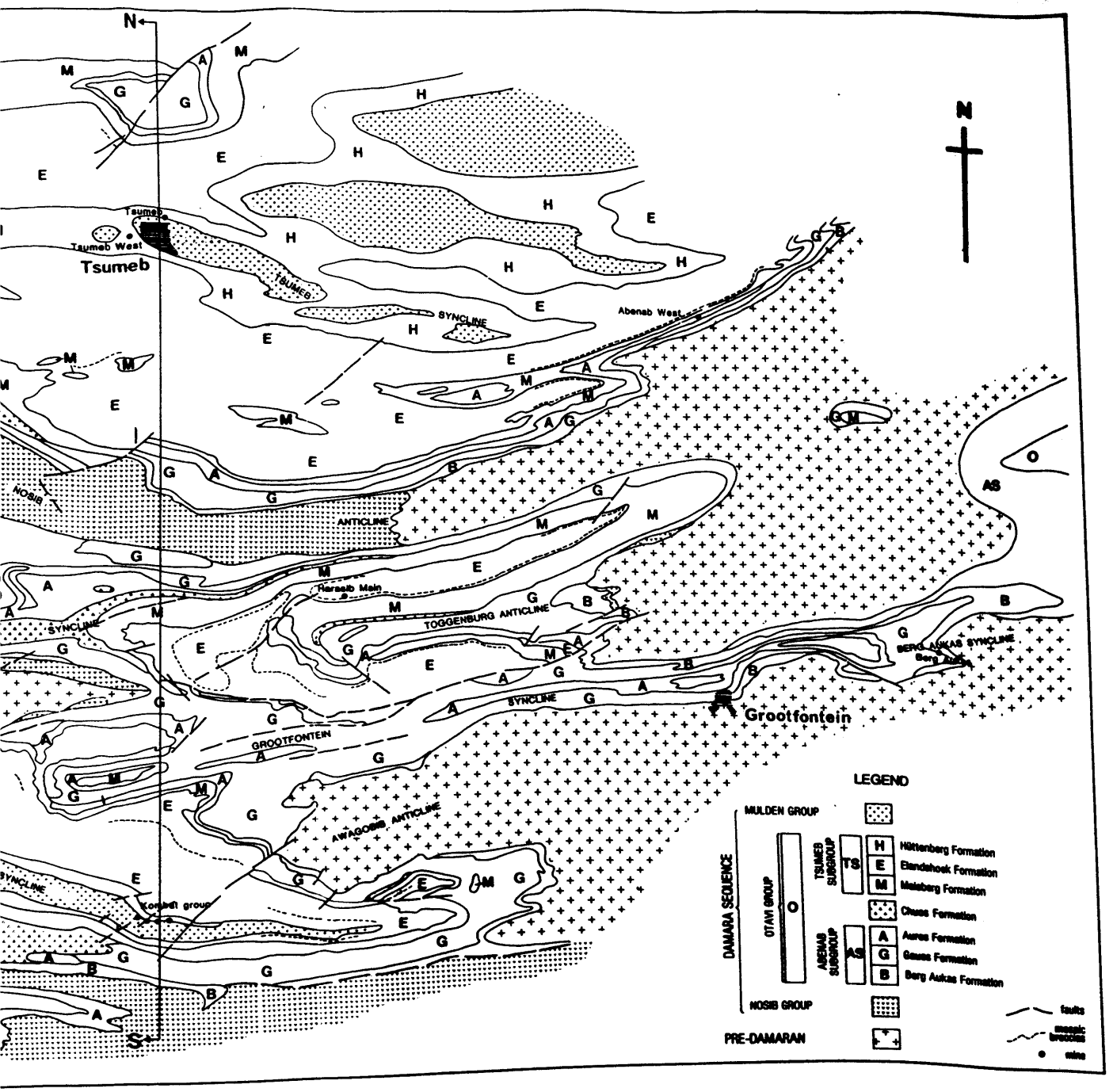

Land. Modified from mapping by Tsumeb Corporation Limited and
tion line N-S.

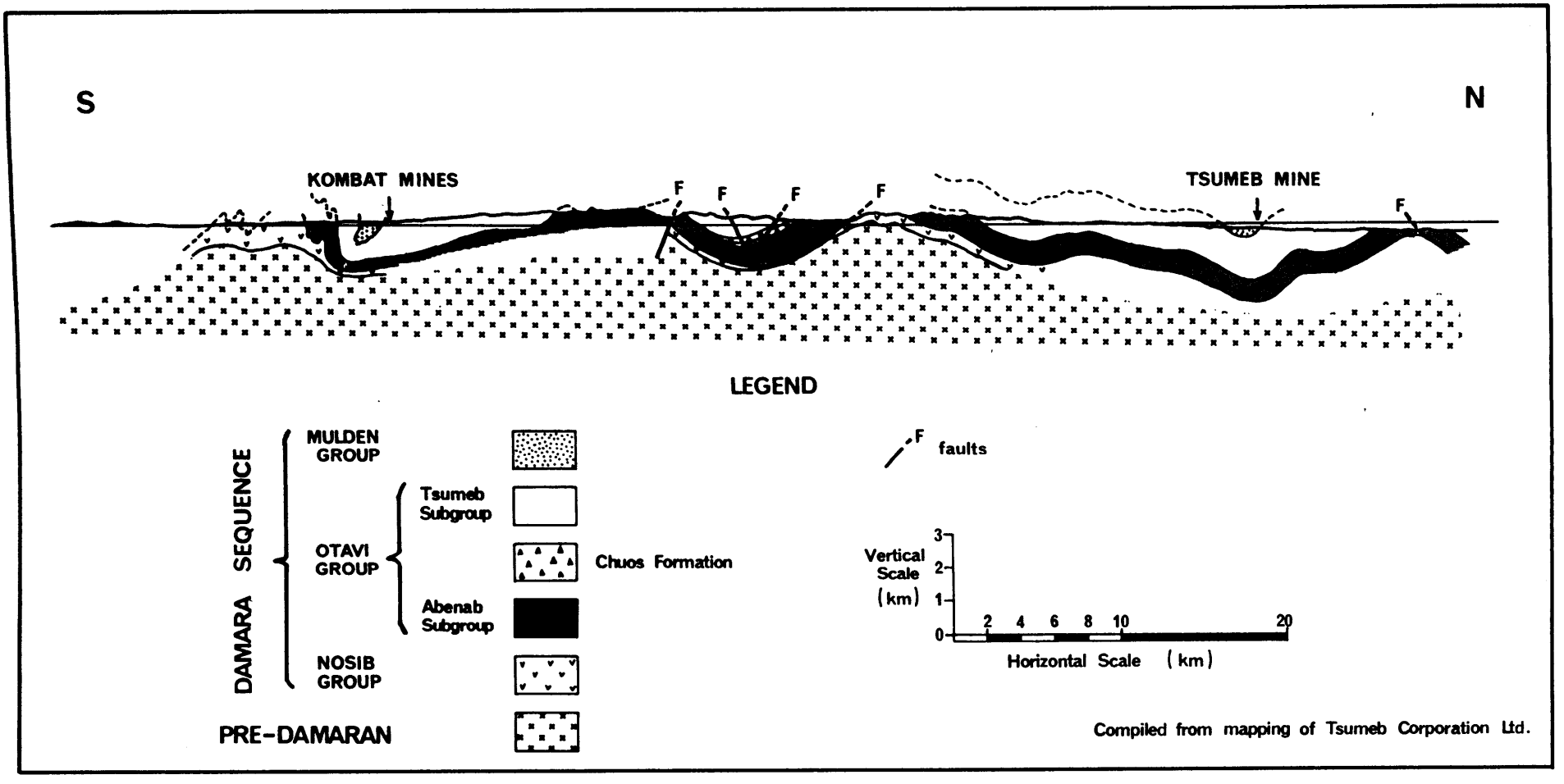

Fig. 4
Geological section N-S, Tsumeb to Kombat (see Fig. 3 for location).

pyritic, argillaceous limestone and dolostone occur at the base of the formation.

The Gauss Formation overlies the Berg Aukas Formation conformably. Its base is marked by the abrupt transition from laminated Berg Aukas dolostone to massive beds typical of the very light to medium grey dolostone of the Gauss Formation. The formation is 476 m thick in the Elandshoek type section. A few lenticular beds of sandstone and arenaceous dolostone occur near the base in places. The lowermost 90 m of the dolostone displays vuggy replacement by finely crystalline quartz and chert to give a colloform appearance. The amount of this replacement quartz increases upwards to become 10 - 50 per cent of the rock. Nodular, siliceous bodies in this rock were interpreted by Hedberg (1979) as possible silicified evaporite nodules. Minor galena and sphalerite are associated with the vugs in some areas (Thirion, 1973b). Massive dolostone, which overlies this colloform dolostone, contains some detrital carbonate grains and minor vugs. The massive dolostone becomes thin-bedded and brecciated towards the top, where it contains a thin oolite bed.

The Auros Formation overlies conformably the Gauss Formation throughout the Otavi Mountain Land. The type section on Elandshoek farm consists of 220 m of variably bedded dolostone, limestone and shale; its base is defined as the lowermost limestone bed (Hedberg, 1979). Limestone and irregular and bedded chert towards the base are overlain by light to medium grey, medium-bedded dolostone which contains ooids. The medium-bedded dolostone is overlain by medium gray, thick-bedded dolostone with silicified stromatolites. This dolostone is succeeded by calcareous shales with minor limestone and dolostone interbeds, followed by a thin stromatolitic, dolomitic limestone. The formation is terminated by 39 m of thick-bedded to massive, light to medium grey dolostone (the "quartz cluster dolomite" of the Abenab West area). The augen-like quartz and dolomite clusters of this rock contain cores of galena and sphalerite in places. These clusters are interpreted in Chapter 2.3.5 as possible former anhydrite nodules. The Auros Formation was eroded in the far western Otavi Mountain Land prior to deposition of the Maieberg Formation. The top of the Auros Formation in the type area is marked by an abrupt change

to thick, paraconformable limestone of the Maieberg Formation. Elsewhere the Chuos Formation is present, or an unconformity occurs at the base of the Maieberg Formation.

2.2.2 Chuos Formation

The Chuos Formation consists predominantly of mixtite which has been variously interpreted as tillite or a mud-flow deposit (Hedberg, 1979). The mixtite contains pebbles of dolostone, limestone, quartzite, chert, gneiss and granite. Fine-grained sandstone, shale beds up to 15 m thick, and a thin dolomitic limestone bed are associated with the mixtite in places. The Chuos Formation is absent from an extensive area in the eastern Otavi Mountain Land (i.e. east of section N-S, Fig. 3).

2.2.3 Tsumeb Subgroup

The Tsumeb Subgroup is composed almost entirely of sedimentary carbonate rocks. These consist of the Maieberg, Elandshoek and Hüttenberg Formations. The Maieberg Formation overlies the Chuos Formation conformably, or overlies older formations paraconformably to unconformably. The stratotype on farm Elandshoek consists of 395 m of thin-bedded and laminated carbonate rocks. The basal contact is a paraconformity which is marked by the change from Auros Formation dolostone to Maieberg Formation limestone. The Maieberg Formation can be divided into lower limestone and subordinate upper dolostone (zones T2 and T3, respectively of Söhnge, 1957), both in the stratotype and elsewhere throughout the Otavi Mountain Land. Contorted bedding and bent breccia clasts occur in the upper dolostone in some areas (Chapter 2.3.2). These were interpreted as penecontemporaneous slump features by Thirion (1973a) and Hedberg (1979).

The Elandshoek Formation is approximately 1000 m thick in the Otavi Mountain Land, where it overlies the Maieberg Formation conformably. It consists of light grey to grey, massive to medium-bedded, variably silicified dolostone with numerous stromatolite horizons. Throughout most of the area it can be divided into the three members of the stratotype (zones T4 to T6 of Söhnge, 1957), but

these interfinger and are replaced by other features to the west. The type sections are on Elandshoek farm and near Tsumeb township. The stratotype begins with the abrupt change from thin-bedded and laminated Maieberg dolostone to the 311 m thick, massive, light grey, basal dolostone member of the Elandshoek Formation (zone T4). This is unbrecciated at the base but becomes moderately brecciated upwards, both at the top of the basal member and in the base of the overlying member, where breccia fragments a centimetre to several metres in diameter occur. The breccias have a secondary quartz and dolomite spar cement which contains disseminated galena and sphalerite. Tectonic (Hedberg, 1979), slump (Söhnge, 1976) and solution brecciation (Thirion, 1973a) origins have been proposed for these breccias, which are interpreted here as solution-collapse breccias (Chapter 2.3.2). The thickness of the lower member decreases in the eastern Otavi Mountain Land, adjacent to the Grootfontein inlier, and its quartz content is higher. Some stromatolites are present in the western Otavi Mountain Land, and a siliceous oolite occurs in the middle of the member, north of Tsumeb.

The second member of the Elandshoek Formation in the type section is a 340 m, thick-bedded, silicified dolostone (zone T5 of Söhnge, 1957). Its base is defined by a change to other than massive bedding, and by the appearance of abundant thin, silicified dolostone and chert layers, a few centimetres to 10 m thick. These contrast with the irregularly silicified zones of the underlying member. Ooids and detrital grains are relatively common within the cherts. Syn-depositional breccias occur in the east-central Otavi Mountain Land. The member is considerably thinner, and the underlying member thicker, in the western Otavi Mountain Land.

The upper member of the Elandshoek Formation stratotype is a 265 m, thick-bedded dolostone with silicified stromatolites (zone T6 of Söhnge, 1957). It is predominantly a light grey, cherty and silicified dolostone which is distinguished by its bedding and its interbedded rock types. Medium grey, locally fetid dolostone beds become increasingly common towards the top of the unit. The basal unit of the member is a two metre thick, stromatolitic, very highly silicified dolostone and chert that constitutes a prominent marker in

the region ("tuten 1" of the mine area; Fig. 5). The stromatolites are laminar mats near the base, but pass rapidly into forms with individual but low relief and very little branching. Numerous thin chert, algal mat and stromatolitic dolostone and chert layers occur higher in this member, but become rare at the top. Some chert layers display ripple marks, ooids and polygonal shrinkage cracks. Three stromatolite horizons are used as markers in the Tsumeb mine area ("tutens 1, 2 and 3"; Fig. 5). The upper member of the Elandshoek Formation contains the North Break zone towards its base in the Tsumeb mine area (Fig. 5). This is a siliceous, manganiferous, calcitized and recrystallized zone which contains very minor copper-lead-zinc mineralization. It has been variously interpreted as: (1) a paleoaquifer with a superimposed tectonic breccia (Söhnge, 1976), (2) an unconformity (Callahan, 1971), or (3) the site of former anhydritic quartz sands (Hopwood, 1975). The top of the Elandshoek Formation is defined in the type section by the conformable transition from medium to light grey dolostone, to the predominantly dark grey units of the overlying Hüttenberg Formation.

The stratotype of the Hüttenberg Formation is in the immediate vicinity of Tsumeb township. The lower member (zone T7 of Söhnge, 1957) is 208 m thick and commences with thin-bedded, dark grey carbonaceous dolostone which contains thin shale and rare chert layers, including some oolitic chert. Thin, dark grey limestone and limy dolostone increase in importance upwards, although dark dolostone predominates at the top of the member in the Tsumeb mine area. The "augen limestone marker", less than one metre thick, occurs in the lower part of this member at Tsumeb mine and for 20 km to the west (Fig. 5). The calcite "augen" of this rock are interpreted here as former "gypsum daisies" after nodular anhydrite (Chapter 2.3.4).

The upper member of the Hüttenberg Formation (zone T8) consists of 175 m of lighter coloured, more siliceous dolostone in the type section. Algal mats are common at the base, but chert beds are rare. Three silicified oolite (including oolitic chert) beds are present in the upper part of the member. These occur over a 40 m interval, the thickest bed being 8 m thick. Phosphate minerals such as apatite crystals and collophane are associated with pyrolusite and disseminated

copper sulphides in these silicified oolite beds at Tsumeb and Kombat. The upper member contains: (1) stromatolites in places, (2) two or more silicified oolite beds in all areas, (3) ripple marks, (4) cross-bedding, and (5) possible desiccation cracks.

Oolitic chert and dolostone, stromatolite layers and dark limestone are present in the Hüttenberg Formation of the Otavi Valley syncline. Thirion (1973a) noted that oolite and chert horizons are more abundant on the north limb of this syncline than on the south limb. However, Innes and Chaplin (in press, 1985) consider that the Hüttenberg Formation is absent from the south limb.

2.2.4 Mulden Group

The stratotype of the Mulden Group consists of a number of exposures in the Tsumeb syncline (Hedberg, 1979). The lower formation consists of 30 m of slate (including calcareous varieties), greywacke and very rare lenses of limestone. Two, 2 m thick beds of sedimentary carbonate breccia are known locally. The lower formation overlies the Hüttenberg Formation with apparent conformity. Hedberg (1979) considered that the Kombat Formation of the Otavi Valley syncline might be partly correlative with this lower formation at Tsumeb. The Kombat Formation consists of slate and phyllite with rare basal sandstone lenses. It possibly exceeds 1300 m in thickness (Innes and Chaplin, in press, 1985).

The upper formation of the Mulden Group in the Tsumeb stratotype, now known as the Tschudi Formation, overlies either the lower formation, or the Hüttenberg Formation, with apparent conformity. However, a basal conglomerate is present 15 km to the west of Tsumeb, near Tschudi. The upper dark grey dolostone of the Hüttenberg Formation is absent in this area, indicating an erosional hiatus (Söhnge, 1976). The Tschudi Formation of the type area consists of approximately 700 m of sub-arkose and quartz arenite. Pyrite is locally abundant. This formation is not represented in the Otavi Valley syncline, although it may correlate with the pelitic Kombat Formation (Chapter 2.3.6).

The Owambo Formation is absent from the Otavi Mountain Land.

2.3 PETROLOGICAL STUDIES

Figure 5 shows the stratigraphic sequence in the Tsumeb mine area. This was compiled for this study from geological maps of the number 6, 7 and De Wet shafts, mine sections, and level plans of Tsumeb Corporation Limited (particularly those of A. Günzel and A. Lombaard). Data from surface geological mapping (Land, 1977b) and from the logs of diamond drill holes 2695 and 2742 were also used. The sequence is similar to that of Hedberg (1979) which was described in the previous section (since his type localities occur in the vicinity of Tsumeb).

Two features of Figure 5 should be noted. The first is that zone T7 is structurally complex in the mine area, and its thickness may therefore have been overestimated. The second is that much of the zone T5 dolostone of the mine area displays fairly massive bedding, and cherts may be less abundant than in the stratotype of Hedberg (1979). Therefore, differentiation into zones T4 and T5 is difficult or meaningless in the mine area, as noted by Hedberg (1979) for the western Otavi Mountain Land in general. This may explain why zone T5 has a thickness of more than 470 m in the mine area, but only 340 m in the nearby stratotype.

The informal zone classification of Söhnge (1957) is retained for convenience throughout this thesis. The following descriptions relate mostly to rocks in the vicinity of Tsumeb mine.

2.3.1 Otavi Group dolostone and chert

Otavi Group dolostone hosts most of the economically important mineralization of the Otavi Mountain Land, including the Tsumeb ore body. The compositions and textures of these rocks are relevant to discussions of the Tsumeb ore body breccias and to isotopic studies.

Carbonate rock of the Otavi Mountain Land is predominantly dolostone, which contains greater than 95 wt % carbonate minerals

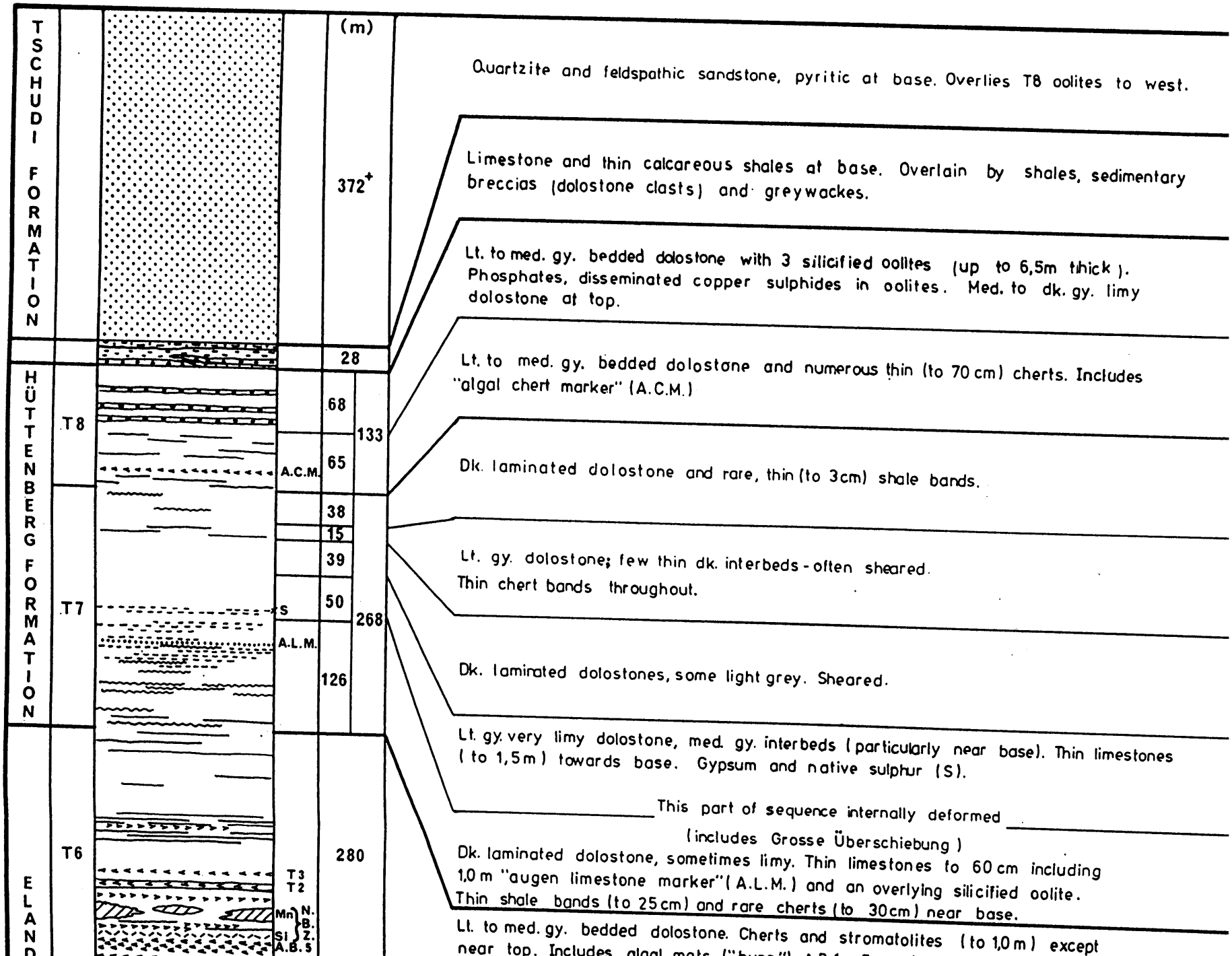
TSCHUDI FORMATION
HÜTTENBERG FORMATION
ELAND
T8
T7
T6
(m)
372+
28
68
65
133
38
15
39
50
268
126
280
A.C.M.
S
A.L.M.
T3
T2
Mn
N.
B.
Si
Z.
A.B.
S
Quartzite and feldspathic sandstone, pyritic at base. Overlies T8 oolites to west.
Limestone and thin calcareous shales at base. Overlain by shales, sedimentary breccias (dolostone clasts) and greywackes.
Lt. to med. gy. bedded dolostone with 3 silicified oolites (up to 6,5m thick). Phosphates, disseminated copper sulphides in oolites. Med. to dk. gy. limy dolostone at top.
Lt. to med. gy. bedded dolostone and numerous thin (to 70 cm) cherts. Includes "algal chert marker" (A.C.M.)
Dk. laminated dolostone and rare, thin (to 3cm) shale bands.
Lt. gy. dolostone; few thin dk. interbeds - often sheared.
Thin chert bands throughout.
Dk. laminated dolostones, some light grey. Sheared.
Lt. gy. very limy dolostone, med. gy. interbeds (particularly near base). Thin limestones (to 1,5m) towards base. Gypsum and native sulphur (S).
This part of sequence internally deformed
(includes Grosse Überschiebung)
Dk. laminated dolostone, sometimes limy. Thin limestones to 60 cm including 1,0 m "augen limestone marker" (A.L.M.) and an overlying silicified oolite.
Thin shale bands (to 25 cm) and rare cherts (to 30cm) near base.
Lt. to med. gy. bedded dolostone. Cherts and stromatolites (to 1,0 m) except

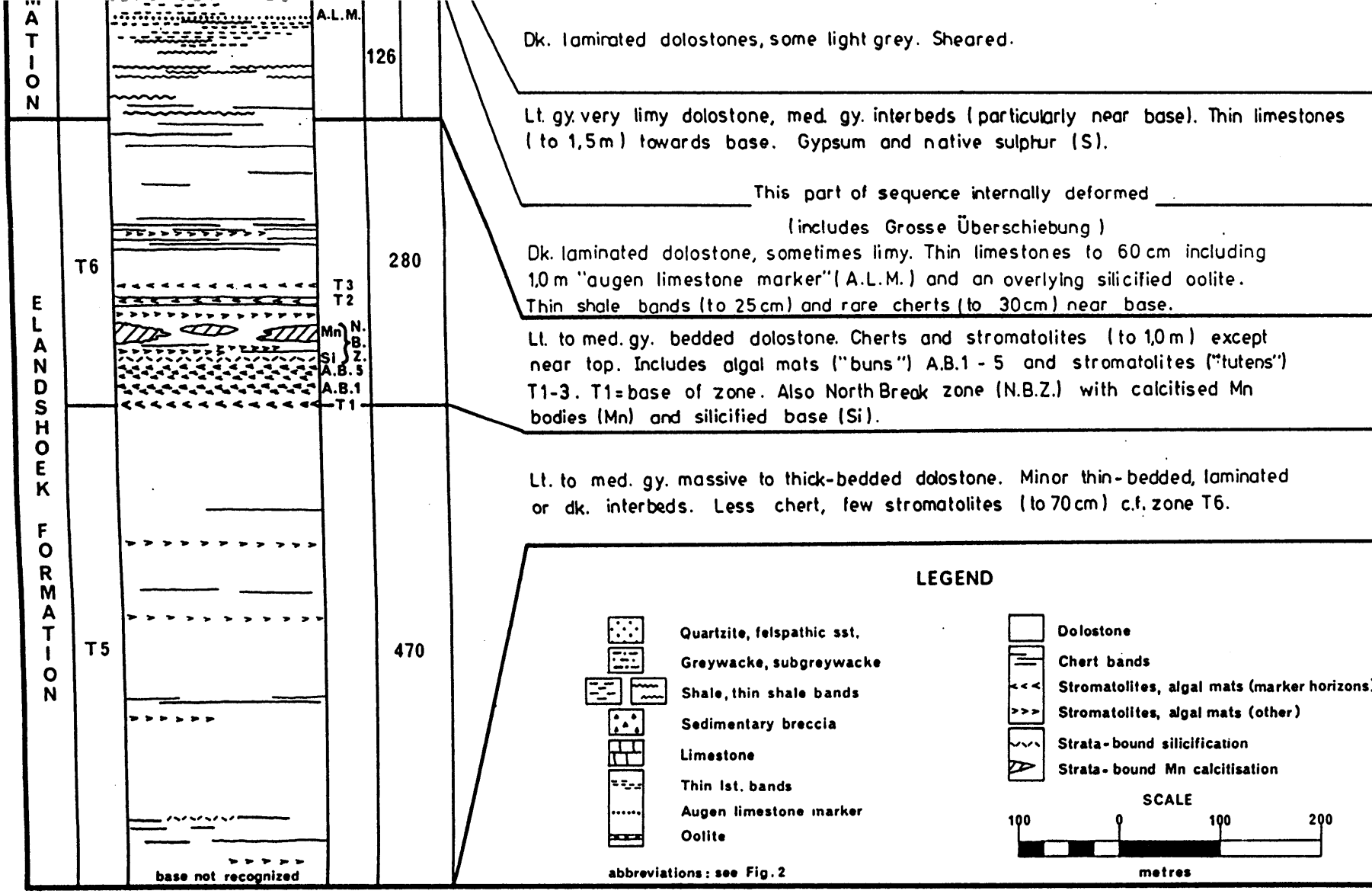

Fig. 5
Stratigraphic sequence, Tsumeb mine area. Compiled from geological maps and sections of Tsumeb Corporation Limited and logs of diamond drill holes 2695 and 2742.

(Table 1 and Schidlowski et al., 1975). Light to medium grey dolostone predominates, and was the only carbonate rock examined in detail during the present study. Specimens were studied from the Berg Aukas, Gauss, Maieberg and Elandshoek Formations, and typical analyses are shown in Table 1 (analyses 5-7). All of the samples are pure dolostones which consist of 5-30 μm microspar dolomite. The microspar has totally replaced the original rock matrix, which was presumably calcitic or dolomitic micrite. Detrital grains such as ooids have similarly been replaced (Fig. 6). Replaced ooids and indeterminate detrital grains are common throughout the mine sequence, but are difficult to distinguish in hand specimen.

Some dolostone specimens are thin bedded or laminated, others are massive. Bedding and laminae are mainly defined by grain-size variation, not compositional variation. Darker laminae consist of fine-grained microspar, and very light layers are coarse-grained dolomite spar (0,1-2,0 mm). The spar occurs as radial crystal aggregates in many specimens, and these project inwards from opposing walls of some layers. The centres of such layers are filled by quartz, microquartz and chlorite, or by single carbonate crystals elongated parallel to the layers. Silica minerals and chlorite are restricted to these sites in most specimens. These cavity-filling textures indicate former solution activity along bedding planes, possibly during dolomitization or late diagenesis. There is no associated sulphide mineralization to indicate that the solutions were ore solutions.

Hopwood (1975) concluded that the colour variation in Otavi Group dolostone beds is a function of their grain size and a grain-boundary effect. He found that dark dolostone has a very fine grain size (1-3 μm), and considered that the grain-boundary effect is caused by finely dispersed clays, which inhibited grain-boundary migration and caused irregular grain shapes. Hopwood (1975) concluded that the dark colour was not directly caused by carbonaceous impurities in most instances. However, carbonaceous material is important in some of these dark carbonate rocks. Analysis 2 (Table 1) shows 1,3 wt % reduced carbon in a dark dolostone, and Brant (1973a, b) noted that some dark dolostone and limestone of zone T7 contains abundant reduced

TABLE 1. ANALYSES OF OTAVI GROUP ROCKS

	HOPWOOD (1975)				THIS THESIS					
	(1)	(2)	(3)	(4)	(5)	(6)	(7)	(8)	(9)	(10)
*SiO_2	1,9	0,08	1,8	0,9	n.d.	n.d.	n.d.			
Al_2O_3	0,35	< 0,05	0,45	0,05	0,49	0,48	0,37			
Fe_2O_3	0,11	0,21	0,23	0,10	0,16	0,11	0,30			
CaO	29,7	32,1	30,3	30,8	30,0	28,7	30,0			
MgO	22,3	21,1	21,4	22,1	21,9	22,3	21,4			
Na_2O	0,05	0,07	0,08	0,05	< 0,01	< 0,01	< 0,01			
K_2O	0,37	0,29	0,37	0,32	< 0,01	< 0,01	< 0,01			
TiO_2	0,03	0,02	0,03	0,02	< 0,01	< 0,01	< 0,01			
P_2O_5	0,05	0,06	0,06	0,08	0,19	0,20	0,18			
MnO	0,05	0,11	0,11	0,05	0,02	< 0,01	0,14			
CO_2	44,8	43,9	44,6	45,0	46,3	47,2	46,6			
C	0,28	1,33	0,55	0,49	0,02	0,02	< 0,01			
TOTAL	100	100	100	100	100	100	100			
$\frac{MgO}{MgO+CaO}$	0,43	0,40	0,41	0,42	0,42	0,44	0,42			
	ppm									
Cu					3,4	2,5		10	36	10
Pb					0,8	2,6		32	19	38
Zn					18	13		51	43	57
Cd					0,2	0,1		0,3	0,02	0,1
Co					0,1	0,2		0,4	1,4	0,1
Ni					6,8	4,6		6,7	80	3,1
Ag					0,2	0,2		0,2	0,6	0,1
Ge					21	173		6	6	2
As					4	5		3	< 0,8	< 0,8
Sb					4 ppb	5 ppb		11 ppb	258 ppb	152 ppb
Ga					0,5	0,2		0,2	0,05	1,0
V					6	0,4		1	5	0,8
Mo					2,8	2,1		1,8	29	3,6
Se					18	13		11	2	4
Ba					< 20	< 20	< 20	n.d.	n.d.	n.d.
U					0,3	0,4		0,4	0,8	0,5
Th					0,1	0,1		0,3	0,2	0,1

1. Bedded grey dolostone, 31 level, Tsumeb.
2. Pyritic dark dolostone, 31 level, Tsumeb (possibly just outside pipe).
3. Indurated grey dolostone, 33 level, Tsumeb (probably just outside pipe).
4. Light coloured dolostone, 35 level, Tsumeb.
5. Massive light grey dolostone, zone T5 (surface sample PB5)
6. Massive light grey dolostone, zone T6 (surface sample PB4)
7. Massive medium grey dolostone, 30 level, Tsumeb (sample 439)
8. Dolostone, zone T8, Tsumeb (sample 837, DDH S56A)
9. Phosphatic dolostone, Kombat (sample 988)
10. Phosphatic dolostone (recrystallized), Kombat (sample 987)

n.d. = not determined
All analyses normalized for major components; analyses 5, 6 and 7 normalized assuming 1 % SiO_2 (as indicated by acid residues). Original analyses, analysts, methods in Appendix 1.1.

FIGURES 6-8

Fig. 6

Thin section of oolitic dolostone from the Elandshoek Formation. Microspar dolomite and dolomite spar have completely replaced the original rock-forming mineral, which was probably calcitic or dolomitic micrite. Detrital grains (probable ooids) have similarly been replaced. Plane polarized light. Sample 833, DDH 3163/38L Tsumeb.

Fig. 7

Hand specimen of phosphatic dolostone from the upper Tsumeb Subgroup. This rock contains angular, elongate, light grey, fragments, pellets and ooids of collophane, and a rounded dolostone clast (D). The fragments are extensively replaced by dolomite spar, and contain coarse-grained apatite crystals (i.e. this is the more altered variety of phosphatic dolostone described in the text). The matrix is medium to light grey dolostone, which consists of dolomite spar. Sample 987, Asis area, Kombat.

Fig. 8

Thin section of sample 987 (Fig. 7) showing large apatite crystals (A) in a matrix of dolomite spar. Crossed nicols.



Fig. 6

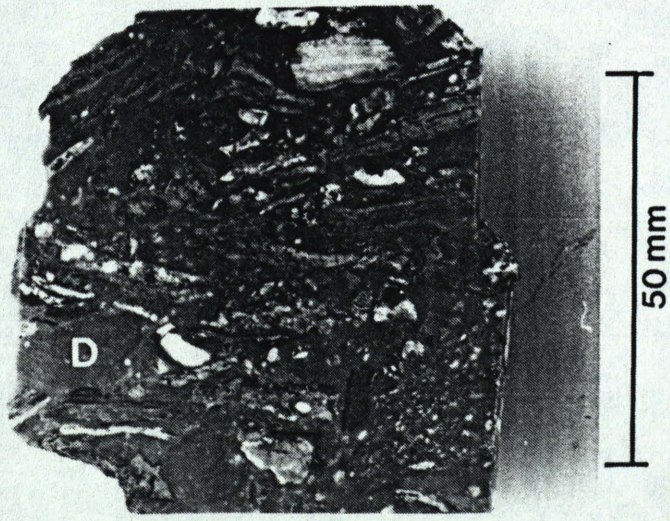

Fig. 7



Fig. 8

carbon (confirmed by analysis).

Bedded chert of the Tsumeb Subgroup consists mainly of microquartz with a grain size of 7-9 μm. Some Elandshoek Formation chert layers contain areas of dolostone, and bedding is continuous from the dolostone to the chert. These chert layers, therefore, replace bedded dolostone. Some chert of this type is associated with silicified stromatolites and algal mats, which themselves grade into chert. Oolite beds of zone T8 are typically silicified. Partly silicified examples consist of microspar dolomite ooids, replaced by silica to varying degrees, in a microspar and spar matrix. Megaquartz (0,1-0,2 mm) is present in addition to microquartz, and chlorite fills some ooid cores. The oolite beds grade into oolitic chert beds.

It is concluded that carbonate rocks of the Otavi Group have undergone a complex diagenetic history. They originally contained clastic, organic and micritic components and in this regard resemble some carbonate rocks of Phanerozoic age. Many interbedded chert layers are of diagenetic replacement type.

2.3.2 Otavi Group breccia

Different types of carbonate rock breccia occur throughout the Otavi Group, and some are important hosts for mineralization. The breccia can be grouped into five types, discussed below. Most of these breccia types were recognized by previous workers (e.g. Bühmann, 1973; Thirion, 1973a; Hopwood, 1975). However, there has been considerable disagreement as to the origin of individual breccia bodies, and some previous interpretations differ from those given here. For example, Bühmann (1973) considered the erosional breccia at locality 51, described below, to be a slump breccia. Hopwood (1975) interpreted the karst breccia of the Tsumeb pipe as a tectonic breccia.

1) Erosional breccia

An erosional breccia immediately underlies Kombat Formation phyllite at locality 51, west of Kombat (Fig. 111a). This polymictic

breccia contains matrix-supported clasts up to tens of centimetres in diameter, within a dolomite matrix. The clasts consist of angular to well rounded oolite, chert, and bedded and massive dolostone. The matrix is dolomite spar and microspar. The Hüttenberg Formation becomes attenuated along strike to the east and west of Kombat, and is absent from the southern limb of the Otavi Valley syncline (Fig. 3), and the upper Elandshoek Formation may also be absent near locality 51. The compositions of the breccia clasts indicate that they were mostly derived from these formations. The breccia is, therefore, interpreted as an erosional sedimentary breccia derived from the underlying and adjacent dolomite sequence. The significance of this erosional event is discussed in Chapter 6.1.4.

2) Slump breccia

Slump breccia is illustrated by breccia bodies in the uppermost Maieberg Formation, 10 km south of Tsumeb. Brecciated horizons are confined between continuous, well-laminated, unbrecciated beds, and the breccia bodies also grade laterally into these undisturbed beds. The elongate fragments of the breccia bodies are curved and bent in a random manner, and bedding in the enclosing rock curves around the fragments. This syn-sedimentary, soft-sediment style of brecciation is thought to be related to slumping (Thirion, 1973a).

3) Solution-collapse breccia

These oligomictic breccia horizons are thought to have formed by dissolution of soluble minerals and horizons, with attendant collapse of interbedded and overlying rocks. Many breccia bodies of this type have a well-defined base but an irregular top; the intensity of brecciation and degree of fragment rotation decreases upwards.

Small-scale solution-collapse breccia bodies are common, and these contain fragments, 1 mm to 1 cm in diameter, which are only slightly displaced and rotated from their original position prior to brecciation. Matrices of coarse-grained dolomite spar and minor quartz constitute only a small proportion of these rocks, and their brecciated nature is not obvious in hand specimen. Many breccia

bodies of this type may be diagenetic and unrelated to mineralization (c.f. solution activity described in Chapter 2.3.1). The other extreme in clast size and breccia distribution is represented by strata-bound, regionally extensive, coarse grained breccia horizons with mineralized matrices, such as occur in zone T4 of the Elandshoek Formation. The solution-collapse origin of these mineralized breccia horizons has been disputed by some workers (Chapter 4.4.7).

4) Karst breccia

Karst breccia forms by sedimentation within pre-existing karst cavities. Sediments are washed into the cavities via solution pipes (e.g. sink-holes) or underground streams. Solution-collapse breccia forms in the same cavities, and clasts from these can be incorporated in the introduced sediment. Karst breccia is commonly discordant to bedding, and contains some components that are foreign to the enclosing rock. The mineralized Tsumeb breccia pipe is interpreted as a karst breccia (Chapter 6.1).

5) Tectonic breccia

Bodies of fault breccia in the Otavi Group were not studied because of their limited exposure and lack of economic importance. Mineralized, breccia-filled fractures associated with the Tsumeb ore body are thought to be related to fracturing associated with solution collapse, not to regional tectonism (Chapter 6.1.2).

In conclusion, solution-collapse and karst breccia bodies are important hosts to hypogene sulphide mineralization in the Otavi Mountain Land. Erosional, slump and tectonic breccia do not form important ore loci, although some mineralized karst features may have developed on pre-existing faults (Chapter 4.4.1).

2.3.3 Phosphatic rocks of the Hüttenberg Formation

Phosphate minerals are relatively abundant in parts of the Hüttenberg Formation. Phosphatic sedimentary rocks throughout the world are characterized by anomalously high concentrations of certain

elements which are unusually enriched in the Tsumeb sulphide ore (Chapter 6.4.1). These rocks are, therefore, possible sources of some elements in the ores.

Bedded collophane (cryptocrystalline apatite) bands and crystallized apatite occur in silicified oolite beds of zone T8 at Tsumeb (Fig. 5). The apatite consists at least partly of dahllite (carbonate apatite) granules, which occur in the centres of silicified ooids (Söhnge, 1957). Phosphatic rocks are also present in the upper part of the Tsumeb Subgroup of the Kombat area (Fig. 3). Very minor collophane also occurs in discordant "pseudo-aplite" bodies at Kombat These bodies are interpreted here as karst-filling Mulden Group quartz arenites (Chapter 4.4).

Phosphatic dolostone from the upper Tsumeb Subgroup of the Kombat area contains angular, elongate fragments which resemble rip-up clasts. Collophane pellets and ooids, and very rare, rounded dolostone intraclasts are also present. Some rocks contain dark brown, isotropic clasts of collophane, and possibly carbonaceous material, in a matrix of dolomite spar. The clasts are partly replaced by quartz and dolomite spar, and contain abundant small apatite inclusions. Other rocks contain white to light grey collophane clasts, which are extensively replaced by coarse-grained dolomite spar identical to that of the matrix (Fig. 7). Coarse-grained apatite is associated with the collophane (Fig. 8).

The lighter coloured rocks are possibly carbonated and recrystallized equivalents of the dark rocks. Cobalt, nickel and molybdenum, elements which may be related to organic material (Chapter 6.4.1), have significantly lower concentrations in a sample of the more altered rock (analyses 9 and 10, Table 1). However, there is otherwise no systematic depletion of minor elements in the more altered rock.

It is concluded that the phosphatic rocks have undergone a complex diagenetic history. This is indicated by recrystallization of these dolomitic rocks and by the presence of apatite cores in ooids of zone T8, and collophane in "pseudo-aplite". The latter indicates that phosphorus was introduced or re-mobilized as late as Mulden Group

times. The complex history of zone T8 phosphatic oolite beds is discussed in Chapter 2.3.4.

2.3.4 Hüttenberg Formation evaporites

An evaporite horizon was recognized in the Hüttenberg Formation of the Tsumeb mine area for the first time during the present study. Similar horizons may be present at the Kombat, Abenab West and Berg Aukas mines. These mines have been the principal metal producers in the Otavi Mountain Land, and the relatively large size of their ore bodies might result from the presence of major sources of sulphur in their immediate vicinities.

A search of the mineral collection of Tsumeb Corporation Limited and of old diamond drill-hole logs revealed that native sulphur, gypsum and anhydrite had been intersected in zone T7 in a number of drill holes at the Tsumeb and Kombat mines. Most samples consist of irregular areas and veinlets of these minerals, in which native sulphur occurs as cores to veins of gypsum or calcite. The stratigraphic position of all recorded occurrences of these minerals within the Tsumeb mine is plotted on Figure 19. The strong stratigraphic control on these minerals is consistent with a sedimentary, evaporitic origin for the sulphate minerals. No sulphide minerals typical of the Tsumeb ore are associated with the sulphate minerals or native sulphur, with the exception of minor pyrite which appears to have replaced gypsum in one sample. There is no evidence that the sulphate minerals or native sulphur formed during the main ore-forming event. A bed of nodular anhydrite has recently been intersected in a similar stratigraphic position during drilling outside the immediate mine area (A. Günzel, pers. comm., 1984). This further supports an evaporitic origin for the sulphate minerals.

A characteristic bed less than one metre thick, the "augen limestone marker", is present in the Tsumeb area (Fig. 5). This bed occurs on both limbs of the Tsumeb syncline and extends for 20 km to the west of Tsumeb (Griffis, 1950). Its distribution coincides with that of sulphide mineralization in the Tsumeb area (Fig. 111a). The "augen limestone marker" contains black, sub-spherical bodies of calcite spar

("augen") in a matrix of black limestone. These bodies consist of aggregates of radiating crystals up to 3 cm in diameter (Fig. 9). The limestone emits a strong odour of H_2S when crushed. The very positive $\delta^{13}C$ values of both the "augen limestone marker" and adjacent dolostone are consistent with an evaporitic environment (Chapter 5.2.1). The "augen limestone marker" occurs only 35 m stratigraphically below most of the native sulphur and gypsum occurrences in the Tsumeb mine area. Hobson (1980; fig. 23) described spherulitic gypsum bodies ("gypsum daisies") of similar appearance from the Permian of England. These form during the hydration of anhydrite nodules. The Tsumeb "augen" might be similar bodies, now replaced by calcite. Other possibilities include replacement of anhydrite nodules by calcite (M.E. Tucker, pers. comm., 1982), or aragonite spherulites, also common in evaporitic sequences (Davies, 1977; D. Shearman, pers. comm., 1982).

Albite crystals are disseminated in several beds of dolostone and limestone between 12 and 18 levels of Tsumeb mine (Fig. 10; Söhnge, 1964). This corresponds to the interval which contains gypsum and native sulphur occurrences and the "augen limestone marker" (Figure 19). Gypsum and pyrite are associated with albite in one sample from the immediate vicinity of the "augen limestone marker", and ore-stage carbonate minerals post-date the albite crystals. Albite has been reported in evaporite-bearing rocks elsewhere in the world, where it is possibly a late diagenetic mineral produced by sodium chloride brines. Porphyroblastic albite has been interpreted as a low grade metamorphic product in salt-bearing marbles and former marls of the French Pyrenees (Moine et al., 1981).

Minor sulphate minerals might also have been associated with the zone T8 oolite beds. Small, radial crystal aggregates of unknown type, now pseudomorphed by silica, occur in some ooid cores (Fig. 11), and similar aggregates occur in phosphatic dolostone of the Kombat area. The delicate nature of the crystal forms indicates that these were diagenetic replacement features, rather than nuclei around which the ooids grew, and they may represent former sulphate minerals. Disseminated chalcocite is widespread in the zone T8 oolite beds westwards from Tsumeb, where it frequently replaces ooid cores, and

FIGURES 9-12

Fig. 9

Hand specimen of olive-black limestone of the "augen limestone marker", showing a spherical calcite body (i.e. one of the "augen"). Elongate blades of calcite radiate outwards from a finer-grained, granular calcite core (C). This was probably originally a "gypsum daisy" after anhydrite, now replaced by calcite; other possibilities are an anhydrite nodule, or an aragonite spherulite. Sample 957, DDH 3189, lower Hüttenberg Formation (central part of zone T7), Tsumeb, approximately 40 m stratigraphically below the zone T7 evaporite horizon.

Fig. 10

Thin section of an albite crystal in medium light grey limestone from lower zone T7. The crystal contains small inclusions of spar, and is rimmed by coarse-grained calcite spar; an euhedral crystal of pyrite is present at the top right. The albite is a possible product of metasomatism by NaCl brines. Sample 623, lower Hüttenberg Formation, Tsumeb, a few tens of metres below the "augen limestone marker" of Figure 9. Crossed nicols.

Fig. 11

Thin section of silicified oolite from upper zone T8. A radial crystal aggregate, now replaced by quartz, occurs in the core of an ooid; apatite and sulphide minerals occur in the cores of ooids in other specimens. The delicate form of the crystal aggregate indicates that it has a diagenetic origin and was not a nucleus about which ooids formed. The mineral might have been anhydrite or aragonite. Sample 788, Hüttenberg Formation, Tsumeb. Plane polarized light.

Fig. 12

Hand specimen of light pinkish dolostone of the "quartz cluster dolomite". The dolostone consists of microspar and spar (the latter filling vugs) and contains "clusters" of coarse-grained, white dolomite spar. The "clusters" have unequal axes in the section shown, and have long axes perpendicular to the figure. The stylolitic boundaries of "clusters" are rimmed by black manganese oxides, and "clusters" from some other localities contain quartz and ore sulphide minerals. The "clusters" are interpreted as former anhydrite nodules. Sample 810, top of Auros Formation, Abenab West.

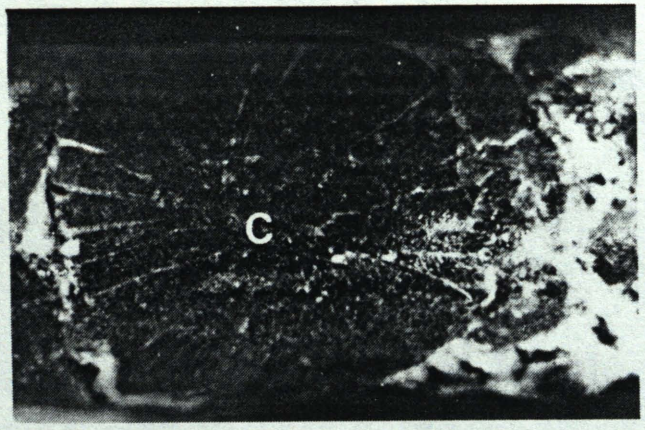

Fig. 9

0 cm 0.8

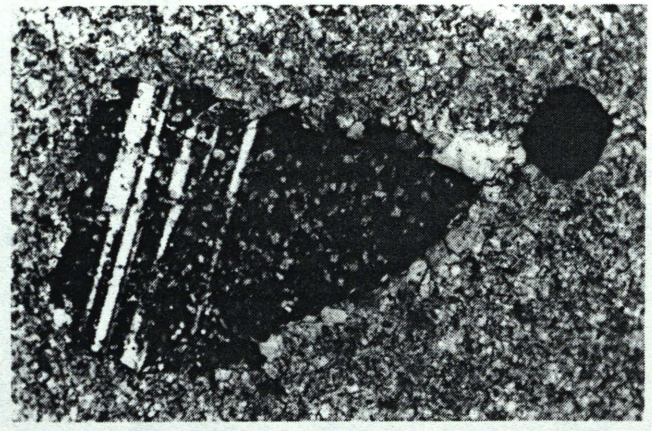

Fig. 10

0 mm 0.2

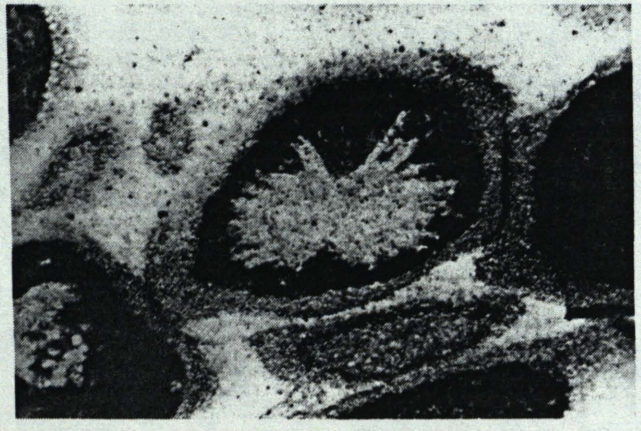

Fig. 11

0 mm 0.2

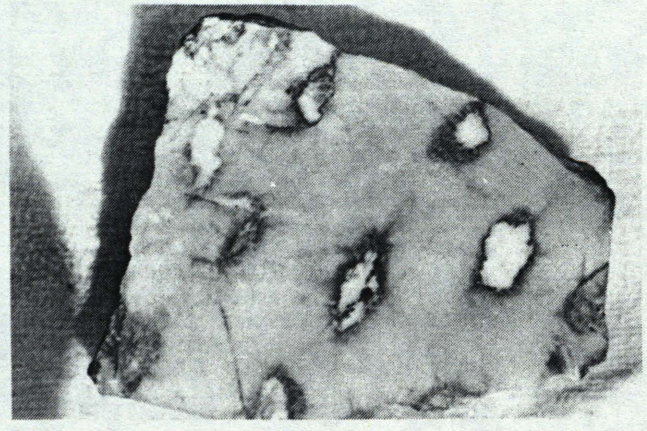

Fig. 12

0 cm 3

hypogene sulphide minerals typical of the Tsumeb ore, including sulvanite, betekhtinite and nickel-carrollite, are also present. Moore and Druckman (1981) recorded replacement of ooids by anhydrite, then pyrite, in the Phosphoria Formation, U.S.A., and a similar process might have operated at Tsumeb.

The zone T8 oolite beds and their equivalents at Kombat have therefore undergone a complex post-depositional history. This included: (1) silicification (prior to Mulden Group deposition; Chapter 2.3.6), (2) recrystallization of carbonate minerals, and replacement by phosphate and possible sulphate minerals (possibly after Mulden Group deposition; Chapter 2.3.3), and (3) replacement by ore sulphides, subsequent to Mulden Group sedimentation (Chapter 6.1). Pyrolusite is also characteristic of the zone T8 oolite beds at Tsumeb and Kombat, but its significance is not known. This complex history is a function of various periods of fluid activity, which probably resulted from the initial high permeability of the oolite beds, and from permeability produced during exposure and karsting, prior to deposition of the Mulden Group (Chapter 2.3.6).

Shallow water to subaerial conditions were characteristic of sedimentation of the upper Tsumeb Subgroup. Lagoonal and sabkha environments are represented by the lower part of zone T7 in the Tsumeb area. These environments are indicated by: (1) the presence of desiccation features (Söhnge, 1957), (2) the discontinuous nature of beds, and (3) the association of dark, carbonaceous dolostone and limestone, pyritic and carbonaceous shale, and sulphate minerals, including nodular anhydrite. The overlying zone T8 oolite beds indicate shallow water conditions, and this was followed by exposure and erosion. Similar environments are preserved near Kombat, in the Otavi Valley syncline (Fig. 3).

2.3.5 Other Otavi Group evaporites

Evaporite minerals might have been present elsewhere in the Otavi Group. The "quartz cluster dolomite" which terminates the Auros Formation is extensively developed between Tsumeb and Abenab, but has been removed by erosion farther to the west. This vuggy-textured

dolostone contains elongate white dolomite bodies ("clusters") of dolomite spar with a grain size of up to 2,5 mm (Fig. 12). The "clusters" in a sample from the Abenab West area are asymmetric in cross-section, with 1-2 cm intermediate axes and 0,6-1,2 cm minor axes. They are extremely elongate perpendicular to this plane, the major axes being 3-4 times the length of the intermediate axes. The major axes of all the "clusters" are parallel. The margins of the "clusters" are surrounded by black manganese oxide halos, and some are stylolitic.

The form of the clusters is similar to that of deformed, elongate anhydrite nodules which Schenk (1969) and Shearman (1978) described from a fossil sabkha in the Carboniferous of Canada. The Auros Formation consists of variable, relatively thin beds of dolostone, chert (some oolitic), stromatolites, calcareous shale and numerous limestone beds. These probably represent lagoonal and other shallow water environments, terminated by a sabkha (the "quartz cluster dolomite"). This was followed by deposition of the Chuos Formation, and erosion prior to sedimentation of the Tsumeb Subgroup.

The "clusters" commonly contain quartz in addition to dolomite, and some have cores of galena and sphalerite. Sulphide-bearing "clusters" of this type occur at the Abenab West mine, in association with sulphide blebs comparable in size to the "clusters" (Verwoerd, (1957). It is therefore probable that sulphide minerals, dolomite and quartz have directly replaced original anhydrite nodules. Sulphide replacement of this type has been described from numerous localities throughout the world (e.g. West et al., 1968; Annels, 1974; Milner, 1976). Possible similar replacement has been described above from zones T7 and T8 of the Hüttenberg Formation (Chapter 2.3.4).

Hedberg (1979) recorded possible silicified evaporite nodules towards the base of the Gauss Formation. There is also an unconfirmed report of anhydrite in this stratigraphic position at the Berg Aukas mine (G.H. Gavine, pers. comm., 1980). Colloform and vuggy dolostone is extensively developed in the basal 90 m of the Gauss Formation. Similar colloform and brecciated rocks, and minor oolite horizons, occur elsewhere in the formation, particularly towards the top. Brecciation and cavity-filling textures have obliterated original

depositional features in the colloform rocks, probably as the result of early dissolution of soluble material in the bedding (Chapter 2.3.1). It is suggested that this soluble material consisted of evaporite minerals, and that evaporite horizons were present at various levels in the Gauss Formation.

Evaporite horizons might also have been present in the North Break zone of the Tsumeb mine area (Chapter 3.4.4), and within zone T4 (Chapter 4.4.7), but there is no direct textural evidence for their former presence.

In summary, the major base metal ore bodies of the Otavi Mountain Land are located in evaporitic sequences. Probable sabkhas occur at the top of the Auros Formation, the top of the Tsumeb Subgroup, and possibly near the base of the Gauss Formation. A similar relationship between economic mineralization of this type and evaporites exists elsewhere in central Africa. The possibility that anhydrite and gypsum provided sulphur for the base metal ores, and that the presence of these minerals was a major control on the location of economic mineralization in the Otavi Mountain Land, is discussed in Chapter 6.2.

2.3.6 Mulden Group sedimentary rocks

Mulden Group sedimentary rocks are important to ore genesis for a number of reasons. A permeable zone developed beneath the base of the Mulden Group as the result of exposure and karsting at the surface of the underlying Tsumeb Subgroup. Karst cavities such as the Tsumeb pipe were filled with sediments of the basal Mulden Group (Chapter 6.1). The permeable unconformity controlled the later flow of ore solutions, and mineralization was deposited in the karst features. Mulden Group arenites and pelites also host major quantities of strata-bound pyrite and minor copper mineralization in the Tsumeb and Kombat areas, and some of this is interpreted as genetically related to the Tsumeb mineralization (Chapter 5.3.2). Mulden Group pelites are also probable sources of metals present in Otavi Mountain Land ores (Chapter 6.4.2).

Mulden Group rocks are preserved in two areas. Arenites dominate in the Tschudi and Tsumeb synclines, near Tsumeb, while pelites dominate in the Otavi Valley syncline, near Kombat (Fig.3).

The contact between the Otavi Group and Mulden Group is broadly conformable in the Tsumeb area, but contact relationships are poorly known because of restricted outcrop. A disconformity is indicated by the absence of the uppermost zone T8 dolostone near Tschudi, 15 km west of Tsumeb, where Mulden Group sediments directly overlie oolitic chert beds of zone T8. The lower, unnamed formation of the Mulden Group averages 30 m in thickness in diamond drill-holes near Tsumeb, and is of variable lithology. Conglomerate, sedimentary breccia and grit constitute part of the lowest few metres. Most shale, marl and thin limestone beds are confined to within 20 m of the base. Greywacke and subgreywacke are mainly restricted to this formation (Lombaard, 1976). The lower formation is overlain by thick sub-arkose and quartz arenite of the Tschudi Formation. The lower formation is absent near Tschudi, and conglomerate forms the base of the Tschudi Formation. This ranges from well-rounded, clast-supported conglomerate to matrix-supported sedimentary breccia.

The Mulden Group of the Kombat area is characterized by a lack of arenite beds. Phyllite and slate of the Kombat Formation immediately overlie dolostone, dolostone breccia or calcareous pelite. The transition from dolostone to slate is typically abrupt. Rare, pebbly sub-arkose lenses form the base of the formation in places (e.g. near the Kombat group of mines). Dolostone breccia horizons, some with a phyllite matrix, which occur on this contact are predominantly erosional (Chapter 2.3.2). However, breccia bodies of solution-collapse, karst and possible tectonic origin occur in the upper part of the underlying dolostones (Chapter 4.4.2).

Mulden Group arenite of the Tsumeb area was described by Botha (1960). It has a 0,2-0,5 mm grain size and contains 60-80 (vol.) % quartz, 10-20 % feldspar, 0-10 % calcite, 0-5 % pyrite and accessory muscovite, sericite (fine-grained white mica), biotite, chlorite, zircon, tourmaline, apatite, iron oxides, ilmenite, rutile and epidote. There is little matrix or cement between the grains, which usually

possess sutured contacts, although some are rounded. A grain elongation and preferred orientation, related to a structural fabric, is common, and this is further accentuated by parallel streaks of sericite. Hedberg (1979) considered that biotite is only present as rounded, detrital grains in these rocks, whereas muscovite is mostly metamorphic. Botha (1960) recorded that microcline is the dominant feldspar, with accessory plagioclase (An_{5-10}) and subordinate orthoclase or microperthite.

Samples of arenite from the Tsumeb area examined during the present study correspond to the above descriptions. However, albite and microperthite dominate over microcline in some samples, and some grains consist of aggregates of plagioclase laths, and might have been derived from an intermediate to basic igneous rock. A carbonate mineral occurs in the arenite matrices and as cross-cutting veinlets. Coarse grained muscovite in the arenite shows no preferred orientation and contains biotite remnants of presumed detrital origin, which it has replaced. Fine grained white mica is aligned parallel to a cleavage. The sulphide minerals are described in Chapter 4.4.1. A typical arenite is illustrated in Figure 25, and whole-rock and minor element analyses are given in Table 2. Some of these rocks have relatively high TiO_2 contents.

Sedimentary rocks of the basal Mulden Group at Tsumeb, and to the west, are variable in composition. Sedimentary breccia from Tsumeb consists of angular dolostone clasts in a matrix of calcite, white mica and angular quartz. The breccia is associated with fine grained sediments of similar composition to the breccia. The breccia clasts appear to be derived from dolostone of the underlying Tsumeb Subgroup. Sedimentary breccia from west of Tsumeb contains angular to sub-angular clasts of chert, quartz arenite and vein quartz in a sub-arkose matrix. Chert clasts are up to 10 cm in diameter, and silicified ooids can be recognized in some clasts. Clast-support conglomerate, with well-rounded pebbles of the above composition, is also present. The chert clasts have been derived from immediately underlying oolitic chert beds of zone T8. The breccia and conglomerate grade into arenite, which contains chert, quartz and feldspar grains.

TABLE 2. ANALYSES OF MULDEN GROUP AND COMPARATIVE SEDIMENTARY ROCKS

	SANDSTONE							PELITE			
	Le Roex (1955)	Hopwood (1975)	This thesis		Pettijohn (1975)			This thesis			Pettijohn (1975)
	(1)	(2)	(3)	(4)	(5)	(6)	(7)	(8)	(9)	(10)	(11)
SiO_2	82,5	67,3	86,7		94,7	77,0	66,2	66,2	56,8		59,0
Al_2O_3	5,6	14,4	6,2		1,1	8,7	13,5	14,6	16,7		15,6
Fe_2O_3	1,49	1,54	0,19		0,6	2,3	5,5	5,5	7,4		6,3
CaO	3,5	0,34	0,58		1,6	2,7	2,5	0,98	0,24		3,2
MgO	0,85	0,16	0,31		0,1	0,5	2,1	2,5	3,6		2,5
Na_2O	0,76	2,1	0,93		0,1	1,5	2,9	2,5	0,91		1,32
K_2O	2,3	5,7	2,7		0,2	2,8	2,0	2,8	3,9		3,3
TiO_2	0,33	0,92	0,11		0,2	0,3	0,6	0,90	0,85		0,66
P_2O_5	0,01	0,14	0,13		-	0,1	0,2	0,22	0,21		0,17
MnO	0,02	0,01	0,01		-	0,2	0,1	0,04	0,16		tr
CO_2	1,78	0,44	0,75		1,1	3,0	1,2	1,26	2,3		2,7
C	n.d.	n.d.	0,05		-	-	0,1	0,12	0,47		0,81
FeS_2	tr	4,0	1,37		-	-	tr	-	2,7		0,81
H_2O^+	0,91	2,9	tr		0,3	0,9	2,4	2,4	3,7		3,7
TOTAL	100	100	100		100	100	100	100	100		100
ppm											
Cu			10	2,9				21		30	
Pb*			7	3				13		7	
Zn			5	9				56		140	
Cd			0,1	0,1				0,4		0,2	
Co			1,7	6				24		29	
Ni			2,1	21				51		59	
Ag			0,1	3,4				0,3		0,1	
Ge			8	97				30		94	
As			0,9	0,5				21		17	
Sb			1 ppb	1 ppb				2 ppb		20 ppb	
Ga			7	14				39		32	
V			8	36				96		122	
Mo			3,9	2,9				45		4,4	
Se			2	4				11		12	
Ba			514	n.d.				439	589	n.d.	
U			1	8				4		4	
Th			3	9				12		9	

1. Tschudi Formation sandstone, Tsumeb area (surface).
2. Tschudi Formation sandstone (pelitic?), drill hole S56, Tsumeb.
3. Tschudi Formation sandstone, drill hole AP39, Tschudi (sample PB1).
4. Tschudi Formation sandstone, drill hole S40, Tsumeb, (sample PB12).
5. Average orthoquartzite.
6. Average arkose.
7. Average greywacke.
8. Kombat Formation slate, drill hole ASW 95G, Otavi Valley (sample PB8).
9. Kombat Formation slate, drill hole AW 68A, Otavi Valley (sample PB10).
10. Kombat Formation slate, drill hole AW 81A, Otavi Valley (sample PB11).
11. Average shale.

n.d. = not determined · tr. = trace
All analyses normalized for major components (original analyses, analysts, methods in Appendix 1.1).
*Tschudi Formation sandstone - 9 ppm Pb (sample PB3).
Kombat Formation slate - 10 ppm Pb, 4 ppm U, 14 ppm Th (sample PB9).

Kombat Formation slate is a fine grained aggregate of chlorite, white mica and subordinate quartz. It contains deformed veinlets and disseminated grains of pyrite, with pyrrhotite overgrowths of probable metamorphic origin. The sulphide minerals are described in Chapter 4.4.5. Analyses of Kombat Formation slate are given in Table 2, together with that of average shale. The Kombat Formation rocks are lower in CaO than the average shale, and contain significantly higher TiO_2 contents and less reduced carbon. They have low to average Zn, Pb and Cu contents, slightly elevated As, Co, Ga and Ni contents, high Mo and Se, and extremely high Ge contents relative to average shale (Table 12).

It is concluded that the contact between the Otavi Group and the Mulden Group marks an erosional hiatus prior to a major change in sedimentary environment. Hedberg (1979) suggested that sedimentation of the Mulden Group was dominantly continental, and this is supported by the presence of basal conglomerates, sedimentary breccias, and rocks locally derived from the upper Tsumeb Subgroup. These were succeeded by sediments of more distant, granitoid provenance. Hedberg (1979) suggested that the Kombat Formation of the Otavi Valley syncline represents a facies change in the Hüttenberg Formation. He considered that the upper part of the Kombat Formation might be partly correlative with the unnamed lower formation of the Mulden Group at Tsumeb. However, the Hüttenberg Formation was deposited in similar shallow water and subaerial environments in both the northern and southern Otavi Mountain Land. It was karsted throughout the Otavi Mountain Land and extensively eroded in the south, prior to the abrupt change to deposition of Kombat Group shale, with basal sandstone lenses (Chapter 6.1.4). It is suggested here that the Kombat Formation is correlative with both the lower and Tschudi Formations of the Mulden Group, but not with any part of the Otavi Group. The change from arenite in the northern Otavi Mountain Land to pelite in the south reflects a transition from continental sedimentation to deeper water, possibly marine sedimentation. The extensive formation of erosional breccias in the south reflects high relief in this area, possibly adjacent to a fault-bounded basin, followed by a rapid marine transgression. This model is developed in a regional framework in Chapter 6.1.4.

CHAPTER THREE

TSUMEB ORE BODY

The Tsumeb ore body is situated on the northern limb of the Tsumeb syncline, which has an easterly trend and plunge in the vicinity of the Tsumeb mine (Fig. 3). Production from 1907 to August, 1974 was 15,6 million tonnes of ore of average grade 5,0 % copper, 27,3 % lead and 5,2 % zinc, and ore reserves in 1974 exceeded 9 million tonnes (of lower average grade). Significant by-product germanium, cadmium and silver were also recovered (Söhnge, 1964; Hopwood, 1975).

Interpretive base plans were compiled for this study from mapping conducted by numerous geologists of Tsumeb Corporation Limited throughout the life of the Tsumeb mine. In particular, these include plans of 19 to 24 level geology and plans and sections from the surface to 20 level compiled by A. Lambaard, together with interpretive plans and sections between 24 and 30 levels compiled by A. Günzel. In the present study this mapping was re-interpreted, using supplementary data which were obtained from numerous mine openings (i.e. stopes and pillars at various elevations below 26 level) and from diamond drill core (Chapter 1.2, Figs. 18-20). Figure 18 shows interpretive plans of the ore body at various elevations. Stopes and pillars are identified by their position relative to a zero datum line (e.g. W20/28L is 20 m west of the datum line, between 27 and 28 levels). The datum line is oriented at 024° (i.e. perpendicular to the long axis of the ore body) and most stopes are elongated in this direction. However, the pipe is mined as northern and southern stopes between 34 and 35 levels, each parallel to the long axis of the ore body (e.g. NORTH/35L). Stopes on ore bodies outside of the pipe have specific names (e.g. S95, S110, North Break). Localities are also identified relative to a square grid pattern, oriented north-south (e.g. 1850N 1950E = metres north and east of a datum point). Figure 19 shows a section through the ore body along section W50, and Figure 20 is an exploded isometric projection of the ore body.

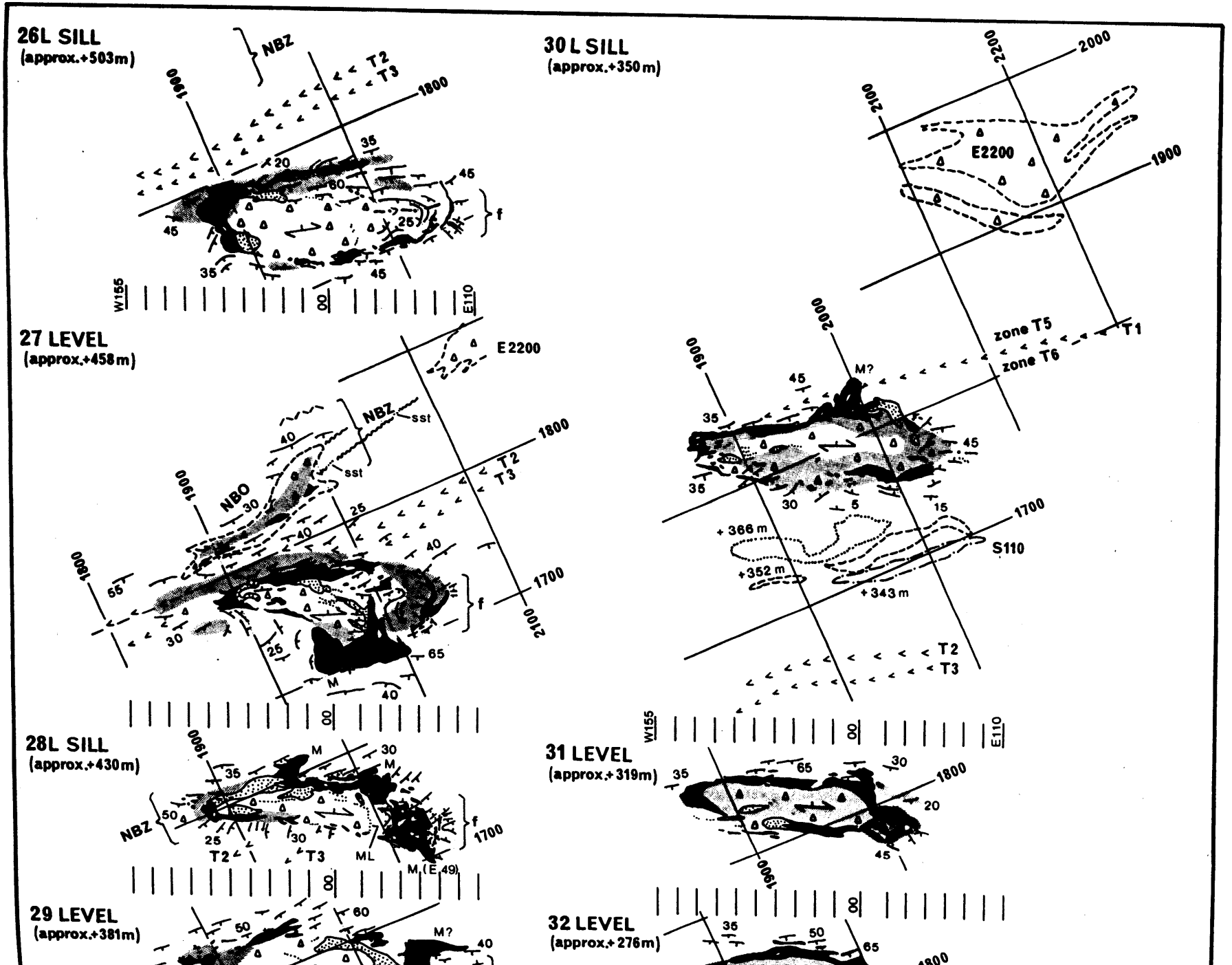
26L SILL
(approx.+503m)
NBZ
T2
T3
1900
1800
W155
E110
27 LEVEL
(approx.+458m)
E2200
NBZ
sst
NBO
T2
T3
1800
1900
1700
2100
f
M
28L SILL
(approx.+430m)
NBZ
T2
T3
ML
M (E49)
1700
29 LEVEL
(approx.+381m)
M?
30 L SILL
(approx.+350m)
2200
2000
2100
E2200
1900
zone T5
zone T6
T1
2000
1900
M?
+366m
+352m
+343m
1700
S110
T2
T3
31 LEVEL
(approx.+319m)
1800
1900
32 LEVEL
(approx.+276m)
1800

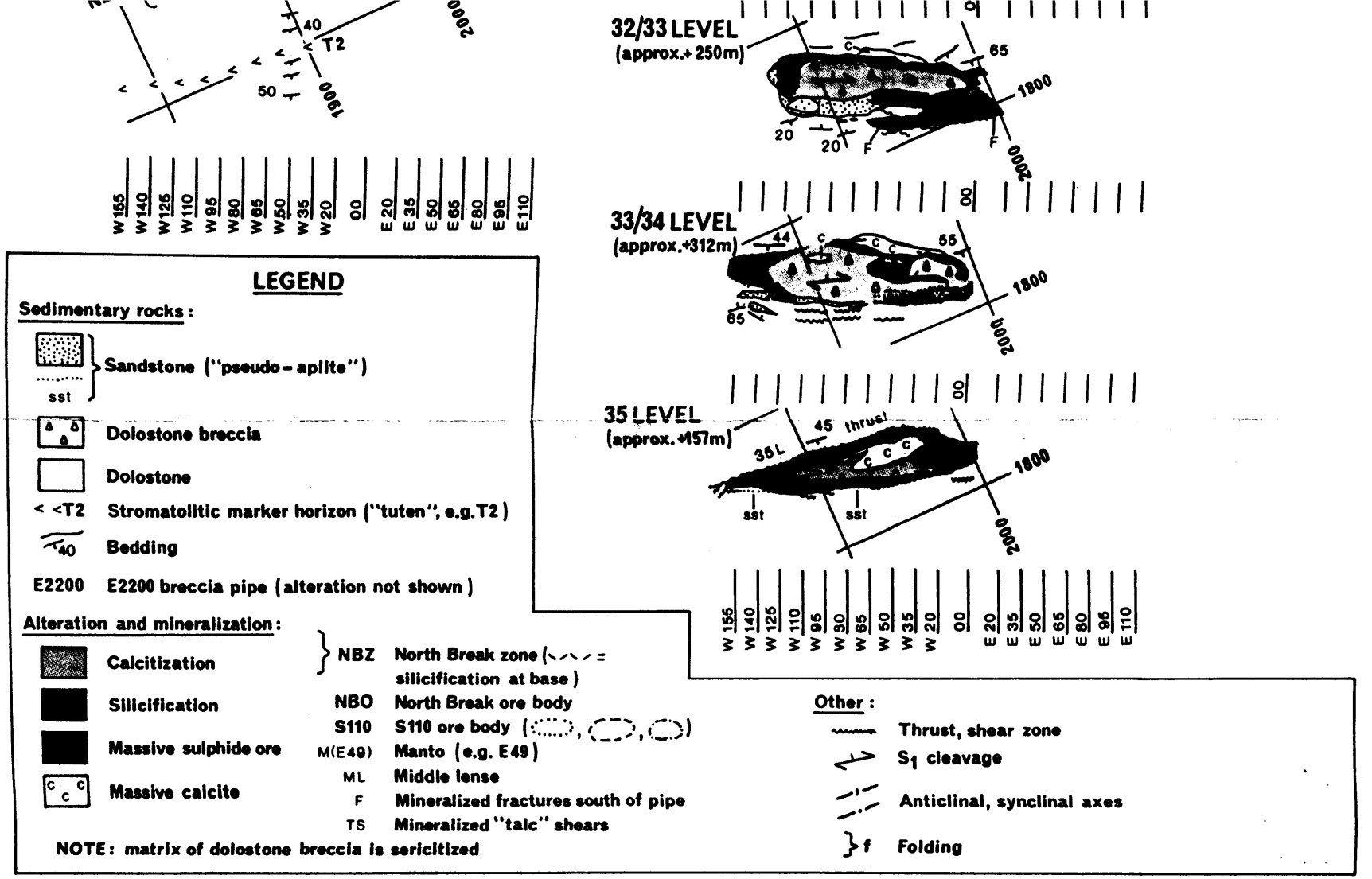

Fig. 18

Plan projection of the Tsumeb ore body at different elevations, reinterpreted from mapping by Tsumeb Corporation Limited (including a compilation by A. Günzel). Disseminated ore is not shown, but is mostly confined to the breccia pipe and its immediate margins, and to alteration zones outside the pipe (e.g. North Break, S110 and S95 ore bodies). The outer margin of the pipe breccia is usually massive ore or a fracture (too narrow to illustrate in all cases).

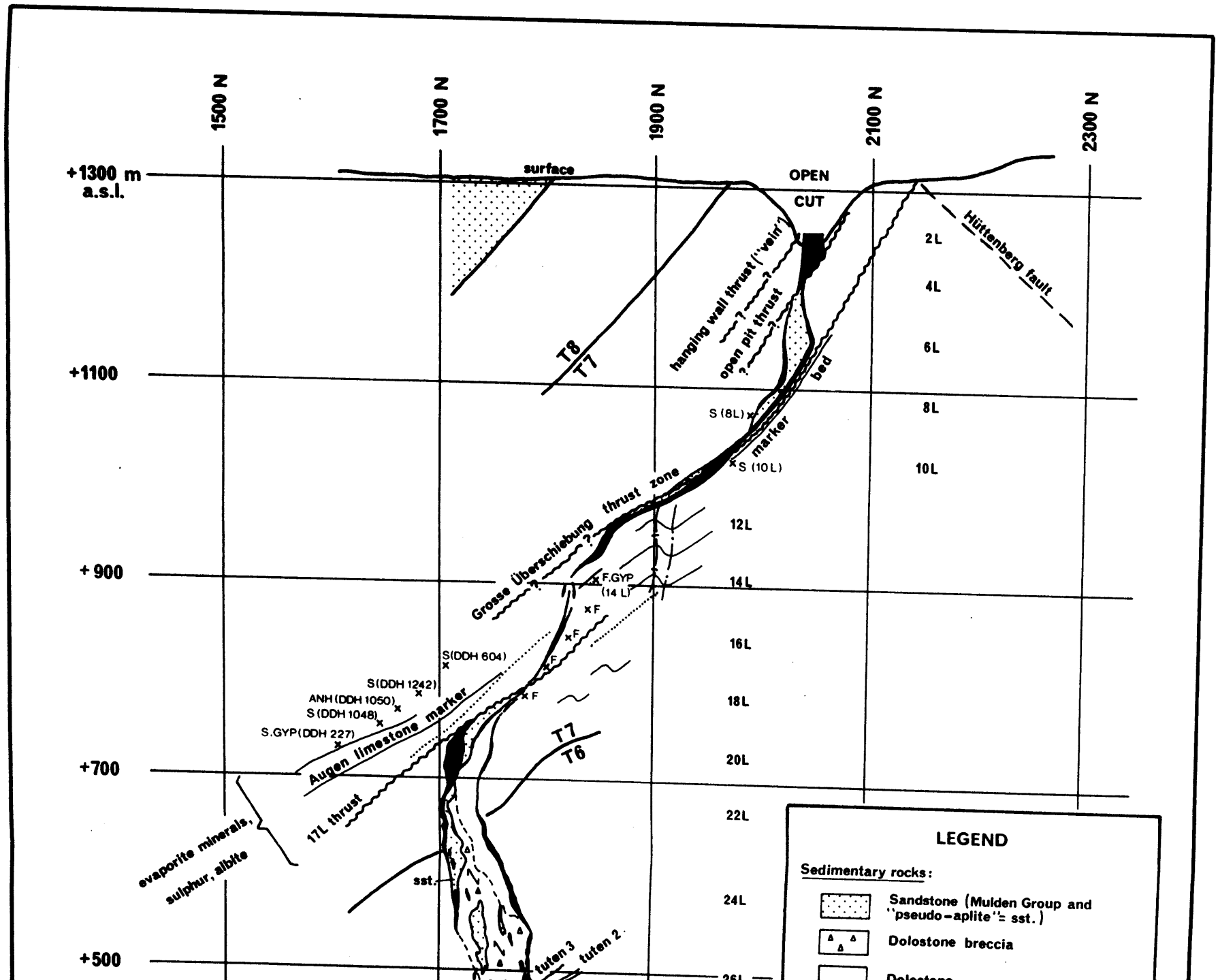
1500 N
1700 N
1900 N
2100 N
2300 N
+1300 m a.s.l.
+1100
+900
+700
+500
surface
OPEN CUT
Hüttenberg fault
hanging wall thrust ("vein")
open pit thrust
bed
marker
T8
T7
T6
S (8L)
S (10L)
Grosse Überschiebung thrust zone
F.GYP (14 L)
F
S(DDH 604)
S(DDH 1242)
ANH (DDH 1050)
S (DDH 1048)
S.GYP (DDH 227)
Augen limestone marker
17L thrust
evaporite minerals, sulphur, albite
sst.
tuten 3
tuten 2
2L
4L
6L
8L
10L
12L
14L
16L
18L
20L
22L
24L
26L
LEGEND
Sedimentary rocks:
Sandstone (Mulden Group and "pseudo-aplite" = sst.)
Dolostone breccia
Dolostone

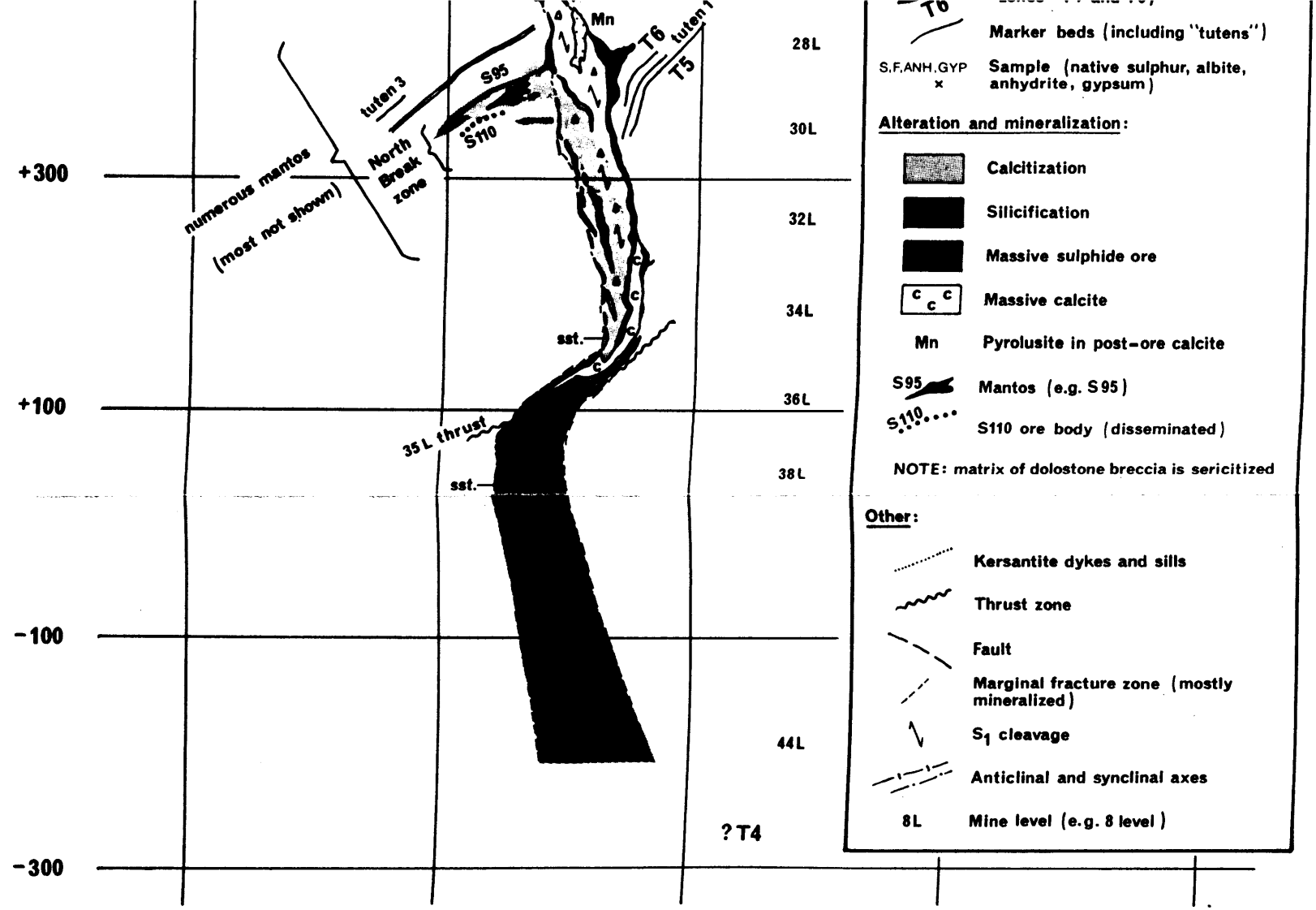

Fig. 19

Cross-section of the Tsumeb ore body along section W50 (azimuth 024°). Reinterpreted from mapping by Tsumeb Corporation Limited, including compilations by A.F. Lombaard and A. Günzel. Disseminated ore not shown (except S110 ore body), but is mostly confined to the breccia pipe and its immediate margins, and to alteration zones outside the pipe (e.g. North Break and S95 ore bodies).

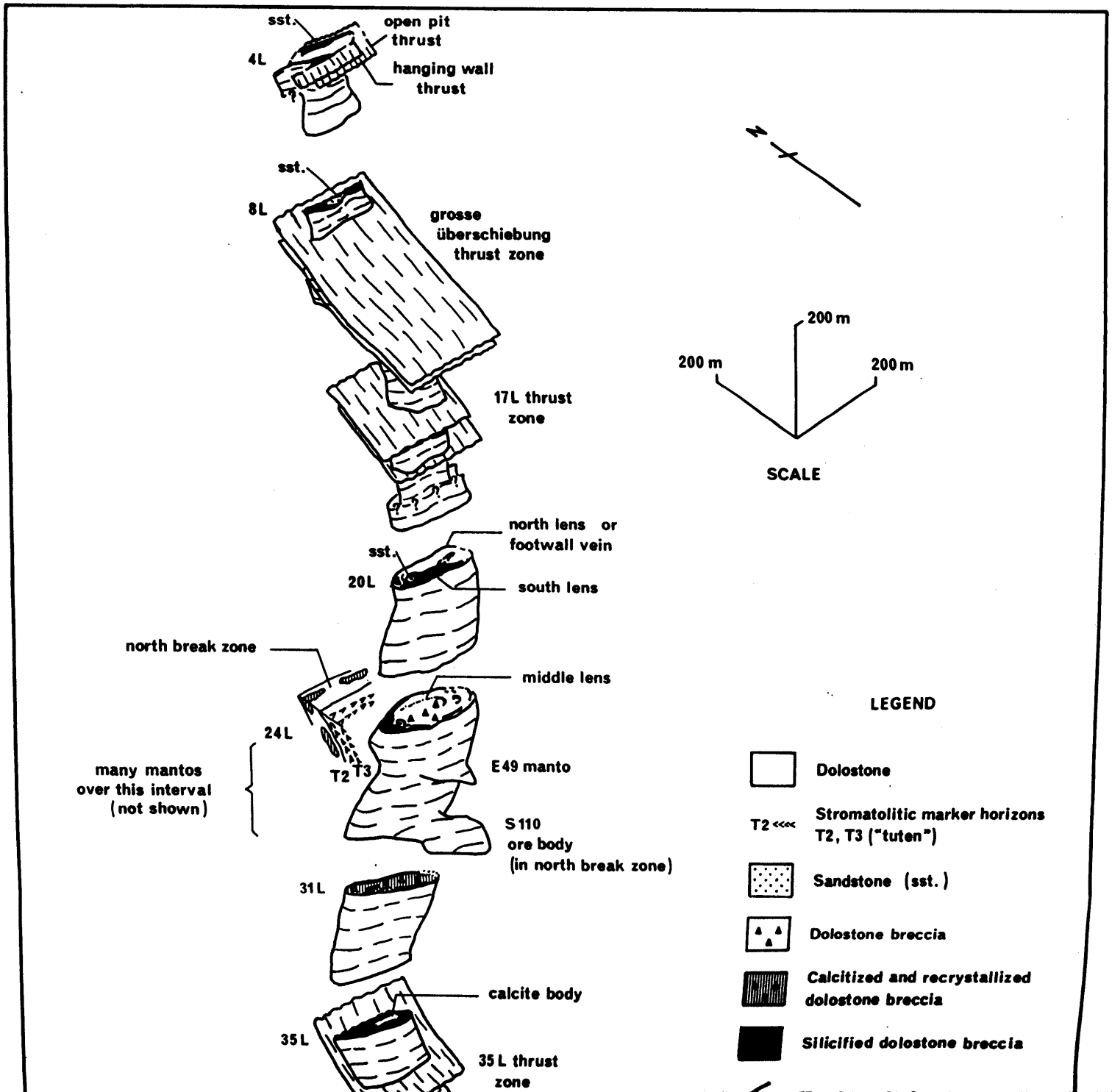
sst.
open pit thrust
4L
hanging wall thrust
sst.
8L
grosse überschiebung thrust zone
17L thrust zone
north lens or footwall vein
sst.
20L
south lens
north break zone
middle lens
24L
many mantos over this interval (not shown)
T2 T3
E49 manto
S110 ore body (in north break zone)
31L
calcite body
35L
35L thrust zone
200 m
200 m
200 m
SCALE
LEGEND
Dolostone
T2 <<<< Stromatolitic marker horizons T2, T3 ("tuten")
Sandstone (sst.)
Dolostone breccia
Calcitized and recrystallized dolostone breccia
Silicified dolostone breccia

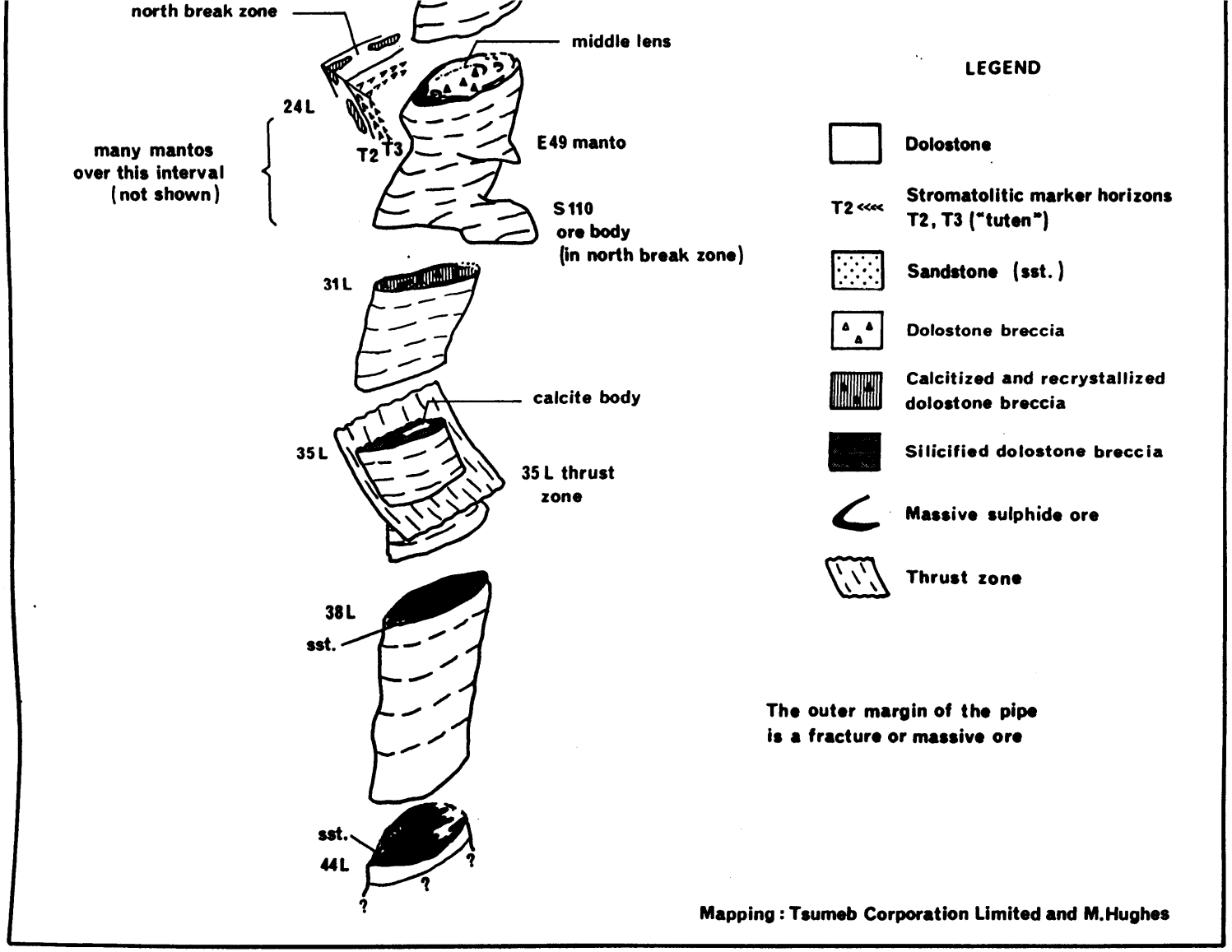

Fig. 20
Exploded isometric projection of the Tsumeb ore body.

3.1 DESCRIPTION

The Tsumeb ore body consists of a breccia pipe which plunges 45° south from the surface to a depth of 550m, and 75° north below this depth (Figs. 19, 20). It crops out in the lower member of the Hüttenberg Formation (zone T7) and penetrates to at least the lower part of the middle member of the Elandshoek Formation (zone T5). The pipe intersects the dolostone bedding at a high angle throughout much of its vertical extent.

Sulphide mineralization from the surface to 6 level is associated with a large, vertical body of "pseudo-aplite" (a quartzo-feldspathic rock of controversial origin). This body is elliptical in plan, and is surrounded by steep, mineralized fractures which are arcuate in places. From 6 level to 14 level the ore body is tabular and dips to the south, approximately parallel to the bedding of the enclosing rocks. The pipe is possibly displaced by post-ore thrusts over this interval (Chapter 3.7.8). The ore body below 14 level is an elongate lens which cuts the bedding at an increasingly larger angle with increasing depth. It gradually changes shape to an elongate ellipse at 21 level, where its plunge becomes northerly. A marginal fracture zone which is fairly continuously mineralized is present again at 20 level. A dolostone breccia body was first documented within the pipe above 21 level (Söhnge, 1964). However, mine plans and descriptions by other workers (e.g. Griffis, 1949a, b) indicate that minor dolostone breccia is present to at least as high as 11 level elevation, although it is very subordinate to "pseudo-aplite" in this upper part of the pipe.

The ore body at 21 level consists of an elliptical, steeply plunging, marginal rim of massive sulphide ore which contains remnants of replaced dolostone breccia and "pseudo-aplite". This rim surrounds a less mineralized core of bedded dolostone, a cylindrical "pseudo-aplite" body, and a dolostone breccia body. The dolostone breccia body is small at 21 level, but exceeds "pseudo-aplite" in volume below 23 level, and constitutes 50 per cent of the plan area of the pipe at 24 level. The northern margin of the breccia body at, and below, 22

level is a fracture zone parallel to, and interior to, the northern margin of the pipe (Lombaard, 1953). This "pseudo-aplite"- and ore-bearing fracture zone, the Middle lens, separates the northern margin of the breccia from bedded dolostone within the pipe. The eastern limit of the breccia is gradational into bedded and massive dolostone to below 26 level, below which the eastern limit of the breccia is an arcuate closure in the Middle lens. The Middle lens merges with the main northern contact and the E49 manto (see below) at 28 level.

The dolostone breccia body increases in plan area to 30 level, concomitant with a decrease in area of the bedded dolostone. The core of the pipe below 30 level consists almost entirely of dolostone breccia and very subordinate "pseudo-aplite". The volume of "pseudo-aplite" diminishes rapidly with depth, until it is confined to narrow, fracture-filling bodies in the marginal fracture zone. The ore body continues to have a steeply-plunging, pipe-like form to the greatest depth accessible during the study (38 level) and probably to the limit of drilling (below 44 level). The interval between 34 and 38 levels, in which the ore body is tabular and parallel to bedding, is an exception. Bedding-parallel thrust faults offset both the pipe and its sulphide ore over this interval (Hughes, 1977).

Numerous, sub-concordant bodies of massive sulphide ore (mantos) occur from above 25 level to 30 level. The mantos extend for up to tens of metres from the pipe margin into the surrounding dolostone. Conformable horizons of calcitization, silicification, brecciation and weak sulphide mineralization (collectively referred to as the North Break zone) intersect the pipe near 29 level (Fig. 20). Concordant and discordant bodies of "pseudo-aplite" are associated with this stratigraphic interval (e.g. S110 ore body), and occur up to 100 metres outside the pipe structure. The strata-bound North Break zone contains traces of mineralization over a 6,5 km strike length at surface. The North Break ore body consists of steep, mineralized fractures and associated breccia bodies which occur within the North Break zone, and which are immediately north of the Tsumeb pipe in the vicinity of 27 level (Figs. 18, 19). Steeply-dipping fractures, some of which contain "pseudo-aplite", occur between the North Break ore body and the

E2200 breccia pipe to the north-east (Fig. 18). The slightly altered and mineralized E2200 pipe may be the faulted extension of the Old Compound breccia at depth (Figs. 107, 108; Hughes, 1977).

Various workers recorded "graphitization" or "carbon alteration" of the pipe breccia below 22 level. Calcitization of the dolostone breccia was first recorded when mining reached 18 level (Söhnge, 1964). Calcitization appears adjacent to massive ore lenses and major fractures of the pipe margins at this elevation, but increases in importance within the pipe core (i.e. within the breccia) with depth. Most of the pipe core is calcitized below 32 level. Silicification of dolostone was first recorded adjacent to ore lenses and mineralized fractures at 24 level (Söhnge, 1964). It is extensive within the pipe core below 33 level, and most of the core is silicified below 34 level. Sericitization of "pseudo-aplite" feldspars (e.g. Geier, 1952), "talc shears" (e.g. below 30 level; e.g. Söhnge, 1964) and "manganese alteration" have also been reported by various workers, and are discussed in Chapter 3.4.

The Pb-Zn-Cu-As sulphide and sulphosalt mineralization is of both open-space filling and replacement type (Geier, 1953). Disseminated sulphide minerals fill breccia interstices and small veinlets. Massive mineralization has replaced the infill and walls of major discordant and concordant fractures. Griffis (1950) considered that much of the massive ore of the marginal fracture zones has replaced dolostone breccia and "pseudo-aplite". Oxidation of the ore body decreases downwards from the surface (i.e. the upper oxidation zone), until at 12 level the ore is largely sulphidic (Söhnge, 1964). Oxidation increases again below 25 level and reaches a maximum below 30 level (i.e. the lower oxidation zone). The ore is increasingly sulphidic at greater depth, and oxidation is insignificant at 38 level.

Narrow, post-ore dykes of olivine kersantite intersect the ore body in the upper levels (Wagner, 1916; Griffis, 1950; Pennebaker, 1952; Söhnge, 1964). These are the only confirmed igneous rocks in the mine area. The dykes post-date a major thrust zone in zone T7, which crops out in the Tsumeb open-cut at surface (Günzel, 1977).

3.2. PREVIOUS STUDIES OF THE TSUMEB ORE BODY

The earliest reports on the geology of the Tsumeb ore body were those of Maucher (1908), Krusch (1911), Wagner (1916), Schneiderhöhn (1919a & b, 1920a & b, 1921, 1929 - see 1958 review) and Stahl (1925, 1926). Unpublished descriptions with particular emphasis on structure include those of Griffis (1949a & b, 1950), Pennebaker (1952, 1954), Lombaard (1953) and Söhnge (1957). Söhnge (1964) reviewed much of this unpublished work, and Hopwood (1975) undertook a detailed structural study of the ore body. Le Roex (1955), Botha (1960) and Hopwood (1975) studied the controversial "pseudo-aplite" which occurs in the ore body. B.H. Geier also reported on "pseudo-aplite", and on Tsumeb mineralogy in general, in unpublished Mineralogical Reports, Mineralogical Notes and Monthly Reports of the Mineral Research Laboratory, Tsumeb Corporation Limited (referenced here as "B.H. Geier, unpubl. rept."). Rock alteration was described by Geier (e.g. 1952), Lombaard (1953), Le Roex (1955) and Hopwood (1975). Previous mineralogical studies are discussed in Chapter 3.6.

The principal models advanced by previous workers are briefly reviewed below and summarized in Table 3. The evidence on which these models are based is discussed in relevant sections of the thesis.

Origins proposed for the "pseudo-aplite" which occurs within the Tsumeb pipe include: (1) *in situ* sedimentation of Mulden Group arenite, (2) syn-tectonic injection of sediment derived from the strata-bound North Break zone, (3) fluidization of Nosib Group sediment by magmatic fluid, or (4) intrusion of an igneous rock. Origins proposed for the Tsumeb ore locus (i.e. the pipe and associated mineralized fractures) can be broadly grouped into magmatic (i.e. related to the intrusion of an adjacent or concealed magma body), tectonic, and solution collapse and karstic. Most workers engaged in structural studies of the ore body proposed magmatic and tectonic origins. Other workers invoked the regional distribution and stratigraphic dependence of mineralization, "pseudo-aplite" bodies and breccia bodies as evidence for a karstic origin. Some workers suggested variations on these

origins. Vellet (1969), for example, proposed that ascending ore solutions stoped upwards to form the breccia pipe. These solutions ultimately reached the Mulden Group contact, and unconsolidated arenites filled the pipe. Pennebaker (1952) and Söhnge (1976) considered the "pseudo-aplite" to be a sediment, but they ascribed a tectonic origin to the breccia pipe. A sedimentary origin for the "pseudo-aplite" and a tectonic origin for the Tsumeb breccia have generally been favoured by Tsumeb mine geologists in recent years. An overall karst hypothesis, in which both breccia and "pseudo-aplite" are considered sediments, had limited support (mainly from N.C. Thirion) when this study commenced.

Most authors who considered the "pseudo-aplite" to be magmatic proposed that the breccia pipe and associated elliptical fracturing were produced by magmatic-hydrothermal fluids, or by local "cauldron subsidence". The magmatic activity and mineralization were ascribed to post-tectonic granitoids of early Cambrian age, or post-Triassic alkaline intrusives. In particular, Lombaard (1953) and Söhnge (1964) suggested that the carbonate gangue and alteration in the pipe might be of post-Triassic carbonatitic origin. This was rejected by Allsopp and Ferguson (1970) on the basis of La and Ce contents and strontium isotope ratios of the carbonate rocks.

Tectonic models have emphasized the importance of shearing parallel to the axial planes of F_1 folds (Griffis, 1950; Pennebaker, 1952, 1954; Söhnge, 1964; Hopwood, 1975). This shearing was considered to have variously controlled brecciation, "pseudo-aplite" injection and mineralization within the Tsumeb pipe. However, Hughes (1977) noted that the plunge of the pipe and its elongation in plan are consistent with the presence of a vertical breccia pipe prior to F_1 folding.

The origin of strata-bound zones of brecciation and alteration has similarly been debated. Those parts of the Tsumeb pipe which are concordant to bedding have been interpreted as mineralized bedding thrusts, or sheared, low-angle axial planes of F_1 folds (e.g. Hopwood, 1975). However, Vellet (1968) proposed post-ore thrusting between 8 and 18 levels. Hughes (1977) recorded reverse faulting at

TABLE 3 ORIGINS PROPOSED FOR THE TSUMEB ORE BODY AND RELATED FEATURES

			DOMINANT ORIGIN OF ORE BODY															
			MAGMATIC					TECTONIC				KARST						
			STAHL, 1925	LOMBAARD, 1953	BOTHA, 1960	SÖHNGE, 1964	ALLSOPP & FERGUSON, 1970	GRIFFIS, 1950	PENNEBAKER, 1952, 1954	HOPWOOD, 1975	SÖHNGE, 1976	STAHL, 1926	SCHNEIDERHÖHN, 1929	LE ROEX, 1955	VELLET 1968, 1969	CALLAHAN, 1971	THIRION, 1973a	HUGHES, 1977
"PSEUDO-APLITE" ORIGIN	IN SITU MULDEN SEDIMENTATION								X		X	X	X	X	X	X	X	X
	SEDIMENT INJECTED FROM NORTH BREAK ZONE									X								
	"FLUIDIZED SEDIMENT" (e.g. NOSIB) WITH MAGMATIC COMPONENT			X		X												
	MAGMATIC ROCK		X		X			X										
BRECCIA PIPE ORIGIN	METEORIC KARST/SOLUTION COLLAPSE								PSA only		PSA only	X	X	X		X	X	X
	HYDROTHERMAL STOPING														X			
	TECTONIC BRECCIATION							X	X	X	Breccia only							
	CRYPTOVOLCANIC/MAGMATIC-HYDROTHERMAL			X	X	X	X											
RELATIVE TIMING OF EVENTS	MINERALIZATION	DAMARAN				Either	Either								X	X	X	X
		POST-TRIASSIC		X														
	BEDDING THRUSTS	PREDOMINANTLY PRE-MINERALIZATION				X		X	X				X					
		SYN-MINERALIZATION								X								
		PREDOMINANTLY POST-MINERALIZATION																X
	F_1 FOLDING	PRE- AND SYN-MINERALIZATION	X	X		X		X	X	X	X		X					
		PREDOMINANTLY POST-MINERALISATION													X	X	X	Either
ORIGIN OF STRATA-BOUND BODIES	MANTOS	BEDDING THRUSTS				X				X	X				X			
		SOLUTION COLLAPSE																
	NORTH BREAK ZONE	BEDDING THRUST				X												
		AQUIFER/COLLAPSE									X				X	X	X	
		ANHYDRITIC ARENITE SOURCE								X								
	KARUCHAS AND MOSAIC BRECCIAS	TECTONIC				X												
		TECTONIC ON INHERITED BRECCIA								X								
		SOLUTION COLLAPSE													X		X	
DARK DOLOSTONE ORIGIN	CARBON ALTERATION			X		X					X							
	ORIGINAL SEDIMENT																	
CALCITE ORIGIN	CARBONATITIC			X		X												
	HYDROTHERMAL						X											

35 level which displaced sulphide mineralization and post-dated the S_1 cleavage (i.e. cleavage axial planar to F_1). The sparsely mineralized, strata-bound North Break alteration zone and the spatially associated massive sulphide mantos have been interpreted as mineralized bedding thrusts (Söhnge, 1964, 1976; Vellet, 1968; Hopwood, 1975). Other workers suggested that the North Break zone was a paleo-aquifer or solution-collapse breccia (Vellet, 1968; Callahan, 1971; Thirion, 1973; Söhnge, 1976), and Hughes (1979) proposed a solution-collapse origin for the mantos. Callahan suggested that the silicified base of the North Break zone was an unconformity surface (Fig. 5).

The timing of mineralization relative to the main, D_1, phase of deformation has also been debated. Geier (1972) concluded from mineragraphic studies that the ore sulphides were only locally deformed. Söhnge (1976) proposed that the sulphide mineralization post-dated folding. However, Ypma (1973a, b) noted that deformation had destroyed much of the fluid inclusion record in the gangue minerals, and concluded that deformation had accompanied or immediately succeeded the mineralizing event. Hopwood (1975) proposed that F_1 folding accompanied but outlasted ore deposition.

The genesis of the ore (as distinct from the ore locus) has only been considered in detail by a few workers. Ypma (1973a, b, c) studied fluid inclusions from Tsumeb gangue minerals and concluded that they formed at 230° - 260° C under relatively shallow conditions (equivalent to a 2500 - 4000 m lithostatic load). Jensen (1973) found that the $\delta^{34}S$ ratios of Tsumeb sulphide minerals were highly positive (+13 to +27‰), and proposed a crustal source for the sulphur (e.g. sedimentary sulphate minerals). Hopwood (1975) suggested that anhydrite had been present in the "pseudo-aplite" prior to mineralization and that its presence subsequently helped to localize the ore. He suggested that the ore fluids were brines, the circulation of which was induced by deep, localized thermal sources such as igneous intrusions or hot spots.

Hopwood (1975) proposed that F_1 deformation and associated hydrothermal activity outlasted deposition of the complex Cu-Pb-Zn-As sulphide minerals which constitute the Tsumeb ore. He suggested that

the temperature of the ore fluids decreased with time, and they became sulphur-deficient and oxidizing. This resulted in recrystallization and differentiation of the original sulphide minerals under hydrothermal conditions. Hopwood (1975) proposed that the sulphide minerals were ultimately oxidized by the ore fluids, to yield the complex oxidic assemblage which other authors have ascribed to the activity of much younger meteoric waters.

Evidence is presented in this thesis that the Tsumeb pipe was initiated as a solution pipe, which formed by meteoric karsting during exposure of the Tsumeb Subgroup. The strata-bound North Break zone and manto fractures formed as part of this karsting event. The breccia which fills the Tsumeb pipe was partly derived by collapse of the pipe walls, and partly by sedimentation from the overlying Mulden Group subsequent to submergence of the pipe. The "pseudo-aplite" is interpreted as a sandstone, which was also derived from the Mulden Group. A model is developed, based on light stable isotope and lead isotope data, in which the ore fluids were brines that migrated northwards from a basin to the south of the Otavi Mountain Land. Metals were leached from the basin rocks and from aquifers within the Otavi Mountain Land. Mineralization was precipitated in karst features such as the Tsumeb pipe, in the vicinity of sulphate-rich horizons which provided sulphur for the ores. The mineralized Tsumeb pipe was subsequently deformed during the D_1 event. Segments of the pipe in the upper levels and below 35 level attained their present tabular, concordant form as the result of thrusting during the D_1 or later events. The ore body was subsequently oxidized by meteoric waters, which formed multiple, superimposed, oxidation and supergene enrichment zones.

3.3 TSUMEB PIPE AND ITS SEDIMENTARY INFILL

Dolostone breccia is closely associated with sandstone breccia and sandstone within the Tsumeb pipe, and all of these rock types are strongly discordant to the bedding of the enclosing dolostone (Figs. 19, 20). There is some compositional gradation between the clasts in the two breccia types, but their matrices are compositionally distinct.

The different rock types display sharply defined contact relationships, and the sandstone and sandstone breccia post-date the dolostone breccia. It should be noted that the rocks of the Otavi Mountain Land have typically undergone some hydrothermal alteration as well as advanced diagenesis (or very low grade metamorphism), so that they contain very fine-grained micas rather than clay minerals. Sedimentary terminology is used throughout the following discussion.

Evidence is presented in the following discussion that these rocks represent successive generations of karst sediment, in large part foreign to the dolostone which encloses the Tsumeb pipe.

3.3.1 Petrology of the dolostone breccia core

The core of the pipe consists of sandstone, sandstone breccia and faulted, but unbrecciated, blocks of the dolostone which surrounds the pipe. These rocks decrease in volume at depth, and dolostone breccia becomes increasingly important until it is the dominant rock within the pipe core (Chapter 3.1, Figs 18-20).

A large volume of the pipe breccia at depth has undergone intense rock alteration which has obscured its original composition, and all of the breccia has subsequently been deformed. The clasts and matrices of large volumes of the least altered breccia have very similar, dark colours, and the outlines of individual clasts in many specimens can only be observed on sawn faces in natural light. Figure 21 shows the monotonous appearance of typical, deformed, dark dolostone breccia. The clasts range up to blocks metres in diameter; in areas where the clasts lack bedding and the matrix is homogeneous, it is difficult to determine whether matrix or clast material is present in underground exposures. These factors make it difficult to determine the original nature of the dolostone breccia. However, evidence is presented below that the matrix of the dolostone breccia, like the sandstone of the pipe, is a sedimentary rock, foreign to the enclosing sequence. Previous arguments for a sedimentary, karstic origin for the breccia have depended on the stratigraphic dependence and discordant nature of the breccia bodies, and their close relationship to "pseudo-aplite" bodies, interpreted as sandstone.

Little-altered and relatively undeformed breccia contains angular, and rarely rounded, light to dark grey dolostone clasts in a dark, fine-grained matrix. Some breccia lacks a matrix, and consists of various compositions of dolostone clast which interlock along stylolitic contacts. Much of the breccia contains different types of dolostone clasts (e.g. massive or well bedded), of differing colours, and rarer, isolated chert clasts (i.e. they are polymictic breccias). The dolostone clasts vary from metres in diameter to microscopic, with a usual range of 0,2 - 10,0 cm (Fig. 22). They typically consist of microspar dolomite, but rare clasts consist of coarse dolomite spar, while others, particularly those darkest in colour, are micritic. Some dolostone clasts are compound fragments, separated by internal stylolites. Bedding within different clasts has a random orientation.

The rare chert clasts are white to black, massive, banded or stromatolitic (Lombaard, 1953; Söhnge, 1964). They are commonly moderately coarse grained, and consist of 0,05 mm megaquartz. Some clasts consist of interbedded chert and dolostone, or quartz siltstone and dolostone. Sandstone ("pseudo-aplite") clasts are completely absent, as also noted by Söhnge (1963). All clasts of the dolostone breccia consist of lithologies typical of the Tsumeb Subgroup rocks which enclose the pipe. The clasts of some areas of the breccia are identical in lithology to the adjacent wall rocks, but most of the breccia contains some clasts foreign to its immediate surroundings. Light grey dolostone fragments are common in the dolostone breccia on 20 level, although the adjacent wall rock consists entirely of dark dolostone (Griffis, 1949a, b). The reverse situation exists between 26 and 28 levels (the dark colour of these clasts is not thought to result from "carbon alteration"; Chapter 3.4.5). The proportion of chert is anomalously low in some dolostone breccia, relative to its wall rock, and oolitic and stromatolitic dolostone clasts present in breccia are absent from adjacent wall rock in other areas of the pipe.

The nature of the dolostone breccia matrices is often difficult to determine. The clasts and matrices are dolomitic in all specimens examined which were not obviously recrystallized and calcitized during alteration related to mineralization. Pressure solution processes at

FIGURES 21-26

Fig. 21

Dark dolostone breccia in the core of the Tsumeb pipe; the monotonous appearance and poor contrast between clasts and matrix is typical of this rock. The dolostone clasts are oriented sub-parallel to the S_1 cleavage, which is confined to the dolomitic siltstone matrix of the breccia. The cleavage curves from top right to bottom left. Minor veins of white calcite post-date both mineralization and the S_1 cleavage (C). The hammer is 31 cm long. W20/29L, +386 m (also see Fig. 81).

Fig. 22

Dark dolostone breccia which contains clasts of medium grey dolostone, most of which show bedding. The clasts consist of microspar dolomite, and the matrix also consists of small clasts of dolostone (i.e. not dolomitic siltstone). The lack of S_1 cleavage is partly attributed to the similar composition of both the clasts and matrix. Sample 850, W70N/29L.

Fig. 23

Dark dolostone breccia which contains angular, medium to dark grey dolostone clasts (C) which are difficult to distinguish from the greyish black, dolomitic siltstone of the matrix (M). The clasts show bedding, and only smaller clasts are oriented sub-parallel to the S_1 cleavage of the matrix. Veinlets of sulphide minerals (V) are confined to the matrix, and are folded and transposed by the S_1 fabric (the white vein consists of plaster). Sample 544, W40N/30L, +372 m (also see Fig. 91).

Fig. 24

Optically continuous, hydrothermal quartz overgrowths on rounded quartz grains in sandstone ("pseudo-aplite") of the Tsumeb pipe. The overgrowths contain inclusions of former matrix minerals. Sample 835, ZERO/33L. Crossed nicols.

Fig. 25

Matrix of pebbly sub-arkose, Tschudi Formation. This sandstone consists of irregular, interlocking grains of quartz, microcline (e.g. top right), albite (bottom left), and microperthite (bottom right). Sample 784, DDH S52, 569', Tsumeb. Crossed nicols.

Fig. 26

Sandstone ("pseudo-aplite") from the Tsumeb pipe. Note the similar texture and mineralogy of this rock (which consists of quartz, albite and microperthite) when compared with sub-arkose of the Tschudi Formation (Fig. 25). Sample 692, 18L. Crossed nicols.



Fig. 21



Fig. 22

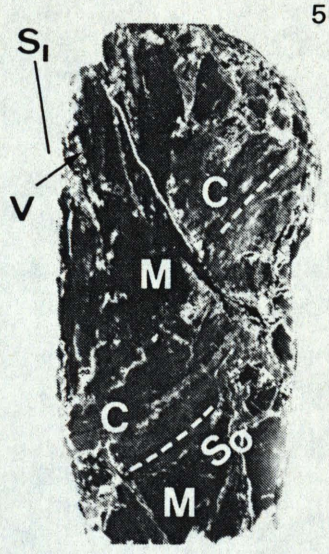

Fig. 23

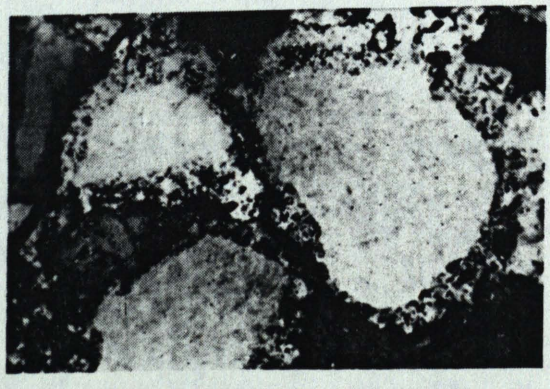

Fig. 24

0 mm 0.2

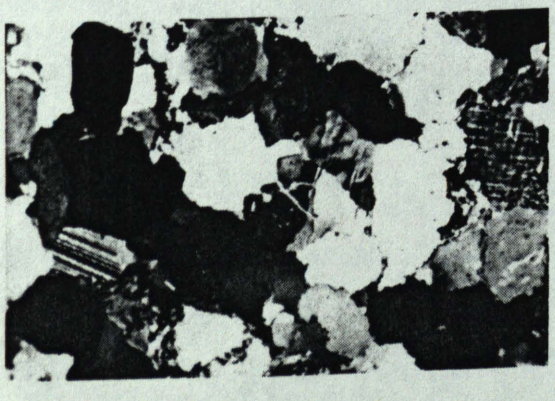

Fig. 25

0 mm 0.5

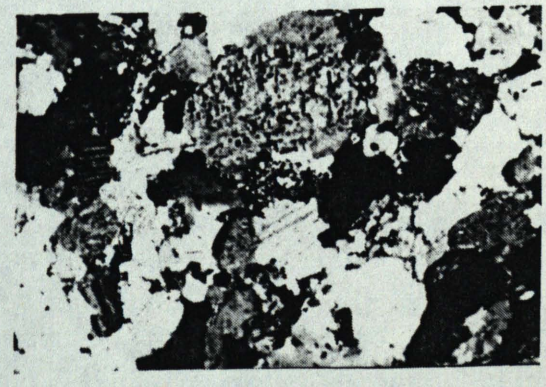

Fig. 26

0 mm 0.5

clast boundaries have obscured the original relationships between the clasts and their matrices in many specimens, and stylocumulate material produced in this manner resembles matrix material. This stylocumulate material contains a high proportion of sericite (fine-grained white mica), and minor amounts of an unidentified, brown, pleochroic, mineral which displays second-order colours (although these colours may be caused by intergrown sericite). Small dolostone clasts became interstitial to larger clasts during the pressure solution process, and the small clasts now resemble sedimentary matrices. A microspar dolostone matrix may be present in some specimens (i.e. a true sedimentary matrix), but its identification as matrix material, rather than former clasts, is uncertain for this reason.

A dolomitic siltstone, which is texturally and compositionally distinct from both the breccia clasts and the adjacent wall rocks, is a widespread matrix to the pipe breccia. The proportion of this matrix exceeds that of clasts within parts of the pipe breccia, and some of this rock is an almost homogeneous, clast-free rock which displays compositional layering in places. This layering drapes around clasts and is interpreted as bedding. The greyish-black matrix shown in Figure 23 is typical of this material. It consists of equal amounts of very fine grained (less than 0,05 mm) quartz and dolomite, greater amounts of sericite, and negligible quantities of the unidentified brown, pleochroic mineral described above. The potassium-rich nature of the rock, and XRD data, show that the sericite is muscovite. The rock is equi-granular, and its texture differs in this respect from much smaller volumes of fine-grained, more phyllosilicate-rich stylocumulate material which occurs between the clasts in many specimens of breccia. Some siltstone matrices are less quartz-rich, contain more abundant, or dominant, sericite and carbonaceous material, and grade into shales.

The chemical composition of the dolomitic siltstone material is shown in analysis 8, Table 4. It contains extremely high SiO_2, Al_2O_3, K_2O, TiO_2, Ba and reduced carbon contents relative to the dolostone enclosing the pipe (Table 1). This reflects the higher quartz, sericite and graphite content, and lower dolomite content, of the siltstone. The high K_2O content of this sample is thought to

TABLE 4. SANDSTONE ("PSEUDO-APLITE") AND SILTSTONE OF THE TSUMEB PIPE

	SANDSTONE						APLITE	SILT-STONE
	HOPWOOD (1975)				THIS THESIS		LE MAITRE	THIS THESIS
	(1)	(2)	(3)	(4)	(5)	(6)	(7)	(8)
SiO_2	82,6	91,5	69,6	83,1	86,8	77,3	72,7	42,1
Al_2O_3	4,9	4,5	3,0	3,8	4,9	5,9	14,3	13,6
Fe_2O_3	-	-	-	2,2	-	-	1,94	1,96
FeS_2	0,19	0,27	0,47	2,3	2,6	0,57	n.d.	n.d.
CaO	3,1	0,63	4,2	0,31	0,31	5,8	1,36	7,5
MgO	0,30	0,53	0,63	0,21	0,24	0,91	0,49	6,5
Na_2O	0,16	0,12	0,06	0,04	2,5	< 0,01	4,2	< 0,01
K_2O	0,38	0,58	0,40	0,34	0,48	1,03	4,1	4,9
TiO_2	0,19	0,22	0,16	0,20	0,22	0,28	0,21	0,83
P_2O_5	0,06	0,06	0,10	0,07	0,09	0,14	0,06	0,24
MnO	0,01	< 0,01	< 0,01	< 0,01	< 0,01	0,01	0,05	0,09
CO_2	3,3	0,17	5,9	1,32	0,17	4,5	0,02	11,3
C	0,01	0,26	0,54	0,24	0,02	0,04	n.d.	0,71
H_2O^+	n.d.	n.d.	n.d.	n.d.	< d	1,67	0,60	1,68
Cu	3,1	1,00	10,4	5,0	0,4	0,84	n.d.	5,1
Pb	0,50	0,06	2,00	0,13	0,2	0,64	n.d.	1,0
Zn	0,16	0,04	0,10	0,40	0,1	0,20	n.d.	0,3
As	0,36	< 0,05	0,16	0,43	0,35	0,15	n.d.	0,77
Other S	0,66	0,02	2,2	-	0,67	0,05	n.d.	1,50
TOTAL	100	100	100	100	100	100	100	100
MgO(MgO+CaO)								0,46
Ba(ppm)					87	166		618

1. Sandstone, 31 level, Tsumeb.
2. Sandstone, 28 level, Tsumeb.
3. Sandstone, 31 level, Tsumeb.
4. Sandstone, 33 level, Tsumeb.
5. Sandstone, 33 level, Tsumeb (sample 522); very slightly altered.
6. Sandstone, 28 level, Tsumeb (sample 196); intensely sericitized.
7. Average aplite (233 analyses), R. le Maitre, University of Melbourne (Hopwood, 1975); for comparison.
8. Altered dolomitic siltstone; matrix of dark dolostone breccia, 30 level, Tsumeb (sample 544).

n.d. = not determined < d = below detection limit

All analyses normalized for major components (original analyses, analysts, methods in Appendix 1.1).

result partly from potassic alteration of an originally clay-rich rock (Chapter 3.4.1).

Magmatic and tectonic origins previously proposed for the breccia require that it was produced by brecciation of the host rocks (Chapter 3.2). A rock of the composition of the dolomitic siltstone matrix of the dolostone breccia could only be produced by dissolution of the dolostones (e.g. by pressure solution during deformation) if more than 90 % of the original mass of the dolostone was removed. This assumes no addition of Al_2O_3, and TiO_2 (SiO_2 is possibly also an original component). Since the proportion of siltstone equals or exceeds that of dolostone clasts within parts of the pipe breccia, this would require the removal of a major proportion of the original rock in those areas. The geometry of the pipe infill relative to the host rocks (Fig. 20), the lack of siltstone fragments within the siltstone matrix, the presence of siltstone fragments in later sandstone (Chapter 3.3.3), the homogeneous nature of much of the matrix, and the presence of probable bedding in the siltstone indicate that it is a sedimentary rock, that was not derived from a consolidated precursor during tectonism.

It is concluded that the dolomitic siltstone matrix of the dolostone breccia is a sedimentary rock, texturally and chemically distinct from the breccia clasts or the enclosing wall rocks, which was introduced to the pipe as an unconsolidated sediment.

3.3.2 Other types of dolostone breccia

Breccia which is not of sedimentary origin occurs in the Tsumeb pipe, but is volumetrically unimportant. This includes breccia formed by fragmentation of the wall rocks of the Tsumeb pipe (during formation of the marginal fracture zone and later reverse faulting) and breccia produced by post-ore solution activity.

The marginal fracture zone which surrounds the pipe is typically filled with sandstone (Chapter 3.3.3), or replaced by massive sulphide ore. Elsewhere, the margin of the pipe consists of a zone of intense fracturing, a maximum of a few metres in width. The fractures are

filled with sulphide minerals, carbonate minerals and quartz, all of which show textures indicative of replacement and open-space filling (Figs 50-52). These fractured rocks grade into breccia which clearly formed as a result of this fracturing. This type of breccia typically consists of calcitized or silicified fragments of dolostone wall rock, with a cement of sulphide or gangue minerals.

Fault breccia formed during post-ore reverse faulting of the pipe. An example is a brecciated zone up to a few tens of centimetres thick in the footwall of a fault surface at 35 level (Chapter 3.7.7). The wall rock dolostone is intensely fractured, but the breccia lacks any matrix or cement.

A third type of breccia is related to oxidation of the ore body in the recent geological past, subsequent to D_1 deformation. Dolostone wall rocks, dolostone breccia, calcitized breccia and large bodies of calcite spar have dissolved, collapsed and been re-cemented by open-space fillings of carbonate minerals. The resulting breccia is vuggy to cavernous, carbonate minerals are compositionally banded or occur as vug-filling crystals, and secondary ore minerals fill vugs and are inter-banded with the carbonate minerals.

The origin of a fourth type of breccia is less obvious. Thin veins of carbonate minerals, anastomosing in places, are superimposed on the pipe breccia and its S_1 structural fabric (Fig. 81). The veins commonly lack vugs, compositional banding or secondary ore minerals. The veining is sufficiently intense to constitute a breccia cement in places, although fragments display little rotation. Isotopic data indicate that these breccia bodies are a variety of the third type of breccia, discussed above (Chapter 5.2.6).

3.3.3 Petrology of sandstone ("pseudo-aplite") and sandstone breccia bodies

Sandstone and sandstone breccia (i.e. breccia with a sandstone matrix) are most abundant in the upper part of the Tsumeb pipe, but decrease in volume with depth until they are confined to narrow veins within the pipe margin (Chapter 3.1). These rocks have previously

been referred to as "pseudo-aplite" because they occur in a pipe-like body which is strongly discordant to the enclosing sedimentary rocks. Also, their textures and mineralogical compositions have been considered ambiguous and consistent with those of either aplogranite (Botha, 1960), or sandstone (le Roex, 1955). It is shown in the following discussions that the composition, texture and mode of occurrence of the "pseudo-aplite" is indicative of a sedimentary origin for these rocks, as proposed by a number of workers in recent years (Table 4; Lombaard et al., in press, 1985).

The petrography of "pseudo-aplite" has been studied by numerous workers (e.g. le Roex, 1955; Botha, 1960; Hopwood, 1975). It is typically a medium light grey to medium grey rock, where it lacks clasts, with a 0,25-1,5 mm grain diameter (rarely 0,1 mm). Texturally and mineralogically it resembles a sandstone, or a breccia with a sandstone matrix (Fig. 26), and its composition corresponds to a sub-arkose, or rarely an arkose or quartz arenite. Its nature has been partly obscured by hydrothermal alteration and deformation. It typically contains 75 per cent quartz and 15-20 per cent feldspar, but the proportion of quartz exceeds 90 per cent in places. Chert grains of sand size are present. Some quartz grains are rounded, and display optically continuous hydrothermal quartz overgrowths (Ypma, 1973a, b), which contain inclusions of former matrix material (Fig. 24). However, interlocking sutured contacts are more common. Compositional layering, interpreted as <u>in situ</u> bedding, is present (Hopwood, 1975). Rare, large quartz grains are grain aggregates within which the component grains show irregular, extremely complex, grain boundary relationships; these resemble the "exaggerated grain growth" textures of some quartzites of high metamorphic grade (Wilson, 1973). They are unlike the polygonal textures of adjacent chert and siltstone grains and fragments.

The feldspars of the "pseudo-aplite" form irregular boundaries with quartz, although some feldspar grains are rounded. They consist of 75 per cent microcline and microcline-perthite and 25 per cent plagioclase (Na-oligoclase to albite). Botha (1960) recorded that plagioclase is typically present as euhedral to subhedral laths, interstitial to the quartz and potassium feldspar, but specimens

examined during this study contain mainly large, equidimensional plagioclase grains. Quartz and feldspar grains interlock in most of the sandstone specimens examined, but more than 50 per cent of fine-grained matrix (quartz, calcite, and sericite) is present in some specimens. This is a secondary matrix formed from pre-existing grains during hydrothermal alteration (Chapter 3.4.6). Accessory minerals of the "pseudo-aplite" are muscovite, biotite, graphite, tourmaline, zircon, rutile, apatite, garnet and opaque ores.

"Pseudo-aplite" compositions range from sandstone to sedimentary breccia with a sandstone matrix (Fig. 27). The breccia clasts include angular fragments and rarer rounded pebbles of sandstone, chert, dolostone and dark siltstone and shale (Figs. 27, 28). Stromatolite fragments, and pebbles which show bedding, are also present. Siltstone clasts consist of equi-granular aggregates of quartz, calcite or dolomite grains. Shale clasts consist of very fine-grained white mica, and chlorite, and some of the dark siltstone and shale clasts contain carbonaceous material.

The "pseudo-aplite breccia" bodies show no resemblance to igneous pebble dykes. Their matrices of "pseudo-aplite" consist typically of equigranular quartzo-feldspathic material of sand size, composed of mineralogically discrete grains rather than grain aggregates. Evidence for former, fine-grained rock flour is absent, and cavity-filling hydrothermal matrix is volumetrically unimportant. Also, there is no evidence of the reaction between clasts and matrices that would be expected if the matrices had crystallized in situ from an igneous melt. The margins of angular clasts of microspar dolostone and phyllosilicate-rich siltstone and shale, in direct contact with the quartzo-feldspathic matrix, show no development of new mineral phases, or recrystallization whatsoever. Ypma (1973a, b) noted that individual quartz grains in the "pseudo-aplite" each have different solid inclusion populations, in terms of the quantity, shape and size of inclusions. He noted that this was indicative of a mechanical mixture of grains, rather than of grains which crystallized from a single igneous body. The pre-Damaran U/Pb ages obtained from "pseudo-aplite" zircons are also considered more consistent with a sedimentary, rather than an igneous, origin (Chapter 5.3.9).

The "pseudo-aplite" has a very high SiO_2 content, and very low Al_2O_3, $Na_2O + K_2O$ and, in some specimens, CaO and MgO contents (Table 4). These values are more consistent with the composition of a sandstone than an igneous rock. This is true even if the effects of rock alteration are considered (Chapter 3.4.6), although analysis 5 is of a rock that is only slightly altered. Hopwood (1975) noted that true aplite has a much higher Na_2O, K_2O and Al_2O_3, and lower SiO_2, content than "pseudo-aplite" (c.f. analysis 7, Table 4). It is, therefore, extremely unlikely that an igneous rock would have a chemical composition which even approaches that of "pseudo-aplite".

It is concluded that "pseudo-aplite" consists of sandstone and sandstone breccia which, like the dolomitic siltstone, was introduced to the Tsumeb pipe as an unconsolidated sediment.

3.3.4 Spatial relationships between breccia bodies of the pipe core

The relationship between the various components of the breccia core was observed in a continuous section through W70 pillar, 29 level (Fig. 31). The northern massive sulphide body is separated from the breccia core of the pipe by 3,5 m of unbrecciated, light to medium grey dolostone. Marginal massive sulphide bodies of this type replace sandstone, sandstone breccia and oligomictic, fracture-generated breccia elsewhere in the mine (Chapter 3.3.2). The contact between the breccia core of the pipe and the dolostone is distinctive. The dolostone becomes increasingly fragmented and veined by a dark, dolomitic siltstone matrix near the contact. The proportion of this matrix ultimately exceeds that of dolostone clasts within 5 m of the contact. The matrix contains small but abundant clasts of variable composition to the south of this point. The proportion and size of clasts increases again 20 m south of the contact. These clasts are variable in composition and include lithologies not represented in the adjacent wall rocks. The proportion of clasts increases southwards, and the S_1 cleavage becomes more obvious. The clasts are elongated in the S_1 surface 25 m south of the contact, and the appearance of the breccia is more typical of the pipe breccia elsewhere in the pipe (e.g. Fig. 21). A breccia with a sandstone matrix dominates from 28 m south to the northern contact of the southern massive sulphide

FIGURES 27-30

Fig. 27

Sedimentary breccia with a sandstone ("pseudo-aplite") matrix (M). Angular to sub-rounded clasts of an earlier generation of sub-arkose (S), chert (C), dolostone (D), dark siltstone and shale are present. Smaller clasts are oriented parallel to the S_1 fabric (parallel to the hammer head). W80S/33L.

Fig. 28

Rounded pebbles of pipe sandstone ("pseudo-aplite"), some of which display bedding, in a darker matrix of similar composition. The dark colour of the matrix is caused by sulphide minerals. The lens cap has a diameter of 54 mm. Sample 589, W50S/34L.

Fig. 29

Sandstone ("pseudo-aplite" : light colour) filling interstices in brecciated dolostone (dark) in the North Break zone, outside the Tsumeb pipe. This is present at the base of a sandstone body which fills a former cavity near the areas shown in Figures 34-35. The brecciation is ascribed to collapse, not hydraulic fracturing (see text). The lens cap has a diameter of 54 mm. S110/30L, +354 m.

Fig. 30

Dark dolostone breccia of the Tsumeb pipe, cut by a later fracture which is filled with sandstone (S, "pseudo-aplite"). The S_1 cleavage can be seen in the top-centre of the figure. Central north part of W70/29L, +393 m (Fig. 31).

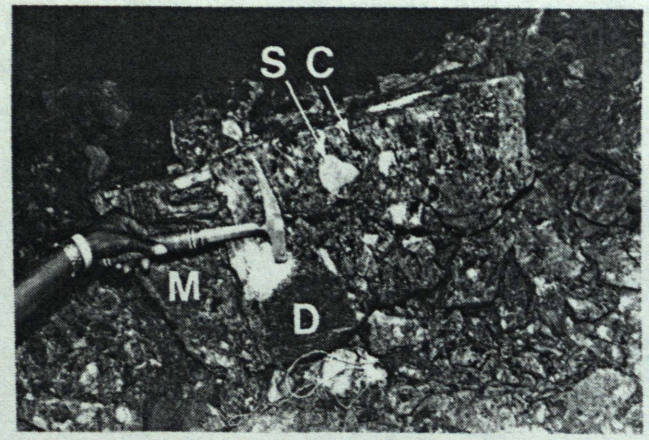

Fig. 27

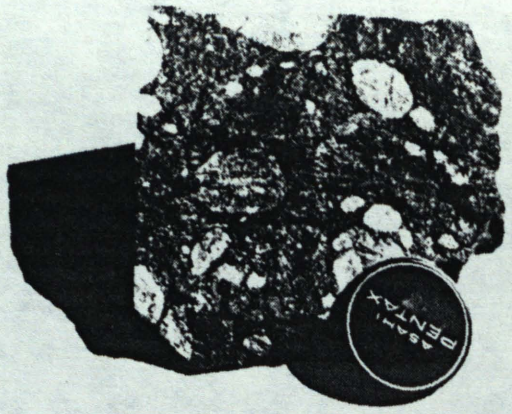

Fig. 28



Fig. 29

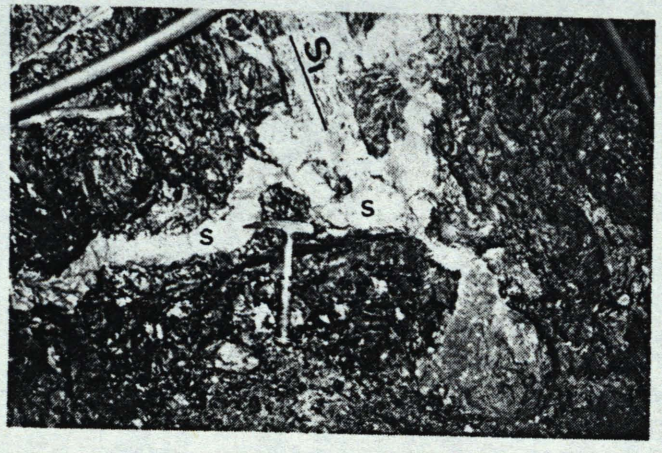

Fig. 30

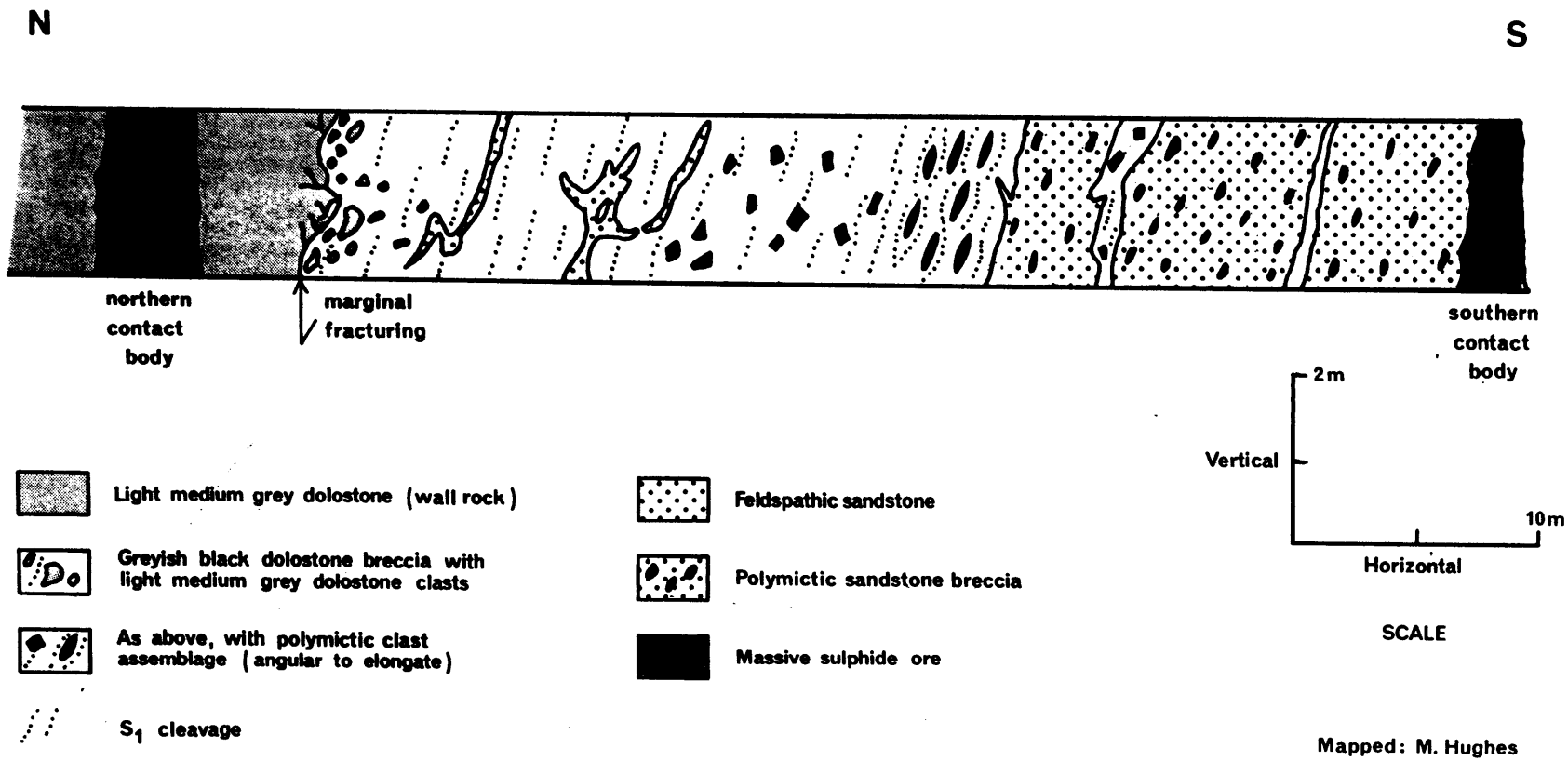

Fig. 31

North-south section through the Tsumeb pipe, showing the different types of sedimentary rock which fill the pipe. The northern and southern contact bodies consist of massive sulphide ore which has replaced the marginal fracture zone (dolostone wall rock occurs south of the southern contact body). The S_1 cleavage has a constant northerly dip throughout the section. Locality: W70 pillar/29 level (+393m).

body at 48 m south. The unbrecciated dolostone wall rock of the pipe is present in the south haulage, immediately south of the section.

Four types of sedimentary infill are therefore present in this traverse (i.e. excluding fracture-generated dolostone breccia which may now be replaced by massive sulphide ore of the northern contact body). These are: (1) dolostone breccia which contains wall-rock clasts, but a matrix foreign to the surroundings, gradational into (2) dolostone breccia in which both the clasts and matrix are foreign, (3) sandstone, and (4) sandstone breccia. It is shown in Chapter 3.3.6 that sandstone and sandstone breccia bodies can be further subdivided on the basis of their composition and temporal relationships.

3.3.5 Temporal relationships between dolostone breccia, sandstone and sandstone breccia

Sandstone and sandstone breccia within the lower part of the Tsumeb pipe occupy systematic fractures which form a continuous margin to the pipe. The sandstone, and to a lesser extent dolostone breccia, are extensively replaced by sulphide ore within these fractures, to form the massive sulphide lenses (Figs. 18-20). These rocks also occur in the Middle lens fracture, and in a narrow fracture which parallels the southern margin of the pipe, immediately external to the pipe structure, between 32 and 33 levels (Fig. 18). Sandstone also occurs in thin, irregular veins within the dolostone breccia core of the pipe, and in steeply-dipping fractures which extend between the North Break ore body and the E2200 breccia pipe (Fig. 18).

Sandstone post-dates the dark dolostone breccia, but was deposited prior to D_1 deformation (Chapter 3.7). Sandstone veins cut the dolostone breccia, but the reverse was not observed. The relationship between the sandstone and the dolostone breccia is clearly displayed in the section represented by Figure 31. Sandstone occurs as veins in the breccia between 9 m and 20 m south of the northern breccia contact, but sandstone bodies are not cut by breccia bodies (Fig. 30). The sandstone breccia between 28 m south and the southern massive sulphide body is related to the marginal fracture zone, which post-dates the dolostone breccia.

A systematic search of the mine workings failed to reveal a single example of sandstone clasts within a dolomitic siltstone or microspar dolostone matrix. Some more altered breccia matrices contain abundant, or predominant, calcite in addition to quartz and feldspar. However, the calcite is coarse calcite spar, which is thought to be an introduced hydrothermal mineral and, or, the alteration product of original small dolostone clasts (Chapter 3.4.6). Rocks of this type are associated with sandstone of the marginal fracture zone.

It is concluded that sandstone and sandstone breccia were deposited within fractures which formed subsequent to lithification of the dolomitic siltstone infill of the Tsumeb pipe.

3.3.6 Relationships between different sandstone and sandstone breccia bodies

Different generations of sandstone can be observed within the Tsumeb pipe. Figure 27 shows a common example of dolostone, chert and sandstone clasts in a later generation of sandstone.

The contact between compositionally-distinct bodies of sandstone-bearing breccia and sandstone was observed near the south-western margin of the pipe (Fig. 32). The earlier sediment is a breccia, with a sub-arkose matrix which has a moderately high feldspar content. The clasts of this breccia consist of dolostone, chert and massive sub-arkose. Angular blocks of bedded graphitic shale and siltstone, up to a metre or more in diameter, are also present (Fig. 33). These resemble the dolomitic siltstone matrix of the dolostone breccia elsewhere in the pipe. Wall rock dolostone, dolomitic siltstone infill of the pipe, and an early generation of sub-arkose (all varieties of which post-date the siltstone elsewhere in the pipe) are, therefore, present within a later matrix of sub-arkose. The second body of sedimentary rock is a massive sub-arkose with a lesser feldspar content, which post-dates the first sub-arkosic breccia body. This second body veins the earlier breccia along their mutual contact, and has partly incorporated some of the larger breccia clasts within its margin.

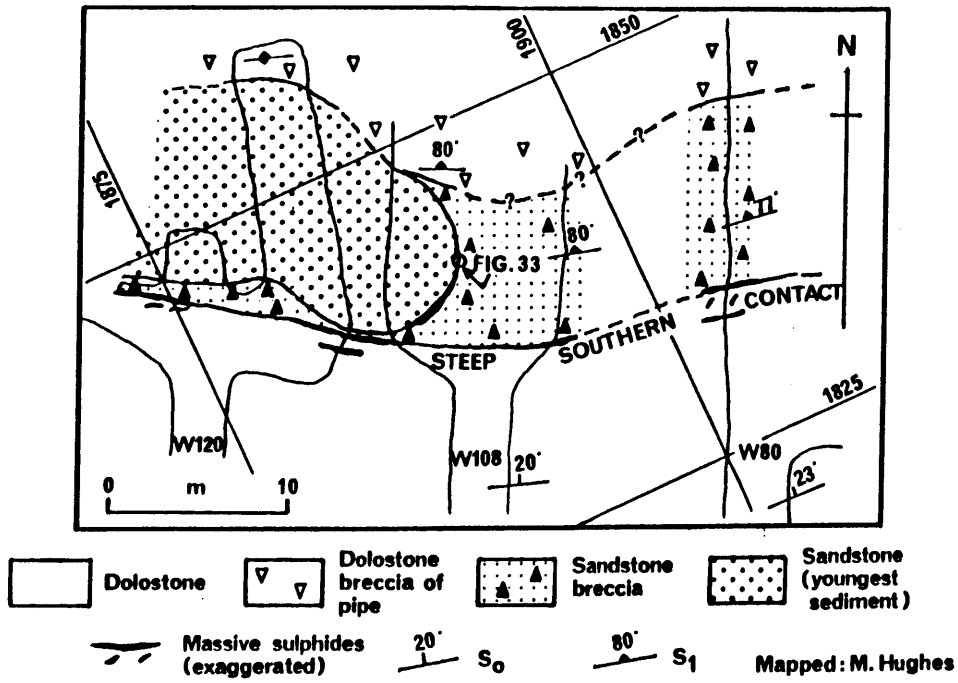

Fig. 32
Multiple generations of sandstone infill at the margin of the Tsumeb pipe (+248m). The sandstone breccia contains clasts of dolostone wall-rock, dolomitic siltstone, and an earlier generation of sub-arkose. The breccia is veined by a later, compositionally distinct sandstone body along their mutual contact.

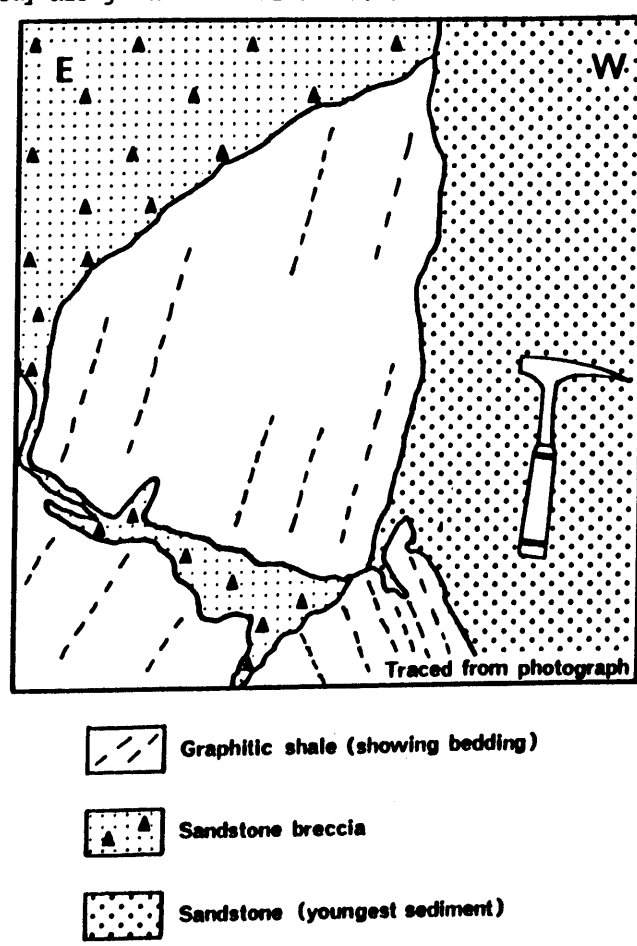

Fig. 33
Detail of the contact between the sandstone breccia and sandstone bodies of Figure 32. A sandstone vein penetrates a large clast contained in the older breccia (i.e. left of hammer).

The second body of sandstone, above, is confined to the marginal fracture zone of the pipe at this elevation (above 33 level). This appears to be the downwards extension of a cylindrical sandstone body which is present within the dark dolostone breccia, interior to the marginal fracture zone, in the south-western corner of the pipe between 18 and 26 levels. The sandstone body is probably fairly continuous down to a short distance above 33 level, where it merges with sandstone of the marginal fracture zone (this is not obvious at all elevations shown in Figure 18, but its presence was confirmed at a number of intermediate elevations). Sandstone continues to be most abundant at the western end of the pipe to below 44 level.

It is concluded that multiple phases of sandstone sedimentation can be recognized in the Tsumeb pipe. The sandstone incorporated fragments of dolostone wall rock, and earlier generations of dolomitic siltstone and sandstone pipe infill, to form breccia with a sandstone matrix. Sandstone in the lower part of the Tsumeb pipe was mainly deposited in the marginal fracture zone, and in a cylindrical body slightly interior to, but connected with, the marginal fracture zone.

3.3.7 Strata-bound sandstone of zone T6

The relationship between strata-bound sandstone, which occurs immediately outside the pipe, and the enclosing zone T6 dolostone was examined in S110 stope at +354 m (Fig. 19). Figure 34 shows a typical exposure, in which the sandstone occurs as discontinuous bodies at the contact between massive, medium grey dolostone and overlying well bedded, medium dark grey dolostone. The sandstone bodies are not interbedded with the dolostone, but occur in irregular bodies which cut the dolostone bedding (e.g. near sample 862). Contact relationships between the two rocks indicate that the discontinuous sandstone bodies are not structurally isolated boudins, but occupy irregular cavities. The contact between the two types of dolostone in Figure 34 is a continuous stylolite, and not a normal sedimentary contact.

Figure 35 is an exposure in a similar stratigraphic position, a few metres to the west of the area shown in Figure 34. Massive, completely chert-free dolostone is overlain by well bedded dolostone,

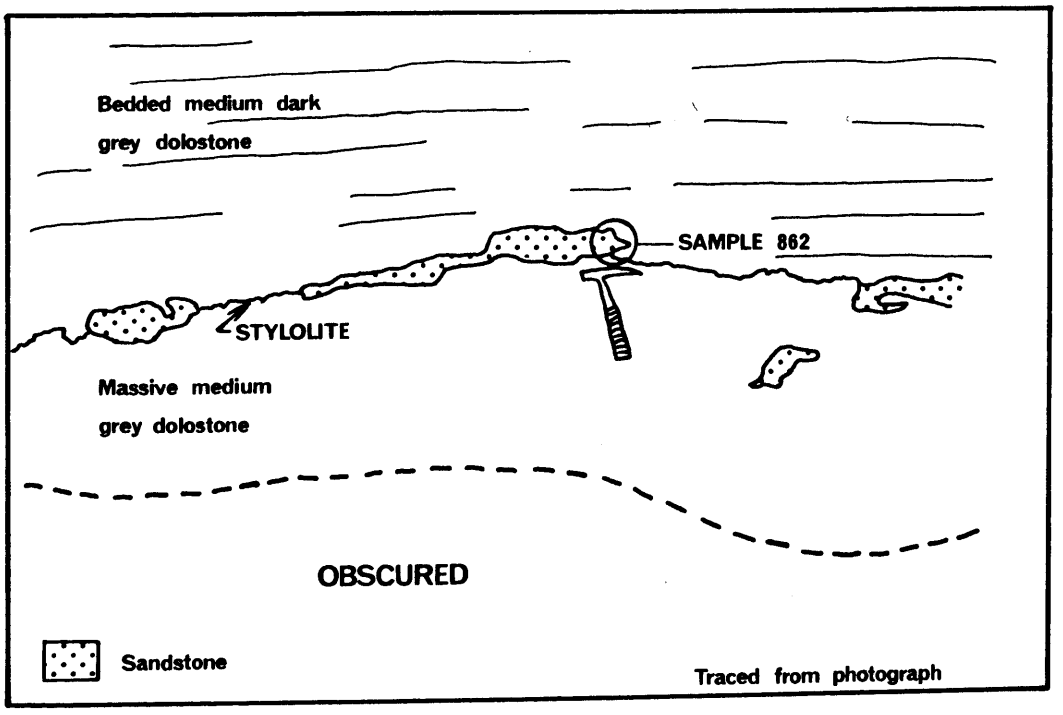

Fig. 34
Strata-bound sandstone in dolostone of zone T6, S110 stope, +354m (looking north-east). The sandstone bodies are not interbedded with the dolostone, but occur in irregular bodies which cut the bedding along high-angle contacts in places.

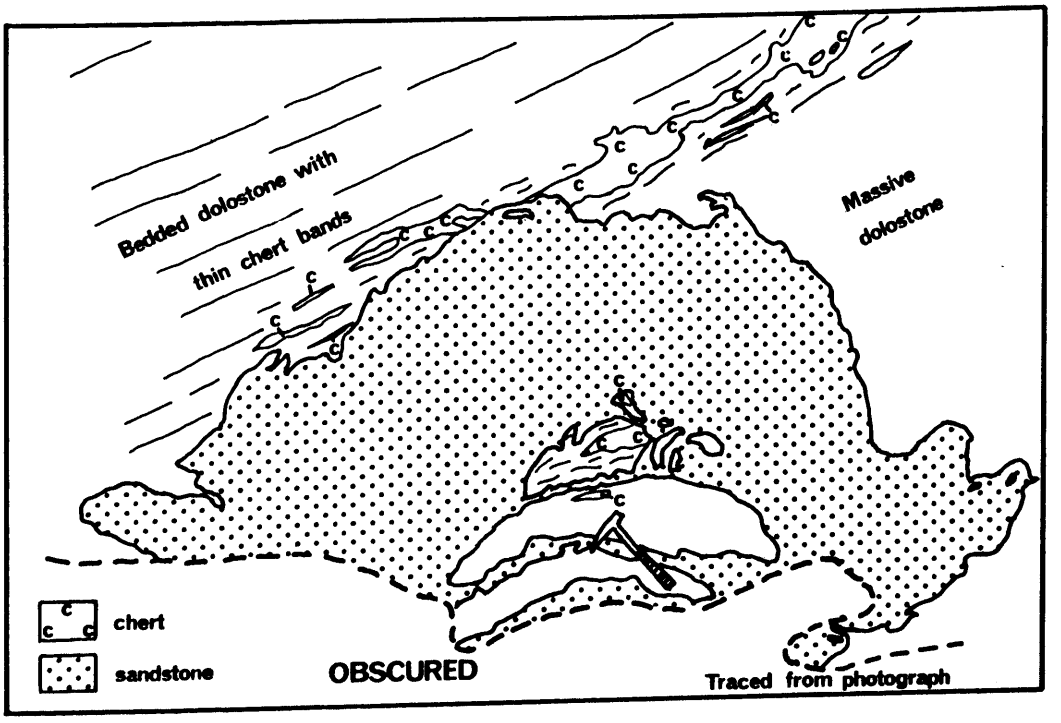

Fig. 35
Cavity-filling sandstone in dolostone of zone T6, S110 stope, +354m (looking north). A fragment of cherty dolostone towards the base of the cavity is identical to a thin bed in the roof, from which it was probably derived.

which contains thin chert bands. The only chert of significant thickness occurs at the contact between the two dolostones. A large body of sandstone occupies an obvious cavity below, and partly transgressive to, this chert. Large blocks of massive dolostone are present within the sandstone at the base of this cavity, and smaller blocks of well bedded, cherty dolostone rest on the massive dolostone blocks. These cherty dolostone blocks include a fragment which was obviously derived from the thick chert in the roof of the cavity. Cavity-filling sandstone bodies elsewhere in S110 stope occur in approximately the same stratigraphic position.

These observations indicate that sandstone sedimentation occurred in irregular, strata-bound cavities. The form of the cavities and their presence in dolostone is consistent with an origin by solution, with attendant roof collapse. The timing of this solution activity, prior to sandstone sedimentation, together with the absence of associated rock alteration in unmineralized areas, indicates that the solution activity was unrelated to the mineralizing event. Therefore, it might have been associated with karsting by meteoric fluids. Breccia bodies which lack sandstone infill, interpreted as solution-collapse breccias, crop out in a similar stratigraphic position outside the mine area (A. Günzel, personal communication).

The textures of some dolostone breccia bodies with sandstone matrices, which Hopwood (1975) interpreted as syn-tectonic bodies formed by hydraulic brecciation, are equally consistent with an origin by karst sedimentation. Figure 29 shows the style of brecciation observed on the contact of a cavity-filling sandstone body, between the areas represented by Figures 34 and 35. Breccia of this type could have been produced by gravitational collapse and fragmentation of dolostone blocks during sandstone sedimentation in a karst cavity, or by the infiltration of sand into pre-existing solution-collapse breccia.

Strata-bound sandstone bodies are thickest and most abundant in the immediate vicinity of the pipe. None are known at distances of more than 100 m from the pipe margins. Hopwood (1975) proposed that the strata-bound sandstone originally occurred as interbeds of sand

within zone T6 dolostone, and was syn-tectonically remobilized into the Tsumeb pipe. However, it is improbable that sand would remain unconsolidated beneath more than 600 m of overlying dolostone, which was sufficiently lithified to fail by brittle fracture prior to the introduction of sand to the marginal fracture zone of the pipe. Observations during the present study are consistent with the introduction of sand from the sand-filled Tsumeb pipe, into strata-bound karst cavities in the immediate vicinity of the pipe. The connection between the pipe cavity and strata-bound zones of solution, together with the pipe contact relations described in Chapter 3.3.4, indicate that the pipe was also formed by solution (e.g. a sinkhole). It is argued in Chapter 6.1.1 that the Tsumeb pipe formed as a result of karsting during exposure of the Otavi Group, and was filled with Mulden Group sediments during subsequent submergence.

3.4 ZONES OF ROCK ALTERATION

Spatial relationships between the major zones of rock alteration in the Tsumeb pipe are described in Chapter 3.1.

3.4.1 Alteration of the dolostone breccia

The dolostone breccia which occurs in the core of the Tsumeb pipe is least altered above 28 level in the mine. Dolostone clasts within the breccia show no compositional change or recrystallization, and sedimentary structures are preserved in detail. The unaltered clasts constitute a major portion of the rock in most areas, and the rock is referred to in this thesis as "unaltered" breccia. However, the matrix of the breccia commonly contains sulphide mineralization, and sericite is the only phyllosilicate mineral present in the matrix of well mineralized specimens (Fig. 23, Chapter 3.3.1). Rocks of this type can contain 5 wt % K_2O, but negligible MgO or CaO except in dolomite (analysis 8, Table 4). Despite this evidence that the ore fluids have extensively penetrated the matrix of the breccia, the carbonate mineral in the matrix is finely granular dolomite. The matrix is therefore considered to have undergone a potassic (i.e. sericitic) alteration by ore fluids which were in equilibrium with dolomite.

3.4.2 Calcitization in the Tsumeb pipe

The dolostone of the pipe breccia has been recrystallized and calcitized to varying degrees in the lower levels of the mine. Similar alteration has affected unbrecciated dolostone that occurs interior (and to a minor extent, exterior) to fractures which form the pipe margins. Calcitization is also present in strata-bound horizons such as the North Break zone (including the related North Break ore body), the S110 ore zone, and the massive sulphide mantos. The distribution of calcitization within the Tsumeb ore body is shown in Figures 18-20. Intense, pervasive alteration is shown; areas of carbonate veining, narrow zones of intense alteration intimately associated with massive sulphide ore, and areas of incipient alteration are excluded. Calcitization of dark dolostone breccia is difficult to map unless systematically verified with acid; the areas shown as calcitized between 26 and 28 level are, therefore, probably minimum areas.

The uppermost level at which calcitization has been reported in the literature is 18 level (Söhnge, 1964). Calcitization was described by Geier (1952, 1953), Lombaard (1953) and Söhnge (1964) at various elevations above 26 level, the uppermost level accessible during the present study. Calcitization in these upper levels is confined to the immediate vicinity of steeply-dipping massive sulphide bodies which are associated with the marginal fracture zone of the pipe. Calcitization only extends for a few metres outwards into the surrounding, unbrecciated wall rock at most elevations (e.g. Fig. 36E). The margins of the pipe are, therefore, sharply defined in most places. Calcitization extends into the pipe core below 28 sill elevation (e.g. along the southern margin at 29L and 30L sill elevations). It affects most of the interior of the pipe, internal to the marginal fracture zone, below 32 level (Fig. 18). Calcitization becomes subordinate to silicification below 34 level.

The original microspar dolostone of the pipe breccia and wall rock has recrystallized to sparry dolomite in places within the calcitized zone. However, alteration and recrystallization to calcite spar is volumetrically far more important. This calcitization has typically preserved the original textural features of the unaltered

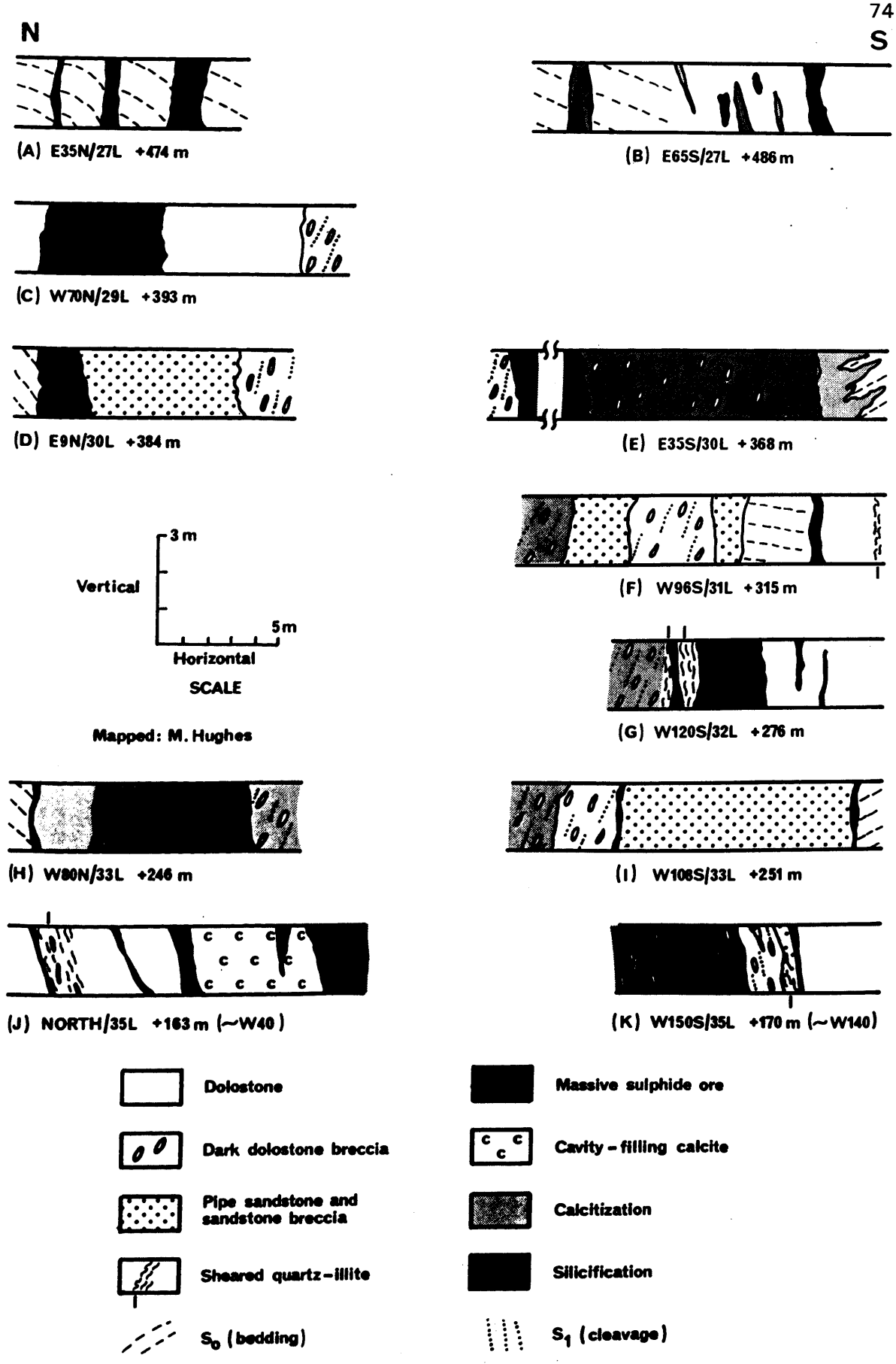

Fig. 36
The contact between the Tsumeb pipe and its wall rocks, showing marginal fractures, alteration zones and massive sulphide bodies.

rock, such as bedding, thin chert layers, and clast boundaries (Figs. 37-38, 40). However, the original nature of some rocks has been obscured. Clasts are typically completely calcitized, but partly, or completely, unaltered dolostone clasts occur in places within completely calcitized matrices (Fig. 37B). The calcitized breccia has undergone greater strain during deformation than "unaltered" dolostone breccia. Breccia clasts in calcitized rocks are in most places elongated, parallel to S_1, to a greater degree than those in less altered rocks. However, large clasts occur which are equidimensional, or which have their long axes oriented at a large angle to S_1 in places (Fig. 37B).

The close spatial relationship between calcitization and sulphide mineralization is best illustrated in areas where sulphide veins cut unaltered dolostone wall rocks, as in parts of the marginal fracture zone. The calcitized rock encloses the vein zone and grades outwards into unaltered dolostone. The calcitized rock grades inwards into coarse-grained calcite spar as individual sulphide mineral and calcite veinlets within the marginal fracture zone are approached. The original texture of the dolostone is partly preserved in many specimens, in which fine-grained spar, inherited from the original dolostone, has recrystallized to grains of calcite spar, millimetres in diameter. These large grains grade from inclusion-free crystals, to crystals which are crowded with inclusions of fine-grained spar. This can be seen at 30 level, where calcitization extends outwards from the mineralized margin of the pipe as irregular, strata-bound zones in the dolostone of the wall rock (Fig. 36E). Calcitized zones of this type are obvious in underground exposures because of their light colour and coarse grain size.

Progressive calcitization occurs over a considerable vertical distance within the pipe breccia. Clasts, and the original matrix of carbonaceous, dolomitic siltstone can still be recognized in some specimens of calcitized sedimentary breccia (Fig. 38). The siltstone matrix has been progressively calcitized, recrystallized, and replaced by calcite spar in such rocks (Fig. 39). Non-carbonate material is concentrated at the margins of the recrystallized spar, or occurs as interstitial films between calcite-rich areas where recrystallization

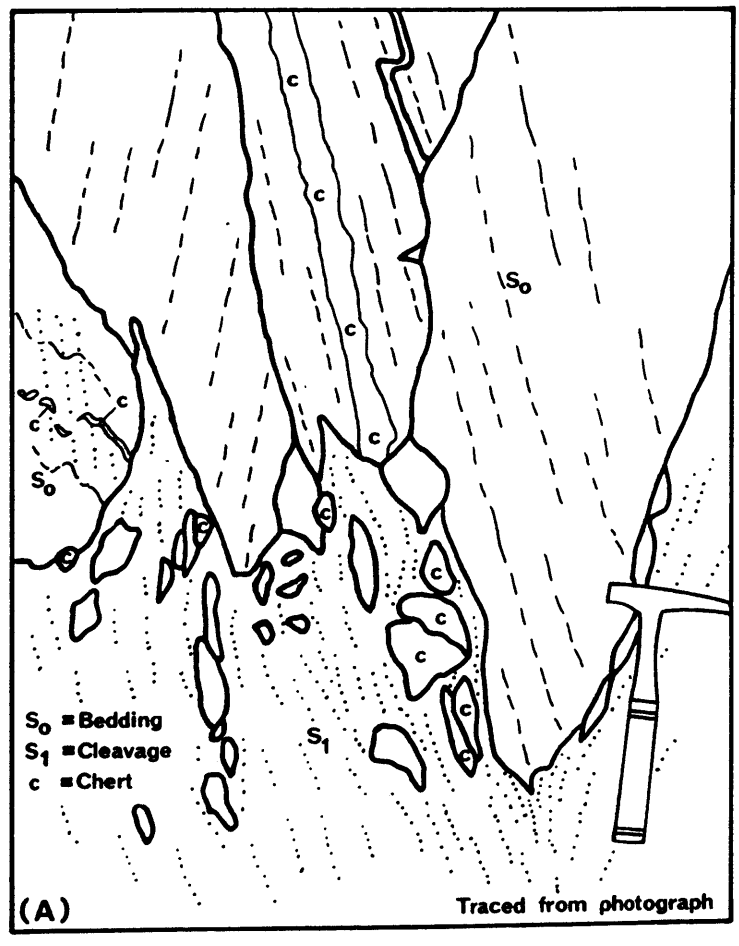

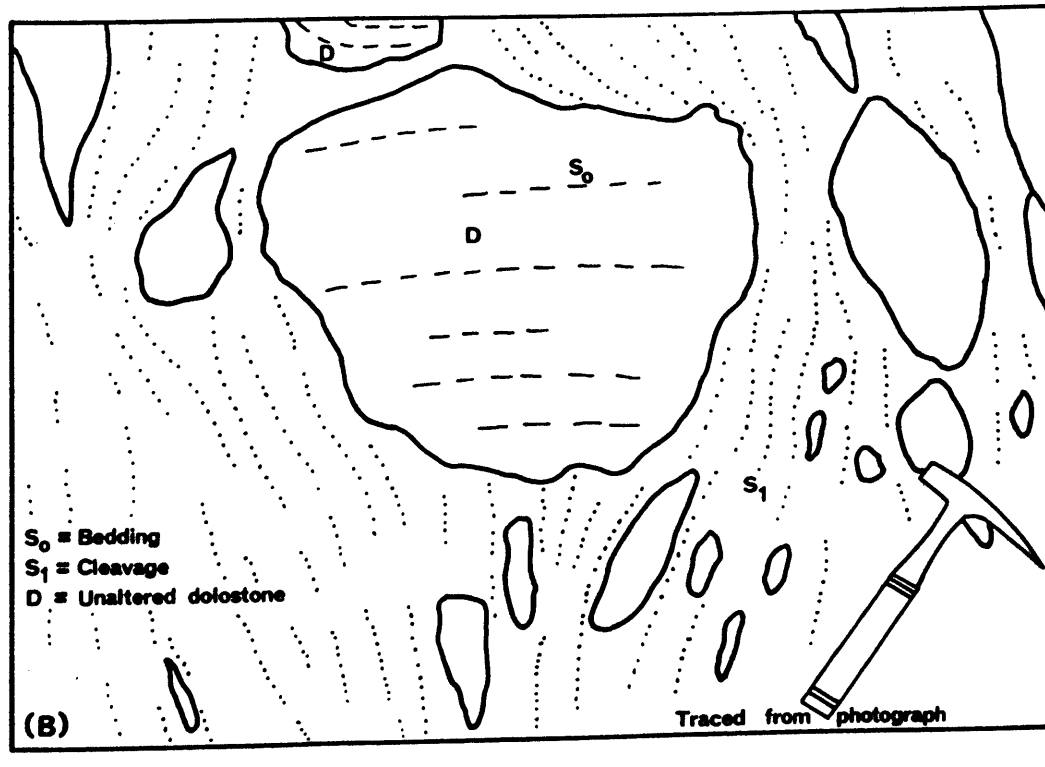

Fig. 37
Calcitized dolostone breccia, W120/32L, +276m (looking west). Clast boundaries (often stylolites), thin chert layers, and randomly - oriented bedding within clasts can be recognized. Many smaller clasts are elongated sub-parallel to the S_1 cleavage, which has a constant orientation. The cleavage penetrates some clasts, in which minor folds are visible (e.g. Figure 37A), but curves around other clasts (e.g. blocks of unaltered dolostone in Figure 37B).

has been extensive. Sulphide minerals occur in the matrix and, to a lesser extent, in clasts. The S_1 structural direction is visible as a cleavage, which disrupts compositional layering (probable bedding) in the dolomitic siltstone, and as an elongation of crystals of calcite spar.

The pipe breccia is more intensely, and extensively, calcitized at greater depth. Figure 40 shows a rock typical of much of the breccia below 30 level, in which angular clasts have been altered to calcite spar or, more rarely, silica; rounded, siliceous fragments are also present. Rounded clasts in the upper, "unaltered" part of the pipe breccia consist of chert, and rounded fragments in calcitized breccia are interpreted to be the same. The matrices of the calcitized rocks consist of calcite spar, and varying amounts of silica; the silica increases with depth in the pipe. Sulphide minerals are more abundant in the matrices than in the clasts. The original nature of the matrix to the pipe breccia has been obscured by alteration throughout most of the calcitized zone, and the relative importance of a siltstone matrix at depth in the pipe is difficult to ascertain.

Coarsely crystalline, light grey to pinkish grey calcite rock is also typical of much of the breccia below 30 level. This type of rock consists predominantly of calcite spar, commonly with a grain size of 1-2 mm, which shows deformation textures and contains relict, finer-grained spar in places (Fig. 41). Elongated grains of quartz and white calcite spar (to 5 mm in length), which lack inclusions of finer-grained spar, occur interstitial to the above calcite spar and are thought to have filled open spaces. This coarsely crystalline rock is termed "marble breccia" by the Tsumeb mine geologists when the rock is obviously a breccia. Clasts are not obvious in some specimens, in which adjacent clasts interlock and are only outlined by sulphide mineralization along clast boundaries. The former bedding direction can be recognized in individual clasts within many areas of "marble breccia"; it can be distinguished by variations in grain size, veining along the bedding direction, and rare, thin, bedded chert layers. The bedding directions in any group of clasts occur randomly oriented, within a matrix which displays a consistent S_1 direction (Fig. 37).

Fig. 38

Hand specimen of calcitized, recrystallized, dark dolostone breccia from the upper part of the calcitized zone of the Tsumeb pipe; a large, light grey clast, now completely altered to calcite spar, is visible on the right. The greyish black, matrix material is carbonaceous, dolomitic siltstone. Medium grey areas of the matrix consist of aggregates of calcite grains, 0,05-0,2 mm (up to 3 mm) in diameter, which have replaced small clasts and the siltstone matrix (Fig. 39). Sample 860, W20/29L.

Fig. 39

Thin section of the fine-grained matrix of sample 860 (Fig. 38); the carbonaceous, dolomitic matrix (D, left) is partly replaced by calcite spar (C, bottom right). Non-carbonate material, such as carbonaceous matter, sericite, and minor amounts of an unidentified, pleochroic brown mineral (Chapter 3.3.1), is concentrated at the margins of the spar, or occurs as interstitial layers between calcite-rich areas where recrystallization has been extensive. The S_1 structural surface is a cleavage which disrupts compositional layering (probable bedding); this surface is also present as an elongation of crystals of calcite spar. Plane polarized light.

Fig. 40

Hand specimen of calcitized, recrystallized (and partly silicified) dolostone breccia from the lower part of the calcitized zone of the Tsumeb pipe. The clasts consist of calcite spar (C) and, more rarely, silica (S); rounded, siliceous clasts are interpreted as cherts of the Tsumeb Subgroup (see text). The original nature of the matrix cannot be determined; it now consists of calcite spar, subordinate silica, and sulphide minerals (which give the matrix its dark colour). Sample 520, W140/34L, +219 m.

Fig. 41

Thin section of calcitized, recrystallized dolostone breccia ("marble breccia"), typical of the calcitized zone of the Tsumeb pipe. Coarse-grained calcite spar (centre), with a grain size of 1-2 mm, shows deformation textures and contains relict, fine-grained spar in places (e.g. dark area, bottom left). Large calcite grains have mutually interlocking boundaries, or are separated by the S_1 stylolitic cleavage (e.g. to left of the chert fragment, C, at lower right). Sulphide minerals, quartz, and minor carbonaceous material are concentrated in the cleavage surface. Elsewhere, quartz and sulphide minerals occur in interstices between grains of calcite. Sample 515, W96/33L, +232 m.

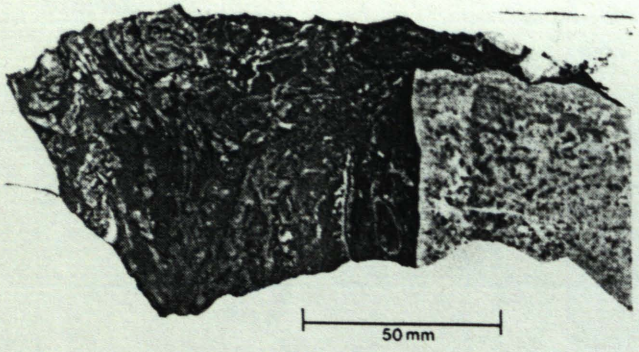

Fig. 38

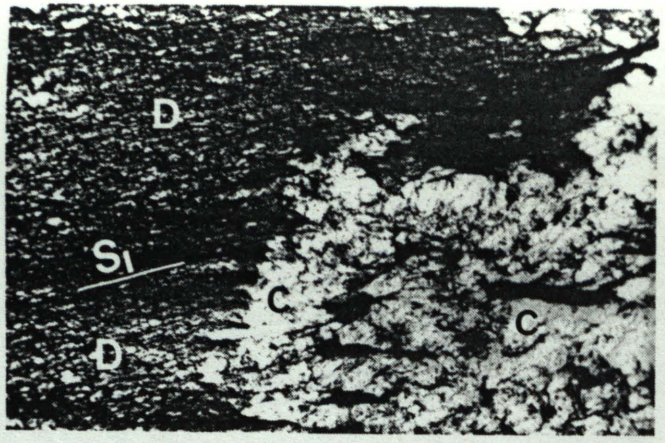

Fig. 39

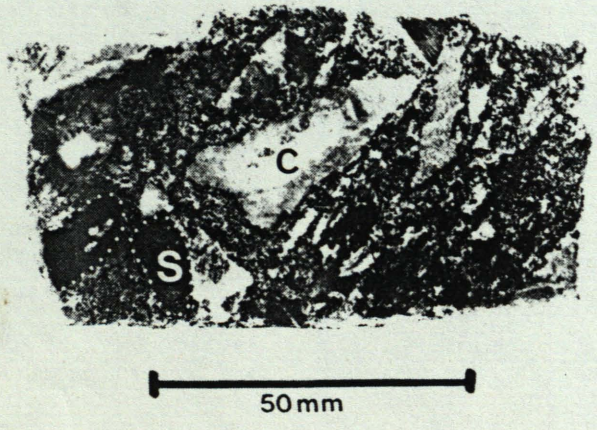

Fig. 40

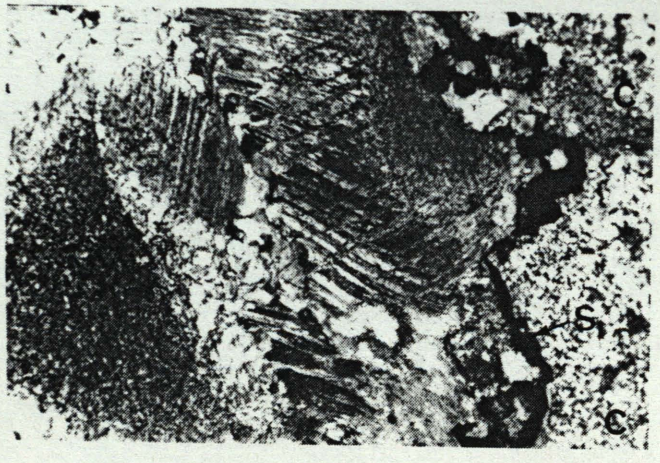

Fig. 41

This direction is represented by cleavage, and by elongation both of grains of calcite spar and clasts.

The chemical changes which occurred during calcitization can be determined by comparing calcitized rock of Table 5 (analyses 1, 3-4) with unaltered dolostone of Table 1. The degree of calcitization is reflected by the MgO/(MgO + CaO) ratios of these rocks. Samples 440 and 439 (analyses 3 and 4, Table 5) are unaltered and calcitized dolostone, respectively, from a single locality. This locality is immediately external to the marginal massive sulphide ore zone of the pipe at E35S/30L, +368 m (Fig. 36E). The only chemical changes in these calcitized rocks, relative to the unaltered rocks, involve addition of CaO, SiO_2 and MnO, and removal of MgO. The MnO content of the calcitized dolostone is at least three times greater than in unaltered dolostone. Discrete manganese minerals are absent, and the calcite which formed during calcitization of the dolostone is, therefore, slightly manganoan.

3.4.3 Silicification in the Tsumeb pipe

Silicification (i.e. replacement of rock by silica) comprises the lowest zone of alteration within the Tsumeb pipe. The uppermost elevation at which silicification has been recorded is 24 level (Söhnge, 1964), although quartz veins (i.e. open-space fillings) occur within ore at higher elevations (e.g. 20L; Lombaard, 1953). Silicification is confined to the vicinity of the massive sulphide margin of the pipe from 24 level to below 31 level, and is most commonly associated with copper-rich ore over this interval. This marginal, silicified zone is too narrow to depict on Figures 18-20, except in the lower part of the pipe. Silicification becomes volumetrically important within the pipe core below 33 level, where it forms an outer rim around the body of calcitized breccia (Fig. 18). Much of the core is silicified below 34 level, and silicification of the entire core is almost complete at 38 level (Figs. 19, 20). Minor white dolomite spar, and rare unaltered dolostone are the only carbonate minerals present at this depth. Calcitization is again locally important below 44 level.

TABLE 5. ALTERED SEDIMENTARY CARBONATE ROCKS OF THE TSUMEB PIPE

	CALCITIZED, RECRYSTALLIZED ROCKS				NORTH BREAK ZONE					SILICIFIED DOLOSTONE	
	HOPWOOD (1975)	THIS THESIS			HOPWOOD (1975)				THIS THESIS	THIS THESIS	
	(1)	(2)	(3)	(4)	(5)	(6)	(7)	(8)	(9)	(10)	(11)
SiO_2	7,5		n.d.	n.d.	2,9	4,7	2,0	37,8	29,9	80,8	78,6
Al_2O_3	0,99		0,54	0,36	0,16	0,15	0,13	0,22	0,58	1,08	0,52
Fe_2O_3	0,07		-	0,30	0,27	0,12	0,21	0,22	0,28	-	-
FeS_2	0,31		0,32	-	-	-	-	-	-	5,7	0,95
CaO	43,9		47,0	29,9	43,4	37,0	38,5	19,0	28,5	2,4	4,9
MgO	3,7		6,1	21,3	8,8	12,5	12,5	13,6	8,1	1,86	2,4
Na_2O	0,12		< 0,01	< 0,01	0,01	< 0,01	0,01	< 0,01	< 0,01	0,08	0,29
K_2O	0,48		< 0,01	< 0,01	0,37	0,03	0,01	0,05	< 0,01	0,17	< 0,01
TiO_2	0,07		< 0,01	< 0,01	n.d.	n.d.	n.d.	n.d.	< 0,01	0,02	< 0,01
P_2O_5	0,07		0,28	0,18	0,08	0,07	0,07	0,12	0,22	0,14	0,12
MnO	0,44		0,45	0,14	0,54	0,53	0,85	0,17	0,42	0,01	0,06
CO_2	40,5		43,8	46,4	43,5	44,0	44,1	28,8	31,4	3,3	7,7
C	0,16		0,05	< 0,01	n.d.	n.d.	n.d.	n.d.	0,03	0,05	0,02
Cu	0,97		0,10	0,10	< 0,01	0,01	0,20	0,03	0,10	0,87	1,28
Pb	0,18		0,10	0,20	< 0,01	0,44	1,19	0,06	0,29	0,29	0,30
Zn	0,15		0,05	< 0,05	< 0,01	0,38	0,28	0,04	0,10	0,38	2,4
As	0,36		0,09	0,10	n.d.	n.d.	n.d.	n.d.	0,05	0,48	0,15
Other S	-		0,07	< 0,01	0,01	n.d.	n.d.	n.d.	< 0,01	2,3	0,28
TOTAL	100		100	100	100	100	100	100	100	100	100
MgO/CaO+MgO	0,08		0,12	0,42	0,17	0,25	0,24	0,42	0,22	0,43	0,33
Ba(ppm)		32	< 20	< 20					366	66	20

1. Calcitized, recrystallized rock, 31 level, Tsumeb.
2. Calcitized, recrystallized rock, 33 level, Tsumeb (sample 492).
3. Calcitized, recrystallized dolostone, 30 level, Tsumeb (sample 440: see (4)).
4. Unaltered massive medium grey dolostone, 30 level, Tsumeb (sample 439: same location as (3) above).
5. Calcitized North Break Zone, 27 level, Tsumeb (supergene calcitization).
6. Calcitized North Break Zone, 28 level, Tsumeb (supergene calcitization).
7. Calcitized North Break Zone, surface, Tsumeb (supergene calcitization).
8. Silicified North Break Zone, surface, Tsumeb.
9. Calcitized and silicified North Break zone, drill hole 3178, Tsumeb (hypogene calcitization).
10. Silicified dolostone, 38 level, Tsumeb (sample 858A): negligible white quartz.
11. Silicified and slightly calcitized dolostone, 35 level, Tsumeb (sample 530): white quartz abundant.

All analyses normalized for major components; analyses 3 and 4 normalized assuming 1 % SiO_2 (as indicated by acid residues). Original analyses, analysts, methods in Appendix 1.
n.d. = not determined

There is an extensive transitional zone between completely calcitized and completely silicified breccia within the pipe core. Clasts of calcitized dolostone occur in matrices which are both silicified and calcitized. Siliceous clasts occur, the original nature of which is indeterminate, but unaltered dolostone clasts are rare. Sulphide minerals are most abundant in the matrices of the breccia, as is minor sericite and carbonaceous matter. The original sedimentary nature of the breccia becomes less obvious with increasing depth, especially where the clasts are strongly elongated parallel to the stylolitic S_1 cleavage. It was this transitional zone that was studied most extensively by Hopwood (1975), who proposed that the breccia was of tectonic origin.

The sequence of alteration zones within the marginal fracture zone is the same as that within the pipe core. However, silicification and calcitization each extend to higher elevations in the marginal zone than the core, and are less systematic in their distributions. One type of alteration commonly predominates at any single locality in the marginal zone. Where both types of alteration are present, silicification and calcitization form separate but adjacent zones (Fig. 36H). Silicification is relatively unimportant in the strata-bound alteration zones, except in the immediate vicinity of the pipe. The exceptions are a thin, but extensive silicified zone at the base of the strata-bound North Break zone, and strata-bound silicification associated with the S95 manto (Fig. 19).

Silica in the silicified rocks commonly has a distinctive form (Fig. 42). Elongated quartz blades of hydrothermal origin are abundant, and are mostly confined to the matrix of silicified breccia. Lath-like quartz of this type has been recorded elsewhere (Lovering, 1972), e.g. in "jasperoid" of the Tri-State zinc district, U.S.A. (McKnight and Fischer, 1970). The quartz blades of the Tsumeb specimens are randomly oriented in some specimens, but sub-parallel to S_1 in others. They display two dominant, opposing directions of shape elongation in some specimens, to form systematic networks. Hopwood (1975) noted that quartz blades from Tsumeb are "length-slow" and suggested, by analogy with "length-slow" chalcedony (Folk and Pittman, 1971), that this indicated the former presence of anhydrite.

However, quartz is typically elongated parallel to its c-axis, and quartz from Tsumeb is therefore not unusual.

The original nature of completely silicified dolostone breccia from the lower part of the pipe core is not obvious at most localities (Fig. 44, and the darker material in Fig. 43). However, silicified clasts (Fig. 45), or less commonly, former bedding in clasts, can be recognized in places and the rock is clearly a breccia. Most clasts are oriented sub-parallel to S_1. Large, angular blocks of completely unaltered dolostone, up to a metre in diameter, occur in a completely silicified matrix in places near the pipe margin (Fig. 43). The margins of some dolostone blocks are completely unaltered, whereas others are partly silicified, and clasts of unaltered dolostone, only a few centimetres in diameter, occur at some localities with clasts that are completely replaced by silica. It is impossible to determine petrographically the original nature of the matrix of completely silicified breccia, or of clasts other than rare, unaltered dolostone clasts. It is also impossible to distinguish between matrix material and small clasts. Exposures of the type shown in Figure 43 are atypical, in that they contain large, unaltered clasts and discrete white quartz veins. The bulk of the breccia is monotonous in appearance, and resembles the darker material in this photograph, or has a mottled appearance (Fig. 44). It is obvious, from the gradational nature of alteration with depth in the pipe, that the rare, unaltered dolostone clasts now present did not constitute the only dolostone in the original breccia, and the precursor to the completely silicified breccia is considered to have been dolostone breccia. Grain size, permeability and subtle compositional differences may have influenced the relative susceptibilities of the matrix and individual clasts to silicification.

Three main components constitute the completely silicified rocks. The first is very light grey, to white silica (the light areas in Figures 43-45) and the second is medium light grey, to grey silica (the dark material in the photographs). The third component is a very subordinate quantity of white dolomite spar (Fig. 44), which is commonly associated with the white silica. All three components display deformation textures. The two types of silica differ

petrographically. The white silica consists of very elongate grains, 2-12 mm in length (average 3-5 mm), with irregular, sutured, mutual boundaries. Sulphide minerals and small aggregates of large dolomite grains (average 5 mm) are the only minerals associated with this type of quartz. The grey silica consists of much finer-grained blades of quartz (0,03-0,20 mm long), and minor sericite. Sulphide minerals and sericite are commonly associated with the S_1 stylolitic cleavage. The most striking feature of these completely silicified rocks is the total absence of calcite, despite the presence of both hydrothermal dolomite spar and relict dolostone.

It is suggested that, prior to replacement, the grey silica consisted of dolostone breccia, and that the white silica and dolomite spar fill former vugs and interstices within this rock. This is apparent in thin sections of the specimens illustrated in Figure 44, in which much of the white quartz forms poorly defined veins which contain rare, large grains of sulphide minerals. Sulphide minerals are also disseminated in the grey silica, parallel to the walls of the white silica veins.

The chemistry of the silicification process is simple; analyses 10-11, Table 5 reflect the replacement of dolostone by SiO_2. The high MgO/(MgO + CaO) ratios of these rocks result from the presence of dolomite, rather than calcite, in these intensely silicified rocks. The increasing importance of silicification with depth can be seen in Figure 49. Samples from a traverse through the unaltered dolostone breccia core of the pipe at 28 level contain 16-30 per cent of material insoluble in HCl. This increases to 29-43 per cent in slightly silicified breccia of the lower calcitized zone, above 34 level. The insoluble content increases significantly to 64-91 per cent in the silicified zone at 38 level.

3.4.4 Rock alteration in the North Break zone

The North Break zone is an approximately 35 m thick horizon within the lower, stromatolitic part of zone T6 (Fig. 19). It can be observed adjacent to the pipe within the mine workings, and for a strike length of 6,5 km at surface. The base of the North Break zone

FIGURES 42-47

Fig. 42

A silica vein with characteristic bladed quartz, from the silicified and mineralized, marginal fracture zone of the Tsumeb pipe. Blades of quartz occur in the vein (bottom), and this is rimmed by coarse-grained calcite spar (centre) which grades into unaltered dolostone (top). Sample 230, E65/28L, +486 m (location: south end of Fig. 36B). Crossed nicols.

Fig. 43

Silicified dolostone breccia, which contains large blocks of unaltered dolostone (D) in a completely silicified matrix (M). The matrix contains smaller, silicified clasts which are difficult to recognize (Fig. 45). Vertical veins of white quartz (Q) contain traces of dolomite spar and sulphide minerals; these veins are deformed and sub-parallel to the S_1 structural surface. The veins are confined to the marginal fracture zone of the Tsumeb pipe. W30S/38L, +34 m. Scale given by geological hammer, bottom centre.

Fig. 44

Matrix to typical silicified dolostone breccia. This consists of (1) very light grey to white, coarse-grained quartz of open-space filling origin, Q, which contains tennantite, (2) very minor white, coarse-grained dolomite spar, D, also filling open spaces, and (3) medium light grey to grey silica (S) which contains sericite, and which is of replacement origin (see text). Left = sample 852B, W50/38L; right = sample 168, W150/35L, +170 m.

Fig. 45

Silicified dolostone breccia with a silicified clast (C) that shows former bedding (S_o). The matrix and clast are medium light grey to grey silica. Very light grey to white quartz veins occur sub-parallel to the S_1 surface, and rim the clast. Sample 858B, W30S/38L, +34 m (same location as Fig. 43).

Fig. 46

Sericitized sandstone ("pseudo-aplite") of the Tsumeb pipe. Most feldspar has altered to sericite (S), although some albite remains unaltered (A, top left, bottom left). The tourmaline (T) shown in Figure 47 is at top right. Sample 517, W140/34L, +219 m. Crossed nicols.

Fig. 47

Rounded brown tourmaline of detrital origin, with a ragged overgrowth of colourless, hydrothermal tourmaline, in the sandstone of Figure 46. Crossed nicols.



Fig. 42 0 mm 0.5

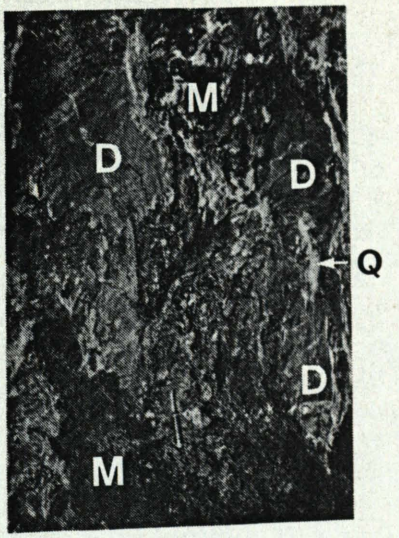

Fig. 43

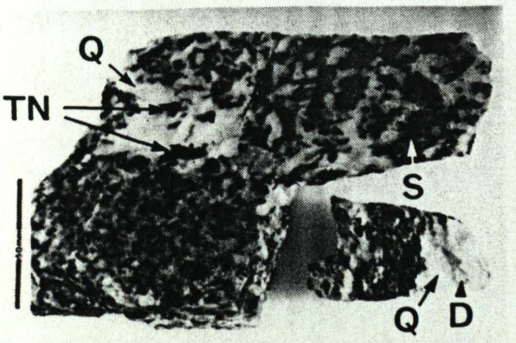

Fig. 44

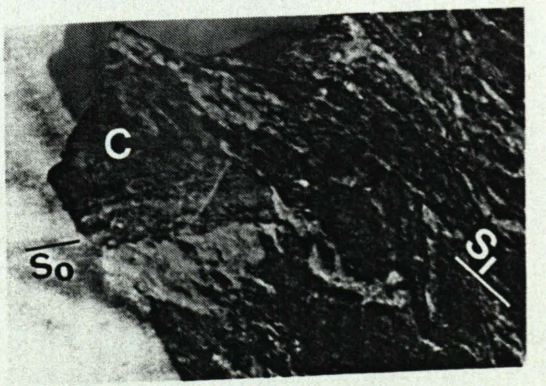

Fig. 45 0 cm 8

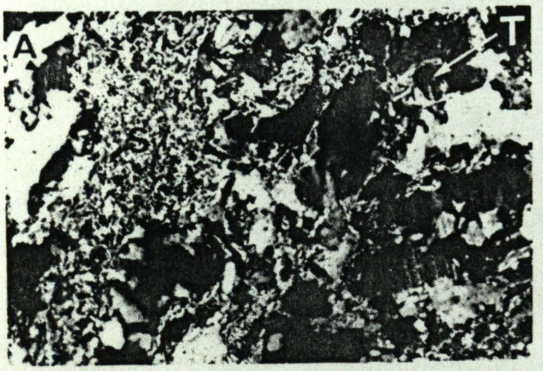

Fig. 46 0 mm 0.2

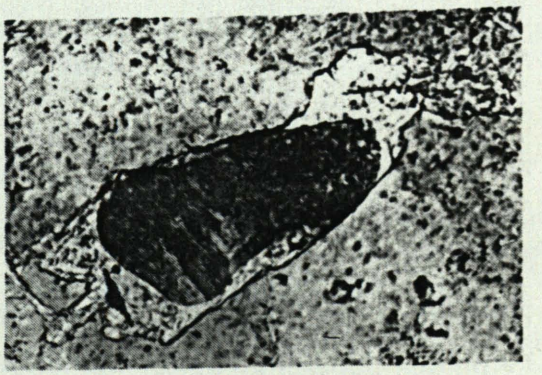

Fig. 47 0 mm 0.05

is defined by a 1-3 m thick silicified horizon (Söhnge, 1976). This horizon is overlain by dolostone that contains large, irregular, strata-bound areas of coarsely crystalline calcite and, in the immediate vicinity of the pipe, mineralization, silicification and brecciation. The mineralized areas include the S95 manto, the S110 ore body and the North Break ore body, all of which are confined to within 100m of the Tsumeb pipe. Paleokarst structures are interpreted to be present within the S110 ore body (Chapter 3.3.7). The definition of the North Break zone used here is more restricted than that of Land (1977b), who defined it as all rocks between the silicified base of the zone and the "tuten 2" stromatolitic marker (Fig. 19).

The basal, silicified and calcitized horizon of the North Break zone contains sparse chalcocite, galena, tennantite and sphalerite mineralization for many kilometres at surface (Land, 1977b), indicating the presence of the same rock alteration and mineralization event that affected the Tsumeb pipe. This is confirmed by the lead isotope ratios in the galena (Chapter 5.3.5). Sulphide mineralization is extremely rare in the overlying calcite bodies, except in the immediate Tsumeb mine area.

The basal silicified horizon was examined in DDH 3178. The contact between unaltered, medium light grey dolostone and overlying fine grained, calcitized dolostone at the base of the silicified and calcitized horizon, is abrupt. The quartz content of the rock increases to 20-35 percent within 2 cm of this calcitized contact. The calcitized dolostone is identical in appearance to that associated with sulphide mineralization in the Tsumeb pipe and ore bodies within the North Break zone. The calcite grains, and many quartz grains, are elongated parallel to the S_1 structural surface, and display deformational textures, and some samples contain randomly oriented quartz blades.

The large, overlying areas of coarsely crystalline calcite rock, where remote from mineralization, differ compositionally and texturally from calcitized rocks in the base of the North Break zone, described above, and in ore bodies of the North Break zone. These unmineralized, strata-bound calcite bodies contain three main components. The first

is pinkish grey, microspar dolostone, and the second is calcite spar (and minor fine-grained dolomite spar) which replaces the microspar dolostone. The third component is coarse grained calcite spar, with an average grain size of a few millimetres, which typically has a dark brown colour caused by numerous small inclusions of pyrolusite. Quartz and minor apatite are associated with the calcite spar. Hopwood (1975) considered that the pyrolusite ("manganese alteration") occurred as granular areas between "blades" of coarse grained calcite spar. However, pyrolusite in samples examined during the present study occurs in the calcite, immediately adjacent to dolostone inclusions. Large areas of calcite spar grade from brown at their margins, closest to dolostone inclusions, to white in their cores. The pyrolusite might, therefore, have formed during calcitization of a pre-existing, manganese-bearing mineral, such as the pinkish grey dolostone.

The manganese-rich nature of these calcitized rocks, some of which contain up to 0,85 % MnO, can be seen in analyses 5-7, Table 5. Analysis 9 is of a dolostone that was calcitized during the earlier, hydrothermal alteration event; this rock has the moderately high MnO content typical of these rocks elsewhere in the pipe, and a moderately high barium content.

Hopwood (1975) noted that the calcite spar in these unmineralized calcite rocks has overgrown the S_1 cleavage in the dolostone. This is consistent with the total absence of deformation textures in all of the calcite examined during the present study. The calcite in these strata-bound bodies is, therefore, thought to be younger than the calcite associated with sulphide mineralization. It post-dates karsting, mineralization and alteration, and D_1 deformation in the North Break zone. The oxygen isotope data of Chapter 5.2.3 support this conclusion and indicate that the calcite formed as the result of supergene processes.

The North Break zone therefore has a number of unique features. These are: (1) the timing of rock alteration and solution, two periods of which occurred prior to deformation (i.e. karsting and

mineralization) and one later, (2) the great strike length of the alteration zone, (3) the presence of paleokarst and manto structures, and (4) the presence of abundant stromatolites with low relief, and rare oolite horizons. These features indicate that the North Break zone was highly permeable, that this permeability existed over an extended period of time, and that the host rocks were deposited in relatively shallow water. These observations are consistent with the former presence of soluble minerals, e.g. evaporite minerals, but also with the presence of paleokarst which was subsequently rejuvenated, or both.

3.4.5 Carbon in the Tsumeb pipe

Various workers have suggested the presence of another type of alteration, "carbon alteration" or "graphitization", below 22 level in the Tsumeb pipe (Geier, 1952; Lombaard, 1953; Söhnge, 1964, 1976). This was invoked to explain the dark grey to black nature of the dolostone breccia (both matrix and clasts) relative to the wall rock dolostone. Geier (1952) also noted the presence of thin, graphite-filled veinlets in dark dolostone breccia. He noted that these rocks contain up to 5 vol. % graphite, but considered that disseminated, opaque material also present in the rock is carbonaceous material inherited from the original rock.

The first appearance of this proposed alteration, and of the dolostone breccia body, was recorded at 22 level (Söhnge, 1964). Subordinate light coloured dolostone clasts occur with abundant dark dolostone clasts in the dolostone breccia at lower elevations, yet the light fragments display no evidence of alteration (Fig. 81). This does not indicate, therefore, that the colour of the dark clasts was caused by "carbon alteration", although the possibility of very selective replacement of clasts exists. It is shown in Chapter 3.3.1 that the dark dolostone breccia is a slightly carbonaceous sedimentary rock, foreign to its surroundings. It is probable, therefore, that much of the carbon is an original sedimentary constituent of the breccia. It is also possible that many of the dark clasts do not contain significant carbon concentrations, but that their dark colour is a grain boundary effect which results from their fine grain size and

the presence of clay minerals or micas (Chapter 2.3.1). Polished sections of breccia clasts made during the present study do not display anisotropic graphite, although fine-grained carbonaceous material within the breccia matrix is sufficient to account for the reduced carbon content shown in analyses of these rocks.

The reduced carbon contents of hand specimens of dolostone breccia were analyzed to investigate the above possibilities. The results are summarized in Figure 48 and listed in full in Appendix 1.3 A bulk sample of medium to dark grey dolostone clasts contains very little reduced carbon, not significantly higher than the content of the wall rocks, or the rocks of the underlying alteration zones. Therefore, the dark colour of these clasts is not caused by reduced carbon. The breccia matrix has a significantly higher, though still low, reduced carbon content. This is comparable to the reduced carbon content of the Mulden Group sediments from which the breccia matrix is thought to have been derived (Chapter 6.1.1).

An attempt was also made to determine if these values are typical of the dolostone breccia as a whole, and to compare altered and "unaltered" breccia. Channel sample and drill core samples were analyzed along "unaltered", calcitized and silicified sections through the pipe (Fig. 49). The average reduced carbon content of the "unaltered" breccia is small, and can be accounted for by the presence of a more carbonaceous matrix. The calcitized and silicified zones have a significantly lesser reduced carbon content than the "unaltered" dark dolostone breccia. The proportion of carbonaceous matrix could have been smaller at depth, resulting in a lower reduced carbon content in these alteration zones. However, it is more probable that the large differences between the traverses, and the consistent values within each traverse, result from the chemical instability of reduced carbon during silicification and calcitization.

Veinlets of graphite are absent from polished sections prepared during the present study. Fine grained, opaque material, dark and isotropic in reflected light, which occurs along stylolite surfaces is carbonaceous material that has become concentrated during stylolitization. The descriptions of Geier (1952) indicate that the

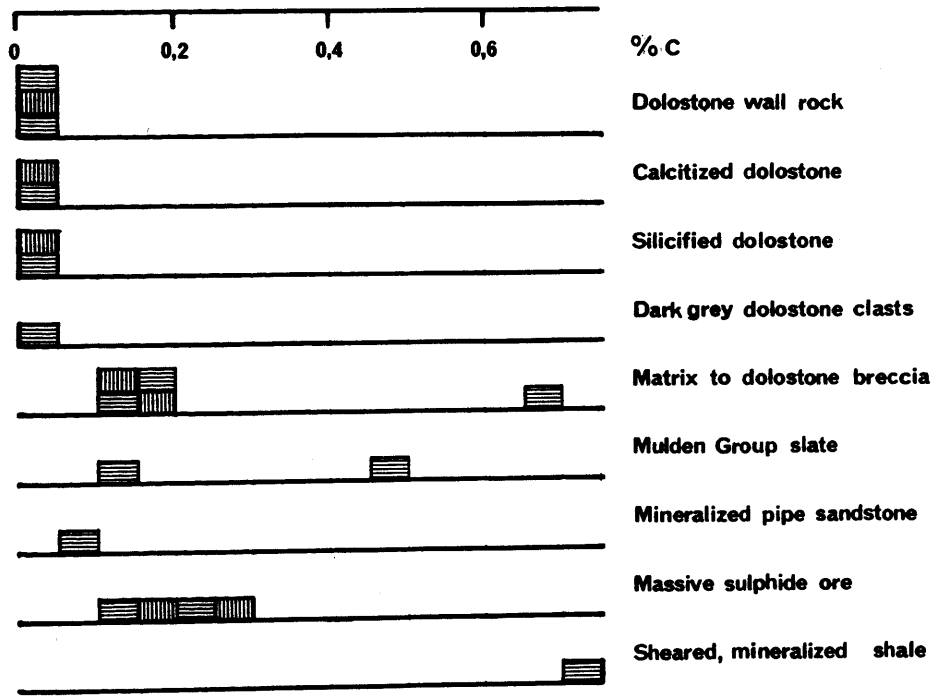

Fig. 48
Reduced carbon content of rock and ore from the Tsumeb ore body.

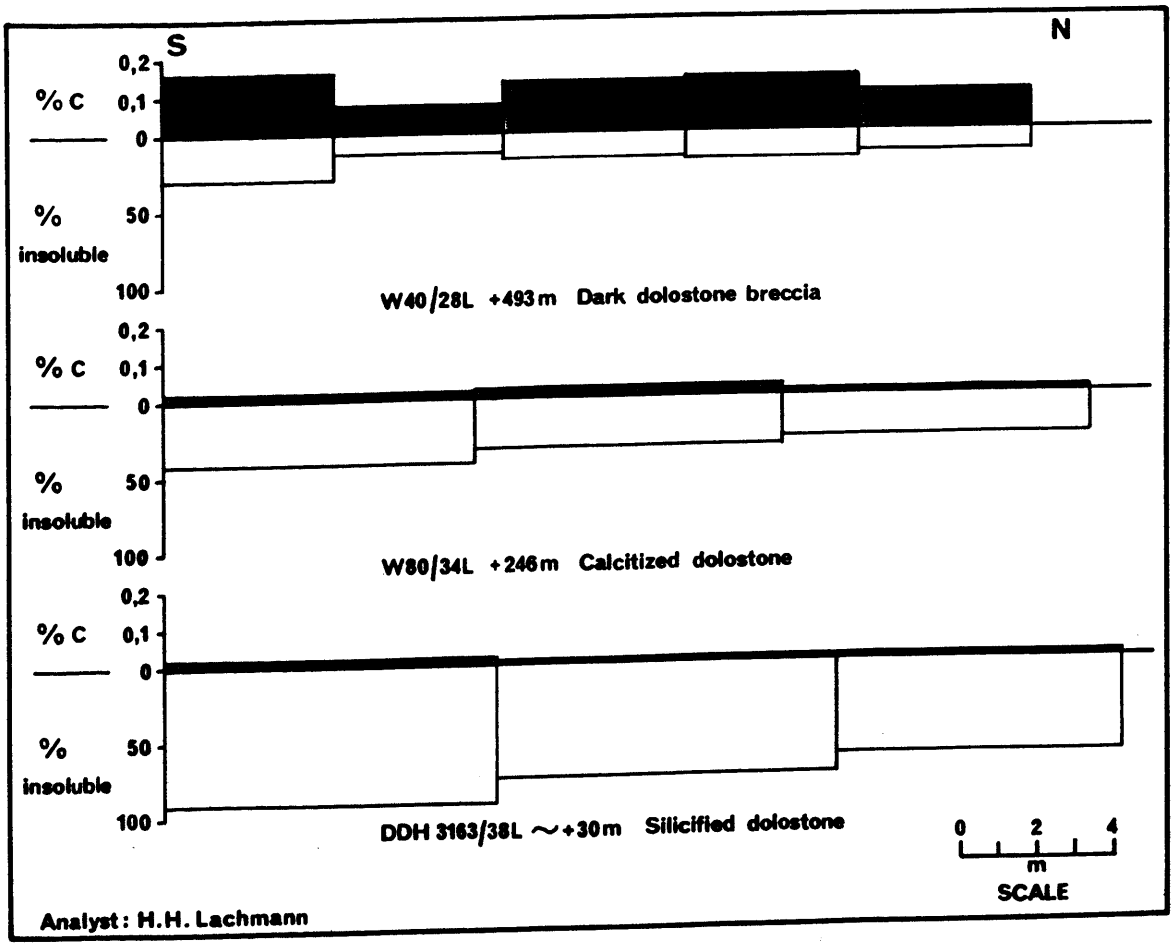

Fig. 49
Variation in the content of reduced carbon and quartz (material insoluble in HCl) in the different alteration zones of the Tsumeb ore body.

pleochroic and anisotropic vein-fillings which he described did consist of graphite, rather than carbonaceous material, and this may have been deposited from an external source (e.g. the ore fluids) as he suggested. However, veinlets of pyrobitumen occur in the breccia, and globules of pleochroic, anisotropic pyrobitumen pre-date sulphide minerals in calcite gangue from 22L (Geier, unpub. rept, 1953; Söhnge, 1964); this material may have been mistaken for graphite because of its optical similarity.

It is concluded that the dark colour of clasts in dark dolostone breccia is not caused by "carbon alteration" or "graphitization". Pyrobitumen may have been introduced to the matrix of the dolostone breccia from an external source, and graphite may have formed during rock alteration in the upper part of the pipe, but these substances occur in small quantities relative to carbonaceous material present in the original rock. Reduced carbon was unstable during calcitization and silicification of rocks within the Tsumeb pipe.

3.4.6 Alteration of the pipe sandstone

Previous workers recognized various types of alteration of the pipe sandstone. These include sericitization of feldspar (Geier, 1952), intense calcitization (Lombaard, 1953), and the formation of clear quartz overgrowths on detrital quartz grains (Pennebaker, 1952). The presence of minor hydrothermal tourmaline was recognized during the present study, and supposed "talc alteration" (Söhnge, 1964; Hopwood, 1975) was found to consist of illite, rather than talc.

Grains within the pipe sandstone mostly interlock along irregular, sutured boundaries. Obvious quartz overgrowths on pre-existing rounded grains occur, but are not abundant (Fig. 24). Ypma (1973a, b) noted that these quartz overgrowths contain fluid inclusions of the type found in the Tsumeb sulphide ore. Fine-grained mosaics of equigranular quartz grains which occur along grain boundaries in some speciments might also be of hydrothermal origin. Some former sandstone is completely replaced by quartz and sericite, and can be mistaken in hand specimen for silicified dolostone. Former feldspars in these rocks consist of intergrown sericite and quartz

blades, continuous with quartz blades in the matrix.

Sericitization and calcitization occur independently or together; in incipiently altered sandstone they are confined to grain boundaries, but where alteration is intense they extensively replace rock minerals (Fig. 46). Sericite has formed after feldspar, and after rare grains of biotite (the original nature of which is now indeterminate, but which is assumed to be of detrital origin). Calcite is less selective as to the grains replaced, but is very abundant in rocks which contain clasts of calcitized dolostone. The potassic nature of the alteration is obvious from analysis 6, Table 4, of a rock in which all feldspars are replaced by sericite. Sericite in altered sandstone, (and coarser-grained blades of white mica disseminated in massive sulphide ore) were confirmed to be potassium aluminium silicate minerals by qualitative energy dispersive microprobe analysis (Analyst: N. Lindsay). Analysis 5, Table 4, is of a sandstone which is incipiently altered, but in which most of the original albite is unaltered, as is reflected in the high Na_2O:K_2O ratio. Sulphide minerals in altered sandstone replace grain margins, rather than the interiors of grains, in sparsely mineralized samples. Extensive chloritization of feldspar is present in a few specimens, but is absent from most specimens and is not obviously related to the main alteration and mineralization event.

Botha (1960) noted that multi-coloured and colourless tourmaline are much more abundant in the Tsumeb pipe "pseudo-aplite" (which he considered magmatic) than in the Mulden Group sandstone. This was one of the mineralogical criteria which he used to distinguish differences between the two rock types. Rounded, strongly coloured (often brown) tourmaline of probable sedimentary origin occurs in both the Mulden Group sandstone and the pipe sandstone. The present study revealed common overgrowths of pale tourmaline on strongly coloured tourmaline in the pipe sandstone. The pale tourmaline occurs alone, commonly as ragged, elongate forms, or as irregular overgrowths on strongly coloured tourmaline (Fig. 47). The irregular form of the pale tourmaline indicates that it has not undergone sedimentary transport. It appears to have precipitated in situ, either alone or as hydrothermal overgrowths on sedimentary tourmaline.

Söhnge (1964) recorded "talc alteration" associated with shear zones in drill holes below 30 level, and Hopwood (1975) noted that this alteration is commonly associated with sheared sandstone. Figures 6D and 6G of Hopwood (1975) depict steep "talcose" shears on the southern margin of the pipe in W136 stope and W120 cross-cut, 33 level. These were examined during the present study in a similar position in W136/W120 stope, 31 level (+343 m), on the south-western margin of the pipe. Remnants of calcite veins and pods of supergene chalcocite occur within "talc" of near-vertical shear zones, tens of centimetres wide, and the calcite pre-dates the shearing. XRD studies of the "talc" reveal that it consists of illite, quartz, minor kaolinite, but no talc. The supposed "talc" is, therefore, illite which has probably been derived from sheared, intensely sericitized pipe sandstone.

3.4.7 Summary

Three main alteration zones can be recognized in the dolostone breccia core of the Tsumeb pipe (Fig. 135). The deepest zone consists of quartz and minor sericite, dolomite spar and unaltered dolostone; it lacks reduced carbon. The overlying calcitized zone consists of slightly manganoan calcite spar and minor sericite, and also lacks reduced carbon. The uppermost alteration zone displays the least alteration; dolomite and reduced carbon were in equilibrium with the ore fluids and the dark dolostone is, therefore, unaltered. However, original clay minerals in the matrix of the dark dolostone breccia were extensively altered to sericite. Some massive sulphide bodies are in direct contact with completely unaltered, bedded dolostone (Fig. 55).

Sub-arkose within the Tsumeb pipe has been calcitized, silicified and sericitized to varying degrees. Feldspar and biotite (of detrital origin) were altered to sericite, and new tourmaline formed. Sericite in the altered dolostone breccia and in the sub-arkose is muscovite (i.e. sericite *sensu stricto*). Chlorite is present within the Tsumeb pipe, but is quantitatively insignificant relative to sericite and is not obviously related to hypogene sulphide mineralization.

Dolostone of the strata-bound North Break alteration zone was

calcitized and silicified during the alteration and mineralization event that affected the Tsumeb pipe. A later, intense and extensive, alteration event produced calcite and pyrolusite within this zone.

3.5 STRUCTURAL AND STRATIGRAPHIC CONTROLS OF MINERALIZATION

Discordant and strata-bound massive sulphide ore of the Tsumeb pipe is controlled by major fractures, while disseminated ore is controlled by minor fractures and by inter-clast and inter-granular permeability. Sulphide mineralization is epigenetic and of both open-space filling and replacement types. Open-space filling is recognized by the presence of sulphide crystals in vugs, by the presence of sharply- defined contacts along some veins, and by symmetrical, crustified veins. Also, sulphide crystals which occur along the walls of some veins have irregular margins where they contact the vein walls, but display well-formed crystal faces which project into the formerly open space of the vein (Fig. 50).

There is also abundant evidence for large-scale replacement of sedimentary rocks by sulphide minerals. Sandstone of the marginal fracture zone, in which sulphide minerals are confined to inter-granular sites, grades into massive sulphide ore in which only rare remnants of well mineralized sandstone remain. Chert fragments, and unaltered or calcitized dolostone fragments which occur in massive sulphide ore, are commonly identical in size, shape and composition to chert and dolostone clasts in adjacent, unreplaced sandstone breccia. Irregular and diffuse margins on many bodies of massive sulphide ore in contact with dolostone indicate that sulphide minerals have replaced the dolostone. Silicified stromatolitic forms of the "tuten 2" marker define a continuous horizon within massive sulphide ore of E49 manto, near "Y" in Figure 54. The matrix to these forms consists entirely of massive sulphide ore in places, indicating that the former dolostone host to the silicified forms has been completely replaced by sulphide minerals.

3.5.1 Steeply dipping massive sulphide bodies

Steeply dipping massive sulphide bodies are mostly confined to a marginal zone which surrounds the pipe (Fig. 18). These bodies vary from tens of centimetres to greater than 10 m in thickness, and commonly contain more than 50 vol. % sulphide minerals (Fig. 51). The marginal massive sulphide bodies occur in two sub-parallel, northern and southern ore zones, which are connected at the eastern and western ends of the pipe. These are termed the North lens (or Footwall vein) and South lens, respectively. It is argued in Chapter 3.7 that the elongate, elliptical shape of the pipe results from post-ore deformation, and that the pipe and its marginal zone of massive sulphide ore were originally nearly circular in plan. The less regular form of the pipe between 31 and 34 levels (Fig. 18) is partly a function of post-ore shearing. The marginal massive sulphide bodies were offset by reverse bedding faults between 6-19 levels and 35-37 levels, subsequent to D_1 deformation. The very elongated form of the pipe at 35 level results from this faulting along the northern margin, and sulphide lenses along this margin now lie in this fault plane. Sandstone and massive sulphide bodies, only tens of centimetres wide, occur on the pipe margin below this faulted segment to at least 38 level, but are too thin to show on Figure 18.

Massive sulphide bodies commonly replace sedimentary rocks which fill the marginal fracture zone of the pipe, or replace breccias generated during formation of the fractures (Chapter 3.3.2). However, some very thin massive sulphide layers occupy fractures which post-date earlier fracture-filling sedimentary rocks, and some thicker bodies may also be of this type. Massive sulphide bodies cut bedding in dolostone at many localities above 30 level (i.e. they have two dolostone walls), e.g. 20L, 27L (Fig. 31), 26L (Figs. 36A, B), 24L (Lombaard, 1953). Sulphide bodies at lower elevations more commonly occur on the contact between unaltered, or altered, sedimentary infill of the pipe and the enclosing wall rocks (Figs. 18, 19, 36G). Most massive sulphide bodies possess sharp outer contacts with the dolostone wall rocks, while their internal contacts vary from sharp to diffuse. The marginal fracture zone has been intensely and pervasively altered, and the rock alteration commonly differs in composition from that present

FIGURES 50-53

Fig. 50

Veins of calcite spar and calcitized dolostone which fill, and occur adjacent to, steeply-dipping fractures in the marginal fracture zone of the Tsumeb pipe. The upper vein and the margin of the lower vein consist of unmineralized, calcitized dolostone (now calcite spar). The central area, and the area above the upper vein, is fine-grained calcite spar (calcitized dolostone) and dolostone, which shows remnant bedding. The lower part of the lower vein is coarse-grained calcite spar and galena. The galena is subhedral except where it is in contact with calcitized dolostone. Diameter of lens cap is 54 mm. W40/30L, +367 m.

Fig. 51

Vertical compositional banding in copper-rich massive sulphide ore of the marginal fracture zone, below the E49 manto (Figure 56). Pyrite (P, light), galena (G, medium), bornite and black silica (dark). Scale given by geological hammer, bottom centre. E49S/28L, +424 m.

Fig. 52

Breccia, interpreted as a collapse breccia, in the footwall of the S95 manto. The lower contact of the sub-horizontal manto is 10 cm above the top of the figure. Slightly disoriented blocks of silicified dolomite, showing bedding, are separated by coarsely crystalline, white calcite spar of cavity-filling origin. Scale given by geological hammer, centre. W20/30L, +362 m.

Fig. 53

Drill core, showing a galena-tennantite-pyrite vein (V) cutting dolostone (D) and dolomite spar (S), adjacent to the silicified zone of the Tsumeb pipe. This illustrates fracturing within the marginal fracture zone, subsequent to rock alteration (and therefore subsequent to deposition of sandstone within the fracture zone). Silicified dolostone breccia (B) with a matrix of massive sulphide ore occurs to the right of the dolomite spar. Sample 925, DDH 3163/38L.

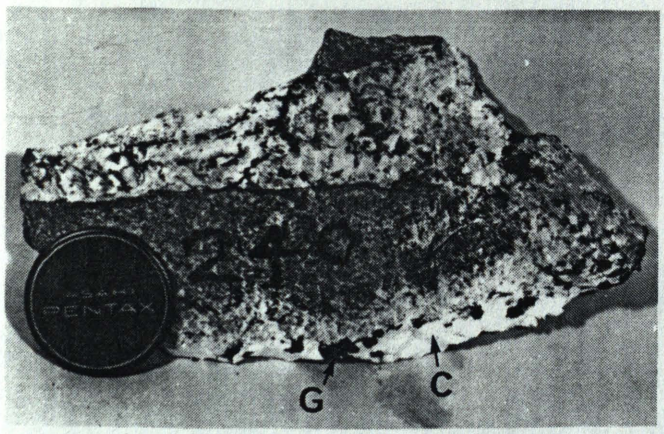

Fig. 50

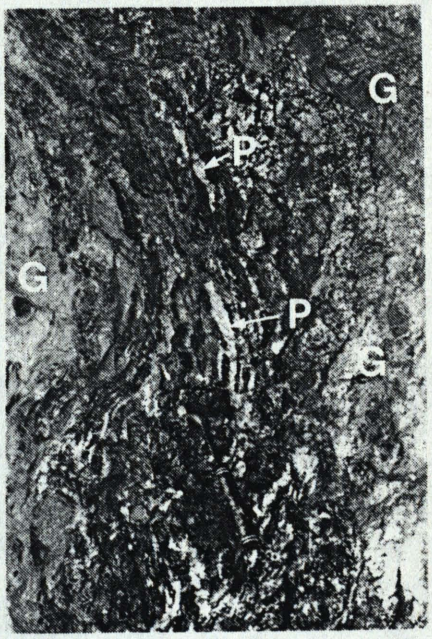

Fig. 51



Fig. 52

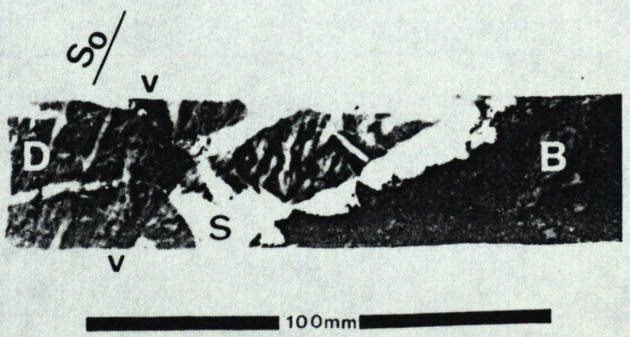

Fig. 53

in the immediately adjacent, altered pipe core. Relatively minor dolomite and calcite veining occurs in the marginal fracture zone. (Fig. 50); this is most abundant on the margins of massive sulphide bodies, or where massive sulphide ore is absent and the fracture zone is represented by rock alteration and brecciation. Thin fractures filled with sulphide minerals post-date deposition of some carbonate gangue minerals (Fig. 53).

It is concluded that fractures associated with the margin of the pipe formed after the deposition of the dark dolostone breccia within the Tsumeb pipe, and before the deposition of sandstone (Chapter 3.3.5). Sulphide minerals filled open cavities within the marginal fracture zone, and replaced its sedimentary rock infill and, to a lesser extent, replaced the wall rocks adjacent to the fracture zone. Further, probably minor, fracturing occurred in the marginal fracture zone after deposition of the sandstone and, at least in part, prior to or simultaneously with sulphide mineralization.

3.5.2 Mantos

Strata-bound mineralization of the Tsumeb pipe includes massive sulphide mantos, disseminated mineralization of the S110 ore body, and sparse mineralization that occurs in the silicified base of the North Break zone. These mineralized bodies occur over a stratigraphic interval of 180 m in the lower, stromatolitic half of zone T6, which corresponds to 25-30 levels in Tsumeb mine (Fig. 19). The thin, silicified horizon and the closely associated S110 copper ore body, occur near the base of this interval. The "tuten 3" stromatolitic chert marker of zone T6 occurs near the top of the more mineralized, lower part of the interval (Fig. 19). The North Break ore body (a discordant body, distinct from the North Break zone) also occurs in this part of the sequence, to the north of the Tsumeb pipe and within the North Break zone.

All mantos of the Tsumeb pipe are, by definition, broadly conformable to the stratigraphy. They are confined to dolostone, where they are closely associated with stromatolite and chert horizons in many places, and do not cut the breccia of the Tsumeb pipe (although

they can occur in dolostone interior to the marginal fracture zone of the pipe). However, mantos typically cut the bedding at a small angle (Fig. 55), and in places dip in the opposite direction to the enclosing rocks. Many mantos mined in the past do not appear on old geological plans because of their sub-horizontal attitude. Also, mantos are very variable in shape and elevation and cannot be easily correlated between drill holes. It proved difficult, therefore, to reconstruct the distribution of previously mined mantos during the present study. However, at least ten mantos are known to have been mined (Söhnge, 1964). Two large mantos and a number of thin (0,5-2 m thick), discontinuous mantos were observed between 26 and 30 levels. The large mantos are the S95 manto, on the southern side of the pipe above the S110 ore body, and the E49 manto, at the eastern end of the pipe above the North Break zone. The E49 manto was mined during the present study and could be mapped in detail, but the previously mined S95 manto was only observed briefly during pillar recovery in the immediate vicinity of the pipe.

Some manto contacts are sharp and unaltered (Fig. 55); this is common in the E49 manto, although more gradational boundaries are also present. Elsewhere, as in the S95 manto (which occurs within the North Break alteration zone), the manto margins are typically sharply defined but are calcitized or silicified. The S95 manto is overlain by calcitized dolostone in E9S/30L (+374 m) and by silicified dolostone in W40S/30L (+368 m). Parallel alteration zones, separated by unaltered dolostone, occur in the underlying and overlying wall rocks. Replacement by sulphide minerals and open-space filling have both been important processes within mantos. However, no sandstone remnants and only minor dolostone fragments were observed within massive ore of mantos, and chert fragments predominate. Breccia clasts within massive sulphide ore of E49 manto are dark grey to black chert, unlike the predominantly white chert of the enclosing sequence. Many chert breccias within mantos consist of large blocks which have fragmented almost in situ. They do not consist of cavity-filling silica which has been disrupted subsequent to formation, since they commonly display prominent bedding surfaces. Breccia bodies are rare immediately above or below mantos, but do occur; e.g., the base of S95 manto immediately overlies a thick horizon of altered breccia in W40S/30L (+368 m) and

W20S/30L (+362 m), i.e. within the North Break zone. This breccia consists of slightly disoriented blocks of silicified dolostone in which former bedding can be recognized. The blocks are separated by large areas of coarsely crystalline white calcite spar (Fig. 52).

3.5.3 E49 manto near 28 level

Figure 54 shows a portion of E49 stope and manto immediately below 28 level. A near-vertical, copper-rich, massive sulphide body occurs along the southern margin of the pipe. A thinner, less continuous, massive lead-zinc body is present along the northern margin of the pipe. The two contact bodies form parts of a single, continuous body which has an arcuate north-south trend to the east of Figure 54. The closure which connects the two bodies occurs in E49E stope (+426 m), between E70 and E80 sections (Fig. 57).

A massive lead-zinc manto occurs at the northern end of E49 stope. This continues as a thin body westwards along the northern margin of the pipe, outside the figure. It connects southwards between the northern and southern contact bodies in E49 stope (i.e. through the core of the pipe). This connection can be seen at the western margin of the stope in Figure 54, and extends further east in this central position at slightly higher elevations. The composition of the manto changes from lead- and zinc-rich to copper-rich, southwards over the central part of the stope. The manto continues as a copper-rich body to the south of the southern contact body, and above the level of Figure 54 (i.e. this southern extension of the manto is not shown). The south-eastern margin of the southern contact body flares upwards at +419 m (near "X"), in the base of the overlying manto. The manto dips eastwards at this point, where it was stoped to below +412 m to the south-east of the pipe. This part of the manto connects with the manto in the northern part of the stope, via the area east of E66 section, and changes to lead- and zinc-rich over this interval (Fig. 57).

The contact between E49 manto and the marginal fracture zone of the pipe was observed in E49 stope at 29 level (Fig. 56), 7 m above point "X" of Figure 54. The steep layering in the bottom left corner

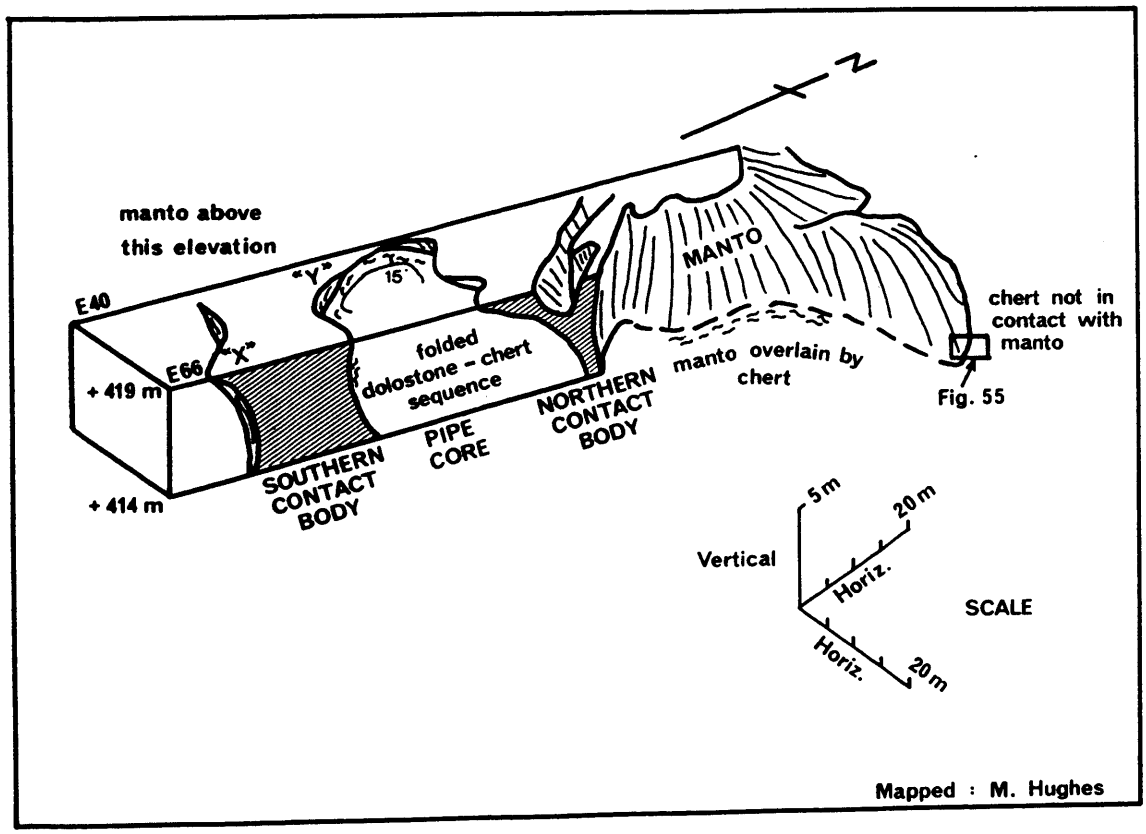

Fig. 54
Isometric projection of part of the E49 manto, showing the relationship between the manto and the vertical contact bodies (E49 stope, immediately below 28L). The two contact bodies are parts of a single, continuous body which has an arcuate, north-south trend farther to the east. The manto joins the southern contact body above "X", and also dips eastwards out of the section from this point.

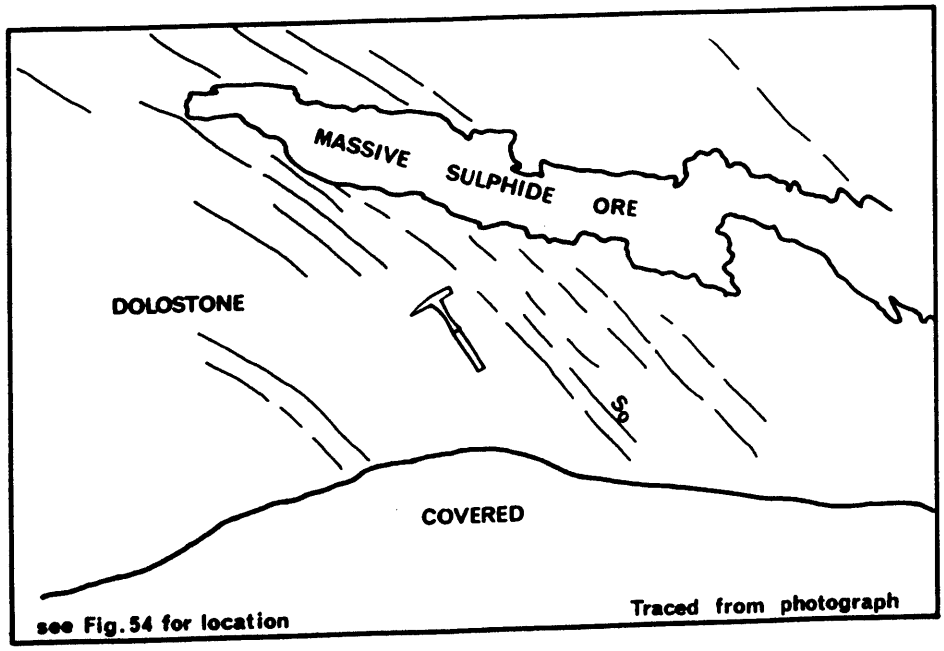

Fig. 55
The termination of the E49 manto in E49N/29L stope, +414m (looking north-east). The manto cross-cuts the bedding but there is no fracture beyond the end of the manto, and no drag occurs in dolostone adjacent to the margins of the manto. The margins are unaltered.

of Figure 56 is illustrated in Figure 51. The margin of the pipe continues steeply downward below this point (i.e. the southern margin of the southern contact body is immediately south of Figure 56). The manto itself continues north and south outside Figure 56. Compositional layering in sulphide ore of the southern contact body bends slightly into the plane of the manto, then terminates abruptly just below the manto roof. The southern contact body, therefore, terminates abruptly upwards at the manto. This interruption in the southern contact body is only slight. Data from old plans of overlying stopes indicate that the contact body continues above the manto, immediately north of Figure 56.

The core of the pipe in E49 stope consists of bedded dolostone and chert (Fig. 54); the dolostone grades from unaltered to calcitized, and silicification is confined to the immediate margin of the southern contact body. The sequence is moderately deformed in the eastern part of the stope, with dips in excess of 45°. It has a regular, shallow dip to the west of only 15°-25° in the western part of the stope. Dark dolostone breccia is absent, but was observed in E9 cross-cut (to the west) and old mapping indicates that it may continue eastwards to at least E20 cross-cut. The western limit of E49 manto, within the pipe core, was not observed in E49 stope, as the manto continues into the western wall at all elevations. All mantos observed within the Tsumeb pipe occur in dolostone, and none cut the dolostone breccia body; mine plans indicate that E49 manto also shows this distribution, and that it terminates to the west at the eastern closure of the Middle lens, on the contact of the breccia body (Fig. 57).

E49 manto is broadly concordant with the enclosing rocks, both inside and outside the pipe. It is closely associated with the "tuten 2" stromatolitic dolostone marker in the central part of E49 stope. It immediately overlies or incorporates the "tuten 2" marker within the core of the pipe. The "tuten 2" marker was also observed in the northern wall of the southern contact body (near "Y" in Figure 54). It was not seen to the south of this body in E49 stope, but was observed south of the contact in E35 pillar at +396 m. This indicates that the marker has been significantly displaced or downfolded along

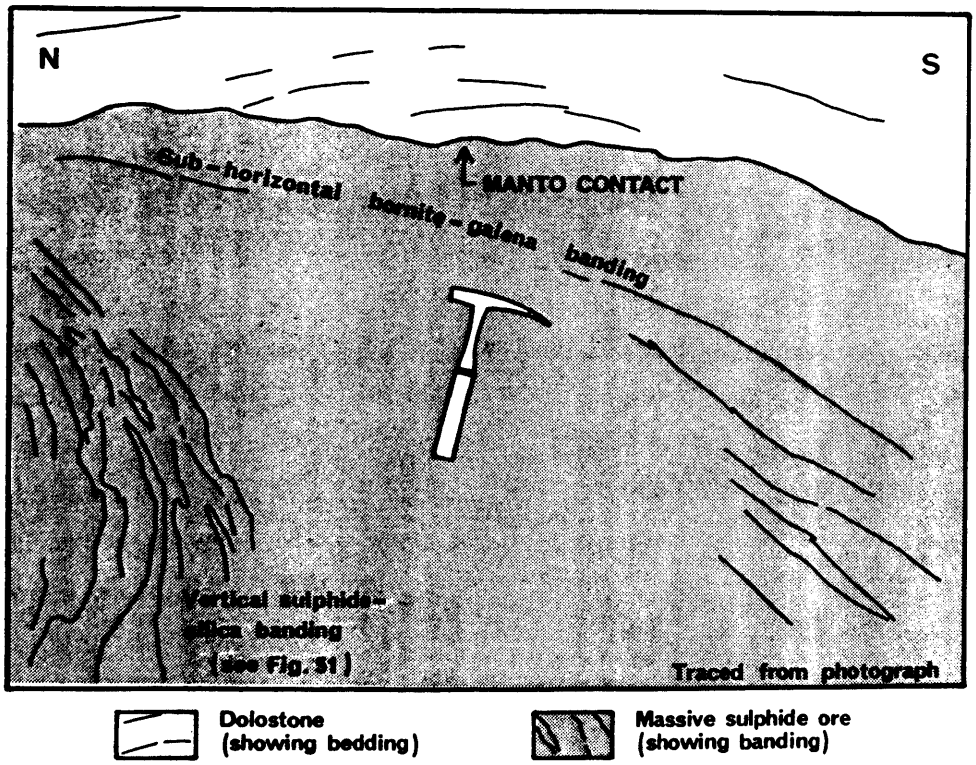

Fig. 56

The contact between E49 manto and the southern contact body of the marginal fracture zone, 7m above point "X" of Figure 54 (E49S/28L, +426m). The southern contact body terminates abruptly upwards at the sub-horizontal manto, but continues steeply downwards below the vertical banding on the north side of the diagram.

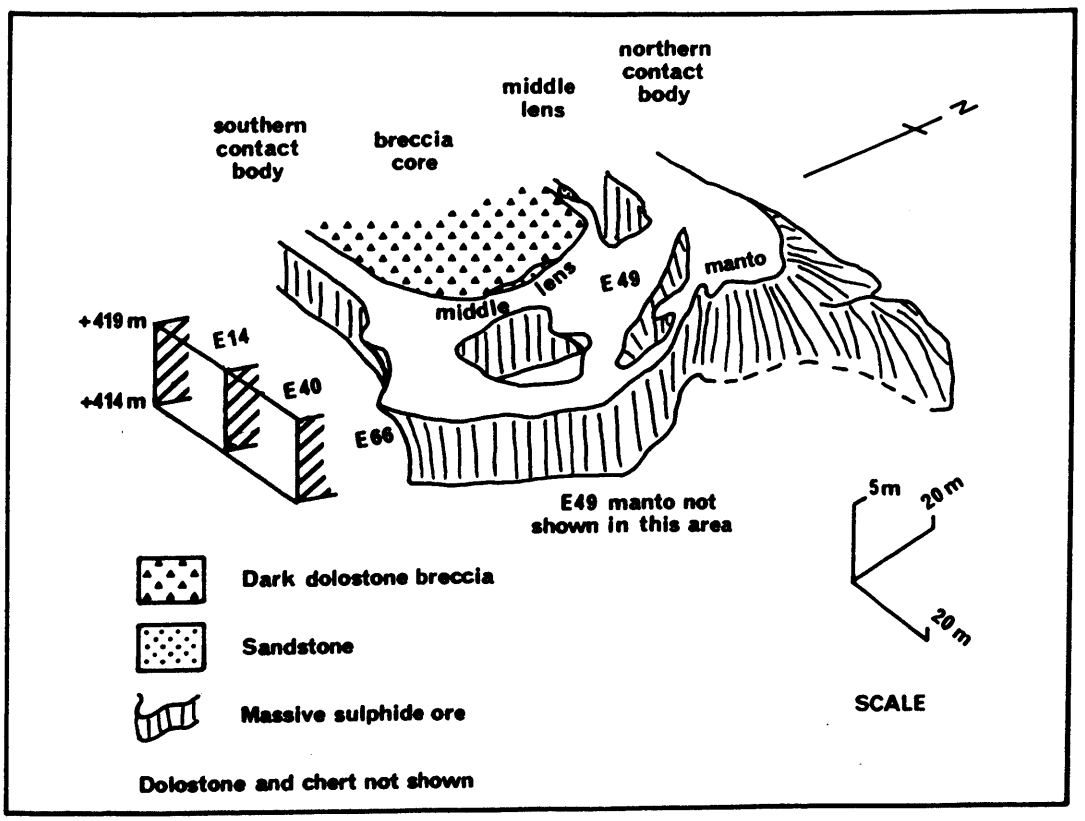

Fig. 57

Interpretive sketch showing the relationship between E49 manto, the contact ore body of the marginal fracture zone, and the Middle ore lens (the margin of the sedimentary breccia at this elevation). The northern contact body, part of the southern contact body, and their arcuate junction farther east, occupy a fracture in dolostone of the wall rock. The E49 manto probably terminates at the Middle lens (i.e. up the dip of the manto, above the section).

the internal contact of the southern contact zone in this area. The E49 manto immediately underlies or incorporates a chert unit in most of the northern part of the stope. The E49 manto is not completely concordant, but cross-cuts bedding at a small angle; this is well illustrated at the termination of E49 manto, 55 m outside the northern margin of the pipe, where the manto cuts the bedding at an angle of approximately thirty degrees (Fig. 55). The manto terminates at the top left-hand corner of the figure, but the bedding continues undisturbed across the projected position of the manto, only centimetres beyond its point of termination. There is no evidence of drag in the dolostone adjacent to any of the cross-cutting manto contacts examined.

The slightly cross-cutting nature of mantos relative to bedding, the sharply defined, parallel walls of many mantos, and the presence of associated breccia bodies, indicates that mantos are controlled by former fractures. The lack of bedding displacement at the termination of E49 manto, and of drag adjacent to manto contacts, indicates that these fractures were not surfaces of significant translational movement of the type proposed by Söhnge (1964) and Hopwood (1975) (Chapter 3.2). This is consistent with the observation that mantos do not penetrate the dark dolostone breccia core of the pipe, but terminate near the breccia contact. Solution activity and karsting are interpreted to have been important both within the pipe and in lower zone T6, and the manto fractures probably formed by collapse related to this activity, although some additional collapse may have occurred during the mineralizing event (Chapters 3.3.7, 3.4.4).

3.5.4 S110 and North Break ore bodies

The low grade S110 ore body occurs towards the base of the North Break zone, where it underlies high grade ore of S95 manto (Fig. 19). Karsting, karst sedimentation and roof collapse were important processes within S110 ore body (Chapter 3.3.7).

The North Break ore body occurs within the manganese-rich, calcitized upper part of the North Break zone, between 26 and 27 levels. The ore body extends from immediately north-west of the Tsumeb

pipe, north-eastwards to the E2200 breccia pipe (Fig. 18). The North Break ore body is a discordant zone of fracturing and rock alteration, which contains breccia bodies. Sandstone bodies greater than 0,5 m wide fill some steeply dipping fractures. Hypogene sulphide mineralization occurs in discordant fractures and, to a subordinate extent, in fractures parallel with bedding. The zone of fracturing has a strike of 076° and a strike length of 260 m, although economic mineralization occurs over only 130 m of this distance.

The North Break ore body is a separate structure from the Tsumeb pipe. The southern margin of the North Break ore body is 25-30 m from the northern margin of the Tsumeb pipe at its closest point, and it terminates towards the base of the North Break zone without intersecting the pipe. Its formation was, therefore, probably related to karsting and solution collapse within the lower part of zone T6.

3.5.5 Disseminated mineralization

Disseminated mineralization is widespread throughout the Tsumeb pipe, but is of much less economic importance than massive sulphide ore of the pipe margin and mantos. Griffis (1950) noted that mineralized sandstone mined above 20 level contained 5-10 percent total combined copper, lead and zinc, and mineralized dolostone had only half this metal content. These grades in the dolostone are also typical of the dolostone breccia which forms the interior of the pipe below 26 level.

True disseminations of sulphide minerals occur interstitial to dolostone breccia clasts, within breccia matrices, and as intergranular areas within the pipe sandstone. Replacement of breccia clasts by sulphide minerals is a very subordinate process. Most thin sulphide veinlets are confined to breccia matrices (Figs. 23, 91) but larger veins cut both matrices and clasts, which are replaced by sulphide minerals adjacent to the margins of these veins. The interstitial nature of these types of mineralization is usually obvious within "unaltered" pipe breccia, but is typically obscured by subsequent deformation within more altered breccia. In particular, sulphide minerals which appear to have mineralized the S_1 cleavage within

altered rocks have actually been transposed into, and concentrated within, this cleavage during deformation (Chapter 3.7).

A second type of disseminated mineralization is open-space fillings of vugs, which is moderately common but of negligible economic importance. Hypogene vug fillings occur within massive sulphide ore and within breccia. Most vugs have been destroyed during deformation, particularly within breccia of the calcitized zone, and these vugs now resemble other types of interstitial mineralization; vugs are best preserved in the silicified zone.

Veins of hypogene sulphide minerals, quartz, or carbonate minerals more than a few centimetres wide contribute to the metal content of low-grade ore. However, these veins are widely spaced and rare within much of the pipe interior, and are absent from some traverses studied through the central part of the pipe. Most veins occur in the marginal fracture zone, or branch off from this zone into the core of the pipe (Lombaard, 1953). Thin, mineralized dolomite veins, not more than a few centimetres wide, fill former open spaces along dolostone bedding surfaces in a few places, interior to the marginal fracture zone of the pipe (e.g. E65/26L).

3.6. ORE CHEMISTRY AND MINERALOGY

It is shown below that supergene sulphide enrichment of the Tsumeb ore was more important than has previously been recognized. This, together with the presence of previously unrecognized deformational textures in the ore, requires that new paragenetic sequences be established, and these differ for different ore types. It is also shown that systematic chemical and mineralogical zoning is present in the hypogene ore.

3.6.1 Mineralogy of the hypogene ore

The hypogene mineralogy of the Tsumeb ore body is very complex. Table 6 lists those minerals which have been confirmed by other than optical techniques, and those which have been reliably identified under

TABLE 6 HYPOGENE SULPHIDE MINERALS IN TSUMEB ORE

Mineral	Composition	XRD	Classical Analysis	Microprobe Analysis	Microprobe Scan	Author
MAJOR						
Galena	PbS					
Sphalerite	ZnS					
Tennantite	$Cu_{12}As_4S_{13}$	x	x			B.H. Geier (unpub.), this thesis
Enargite	Cu_3AsS_4			x		This thesis
Bornite	Cu_5FeS_4	x		x		This thesis
Chalcocite *	Cu_2S	x		x		This thesis
Digenite *	Cu_2S			x		This thesis
Djurleite *	Cu_2S	x				Roseboom Jr. (1962)
Pyrite	FeS_2	x		x		This thesis
Chalcopyrite	$CuFeS_2$	x		x		This thesis
SIGNIFICANT TRACE						
Germanite	$Cu_3(Fe,Ge)S_4$	x		x		Geier & Ottemann (1970a, b), this thesis
Renierite	$Cu_{2,5}Ge_{0,5}FeS_4$	x	x	x		Sclar & Geier (1957), this thesis
Briarite	$Cu_2(Fe,Zn)GeS_4$	x		x		Geier & Ottemann (1972), Francotte et al. (1965)
Cd-wurzite	(Zn,Cd)S	x	x			Hurlbut (1957)
Gallite	$CuGaS_2$	x		x		Geier & Ottemann (1970a), Strunz et al. (1959), this thesis
Betekhtinite	$Pb_2(Cu,Fe)_{21}S_{15}$			x		Geier & Ottemann (1970a), this thesis
Ni-carrollite	$CuCo_2S_4$ (+Ni)			x		This thesis
Luzonite	Cu_3AsS_4					
Molybdenite	MoS_2				x	Geier & Ottemann (1970b)
RARE						
Sulvanite	$Cu_3(V,Ge)S_4$			Dairy Prospect (x)		Geier & Ottemann (1970a)
Linnaeite	Co_3S_4 (possibly Ni-carrollite)					
Acanthite	Ag_2S					
Tungstenite	WS_2				x	Geier & Ottemann (1970b)
Metacinnabar	HgS					
Ge-mawsonite	$(Cu,Ge)_7(Fe,Zn)_2(Sn,As)S_{10}$	x		x		Geier & Ottemann (1970a), Ottemann et al. (1977)
Ge-stannite? ("Lu")	$Cu_2(Fe,Zn)SnS_4$+Ge			x		Geier & Ottemann (1970a)
Gratonite	$PbgAs_4S_{15}$	(occurrence probable: requires verification)				B.H. Geier (unpub.)
Seligmannite	$CuPbAsS_3$	(occurrence uncertain: requires verification)				B.H. Geier (unpub.)
Glaucodot	(Fe,Co)AsS	(occurrence uncertain: requires verification)				B.H. Geier (unpub.)
Patronite	VS_4	(occurrence uncertain: requires verification)				B.H. Geier (unpub.)

* Probably mostly supergene x - analysis

the microscope. The dominant sulphide and sulphosalt minerals are galena, sphalerite, tennantite, enargite and subordinate bornite. Pyrite is widespread, but is not a major component of the ore. Chalcocite, digenite and djurleite are probably mostly supergene sulphide phases, although minor hypogene Cu_2S is thought to occur (Chapter 3.6.3). Chalcopyrite is sparse, and where present it occurs as microscopic grains in most areas. Arsenopyrite is absent from this arsenic-rich ore body.

Trace mineral species which are of widespread occurrence, or which occur as significant minor phases in places, include germanite, renierite, briartite, cadmium-wurtzite, gallite and betekhtinite. Nickel-carrollite, luzonite (the low temperature polymorph of enargite), and molybdenite are less common. Rare grains of linnaeite were identified optically by Geier (unpub. rept.), but this might be nickel-carrollite. Acanthite, after argentite, has rarely been observed. Very rare minerals include sulvanite, germanium-mawsonite, tungstenite, metacinnabar and probable germanium-stannite and gratonite.

The germanium-, gallium- and vanadium-bearing sulphide mineral assemblage which occurs in the Tsumeb ore body is extremely rare outside central Africa. However, germanium-bearing minerals occur in unusually large, local concentrations at Tsumeb, and in the Kipushi ore body, Zaïre (Fig. 123). Bodies of massive germanite were stoped from 5 and 6 levels at Tsumeb, including 100 tonnes of massive germanite, and veinlets, up to a few centimetres thick, of massive germanite and renierite occur in places throughout the mine. Briartite is rare. Germanite was first described from Tsumeb (Pufahl, 1922) and renierite from Kipushi (Vaes, 1948). Briartite (Francotte et al., 1965) and gallite (Strunz et al., 1959) were first described simultaneously from both Tsumeb and Kipushi.

The existence of a number of minerals identified optically by previous workers is doubtful or insufficiently substantiated. These include cubanite, glaucodot, seligmannite, "mineral S" ($(Ni,Cu)_2GeS_4$ of Strunz, 1959), native gold, patronite, wittichenite (probably betekhtinite) and famatinite, i.e. stibioluzonite (probably luzonite).

Geier (unpub. repts.) revised a number of his early, tentative identifications as more data became available. These include lautite and "pseudo-lautite" (subsequently confirmed as betekhtinite), voltzite (zinc-greenockite) and colusite (details unknown, possibly sulvanite).

Gangue minerals other than quartz, calcite and dolomite include a couple of recorded occurrences of fluorite, of microscopic size, and barite. However, rare barite observed during this study is well crystallized and undeformed, and is not thought to belong to the hypogene phase of mineralization.

3.6.2 Chemistry of the hypogene ore minerals

Lead is the most abundant metal in the Tsumeb ore body, followed by copper and zinc, and the ore is arsenic-rich and relatively iron-poor. Cadmium and silver occur in important quantities, and molybdenum, germanium and mercury are significant trace elements. Table 7 shows the average composition of ore milled over a ten year period (order of magnitude only).

Enargite and tennantite in the Tsumeb ore body have a very low antimony content, typically less than one per cent, and approximate to the arsenic end-members of these minerals (Moritz, 1933; Geier, unpub. repts). The antimony content of ore samples is also low (Appendix 1.3). Three varieties of tennantite are present. Nearly all of the tennantite is zincian tennantite, with an average of 0,8 per cent iron and 8 per cent zinc. A second, rare, zinc-poor but iron-rich tennantite, which occurs in association with germanium minerals, was identified by Geier (unpub. rept.; Appendix 1.2). He incorrectly identified this as lead-bearing, as well as iron-bearing, because of a computational error. An iron-rich tennantite was also observed during the present study (analysis 6). Schneiderhöhn (1929) noted "green enargite" as an alteration product of enargite, and Moritz (1933) subsequently identified this as an optically distinct variety of tennantite of unknown composition. It is not certain that this third variety of tennantite is a hypogene mineral (Ramdohr, 1980).

Bornite analyzed during the present study is normal bornite or

slightly sulphur-rich "x-bornite". It is compositionally distinct from the sulphur-rich "anomalous bornite" of supergene oxidation origin described by Sillitoe and Clark (1969). Chalcopyrite is normal chalcopyrite, not talnakhite, mooihoekite or haycockite (Appendix 1.2).

Sphalerite is typically a grey variety with 0,2 per cent iron. Subordinate brown sphalerite, with 0,3 per cent iron, and a distinctive light green sphalerite, with 0,2-2,2 per cent iron, are present. Grey sphalerite from the deeper levels of the mine may be more iron-rich (Geier, unpub. repts.). Green sphalerite constitutes only a small percentage of the total sphalerite at any elevation, e.g. 5 vol.% of the sphalerite in all ore types (massive and disseminated) from 21 to 24 level. Mercury is present in anomalous concentrations in the ore body, and metacinnabar inclusions occur in some sphalerite grains (Geier, unpub. rept.); ore samples collected during the present study average 100-200 ppm mercury (Appendix 1.3). Mercury-bearing sphalerite from other localities is fluorescent (Tauson and Abramovich, 1980), and this may be the reason for the fluorescence of some sphalerite from the Tsumeb ore body..

All varieties of sphalerite from Tsumeb contain less than 3 per cent cadmium. There is a strong correlation between cadmium and zinc in the ore samples from below 26 level (Fig. 58b). This corresponds to 1,2 wt.% Cd in pure sphalerite (1,8 wt.% Cd if the two most cadmium-rich samples are included). Griffis and McCue (1950) recorded average cadmium and zinc grades between 12 and 24 levels equivalent to 2,0 wt.% Cd in sphalerite. The rare mineral, cadmium-wurtzite, is moderately abundant at the western end of the ore body between 17 and 20 levels. Ore samples average 13 per cent cadmium, c.f. 0,2 per cent cadmium in average ore, at this elevation. The cadmium-wurtzite contains 42-58 mole % CdS (Hurlbut, 1957).

Pyrite occurs in at least three varieties. The first, and according to Geier (unpub. rept.), the earliest, variety is a rare, fine grained variety of pyrite with a moderate cobalt content (e.g. 1,0 per cent cobalt). This variety is associated with nickel-carrollite. A coarse grained, possibly younger, pyrite with less than 0,1 per cent

cobalt, is the dominant variety in the Tsumeb ore body (Geier, unpub. rept.). Ottemann (1978) described a third variety of pyrite, a finely banded, stalactitic "gelpyrite" which contains 7 per cent arsenic and 2 per cent copper. It is not known if this last variety forms part of the hypogene sulphide assemblage.

Analyses of nickel-carrollite made during the present study confirm the optical and micro-chemical identification of this thiospinel by Geier (unpub. rept.; analyses 3-6, Appendix 1.2). The cobalt content of this mineral is constant, but the nickel and copper contents vary sympathetically as the result of mutual substitutions of these elements in the tetrahedral sites. Samples of ore contain less than 10 ppm cobalt and 5-200 ppm nickel (Appendix 1.3).

There is no relationship between the germanium and zinc contents of the ore (Appendix 1.3). This reflects the importance of discrete germanium minerals in the ore, and contrasts with the common occurrence of germanium in the sphalerite of Mississippi Valley-type ore bodies. There is also no relationship between the germanium content of the ore and the content of any of the elements copper, lead, arsenic or iron. The majority of samples collected during the study contain less than 200 ppm germanium.

Hypogene silver minerals have rarely been recorded in the Tsumeb ore, but silver is enriched in a number of hypogene and supergene minerals. Galena averages 40 ppm silver, chalcocite of possible hypogene origin averages 1400 ppm silver, tennantite averages 290-570 ppm silver, and a single analyzed specimen of bornite contained 1500 ppm silver (Geier, unpub. repts.). Betekhtinite contains up to 11 per cent silver (Geier and Ottemann, 1973). Figure 58c shows that the silver content of the ore is proportional to its copper content; this corresponds to more than 100 ppm silver per 10 per cent copper. However, the silver content is inversely proportional to the lead content, reflecting the low lead content of the ore relative to copper minerals, and the low silver content of galena (Fig. 61d).

The contents of other trace elements in the ore are listed in Appendix 1.3. Samples collected during the present study contain less

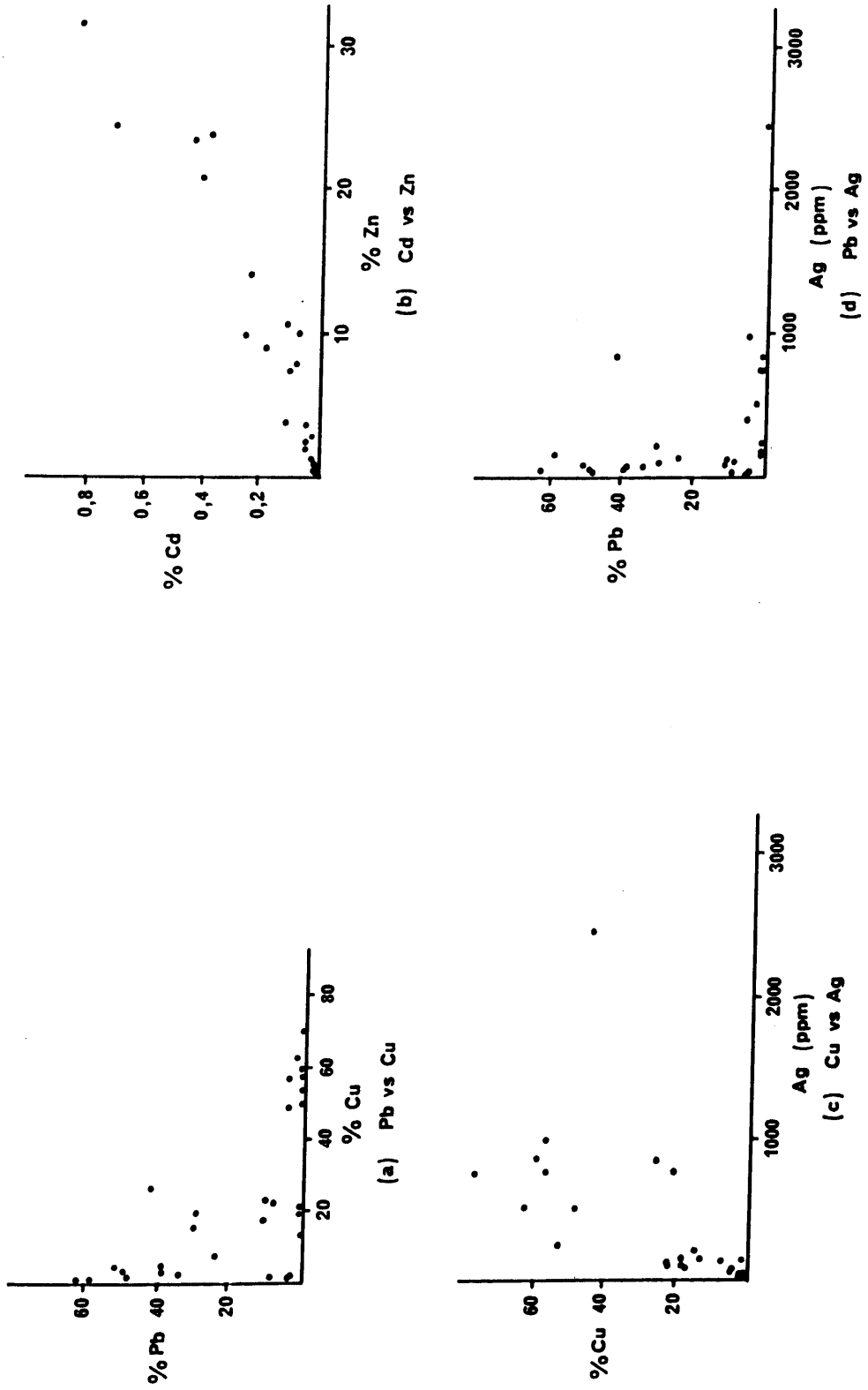

Fig. 58
Relationships between the abundances of some major and minor elements in the Tsumeb ore.

than 5 ppm Bi, Ga, Tl and U, less than 20 ppm W, 5-200 ppm Sn and Ba and, in some samples, more than 200 ppm Mo.

Total mineral analyses of enargite, betekhtinite, renierite, germanite, gallite and pyrite are listed in Appendix 1.2.

3.6.3 Supergene sulphide enrichment and oxidation

Oxidation of the hypogene sulphide ore has long been recognized to extend to below 30 level of Tsumeb mine (Söhnge, 1964), but the distribution of ore formed by supergene sulphide enrichment has not been as well documented. Schneiderhöhn (e.g. 1920a,b, 1929) recognized supergene ("granular") chalcocite between 2 and 5 levels, which had replaced pyrite, and which contained skeletal bornite bodies (Fig. 59). He recorded a second, "lamellar" type of chalcocite, which had not replaced pyrite, and which contained oval to circular bornite grains, to be the predominant variety below 5 level. This variety showed textural evidence of inversion from a higher-temperature form. He concluded that "lamellar" chalcocite and associated digenite were hypogene sulphide minerals, although this was questioned by Stahl (1925). Later workers commonly assumed most Cu_2S phases which occur at lower levels in the mine to be hypogene minerals.

Observations made during the present study indicate that supergene sulphide ore is extensively developed at depth in the Tsumeb mine. It is probable that Cu_2S phases, bornite and possibly even chalcopyrite, both above and below 26 level, have in many instances been incorrectly assigned to the hypogene sulphide assemblage by previous workers. For example, Hopwood (1975) considered that both chalcocite, and pods of massive galena which the chalcocite replaces, result from a single, hypogene, mineralizing event. The deformed galena pods are considered here to be hypogene, but the undeformed chalcocite is interpreted as the product of later supergene sulphide enrichment (Fig. 60). The following arguments for a supergene origin of most Cu_2S phases, and some bornite, are based on textural relationships and the distribution of these phases within the Tsumeb pipe.

The following textures, produced by supergene sulphide enrichment, should be compared with the hypogene ore textures of Figures 75-80.

Fig. 59

Intergrowth between bornite (black) and Cu_2S (grey). This is interpreted as the replacement of a grain of hypogene bornite by supergene Cu_2S (Schneiderhöhn, 1920, interpreted such textures similarly). Sample 1125, S95/30L. Plane polarized light.

Fig. 60

Supergene Cu_2S (mostly tarnished) which has partly replaced grains of galena. Note the irregular grain boundaries between the two minerals, typical of supergene replacement textures in ore from the Tsumeb ore body. Sample 554, E9/32L. Plane polarized light.

Fig. 61

Hypogene chalcopyrite (CP), veined and replaced along its margins by bornite (BN) and Cu_2S (CC) of supergene origin. Irregular grain boundaries of this type are typical of supergene ore. Sample 1126, DDH 1560/29L. Plane polarized light.

Fig. 62

This figure shows the contrast between hypogene ore textures and textures produced by supergene sulphide enrichment. Galena (GN, tarnished) and bornite (BN) have smooth, curving contacts, which are interpreted as annealing textures. Supergene Cu_2S (CC) has irregular contacts with these minerals (e.g. bornite, top right), which it also veins. Sample 434E, E49/29L. Plane polarized light.

Fig. 63

Euhedral pyrite (PY) of hypogene origin in a matrix of supergene Cu_2S (CC). This shows that the presence of euhedral pyrite within a matrix of Cu_2S is not diagnostic of a hypogene origin for the Cu_2S. Hypogene sulphide minerals, other than pyrite, have been completely replaced by Cu_2S (traces remain elsewhere in the sample), but pyrite replacement has been restricted to a very few grain boundaries (arrows). Sample 176, W40/31L. Plane polarized light.

Fig. 64

Bornite (BN) partly replaced by an intergrowth of chalcopyrite (CP, white) and covellite (CV, black). Textures of this type are interpreted to be of supergene oxidation origin (c.f. Sillitoe and Clark, 1969). They probably form by reactions of the type:

$$\underset{\text{bornite}}{2Cu_5FeS_4} + 8H^+ + 2O_2 \rightleftharpoons \underset{\text{chalcopyrite}}{2CuFeS_2} + \underset{\text{covellite}}{4CuS} + 4Cu^{2+} + 4H_2O$$

Sample 736, 21L. Plane polarized light.

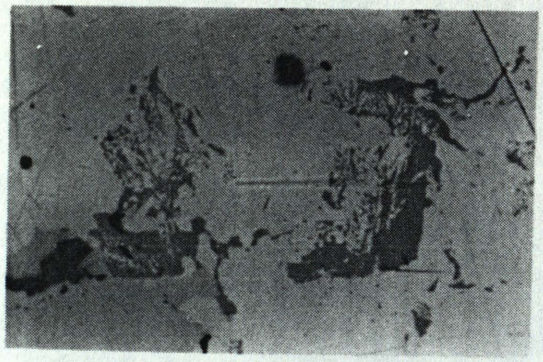

Fig. 59

0 mm 0.2

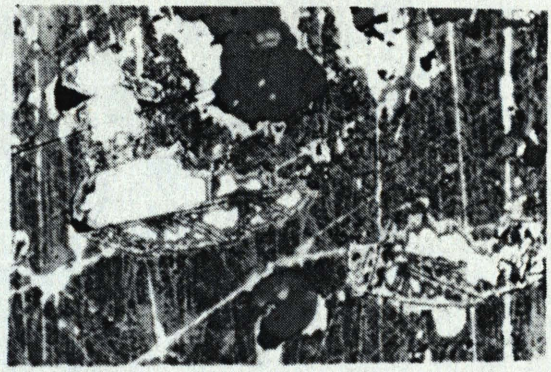

Fig. 60

0 mm 0.2

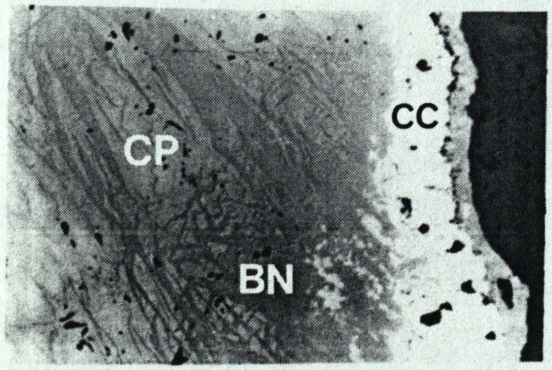

Fig. 61

0 mm 0.2

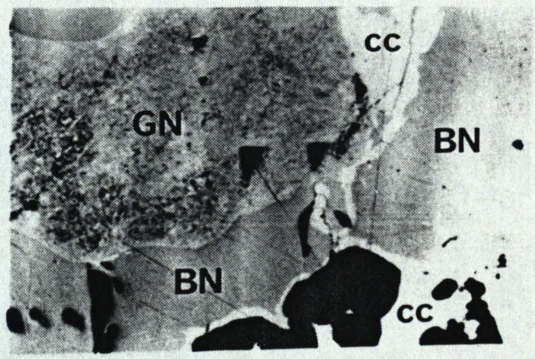

Fig. 62

0 mm 0.2

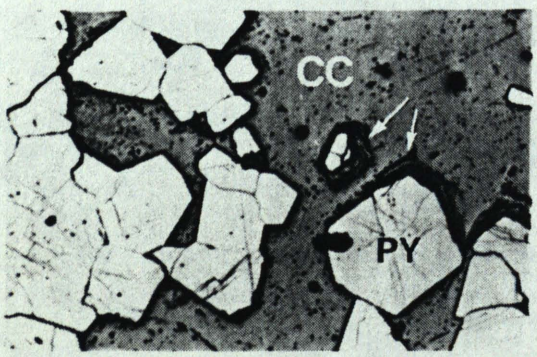

Fig. 63

0 mm 0.2

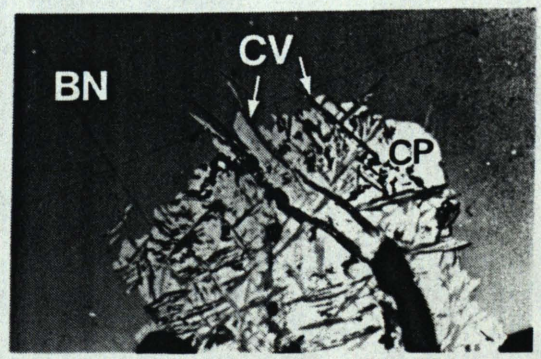

Fig. 64

0 mm 0.2

Ore textures can be used to group sulphide minerals which occur within massive ore into deformed and undeformed mineral assemblages (Chapter 3.7.3). Deformed minerals include nearly all sulphide minerals, including most bornite. The major exceptions are the Cu_2S phases, which are undeformed in all specimens examined. However, textures which consist of oval to circular bornite grains in chalcocite, described by Schneiderhöhn (1920b), may be deformation textures. Undeformed sulphide minerals all consist of species which can form from supergene sulphide enrichment or oxidation, i.e. Cu_2S phases, some bornite and minor chalcopyrite. The deformed and undeformed mineral assemblages are considered, therefore, to be hypogene and supergene, respectively.

Bornite is considered hypogene where it displays a characteristic texture, interpreted as a deformation texture in Chapter 3.7.3. Bornite of this type forms smooth, curved and cuspate boundaries with galena (Fig. 96). Most ore which contains galena and bornite shows these textures. None of this bornite contains remnants of unreplaced chalcopyrite, enargite or tennantite, and enargite and tennantite do not form textures with galena similar to that formed by bornite. The bornite is not, therefore, a supergene mineral which has replaced an earlier, hypogene, copper-bearing mineral. Undeformed bornite of probable supergene origin does occur in the ore body, but is very subordinate to hypogene bornite; bornite of this type veins and replaces chalcopyrite in the North Break ore body (Fig. 61).

The Cu_2S minerals consist of chalcocite or fine, bladed intergrowths of chalcocite and digenite (Appendix 1.2). Much of the "chalcocite" may be djurleite, a mineral which was recognized first at Tsumeb (and other localities) by Roseboom (1962); the "digenite" may be anilite. These minerals typically occur in skeletal intergrowths with bornite, which they appear to replace (Fig. 59). Schneiderhöhn (1920b) considered intergrowths of this type to be of supergene ("deszendenten Zementation") origin. The Cu_2S minerals can also show a textural relationship to galena of the type described above for hypogene bornite and galena. However, the Cu_2S minerals also display cross-cutting and irregular replacement relationships to galena and bornite in the same specimens (Figs. 60, 62). Therefore, Cu_2S

minerals of this type are considered supergene, and their textures are partly inherited from the bornite which they replace. The presence of euhedral pyrite which is enclosed by Cu_2S minerals is not diagnostic of a hypogene origin for the latter. This is because pyrite is replaced later than other sulphide minerals during supergene enrichment (Fig. 63). The sequence in which Cu_2S minerals replace sulphide minerals in the Tsumeb ore is interpreted as: (1) bornite, chalcopyrite, (2) galena, tennantite, (3) sphalerite, pyrite.

The above evidence for supergene sulphide enrichment at great depth in the Tsumeb ore body is consistent with the observation that oxidation has extended to great depth; i.e. conditions suitable for supergene enrichment were potentially present. Mineral specimens from the upper levels were examined during the present study, together with unpublished reports of Tsumeb Corporation Limited and systematic samples collected from the lower levels. These indicate that sulphide minerals which display textures interpreted as supergene textures are most abundant below each of the oxidation zones recognized by previous workers (e.g. Söhnge, 1964). The upper oxidation zone occurs from surface to above 12 level (Söhnge, 1964), and the underlying supergene sulphide zone extends to below 16 level (and 20 level in places). The lower oxidation zone commences above 25 level and increases in intensity downwards to a maximum below 30 level. This oxidation zone may be related to the flow of oxygenated meteoric water in the strata-bound North Break zone (Söhnge, 1964), and possibly also in steeply dipping faults which connect the North Break ore body and the E2200 breccia pipe (e.g. 27 level, Fig. 18). The lower zone of supergene sulphide enrichment is well represented to below 34 level. It is still present at 35 level, in a restricted area which is associated with a zone of reverse faulting along the northern margin of the pipe. This fault zone post-dates some of the hypogene sulphide ore, and also the later, S_1, deformational fabric (Chapter 3.7.7).

Some chalcopyrite-bearing assemblages are interpreted here to have resulted from supergene sulphide oxidation. A common example is the oxidation of bornite to chalcopyrite and covellite in samples from 21 level (Fig. 64), described from Chile by Sillitoe and Clark (1969). This alteration penetrates inwards from the margins of bornite grains,

and is texturally distinct from very rare, lamellar intergrowths of chalcopyrite along (111) planes in bornite (Fig. 73), which also occur on 21 level. The lamellar intergrowths lack covellite, but are associated with minor chalcocite. They resemble hypogene exsolution textures, illustrated by Brett (1964), but their vein-like nature in some specimens (Fig. 74), and their close association with chalcopyrite of supergene oxidation origin, indicates that they may, like the chalcopyrite-covellite intergrowths, result from oxidation of bornite. B.H. Geier recorded idaite, a probable oxidation product of bornite (Sillitoe and Clark, 1969), in association with chalcopyrite and bornite on 20 level.

Other sulphide minerals and metals associated with oxidation and supergene sulphide enrichment in the Tsumeb ore body include realgar, native silver, native copper, stromeyerite, greenockite, cinnabar and millerite (after nickel-carrollite). Algodonite and umangite have been identified optically, but their identities remain to be confirmed by other techniques (Geier, unpub. repts.,; Strunz and Tennyson, 1967).

It is concluded that supergene sulphide minerals extend to great depths in the Tsumeb ore body, in association with two, discrete zones of oxidation. These minerals post-date deformational textures in the ore, and some are spatially associated with permeable zones which post-date both the hypogene sulphide ores and the subsequent, S_1, deformational fabric. Most Cu_2S phases, some bornite, and minor amounts of chalcopyrite, have a supergene enrichment or oxidation origin.

3.6.4 Contrasting metal ratios in disseminated and massive ore

The ratios of copper, lead and zinc in hand specimens of massive ore and channel samples of disseminated and massive ore, are shown in Figures 65, 66 and 68 (also see Appendix 1.3). Samples of massive ore, including all but one sample taken from mantos, plot mostly along the copper-rich end of the copper-zinc and copper-lead joins, or to a lesser extent along the lead-rich end of the lead-zinc join (Figs. 65, 68). There is a paucity of zinc-rich samples, or samples with

copper, lead and zinc in similar proportions, in either massive or disseminated ore. Disseminated ore plots along the copper-zinc and copper-lead joins, but few samples of disseminated ore plot close to the copper apex, and none plot along the lead-zinc join. Arsenic: copper ratios indicate that tennantite is the dominant copper mineral in massive lead-zinc ore, but bornite, or supergene chalcocite after bornite, is common (in addition to tennantite) in massive copper ore (Fig. 65).

Figure 58a shows the actual lead and copper contents, rather than metal ratios, in disseminated and massive ore samples. This illustrates more clearly the antipathetic relationship that exists at hand specimen scale between copper and lead in samples of massive ore (i.e. samples tend to be copper-rich or lead-rich, but not both). This bimodal nature of massive sulphide ore also occurs on a larger scale. The two types of ore can be commonly observed in a single traverse through one ore lens, where they form adjacent, mineralogically distinct domains.

3.6.5 Mineralogical and chemical zoning in the pipe core

Nine channel sample traverses were selected to examine geochemical zoning in disseminated sulphide ore of the pipe core. Channel samples were taken at one to two metre intervals through "unaltered", calcitized and silicified rocks at various elevations (Figs. 66a-i). The traverses constitute continuous sections in areas where oxidation, supergene enrichment and vein-type mineralization are minor.

The change in metal ratios with elevation is gradational, similar to the change in the dominant type of rock alteration. However, metal ratios display a marked dependence on wall rock composition. The lowermost alteration zone, the silicified zone, contains copper-zinc mineralization, and the lead content is negligible (Figs. 66a,b). Copper-lead mineralization dominates where calcitization appears higher in the pipe (Fig. 66c). The zinc content of the mineralization is also minor within the calcitized zone (Figs. 66c-e), although two zinc-rich samples occur within sandstone bodies

TABLE 7 AVERAGE COMPOSITION OF ORE MILLED, 1964-1974
(Order of magnitude only)

	%	ppm		%	ppm
Cu	4		Sn		10
Pb	12		Mo		500
Zn	3		Hg		100
As	1		Co		5
Fe	1,5		Ni		20
S	4		V		10
			Tl		5
Cd		400	In		< 1
Ge		50	Se		50
Ag		100	Te		20
Au		0,01	Mn		100
Bi		1	Re		< 1
Sb		150	P		10
Ga		< 1	F		50

Source of data: Mine Laboratory, Tsumeb Corporation Limited

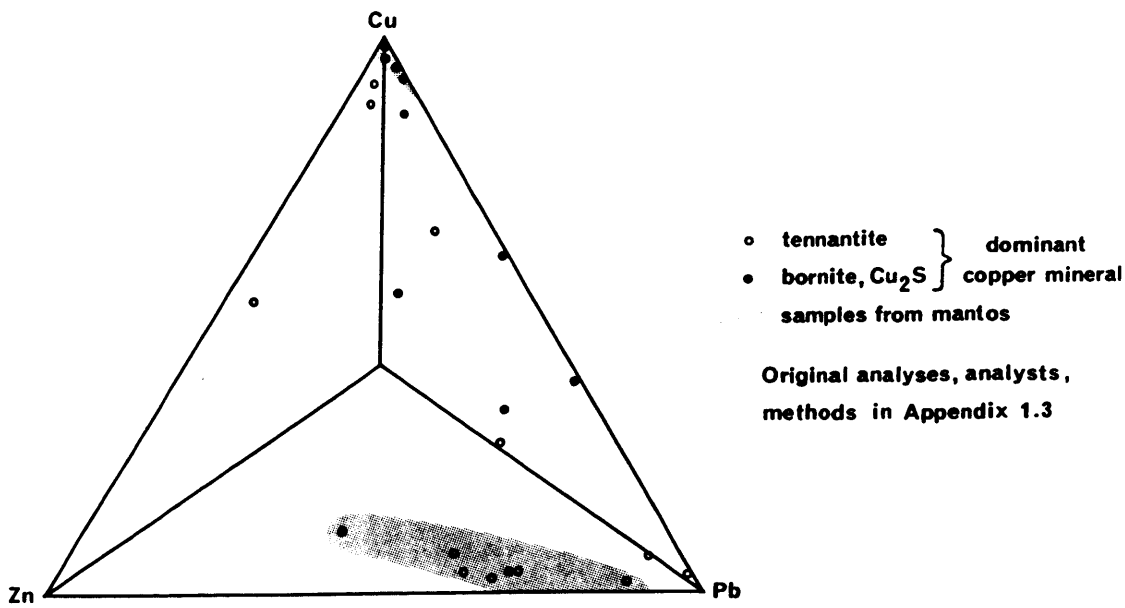

Fig. 65
Variations in the major element composition of massive and high grade ore from below 26 level (hand specimens). Zinc-rich ore is absent, massive ore with copper, lead and zinc is rare, and ore from mantos is mostly copper-rich, or is lead-zinc ore.

(Fig. 66d). The mineralization is significantly more copper-rich where calcitization decreases upwards in the breccia core (Figs. 66f-h). Unpublished data of Tsumeb Corporation Limited indicate that this is still the situation at 23 level. Lead-zinc mineralization is notably absent from all disseminated ore.

Arsenic-copper ratios at different elevations in the pipe indicate that copper in disseminated ore of the silicified zone is almost exclusively contained in tennantite (Fig. 67). Mineragraphic studies show that this ore consists almost exclusively of tennantite, pyrite and sphalerite. Galena is an important additional component in the overlying calcitized zone, and bornite is an important copper mineral in addition to tennantite. Galena then becomes a minor constituent of disseminated ore above the calcitized zone.

Two associations of sulphide minerals are present in "unaltered" rocks above the calcitized zone. The first consists of disseminated tennantite and pyrite, with subordinate galena and very minor sphalerite and germanite. This typically occurs in light medium grey dolostone. Bornite is probably only important in this ore immediately above the calcitized zone, but insufficient specimens are available to accurately determine its distribution (no specimens of disseminated ore were available from above 20 level, so it is also not known if enargite occurs in disseminated ore at higher elevations). The second association of sulphide minerals is mineralogically complex, and occurs typically in the dark dolostone breccia. It consists of pyrite, tennantite, light green sphalerite, germanite, renierite, gallite, molybdenite and sulvanite. Minor bornite, galena and hypogene chalcopyrite are present in places, and germanium minerals are widely distributed and can exceed copper minerals. Green sphalerite is almost completely absent from the marginal massive ore zone, and is confined to the dark dolostone breccia.

Disseminated mineralization in the sandstone bodies does not have a unique composition, and insufficient samples were analyzed to determine if vertical zoning is present. The only zinc-rich samples in Figure 66d are both arenites, but copper-lead mineralization is present in both the calcitized dolostone and the arenite of Figure 66e.

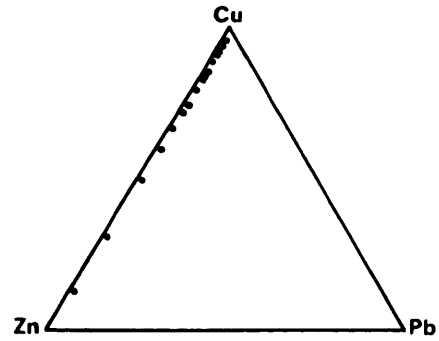

(a) Silicified dolostone breccia
DDH 2644/42 L ~ -116 m
length 50 m (horiz. projection)

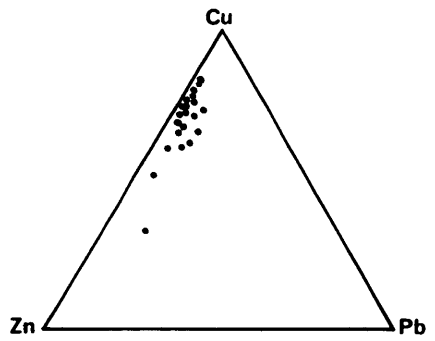

(b) Silicified dolostone breccia
DDH 3163/38 L ~ +30 m
length 23 m (horiz. projection)

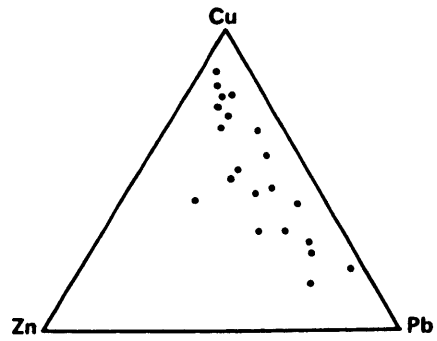

(c) Silicified and calcitized dolostone breccia
W110/35 L +163 m length 23 m

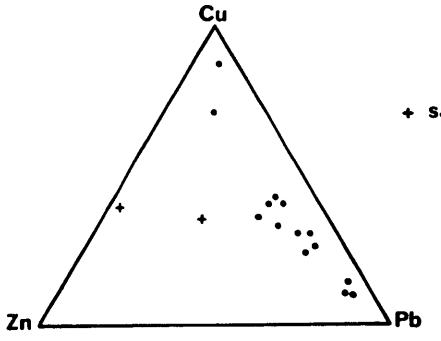

+ sandstone

(d) Calcitized dolostone breccia and sandstone
W96/33 L +220 m length 34 m

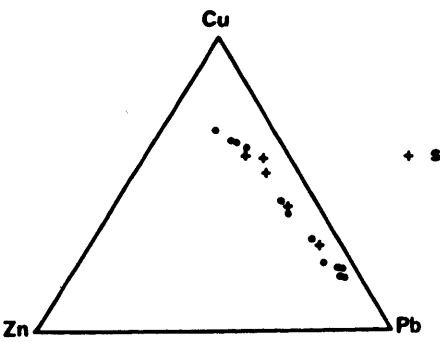

+ sandstone

(e) Calcitized dolostone breccia and sandstone
W80/34 L +246 m length 36 m

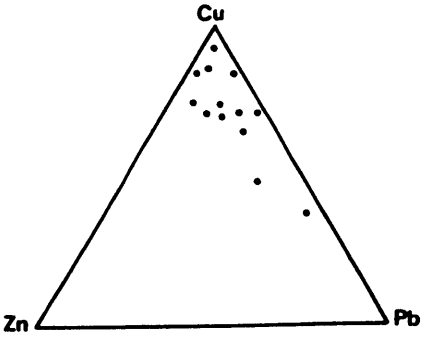

(f) Calcitized and dark dolostone breccia
W120/32 L +277 m length 28 m
(W108/32 L +274 m identical)

(continued next page)

Fig. 66
Variations in the major element composition of disseminated ore from below 26 level (samples from traverses at different elevations). Disseminated copper-lead-zinc ore is rare, and lead-zinc ore is absent. Copper-zinc ore of the silicified zone is succeeded by copper-lead ore in the overlying calcitized zone, and the ore is more copper-rich in dark dolostone breccia of higher elevations.

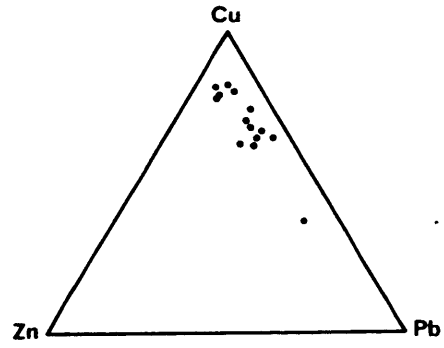

(g) Dark dolostone breccia
E9/29 L +381 m length 28 m

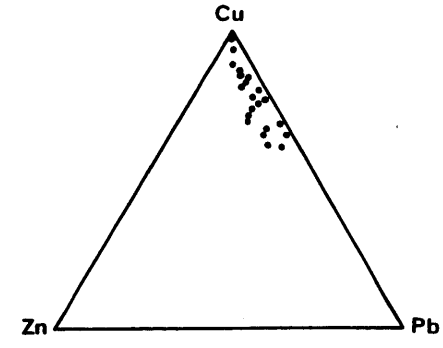

(h) Dark dolostone breccia and sandstone (undifferentiated)
W70/29 L +410 m length 24 m

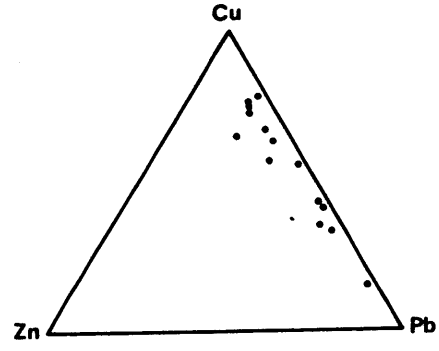

(i) Dark dolostone breccia
W40/26 L +495 m length 28 m
(traverse 4m east, +493 m identical)

XRF analyses,
Tsumeb Corporation Limited

Fig. 66 (continued)

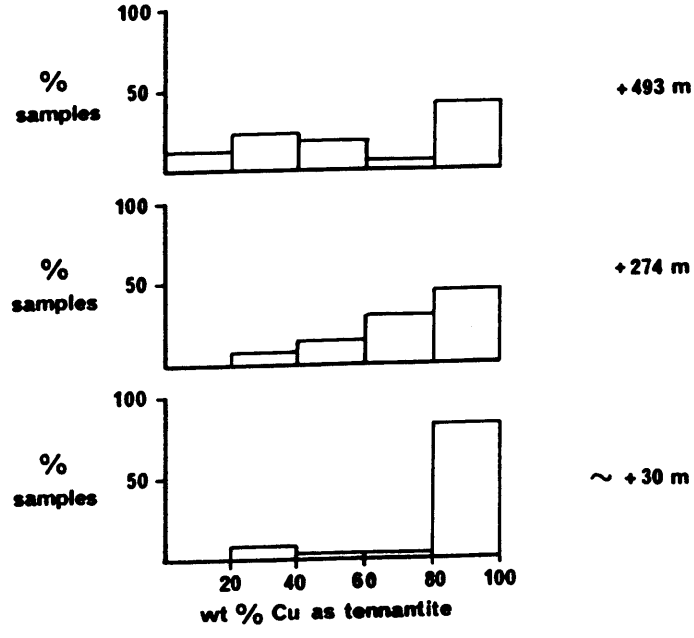

Fig. 67
The proportion of tennantite relative to other copper minerals in traverses from the silicified zone (+30m), calcitized zone (+274m), and dark dolostone breccia of the Tsumeb pipe (+493m).

Mineragraphic studies indicate that bornite-rich ore and supergene Cu_2S phases are very common in sandstone of both the calcitized and "unaltered" zones.

3.6.6 Chemical zoning in massive sulphide ore

Figure 68 shows six, north-south geochemical sections through the pipe at different elevations, from approximately +30 to +493 m. These were designed to sample ore associated with "unaltered", calcitized and silicified dolostone, and some samples shown in Figure 66 were selected from parts of these traverses. The lithology, ore type and total metal (Cu + Pb + Zn) profile has been plotted for each traverse.

The geochemical sections are incomplete along some profiles as a result of faulting or incomplete sampling. However, a pattern is evident in which most of the metal is associated with the north and south margins of the pipe (i.e. the massive ore zones of Figures 68 and 69). The breccia core contains low, often fairly consistent metal values. Increased ore grades occur within the breccia core adjacent to zones which were formerly permeable (e.g. the sandstone at +274 m). The large massive sulphide body at +409 m elevation occurs where a manto intersects the pipe from the north. Post-ore faulting has removed the northern massive sulphide contact body at +163 m and has probably also diminished the southern contact body at +493 m. The presence of this southern contact is reflected in the total Pb curve of Figure 69c. The southern contact body at +246 m is clearly shown on the total zinc curve (not plotted), and is indicated by a change in ore type on Figure 68.

The chemical zoning patterns present in the more restricted traverses of Figures 66a-i are present throughout all of the traverses of Figures 68 and 69 (i.e. copper-zinc, then copper-lead becoming more copper-rich in the upper levels). The composition of high grade ore of the marginal fracture zones is significantly different in many places from the composition of mineralization in adjacent parts of the pipe core. Lead-zinc ore is confined completely to the highly mineralized marginal fracture zones, and occurs at all elevations. Copper-zinc

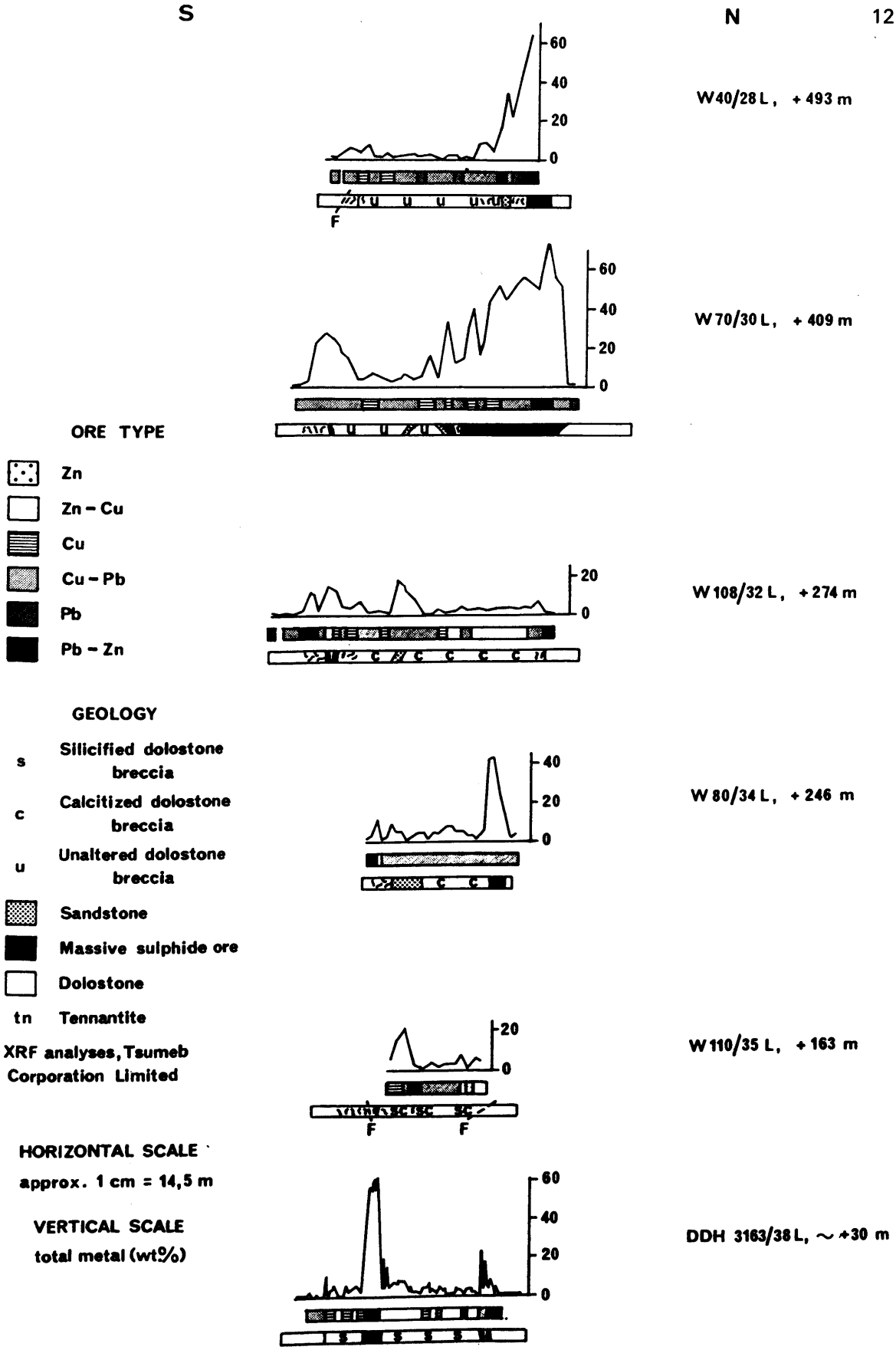

Fig. 68
Sections through the Tsumeb pipe at different elevations, showing metal concentration (total Cu+Pb+Zn), ore type and lithology. Most metal is concentrated at the margins of the pipe.

ore is confined to the lower levels, both in the marginal fractures and in the breccia core. Ore in which zinc is the dominant metal is completely absent from both the pipe core and its margins at all elevations sampled.

Individual copper, lead and zinc analyses for three of the above traverses, selected to represent the silicified, calcitized and "unaltered" zones of the pipe, are shown in Figures 69 a-c. The estimated weight per cent of total copper in minerals other than tennantite is also shown, and this increases upwards in the pipe core. The curves for individual elements indicate complex zoning, particularly the common presence of adjacent copper- and lead-rich ore, in the marginal massive sulphide bodies. The southern margin at an elevation of approximately +30 m is a good example of this; lead and lead-zinc ore are bounded by thin margins of copper and copper-zinc ore (Fig. 69a). A similar situation exists on the southern margin at +274 m (Fig. 69b) and on the northern margin at +493 m (Fig. 69c), where lead-zinc ore occurs external to copper-rich ore. This pattern of lead-zinc ore external to copper ore was also reported from 21, 22 and 24 levels by Lombaard (1953).

3.6.7 Mineralogical classification of massive ore types

It is shown above that massive sulphide ore can be classified chemically into lead-zinc, lead-copper, copper, and copper-zinc varieties, which occur separately, either at different elevations or as adjacent parts of single sulphide bodies. Mineragraphic studies were made of approximately 170 polished sections from below 26 level and 105 sections from above, and hundreds more from the collection of Tsumeb Corporation Limited were briefly examined. Data from these were combined with underground observations and data from previous mineragraphic studies. The chemical groupings given above are found to correspond to a continuous mineralogical gradation, from galena-sphalerite-tennantite (or -enargite) ore (i.e. lead-zinc ore, type 1) via sphalerite-poor, and sphalerite- and galena-poor, varieties (types 2 and 3) to tennantite-sphalerite ore (i.e. copper-zinc ore, type 4). No important gradations are observed between lead-zinc and copper-zinc ore at any locality; although some examples are known from the lower

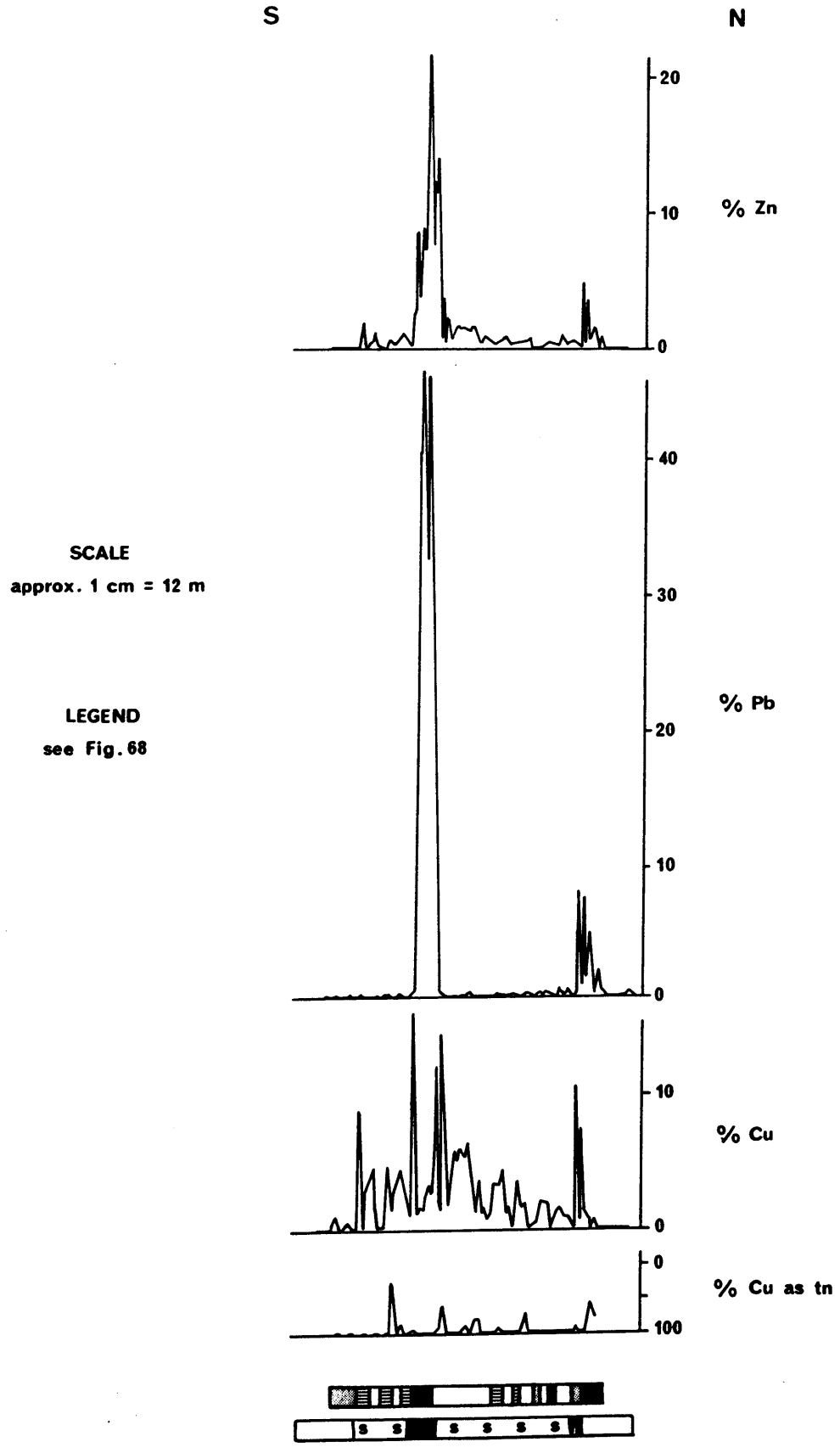

Fig. 69a
Geochemical sections through the silicified zone of the Tsumeb pipe (DDH 3163/38L, ~+30m). Note the presence of adjacent copper-rich and lead- and zinc-rich zones at the southern end of the pipe. Most copper occurs in the mineral tennantite (c.f. Figures 69b,c).

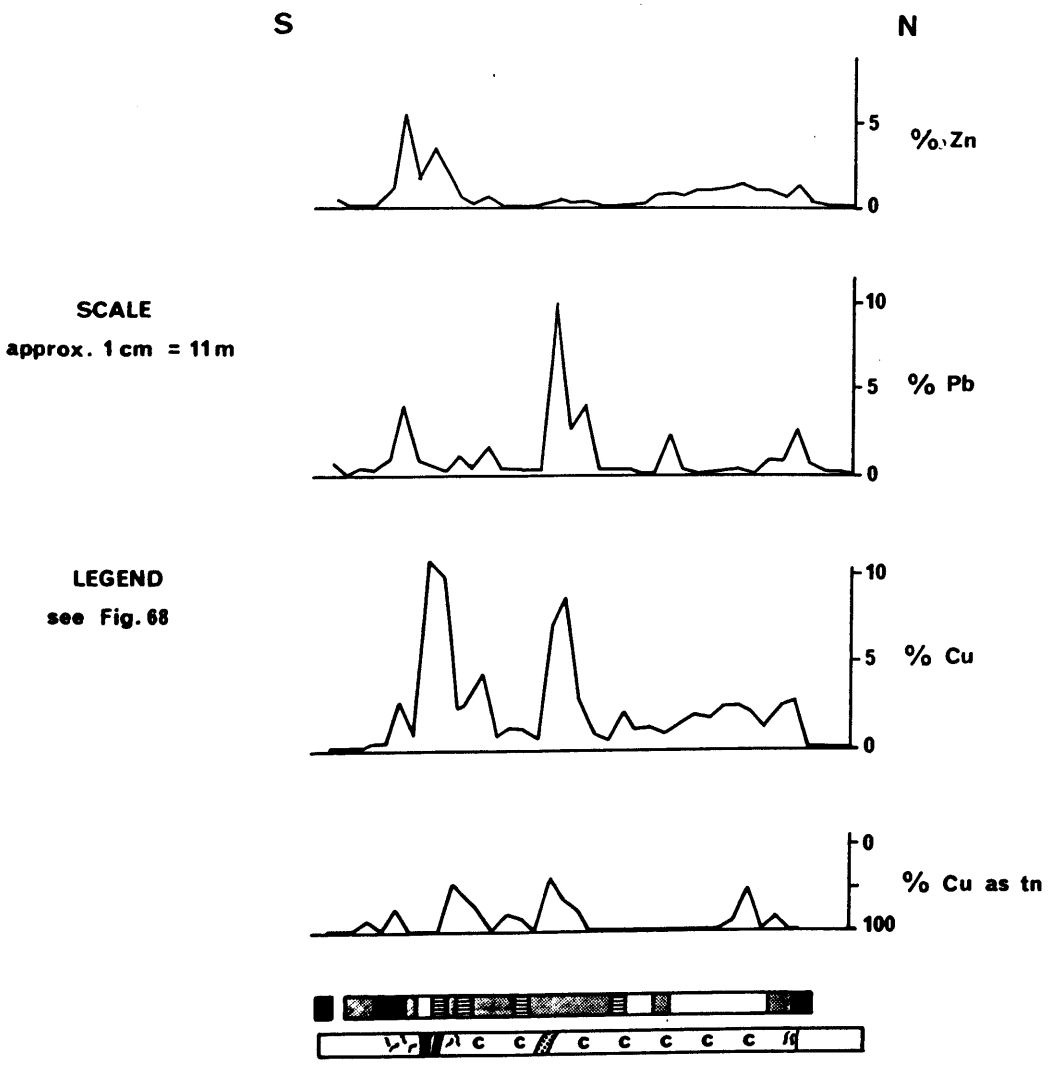

Fig. 69b
Geochemical sections through the calcitized zone of the Tsumeb pipe (W108/32L, +274m). Compare with Figures 69a,c.

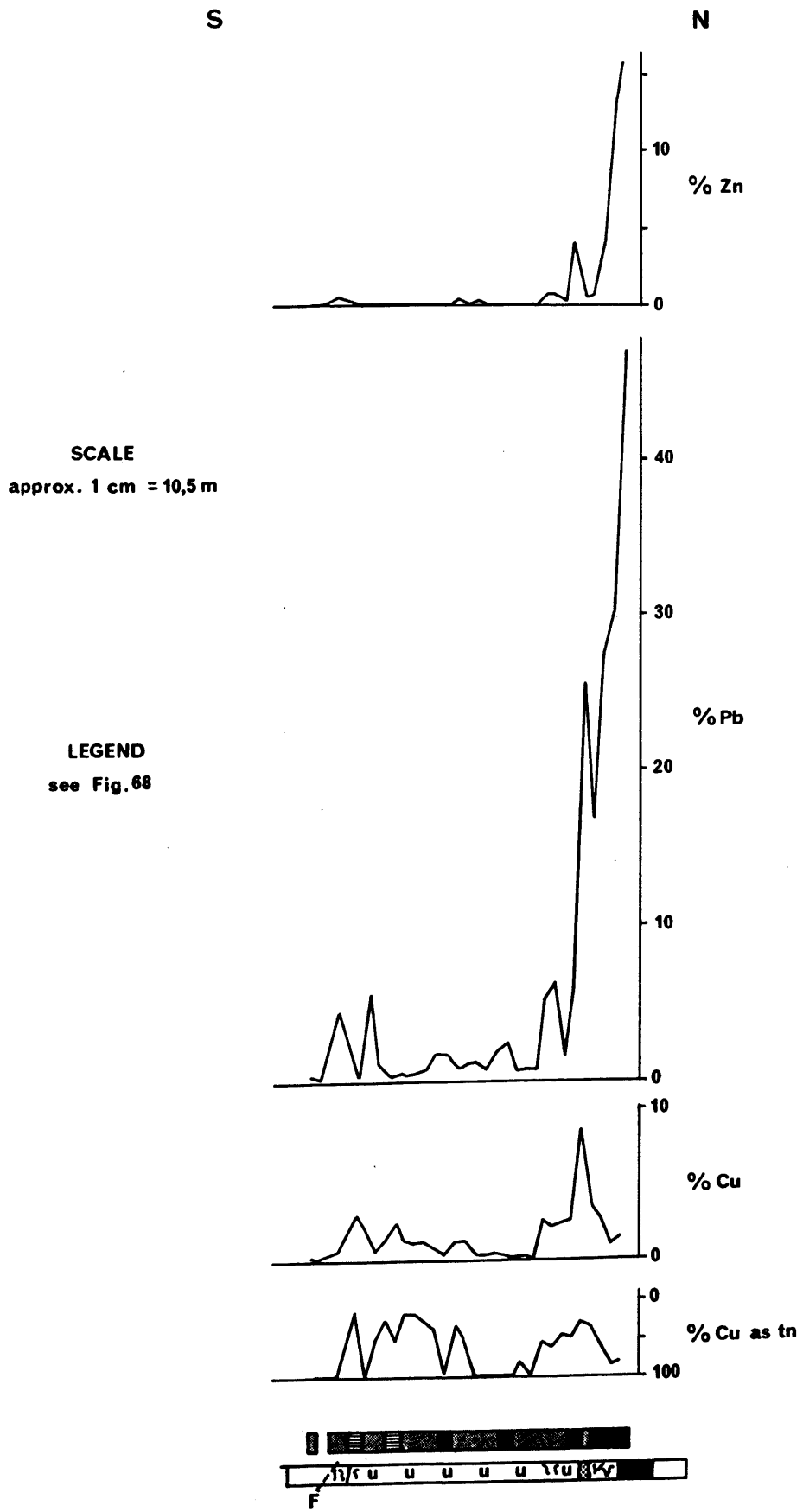

Fig. 69c
Geochemical sections through the dark dolostone breccia of the Tsumeb pipe (W40/28L, +493m). Note the presence of adjacent copper-rich and lead- and zinc-rich zones at the northern end of the pipe. Much copper occurs in copper minerals other than tennantite (mostly bornite, c.f. Figures 69a,b).

part of the pipe, minor paragenetic differences exist between the ore types (Chapter 3.6.12). Ore types are subdivided further into types A and B, using the dominant copper-arsenic-sulphide phase (Fig. 70). Gradations also exist between ore types in which tennantite, bornite, or chalcopyrite is the dominant copper mineral (types 3B, 3C and 3D, respectively).

1) Galena-sphalerite-tennantite (or enargite)-pyrite.

Bornite, and less commonly chalcopyrite, are moderately rare and minor constituents in lead-zinc ore, in which tennantite or enargite occur with galena, sphalerite and pyrite. Trace amounts of germanium minerals, gallite and molybdenite are present in places. These trace minerals are associated with the light green variety of sphalerite, which is subordinate to other types of sphalerite in this ore. Renierite and germanite, in extremely small quantities, are the only common trace minerals where green sphalerite is absent. Lead-zinc ore of types 1A and 1B grades through a variety which lacks sphalerite (2) into ore which lacks both sphalerite and galena (3A and 3B). These ore types have a similar distribution and form a continuous series in the marginal fracture zones. Enargite-bearing varieties of these ore types, with or without tennantite, and commonly with only minor pyrite, are confined to the upper levels of the mine. Tennantite-dominant, enargite-free varieties, which contain pyrite, are confined to the lower levels.

2) Galena-tennantite (or enargite)-pyrite.

This ore type is gradational between type 1 and type 3.

3A, B) Enargite (or tennantite)-pyrite.

Mineralogically simple, type 3A and 3B ores grade into type 2. Type 3B grades into type 4, and also into bornite-rich and chalcopyrite-rich ores (3C and 3D) in places, although intermediate compositions are volumetrically unimportant.

3C) Bornite-rich ore.

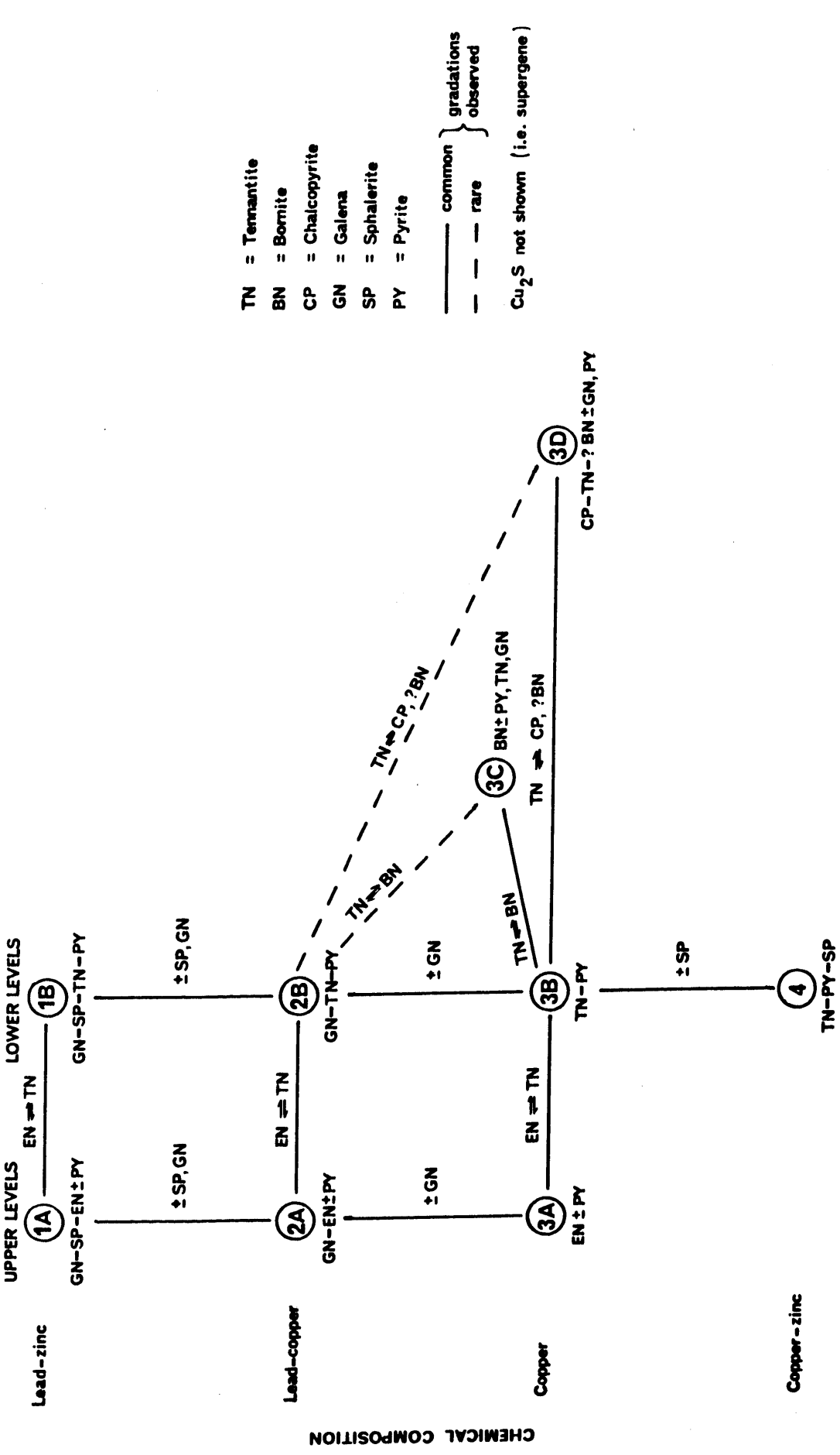

Fig. 70 Chemical and mineralogical variations between different types of massive sulphide ore.

This includes tennantite-bornite, bornite-tennantite-pyrite, bornite-pyrite and Cu_2S-bearing varieties, with or without pyrite. The Cu_2S minerals in the samples studied are thought to be mostly, or entirely, supergene. Galena-rich varieties of type 3C ore are volumetrically unimportant, and many of these contain betekhtinite. Sphalerite-rich varieties are very rare. Germanium minerals and gallite are coarse-grained and abundant in places. Type 3C ore forms a subordinate, but significant, proportion of the ore in the marginal fracture zone, particularly at intermediate elevations. It is characteristic of the copper-rich mantos, and also forms semi-massive ore within the margins of large sandstone bodies.

3D) Chalcopyrite-tennantite-?bornite.

This rare ore type is well represented in the North Break ore body. Much of the bornite is supergene, but hypogene bornite is probably also present.

4) Tennantite-pyrite-sphalerite.

Massive ore of this type is confined mostly to silicified dolostone in the lower levels of the mine. Both zinc-rich and zinc-poor varieties are common in disseminated ore and small massive sulphide veins at this depth. However, a zinc-poor variety is typical of the few specimens of this ore type examined from large massive bodies between 34 and 38 levels. This ore type is transitional to type 3B and is associated with types 1 and 2 (both of which are paragenetically distinct). Type 4 ore is mineralogically simple, and specimens examined lack the Tsumeb trace mineral suite.

Pyrite is only a minor constituent of all ore types in the Tsumeb mine (e.g. it only constitutes 5 vol. % of the sulphide minerals in type 2 ore between 21 and 24 levels). Enargite-bearing ore of the upper levels is even less pyritic. Pyrite increases in abundance below 26 level (particularly below 30 level). It is abundant and coarse grained in some bornite ore (e.g. 33 level and E49/28-30 levels).

3.6.8 Distribution of massive ore types

The distribution of the different types of massive sulphide ore can be discussed in terms of the northern, southern, eastern and western margins of the pipe, the Middle lens, sandstone bodies within the pipe structure, and the mantos. Lead-zinc ore (type 1) is characteristic of the area west of the sandstone body between 5 and 20 levels (Fig. 20). Copper-lead ore of variable composition occurs east of the sandstone body. Enargite-bearing ore (types 1A, 2A and 3A) is only important above 20 level (mainly above 17 level). Any further attempt at subdivision of the ore above 20 level is meaningless, because supergene sulphide ore dominates near surface, and the form of the ore body has probably been greatly modified by post-ore thrusting in the upper levels of the mine (which are now inaccessible).

Lead-zinc ore (type 1) is typical of the marginal fracture zone and the Middle lens between 20 and 38 levels. It is the dominant ore type along the northern margin of the pipe between 20 and 28 levels, and occurs, as a zinc-rich variety, along the western margin of the pipe between 20 and 25 levels. Ore which contains cadmium-wurtzite is confined to lead-rich (rather than zinc-rich) ore in this part of the ore body. Lead-zinc ore grades through type 2B ore into tennantite-rich copper ore (type 3B) which dominates along the southern and eastern margins of the ore body. Lead-zinc ore gradually decreases in volume throughout the pipe with depth below 30 level. It is most abundant along the eastern margin below this level, but also becomes minor in this position below 38 level.

Below 20 level, tennantite-rich copper ore (type 3B) is important along the southern and eastern margins of the pipe to 24 and 26 levels, respectively. This ore appears in places along the lead- and zinc-rich northern margin below 29 level. It occurs for significant distances along this margin by 30 level, together with pods of bornite-rich ore (type 3C). Bornite-rich ore appears on the inner side of the tennantite-rich southern margin at depth. It is the dominant ore along this margin below 24 level, and along the western margin below 26 level, and is locally important along the eastern margin (e.g. 26 and 29 levels). Bornite-rich ore is also associated

with sandstone bodies, particularly their margins, at a number of elevations below 20 level (e.g. the south-western margin of the pipe, 21-24 levels).

Bornite-rich copper ore is unimportant in the marginal zone below 33 level. Mineralogically simple, tennantite-bearing lead-copper and copper ores (types 2B and 3B), and lead-zinc ore, are typical of massive sulphide ore within the central and western margins of the pipe below 34 level. Copper-zinc ore (type 4) of the marginal zone is confined to below 34 level.

Ore in the mantos is compositionally similar to ore in the immediately adjacent marginal fracture zone (e.g. E49 manto, Chapter 3.5.3). Copper-rich mantos are, therefore, typical of the southern margin of the pipe, and lead-zinc mantos are typical of the northern margin. Bornite ore dominates over type 2 and 3 copper ore in copper-rich mantos.

Figure 71 shows the distribution and very approximate variation in abundances of sulphide and sulphosalt minerals within massive and high grade ore of the Tsumeb pipe. The figure was compiled from Griffis and McCue (1950), Geier (1953, unpub. repts), Söhnge (1964, 1976), Hopwood (1975) and the present study. The important features are as follows. The greatest concentration of metal occurs in the intermediate levels of the mine, in the vicinity of the North Break zone. A major, but subordinate, concentration is present in the overlying pipe, and a major decrease occurs in the quantities of all major ore minerals in the lower levels of the mine. Enargite and cadmium-wurtzite are confined to the upper levels, and bornite is important in the vicinity of the North Break zone. Cu_2S phases are abundant above 20 level and in the vicinity of the North Break zone. However, these are thought to be mostly supergene sulphide minerals, and they have been largely omitted from Figure 71. Most copper in ore below 20 level occurs in tennantite, and pyrite increases in abundance in the lower levels.

The depth distribution of the trace minerals is poorly known. Many are characteristic of the breccia core of the pipe, rather than of

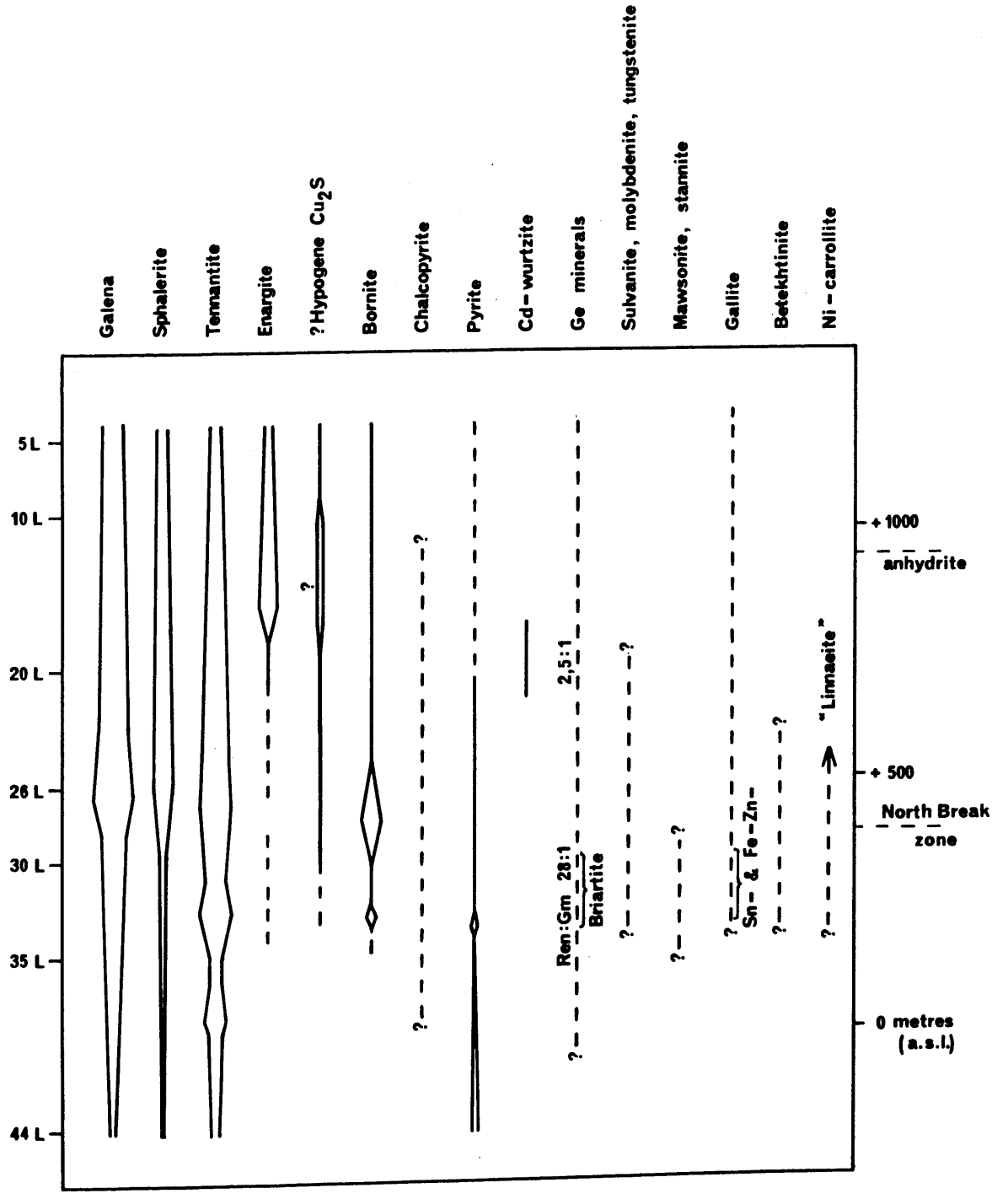

Fig. 71
Distributions and relative abundances of hypogene minerals with depth in the Tsumeb ore body. Note the zoning of copper minerals (e.g. enargite versus tennantite), Cd-wurtzite, and germanium minerals (germanite versus renierite), and the decrease in galena and probable increase in pyrite with depth. Compiled from Griffis and McCue (1950), Geier (1953, unpub. repts.), Sohnge (1964, 1977), Hopwood (1975), and this study.

the massive sulphide bodies, but it is impossible to subdivide the data. Some may occur in the upper levels, but might not have been recognised at the time of mining (some were undescribed species at that time). Germanite and renierite are volumetrically minor, but widely distributed, within the pipe. The increase in the renierite : germanite ratio with depth (Geier, unpub. repts.) is, therefore reliably established (Fig. 71). Insufficient studies have been made on the largely unmined ore below 34 level for the distribution of trace minerals to be known at depth, but observations made during the present study indicate that they are very rare.

3.6.9 Zoning of gangue minerals

The compositions of cavity-filling gangue minerals, which are associated with sulphide mineralization in the core and margins of the pipe, are related to the dominant alteration type in the enclosing rock. Quartz occurs as veins, disseminations and vug fillings in the silicified zone. Minor coarse grained dolomite spar is associated with this quartz, but hypogene calcite is negligible. Calcite spar is the dominant vein and vug mineral in the calcitized zone, and a large massive calcite body, in excess of 10 m thick in places, extends from just below 32 level to slightly above 36 level (Fig. 18). However, dolomite spar is moderately abundant in veins and vugs. The proportion of dolomite spar relative to calcite increases upwards in the pipe as the intensity of calcitization decreases. Dolomite is the dominant vein mineral in the unaltered dark dolostone breccia, and in adjacent, bedded dolostone. Schneiderhöhn (1920c) noted that gangue minerals in the upper levels of the mine consist equally of dolomite and quartz, with only minor calcite.

3.6.10 Previous paragenetic studies and present approach

It is difficult to evaluate previous studies of sulphide and gangue parageneses for a number of reasons. The most important of these is that the ubiquitous presence of deformational textures in massive sulphide ore was not recognized by previous workers. Also, the inhomogeneous nature of deformation within the Tsumeb pipe was not fully appreciated (Chapter 3.7). For example, the paragenetic

sequence of Geier (unpub. repts.) depends on deformational events which are not recognized in the present study. The argument advanced in Chapter 3.6.3, that most chalcocite, some bornite, and a minor quantity of chalcopyrite are not hypogene, differs from previous interpretations. It is also shown in the following discussion that no single paragenetic sequence is representative of all ore types. This, and confusion over hypogene versus supergene phases, are probably the reasons for major disagreement by previous workers as to the relative timing of sphalerite, bornite, Cu_2S phases and galena (e.g. Schneiderhöhn, 1920c; Moritz, 1933; Sclar and Geier, 1957; Geier, unpub. repts.).

Previous paragenetic studies are, therefore, of limited use, and a new study was undertaken. Polished ore sections, and hand specimens from vugs and veins, were used to determine the paragenetic sequence in each of the different ore types. The presence of deformational textures in massive sulphide ore imposed limitations on the study. The relative ages of two brittle sulphide minerals (i.e. minerals which have deformed by cataclasis, such as pyrite and sphalerite) can be determined by the consistent presence of inclusions of one mineral in the other; the minerals may be contemporaneous (or sequential if reaction relations are indicated). It is more difficult to interpret the relative ages of a brittle mineral and its ductile matrix (e.g. pyrite in galena). The brittle mineral is interpreted as the earlier phase where it is bounded by a continuous, irregular but smooth margin which indicates replacement by the enclosing phase (e.g. crystals which resemble the pyrite shape in Fig. 80). The brittle mineral is interpreted as earlier than, or simultaneous with, the matrix where its crystals are typically euhedral, since there is no evidence of porphyroblastic sulphide minerals in the Tsumeb ore. However, it is impossible to interpret the relative ages of the minerals where the brittle mineral shows cataclastic boundaries. It is also impossible to interpret the relative ages of two ductile minerals, such as galena and bornite.

3.6.11 Paragenesis of massive sulphide ore

The paragenetic sequence for each type of ore summarized in Figure 70 is shown in Figure 72.

The paragenesis of type 1B, tennantite-bearing lead-zinc ore is shown in (B) and (C). Pyrite occurs as anhedral, or subhedral to euhedral, grains in tennantite and sphalerite (Fig. 75), and tennantite pre-dates sphalerite in the majority of specimens. There is evidence of continuing, or multiple events of pyrite precipitation in some specimens, e.g. after tennantite but prior to sphalerite (paragenesis C). Galena has replaced pyrite grains in some specimens. The paragenesis of type 1A, enargite-bearing lead-zinc ore resembles paragenesis (B), in that both sphalerite and galena are late phases. Enargite has been consistently replaced along its margins by tennantite, rather than vice-versa, in all enargite-bearing ore types (Fig. 76). Enargite has also been replaced by galena, and some enargite has undergone pervasive alteration to the "green enargite" (i.e. tennantite) of Schneiderhöhn (1929). The paragenesis of type 4 copper-zinc ore (Fig. 77) is shown in (J). Pyrite is commonly enclosed by sphalerite, and sphalerite by tennantite, and the enclosed phases have been replaced by the surrounding minerals. Pyrite precipitation occurred between that of sphalerite and tennantite in some specimens (Fig. 78).

Type 3C bornite ore (paragenesis H) contains subhedral to euhedral and less commonly, anhedral, grains of pyrite in tennantite. Anhedral pyrite occurs enclosed in bornite and galena, but subhedral to euhedral pyrite is more common (Fig. 79). Some specimens contain tennantite which is slightly darker in colour than normal; one such tennantite lacks inclusions and is rimmed by germanite and renierite. The tennantite is possibly iron-rich tennantite, which has been observed elsewhere in association with germanium minerals (Chapter 3.6.2). The dark tennantite and germanium minerals are enclosed by normal tennantite, which contains numerous inclusions of germanite (including tungsten-germanite) rimmed by renierite. Germanite with renierite rims is common in type 3C ore, e.g. with gallite, within bornite. Nickel-carrollite is intergrown with, and replaced by,

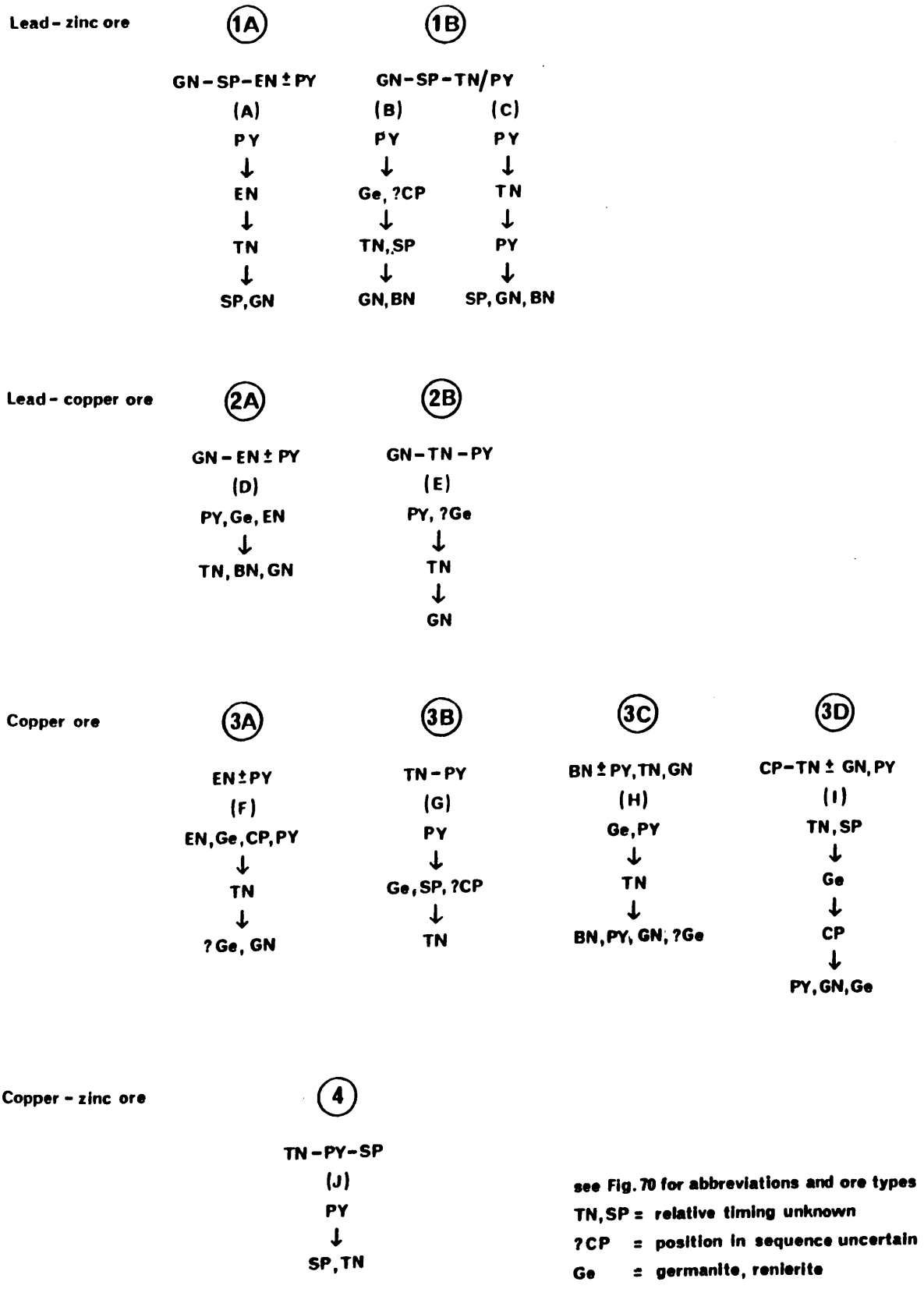

Fig. 72
Paragenetic sequences in different types of massive sulphide ore from the Tsumeb ore body. Note that tennantite post-dates enargite in enargite-bearing ore, galena is a late mineral in all ore types, and the relative timing of pyrite, sphalerite and tennantite varies in different types of ore.

FIGURES 73-80

Fig. 73

Basket-weave texture of chalcopyrite along (III) planes in bornite. This resembles a hypogene exsolution texture, but it is interpreted as a supergene oxidation texture. Chalcopyrite of supergene oxidation origin is present at this elevation in the mine (Fig. 64), and the basket-weave texture grades into chalcopyrite veins elsewhere in the sample (Fig. 74). Sample 1117, W35/21L. Plane polarized light.

Fig. 74

Chalcopyrite veining in bornite; same sample as Fig. 73. The chalcopyrite, of probable supergene oxidation origin, has partly veined the (III) planes in the bornite adjacent to the large veins, and grades into a basket-weave texture elsewhere in the sample. Plane polarized light.

Fig. 75

Type 1B galena-sphalerite-tennantite-pyrite ore. Euhedral to subhedral pyrite (PY) is enclosed by tennantite (TN) and sphalerite (SP) in a matrix of galena (GN). Sample 316, W20/30L. Plane polarized light.

Fig. 76

Enargite (white) enclosed and replaced by tennantite (dark grey) in germanium-rich tennantite-enargite-chalcopyrite ore (a variety of type 3). Sample 1121, W35/22L. Crossed nicols.

Fig. 77

Type 4 tennantite-pyrite-sphalerite ore, in which pyrite (PY) and sphalerite (SP) are enclosed in tennantite (TN). Sample 884, DDH 3163/38L. Plane polarized light.

Fig. 78

Chains of pyrite grains (PY) occur at the interface between tennantite (TN) and sphalerite (SP) in type 4 tennantite-pyrite-sphalerite ore. Some sphalerite has been bleached during supergene alteration. Sample 1123, W150/34L. Plane polarized light.

Fig. 79

Type 3C bornite ore which contains euhedral to subhedral pyrite (PY) within bornite (BN), galena (GN), and Cu_2S (CC) of probable supergene origin. The bornite-galena and galena-Cu_2S contacts are smooth and curving; however, Cu_2S forms irregular contacts with bornite, which it has replaced. Sample 124, W70/30L. Plane polarized light.

Fig. 80

Type 3A enargite-pyrite ore with minor germanite (GM) and galena (GN). Pyrite (PY) has been replaced by enargite (EN). Sample 975, 16L. Plane polarized light.

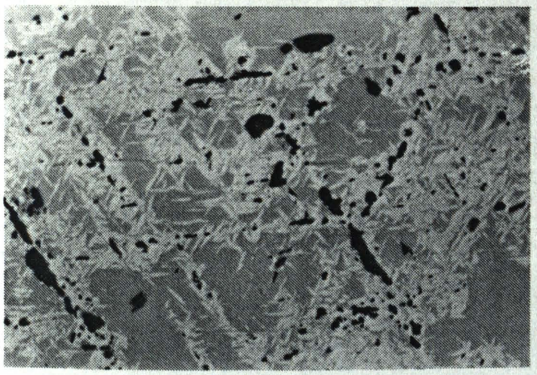

Fig. 73 0 mm 0.1

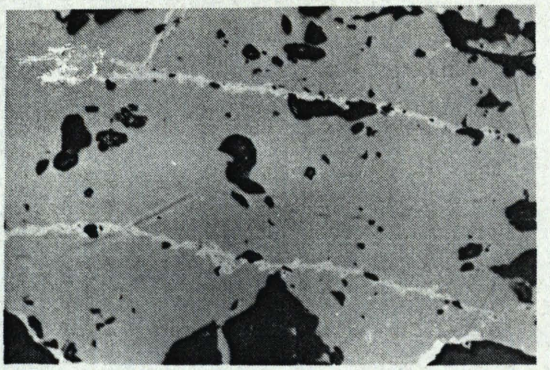

Fig. 74 0 mm 0.1

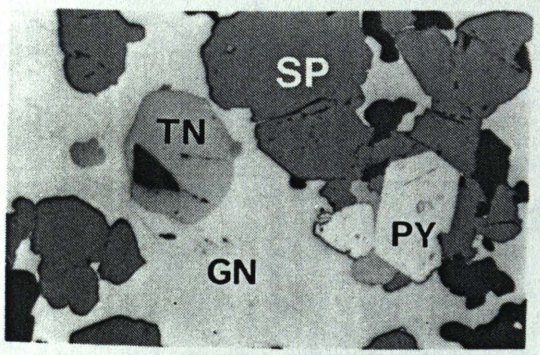

Fig. 75 0 mm 0.2



Fig. 76 0 mm 0.2

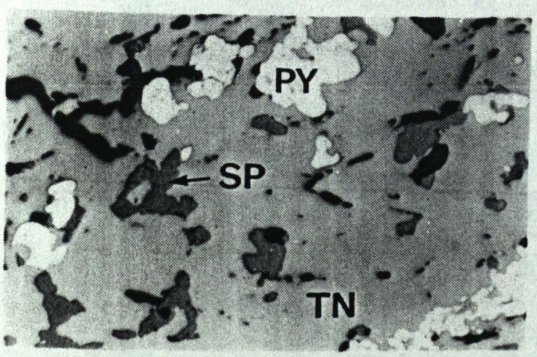

Fig. 77 0 mm 0.2

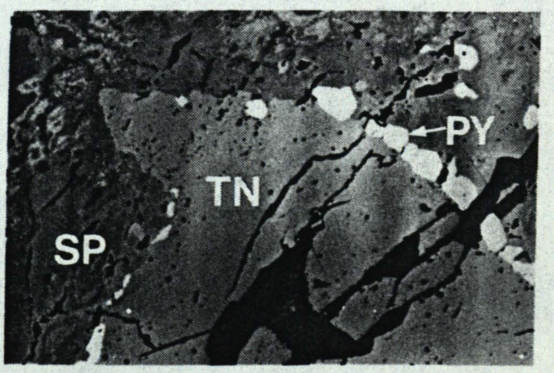

Fig. 78 0 mm 0.2

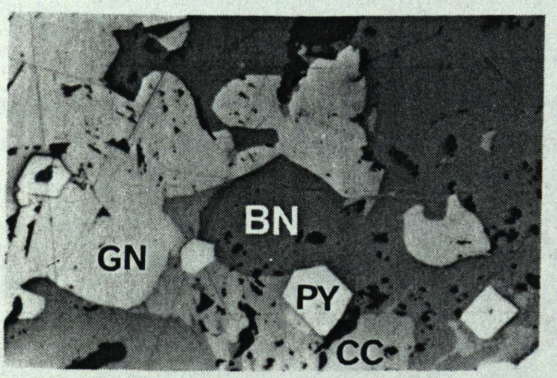

Fig. 79 0 mm 0.2

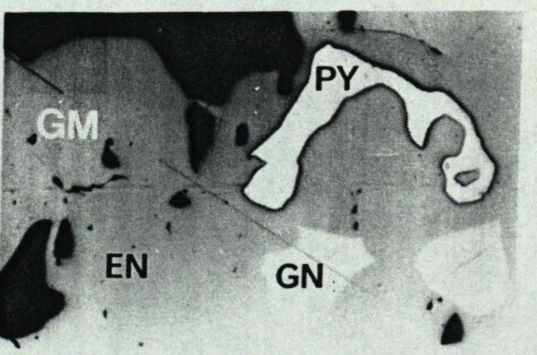

Fig. 80 0 mm 0.2

galena in some specimens, and occurs as skeletal and subhedral grains in bornite. Betekhtinite was only observed in type 3B ore, where it occurs in contact with, but not intergrown with, both bornite and galena in every instance.

Type 3D chalcopyrite ore (paragenesis I) of the North Break ore body contains germanite, tennantite and sphalerite within chalcopyrite. Germanite grains are partly enclosed by the margins of tennantite grains in some specimens. This contrasts with type 3A ore (Fig. 80), in which chalcopyrite and germanium minerals pre-date tennantite, but are enclosed by or post-date enargite.

Grey sphalerite is the dominant sphalerite type in massive ore, particularly in lead-zinc ore, in which it is a late mineral. Brown sphalerite occurs most frequently in specimens from the upper levels of the mine, typically in enargite-rich lead-copper and copper ores. Green sphalerite is rare, and occurs mostly in germanium-rich associations. B.H. Geier (unpub. repts.) proposed that different generations of sphalerite precipitated at different times, and considered green sphalerite to be a paragenetically early variety of sphalerite.

3.6.12 Paragenesis of disseminated ore

Paragenetic sequences within disseminated mineralization could not be studied in detail, because sulphide aggregates are small and textures are not diagnostic in many specimens. Disseminated copper-zinc ore of the silicified zone is mineralogically identical to massive sulphide ore of type 4 (Fig. 70), and sphalerite pre-dates tennantite in many specimens. Copper-lead ore of the calcitized zone is mineralogically similar to type 2B massive ore, although some varieties are bornite-rich. The overlying copper-rich ore is mineralogically similar to type 3B massive ore.

Vug-filling sulphide mineral assemblages provide little information on sulphide parageneses. This is because they are volumetrically minor, they cannot be definitely related to the main phase of sulphide ore deposition (i.e. they may be paragenetically

late), and they are mineralogically simple and cannot be easily related to any of the types of massive sulphide ore. A tennantite crystal in one specimen contains a core of galena, the reverse of the paragenetic sequence interpreted for the different types of massive ore. Late pyrite post-dates galena and tennantite crystals in some vugs.

3.6.13 Paragenesis of trace minerals

The paragenesis of the rarer, trace minerals has been studied in detail in the past, and depositional sequences which have been established previously agree with observations made during the present study.

Renierite post-dates and replaces germanite (Sclar and Geier, 1957), and some sulvanite is closely associated with renierite (Geier and Ottemann, 1970a). Briarite forms myrmekitic and graphic intergrowths with tennantite, sphalerite and renierite (Strunz and Tennyson, 1967; Geier and Ottemann, 1972). Germanium-mawsonite occurs as rims on probable germanium-stannite; it is enclosed by tennantite, sphalerite and bornite, and occurs in a probable exsolution intergrowth with briartite. Gallite occurs as inclusions in germanite and renierite, and as lamellae (i.e. apparent exsolutions) in sphalerite (Strunz et al., 1959). The variety of sphalerite associated with germanium minerals, gallite, tin minerals, cadmium-wurtzite, sulvanite, molybdenite and tungstenite is invariably the rare, light green type (Geier, unpub. repts.).

The above studies, together with those of Schneiderhöhn (1920c), Moritz (1933), Ottemann et al. (1977) and the present study, indicate that germanium, gallium, tin, molybdenum, tungsten, vanadium and cobalt minerals are paragenetically early. However, germanium minerals post-date tennantite in type 3D chalcopyrite ore, and a second generation of germanium minerals may post-date tennantite in bornite ore of type 3C. Germanium minerals crystallized subsequent to an unidentified, possibly iron-rich, variety of tennantite in type 3C ore (Chapter 3.6.2).

3.6.14 Paragenesis of gangue minerals

The paragenetic sequence of carbonate minerals, quartz and sulphide minerals was examined in veins and vugs. Galena, tennantite and rare enargite crystals post-date quartz crystals in SOUTH/35L, within the silicified zone. Some massive tennantite pre-dates crystals of dolomite spar, but galena and tennantite crystals post-date crystals of dolomite spar in the silicified zone. Dolomite crystals post-date quartz at a few localities.

Some vein-filling calcite post-dates galena crystals in the calcitized zone (Fig. 50). Small pods of deformed calcite spar within massive sulphide ore may be either former vug-fillings or, more probably, remnants of larger calcite bodies which have been replaced by galena. The large calcite body which occurs in the lower levels of the mine (Chapter 3.6.9) appears to be replaced by galena, but relationships are equivocal. Calcite spar also forms the matrix of silicified dolostone blocks in S95 manto (Fig. 52). The relationship between hypogene calcite and dolomite gangue could not be determined as the two minerals were not observed together in veins. Tennantite and galena crystals post-date dolomite crystals in some vugs within the calcitized zone, although some dolomite precipitation outlasted that of tennantite.

Dolomite spar and crystals post-date tennantite in some veins of the overlying "unaltered" zone, but tennantite-galena veinlets also post-date dolomite spar. Lambaard (1953) recorded remnants of quartz-calcite-dolomite vein material in ore from 21 level, which were surrounded successively by pyrite, copper minerals and galena-sphalerite ore. He concluded that most sulphide minerals post-date quartz-dolomite veins at this elevation.

It is concluded that much calcitization and silicification preceded deposition of the sulphide ore, but that hypogene carbonate minerals and quartz were also deposited with sulphide minerals in vugs and veins which formed subsequent to the main phase of ore deposition. Carbonate minerals post-date quartz in these late veins, but not vice-versa.

3.6.15 Summary

Tsumeb ore contains major quantities of Cu, Pb, Zn, Fe and As, and anomalous concentrations of Ag, Cd, Hg, Mo and Ge. It also contains a number of rare Ga, V, W and Sn minerals. Tennantite, enargite, bornite, galena, sphalerite and pyrite are the major sulphide phases. The iron content of the ore is low relative to that of the other major metals, and this is reflected in the low pyrite content of the ore.

Chemical and mineralogical zoning is well developed in the ore (Fig. 135). The composition of disseminated ore within the core of the pipe differs from that of massive sulphide ore, and is closely related to the composition of alteration in rock which hosts the disseminated ore. Disseminated copper-zinc ore occurs in the silicified zone, together with open-space fillings of quartz and minor dolomite. This mineralization is overlain by disseminated copper-lead ore in the calcitized zone, where dolomite is subordinate to calcite in open space fillings. Disseminated copper ore occurs in the "unaltered" zone, and is commonly mineralogically complex;. open spaces are mostly filled by dolomite. Lead-zinc ore is not represented among the disseminated ore types. Dolomite and calcite post-date quartz in open space fillings within both disseminated and massive ore, and carbonate minerals can pre-date or post-date sulphide minerals.

Zoning also occurs within massive sulphide ore of the fracture zones and mantos. Volumetrically minor copper-zinc ore (type 4) occurs adjacent to the lowermost, silicified zone. Galena is rare in both this and the mineralogically equivalent, disseminated ore of the pipe core at this elevation. Bornite-rich ore of type 3C and volumetrically unimportant chalcopyrite-rich ore of type 3D are mostly confined to intermediate levels, in the vicinity of the calcitized zone and the North Break zone (and, in the case of chalcopyrite-rich ore, outside the pipe). Galena is minor and sphalerite is rare in these ore types, which differ from tennantite-pyrite ore of type 3B in that major amounts of chalcopyrite and bornite (including bornite plus euhedral pyrite) have crystallized after tennantite. Lead-zinc ore is separate from, but gradational into copper-rich ore types which contain

tennantite and enargite. Tennantite-bearing copper ore occurs at lower and intermediate levels, but enargite is important in the upper levels of the mine. Germanium-rich ore is best developed in the upper levels, and the ratio of renierite to germanite increases at depth. Cadmium-rich wurtzite is confined to the upper levels.

It is concluded that different paragenetic sequences are present in different ore types (Fig. 72). Sphalerite and chalcopyrite can both pre-date and post-date tennantite deposition, but in different ore types. Tennantite post-dates enargite in all samples in which both minerals occur, and enargite is partly altered to tennantite in many samples; this agrees with the observations of Schneiderhöhn (1929), Moritz (1933), and Geier (unpub. repts.). Pyrite was early to crystallize in all pyrite-bearing ore. However, only minor pyrite crystallized (or remains unreplaced) from this event in much of the ore, and most of the pyrite now present in the ore precipitated at an intermediate or late stage. This is particularly true of type 3C bornite ore, in which pyrite is typically late and enclosed by bornite.

The relative timing of, and the inter-relationship between, the different types of massive ore is complex. Type 3A enargite-bearing copper ore is transitional to type 2A copper-lead ore and type 1A lead-zinc ore, concomitant with an increase in galena and sphalerite, respectively. These two minerals are paragenetically late in type 1A ore. A similar relationship exists between tennantite-bearing ores of types 3B, 2B and 1B. Ore of types 3A and 1A occur as separate, but commonly adjacent, bodies and type 2A ore is volumetrically unimportant. This sequence is interpreted as a temporal progression in which galena, and galena plus sphalerite, have progressively replaced pre-existing copper mineralization.

The relationship between enargite-bearing ore of the upper levels of the mine (types 3A to 1A) and enargite-free ore of the lower levels (types 3B and 1B) is more complex. Enargite is replaced by tennantite to varying degrees in the upper level ore. However, tennantite is a negligible constituent of some enargite-bearing lead-zinc ore of type 1A (i.e. paragenetically late galena and

sphalerite occur in ore in which enargite has not been replaced by tennantite). Enargite is extremely rare in the lower levels, and there is no evidence that it was ever present in most of this ore. Therefore, there is a spatial variation which involves enargite and tennantite, upon which two temporal variations have been superimposed. These are the replacement of enargite by tennantite, and the change from precipitation of copper minerals to that of galena and sphalerite. The copper sulpharsenide paragenesis is possibly more complex than this within minor volumes of ore. Iron-rich tennantite may occur in some germanium-rich ore, and this may be paragenetically early relative to normal, zinc-rich tennantite.

3.7 DEFORMATION OF THE TSUMEB ORE BODY

Major, F_1, folds of the Otavi Mountain Land have an easterly trend, with shallow plunges to the east and west, and are open and approximately symmetrical in cross-section, with limbs that dip at 20° to 60° (Figs. 3, 4). However, in the southern Otavi Mountain Land folds vary from symmetrical, to overturned with southerly dipping axial planes, similar to folds elsewhere along the southern margin of the Owambo basin (Chapter 2.1; Söhnge, 1957; Hopwood, 1975). F_1 folding occurred during D_1, the earliest deformational event recognized in the Otavi Mountain Land; this was the only major deformational event that affected the Tsumeb Subgroup in the vicinity of Tsumeb. A later phase of folding, F_2, is important in the southern Otavi Mountain Land, where a minor F_3 phase can also be recognized (Chapter 4.4.4). The Tsumeb ore body is situated on the northern limb of an F_1 fold, the Tsumeb syncline (Fig. 112). The F_1 folding has resulted predominantly from flexural slip in weaker, phyllosilicate-rich or calcareous layers within the dolostone (Hopwood, 1975).

Minor folds in the Tsumeb Subgroup, immediately to the west of Tsumeb, are mostly sub-parallel to the Tsumeb syncline, with trends of 116° and plunges of 10°-15° east (Griffis, 1949). A cleavage, axial planar to these minor folds in the Tsumeb West area, has a strike of 105° and dips vary from 70°N to 70°S (Fig. 112). This cleavage, which

occurs as a "flow cleavage" in limestone, but as a "fracture cleavage" in dolostone (Berning, 1951; le Roex, 1951), was termed S_2 by Hopwood (1975) but is re-defined here as S_1, using the terminology of Hobbs et al (1976).

Most previous workers who studied the structure of the Tsumeb ore body considered that shearing parallel to the axial plane of the syncline (i.e. parallel to S_1) controlled brecciation, injection of "pseudo-aplite" (from elsewhere in the Tsumeb Subgroup) and mineralization, within the Tsumeb pipe (Chapter 3.2). It is argued in Chapter 3.3 that most of the breccia in the Tsumeb pipe is a sedimentary breccia, not a tectonic breccia, and that "pseudo-aplite" is sandstone which was deposited within the pipe cavity. It is demonstrated in the following discussion that the breccia and sandstone were deformed by the D_1 deformational event, and that hydrothermal alteration and sulphide mineralization formed prior to cessation of this event, and possibly prior to its commencement.

3.7.1 S_1 cleavage in the Tsumeb pipe

The S_1 cleavage occurs as a close-spaced penetrative fabric in limestone, calcitized dolostone, and in the calcitized or sericitic matrices of breccia bodies. The cleavage does not commonly penetrate unaltered dolostone clasts within breccia bodies, but is mostly confined to the matrix, where it varies in intensity (e.g. in the Tsumeb pipe). Breccia clasts are elongated within the S_1 plane at many localities within the Tsumeb pipe (Figs. 21, 27, 31, 37, 43, 81), and probable ooids in the Elandshoek Formation, which crop out in the North Break zone to the north of the Tsumeb mine, are also elongated in this plane (Hopwood, 1975).

The S_1 cleavage is not as obvious in the immediate vicinity of Tsumeb as at Tsumeb West (Fig. 112). The cleavage is commonly not visible in dolostone at Tsumeb and, where present, it is a weak, spaced cleavage with a variable strike (085°-115°). Because the S_1 cleavage can rarely be observed within the dolostone wall rock of the Tsumeb pipe, or in bedded dolostone which occurs inside the pipe, it cannot be

FIGURES 81 - 88

Fig. 81

Dark dolostone breccia from the area shown in Figure 21. This rock consists of unaltered clasts of both light grey and dark grey dolostone, in a matrix of sericitized, carbonaceous, dolomitic siltstone which shows a well developed S_1 cleavage. Some dolostone clasts interlock along stylolitic contacts with no intervening matrix. Calcite veins (C) are of supergene origin and post-date the S_1 cleavage (Chapter 5.2.5). Sample 844B, W20/29L.

Fig. 82

A thin section of dark dolostone breccia, showing clasts which interlock along the stylolitic, S_1, cleavage with no intervening sedimentary matrix. The orientation of bedding, S_o, varies in adjacent clasts. Minor amounts of sulphide minerals and other insoluble material have accumulated in the stylolites, and are interpreted as a stylocumulate residue. Sample 549A, E9/30L. Plane polarized light.

Fig. 83

A polished surface of dark dolostone breccia, showing the form of the contact between a clast of light to medium grey dolostone and its matrix of carbonaceous, dolomitic siltstone. The S_1 cleavage is mostly confined to the matrix, and only penetrates the outer one millimetre of the clast. Sample 653, 16L.

Fig. 84

Calcitized dolostone breccia, showing recrystallized compositional banding (i.e. bedding, S_o) which has a constant orientation within individual clasts. The stylolitic S_1 cleavage has a constant orientation throughout the core, and is confined to the matrix and to the contacts between clasts. The S_1 cleavage is the only important cleavage within the Tsumeb pipe, but bedding of the type illustrated was probably interpreted as an early cleavage by some previous workers (e.g. Hopwood, 1975). Sample 955, DDH 2946/30L.

Fig. 85

Deformation cleavage (C) and kinked twin planes (T) in calcite grains which comprise calcitized dolostone breccia. Sample 565, W120/32L. Crossed nicols.

Fig. 86

Deformation features in silicified dolostone breccia. Many grains, particularly smaller grains, are oriented sub-parallel to the S_1 structural direction. Individual quartz grains show deformation lamellae (D). Sample 910, DDH 3163/38L.

Fig. 87

Folded inclusions of carbonaceous material in massive tennantite (a texture common in massive sulphide ore). This texture alone is not diagnostic of post-ore deformation because the tennantite could have replaced previously folded rock. Sample 512, W120/33L. Plane polarized light.

Fig. 88

Pressure shadows of tennantite (TN), adjacent to grains of pyrite (PY), in dark dolostone breccia which shows compositional banding. The pressure shadows are oriented in the plane of the S_1 cleavage. This indicates that the deformational event which formed S_1 was synchronous with, or subsequent to, the mineralizing event. Sample S845,3, 22L. Oblique natural light.



Fig. 81 0 cm 5

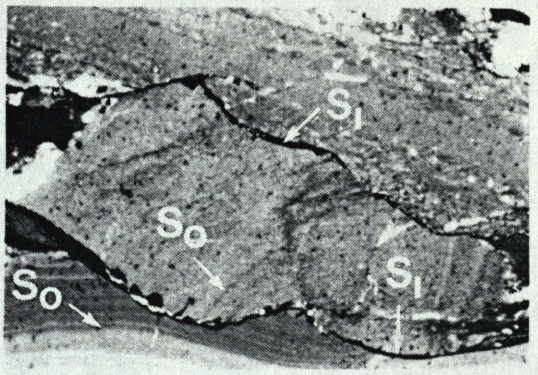

Fig. 82 0 mm 2

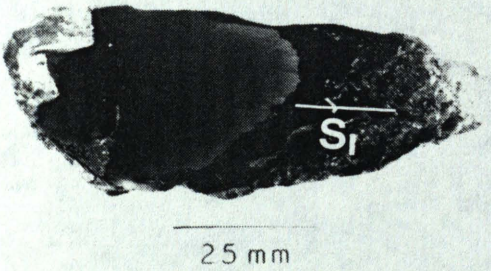

Fig. 83

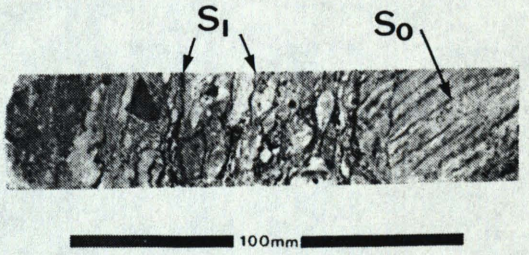

Fig. 84

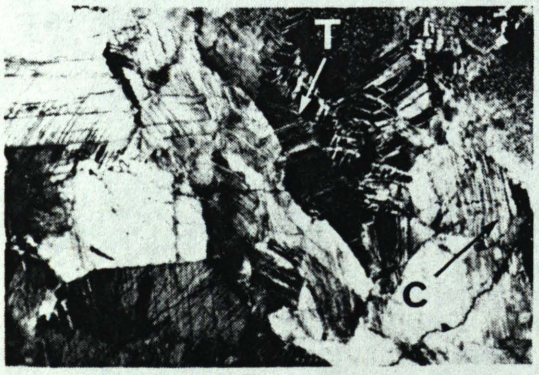

Fig. 85 0 mm 2

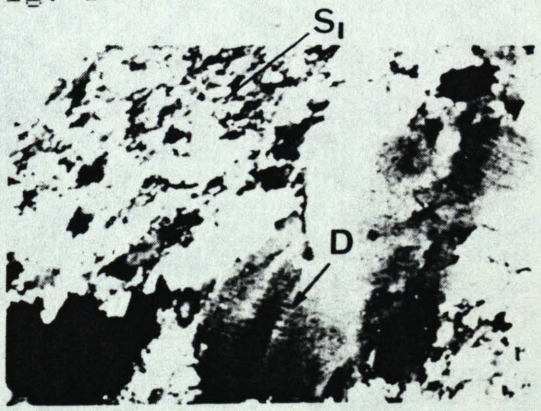

Fig. 86 0 mm 0.4

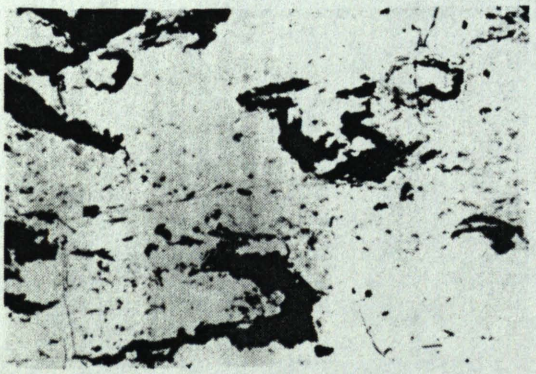

Fig. 87 0 mm 0.4

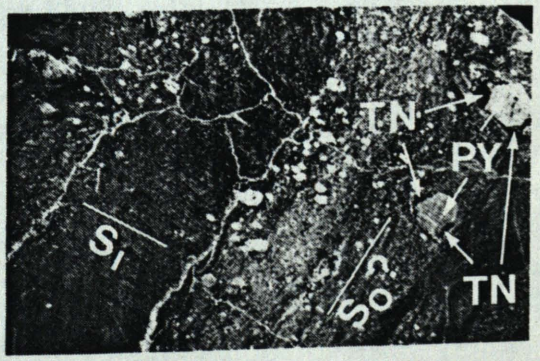

Fig. 88 0 cm 0.5

positively identified by its relationship to minor F_1 folds at most underground localities. However, the dominant cleavage within the pipe breccia is considered to be S_1, because it is oriented parallel to unequivocal S_1 cleavage present at surface and in rare underground exposures. The S_1 cleavage has a consistent orientation which can be observed continuously along complete sections through the Tsumeb pipe in some stopes (Fig. 31). The S_1 cleavage curves around large clasts in the breccia of the Tsumeb pipe, so cleavage measurements shown in Figure 89a-f were confined to areas where small clasts and abundant matrix predominate. Each measurement is representative of a minimum of approximately one metre width of breccia, measured perpendicular to cleavage, therefore the number of suitable points which could be measured at any one locality, e.g. a stope or pillar, was limited. The number of localities at which measurements could be taken at any given elevation was also limited, particularly above 30 level where mining was confined to pillar recovery, and this restricted any rigorous structural study. The S_1 cleavage has a similar orientation at Tsumeb, Tsumeb West, and farther to the south (Figs. 89h, i, 112). It is the only cleavage present at most localities in the Tsumeb mine (Chapter 3.7.10). The multiple, disoriented cleavages which Hopwood (1975) considered to be present in the pipe breccia are almost certainly compositional banding inherited from former bedding, of the type observed during the present study (Figs. 37A, 84).

The S_1 cleavage has an average strike of 109°, and dip of 78°N within the Tsumeb pipe above 33 level (Fig. 89a-e). The cleavage is approximately parallel to the elongation of the pipe in plan (i.e. 100°-110°). It is perpendicular to the vertical plane within which all variations in the plunge of the pipe lie (except between 9 and 12 levels, and between 30 and 36 levels, in the vicinity of bedding faults; Chapters 3.7.7, 3.7.8; Fig. 90). The dip of the S_1 cleavage varies from 68°-79°N between 26 and 33 levels, but averages 78°N, slightly steeper than the plunge of the pipe (observations at numerous elevations, other than those at which systematic measurements were made, indicate that this average dip is probably less than estimated because of the small sample size). The dip of the S_1 cleavage reverses to the south from above 2 sub-level/35L (+165 m), to

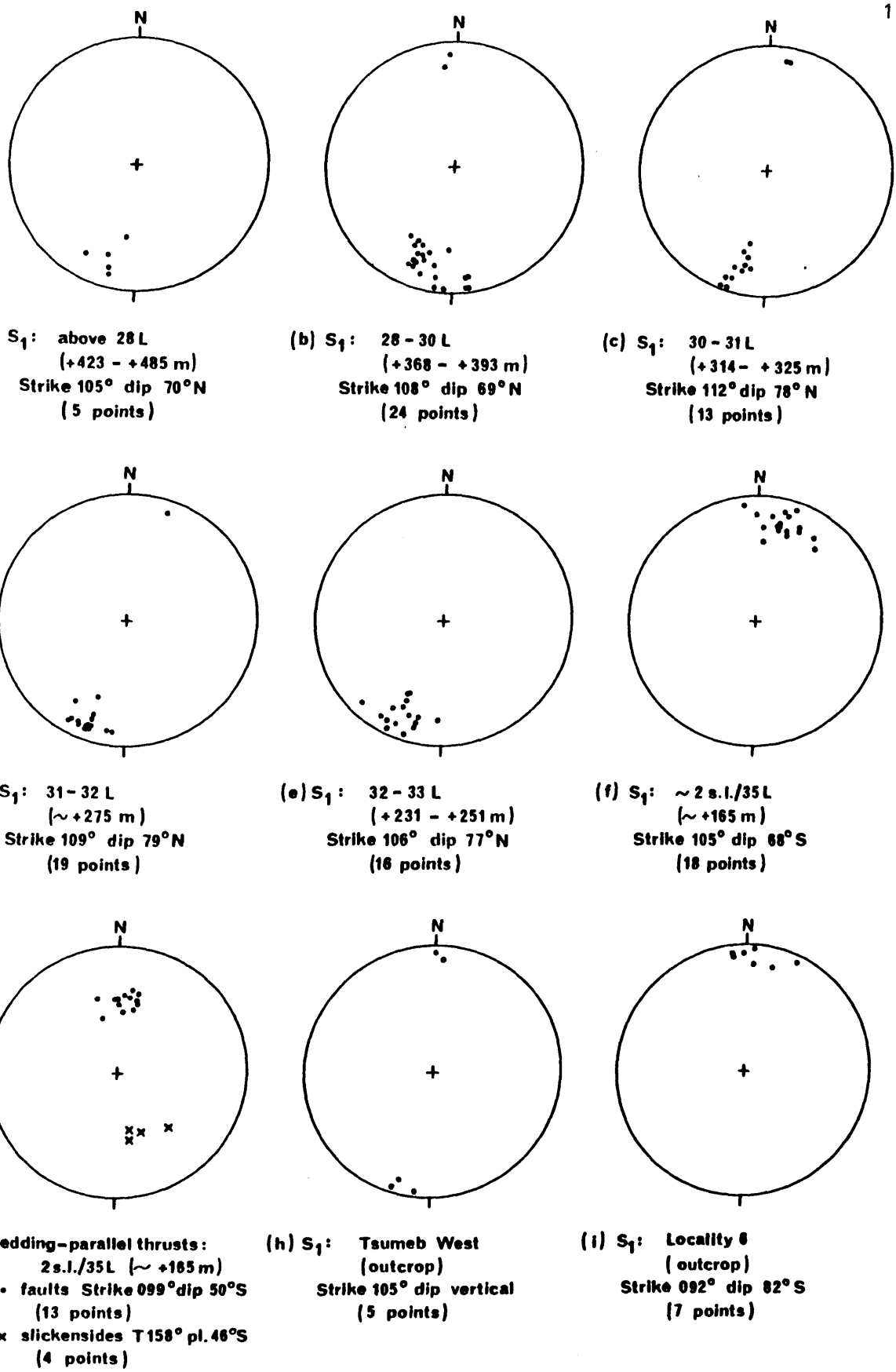

Fig 89.

Equal area plots of poles to the S_1 cleavage and 35L thrust faults, Tsumeb ore body. Average orientations are also given. The S_1 cleavage within the ore body dips north above 34 level (a-e), but reverses to the south between 34 level and 37 level (f). Data from the Tsumeb West and locality 6 occurrences (Fig.111a) are also shown.

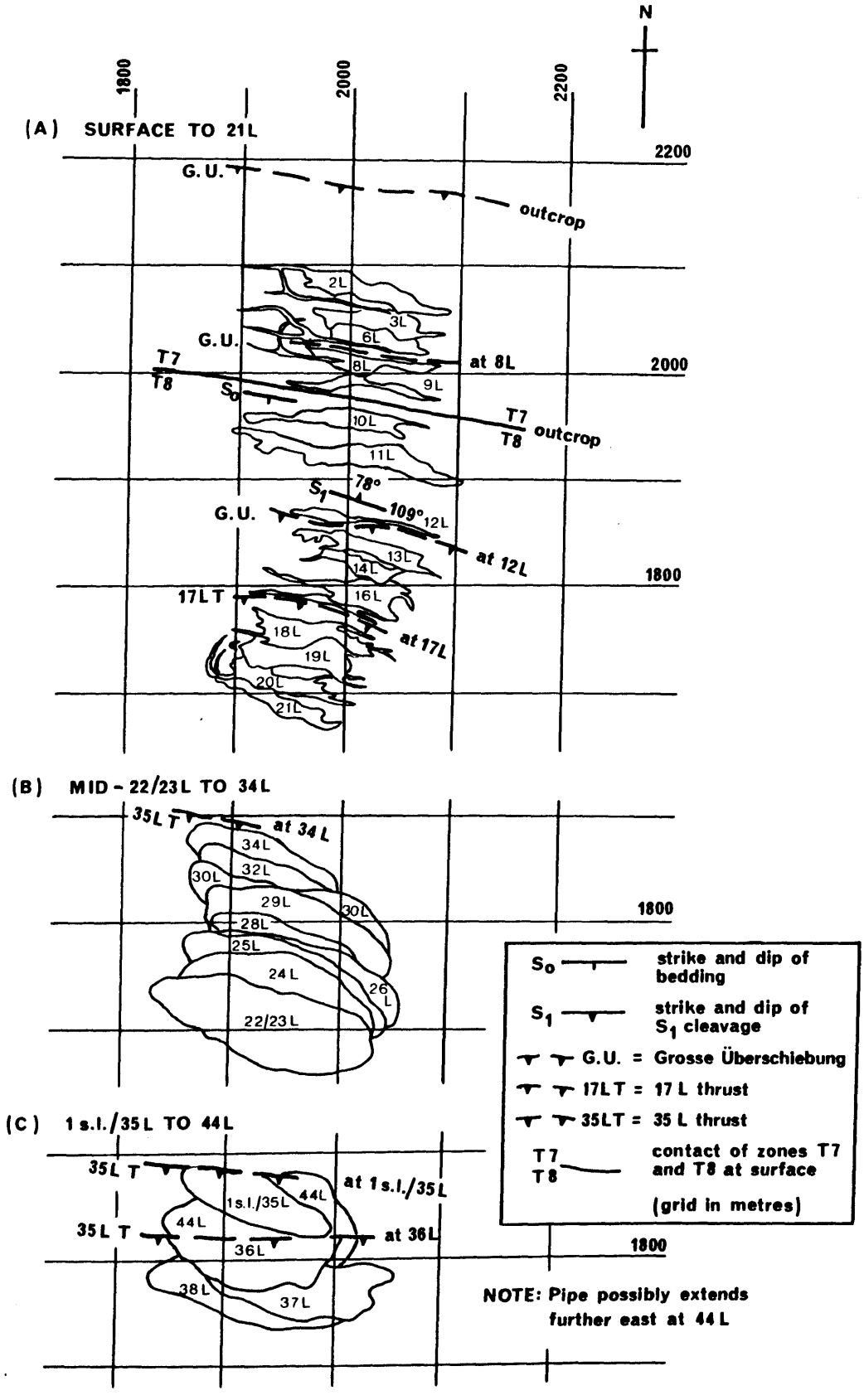

Fig. 90

Plan projections of the Tsumeb ore body at various elevations. All variations in the plunge of the pipe lie in a vertical plane except between 9 and 12 levels, and 30 and 36 levels (in the vicinity of bedding-parallel thrusts; Fig. 19). The S_1 cleavage is approximately perpendicular to this plane, and parallel to the elongation of the pipe.

below 35 level (+151 m), the lowest elevation examined in detail, as the result of thrusting which post-dates the cleavage (Fig. 89f; Chapter 3.7.7). Observations in a limited area exposed at 38 level showed that the dip of S_1 is variable, but consistently steeper than at 35 level (e.g. strike 104°, dip vertical).

The ubiquitous presence of the S_1 cleavage in the breccia matrix excludes an origin in which the pipe breccia formed subsequent to D_1 deformation. The systematic angular relationships between S_1 cleavage, elongation of the pipe, and the plane within which the pipe plunges, indicate that the present shape and attitude of the pipe was attained during the D_1 deformational event (Hughes, 1977). The mechanisms by which this occurred are discussed below.

3.7.2 Contrasting deformation mechanisms during F_1 folding

All rocks within the Tsumeb pipe, whether hydrothermally altered or unaltered, were deformed during F_1 folding. However, the style and intensity of deformation varies in different rock types. Although rocks such as sandstone, dolostone and silicified dolostone show low strain in places, this can be ascribed to the inhomogeneous nature of deformation, which resulted from the variable distribution of different lithologies that deformed by different mechanisms (also see Hopwood, 1975). These differences are most obvious between massive rock and breccia.

Bedded and massive, unbrecciated dolostone commonly lacks the S_1 cleavage and shows only minor, open folds (except in the immediate vicinity of the pipe; Chapter 3.7.4). Grains of microspar dolomite are elongated parallel to S_1 in a few specimens, but the presence of folded quartz and carbonate veinlets in specimens which consist of equant microspar indicates that some internal deformation has also occurred in rocks which lack any obvious fabric. Nevertheless, flexural slip was probably an important mechanism of folding (Hopwood, 1975), because many folds have a true parallel form, and thin shale and limestone beds exist along which slip could have occurred. In contrast to the above dolostone, the pipe breccia shows the S_1

cleavage throughout, although the intensity of the cleavage is variable, and clasts are commonly elongated in the S_1 direction. The cleavage generally curves around clasts (Figs. 21, 37), but it can penetrate the margins of unaltered dolostone clasts for 1-2 mm (Fig. 83), and is strongly penetrative within some clasts of calcitized dolostone (Fig. 37A). This contrasting behaviour of different rock types is relevant to the origin of folding in the vicinity of the pipe, and to the time of formation of the marginal fracture zone (Chapter 3.7.5). The different deformational mechanisms which operated in dark dolostone breccia, calcitized dolostone breccia, silicified dolostone breccia, and the pipe sandstone are discussed in more detail below.

Deformational mechanisms, and the intensity of deformation, vary with the composition of the rocks which fill the Tsumeb pipe at any locality. The altered matrix of the dark dolostone breccia is commonly strongly cleaved, grains in the matrix are elongated, and large total strains are indicated in many places by veinlets of sulphide minerals folded in S_1 (Figs. 23, 91). However, few clasts show signs of internal deformation (e.g. the presence of cleavage, or folded bedding), although different clasts commonly interlock along stylolitic surfaces (Figs. 81, 82), and in places such clasts can comprise the entire rock. Exceptions occur in which both the dolomitic matrix and clasts show similar (and low) total strain, and a spaced, planar or stylolitic S_1 cleavage can penetrate the entire rock in these areas.

Calcitized dolostone breccia commonly contains a stylolitic S_1 cleavage which forms the contacts between different clasts (Figs. 41, 92). The S_1 cleavage consists typically of abundant, continuous, systematically-oriented stylolites, individually up to more than a metre in length; other, randomly oriented stylolites are at most centimetres long, and terminate at the S_1 stylolites (the exception being stylolites which form the contacts between very large clasts, as in Figure 37A). The S_1 cleavage can take other forms; it is most penetrative in the fine-grained matrix of calcitized breccia, where a matrix is present (Figs. 38, 39), but it can also penetrate large, completely calcitized clasts in which it folds former bedding (Fig.

FIGURES 91 - 98

Fig. 91

Dolomitic siltstone matrix of the dark dolostone breccia shown in figure 23, in which tennantite veinlets have been folded and transposed by the S_1 cleavage. The cleavage clearly post-dates the sulphide minerals in thin section, and mineralization therefore pre-dated the close of development of this cleavage. Sample 544, W40N/30L.

Fig. 92

Sulphide minerals within the S_1 stylolitic cleavage of calcitized dolostone breccia. The cleavage contains carbonaceous material (C) at the contact between two clasts of calcitized dolostone. Pyrite (PY) within the upper clast shows crystal faces, but adjacent to the stylolitic cleavage the pyrite aggregate has a smoothly curving margin which follows a stylolitic cleavage surface. This smooth margin is interpreted as the result of the dissolution of pre-existing pyrite within the later, stylolitic cleavage surface, so that the pyrite within the cleavage has a stylocumulate origin similar to that of the carbonaceous material. The pyrite was not, therefore, precipitated along the cleavage. This interpretation is supported by the presence in other specimens of well-defined sulphide veinlets, perpendicular to the cleavage, which terminate abruptly at stylolitic contacts in a similar manner. Sample 492, W80/33L. Plane polarized light.

Fig. 93

Galena crystals from a vug in silicified dolostone. Smoothly curving grain boundaries are present within single crystals, and the trace of these boundaries (G) can be seen on single crystal faces. This feature, anomalous interfacial angles, and curved crystal faces, are interpreted as deformation features. Sample 845, NORTH/35L.

Fig. 94

Deformation and recovery textures in massive galena. Elongated grains of galena, which show sub-grains in their interiors and at their margins, occur at bottom left. These grade into a sub-grain mosaic (foam texture) at top right. These textures are

most consistent with low-temperature deformation, subsequent to mineralization. Sample 423, 2 sub-level /35L. Plane polarized light. Etched with HCl + thiourea.

Fig. 95

Elongated grains of galena, with more regular boundaries than the galena of Figure 94, and sub-equant grains of sphalerite (SP). This is possibly a recovery texture in formerly schistose ore (see text). Sample 326A, ZERO/33L. Plane polarized light. Etched with HCl + thiourea.

Fig. 96

Smoothly curving and cuspate grain boundaries between elongated grains of galena (GN) and bornite (BN). The cleavage in the galena is continuous, and does not show folding or kinking, and the texture is interpreted as the result of mutual deformation of the two sulphide minerals followed by recovery. Sample 595C, E49S/29L. Plane polarized light.

Fig. 97

The most common texture in lead-zinc ore from Tsumeb. Galena (light) occurs as sub-equant grains, only a few of which show sub-grains. Sphalerite (dark) consists of growth twins, some of which are bent, and rare deformation twins. The paucity of deformation twins is interpreted as the result of the ductile nature of the galena matrix (which has undergone partial recovery since deformation), relative to the sphalerite inclusions. Sample 749, 22L. Plane polarized light. Etched with HCl + thiourea.

Fig. 98

Well developed foam texture in enargite (E, larger grains) which is disseminated in a calcite-rich rock (C, smaller grains). Complete equilibrium of this type, in which grain boundaries are straight and 120° triple junctions are present, is rare except in sub-grain mosaics of the type shown in Figure 94. The enargite was identified by its optical properties, reflectance, microhardness, and the presence of Cu, As and S (energy-dispersive microprobe analysis; N. Lindsay, 1985). Sample 387, E35/28L. Crossed nicols.

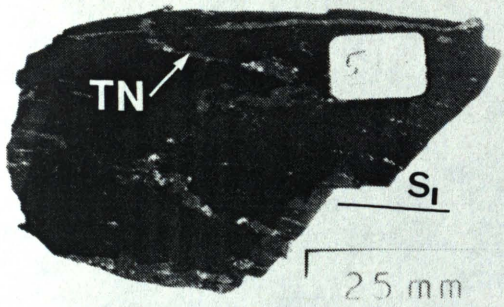

Fig. 91



Fig. 92

0 mm 0.4

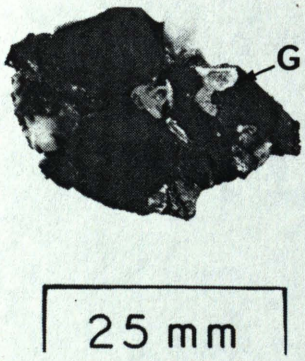

Fig. 93



Fig. 94

0 mm 0.4

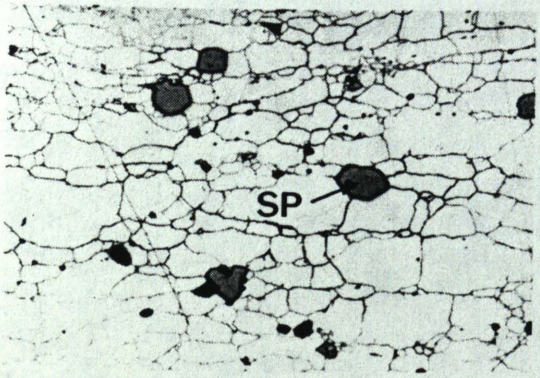

Fig. 95

0 mm 0.4

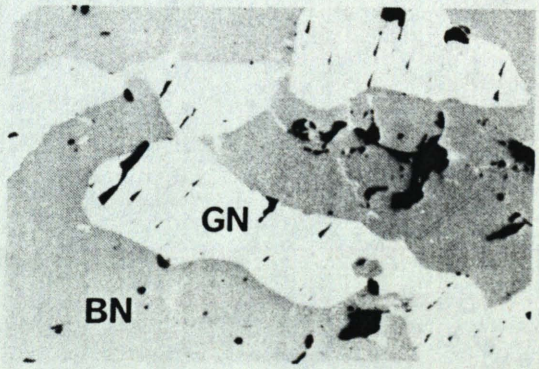

Fig. 96

0 mm 0.2



Fig. 97

0 mm 0.4



Fig. 98

0 mm 0.2

37A). Thin bodies of less calcitized rock can form pinch-and-swell structures which plunge at small angles within the S_1 surface of calcitized dolostone breccia. This competency contrast between rocks composed of dolomite and calcite is also seen within folds in interbedded dolostone and limestone of stratigraphic zone T7, in which only the limestone beds vary in thickness (Hopwood, 1975; Fig. 106). This behaviour is consistent with the relative ductilities of these rocks observed in experimental studies (Handin et al., 1963). Clasts of calcitized dolostone differ from clasts of unaltered or silicified dolostone in their greater degree of elongation in the S_1 direction (i.e. their axial ratios), and in the ubiquitous presence of intra-granular deformation within individual clasts. The calcite grains which comprise single clasts show serrated contacts, and are elongated parallel to S_1 in places; deformation twinning is present in all specimens examined, although it varies in intensity, and twin planes can be kinked (Fig. 85).

Completely silicified dolostone breccia contains a widely spaced, stylolitic, S_1 cleavage, which is only weakly oriented in places, although this cleavage is closely spaced and penetrative where the breccia is only partly silicified. Clasts in completely silicified rock are less strongly elongated in the S_1 surface compared with clasts in calcitized rock (Fig. 45), and the matrix and clasts do not appear to have deformed as separate components to the extent observed in other types of breccia. Individual quartz grains in both matrix and clasts show serrated contacts, undulatory extinction, deformation bands, and deformation lamellae, and most grains are elongated sub-parallel to S_1 (Fig. 86). Fine-grained, equigranular quartz of uncertain origin has a polygonal (foam) texture. However, strain is inhomogeneous in the body of silicified breccia as a whole, and areas of low strain exist.

The pipe sandstone does not commonly display obvious S_1 cleavage, although oriented quartz grains and flakes of sericite occur at some localities. However, there is widespread evidence that this rock was deformed during F_1 folding. Undulose extinction is present in many quartz grains, and clasts are oriented in the S_1 surface in

bodies of sandstone breccia (Fig. 27). Near-vertical veins of sandstone, tens of centimetres thick, can form pinch-and-swell structures, or even boudins, within the S_1 surface in dark dolostone breccia or calcitized breccia; these structures plunge at shallow angles, and quartz-carbonate bodies can occur in the necks between individual boudins (Botha, 1960; plates 1 and 2).

The widespread presence, in sandstone and hydrothermally altered rocks of the Tsumeb pipe, of deformation features related to the formation of the S_1 cleavage indicates that all of these rocks were deformed during F_1 folding. The dominant type of deformation mechanism present in a particular rock was a function of the massive, bedded or fragmental nature of the rock, its grain size and its composition. These variables in turn controlled the relative importance of trans-granular, intergranular and intra-granular deformation processes,. e.g. flexural slip folding, pressure solution (along stylolite and grain boundaries) and deformation twinning. The presence of deformation twinning in calcite, and the importance of pressure solution processes, is consistent with the very low temperature of metamorphism (or lack of metamorphism) interpreted for the Tsumeb ore body (Chapter 3.7.11; McClay, 1977; Groshong et al., 1984).

3.7.3 Deformation of sulphide ore

Previous studies have proposed that the Tsumeb sulphide ore (1) post-dated major deformation (e.g. Geier, 1972; Söhnge, 1976), (2) accompanied, but was outlasted by (or immediately preceded) deformation (Ypma, 1973a, b; Hopwood, 1975), or (3) accompanied but outlasted deformation (B.H. Geier, unpub. rept.). Models (1) and (3) depend on the assumed homogeneous nature of deformation within the Tsumeb pipe, and on the interpreted lack of deformational and recrystallization effects in part, or most, of the ore. Evidence advanced for this includes the presence of undeformed sulphide minerals in both vugs and massive sulphide ore (the latter is considered here to be partly of supergene origin; Chapter 3.6.3). The evidence advanced for model (2) does not preclude the possibility that mineralization pre-dated

deformation entirely. It is demonstrated here that typical ore from the Tsumeb pipe shows textures consistent with deformation and recovery at moderately low temperatures. The F_1 fold event outlasted or post-dated sulphide mineralization, and there is no evidence that the two events were necessarily related.

The deformational textures and fabrics in Tsumeb sulphide ore include: (A) features which could pre-date or post-date sulphide deformation, and (B) features which indicate that sulphide minerals formed prior to, or synchronous with, F_1 folding. The first group of features occurs in massive sulphide ore and includes: (1) folded chert bands (Fig. 99), (2) tightly folded, graphitic and shaly inclusions (Fig. 87), (3) replaced bodies of sedimentary breccia with clasts oriented parallel to S_1 (Chapter 3.5), and (4) bodies of brecciated chert. None of these features alone is conclusive evidence for deformation of the sulphide ore, because the sulphide minerals might have replaced pre-existing folds and breccia bodies. However, it is shown below that the sulphide minerals display microtextures which are indicative of deformation and recovery. It could be argued that the sulphide minerals replaced rocks deformed by the F_1 event, and were subsequently deformed during a second phase of deformation. However, there is no evidence for superimposed structural fabrics (e.g. re-orientation of clasts in ductile galena ore), and many sulphide veinlets within disseminated ore can be shown to pre-date the close of S_1 cleavage development. It is therefore probable that the above features were produced during F_1 folding of the sulphide ore.

Features which indicate that sulphide minerals were emplaced prior to, or synchronous with, major deformation are deformation and annealing textures in massive sulphide ore. Galena is the most sensitive indicator of deformational conditions in the Tsumeb ore. Many samples of massive sulphide ore which consist predominantly of galena, contain elongated grains of galena with either irregular or smooth boundaries (Figs. 94 and 95, respectively). The irregular boundaries consist of polygonal sub-grains, and the interiors of the grains show evidence of strain (indicated by the uneven, banded nature of the etch on single grains). The interiors of the grains show all

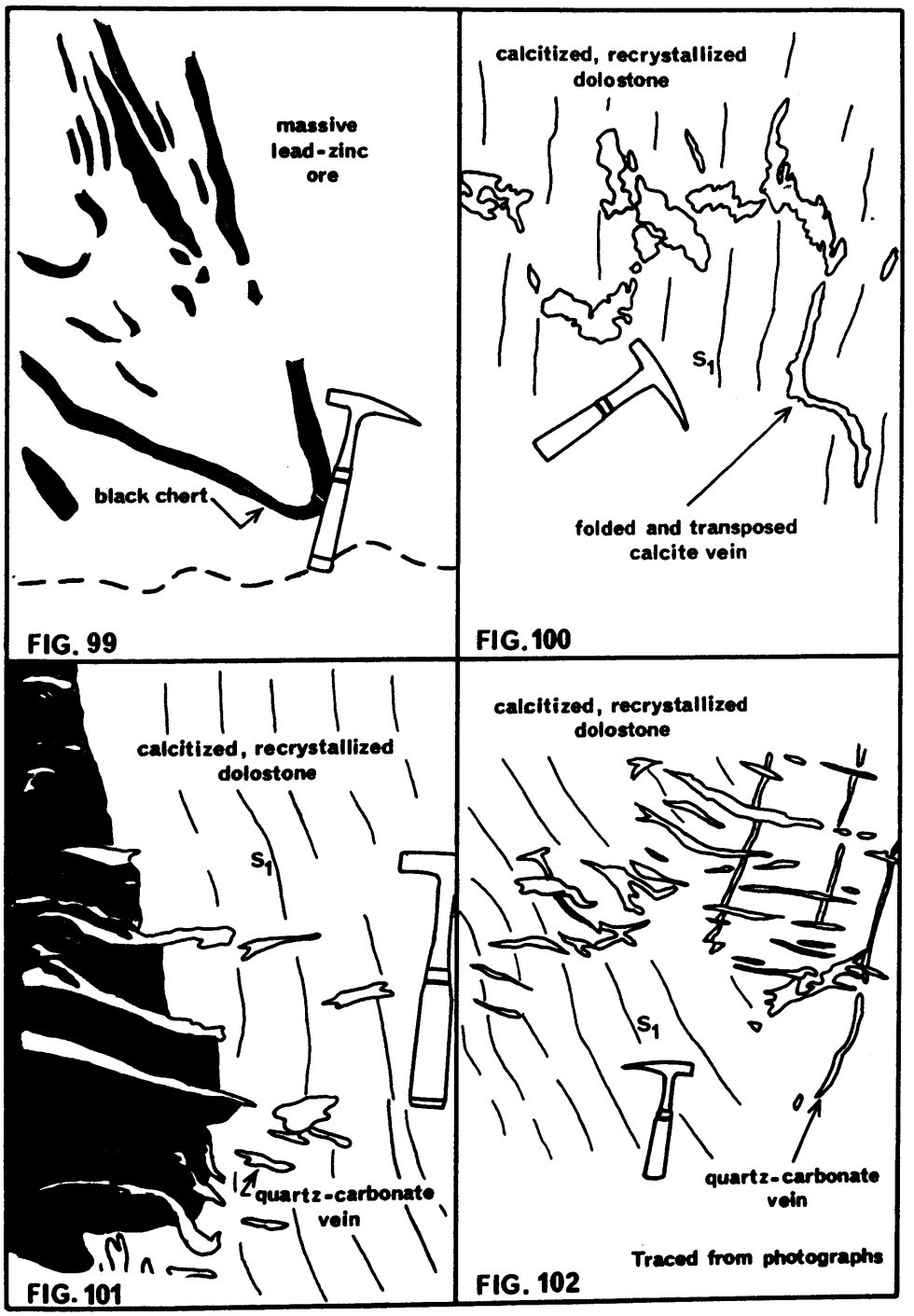

Fig. 99
Folded chert bands in massive lead-zinc ore; the ore shows deformation and recovery textures.
Fig. 100
Calcite vein (with minor galena) folded and transposed by the S_1 cleavage.
Fig. 101
Unmineralized, en echelon, quartz-carbonate veins in a large dolostone clast. The veins are perpendicular to the S_1 cleavage, which they cut outside the clast.
Fig. 102
Unmineralized, en echelon, quartz-carbonate veins which post-date the S_1 cleavage. The vein zone cuts the cleavage at a large angle.
The hammer is 31cm long.

stages of recovery and primary recrystallization. These range from incipient sub-grains, through equigranular aggregates of sub-grains in which the elongate grain boundaries can still be recognized, into equigranular aggregates in which the original grain boundaries have been completely destroyed. These last aggregates have probably formed by syntectonic recovery, to give polygonal aggregates of new grains which are the size of the sub-grains from which they formed (i.e. foam texture, Fig. 94; Stanton, 1972). The origin of elongated grains with smooth boundaries is less obvious (Fig. 95); these may be grains which have partly recrystallized, but which have inherited part of the original deformational fabric (Stanton and Willey, 1972). This origin, rather than a simple deformational origin of the elongation, is indicated by the smooth grain boundaries, by the lack of both sub-grains and evidence for internal strain, and by the presence of aggregates of elongated galena and bornite grains, with smooth, cuspate contacts, in which the galena cleavage is undeformed (Fig. 96).

Other examples of galena-rich ore lack elongated grains, and the galena forms mosaics of equi-dimensional or irregular grain size, in which the grains have smooth, curving boundaries, and in which sub-grains are absent. A variety of this texture, in which incipient sub-grains can occur, is typical of more sphalerite-rich ore. The sphalerite grains are most commonly irregular, and consist of undeformed, or bent, growth twins and rarer deformation twins (some of which can be recognized as single, broken grains), although sphalerite with smooth, curving boundaries can occur. Tennantite grains are even more commonly irregular in form, and pyrite is euhedral, or displays cataclastic textures, in all specimens. The galena, and possibly some of the sphalerite and tennantite grains with smooth, curving boundaries, are considered to show normal grain growth, without attainment of complete equilibrium (Stanton, 1972). These textures, the paucity of deformation twinning in sphalerite, and the lack of recovery of sphalerite grains in much of the ore, indicate (1) low temperatures of deformation and recovery, at less than greenschist facies conditions (Mills, 1976; McClay and Atkinson, 1977), and (2) the ductile nature of the galena matrix, relative to inclusions of sphalerite. Complete equilibrium, in which grain boundaries are

straight and 120° triple junctions are present (i.e. foam texture), has been reached in galena (and more rarely, enargite) in only a very few of the specimens examined (Fig. 98). The sequence of decreasing ductility shown by the sulphide minerals, i.e. (1) galena, bornite, (2) sphalerite, enargite, tennantite, and (3) pyrite, agrees with experimental studies and observations from other ore bodies (McDonald, 1967; Stanton and Willey, 1970; Cox et al., 1981).

Other features are diagnostic of the relative timing of deformation and sulphide mineralization; these include textures in which more ductile sulphide minerals occur in pressure shadows about less ductile sulphide minerals, indicating that mineralization was prior to, or synchronous with, development of the S_1 cleavage (Fig. 88). Other textures, which show that veinlets of sulphide minerals were present prior to the close of development of the S_1 cleavage, are common throughout the breccia core of the Tsumeb pipe (Figs. 91, 92). An extensive search failed to reveal a single example of hypogene sulphide minerals which mineralize, or cut, the S_1 cleavage (although this impression can be obtained from hand specimens of the samples illustrated in Figures 91 and 92; e.g. see Figure 23). Sulphide minerals and the stylolitic cleavage are closely associated because both are confined to the matrix and not to the clasts of the breccia. Also, many stylolites probably formed at the contact between sulphide minerals and grains, or small clasts, of calcite. The concentration of ore minerals in later stylolites has been recorded from many types of ore deposit (e.g. Mississippi Valley type; Park and Schot, 1968).

Most galena, tennantite and quartz crystals that occur in vugs are at least slightly deformed, although some crystals retain their original shape. Quartz crystals show basal slip. Deformed crystals of galena show anomalous inter-facial angles, and curved faces, and single crystals now consist of multiple grains, the smoothly curving contacts of which can be observed on single crystal faces (Fig. 93). The vugs which contain the crystals are elongated parallel to the S_1 structural surface, and vugs are open and least elongated, and vug crystals are only slightly deformed, where the S_1 cleavage is least

obvious; no hypogene vugs cut the S_1 cleavage. Most vugs observed during the present study were in silicified dolostone (but not only in the silicified zone of the pipe), and no vugs were seen in dolostone that has been extensively calcitized and recrystallized. Vug-filling sulphide minerals, which constitute a negligible proportion of the sulphide ore, are the only sulphide minerals which might have formed during the waning stages of deformation. However, there is no process known to the writer by which single crystals (and single crystal faces) could have become aggregates of grains unless they were strained. This could not have occurred in open cavities, because unfilled cavities could not have remained open during deformation and diagenesis under the conditions indicated at Tsumeb (unless the depth of burial has been greatly overestimated; Chapter 3.7.11). The vugs must have been filled when deformation occurred, and the crystallized form of vug-filling crystals could have survived deformation in areas of low differential strain (e.g. the subhedral form of galena crystals, enclosed in calcite, has been retained at one locality elsewhere in the pipe; Fig. 50). There is no evidence for the nature of the material which filled the vugs; however, the crystals would have been subjected to differential strain even in fluid-filled vugs, because the crystals were attached to vug walls which underwent differential strain. The volumetrically-insignificant sulphide minerals which fill vugs might therefore have pre-dated deformation, as might all sulphide minerals in the ore body, and there is no unequivocal evidence for syntectonic mineralization.

Hydrothermally altered rock of the silicified and calcitized zones of the Tsumeb pipe has been over-printed by the S_1 cleavage, and clasts are oriented parallel to this surface (Chapter 3.7.2). This is important evidence for extensive hydrothermal activity prior to the close of development of the S_1 cleavage. Mineralized calcite veins and quartz veins of cavity-filling origin are folded and transposed by the S_1 cleavage (Fig. 100), and no veins of this type cut the cleavage. Many veins of quartz, calcite and sulphide minerals which now appear parallel to the S_1 structural direction are deformed in the S_1 surface (e.g. Fig. 43), and probably formed parallel to the marginal fracture zone, as the result of renewed movement on this zone

during the mineralizing event (Chapter 3.5.1, Fig. 53). These veins were flattened during the D_1 deformation and, like the northern and southern margins of the pipe, are now sub-parallel to S_1 (Fig. 109b).

It is concluded that hydrothermal alteration and hypogene sulphide mineralization of the Tsumeb pipe occurred prior to the close of development of the S_1 cleavage, and therefore prior to the close of F_1 folding. Although this hydrothermal event might have occurred during the early stages of folding, it is equally possible that it occurred during an event prior to, and unrelated to, deformation of the enclosing Otavi Group rocks. Metamorphism of the ore body, if it occurred, did not reach greenschist facies conditions.

3.7.4 Minor folds associated with the Tsumeb pipe

Most minor folds which occur within the Tsumeb pipe, and in its immediate vicinity, cannot be identified unequivocally as F_1 folds because no S_1 cleavage was observed during the present study in the few folds exposed below 26 level (Figs. 18, 103, 104; also Map 7 of Botha, 1960). However, the fold axes are sub-parallel to both the strike of the S_1 cleavage, and the elongation of the Tsumeb pipe in plan, and are probably F_1 folds. Most of the folds are moderately open and symmetrical in form.

Lombaard (1953) and Söhnge (1964, 1976) recorded an "ore body syncline" within the pipe below 18 level (i.e. below that part of the pipe considered here to be disrupted by thrusting). This fold is internal to the marginal fracture zone to at least 29 level (Fig. 18, 26 to 28 levels; Fig. 104). Söhnge (1964, 1976) considered that an anticline, which adjoins the "ore body syncline" to the south at some elevations, contains the "south vein" (i.e. the marginal ore body along the southern contact of the pipe), near or within its ruptured axial zone. Some workers suggested that this anticline and syncline controlled the later development of the ore body (e.g. Pennebaker, 1954). The "ore body syncline" occurs immediately interior to the western closure of the marginal ore zone at 19 and 20 levels (Lombaard,

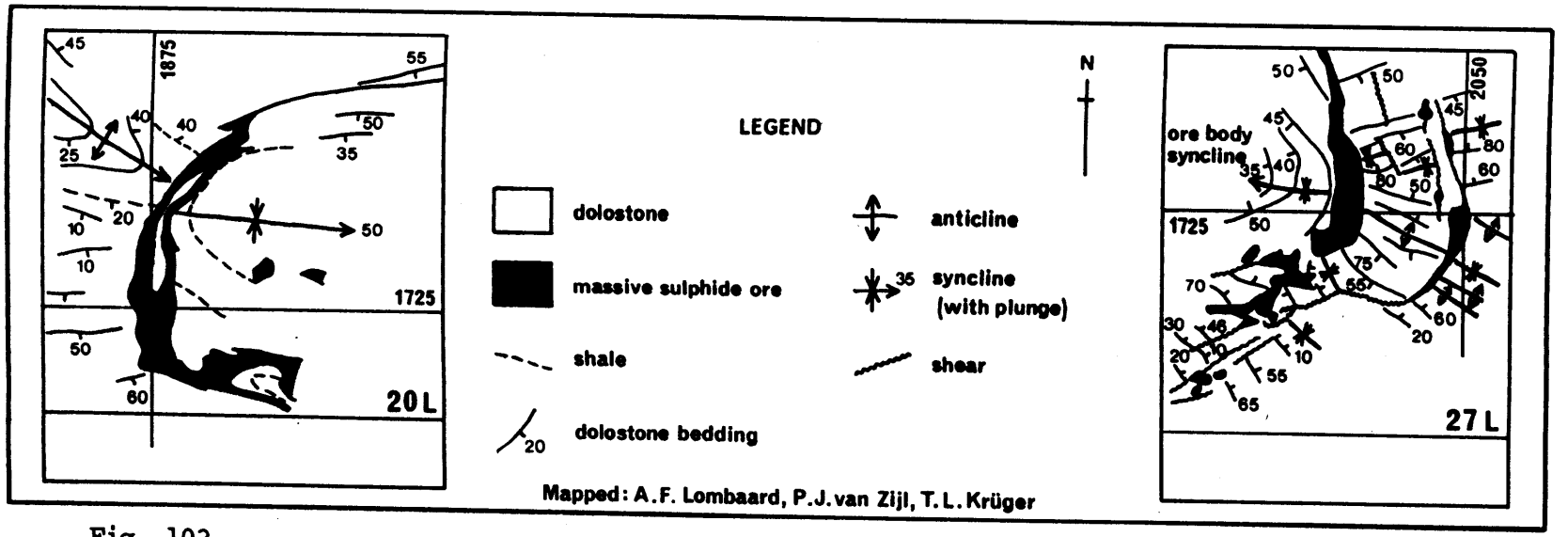

Fig. 103

Geological plan of steeply-dipping massive sulphide bodies of the marginal fracture zone, showing arcuate closures at the western and eastern ends of the Tsumeb pipe. The "ore body syncline" occurs within the pipe, and minor folds occur external to the ends of the pipe, but there is no continuity of fold axes across the marginal fracture zone.

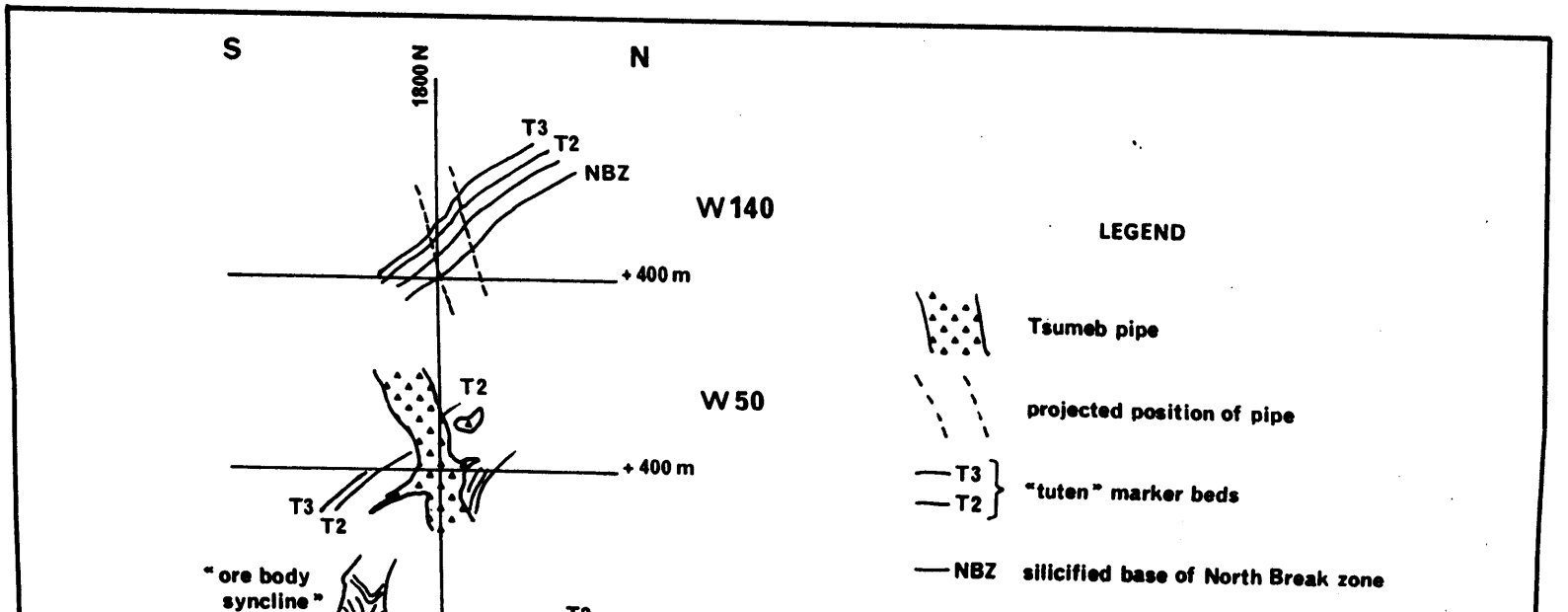

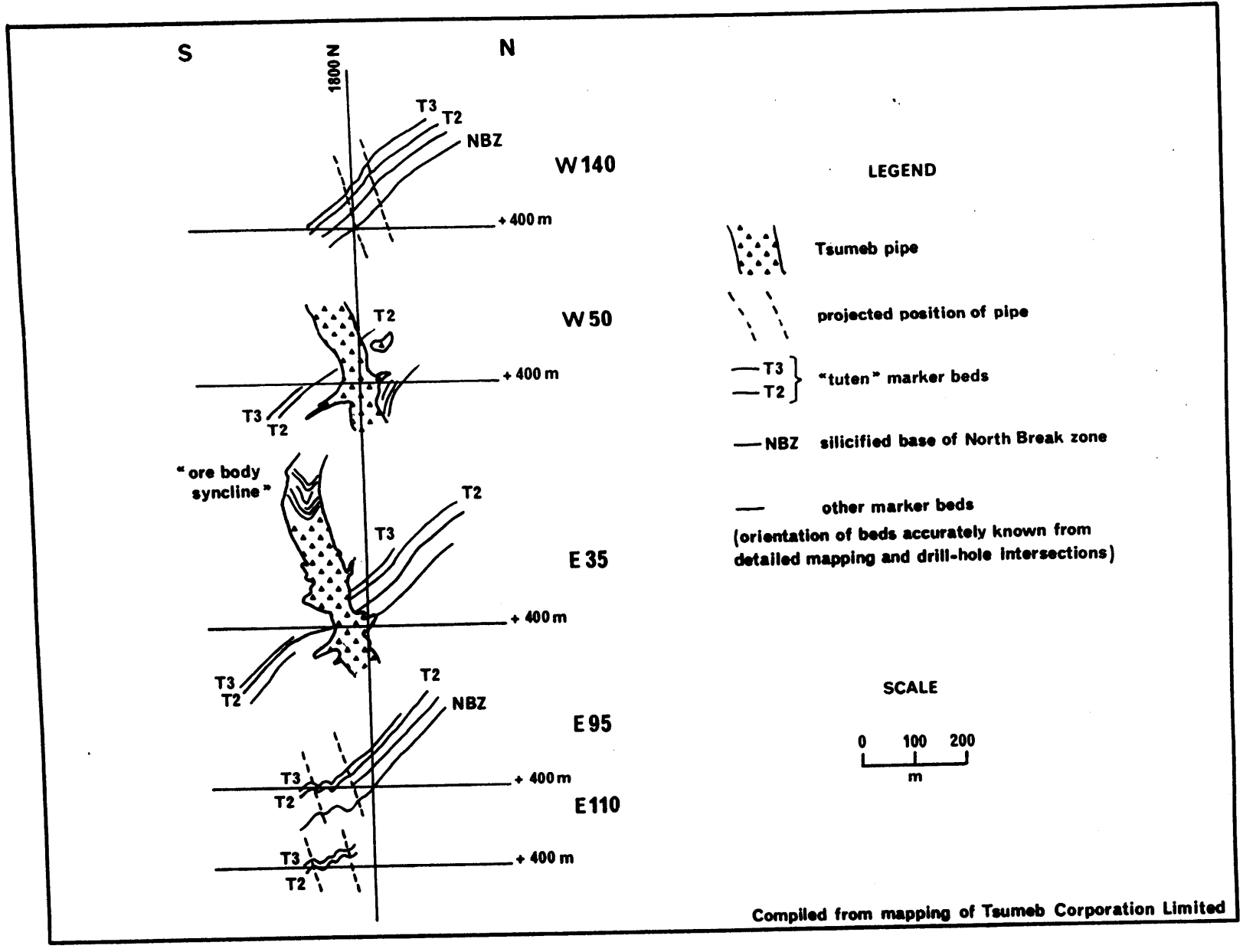

Fig. 104

Geological sections through the Tsumeb pipe, showing open folding adjacent to the pipe (e.g.E35), numerous minor folds outside the eastern end of the pipe (e.g.E95), and the "ore body syncline" within the pipe (E35).

1953), and an anticline with a similar trend (not that discussed above) occurs immediately to the west of the ore zone at 20 level (Fig. 103). Both folds terminate at the ore zone, which cuts the dolostone in both strike and dip. Lombaard (1953) concluded that the fold axes were displaced by the marginal fractures, and that this fracturing pre-dated ore deposition, but post-dated the main folding (a conclusion which is questioned in Chapter 3.7.5). Botha (1960) described a similar example at the eastern closure of the marginal ore zone in E79/28L (Fig. 18), and concluded that "the main ore locus wanders across the minor folds in a manner suggesting that the breccia forming the core could not have developed as a result of folding".

Minor folds of the above type, which occur immediately external to the eastern and western margins of the pipe, are relatively common and are best developed at the eastern end of the pipe. Previous mapping by the staff of Tsumeb Corporation Limited indicates that the axes of these folds are not parallel, but radiate outwards slightly from the eastern end of the pipe (e.g. E79/28L, Fig. 18; Fig. 103). This could not be confirmed during the present study, because of a lack of suitable exposures. Minor folds were observed outside of the eastern end of the pipe at only one location (ZERO/33L), and the profiles of these folds were unusual in that they approached the form of box folds, despite the moderately massive nature of the host dolostone.

3.7.5 Origin of the marginal fracture zone and minor folds

Hopwood (1975) concluded that massive sulphide ore on the pipe margins (Chapter 3.5.1) has replaced planar, S_1 foliation zones, which were subsequently re-folded by steeply-plunging F_2 folds to form closures at the eastern and western ends of the pipe. The structural relationships at the eastern and western ends of the pipe, described above, are not consistent with this origin, and no important F_2 event is recognized. This origin is also inconsistent with the strongly cross-cutting nature of the pipe below 19 level, relative to bedding in adjoining rocks, and the relatively simple structure of the host dolostone (demonstrated in plans and sections compiled by

A. Günzel, subsequent to the study of Hopwood, 1975; Figs. 19, 20). Further evidence is provided by the S_1 cleavage. This cleavage is sub-parallel to the marginal fracture zone, including its contained ore and sandstone, in the central part of the pipe (i.e. away from the ends of the pipe). However, it maintains the same strike at the ends of the pipe, near its intersection with the marginal fracture zone, and the cleavage has therefore not been folded by an F_2 event. An alternative origin for the marginal fracture zone must therefore be considered.

Other evidence for timing of the marginal fracture zone, relative to D_1 deformation, appears to be contradictory. Lombaard (1953) concluded that fracture formation post-dated major folding because he considered that the marginal fractures displaced minor folds (Chapter 3.7.4). However, there is evidence that the fractures formed prior to the close of the D_1 deformational event because: (1) massive sulphide ore of the marginal fracture zone is deformed, and hydrothermally altered rock in the marginal fracture zone, and the same rock and minor sulphide veinlets in the core of the pipe, predate the close of formation of the S_1 cleavage, (2) the marginal fracture zone defines the shape of the Tsumeb pipe, which in turn shows a systematic geometrical relationship to structural features, consistent with deformation of the pipe during the D_1 deformational event (Chapter 3.7.1), and (3) the fractures are filled with sandstone, consistent with an origin synchronous with sedimentation within the Tsumeb pipe.

The apparent contradiction discussed above can be explained by the contrasting deformational mechanisms which operated interior to, and outside, the marginal fracture zone of the pipe. The above evidence, and the lack of any obvious geometrical relationship between F_1 folding and the closures at the end of the pipe, indicate that the marginal fracture zone formed prior to D_1 deformation, during an unrelated event (Figs. 109a, 110a). The S_1 cleavage is rare in the dolostone which hosts the pipe, and is only intense and extensively developed within the Tsumeb pipe itself. Shortening occurred perpendicular to the cleavage, and to the present elongation of the pipe, and as a result the breccia body of the pipe core was affected by

pressure solution and intra-granular deformation processes during the development of the S_1 cleavage. Bedded dolostone internal to the marginal fracture zone, and the dolostone sequence external to the marginal fracture zone, were folded by a mechanism of flexural slip and buckling, and minor folds formed at the ends of the pipe to accommodate strain across the pipe structure (Fig. 109b). The angle of intersection between the Tsumeb pipe and bedding in the enclosing dolostone is consistent with rotation of the pipe, during formation of the Tsumeb syncline by a process of flexural slip folding (Fig. 19, 110b). The marginal fracture zone and its contained sulphide ore acted as a major structural discontinuity during folding, so that there is no correspondence between fold axes on either side of the marginal fracture zone. Söhnge (1976) suggested a similar origin, in which the minor folds were localized by a pre-existing sandstone body, but he considered the pipe breccia to have formed during deformation.

It can be concluded from the above that the fractures which define the margin of the Tsumeb pipe formed subsequent to lithification of the dolostone breccia core of the pipe and its siltstone matrix, but prior to deposition of sandstone within the pipe and subsequent deformation. The source of the sandstone is interpreted as the base of the Mulden Group (Chapter 6.1.1) and, if this is accepted, most fracturing occurred at depths of less than a kilometre. Most fractures are at, or a few metres outside, the contact between the breccia pipe and the dolostone wall rock, although parallel fractures occur external to these contact fractures in the upper part of the pipe (Figs. 18, 20, 31-32, 36, 57). The marginal fractures are interrupted in at least one locality where they pass through a manto fracture, and these two types of fracture may have a related origin (Chapter 3.5.3). The mechanism for the fracturing is not obvious, but similar fractures occur at the margins of breccia pipes formed by karsting and solution collapse in geologically young, undeformed sedimentary rocks (Chapter 6.1.5). A possible origin is by subsidence and collapse of the unsupported breccia column as the result of rock dissolution at depth (Chapter 6.1.2).

3.7.6 Strain across the Tsumeb pipe caused by F_1 folding

The total strain across the pipe breccia caused by F_1 folding is difficult to determine because of the inhomogeneous nature of the strain, and the paucity of suitable strain markers. Folded veins of sulphide minerals within the matrix of the dark dolostone breccia, and folded calcite veins within calcitized breccia, indicate the presence of compressional strains as high as 65 per cent, measured perpendicular to the S_1 cleavage (e.g. Figs. 23, 100). This is similar to the value indicated by the divergence of the pressure solution cleavage around undeformed dolostone blocks in calcitized breccia (e.g. Fig. 37). Estimates of the strain in breccia which contains the stylolitic cleavage, determined from the sum of the widths of individual stylolites (but ignoring intra-granular deformation), range from less than 30 per cent, to a maximum of 50 per cent (the latter in rocks which contain an average of 2-5 stylolites/cm). The profile of the ore body syncline indicates 50 per cent strain, if the origin proposed here for this fold is accepted.

Total strain across the pipe can also be approximated by assuming that the pipe had a circular cross-section prior to deformation. Estimates range from 45-65 per cent bulk strain, depending on the rock type and the deformation mechanism. Values of 45 per cent and 55 per cent are typical of the dark dolostone breccia and silicified breccia, and the calcitized breccia, respectively, if it is assumed that material dissolved during formation of cleavage was redeposited within the pipe structure. These values are 60 per cent and 65 per cent if a completely open system is assumed. Petrographic evidence indicates that the calcitized breccia (at least) may have behaved as a partly open system, as has been proposed elsewhere for cleavage formation in sedimentary carbonate rocks (Geiser and Sansone, 1981). The best estimate from all of the above evidence is that an average compressional strain of 55 per cent occurred across the pipe (c.f. 22 per cent across the Tsumeb syncline, estimated from the fold profile).

3.7.7 Thrusting in zone T5

The reversal in plunge of the Tsumeb pipe that occurs from above 35 level, to 37 level, is associated with a zone of reverse faulting, parallel to the bedding of the enclosing dolostone (Hughes, 1977; Figs. 19, 105a). This interval was only accessible down to 35 level during the present study. The pipe retains its 110° elongation from where it is first intersected by the fault zone above 1 s.l./35L, to below 35 level (Fig. 105b). The northern boundary of the pipe becomes progressively straighter in plan, parallel to the strike of the fault zone, and the western end of the pipe becomes increasingly attenuated with depth. These observations are consistent with an origin for the faulting subsequent to deformation of the pipe (i.e. subsequent to the pipe attaining its elongated form). Other evidence for this origin is proposed below.

The main surface of movement within the fault zone has a true width of at least three metres, and an average of three, well-defined fault surfaces occur over this width (Fig. 105a). The fault surfaces are not parallel, but converge in plan and section (Fig. 105c). Fracturing occurs in the footwall of at least one fault, where it occurs in dolostone, but no breccia which resembles the pipe breccia is present. At least one further, isolated fault surface occurs a few metres above this, on 2 s.l./35L (Fig. 105a). The fault surfaces can be recognized within larger, massive sulphide bodies, and form one or both contacts of such bodies in places (Figs. 105c,d,e), but most fault surfaces are not obvious where they are confined to the bedding surface of dolostone outside the pipe. Parallel, slickensided fault surfaces occur within the large calcite body at 35 level, and these are parallel to, and immediately overlie, the main zone of reverse faulting. It is possible that the fault zone is even wider than described above, as the base of the zone might not have been observed, because of the distribution of mine openings and lack of access below 35 level. The fault surfaces on 2 s.l./35L have a strike of 099° and dip 50°S, parallel to bedding (Fig. 89g). Geological sections constructed through the ore body indicate that the average dip is closer to 42° between 34 and 36 levels. The fault zone forms much of the northern

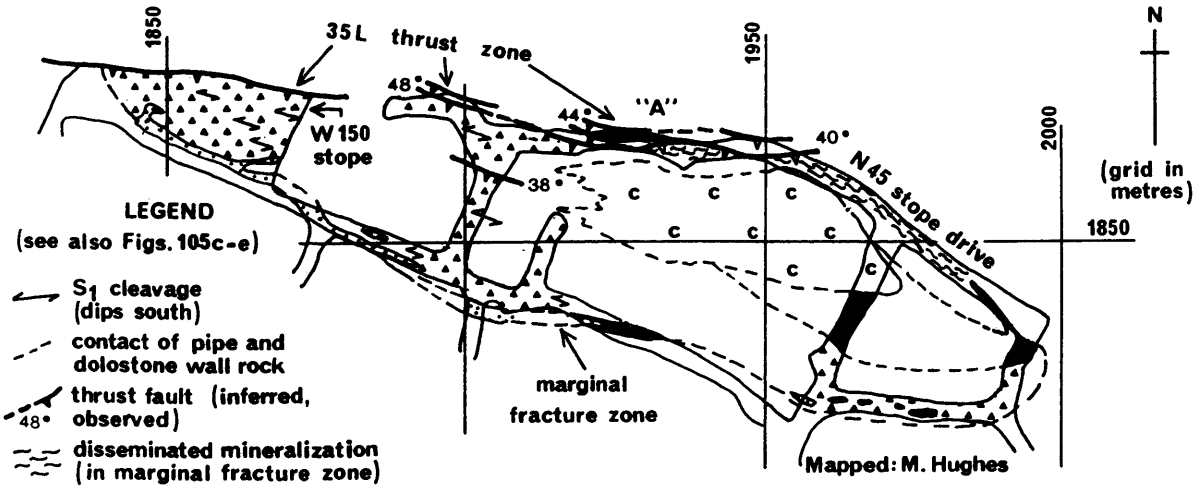

Fig. 105a
Geological plan showing how the Tsumeb pipe (including its marginal fracture zone in N45 stope drive) is truncated by the 35L thrust zone. Locality: W150 stope and no. 2 sub-level, 35 level (+163m).

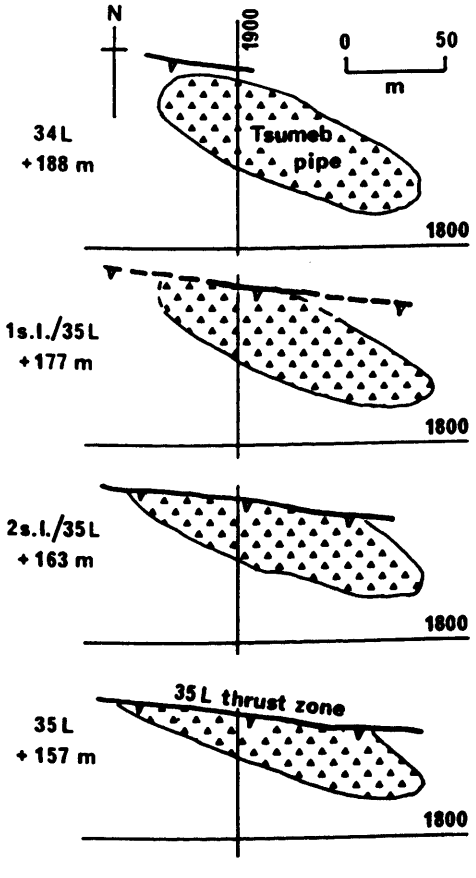

FIG. 105b

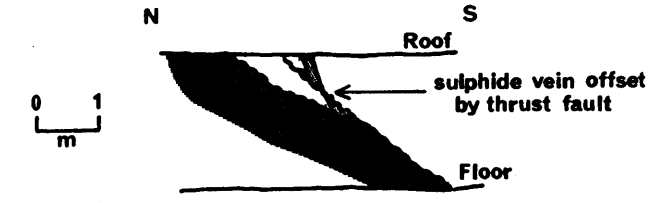

FIG. 105c

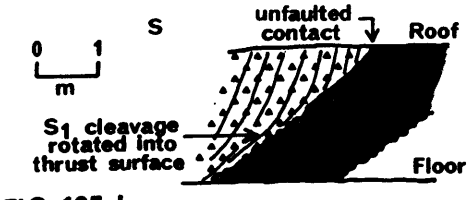

FIG. 105d

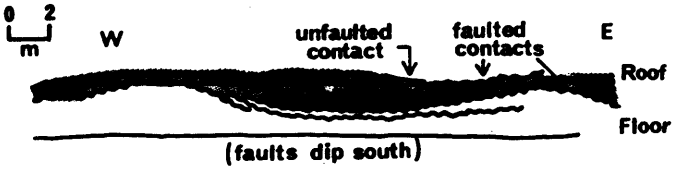

FIG. 105e

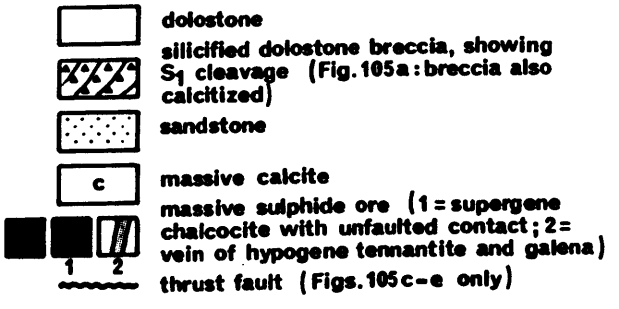

Fig. 105b
Plan view of the Tsumeb pipe at different elevations, showing how the Tsumeb pipe is increasingly truncated by the 35L thrust zone with increasing depth.

Figs. 105c-e
Faulted and unfaulted contacts of massive ore: (c) North stope/35L, +160m, central part of the northern contact of the pipe (near "A", Fig. 105a). Bifurcating faults offset ore veins. (d) same locality but farther west; fault, both within the ore and on its contact, which rotates the S_1 cleavage. (e) N45 stope drive in Fig. 105a, near "A"; the upper contact of the massive ore body is unfaulted throughout much of this area.

margin of the ore body to approximately 36 level, below which its dip, interpreted from drill hole data, flattens to a minimum of 21° above 37 level. The fault zone probably passes through the ore body between 36 and 37 levels (which were not accessible during the present study), and passes out of the southern boundary of the ore body above 37 level (Fig. 19).

Slickensides which occur on fault surfaces at 2 s.l./35L have a trend of 158° and plunge 46°S (Fig. 89g), parallel to the offset in the plunge of the pipe between 30 and 36 levels (Chapter 3.7.1; Fig. 90). Reverse movement is indicated where the surfaces offset steeply-dipping massive sulphide bodies and cause drag on the S_1 cleavage. Sulphide veins up to 10 cm thick, within the marginal fracture zone, are off-set by as much as 30 cm within the plane of individual fault surfaces (Fig. 105c), and the total displacement of the pipe is 100 m (measured parallel to bedding). Hypogene copper ore within the thrust zone (now extensively replaced by supergene sulphide minerals) has a cataclastic texture, but it was impossible to obtain suitable samples of galena to determine if thrusting post-dated recovery of galena, subsequent to its deformation during F_1 folding. The S_1 cleavage has been rotated into individual fault surfaces within the main fault zone, and the dip of the cleavage decreases by at least twenty degrees adjacent to such faults (Fig. 105d). Clasts of calcitized dolostone within the breccia body show extreme flattening in the south-dipping S_1 surface.

It can be concluded that reverse faulting in zone T5 post-dates sulphide mineralization and the subsequent S_1 cleavage (and therefore the pipe structure).

3.7.8. Thrusting in zone T7

The shape of the Tsumeb ore body above 19 level is controlled by a number of zones of thrust faulting (Fig. 19). These include, in order of increasing depth:

(1) The Hanging Wall thrust, or "vein"; this vein, classed as a thrust fault by Stahl (1925), is concordant to bedding, possibly

because the marginal fracture zone of the pipe has been rotated (i.e. dragged) into a thrust surface (see below). The thrust surface may correspond to an unmineralized bedding fault observed at the base of the southern face of the Tsumeb open pit during the present study. The bedding in rocks which underlie this fault intersects the fault plane at a large angle.

(2) The Open Pit thrust (or 85 m level thrust), which crops out in the northern face of the Tsumeb open pit.

(3) One or two unnamed thrust faults of probable minor significance, described by Stahl (1925) in the vicinity of 7 and 8 levels.

(4) The Grosse Überschiebung (also called the Grosse Steinbruchüberschiebung, or 6 level thrust). This major thrust zone crops out in the southern part of the old fill quarry, north-west of the Tsumeb open pit, where the thrust zone occurs in the uppermost limestone beds of zone T7 (Fig. 106). Stahl (1925) noted that this fault intersects the ore body at 6 level and remains in its footwall to below 8 level. Recent mapping by A. Lombaard (unpub.) confirmed the presence of a fault belonging to this thrust zone in the footwall of the ore body between 6 and 9 levels. It occurs within the ore zone at 9 and 10 levels, as indicated by heavily deformed dolomite layers within the sulphide ore and the undeformed nature of the footwall of the ore body at 10 level. It appears in the hanging wall of the ore body at 12 level.

(5) The 17 level thrust, indicated on old geological plans and sections, and described by Griffis (1949a & b, 1950). Its extension to the south of the ore body at depth is possibly indicated by shearing and quartz-carbonate veining in DDH 3169 (Fig. 19).

The existence and locations of these thrust faults, particularly (1), (2) and (4), are well established (Stahl, 1925). The descriptions of Stahl (1925) and Griffis (1950), when considered in conjunction with mapping by A. Lombaard, indicate that individual thrust zones consist of multiple planes of movement (as observed in the 35L thrust zone).

The upper levels of the mine are now inaccessible, and the ore body has been stoped out in the vicinity of the thrust faults. It was therefore impossible to determine the timing of thrusting, relative to formation of the pipe structure, mineralization, and F_1 folding. Early descriptions indicate that sandstone in the upper levels of the mine was sheared and displaced by thrust surfaces (Stahl, 1925; Schneiderhöhn, 1929). Sandstone was therefore present prior to the termination of thrusting, consistent with the pre-deformational origin of the pipe and its contained sedimentary rocks proposed here. Minor folding is closely associated with the thrust faults. Sub-zone D of zone T7, which corresponds to the immediate footwall of the Grosse Überschiebung, is internally deformed in outcrop (Land, 1977b). Folds within this stratigraphic sub-zone have axial planes parallel to bedding, and quartz-carbonate veining is abundant. Fold limbs are parallel, and fold closures are tightest, adjacent to the thrust plane, and thickening and thinning occur in limestone beds (Fig. 106). Fold axes plunge to the west, rather than the east, in this area. These folds contrast with those elsewhere, which are oblique to bedding and which fold more than one sub-zone. Folding also occurs in the footwall of the Grosse Überschiebung at depth within the Tsumeb mine (e.g. 12 to 14 levels).

The pipe has been displaced approximately 20 m on the Open Pit thrust, 250 m on the Grosse Überschiebung and 90 m on the 17 level thrust, measured parallel to bedding. The total known offset of the pipe in zone T7 is approximately 520 m. The displacement of the pipe by the thrust surfaces is not strictly co-planar with the rotation of the pipe interpreted to result from F_1 flexural slip folding (Chapter 3.7.1, Fig. 90). Above 12 level (the lowest point at which the Grosse Überschiebung intersects the pipe) the pipe is offset in a northerly direction. A similar situation exists between 30 and 36 levels, above the zone of reverse faulting in zone T5. This is not observed above the 17 level thrust, although the plunge of the pipe does not reverse until below 21 level. There is no evidence that the thrust zones are parallel to the axial planes of F_1 folds, as proposed by Hopwood (1975), nor even that thrusting occurred during the first (i.e. D_1) deformational event.

Schneiderhöhn (1929) considered that thrusting pre-dated deposition of the sulphide ore. However, Griffis (1949a, b) observed that the ore was cut by thrusts parallel to the dolomite bedding. He noted that earlier workers had explained the decrease in the volume of ore at the second, ninth, twelfth and seventeenth levels as the result of thrusting, which dislocated the ore and elongated the ore body. He recorded that sulphide ore is not localized on the thrusts, and suggested that considerable post-ore movement might have occurred on these surfaces. For example, a remnant of ore on 10 level is cut by a later fault with a 30 m displacement (Griffis, 1950); this is possibly a thrust fault which forms part of the Grosse Überschiebung thrust zone. Griffis (1949a, b) was undecided as to whether thrusts were primary controls of brecciation and ore deposition, or alternatively post-ore features. He subsequently adopted a model in which the thrusts were the unmineralized set of two, conjugate, shear directions (the mineralized fractures, interpreted here as the marginal fracture zone, formed the second set; Griffis, 1950).

The argument that thrusting occurred prior to mineralization has been based mostly on the supposedly undeformed nature of the ore within the thrust zones. Ore of the intermediate and lower levels of the mine, which is shown here to be deformed (Chapter 3.7.3), was also considered by many previous workers to be undeformed. Also, supergene sulphide enrichment was important in the upper levels of the mine, and this might have partly obliterated earlier deformational textures. The observations of Griffis (1949a & b, 1950), described above, indicate that at least some sulphide ore was displaced by later thrusts. B.H. Geier (pers comm., 1979) noted that "steel" galena is abundant in the vicinity of thrust faults in the upper levels of the mine, and considered that thrusting post-dated ore deposition (the term "steel" galena has been used by B.H. Geier in some unpublished reports to describe galena with a grain size of less than 17 μm). It is therefore possible that thrusting was a late event, that post-dated recovery of ore previously deformed during the D_1 event, but there is no direct evidence for this. Thrust faulting in zone T7 may therefore have occurred at the same time as reverse faulting in zone T5 (Fig. 110c). This is supported by the offset in the plunge of the pipe above the

Grosse Überschiebung thrust zone; this offset is parallel to a similar offset above the 35L thrust zone, and to slickensides on the surfaces of thrust faults within the 35L thrust zone (Chapter 3.7.7).

3.7.9 Relationship between the E2200 and Old Compound breccia bodies

Hughes (1977) tested the model proposed here, in which thrusting and F_1 folding post-date the formation of the breccia pipe, by considering the effect of such deformation on another breccia body, the Old Compound breccia, to the north-east of the Tsumeb pipe. The predicted position of this breccia at depth was found to correspond closely to that of the E2200 breccia (Figs. 107, 108). This latter body, intersected in holes drilled to the north-east of the Tsumeb pipe between 24 and 30 levels, has a plunge parallel to that of the Tsumeb pipe. The reconstruction is consistent with the Old Compound breccia and the E2200 breccia being a single body, which was deformed in the same manner as the Tsumeb pipe (a relationship that was previously unsuspected).

3.7.10 Other deformation

Numerous sets of en echelon, unmineralized, quartz-carbonate veins of unknown origin occur within the Tsumeb mine. The most common occurrences are fracture sets confined to large clasts, in which individual fractures are perpendicular to the S_1 cleavage, which they cut outside the boundaries of the clasts. An origin by shearing parallel to S_1 is therefore indicated (Fig. 101). These fracture sets differ from an earlier generation of sparsely mineralized, en echelon veins of similar appearance which pre-date S_1, and which are mostly confined to large clasts in the vicinity of the marginal fracture zone, to which they are probably genetically related. Large sets of unmineralized, en echelon, quartz-carbonate veins, are superimposed on both clasts and matrix, and cut S_1 at a large angle (Fig. 102). There is no evidence for the time of formation of these fractures relative to the thrusting event, although they might have formed at this time.

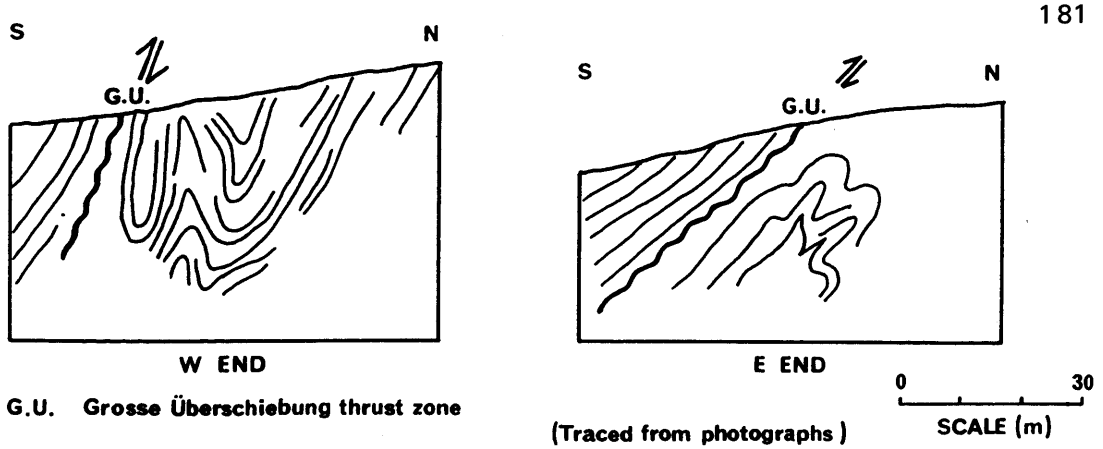

Fig. 106
Folding in footwall rocks of the Grosse Überschiebung thrust zone, Old fill quarry, Tsumeb (north-west of the Tsumeb open cut; Fig. 107). Dolostone beds have a constant thickness, but limestone beds are thickest in fold apices.

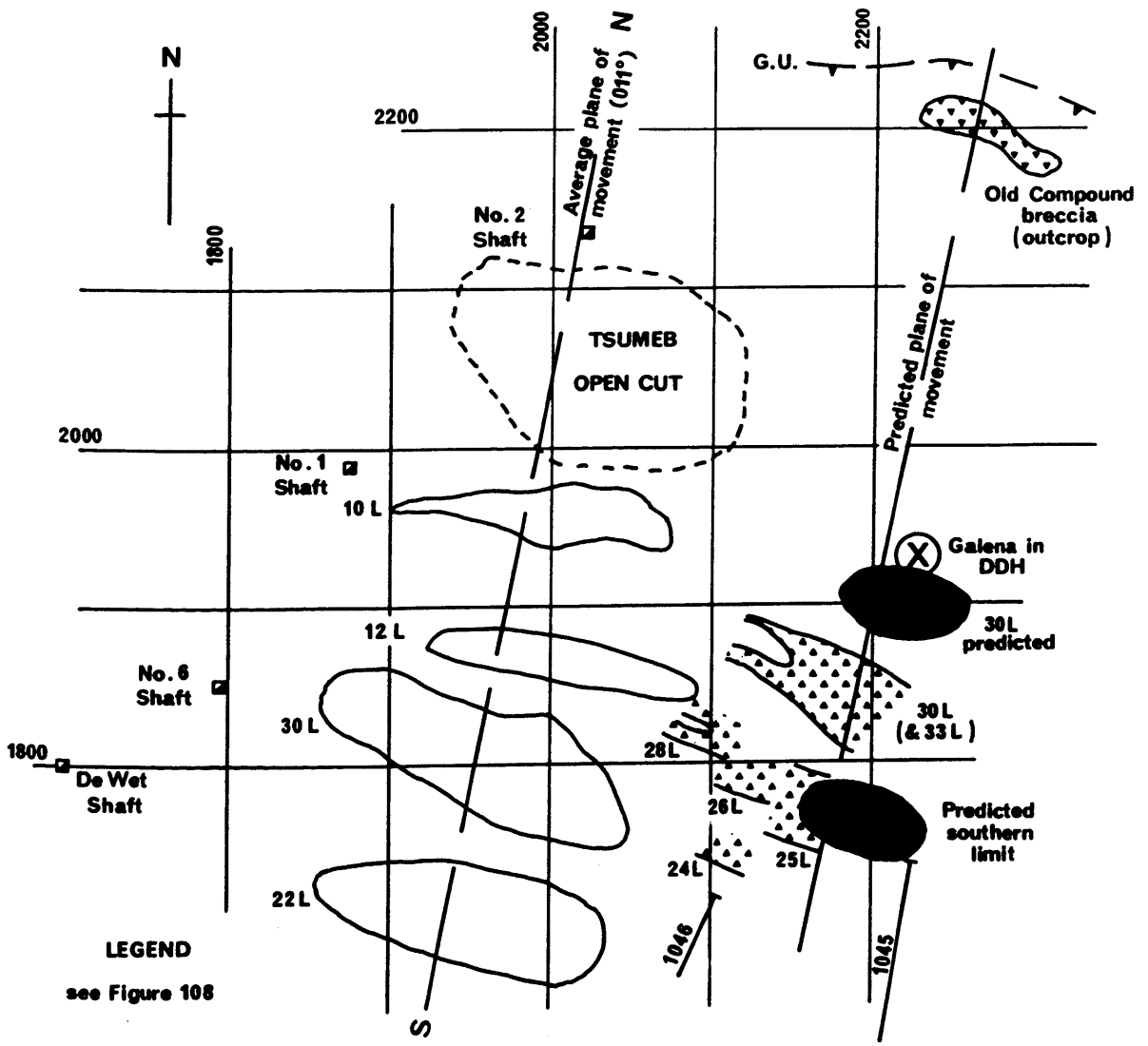

Fig. 107
Plan projection of the Tsumeb pipe, E2200 breccia body, and Old Compound breccia body, showing that the latter two bodies may be a single body. The Old Compound breccia is assumed to have been folded and faulted in the manner proposed for the Tsumeb ore body, and its predicted position at depth coincides with the known position of the E2200 breccia body (see Fig. 108 for section N-S).

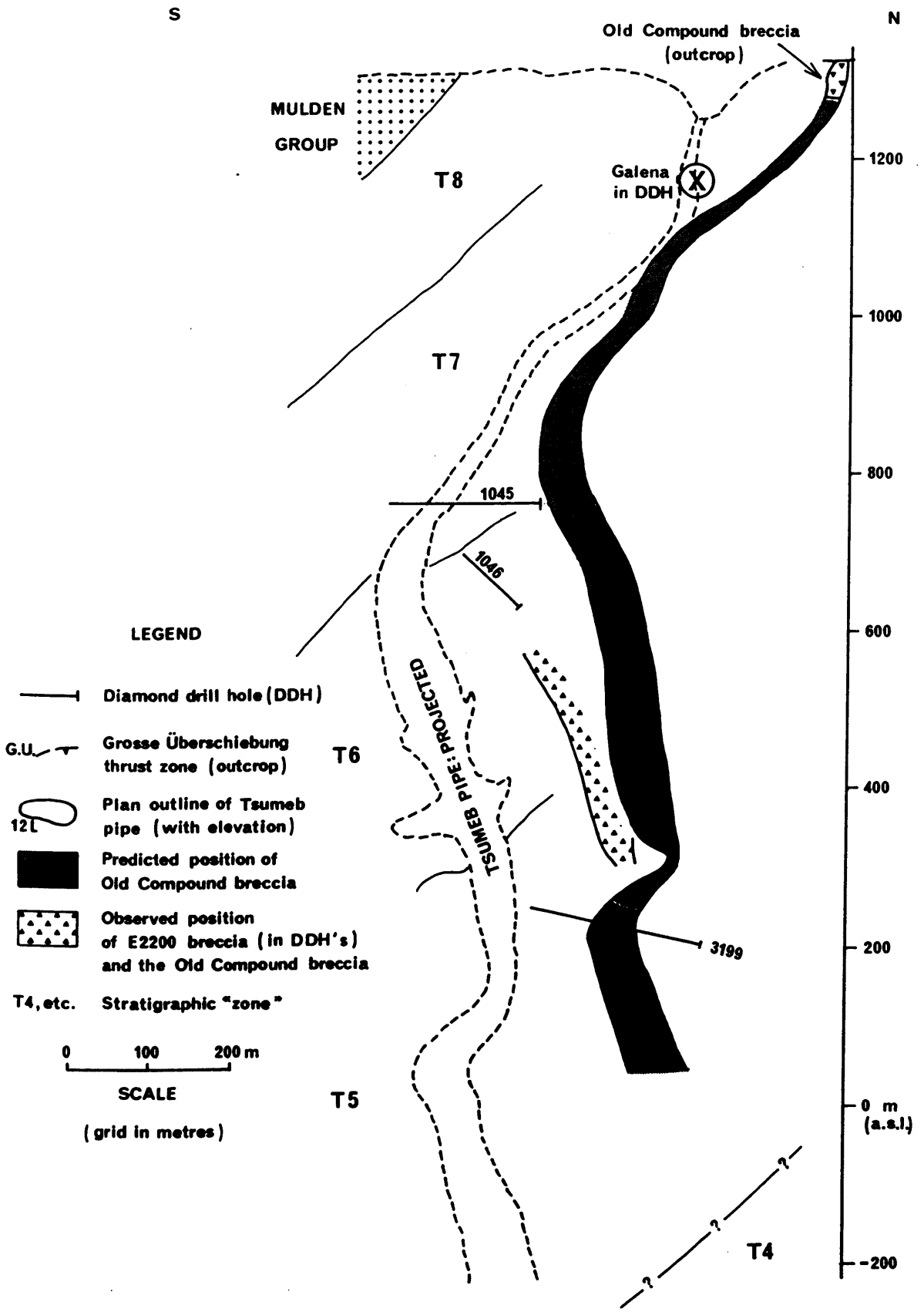

Fig. 108
Cross-section N-S of the Tsumeb pipe, E2200 breccia body, and Old Compound breccia body (see Fig. 107 for explanation).

There is evidence for a second, post-S_1, phase of folding near Tsumeb, particularly in the vicinity of the Tsumeb West fracture zone (Chapter 4.4.1). Rare, open folds with a widely spaced, axial planar cleavage (non-penetrative at hand specimen scale) trend at 055°, and the cleavage is sporadically, but more widely, distributed with strike 050°-065° and dip 70°N-80°S. Cleavage with a similar orientation post-dates the S_1 cleavage near Tsumeb West, and was observed at one locality within the Tsumeb pipe. However, the sporadic distribution of this cleavage and the rarity of associated folding makes the identification of a single, widespread folding event uncertain; any such event, if present, was of negligible intensity.

3.7.11 Metamorphism of Otavi Group and Mulden Group rocks

Otavi Group and Mulden Group rocks of the Owambo basin have undergone only diagenesis, to low grade (probably mostly very low grade) metamorphism (i.e. in the sense of Winkler, 1976). Rocks of the Mulden Group possibly show a systematic regional variation in metamorphic grade (although unequivocal mineral assemblages are absent), with the lowest grade (possibly diagenetically altered) rocks in the vicinity of Tsumeb and westwards, and higher grade rocks many tens of kilometres to the north and south. Greenschist facies assemblages (i.e. temperatures above approximately 320°C) occur only in the extreme south of the Otavi Mountain Land, and the biotite isograd is reached outside of the southern and western boundaries of the Owambo basin (Fig. 1; Clifford, 1967). Sedimentary carbonate rocks of the Otavi Group lack diagnostic mineral assemblages, although the presence throughout the Otavi Mountain Land of dolomite plus quartz and the absence of talc and tremolite, indicate that the metamorphism of these rocks was low grade (Winkler, 1976).

Mulden Group pelite, studied 150-300 km to the north and north-west of Tsumeb, contains three different metamorphic assemblages: (1) illite, chlorite, quartz, albite and, in places, smectite of probable later origin, (2) the first assemblage, plus microcline and pyrite, and (3) the second assemblage plus stilpnomelane (Clauer and Kröner, 1979). The Rb-Sr and K-Ar isotope systems in the rocks were isotopically re-set at 535 m.y. and 455 m.y., and Clauer and Kröner (1979) proposed two metamorphic events at these times, with temperatures between 250°C and 300°C and pressures of up to 2 kbar. The evidence advanced for this was: (1) illite occurs only as the high

temperature, 2M polymorph, indicating a minimum metamorphic temperature of 200°C, (2) the crystallinity index of illite is low (i.e. 3,5-4), (3) stilpnomelane is present (indicating temperatures of 200° - 300°C and a pressure of 2 kbar), (4) the Rb-Sr system in clay minerals is isotopically re-set (i.e. homogenized, indicating temperatures of 250°C), and (5) biotite is absent (indicating temperatures of less than 300°C). Clauer and Kröner (1979) also noted that stilpnomelane elsewhere in the world has formed at the limit between the zeolite facies and the prehnite-pumpellyite facies (i.e. at approximately 250°C).

Although Clauer and Kröner (1979) considered that the absence of biotite indicated an upper temperature limit of 300°C, biotite crystallization can possibly be delayed until higher temperatures (Winkler, 1976); however, the crystallinity index of illite, and the presence of stilpnomelane, confirm a temperature close to 250°C. The pressure is not well established by the data, but must have exceeded 1 kbar if a geothermal gradient of not more than 50°C/km was present in the Owambo basin (a realistic maximum for most epicontinental basins). A metamorphic temperature of approximately 250°C and a pressure in excess of 1 kbar is therefore strongly indicated for the Mulden Group, in the area north of the east-north-east trending basement ridge which existed between the Kamanjab inlier and Tsumeb (Fig. 1; Chapter 2.1).

Mulden Group sandstone which overlies the Kamanjab-Tsumeb basement ridge, to the south of the above area, contains widespread and moderately common detrital biotite. Unaltered, detrital biotite in the Tschudi Formation of the Tsumeb area is most commonly present as perfectly rounded cleavage flakes, and rounded, unaltered forms also occur in the discordant sandstone of the Tsumeb pipe (Botha, 1960). Biotite has also been recorded from Mulden Group sandstone immediately north of the Kamanjab inlier, and between the inlier and Tsumeb, but is absent (e.g. altered to chlorite) to the north and south of the basement ridge (Hedberg, 1979). The survival of a detrital mineral is not diagnostic of metamorphic conditions, but the systematic areal distribution of detrital biotite in a single rock type indicates that differences in metamorphic grade probably existed on a regional scale.

It also indicates that the lowest metamorphic grade (possibly even diagenetic conditions, i.e. below 200°C) occurred in Mulden Group sedimentary rocks which overlie the Kamanjab-Tsumeb basement ridge. The deformation and annealing textures in the Tsumeb ore are consistent with this conclusion (Chapter 3.7.3). The very low grade, or lack, of metamorphism in these rocks may have resulted from: (1) a lower geothermal gradient above the basement high (typical of most sedimentary basins), and (2) a lesser depth of burial of Mulden Group rocks because of reduced sedimentation above the basement ridge (Chapter 2.1).

The metamorphic grade of Mulden Group rocks probably increases southwards towards Kombat, in the southern Otavi Mountain Land, although this cannot be demonstrated conclusively (Fig. 3). The Kombat Formation of the Otavi Valley area consists of slate, a sericite-chlorite-quartz-feldspar rock, which lacks biotite. The phyllosilicate minerals are much coarser grained than in pelitic rocks further to the north, pyrite has altered partly to pyrrhotite (Chapter 4.4.5), and galena typically shows annealing textures in which grains are perfectly polygonal (these are rare at Tsumeb). These features may result partly from the more intense deformation (i.e. higher strain) in the southern Otavi Mountain Land, or the presence of larger volumes of fluid during metamorphism (Ferry, 1981), rather than from a higher grade of metamorphism. However, biotite appears in pelite immediately to the south of the Otavi Valley (Fig. 1), and the metamorphic grade of Mulden Group rocks at Kombat is probably equal or higher, therefore, than that of equivalent rocks north of the Kamanjab-Tsumeb basement ridge.

3.7.12 Timing of mineralization, deformation and metamorphism

The timing of mineralization, deformation and metamorphism can be established with reasonable certainty. Sedimentary carbonate rocks of the Otavi Group overlie volcanic rocks of the Nosib Group, which yield a U-Pb zircon age of 728 $\pm$ 40 m.y. (2σ) to the south of the Owambo Basin (Miller and Burger, 1983a). An important erosional break occurs at the top of the Tsumeb Subgroup in the Otavi Mountain Land,

below the Mulden Group contact (Chapter 6.1.4). Also, metamorphism and deformation of the Khomas Subgroup, the probable pelitic equivalent of the Tsumeb Subgroup, occurred prior to deposition of the Mulden Group along the western and southern margin of the Owambo basin (Frets, 1969). It is therefore highly probable that the Otavi Group underwent low grade metamorphism at this time, or diagenesis during subsequent uplift and erosion. The most probable cause of the 640 $\pm$ 200 m.y. (2σ) U-Pb whole rock isochron age obtained from these rocks during the present study is thought to be early diagenesis or dolomitization, but the possibility that this represents the above event cannot be completely excluded (Chapter 5.3.6).

Evidence is presented here that mineralization at Tsumeb pre-dated the first major deformational event which affected Otavi Group and Mulden Group rocks of the Otavi Mountain Land (or the close of this event). A U-Pb zircon age of 589 $\pm$ 50 m.y. (2σ) was obtained for a granitoid intrusion that post-dates the major phase of folding and metamorphism in the Kuiseb Formation, to the south of the Owambo basin (Miller and Burger, 1983b). This phase corresponds to the F_1 event in Mulden Group rocks of the south-western Owambo basin (and probably also the Tsumeb area). A similar age of 577 $\pm$ 20 m.y. was obtained for a granite which has intruded Mulden Group rocks farther to the west. These ages do not differ greatly from the Rb-Sr isochron age of 537 $\pm$ 7 m.y. obtained from metamorphosed Mulden Group rocks north-west of Tsumeb (Clauer and Kröner, 1979). Therefore, the best estimate of the age of Tsumeb mineralization, and of the subsequent D_1 event in the Tsumeb area, is that these occurred between 730 and 590 m.y. (the time of closure of the U-Pb system in zircons within granitoids which post-date the D_1 event).

3.7.13 Conclusions

The Otavi Group was deposited subsequent to 730 m.y., and the Tsumeb pipe formed, was mineralized and then deformed prior to approximately 590 m.y. The highest grade of metamorphism reached in the host rocks of the ore body, subsequent to ore deposition, was very low grade (e.g. 250°C), but it is possible that temperatures did not

exceed those of diagenesis (i.e. less than 200°C).

The marginal fracture zone of the Tsumeb pipe formed during sedimentation within the pipe structure, at depths of less than one kilometre, prior to burial, mineralization and deformation (Figs. 109a, 110a). The sedimentary rocks of the Tsumeb pipe, their hydrothermally altered equivalents, and the sulphide ore, were deformed by the first major phase of folding in the southern Owambo basin. The mineralizing event may have completely pre-dated this deformational event, and been unrelated to it. The deformation was inhomogeneous; massive and bedded dolostone deformed mostly by flexural slip, but the breccia pipe underwent a compressional strain of approximately 55 per cent perpendicular to a pressure solution cleavage (S_1), and intragranular deformation was important in hydrothermally altered rock. The Tsumeb pipe rotated relative to bedding during this F_1 folding, and minor folds formed at the eastern and western ends of the pipe (Figs. 109b, 110b).

The Tsumeb pipe was also deformed by thrusting, at least partly after formation of the S_1 cleavage (i.e. during the late stages of D_1 deformation, or during a later event). This, and the preceding folding, extended the length of the pipe, from 1300 m vertically above its probable base in zone T4, to more than 1600 m above its base (Fig. 110c).

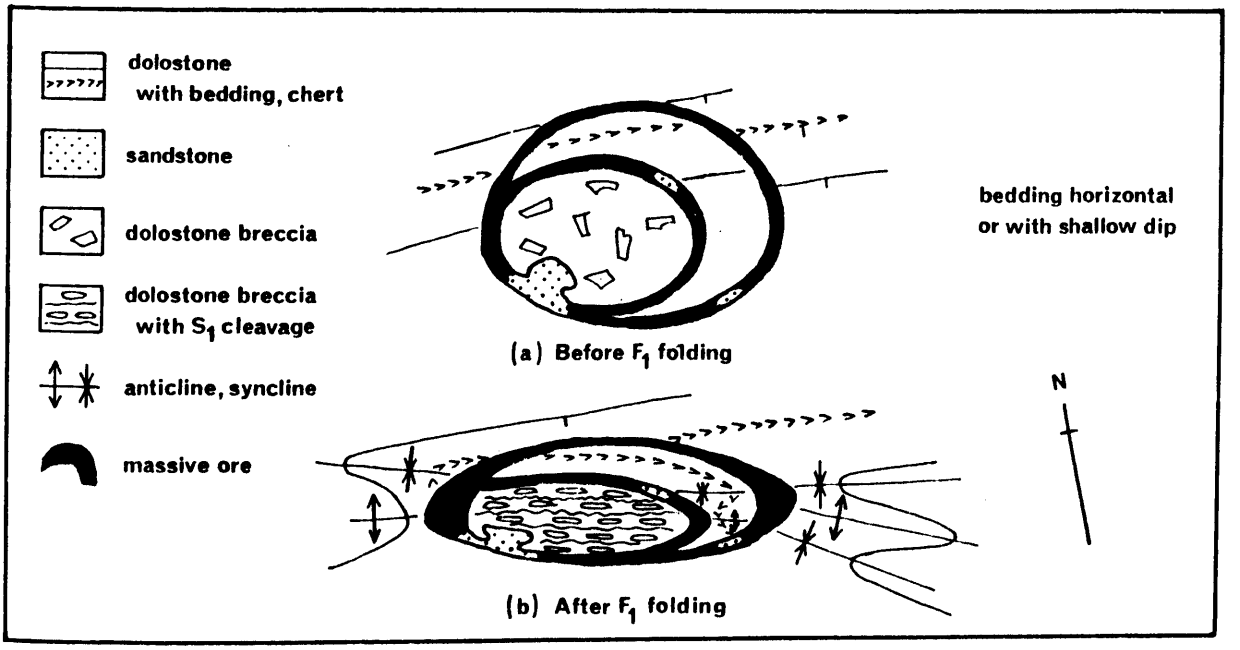

Fig. 109
Plan of the Tsumeb pipe, before and after F_1 folding. The pipe became elongated during the F_1 event, and the S_1 cleavage and minor folds were formed.

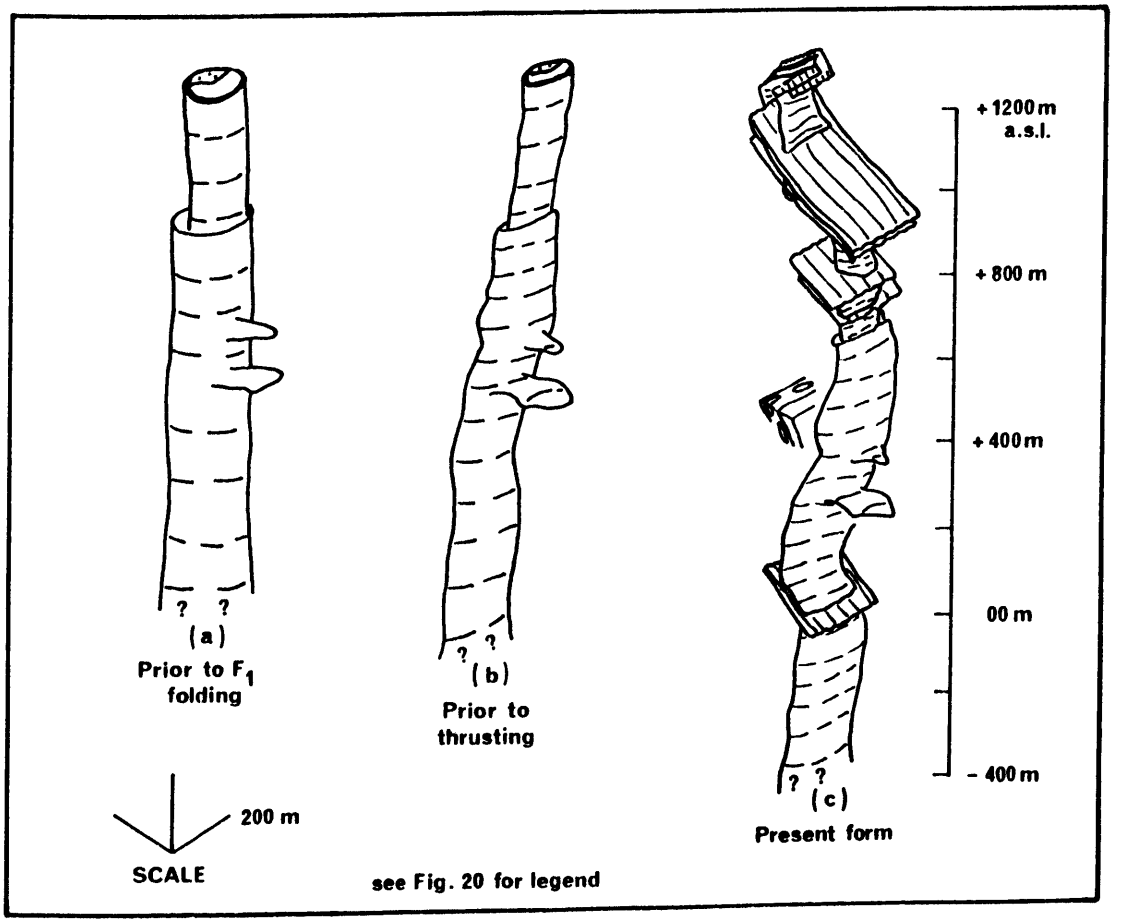

Fig. 110
Isometric projection of the Tsumeb pipe, before and after F_1 folding (a,b) and after thrusting (c).

CHAPTER FOUR

MINERALIZATION IN THE OTAVI MOUNTAIN LAND

Mineralization throughout the Otavi Mountain Land is examined and reviewed for comparison with the Tsumeb ore body, and to determine regional controls on the mineralizing event which formed the Tsumeb ore body. Comparisons are made with ore bodies elsewhere in Africa, and other continents. This chapter also provides the geological framework for the isotope studies of Chapter 5.

4.1 PREVIOUS STUDIES

The earliest descriptions of mines and prospects in the Otavi Mountain Land are those of Krusch (1911), Schneiderhöhn (1921, 1929) and Stahl (1926). These contain only brief descriptions of mineral occurrences other than Tsumeb. Later, general reviews of Otavi Mountain Land mineralization are contained in Schwellnus et al. (1944), Söhnge (1957, 1972), Callahan (1971), Thirion (1974) and Hopwood (1975). There have been few intensive studies of ore body structure and mineralization controls in mines other than Tsumeb. Mines studied in most detail are Abenab West (Verwoerd, 1957) and the Kombat group (Lombaard, 1973; Hopwood, 1975; Innes and Chaplin, in press, 1985). The localities of mines and prospects in the Otavi Mountain Land are shown in Figure 111a.

Controversies about the origin and structural history of the Tsumeb ore body have extended to other mines and prospects of the Otavi Mountain Land. Workers who studied mineralization controls in individual mines and prospects generally favoured shearing and fracturing, synchronous with, or subsequent to folding, as the mineralization control (Simpson, 1956; van Zyl, 1961a, b; Hälbich, 1967; Hopwood, 1975). Other workers were influenced by the distribution of transgressive sandstone ("pseudo-aplite") bodies,

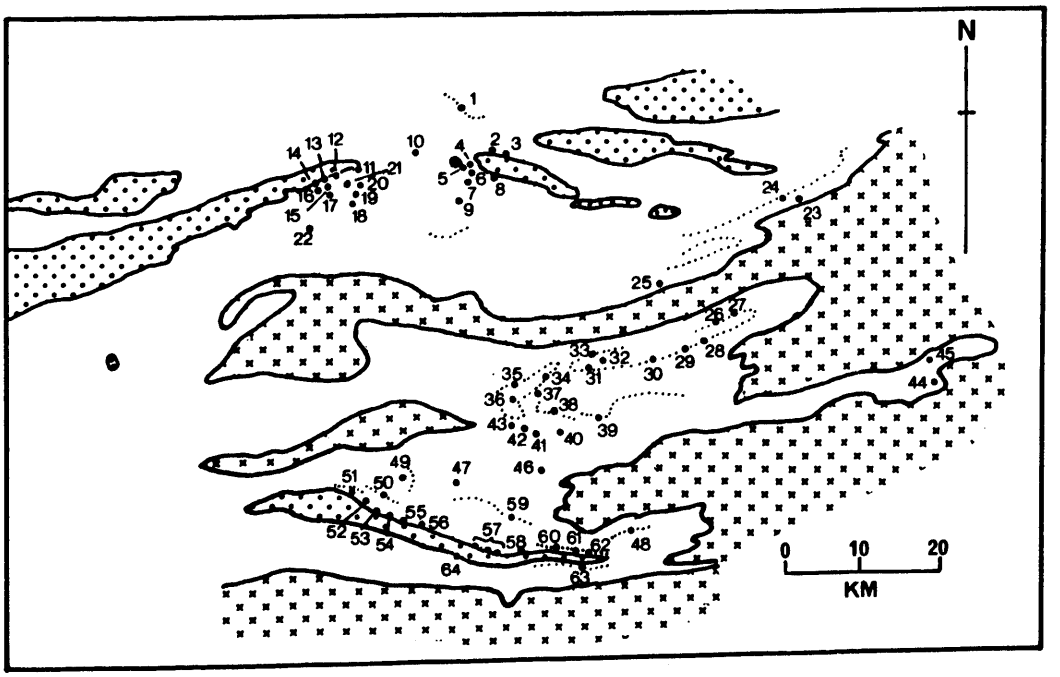

FIG. 111 (a) Mines and prospects of the Otavi Mountain Land

Mulden Group
Otavi Group
Nosib Group and pre-Damara Group
Strata-bound breccia, zone T4
Mine or prospect

2 Tsumeb
23 Abenab West
53 Kupferberg
3 Dairy Lead Prospect
31 Harasib Main
57 Kombat Group
4 Tsumeb West
44 Berg Aukas
(Asis West to Asis Ost)

(geology simplified from FIG. 111c)

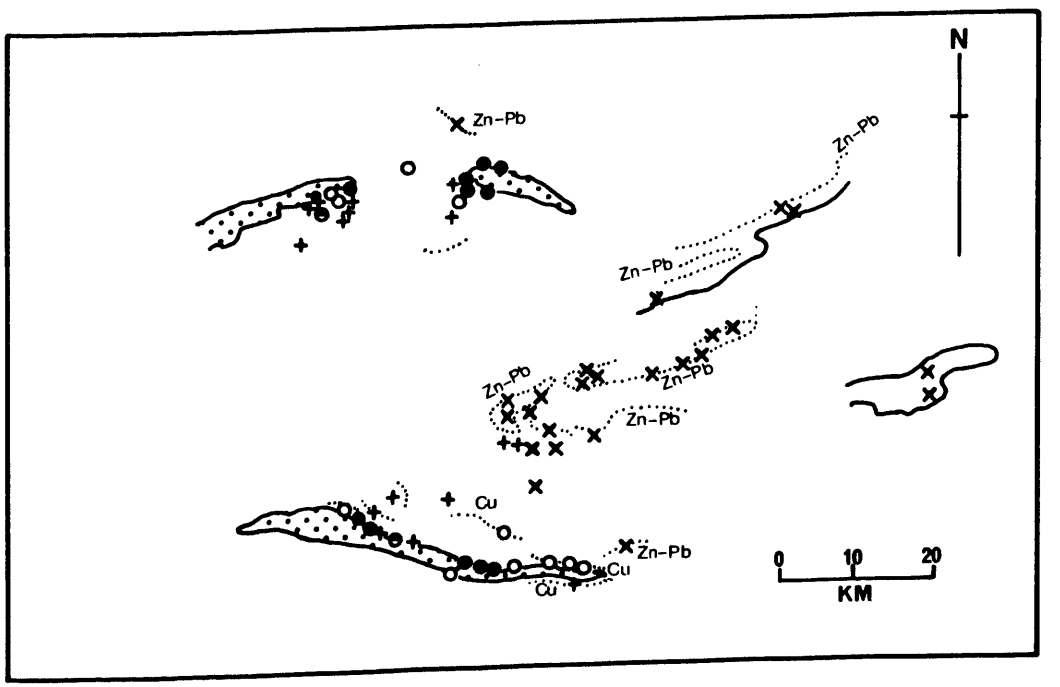

FIG. 111 (b) Mineralogical classification of mines and prospects

(I) Copper significant (± Pb, Zn)
- Tsumeb type (sensu stricto)
- Other: Cu major
- Other: Cu significant
- Tschudi type

(II) Zn-Pb
- Zn-Pb or Cu in strata-bound breccia
- Larger occurrences (mainly discordant breccia)

(III) + Unclassified

(minor geological detail included from Fig. 111a)

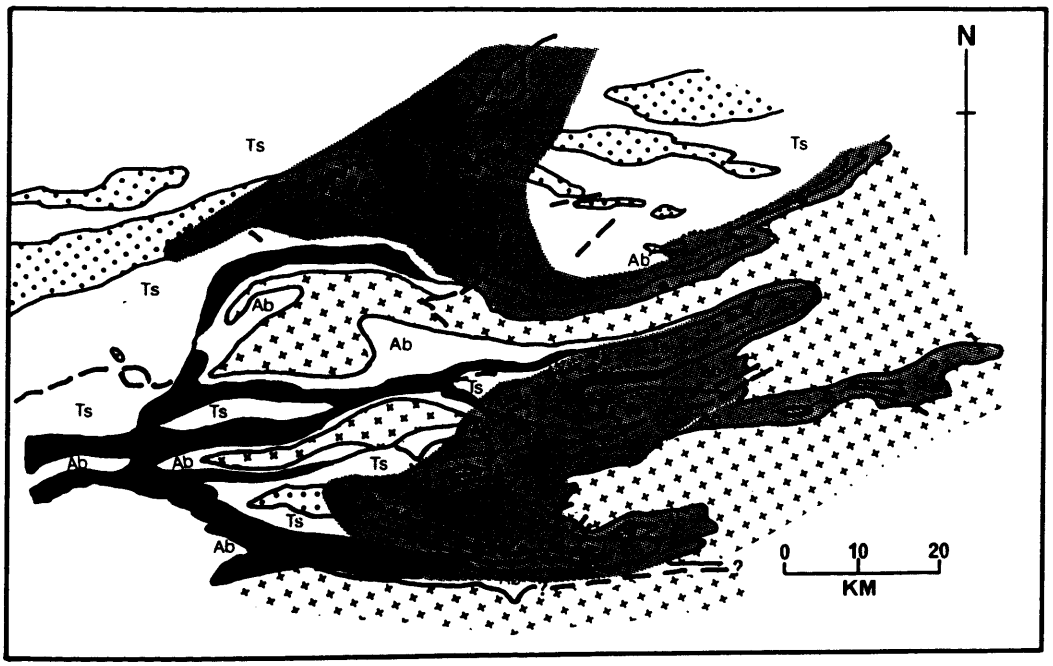

FIG.111 (c) Stratigraphic position of mines and prospects

- Mines and prospects
- Base metal occurrences
- Faults
- Mulden Group
- Ts — Tsumeb Subgroup
- Chuos Formation
- Ab — Abenab Subgroup
- Nosib Group and pre-Damaran rocks

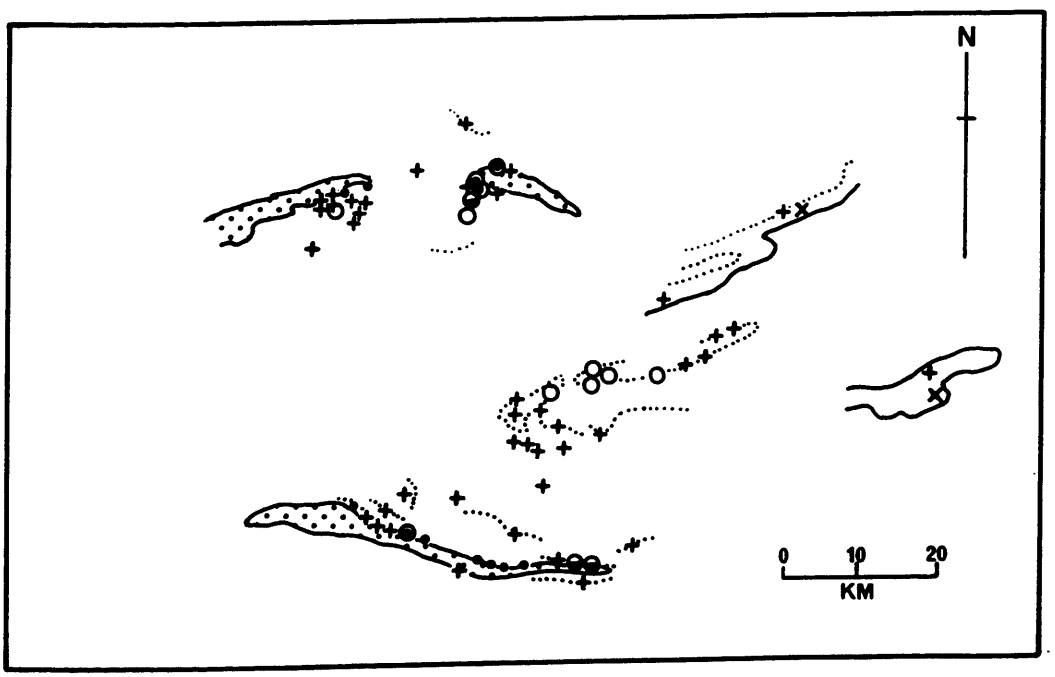

FIG.111 (d) Classification of mineralization loci

- × Major strata-bound ore
- O Breccia pipe (in part)
- • Discordant and conformable sandstone
- ● Discordant sandstone in breccia pipe
- O Other discordant, polymictic breccia bodies
- \+ Not described
- ····· Strata-bound breccia

(minor geological detail included from Fig. 111a)

breccia bodies and mineralization, relative to their stratigraphic position in the Otavi Group. The distribution of these features, particularly their positions relative to unconformities, prompted some authors to propose karst origins for mineralized sites; these were considered to have formed either prior, or subsequent, to F_1 folding (Stahl, 1926; Schneiderhöhn, 1929, 1958; le Roex, 1955; Callahan, 1971; Thirion, 1973a). Some of these workers considered mineralized, strata-bound horizons, such as the North Break and Karuchas zones (Chapter 2.2.3), to be paleoaquifers. Discordant breccia bodies such as those at Tsumeb and Harasib were thought to have been produced by dolostone dissolution and associated collapse (Thirion, 1973a).

Routine mineragraphic investigations of mineralization from Otavi Mountain Land mines and prospects, mainly by B.H. Geier, are recorded in unpublished reports of the Mineral Research Laboratory, Tsumeb Corporation Limited. Published mineragraphic studies are those of Abenab West (Verwoerd, 1957), Kupferberg (Markham, 1959), Dairy Lead prospect (Geier and Ottemann, 1970a) and the Otavi Mountain Land in general (Emslie, 1978, 1979). Jensen (1973) studied sulphur isotope ratios in sulphide minerals from a number of Otavi Mountain Land mines and prospects.

Calcitization, silicification and "carbon alteration" are associated with sulphide mineralization throughout the Otavi Mountain Land (Söhnge, 1957, 1976). Non-sulphide, gangue minerals are quartz, calcite and dolomite. Occurrences of hypogene barite (Kombat and localities 55, 56) and fluorite (Tsumeb and locality 11) are restricted, and fluorite has only been reported in a few hand specimens (Fig. 111a). The Kombat group of mines differ from other mines of the Otavi Mountain Land, in that they contain a volumetrically important, and mineralogically diverse, assemblage of minerals other than sulphide minerals (Innes and Chaplin, in press, 1985).

4.2. TYPES OF MINERALIZATION

Four main types of base metal mineralization occur in the Otavi

Mountain Land. The first is an uneconomic, copper-lead-zinc mineralization in metavolcanic rocks of the Nosib Group; negligible information is available about this type of mineralization, and it is not considered further. The second type is a mineralogically simple, galena-sphalerite-pyrite mineralization, similar to that of the Mississippi Valley-type ore association. The third type of mineralization consists of copper, copper-lead and copper-lead-zinc occurrences (including Tsumeb and Kombat mines) which, together with the second type, are confined to sedimentary carbonate rocks of the Otavi Group. The fourth type is a stratiform copper-pyrite $\pm$ pyrrhotite mineralization in rocks of the basal Mulden Group. "Sand-sack" vanadium deposits, related to Cainozoic weathering and karsting, are excluded from this discussion (Schwellnus et al., 1944).

The locations of mines and mineral prospects of types two to four are shown in Figure 111a. All existing mines, some of the larger prospects, and occurrences cited in published reports have been identified on this figure. The names and exact locations of all other numbered occurrences are in the possession of the Tsumeb Corporation Limited.

The mineralogically simple lead-zinc mineralization (i.e. the second type) is named the Berg Aukas mineralogical type, after the largest and best studied member of the group. This ore type consists of sphalerite, galena and pyrite, with sphalerite equal to, or greater than, galena. Some examples of this ore are lead-rich relative to Mississippi Valley-type ore, other than ore from south-east Missouri, U.S.A., and massive sulphide ore is more common in the Berg Aukas type. Trace amounts of chalcopyrite, enargite, pyrrhotite, jordanite and tennantite (or "tetrahedrite") are present in the Berg Aukas type of ore. The lead isotope study demonstrates that this mineralization is isotopically distinct from the copper-rich type (Chapter 5.3.2).

The third, copper-rich type of mineralization commonly contains tennantite, pyrite, sphalerite and galena in common with the Berg Aukas type, but also contains other copper minerals. It can be subdivided using the mineralogical data of Emslie (1978) and B.H. Geier (unpubl.

repts; Fig. 111b). These subdivisions are: (a) Tsumeb-type mineralization sensu stricto, defined by the presence of germanium- and gallium-bearing sulphide minerals, or the rare minerals sulvanite (Cu_3VS_4) or betekhtinite ($Pb_2(Cu,Fe)_{21}S_{15}$), (b) occurrences which contain significant quantities of chalcopyrite and bornite, (c) occurrences in which copper is the element of economic interest (i.e. the hypogene mineralogy is unknown, but lead-zinc mineralization is not thought to be volumetrically important). Representative prospects from all three types of copper mineralization are of one lead isotopic type (Chapter 5.3.2), and all copper prospects would probably prove to be of a single mineralogical type if hypogene ore was available for study from every locality (it does not follow that all lead-zinc prospects are of Berg Aukas-type). Therefore, these three subdivisions of copper-rich ore will be referred to as Tsumeb-type ore during subsequent discussions. A limited, very rare group of minerals is used above to define the Tsumeb-type mineralization, but other sulphide minerals might also be characteristic of this type (e.g. nickel-carrollite, found at Tsumeb, Kombat and locality 8). The Tsumeb type of mineralization can be subdivided into two sub-types, of significantly different mineralogical composition, represented by Tsumeb mine and the Kombat group of mines (Asis West to Asis Ost), respectively. The distinctions between these sub-types are discussed in Chapters 4.3. and 4.4.3.

The fourth type of mineralization, which consists of both disseminated and massive, stratiform, copper and iron sulphide mineralization, occurs in lower Mulden Group rocks at Tsumeb, locality 14, and in the Otavi Valley (Veldsman, 1979; Innes and Chaplin, in press, 1985; Chapter 2.3.6). This is a classical disseminated, stratiform copper mineralization at some localities, of the type that occurs elsewhere in central Africa (e.g. Zambia). It is named Tschudi-type mineralization, and is isotopically similar to the Tsumeb type of mineralization (Chapter 5.3.2).

It is shown in Chapter 5 that there are isotopic relationships between the Berg Aukas, Tsumeb and Tschudi types of mineralization, and this is thought to indicate a genetic relationship. These types of

mineralization, all of which are present elsewhere in central Africa, are referred to collectively as the Owambo basin ore association.

4.3 DISTRIBUTION OF MINERALIZATION

Mineralization displays a strong stratigraphic dependence throughout the Otavi Mountain Land (Söhnge, 1957). Copper mineralization is confined to the upper Tsumeb Subgroup, particularly in the vicinity of the Mulden Group contact (Tsumeb type), and in the base of the Mulden Group itself (Tschudi type; Figs. 111b-c). It is also geographically confined to northern and southern areas, in which the Mulden Group is preserved. Lead is more important in copper ore of the northern area, and barite, magnetite and silicate gangue minerals are largely confined to copper ore of the southern area. These correspond to the two subdivisions of Tsumeb-type mineralization, represented by the Tsumeb ore body and the Kombat group of ore bodies, respectively.

Söhnge (1957) noted a close association between copper mineralization and discordant sandstone ("pseudo-aplite") bodies which, like copper mineralization, are confined to the vicinity of the contact between the Otavi Group and Mulden Group (Fig. 111d). Most other copper mineralization is associated with polymictic breccias (including breccia pipes), and pipes and irregular bodies of altered sedimentary carbonate rock. Strata-bound mineralization is also known within the sedimentary carbonate rocks, and includes: (1) the North Break zone, Tsumeb (Chapter 3.4.4), (2) disseminated mineralization in silicified oolites of zone T8, at Tsumeb, Kombat, and localities 8 and 20 (Chapter 2.3.4), and (3) strata-bound breccia of the lower Elandshoek Formation (Chapter 4.4.7).

Lead-zinc mineralization of Berg Aukas type is also geographically and stratigraphically controlled. It is confined to the margins of the Nosib, Toggenburg and Awagobib anticlines in the central and eastern Otavi Mountain Land (Figs. 3, 111b). It occurs within, and stratigraphically lower than, the lower Elandshoek Formation of the Tsumeb Subgroup. Berg Aukas-type mineralization is most abundant in

this formation, and in the Gauss and Auros Formations of the Abenab Subgroup. It occurs both in strata-bound breccia, and in discordant breccia pipes (Fig. 111d).

Disseminated, strata-bound, Berg Aukas-type mineralization of the lower Elandshoek Formation crops out from 3 km east, to at least 20 km west of Abenab, and possibly continues westwards to connect with an occurrence south of locality 9 (Figs. 111a, b). It is also present at locality 1, but its extent in this area is not known because of very restricted outcrop. It crops out eastwards from locality 27, around the closure of the Maieberg syncline, then westwards through the Harasib Main area to occurrences 35 and 36, then eastwards around the closure of the Toggenburg anticline to at least locality 39. Similar mineralization occurs south of the Awagobib anticline at locality 48.

Strata-bound, copper-bearing mineralization of possible Tsumeb type occurs in a similar stratigraphic position to the above Berg Aukas-type mineralization, in an area north of the Otavi Valley (e.g. occurrence 59). This horizon occurs close to the contact with the Mulden Group at the eastern end, and on the southern limb, of the Otavi Valley Syncline. It is not known if its close proximity to the contact results from extensive erosion of the Otavi Group, prior to Mulden Group deposition, or if the strata-bound breccia is slightly discordant to the stratigraphy, and occurs higher in the sequence towards the south. The only Berg Aukas-type mineralization known south of the Gauss fault in this stratigraphic position (Fig. 3) is at locality 48. All other Berg Aukas-type occurrences in the southern Otavi Mountain Land occur lower than this in the sequence.

Thirion (1973a) described Berg Aukas-type mineralization in discordant, polymictic breccia pipes which occur in the Harasib area, slightly higher in the sequence than the strata-bound, oligomictic breccia bodies (Fig. 111d). Some of these pipes terminate downwards in the strata-bound breccia, e.g. Harasib Main. Berg Aukas-type mineralization occurs in the Auros Formation at Abenab West mine, and towards the base of the Gauss Formation at Berg Aukas mine. Berg Aukas-type mineralization also occurs higher in the Gauss Formation, at localities 41, 45 and 46.

4.4 DESCRIPTIONS OF INDIVIDUAL AREAS

A number of mines and prospects in the Otavi Mountain Land were briefly examined for comparison with the Tsumeb ore body, and in particular to determine if any occurrences show features inconsistent with the origin proposed for Tsumeb. It is shown below that some of the ore loci in sedimentary carbonate rocks are best explained by a karst and solution collapse origin. Limited observations from other bodies are consistent with this origin, although alternative origins are not precluded.

4.4.1 Tsumeb area

Mineralization of the Tsumeb area (Fig. 112) is of both Tsumeb and Tschudi mineralogical types. A north-south zone of breccia bodies and fracturing, which contains Tsumeb-type mineralization, was examined to the west of Tsumeb. This zone, the "Tsumeb crosswarp" of Berning (1951), is referred to here as the Tsumeb West fracture zone. It can be traced for at least eight kilometres, to near the contact between zone T4 and zone T5, and it contains a number of polymictic breccias over this distance (e.g. Tsumeb West, localities 6 and 7; Fig. 112). Berning (1951) noted that a north-south fracture which he observed within the Tsumeb West fracture zone does not off-set the axes of minor F_1 folds that cross it, and suggested that the fracture zone was produced by post-F_1 "arching" of the sequence. Hälbich (1967) considered the zone, and its contained breccia bodies, to be syntectonic.

An examination of the Tsumeb West and locality 6 occurrences confirmed that they both contain steeply plunging bodies of sandstone and polymictic breccia (as indicated by mapping of Tsumeb Corporation Limited; Figs. 113, 114). Pennebaker (1952) recorded rounded pebbles of white vein quartz and granite from the sandstone body at Tsumeb West. The S_1 cleavage occurs within both bodies (Figs. 89h, i), and a later fracture cleavage, with strike 051° and dip 80°S, is superimposed on S_1 in outcrops of weakly calcitized dolostone, approxi-

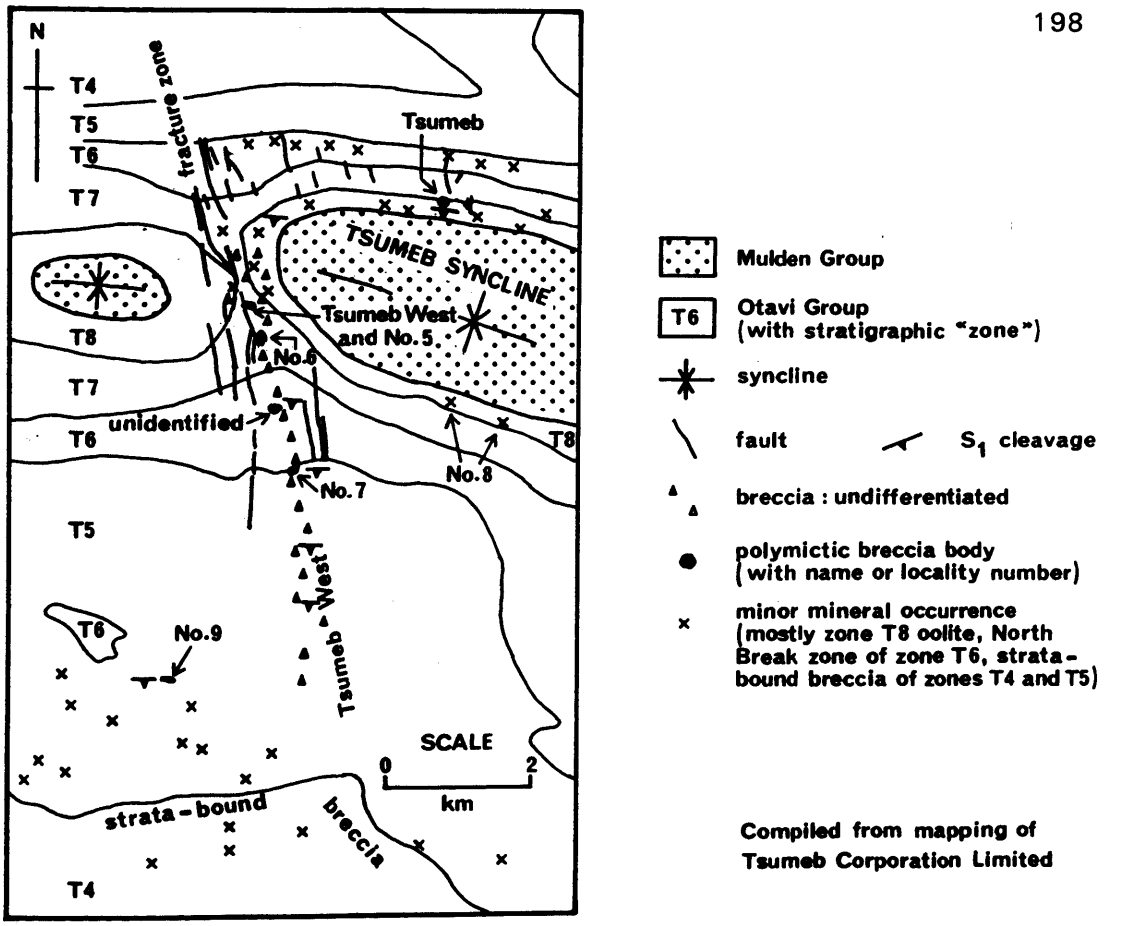

Fig. 112
Geological plan of the Tsumeb area, showing the Tsumeb West fracture zone, polymictic breccia bodies, and mineral occurrences.

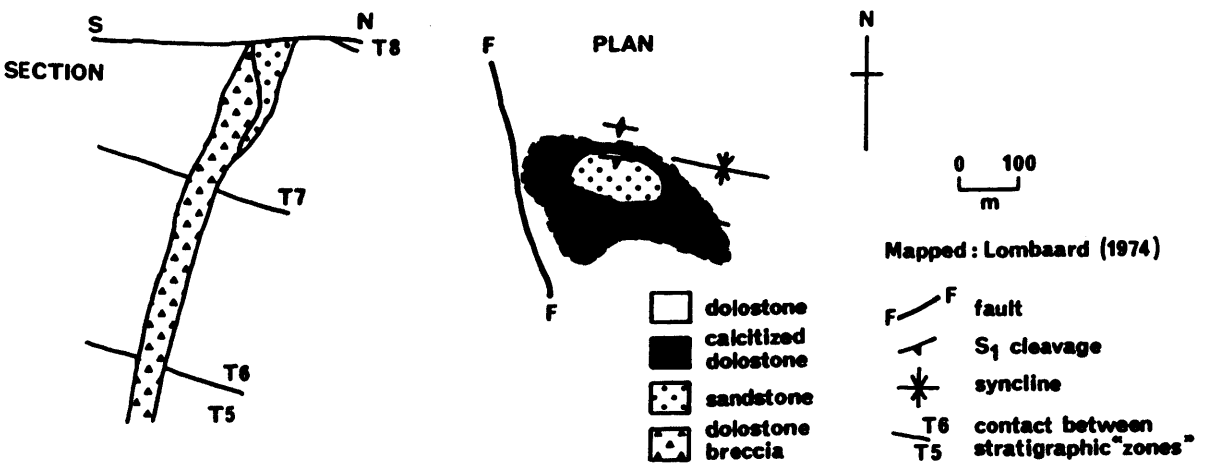

Fig. 113
Geological plan and section of the Tsumeb West prospect, south-west of Tsumeb, showing the decrease in volume of sandstone ("pseudo-aplite") with depth in this pipe-like body.

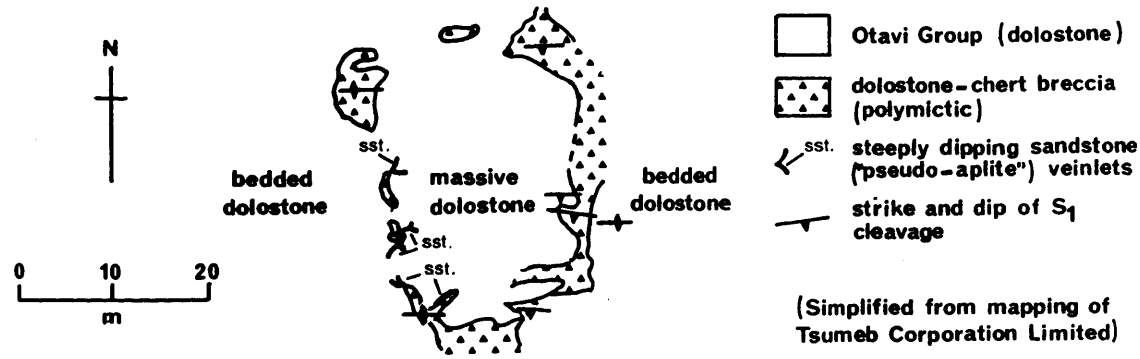

Fig. 114
Geological plan of locality 6, south-west of Tsumeb. The strike of the S_1 cleavage is perpendicular to the strike of both the breccia bodies and the Tsumeb West fracture zone (Fig. 112).

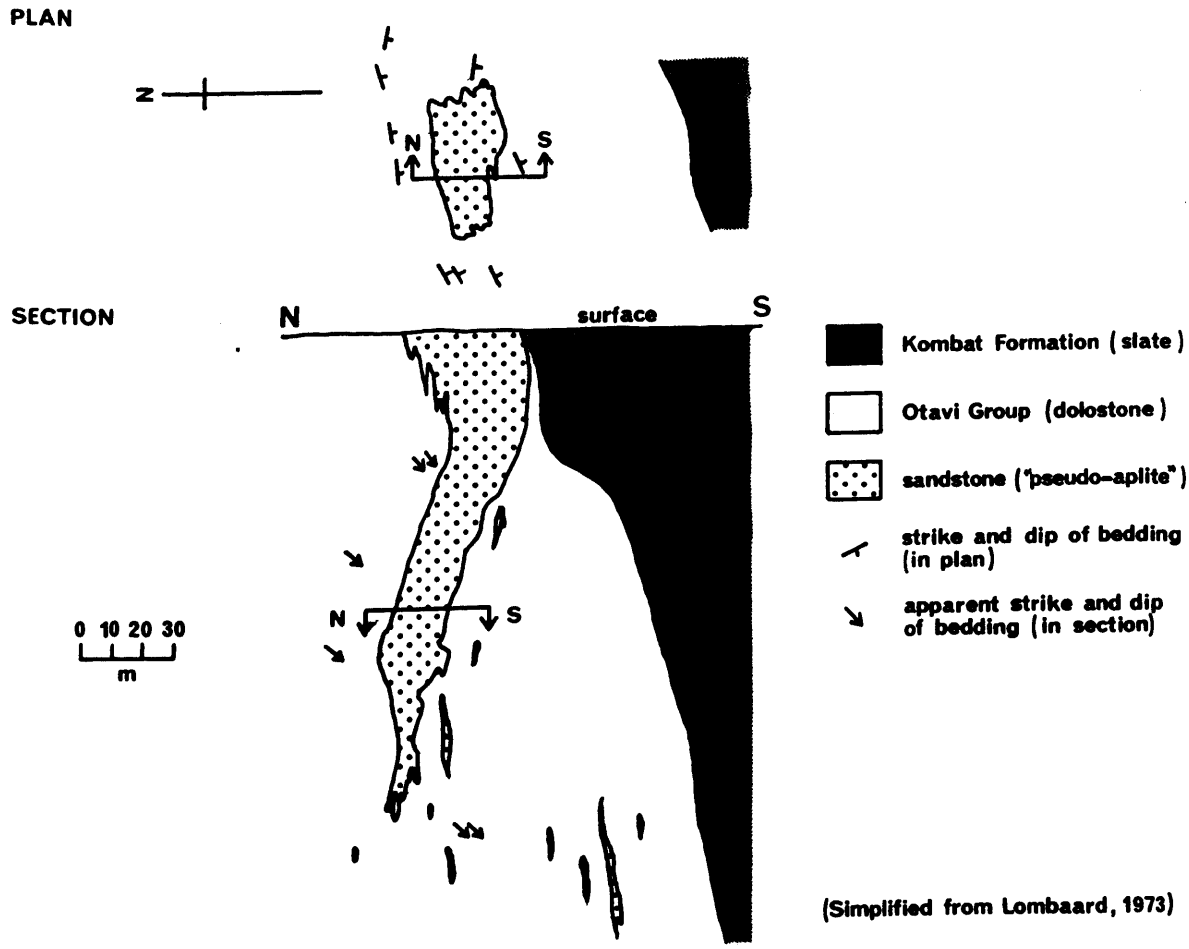

Fig. 115
Geological plan and section of the Kombat East ore body, section E595, showing the decrease in volume of the discordant sandstone body with depth below the overlying slate.

mately 100 m north-north-east of the Tsumeb West opencut. The sandstone body which is present in outcrop at the Tsumeb West prospect decreases in size with depth (proven by drilling), and a cleaved dolostone breccia continues below the sandstone (Fig. 113). The locality 6 occurrence consists of a steeply-dipping, cylindrical body of chert breccia and very minor sandstone, which surrounds a core of featureless, medium grey dolostone; these are enclosed by medium to light grey dolostone (Fig. 114). The breccia body contains some algal chert fragments, foreign to the host rocks, and the S_1 cleavage was found to have a strike perpendicular to the elongation of the breccia body; these observations, together with the presence of sandstone, indicate that this is also a body of sedimentary breccia.

Discordant occurrences of sandstone have been recorded elsewhere within the Tsumeb West fracture zone, north of Tsumeb West and south of locality 6. A breccia, which consists of oolitic chert fragments, occurs 20-150 m stratigraphically below the oolitic chert horizons of zone T8 near Tsumeb West (Botha, 1960).

The importance of tectonic brecciation within the Tsumeb West fracture zone is unknown. However, it is shown above that many mineralized breccia bodies are polymictic, and some are closely associated with sandstone bodies which steeply cut the host rocks. At least one north-south fracture within the zone does not offset the axes of minor folds that cross it, and the S_1 cleavage is superimposed on the bodies of sandstone and polymictic breccia which are distributed along the length of the fracture zone. It is suggested here that the Tsumeb West fracture zone formed as a broad fracture zone of limited displacement. This was the site of subsequent major karsting and solution collapse, and then of karst sedimentation during later submergence, as at Tsumeb.

Tsumeb-type mineralization is known elsewhere in the Tsumeb area at the Dairy Lead prospect (in zone T7), and strata-bound in the North Break zone, both on the northern limb of the Tsumeb syncline. Strata-bound mineralization also occurs on the southern limb of the Tsumeb syncline at locality 8, in oolitic chert of zone T8. Shale and

sandstone occur in cross-cutting and conformable lenses in the vicinity of the oolitic chert horizons, and some of these cross-cutting bodies occur to within a few tens of metres of the contact between the Otavi Group and Mulden Group (Botha, 1960).

The second type of mineralization in the Tsumeb area is the Tschudi type of mineralization, which occurs in the basal Mulden Group. This mineralization consists mostly of disseminated pyrite, but stratiform chalcocite mineralization is associated with the pyrite west of Tsumeb (Veldsman, 1979). Traces of chalcopyrite and bornite occur with abundant pyrite in the vicinity of Tsumeb, where disseminated pyrite occurs over a stratigraphic interval of more than 200 m towards the base of the Mulden Group. Diamond drill hole intersections of up to 30 m of 12 vol. % pyrite have been obtained in this area. Fibrous quartz and pressure shadows of mica, which fringe subhedral to euhedral pyrite grains, are oriented parallel to a cleavage which is thought to be S_1. This indicates that pyrite was present prior to the close of this deformational event. Some pyrite has replaced ilmenite, now leucoxene, and original biotite, now mostly altered to muscovite plus rutile.

Lead and sulphur isotope data from pyrite associated with Tschudi-type copper mineralization is consistent with a late diagenetic origin for the pyrite. Lead isotope data from associated galena indicate that the galena formed during a separate event, from the same solutions as the Tsumeb-type mineralization (Chapter 5).

4.4.2 Ore controls in the Otavi Valley area

Mineralization of the Otavi Valley area is of both Tsumeb and Tschudi mineralogical types. The Kombat group of mines are economically important, with production and reserves of 8,0 million tonnes of 2,5% Cu, 2,1% Pb, and 18 g/t Ag, to December, 1981 (Innes and Chaplin, in press, 1985). Tsumeb-type mineralization of these mines occurs within dolostone of the Tsumeb Subgroup, along a 5 km strike length of the contact between the dolostone and the overlying Kombat Formation (i.e. Mulden Group) slate. The ore loci are steeply-dipping, fractured and sheared zones, which contain dolostone breccia bodies and

discordant veinlets and bodies of sandstone (Fig. 115). The mineralized zones extend up to 150 m (typically less than 100 m) stratigraphically below the contact between the Otavi Group and the Mulden Group. Sulphide mineralization is massive, vein-like and disseminated, and is of both cavity-filling and replacement types. Sulphide ore and iron oxide and manganese oxide minerals partly, to completely, replace the matrices of dolostone breccia and sandstone bodies (Innes and Chaplin, in press, 1985).

The ore bodies are cleaved and boudinaged parallel to their strike, and a steeply plunging mineral lineation is developed. The long axes of clasts in some breccia bodies display a preferred orientation, and thinner sulphide veins are transposed in a cleavage. Annealed sulphide minerals and calcite are present, and some sulphide minerals occur as stylocumulate residues along the stylolitic contacts of breccia clasts (Innes and Chaplin, in press, 1985). Samples of sulphide ore examined during the present study show annealing textures between galena and bornite, but not between galena and chalcopyrite (although annealed chalcopyrite has been recorded by Innes and Chaplin, in press, 1985). The galena shows perfect 120° triple junctions, unlike galena from the Tsumeb ore body, and none of the galena or bornite grains are elongated (Fig. 120). Steeply dipping, north-east to east-trending zones of intense deformation contain many of the mineralized bodies, and some workers have emphasized the importance of these zones as sites of syntectonic mineralization (Hopwood, 1975; Innes and Chaplin, in press, 1985).

Hopwood (1975) considered that zones of sandstone emplacement, rock alteration and sulphide mineralization in the Kombat ore bodies were synchronous with F_1 folding and associated S_1 foliation, brecciation and shearing. Hopwood (1975) and Innes and Chaplin (in press, 1985) considered these zones to be shear extensions of attenuated fold hinges. Innes and Chaplin (in press, 1985) proposed two different mineralizing events. The first involved subaqueous deposition of carbonate minerals and hydrous oxides of iron and manganese, and possibly barite layers. This occurred concurrently with, and in association with, deposition of sandstone at the base of

the Kombat Formation. This was followed by F_1 and F_2 folding; foliated, sheared and brecciated zones were subsequently produced during F_3 (or possibly F_2) folding, and a non-penetrative S_3 fracture cleavage was developed. Sulphide minerals were emplaced in these structural zones during F_3 folding, concurrent with calcitization of the dolostone and hydrothermal reworking of the iron-manganese bodies into oxide and silicate assemblages. Calcitization and sulphide mineralization outlasted F_3 folding.

Figure 14 of Hopwood (1975), reproduced here as Figure 116, and photographs contained in his report (plates 6.1A,B and 6.2) show identical features to those observed at Tsumeb mine during the present study. There is the same, abrupt change from open folding in dolostone to strong, vertical fracturing and cleavage in the ore zone. The ore zone consists of calcitized and strongly cleaved dolostone, dolostone breccia and sandstone lenses, including dolostone breccia with a sandstone matrix. Sandstone bodies show crosscutting or anastomosing relationships (Innes and Chaplin, in press, 1985; figs. 3, 4). The ore zones are not elongated in the Kombat East area, where pipe-like bodies of sandstone are known (Innes and Chaplin, in press, 1985; Fig. 115). The cleavage is approximately parallel to the sandstone bodies within more elongate ore zones. Therefore, the Kombat ore bodies display many of the same features as the Tsumeb ore body, and it is proposed here that they have a similar, pre-deformational, origin.

Brief surface and underground examinations were made of the Kombat mines during the present study. These were sufficient to show that an alternative model of pre-deformational karsting and sulphide mineralization is consistent with the data, and to indicate some disagreement with the structural relationships on which the argument for syn-F_3 mineralization is based (Chapter 4.4.4).

4.4.3 Mineralogy of the Kombat ore bodies

Tsumeb-type mineralization of the Otavi Valley area differs from that of the northern Otavi Mountain Land (e.g. Tsumeb). Lead is less

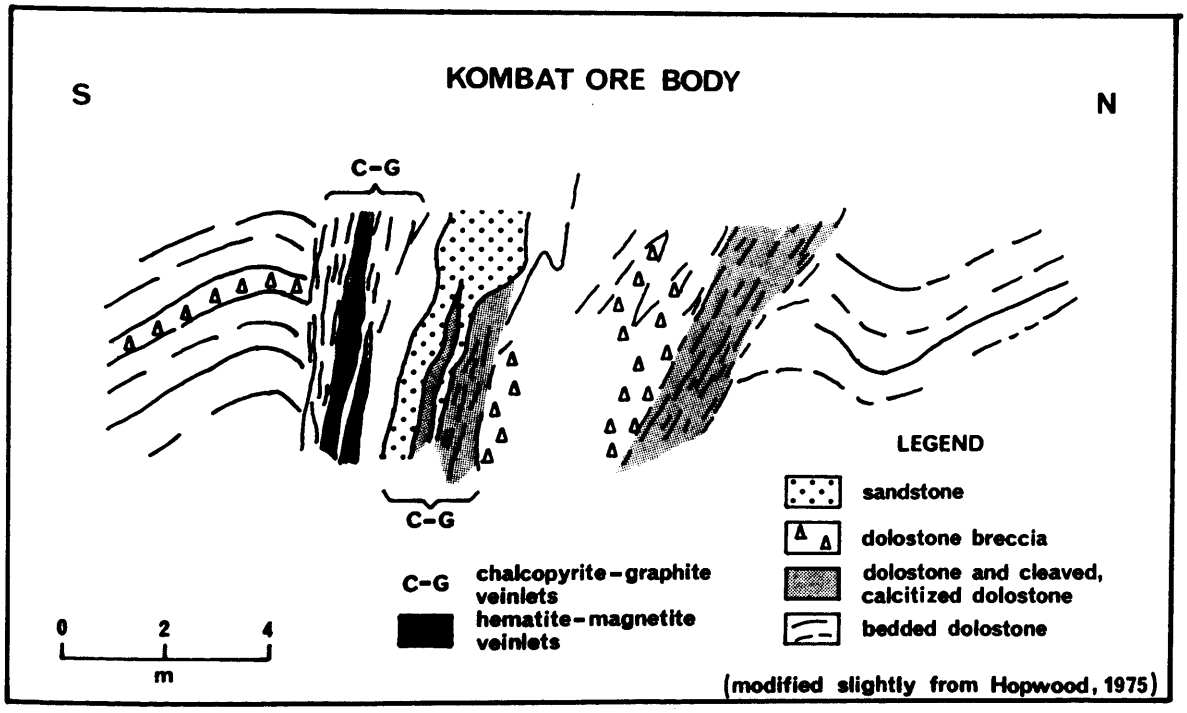

Fig. 116
Cross-section of the Kombat ore body, W70-4 stope, Kombat mine. Dolostone breccia, calcitized dolostone and sandstone are present, as in the Tsumeb ore body. Note the abrupt change from open folding in dolostone to sub-parallel fracturing and cleavage within the ore zone.

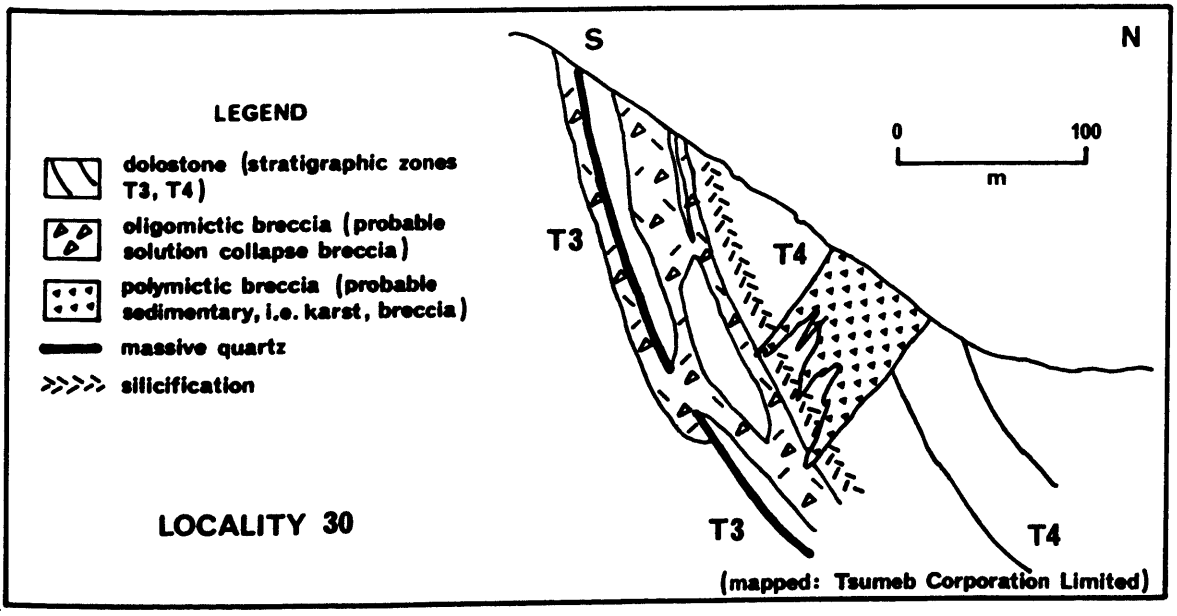

Fig. 117
Cross-section of locality 30, showing a pipe-like body of polymictic breccia which cross-cuts sedimentary carbonate rocks. The pipe terminates downwards in strata-bound, oligomictic, dolostone breccia towards the base of stratigraphic zone T4. This is typical of Berg Aukas - type mineralization in the Elandshoek Formation.

important in the Otavi Valley area, barite, magnetite, hematite, manganese oxide, and silicate gangue minerals are present, and there are differences in the sulphide mineralogy.

This Kombat sub-type of the Tsumeb type of mineralization has been studied in detail in the Kombat group of mines, where it can be divided into two main types (Innes and Chaplin, in press, 1985). The first, and only economically important, mineralization consists of base metal sulphide minerals in sedimentary carbonate rocks. Calcitization is the dominant wall rock alteration, and gangue minerals consist of minor calcite, dolomite, very minor quartz and rare barite (the barite occurring in iron oxide bodies, but also in sulphide ore and bodies of pyrobitumen). The sulphide ore contains copper and subordinate lead (c.f. lead and subordinate copper at Tsumeb) and, like Tsumeb ore, it shows a strong association between silver and copper. However, the silver content of the ore is lower than at Tsumeb, arsenic is minor, and zinc rarely exceeds a few thousand ppm. Molybdenum and germanium are present to a few hundred ppm, as at Tsumeb. However, massive bodies of germanium ores are absent, although germanium is locally enriched in schungite (pyrobitumen) bodies, and in some bornite and chalcopyrite ore.

The geochemical differences between Tsumeb and Kombat sulphide ores are reflected in their mineralogy (Table 8). The Kombat ore consists of chalcopyrite and bornite (c.f. bornite and tennantite at Tsumeb), galena and pyrite. Iron-rich, zinc-poor tennantite and iron-rich sphalerite (e.g. 6-9 wt.% Fe), are minor phases (B. H. Geier, unpubl. repts.; Innes and Chaplin, in press, 1985). Arsenopyrite, molybdenite, enargite, betekhtinite, renierite, glaucodot, nickel-carrollite and cadmium-wurtzite have been recorded, mainly by B.H. Geier. Tennantite and enargite occur in bornite-rich ore. Arsenopyrite, which occurs in chalcopyrite-pyrite ore at Kombat, is absent from Tsumeb, and renierite is not widely distributed at Kombat. Lautite and colusite have also been recorded, but these were tentative identifications by B.H. Geier which were probably subsequently revised (e.g. betekhtinite was formerly identified as lautite).

TABLE 8 MINERALOGY OF TSUMEB-TYPE ORE BODIES

	Tsumeb, SWA/Namibia	Kombat, SWA/Namibia	Kipushi, Zaire	Mumbwa, Zambia	M'Passa Congo Republic
Pyrite FeS_2	1	1	1	1	1
Sphalerite ZnS	1	2	1	2	1
Cd-wurtzite (Cd,Zn)S	2	4	-	-	-
Galena PbS	1	1	2	-	1
Chalcopyrite $CuFeS_2$	2	1	1	1	3
Bornite (hypogene) Cu_5FeS_4	1	1	1	1	2
Chalcocite (hypogene) Cu_2S	3	?	3	?	?
Tennantite $Cu_{12}As_4S_{13}$	1	2	2	1	1
Enargite Cu_3AsS_4	1	3	3	-	3
Arsenopyrite FeAsS	-	3	2	2	3
Magnetite Fe_3O_4	-	1	-	-	-
Barite $BaSO_4$	-	2	4	-	-
Pyrobitumen	4	3	3	-	4?
Betekhtinite $Pb_2(Cu,Fe)_{21}S_{15}$	3	4	4	-	-
Germanite $Cu_3(Fe,Ge)S_4$	3	-	4	?	4
Renierite $Cu_{2,5}Ge_{0,5}FeS_4$	3	4	3	4?	4
Briarite $Cu_2(Fe,Zn)GeS_4$	4	-	4	?	4?
Gallite $CuGaS_2$	3	-	3	-	-
Molybdenite MoS_2	3	4	2	-	3
Tungstenite WS_2	4	-	4	-	-
Unnamed $(Mo,Re)S_2$	-	-	4	-	-
Carrollite/linnaeite $Co_3S_4 \pm Ni,Cu$	3	4	3	?	-
Cobaltite CoAsS	-	-	3	?	4
Other, & unidentified Co,Ni minerals	-	?	-	3	3
Ge-mawsonite $(Cu,Ge)_7(Fe,Zn)_2(Sn,As)S_{10}$	4	-	4	-	-
Ge-stannite? $Cu_2(Fe,Zn)SnS_4 \pm Ge$	4	-	-	-	-
Metacinnabar HgS	4	-	-	-	-
B, Li or Be minerals	4	4	-	-	-
Gratonite $Pb_9As_4S_{15}$	4?	-	-	-	-
Sulvanite $Cu_3(V,Ge)S_4$	4	-	4	-	-
Cosalite $(Pb_2Bi_2S_5)$	-	-	4	-	-
Bismuthinite (Bi_2S_3)	-	-	4	-	-
Wittichenite (Cu_3BiS_3)	-	-	4	-	-
Emplectite $(CuBiS_2)$	-	-	4	-	-
Aikinite $(PbCuBiS_3)$	-	-	4	-	-
REFERENCES	Table x	a b	c d e	f	g h

1 = major
2 = minor, widespread or locally concentrated
3 = trace, widespread
4 = trace, rare
- = not recorded
? = presence uncertain, or identification doubtful

a B.H. Geier (unpub. repts.)
b Innes & Chaplin (in press, 1985)
c Intiomale & Oosterbosch (1974)
d de Vos et al.(1974)
e Dimanche (1974)
f Cikin & Drysdale (1968)
g Bigotte (1959)
h Scolari (1965)

The second, uneconomic mineralization in the Kombat group of mines consists of massive bodies of iron and manganese oxide, and silicate, minerals which occur as separate but adjacent bodies. This mineralization is always associated with sandstone, and is confined to the contact between slate and dolostone. The mineralization consists of tectonically interlayered magnetite, hausmannite (Mn_3O_4), hematite, tephroite (Mn_2SiO_4), rhodonite ($MnSiO_3$), leucophoenicite ($Mn_7(SiO_4)_3(OH)_2$), barite, kutnahorite ($Ca(Mn,Mg,Fe^{2+})(CO_3)_2$), hypogene native copper, an undescribed Pb-Ca silicate, helvite ($Mn_4Be_3(SiO_4)_3S$) and garnet (possibly calderite; Innes and Chaplin, in press, 1985). Minor pyrite, chalcopyrite and galena are associated with this assemblage. B.H. Geier also recorded hauerite (MnS_2) and hollandite ($BaMn_8O_{16}.xH_2O$) from the Kombat mines, but it is not known if the identities of these minerals were confirmed.

Pyrite-sericite-kaolinite (and minor pyrophyllite) occur elsewhere in sandstone, and silicification is important in places (Innes and Chaplin, in press, 1985). Large masses of chalcopyrite-bearing schungite (pyrobitumen) occur as cross-cutting bodies in places on the dolostone-slate contact (Hopwood, 1975). Crustiform veins within the Kombat ore body contain galena, helvite, rhodochrosite ($MnCO_3$), barite, manganite ($MnO(OH)$), nambulite ($NaLiMn_3Si_{10}O_{28}(OH)_2$), sérandite ($Na(Mn^{2+},Ca)_2Si_8(OH)$), cahnite ($Ca_2B(AsO_4(OH)_4$), brushite ($CaHPO_4.2H_2O$), kentrolite ($Pb_2Mn^{3+}Si_2O_9$), calcite and gypsum; Innes and Chaplin (in press, 1985) consider these veins to be paragenetically late.

4.4.4 Deformation of the Kombat ore bodies

Innes and Chaplin (in press, 1985) recognized isoclinal folds (F_1) with an east-trending, axial planar cleavage (S_1). This is a slaty cleavage and schistosity in slate and phyllite of the Kombat Formation, throughout the Otavi Valley, in which the S_1 cleavage transposes sulphide layering and colour lamination (S_0). The S_1 surfaces are refolded by a second phase of nearly co-axial, concentric

folds (F_2), and the S_1 surfaces are post-dated by an S_2 crenulation cleavage, axial planar to F_2. S_1 and S_2 are near-vertical cleavages which are sub-parallel to the slate-dolostone contact in the Kombat group of mines. A late fracture cleavage, S_3, is non-penetrative on the mesoscopic scale and is axial planar to minor, chevron-style folds (F_3) and parallel to kink bands. Innes and Chaplin (in press, 1985) considered that F_3 structures might be related to north-east trending, dip- and strike-slip faults of the Kombat area. The relations observed between F_1 and F_2 folds, and S_1 and S_2 cleavages, during the present study correspond to those above.

The evidence which has been advanced for syntectonic mineralization is that: (1) fracturing and brecciation which host the mineralization and associated rock alteration are associated with attenuated fold hinges (Hopwood, 1975; Innes and Chaplin, in press, 1985), and (2) microtextural relationships show that mineralization was synchronous with, and outlasted, (a) S_1 (Hopwood, 1975), or (b) S_2 or S_3, cleavage development (Innes and Chaplin, in press, 1985).

The first type of evidence is based on the observation that a systematic geometric relationship exists between fractures, breccia bodies, boudins, cleavages and minor folds. This does not demonstrate that these features all formed at the same time, by a related process, although this would commonly be assumed in the absence of conflicting evidence. This conflicting evidence is that discordant sandstone bodies which fill fractures are present, and some of these bodies show no obvious association with minor folding (Fig. 115). Innes and Chaplin (in press, 1985) interpreted the sandstone which occurs in the Kombat mines as Mulden Group rock, and although they favoured transposition of the sandstone bodies into the dolostone along attenuated folds, they did not consider that the evidence precludes the possibility of a karst-fill origin. Similar sandstone in the Tsumeb pipe is interpreted here as karst-fill sediment. Innes and Chaplin (in press, 1985) favoured a tectonic origin for the majority of Kombat breccia bodies, but considered some to be sedimentary, indicating further possible analogies with the Tsumeb pipe. The first type of evidence is,

therefore, inconclusive. It is equally consistent with a karst-fill origin for the Kombat ore loci, followed by mineralization, and then by inhomogeneous deformation which was concentrated within the calcitized and mineralized zones.

The other evidence for syntectonic mineralization is micro-textural. Innes and Chaplin (in press, 1985) noted that compositional layering in the iron-manganese bodies is transposed by the S_1 and S_2 cleavages, with the development of axial planar amphibole. Therefore, they considered that this mineralization pre-dated deformation. However, they proposed that the sulphide mineralization was introduced synchronously with development of the S_3 cleavage. It is argued in the following discussion that the sulphide mineralization was also deposited prior to the close of formation of the S_1 cleavage, and that it is genetically related to the iron-manganese mineralization.

Innes and Chaplin (in press, 1985) noted that "It is difficult to correlate structural events between ... [slate and dolostone] which exhibit such different responses to stress." Fabrics which are well developed in the slate become indistinct, or disappear, in the dolostone. Innes and Chaplin (in press, 1985) mainly obtained their evidence for the timing of mineralization from structural relationships in the contact zone between slate and "marl" (i.e. metamorphosed sedimentary carbonate rock which contains abundant phyllosilicate minerals) of the Asis West mine, where structural fabrics are better developed than in the dolostone away from the contact. They recognized a steeply dipping, S_3, fracture cleavage, with an east-north-east strike, in both dolostone and "marl" on the slate contact. This has the same attitude as a strongly penetrative cleavage in the adjacent slate, which they identified as S_2. The "marl" contains veinlets of chalcopyrite, pyrite and pyrrhotite within surfaces that Innes and Chaplin (in press, 1985) interpreted as folded S_2 surfaces. They considered that these veinlets were not folded by the event which folded the S_2 cleavage, but that the veinlets formed in S_2 subsequent to this event. They noted that chalcopyrite also occurs along S_3 fracture cleavages in dolostone, and concluded, therefore,

that mineralization was synchronous with the formation of S_3 cleavage.

The area illustrated in Figure 4 of Innes and Chaplin (in press, 1985) was visited during the present study. Cleavage in the dolostone and "marl" ("S_3" of Innes and Chaplin, in press, 1985) and slate ("S_2") has a single orientation. It only varies in the degree to which it is penetrative, its penetrative nature increasing with increasing mica content of the rock. The same cleavage is continuous from the slate to the dolostone (Fig. 118), and "S_2" and "S_3" are considered here to be a single cleavage. Sulphide veinlets in the "marl", and in other sericite-rich but chlorite-poor rocks of the contact zone, form intra-folial closures within the cleavage surface. The only veinlets which lie in this surface appear to have been transposed into that position, and not to have formed subsequent to the cleavage (Fig. 119). There is no evidence as to the original nature of the fractures which are now filled by sulphide veinlets.

The penetrative "S_2" cleavage in the slate resembles the S_1 cleavage present at other localities. F_2 folding was observed in slate outcrops at two localities farther west in the Otavi Valley, and the S_1 and S_2 cleavages in slate were examined microscopically from drill core in the Asis West area. The S_1 cleavage is not transposed into S_2 at any of these localities. S_2 is a well developed crenulation cleavage which does not displace S_1, and negligible growth of new mica has occurred in the S_2 surface. The "S_2" and "S_3" cleavages of Innes and Chaplin (in press, 1985), re-defined as a single, penetrative cleavage above, are therefore considered to be a single, S_1, cleavage at the locality which they describe at Asis West. The sulphide veinlets were present prior to the close of S_1 cleavage development, and possibly D_1 deformation, consistent with the timing of sulphide veinlets in slate of the Kombat Formation (Chapter 4.4.5). Extensive and intense deformation of massive sulphide ore is indicated by the widespread occurrence of deformation and annealing textures in this ore.

It is concluded that the ore loci are paleokarst and collapse

Fig. 118

The contact of dolostone of the Tsumeb Subgroup (TS) and slate of the Kombat Formation (KF). Slaty cleavage in the Kombat Formation, interpreted as S_1 cleavage, is a less penetrative fracture cleavage in the adjacent dolostone. The cleavage is not parallel to the contact but intersects it at a small angle, defined by the parallel orientation of dolostone clasts in the slate at the contact. The scale is given by the hammer at bottom right. Asis West ore body, W1150-10 stope, + 1284m.

Fig. 119

Sericite-rich rock from the vicinity of the above contact. Sulphide-quartz veinlets in this rock appear to have been folded, transposed and boudined in the S_1 cleavage, rather than been precipitated within it. Sample 1020, Asis West ore body, W1150-10 stope.

Fig. 120

Foam texture in galena, indicating syn-deformational or post-deformational annealing of sulphide ore. This texture is more common in the Kombat group of ore bodies than in the Tsumeb ore body. Sample 1009, Kombat West ore body, 6-4 stope, + 1493m. Plane polarized light. Etched with HCl + thiourea.

Fig. 121

Strata-bound, oligomictic breccia of the type developed on a regional scale in zone T4 of the Elandshoek Formation (Chapter 4.4.7). This example is immediately adjacent to, and underlies, the polymictic breccia pipe of the Harasib Main prospect. The matrix of the strata-bound breccia is a hydrothermal cement, which consists of dolomite, minor quartz and traces of galena and sphalerite. This is mostly an <u>in situ</u> brecciation which is interpreted to have formed by solution collapse above, and within, soluble horizons (possibly during the mineralizing event). The breccia has undergone low strain, and some quartz is elongated in the S_1 structural direction. The hammer is 31cm long.

Fig. 122

Deformation and recovery textures in massive sphalerite of the Abenab West ore body. Deformation twins are present in all large grains, and small annealing twins have formed along fractures and grain boundaries. Galena elsewhere in the section shows foam texture (not shown). Sample 573F. Plane polarized light. Etched with HCl + thiourea.

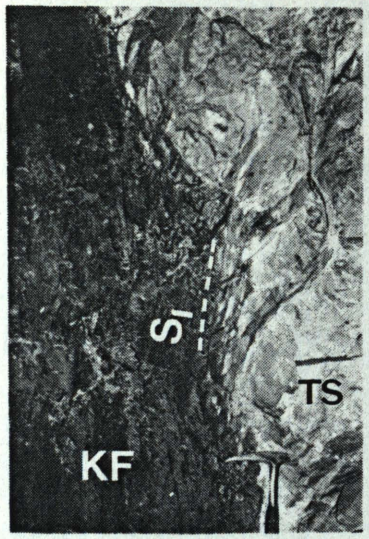

Fig. 118

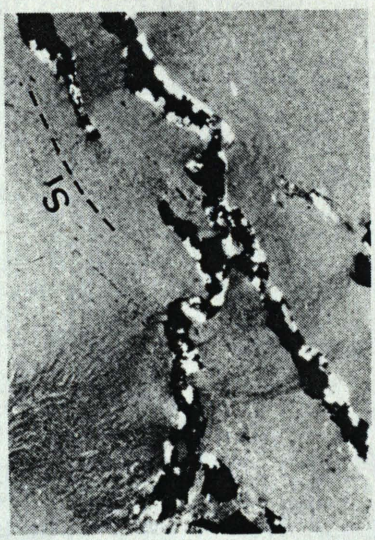

Fig. 119 0 mm 2



Fig. 120 0 mm 0.4

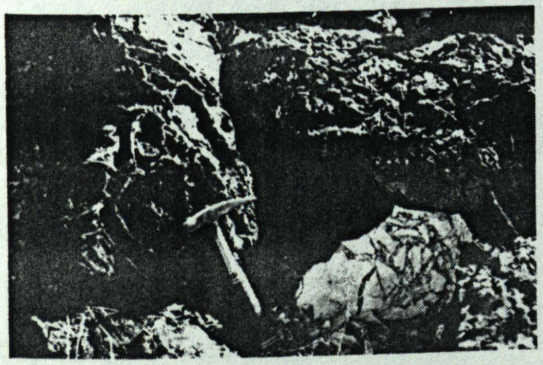

Fig. 121

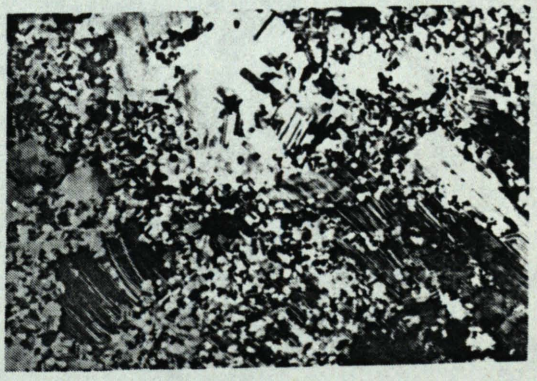

Fig. 122 0 mm 0.4

features, filled with Mulden Group sediment, which formed at the top of the Tsumeb Subgroup. These features formed contemporaneously with those at Tsumeb, but were confined to shallower depths. Both the iron-manganese bodies (or at least the magnetite bodies examined during the present study) and the sulphide ore bodies were deposited within these features by hydrothermal processes, prior to the close of D_1 deformation. It is argued in Chapter 5.1.2 that they were deposited during a single mineralizing event.

4.4.5 Mineralization in the Kombat Formation

Tschudi-type mineralization of the Otavi Valley area consists of disseminated and massive pyrite, and pyrrhotite of metamorphic origin, in the basal Kombat Formation. Traces of chalcopyrite, sphalerite and galena, and rarely bornite, are associated with the pyrite and pyrrhotite. The sulphide minerals constitute 2-5 vol. % of the slate over significant areas, and up to 60 vol. % over widths of up to 5 m in places (Innes and Chaplin, in press, 1985).

Compositional layers and sulphide layers in slate of the Kombat Formation are transposed by the S_1 cleavage and, less commonly, occur as intrafolial folds within S_1. Muscovite, chlorite, quartz, sulphide minerals, and boudins of quartzo-feldspathic material are elongated in the S_1 surface. Layering within bodies of fine grained pyrite is commonly at a small angle to S_1. However, large bodies of pyrite have been pulled apart along surfaces which are al igned at a high angle to S_1 (i.e. extension has occurred, sub-parallel to S_1). The resulting segments consist of aggregates of coarse grained pyrite grains, and the segments are bounded by the euhedral crystal faces of their component grains; therefore, the pyrite recrystallized during, or subsequent to, fragmentation. The pyrite bodies are veined by pyrrhotite, and have pressure shadows of pyrrhotite, quartz, and calcite, which are elongated in the S_1 surface.

The S_1 cleavage is kinked, but not transposed, by an S_2 crenulation cleavage, and only very minor amounts of new mica have grown in the S_2 surfaces. Some thin sulphide layers are kinked by

the S_2 cleavage.

It is concluded that the S_1 cleavage transposes earlier sulphide layers, which therefore pre-date, or were emplaced during, the F_1 folding. The presence of fragmented, recrystallized pyrite bodies, rimmed by pressure shadows of pyrrhotite, within the S_1 surface, indicates that metamorphism was associated with the F_1 event.

4.4.6 Harasib area

Discordant, polymictic breccia pipes of the central Otavi Mountain Land contain Berg Aukas-type mineralization (Figs. 111b, d). Breccia of the Harasib Main breccia pipe contains light and dark grey dolostone clasts, some of which display bedding, in a matrix of dark grey, dolomitic siltstone and light grey dolostone (locality 31, Fig. 111a). Quartz veins which contain dolomite spar and galena occur within the breccia, both in its matrix and along the bedding planes of clasts. A cleavage (commonly stylolitic), with strike 096° and a steep dip, is superimposed on the matrix and on some clasts, and also occurs in dolostone of the surrounding area; this probably corresponds to the S_1 cleavage of the Tsumeb area. Clasts are strongly elongated within this cleavage in places, and some aggregates of galena grains have boundaries formed entirely by the stylolitic cleavage. This indicates that the galena was present prior to the close of formation of the S_1 cleavage.

Drilling has shown that the Harasib Main breccia pipe cross-cuts the enclosing sedimentary carbonate rocks and terminates in underlying, strata-bound, oligomictic, dolostone breccia bodies of the lower Elandshoek Formation. Other polymictic breccia pipes of the central Otavi Mountain Land which contain Berg Aukas-type mineralization show similar discordant relationships (Figs. 111d, 117).

The compositions, shapes and structural relationships of these breccia pipes and their contained mineralization are consistent with karsting, karst sedimentation and mineralization, prior to D_1

deformation.

4.4.7 Strata-bound breccia of the Elandshoek Formation

Strata-bound, oligomictic, dolostone breccia bodies which contain a sparse, disseminated, Berg Aukas-type mineralization are widespread in the lower Elandshoek Formation of the eastern Otavi Mountain Land (Chapter 4.3). These oligomictic breccia bodies consist of angular dolostone fragments with a hydrothermal cement of quartz, with dolomite and rare calcite in places; galena and sphalerite occur on the walls of this cavity-filling cement (Fig. 121). Some veins are crustiform, and vugs within the cement contain quartz crystals which show crystal forms. Breccia bodies which have a dolostone matrix, and breccia bodies which consist entirely of interlocking clasts, are associated with the hydrothermal breccia bodies in places.

Strata-bound breccia bodies have fairly abrupt lower contacts at some localities, but their upper limits are indefinite and extend into the overlying member of the Elandshoek Formation (zone T5). Breccia fragments have commonly formed by brecciation in situ, and display little rotation. Cement-filled fractures of the type illustrated in Fig. 121 grade into more systematic networks of quartz veins which do not displace bedding planes. They also grade into completely silicified, strata-bound horizons, metres thick, locally termed "jasperoid" (Thirion, 1973a).

The strata-bound breccia bodies have been deformed. Quartz grains show strain extinction, and laths of quartz are bent, or are elongated in the S_1 direction; some galena shows foam texture. Quartz veins in breccia bodies between locality 61 and the Mulden Group of the Otavi Valley, to the south, form intra-folial closures in a steeply dipping cleavage with an easterly strike (Fig. 111a). The quartz veins are increasingly transposed in the cleavage as the Otavi Valley is approached. This cleavage is probably the S_1 cleavage of the Otavi Valley area.

Hedberg (1979) interpreted the host rock of the breccia bodies

as massive, monotonous dolostone which formed in deep water. However, he noted that stromatolites and lenticular oolite lenses occur in equivalent rocks of the western Otavi Mountain Land, and north of Tsumeb. Sedimentary breccia which contains angular dolostone blocks, including oolite fragments, in a dolostone matrix is closely associated with hydrothermal breccia between Abenab West and locality 24; this is termed the Karuchas zone (Fig. 111a). Indeterminate spheroidal bodies, which may have formerly been ooids, occur in recrystallized breccia at Harasib. The presence of these lithologies indicates that moderately shallow water conditions might have existed in places; other evidence for shallow water conditions could have been obliterated in areas of intense brecciation, recrystallization and silicification, due to the more soluble nature of such rocks. The environment of deposition of the rocks in the immediate vicinity of breccia bodies, and their former solubility, is therefore unknown.

Some workers proposed a tectonic origin for the strata-bound breccia bodies, e.g. Hopwood (1975) suggested that the massive dolostone was hydraulically fractured during F_1 folding. Alternatively, Thirion (1973a) proposed that the breccia bodies formed above soluble horizons in the dolostones by a regional solution collapse mechanism. The underlying Maieberg Formation contains abundant limestone, and limestone lenses occur in the Elandshoek Formation of the western Otavi Mountain Land; similar soluble horizons may have existed in the Harasib area.

The following must be considered:-

1) Many transgressive, polymictic, breccia pipes of the central Otavi Mountain Land contain dark matrix material, foreign to their surroundings, and terminate in underlying, strata-bound breccia horizons. This is consistent with karsting above a horizon that was permeable prior to mineralization of the strata-bound and pipe breccia bodies.

2) Hydrothermal brecciation, of the type that is abundant in the strata-bound breccia, is also superimposed on the pipes of

polymictic breccia. The lead isotopic data shows that the galena in the hydrothermal breccias is of the same type in bodies of both the strata-bound and pipe breccia (Chapter 5). Therefore, a single mineralizing event is indicated, subsequent to 1).

3) The hydrothermal, strata-bound breccia bodies are not spatially related to structural features. The formation of both these and the pipe breccias, and their contained mineralization, occurred prior to the close of formation of the S_1 cleavage.

These observations are consistent with a similar origin for the two breccia types, related to karsting and solution collapse on a regional scale above soluble horizons within, or immediately below, zone T4. Thirion (1973a) considered that the breccia pipes formed by upward stoping from the strata-bound breccia. However, it is possible that they formed during the karst event that occurred during exposure of the Tsumeb Subgroup, and that they connected with this surface. This is supported by the presence of three cross-cutting bodies of sandstone and phyllite in dolostone of the Harasib area (Botha, 1960). The nature of the soluble rock is unknown; solution of carbonate rock, as proposed by Thirion (1973a) is possible, but some of the strata-bound breccia also resembles breccia described from areas of salt solution (Chapter 6.1.5). A second period of breccia formation was related to collapse which occurred while ore solutions were migrating through the soluble, strata-bound horizons.

4.4.8. Mineralization in the Auros Formation

The Abenab West ore body produced approximately 50 000 tonnes of lead metal and 5 000 tonnes of V_2O_5 from high-grade ore to 1952 (Verwoerd, 1957). The ore body consists of massive, strata-bound sulphide lenses in pink dolostone of the Auros Formation (i.e. the dolostone overlying the "quartz cluster dolomite"). Disseminated mineralization occurs in the cores of the "clusters" of the latter horizon, which are interpreted as replaced anhydrite nodules (Chapter 2.3.5). Disseminations and veinlets of sulphide also occur in the underlying "breccia limestone". The galena is foliated in places

(Verwoerd, 1957); samples of ore examined during the present study show foam texture in galena, and deformation and annealing twins in sphalerite (Fig. 122).

The lead isotope data show that lead in the Abenab West galena is isotopically distinct from that of all other mineralization in the Otavi Mountain Land, including the Karuchas zone (which occurs 200 m stratigraphically above the Abenab West ore body in the same area). The origin of the Abenab West ore locus is unknown, but dissolution of evaporites and proximity to an unconformity at the base of the overlying Elandshoek Formation were possibly important; anhydrite was a probable source of sulphur in the sulphide ore.

4.4.9 Mineralization in the Gauss Formation

Berg Aukas-type mineralization occurs in the Gauss and Auros Formations of the Abenab Subgroup. The most important occurrence is the Berg Aukas ore body, a zinc-rich ore body containing at least 1,9 million tonnes of lead and zinc metal in ore with a total metal content greater than 25 per cent (as well as economically important vanadium; Hopwood, 1975). The Berg Aukas ore body is located in recrystallized dolostone near the base of the Gauss Formation. The massive sulphide ore lenses occur as strata-bound bodies, and as discordant veins which extend into the hanging wall of the strata-bound bodies and die out upwards. None of these veins extend into the footwall of the strata-bound bodies. Boudinage was observed in some veins of massive sulphide ore, and samples of galena examined during this study show foam texture; this indicates that at least some deformation outlasted or post-dated mineralization.

The Gauss Formation is noted for its recrystallized, colloform and vuggy nature. Colloform dolostone which occurs along strike from, and overlies, the Berg Aukas ore body contains mineralized vugs in the area between Berg Aukas and the central Otavi Mountain Land (e.g. localities 41, 45, 46). The sulphide minerals occur as vug fillings associated with carbonate spar, and in dolomitic outgrowths on angular breccia fragments. Soluble material appears to have been extensively

leached along the bedding direction.

Nodular anhydrite was possibly originally present at the stratigraphic level of the Berg Aukas ore body (Chapter 2.3.5). Leaching of anhydrite might have produced the above features, and also supplied sulphur to the ores. The very limited data available on ore controls are consistent with an origin for the Berg Aukas ore body as strata-bound karst cavities. The hanging-wall veins could result from collapse of the roofs of cavities, prior to mineralization and folding of the sequence.

4.5 SUMMARY OF MINERALIZATION IN THE OTAVI MOUNTAIN LAND

Mineralization in sedimentary carbonate rocks of the Otavi Group is hosted by: (1) discordant sandstone bodies, which occur on a regional scale, but which are confined to the vicinity of the contact between the Otavi Group and Mulden Group, (2) polymictic breccia bodies (including breccia pipes), (3) pipes and irregular bodies of altered sedimentary carbonate rock, and (4) permeable lithologies, such as horizons of oolite and strata-bound breccia. The sandstone bodies decrease in size with depth within the Tsumeb Subgroup at Tsumeb, Tsumeb West and Kombat, consistent with derivation of these rocks from Mulden Group sandstone. The form and composition of the various types of mineralized body is indicative of, or consistent with, a karst and solution collapse origin, prior to D_1 deformation, the first major phase of deformation in the Otavi Mountain Land.

Three types of base metal sulphide mineralization present in the Otavi Group and Mulden Group are referred to collectively as the Owambo basin ore association. These are a simple, zinc-lead mineralization (Berg Aukas type), a mineralogically complex, copper-rich, polymetallic mineralization (Tsumeb type), and a mineralogically simple, stratiform copper mineralization (Tschudi type). These all display strong, regional stratigraphic controls, indicating extensive lateral flow of the ore solutions which formed the first two types of mineralization of obvious epigenetic type. All three types of mineralization pre-date

the close, and possibly the onset, of formation of the S_1 cleavage.

Tschudi-type and Tsumeb-type mineralization are confined to the Mulden Group and upper Tsumeb Subgroup, respectively. Lead, and to a lesser extent arsenic, is more important in Tsumeb-type ore of the northern Otavi Mountain Land (Tsumeb sub-type) than in the south. Barite, magnetite and silicate gangue minerals are confined to the southern area (Kombat sub-type). The two sub-types also differ from each other in their proportions of major, copper-bearing, sulphide minerals, such as tennantite, bornite and chalcopyrite. However, they have their polymetallic nature and a number of rare sulphide minerals in common.

Berg Aukas-type mineralization occurs within, and stratigraphically lower than, the lower Elandshoek Formation of the Tsumeb Subgroup. An oligomictic, strata-bound breccia in zone T4 underlies at least 2500 sq. km of the Otavi Mountain Land. This breccia contains Berg Aukas-type mineralization, except in part of the southern Otavi Mountain Land where a copper mineralization is present (Berg Aukas-type mineralization is confined to the underlying Abenab Subgroup throughout most of this southern area). Pipes of polymictic, dolostone breccia, which contain Berg Aukas-type mineralization, terminate in the strata-bound breccia in the central Otavi Mountain Land. The strata-bound breccia and the breccia pipes are interpreted as solution collapse and karst features, related to the presence of soluble lithologies.

The permeable pathways taken by the Tschudi-type and Tsumeb-type ore solutions are interpreted to include the basal Mulden Group sandstone, and the paleokarst topography at the top of the underlying Tsumeb Subgroup (these pathways were probably interconnected). The paleokarst topography formed to a depth of at least 1300 m at Tsumeb, but was probably confined to within 150 m of the former surface at Kombat. Early, near-vertical, faults might also have been important in controlling fluid flow within the Otavi Group. The Tsumeb West fracture zone is interpreted as a karsted fracture zone, and some of the linear, mineralized zones in the Kombat group of mines may be of

similar type. Fracture zones unrelated to karsting or solution collapse are not important ore loci. The strata-bound breccia in zone T4 was an important pathway for the solutions which formed much of the Berg Aukas-type mineralization. Some strata-bound permeability may have also been associated with rocks which underlie the unconformity that post-dates the Abenab Subgroup, e.g. at Abenab West.

Evaporite minerals occur in zone T7 of the Tsumeb Subgroup (e.g. Tsumeb, Kombat), and there is evidence for their former presence in the Auros Formation (Abenab West) and the Gauss Formation (Berg Aukas). They might also have been present in zone T4, although there is no direct evidence for this other than the former existence of soluble horizons. Anhydrite and gypsum were probably important sulphur sources for sulphide minerals in the ore bodies, and permeable fluid pathways and sites of ore deposition were possibly provided by dissolution of these evaporite minerals.

4.6 COMPARISONS WITH AREAS OUTSIDE THE OTAVI MOUNTAIN LAND

The presence of similar, rare mineralogical associations in different ore deposits may indicate that those ore deposits have related origins. Similarities in mineralogy and elemental composition may result from similar (or common) metal sources, ore fluid compositions, and physico-chemical conditions at the sites of ore deposition. The mineralogical composition can also be a function of subsequent metamorphic conditions, but this is probably not an important factor in most of the ore deposits discussed below, because these ore bodies are either unmetamorphosed, or have been metamorphosed under a maximum of low grade conditions. The unusual mineralogies of these ore bodies probably result mostly from the unusual elemental compositions of their ore fluids.

Germanium-bearing sulphide minerals are rare throughout the world, but have been recorded from ore deposits of a number of different genetic types. These ore deposits can be divided into two mineralogical groups, those which contain the argyrodite-canfieldite

mineral series (Ag_8GeS_6-Ag_8SnS_6) and those which contain germanite, briartite or renierite. Germanium is quadrivalent in the first group of ore deposits, and divalent in the second group; minerals from the two groups do not occur together in individual ore deposits, although they can occur within single mineral provinces in separate ore deposits which may be genetically related. Ore deposits which contain the argyrodite-canfieldite mineral series are not considered in detail here, but include the Saxonic vein association and veins which cut strata-bound base metal mineralization of the Kupferschiefer (Chapter 4.6.5).

Most ore deposits which contain germanite, briartite or renierite contain significant quantities of arsenic-bearing minerals. These ore deposits are confined to three environments (Table 9). The first is a calc-alkaline, magmatic environment which contains ore deposits hosted by, or marginal to, felsic intrusive bodies or volcanic rocks. The second environment is the submarine exhalative environment, in which germanium minerals occur in massive, strata-bound sulphide ore bodies. Germanium minerals never occur in significant quantities in these first two environments. The third environment is a relatively shallow water, non-magmatic, epicontinental environment (i.e. sedimentary platform or intra-cratonic basin). Germanium minerals are more widespread and abundant within this environment than any other, although they are, in all cases, a minor constituent of the sulphide ore in which they occur. This third environment includes ore deposits of the Owambo basin, and deposits of similar mineralogical type and age throughout central Africa; it also includes strata-bound and breccia-hosted ore deposits in western Europe, Sardinia, Alaska and China.

4.6.1 Tsumeb-type mineralization of central Africa: stratigraphic position

Germanium-bearing ore deposits of Tsumeb type are present in the Damaran fold belt (i.e. the Otavi Mountain Land), the Katangan fold belt (e.g. Kipushi ore body, Zaïre) and the West Congolian fold belt (e.g. M'Passa ore body, Congo Republic). The ore deposits occur in

TABLE 9 OCCURRENCES OF GERMANITE, RENIERITE AND BRIARTITE

MINERAL	LOCALITY	ORE DEPOSIT TYPE	COMMENTS	REFERENCES
Germanite, renierite	Dastakert, U.S.S.R.	Molybdenum-copper in plutons	enargite, tennantite	Karamjan (1959)
Germanite	Toroiaga-Baia Borsa, Rumania	Copper-zinc in andesite and diorite	tetrahedrite-tennantite	Steclaci (1961)
Germanite, renierite	Meat Cove, Nova Scotia	Base metal-magnetite skarn	stannite	Chatterjee (1979)
Germanite, renierite	Chelopech, Bulgaria	Copper vein in volcanic rocks	tennantite, luzonite, enargite	Terziyev (1966)
Germanite?	Kamikata mine, Japan	Volcanogenic copper-zinc	enargite, luzonite tetrahedrite-tennantite	Takeuchi et al. (1956)
Germanite, renierite?	Daluis gorge, France	Copper replacement in conglomerate	tennantite, luzonite, enargite	Picot (1970)
Germanite	Ruby Creek, Alaska	Copper-lead-zinc replacement of sedimentary carbonate rocks	tennantite, tetrahedrite, carrollite	Runnels (1969)
Renierite, briartite, germanite	Kipushi, Zaïre	Copper-lead-zinc replacement of sedimentary carbonate rocks	Tsumeb type, including betekhtinite, sulvanite, ReS_2?	Dimanche (1974), De Vos et al. (1974)
Renierite, germanite, briartite?	M'Passa, Congo Republic	Copper-lead-zinc replacement of sedimentary carbonate rocks	Tsumeb type	Picot et al. (1963), Scolari (1965)
Germanite, renierite	Mindouli, Congo Republic	Copper-lead-zinc replacement of sedimentary carbonate rocks		Scolari (1965)
Renierite?	Sable Antelope, Zambia	Copper-zinc replacement of sedimentary carbonate rocks	tennantite	Cikin and Drysdale (1971)
Renierite	Iglesiente, Sardinia	Open-space fillings of zinc-lead-barite in sedimentary carbonate rocks		Lauzac (1965)
Germanite?	Dongchuan, China	Stratiform copper in arenite	enargite	Wang (1983)

rocks that were deposited in a platform or shelf environment, which separated the Congo craton from areas of deeper-water deposition (Fig. 123). It has been proposed that the deeper basins were controlled by ensialic rift zones in the West Congolian fold belt, and in the north-east trending branch of the Damaran fold belt and its probable extension as the Katangan fold belt (Martin and Porada, 1977a; Porada, 1979).

The germanium-bearing ore deposits which occur in these fold belts are entirely confined to the top of thick sequences of sedimentary carbonate rocks, and to the base of overlying sequences of arenite and pelite. The ore deposits are mostly confined to the top of sedimentary carbonate rocks of the Otavi Group, the Lower Kundelungu Supergroup, and the Schisto-calcaire Group, in the Damaran, Katangan and West Congolian fold belts, respectively. The sedimentary carbonate rocks are separated by unconformities and disconformities from overlying arenitic and pelitic rocks of the Mulden Group, Upper Kundelungu Supergroup, and Mpioka and Inkisi Groups (Table 10). Only a small number of ore deposits are known in these overlying rocks, including parts of the M'Passa and Bamba Kilenda ore bodies. Ore deposits of the West Congolian fold belt can be further subdivided into those of the Niari basin and Bungo basin, on the northern and southern margins of the Mbridge-Mbanzu Ngungu ridge (Fig. 123). This ridge was a positive feature at various times during deposition of the West Congo Sequence (Cahen, 1978).

The sedimentary rocks in which the ore deposits occur have undergone negligible, to low grade, metamorphism (i.e. mostly to below greenschist facies). The highest metamorphic grade occurs in biotite-bearing rocks which host ore deposits of the Katangan fold belt (e.g. Kipushi). Ore deposits of the Owambo basin, and possibly the M'Passa ore deposit of the Niari basin, were deformed by the first major deformational events in those areas (D.M. Baka, pers. comm., 1978). Intiomale and Oosterbosch (1974) recorded abundant small folds in ore of the Kipushi mine, Zaïre, but it is not clear from their description whether they considered that the sulphide minerals had replaced rock which had already been deformed. Igneous intrusive activity was

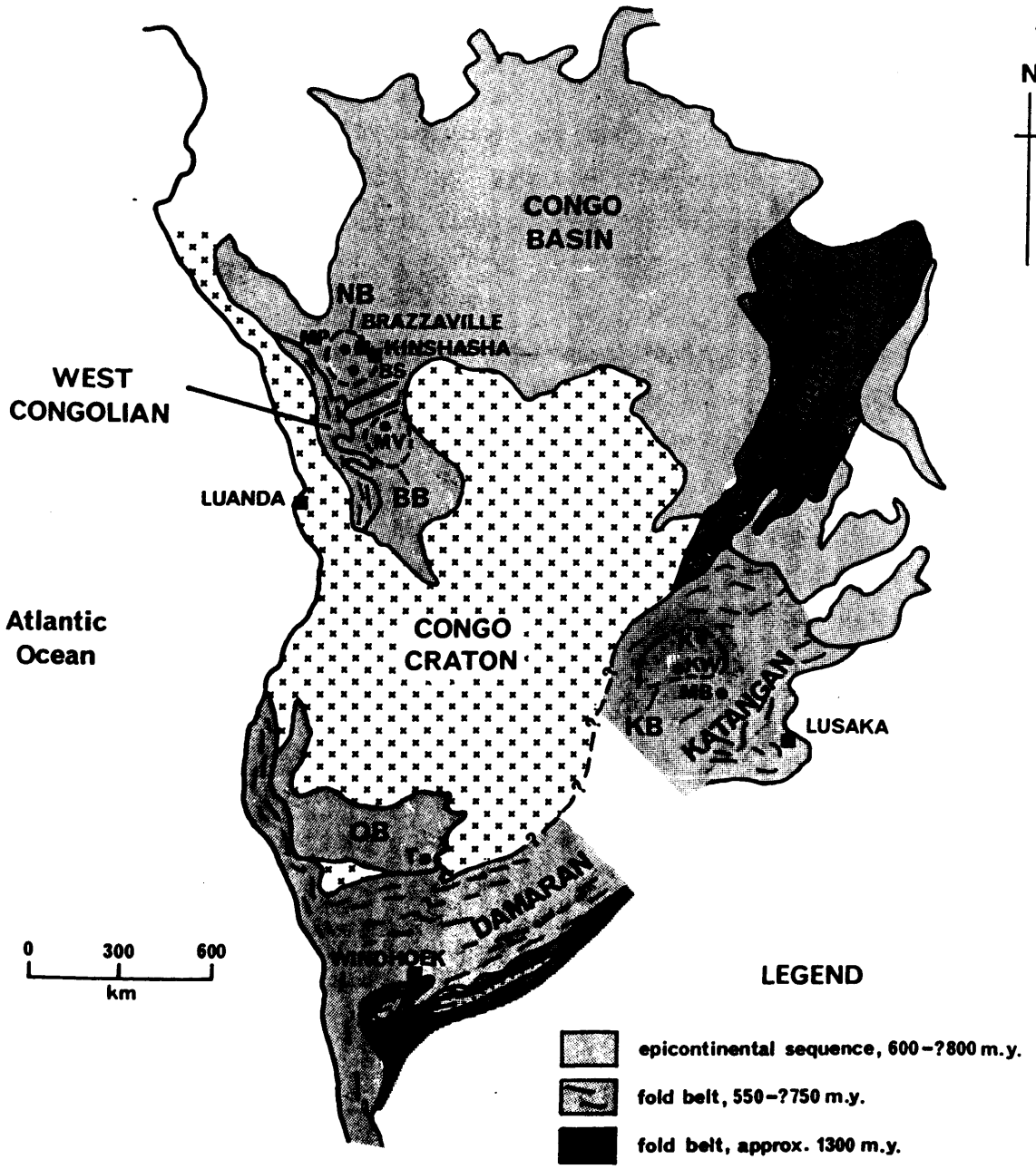

ORE BODIES

(1) Strata-bound in sedimentary carbonate rocks

- T Tsumeb (and other ore deposits of the Otavi Mountain Land)
- MB Mumbwa (also Kabwe, Kiseba)
- K Kipushi (also Lombe, Kengere, Bukanda, Ndola)
- MP,BS M'passa, Boko-Songho (also Mindouli, Hapilo, Diangolo, Djenguilé, Yanga-Koubanza)
- MV Mavoio (also Mangulu, Mavungu, Bamba-Kilenda)

(2) Stratiform copper deposits

- KW Kalengwa (Kundelungu Supergroup?)
- Roan Supergroup and probable equivalents

Fig. 123

Ore deposits of the Owambo basin-type ore association, central Africa. The mineral districts are confined to epicontinental rocks of Late Proterozoic age, adjacent to the Congo craton. Sources of data: Cikin and Drysdale (1971), Intiomale and Oosterbosch (1974), Pauly (1966), Scolari (1965).

negligible in the shelf sequences of each of the fold belts, with the exception of some granite and syenite intrusions in southern Zambia, and only rare dolerite and lamprophyre dykes occur in the vicinity of most ore bodies.

The ages of the sedimentary sequences in each of the fold belts are broadly similar, although poorly known, and the main deformational events and final thermal events can be closely correlated (Table 10). The Roan Supergroup may be older than shown, because an 843 m.y. U/Pb (zircon) age has been obtained from the Lusaka granite, Zambia; however, it is not certain that this granite intrudes rocks of the Katanga Sequence (Barr et al., 1977). A depositional age of approximately 1050 m.y., proposed for the Roan Supergroup by Cahen (1974), is not considered here to be reliably established, because it is based entirely upon the above evidence, on two and three point Rb-Sr "isochrons" from microcline veins near the base of the supergroup, on lithological correlations with the Bushimay Supergroup of Zaïre, and on world-wide comparisons of stromatolite forms. Even if this age is correct, there is no evidence that it is applicable to the Kundelungu Supergroup, as an angular unconformity exists between the Roan and Kundelungu Supergroups in some areas (Ramsay and Ridgeway, 1977).

Mixtites, including possible tillites, occur in the sedimentary sequences of all three fold belts. Gypsum and anhydrite horizons, and probable paleokarst features, are present in sedimentary carbonate rocks a short distance below the base of each of the overlying clastic sedimentary sequences. These overlying sequences include arkoses, and may represent a molasse in each fold belt. Buffard (1977) suggested that the change from sedimentary carbonate rocks to arenite and pelite represents the same event in the Damaran and Katangan fold belts. It can be concluded that parallel, broadly contemporaneous depositional histories are recorded in each fold belt.

The close association between mineralization and sedimentary gypsum and anhydrite in the Otavi Mountain Land is discussed in Chapter 2.3. A similar association is present in the Katangan fold belt. The Kipushi evaporite basin formed during the final stages of

TABLE 10

CORRELATION OF LATE PRECAMBRIAN SEQUENCES OF CENTRAL AFRICA

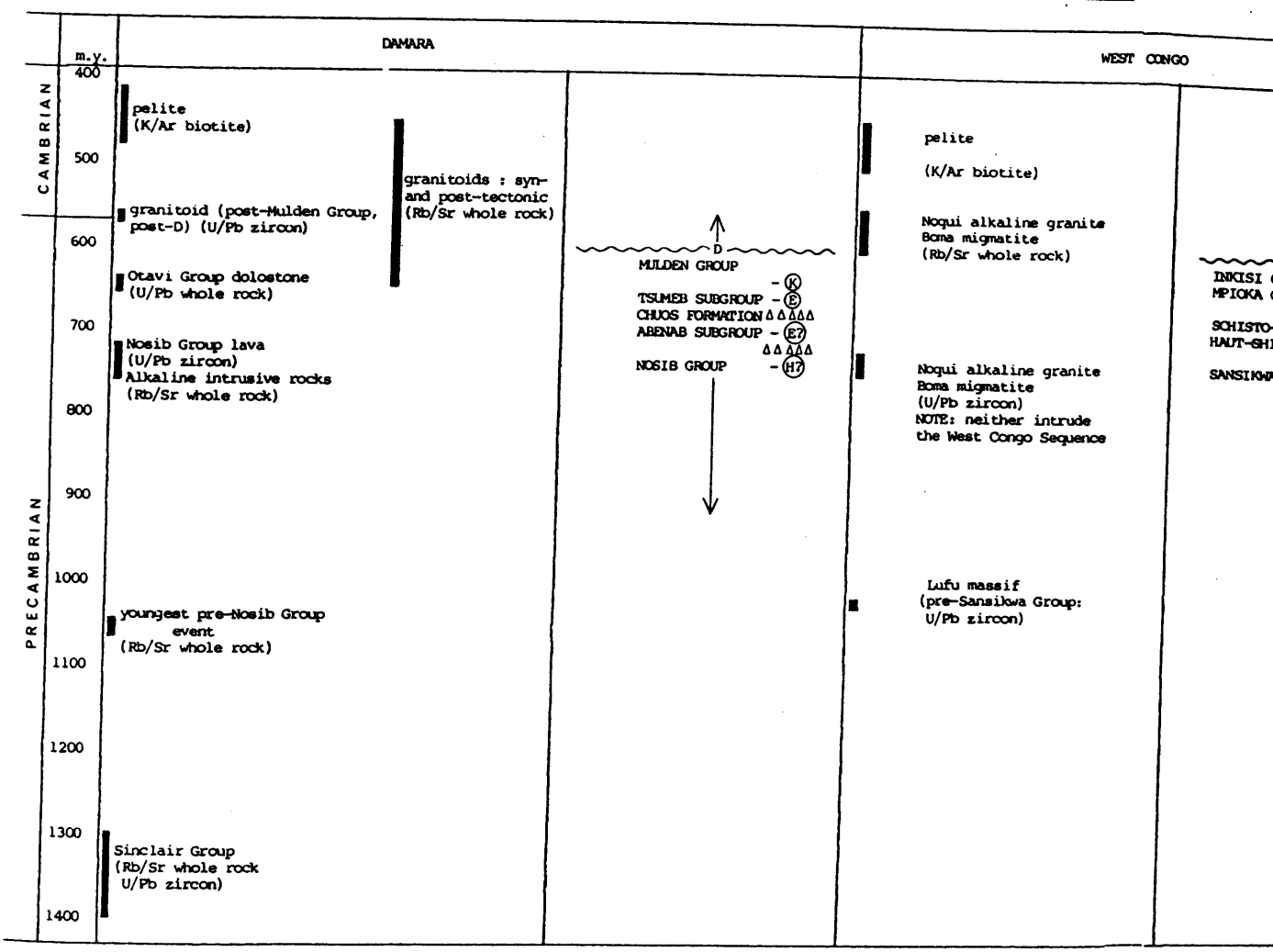

REFERENCES:
Kröner et al. (1978)
Kröner (1982)
Watters (1982)
Miller and Burger (1983a, b)

REFERENCES:
Cahen et al. (1976)
Cahen (1978)

TABLE 10

CORRELATION OF LATE PRECAMBRIAN SEQUENCES OF CE

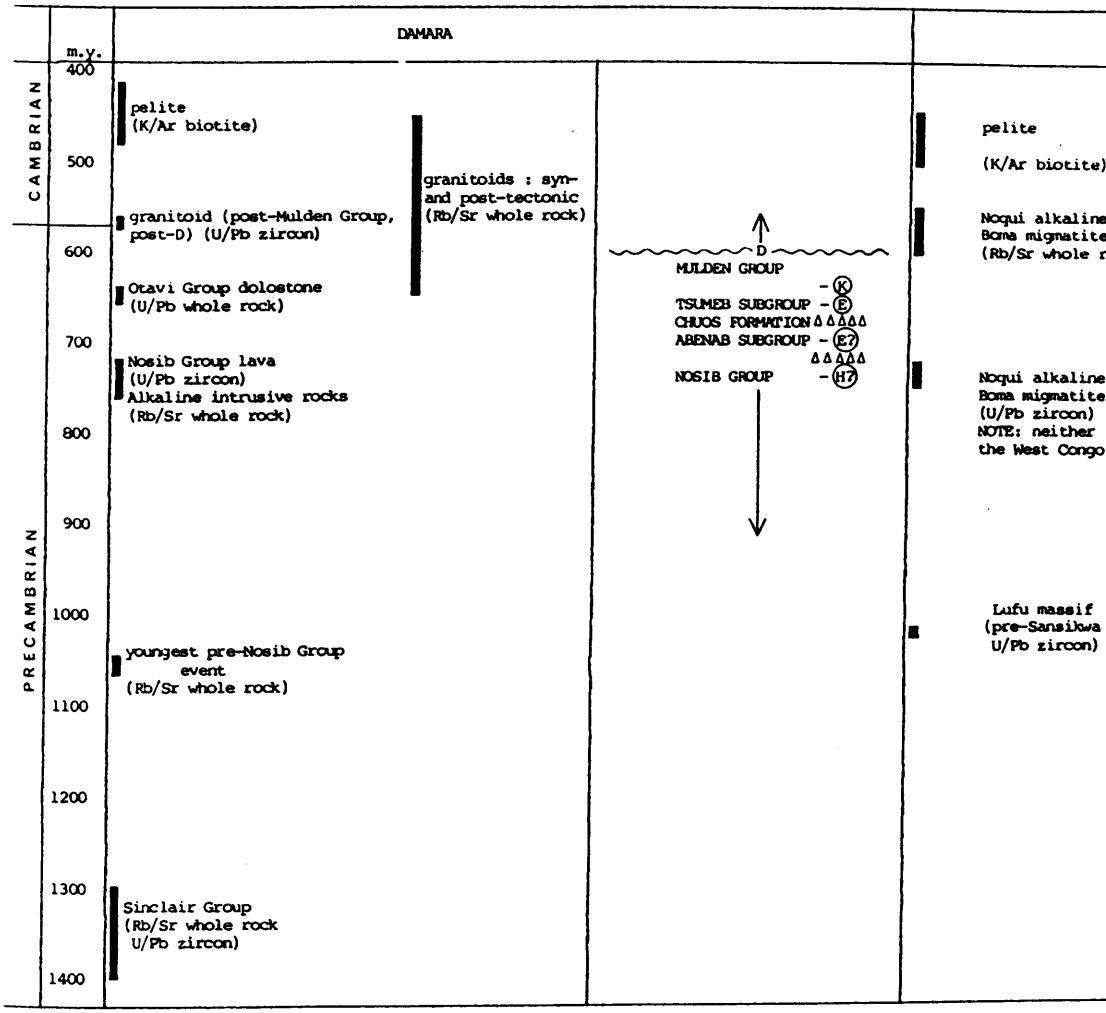

REFERENCES:
Kröner et al. (1978)
Kröner (1982)
Watters (1982)
Miller and Burger (1983a, b)

REFERENCES:
Cahen et al. (19
Cahen (1978)

TABLE 10

CORRELATION OF LATE PRECAMBRIAN SEQUENCES OF CENTRAL AFRICA

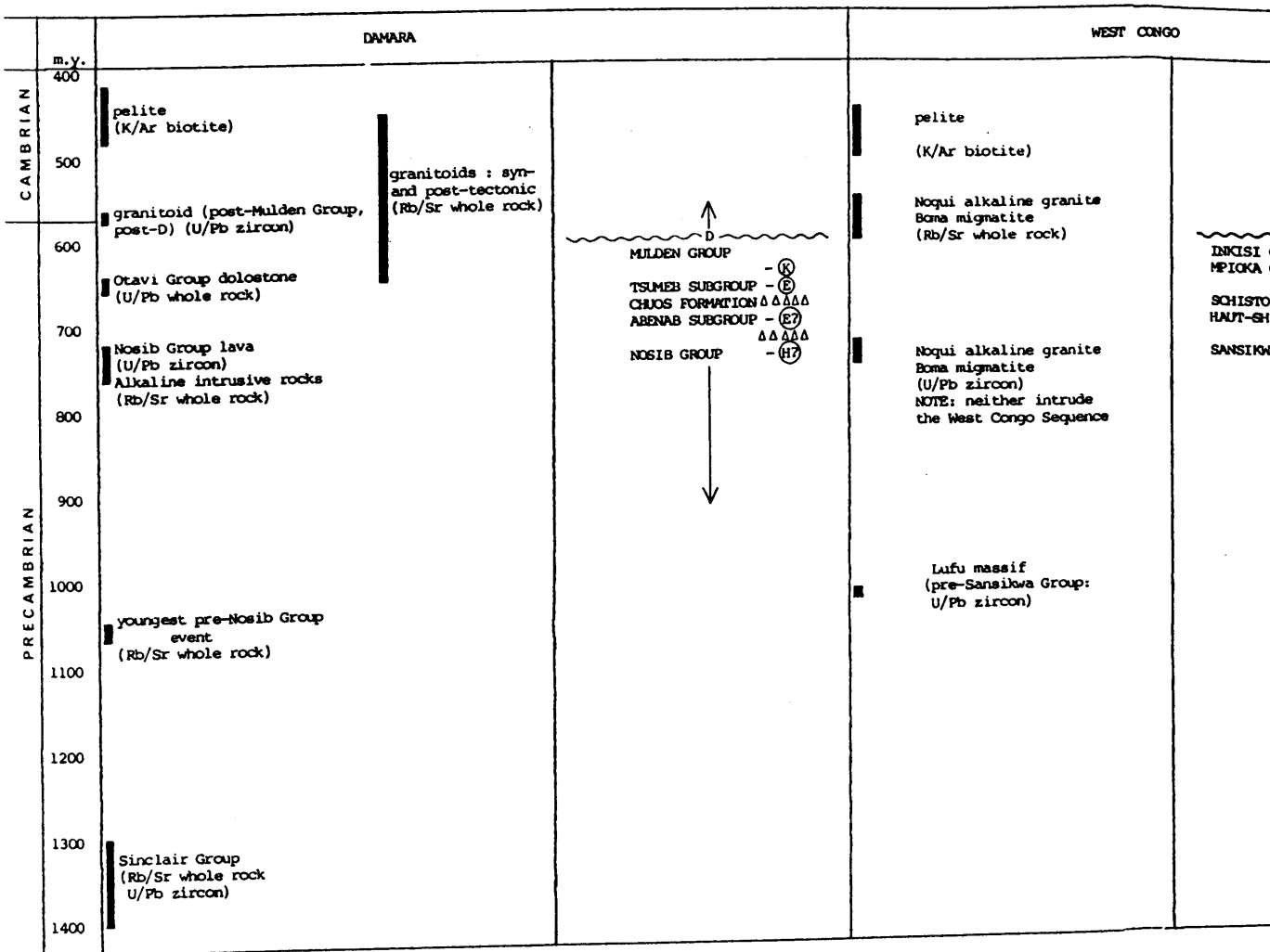

REFERENCES:

Kröner et al. (1978)
Kröner (1982)
Watters (1982)
Miller and Burger (1983a, b)

REFERENCES:

Cahen et al. (1976)
Cahen (1978)

associated with the margins of pipe-like breccia bodies (Murray-Hughes and Fitch, 1929; Brandt, 1955; Reeve, 1963; Cikin and Drysdale, 1971). Mineralization of the Niari basin and Bungo basin is closely associated with minor, north-east trending faults. However, it is typically confined to breccia and manto bodies in rock adjacent to the faults, rather than to the faults themselves (Stam, 1960; Scolari, 1965; Pauly, 1966; Mouzita, 1979). Baka (1975) interpreted the ore controls at M'Passa mine to be karsted fractures and soluble horizons in the Schisto-calcaire Group, less than 15 m below its contact with the Mpioka Group (Table 10).

Mineralization within arenaceous rocks, which overlie the sedimentary carbonate rocks in each of the fold belts, commonly occurs in irregular and strata-bound bodies which extend outwards from fault zones, e.g. n'Zala-Diangala and n'Zala-Mimbodi, Congo Republic (Scolari, 1965). This is also true of Mavoio, Angola, where mineralization also occurs in the underlying sedimentary carbonate rocks (Pauly, 1966). Berg Aukas-type mineralization of the Kabwe mine, Zambia, occurs in breccia pipes which are broadly strata-bound within dolostone (Reeve, 1963).

4.6.3 Tsumeb-type mineralization of central Africa: mineralogy

Tsumeb-type mineralization of the West Congolian and Katangan fold belts is very similar mineralogically to that of the Otavi Mountain Land (Table 8), and Scolari (1965) proposed a germanium-rich province in central Africa. The Tsumeb ore body, and the Kipushi ore body of Shaba, Zaïre, are economically the most important mines in these fold belts (Fig. 123). Production from Kipushi mine to 1981 was 45 million tonnes of ore with an average grade of 12 per cent zinc, 8 per cent copper, 0,9 per cent lead and an estimated 130 grams/tonne silver. The Kipushi ore body is zoned mineralogically, e.g. bornite-rich ore is more abundant in the anhydrite-bearing Série Récurrente than in the underlying Kakontwe Limestone, in which chalcopyrite is important. Minor mineralogical differences exist between the Kipushi and Tsumeb ore bodies (Table 8). Arsenopyrite is widespread at Kipushi, and cobaltite is present in chalcopyrite ore, although

carrollite occurs in bornite ore. Traces of bismuth minerals are present. Enargite is rare, barite is very rare, and germanite is very rare relative to renierite. Molybdenite is more abundant at Kipushi than at Tsumeb, and a probable rhenium-rich molybdenum sulphide is present (Intiomale and Oosterbosch, 1974). Mineralogically-simple, lead-zinc mineralization occurs elsewhere within the Kakontwe Limestone of Shaba, at the Lombe and Kengere occurrences.

Mineralization of probable Tsumeb type is also present in the Katangan fold belt at Mumbwa, Zambia. Production from this area occurred prior to 1925, and consisted of 4250 tonnes copper and 2000 kg silver. Copper ore consists of chalcopyrite, bornite and tennantite, with some arsenopyrite. "Orange bornite" that occurs in germanium-bearing ore from this locality (Cikin and Drysdale, 1968) is probably renierite. Mineralogically-simple, sphalerite-galena-pyrite ore of Berg Aukas type was mined from the economically important Kabwe (Broken Hill) mine, further to the east. Production and reserves at Kabwe, to the end of 1970, were approximately 1 million tonnes of lead and 1,5 million tonnes of zinc (Reeve, 1963; Kortman, 1972).

Ore bodies of the Niari basin, in the West Congolian fold belt, produced approximately 100 000 tonnes lead, 35 000 tonnes zinc, 20 000 tonnes copper, and an unknown but large quantity of silver to 1978. Production from mines of the Bungo basin is unknown, but was small. The mineralogy of ore bodies in both basins has been described by Bigotte (1959), Stam (1960), de Kun (1965), Scolari (1965), Pauly (1966) and la Direction de la Geologie (1968). Minerals which are diagnostic of Tsumeb-type mineralization are confined to occurrences in the Niari basin. M'Passa ore body is the best described; this consists of tennantite, bornite and subordinate chalcopyrite, with very minor enargite and arsenopyrite. The ore contains a suite of cobalt minerals which includes cobaltite but not carrollite (Table 8). Germanite and renierite are present at both M'Passa and Mindouli mines. Mineralogical data from other mines is limited, but chalcopyrite and tennantite are probably the dominant copper minerals in the Niari basin, and minor arsenopyrite is widely distributed. Arsenopyrite and tennantite are also present in mineralization which occurs in overlying

arenite (e.g. N'Zala-Diangala). Cobalt and nickel are important elements in arsenical base metal ore of the Bungo basin, e.g. Mavoio ore body (Pauly, 1966).

4.6.4 Tsumeb-type mineralization of central Africa : timing and conclusions

Tsumeb-type mineralization of the Damaran fold belt post-dated initial deposition of sediments of the Mulden Group, because these are mineralized within the Tsumeb pipe. Mineralization of the Katangan fold belt probably post-dated deposition of most of the Upper Kundelungu Supergroup, because breccia bodies of the type which occur adjacent to mineralization at Kipushi post-date these rocks. Some Tsumeb-type mineralization of the West Congolian fold belt occurs adjacent to, and appears to be controlled by, faults which displace the Inkisi Group. Therefore, although mineralization is spatially related to the contact between sedimentary carbonate rocks and overlying arenite-pelite sequences in each of the fold belts, it occurred subsequent to significant sedimentation above this contact. The Mulden Group, and therefore the Tsumeb ore body, was deformed prior to 589 $\pm$ 40 m.y. (Miller and Burger, 1983b), and the Upper Kundelungu Supergroup prior to 602 m.y. (Cahen, 1974). The West Congo Sequence may also have been affected by a tectono-thermal event at this time (Cahen et al., 1976). The Otavi Group was deposited subsequent to 728 $\pm$ 40 m.y. (Miller and Burger, 1983a). Therefore, Tsumeb-type mineralization occurred between 730 m.y. and 590 m.y. in the Owambo basin, and data from the other fold belts is consistent with a similar age of mineralization.

It is concluded that the Owambo basin-type ore association (including the Tsumeb type of mineralization) defines a mineral province which extends throughout the Damaran, Katangan and West Congolian fold belts, around the margin of the Congo craton. The Tsumeb type of mineralization occurs in identical lithologies, deposited in similar sedimentary and tectonic environments, in each of the fold belts. This mineralization is closely associated with unconformity and disconformity surfaces of broadly similar age, which

mark major lithological changes in all three fold belts, from sedimentary carbonate rocks to overlying arenite-pelite sequences. However, mineralization occurred subsequent to major sedimentation in these overlying sequences. Evaporite horizons were deposited near the top of the sedimentary carbonate rocks, and paleokarst features also occur in this stratigraphic position. This karsting event pre-dated deposition of overlying arenite, at least in the Damaran fold belt.

The Berg Aukas type of mineralization occurs lower in the sequence than the Tsumeb type in both the Damaran and Katangan fold belts. Mineralization also occurs in the base of the arenite-pelite sequences which overlie Tsumeb-type mineralization in each of the fold belts. This mineralization includes stratiform copper mineralization, and irregular, polymetallic and vein-like bodies, some of which are spatially related to the same faults which appear to control the underlying Tsumeb type of mineralization. Mineralization was mined from both the sedimentary carbonate rocks and overlying arenite in some mines (e.g. Mavoio, Angola). Mineralization of the Damaran fold belt was deformed by an early, major phase of folding, and mineralization in the other fold belts may also have been deformed by folding events.

4.6.5 Mineralogically similar occurrences outside central Africa

Ore bodies which are mineralogically similar to Tsumeb-type mineralization are not confined to central Africa. The germanite- and renierite-bearing, arsenical copper mineralization of Daluis gorge, France, occurs immediately east of the Triassic salt basin of south-eastern France and its northern extension as the Bunter Sandstone basin. Pyrite, chalcopyrite, tennantite and rarer enargite and galena occur as veinlets and impregnations in basal Triassic conglomerate, which underlies an evaporite sequence (Picot, 1970). Saxonic veins (see following discussion) and mineralogically similar arsenical mineralization, some of which contains argyrodite and betekhtinite, occurs in basement rock and Triassic dolostone further to the east (in one instance associated with an anhydrite deposit; Hüttenlocher, 1936; Bachtiger, 1963; Graeser, 1965; Tufar, 1982).

The economically important Largentière and Malines ore deposits occur on the north-western margin of the Triassic salt basin described above, and the major germanium producer, Saint Salvy, occurs farther to the south. The Malines deposit, of Mississippi Valley (or "Alpine") type occurs in paleokarst features in dolostone, and in underlying basal Triassic conglomerate (Foglierini et al, 1980a). The Largentière deposit, of sandstone lead type, occurs in sandstone at the base of the Triassic sequence; very minor mineralization is present in overlying dolostone (Foglierini et al, 1980b). Gypsum, including nodular gypsum, is closely associated with some ore at Largentière and Malines. The sphalerite veins of Saint Salvy occur in Cambrian carbonaceous schist, which contains phosphate nodules. The high grade zinc ore is rich in silver, germanium, cadmium and possibly gallium (see analysis in Geldron, 1983), and Saint Salvy is the most productive germanium mine in the world. Germanium is especially concentrated in veins which cut beds rich in organic matter (Geldron, 1983).

Renierite-bearing lead-zinc deposits of the southern part of the Iglesias district, Sardinia, are similar to Mississippi Valley-type deposits. A mineralogically simple, sphalerite, galena and barite mineralization was deposited in paleokarst structures, which developed on Cambrian limestone prior to the deposition of Ordovician shale (Lauzac, 1965; Jensen and Dessau, 1966).

Germanite-bearing copper-zinc mineralization of Ruby Creek, Alaska shows mineralogical similarities to Tsumeb-type mineralization. Mineralization occurs with dolomite gangue in strata-bound breccia bodies, within a Middle Devonian reef complex which is associated with a pelitic sequence (Runnels, 1969). The sedimentary carbonate rocks are associated with a former rifted continental margin which had a horst and graben structure; carbonate sedimentation occurred on the horsts, and pelitic sedimentation and minor volcanism occurred in the grabens. The mineralization consists of massive pyrite, including cobaltian pyrite, chalcopyrite, bornite, tennantite-tetrahedrite, chalcocite, sphalerite, galena, silver minerals, and minor carrollite and barite.

The Dongchuan copper deposit of Yunan, China, occurs in rocks of Late Proterozoic age (Wang, 1985). The mineralization is stratiform

within argillaceous and arenaceous dolostones which are associated with a slate and dolostone, in part sabkha, sequence. The ore displays the zoning of copper and iron sulphide minerals that is characteristic of many stratiform copper deposits (Mendelsohn, 1961). Germanium occurs in anomalous concentrations, possibly as germanite, within enargite-chalcopyrite veins in dolostone of the hanging wall of the deposit (Wang, 1985, considered these veins to be of metamorphic origin).

The deposits discussed above show similarities to both Tsumeb-type mineralization, and the Owambo basin-type ore association. "Tsumeb-type mineralization" is used here in the very restricted sense of an arsenical base metal mineralization, hosted by sedimentary carbonate rocks, which contains at least one type of germanium-bearing sulphide mineral. The above list can be extended to include all occurrences of the rare minerals betekhtinite and sulvanite, which occur in deposits of the Owambo basin, and sulphide minerals which contain essential rhenium (i.e. a rhenium-bearing sulphide mineral, possibly $(Re,Mo)S_2$, is thought to occur in the Kipushi ore body; Intiomale and Oosterbosch, 1974).

Betekhtinite is a low temperature mineral (Markham and Ottemann, 1968), and the possibility that it can form during very low grade metamorphism of copper-lead ore cannot be excluded. However, the absence of betekhtinite in many ore bodies of this type, and the common association of betekhtinite with other rare sulphide minerals characteristic of Tsumeb-type mineralization, is consistent with a primary, hypogene origin for this mineral. Betekhtinite occurs in some volcanogenic massive sulphide deposits (Markham and Ottemann, 1968; Matsukuma, 1971), and is also present in ore deposits which occur in rocks formed in a relatively shallow water, non-magmatic environment. Betekhtinite occurs in stratiform copper-lead-zinc ore of Kazakhstan, U.S.S.R., together with arsenic, cobalt, nickel and silver minerals, molybdenite and djezkazganite, and very minor quantities of bismuth, gold and mercury (Popov, 1955; Vlasov, 1966; Markham and Ottemann, 1968). Djezkazganite was identified as $CuReS_4$, but may be (Re, Mo) S_2 (Morris and Short, 1966). Beds of gypsum and halite immediately overlie the ore-bearing beds in Kazakhstan (Popov, 1962). The Kazakhstan ore shows classical zoning of copper and iron sulphide minerals.

Betekhtinite was first described from base metal veins (Rücken) which cut the stratiform Cu-Pb-Zn mineralization of the Kupferschiefer, Germany, which like the Kazakhstan mineralization shows zoning of copper and iron sulphide minerals. The Kupferschiefer mineralization occurs to the south of the Zechstein salt basin (Zeigler, 1975) and is overlain almost immediately by anhydrite; there is evidence that the mineralization does not have a simple syngenetic origin, despite its stratiform nature and regional extent (Rentzsch, 1974). The Kupferschiefer is a shale with a high pyrobitumen content, and lenses of calcium phosphate and magnesium borate minerals are present in places (Kucha, 1982). Minerals in the Rücken include tennantite, molybdenite, Ni-Co-As minerals, wittichenite, uraninite and possibly (Re, Mo)S_2 (Schüller and Wohlmann, 1955; Schüller, 1959). The Re:Mo content of the Kupferschiefer itself is very high (Haranczyk, 1972), and it contains arsenic, silver, nickel, cobalt, mercury, uranium, selenium, tellurium and bismuth minerals, gold, platinum group elements, and the quadrivalent germanium mineral, argyrodite (Nhan, 1970; Kucha, 1982). This indicates a possible genetic link with argyrodite-bearing veins of the Ag-Bi-Co-Ni-As vein association (Saxonic association), which occur in basement rocks farther to the south-east, at Freiberg. Chalcocite-galena intergrowths from some other areas may be after betekhtinite, although they have not been interpreted as such (e.g. in Saxonic veins of Cobalt, Ontario; Petruk et al., 1971).

Sulvanite occurs in association with copper mineralization in sedimentary carbonate rocks of Italy (Orlandi et al., 1981), Utah (Schempp and Schaller, 1931; Dolanski, 1974) and South Australia (Dolanski, 1974). The South Australian occurrence occurs in a district which contains stratiform copper mineralization with minor gold, arsenic, and cobalt, and also similar mineralization which is hosted by breccia bodies in sedimentary carbonate rocks, e.g. Burra (Johnson, 1965).

A final example of an ore deposit which may prove to be of Tsumeb type, but in which no sulphide ore has yet been observed, is the Apex mine, Utah. Oxidized copper-zinc-silver ore, which contains minor quantities of As, Sb, Bi, Cd, Co, Pb, Mo, Ni, W, Ge, Ga and Ag is

currently being exploited in a pipe-like body of iron oxide minerals (probable gossan) within sedimentary carbonate rocks of Pennsylvanian age. This ore body is unique in that it is primarily being exploited for its contained germanium and gallium (Musto Explorations Limited, unpub. rept., 1984). Evaporite horizons are present within Pennsylvanian rocks of the surrounding region, and uranium deposits with molybdenum and rhenium are present in younger rocks.

All of the occurrences discussed above show some mineralogical similarities, in addition to the presence of the rare minerals discussed. There is also a distinct elemental association (characterized mainly by its diversity) of Cu, Pb, Zn, As, Cd, Ag, Mo, Ge, Ga, Co, Ni, Mo, Ba and, less abundantly or less commonly, Sb, U, V, W, Sn, Hg, Bi, Re, Au and PGE. A similar elemental association occurs in Mississippi Valley-type deposits, in which Pb, Zn, Ag, Co, Cd, Ge, Ga and possibly Mo are important (Heyl, 1967; Foss et al., 1983; Geldron, 1983), and in stratiform copper deposits of Zambia and Zaïre, which contain Cu, Co, Ni, Mo, U, W, As, Ni, Ag, Au, PGE, Bi and Te minerals (Annels, 1984). Sedex (sedimentary exhalative) and related vein mineralization of Ireland contains Cu, Pb, Zn, As, Sb, Ni, Co and Hg (Morrissey et al., 1971).

4.6.6 Other similarities between ore deposits of sedimentary basins

The ore bodies discussed above show other features in common with each other, or with the Owambo basin-type ore association. These include: (1) the presence of paleokarst features, sabkhas, salt basins, and rifted environments, (2) the close spatial association of stratiform copper mineralization and mineralization hosted by veins and breccia bodies in sedimentary carbonate rocks, and (3) the close spatial association of strata-bound ore bodies and some vein-type deposits in adjacent basement rocks. It is shown in the following chapters that these features may all have genetic significance, and that these different types of mineralization (including Tsumeb-type mineralization), and other types of ore deposit in sedimentary basins, are closely associated spatially and may have related origins. Numerous origins have been proposed for the ore deposits discussed, but an origin related to the circulation of stratal fluids is widely accepted for these ore deposits (with the exception of Saxonic vein mineralization and, to a

lesser extent, stratiform copper mineralization).

Different types of base metal mineralization, of broadly similar age, are commonly present within a single sedimentary basin (although only one type may be economically important), and similar groupings of ore deposits can be repeated within adjacent, tectonically-related basins. This constant spatial and temporal association of certain types of ore deposit is consistent with a similar or common origin for these deposits. Examples are the Owambo Basin-type association of central Africa, and the Lower Cretaceous sandstone lead, and stratiform copper, province of western and north-western Africa (Caïa, 1976). Another example is the Triassic mineral province of south-eastern France discussed in Chapter 4.6.5, which forms part of a larger, Triassic lead-zinc province that extends eastwards across southern Europe to Poland (Brigo et al., 1977; Kantor, 1977; Sass-Gustkiewicz et al., 1982) and northwards via the Bunter Sandstone basin into West Germany (Bjorlykke and Sangster, 1981). This province, which is also represented in north-western Africa (e.g. Tunisia) and northern Spain (Rouvier et al., 1985) includes Mississippi Valley-type deposits, sedex (sedimentary exhalative) deposits, sandstone lead deposits, Tsumeb-type mineralization, Saxonic veins and germanium-rich base metal veins. The Mississippi Valley region of the U.S.A., which contains both zinc and lead ores, as well as very minor sandstone lead and copper mineralization, is a further example (Snyder and Gerdemann, 1968). This mineral province may be of early Permian age (e.g. Wu and Beales, 1981), although there is no conclusive evidence that these deposits formed during a single event, restricted in time. There is also a close spatial relationship between Mississippi Valley-type mineralization and sedex mineralization in the Selwyn basin, Canada, and at McArthur River, Australia (Godwin et al., 1982; Walker et al., 1983).

Saxonic vein mineralization and basalt-hosted native copper deposits are common members of associations of the above type. The Michigan copper province, of late Proterozoic age, contains economically unimportant Saxonic vein mineralization (Oja, 1966), in addition to volcanic-hosted native copper and stratiform copper (i.e. copper shale) deposits. Stratiform copper-lead-zinc mineralization (the Kupferschiefer) and Saxonic vein mineralization occur in the Permian mineral province of north-western Europe (Chapter 4.6.7), and economically unimportant native copper mineralization is present in

volcanic rocks of the Rotliegende, which immediately underlies the Kupferschiefer bed (Beck, 1905). Mineralization and rock alteration (Rote Faüle) associated with the Kupferschiefer mineralization also occur in the Rotliegende (Rentzsch, 1974). Native copper mineralization is present farther to the north, in Permian basalt of the Oslo rift, where it occurs adjacent to Saxonic vein mineralization (Vokes and Gale, 1976). The massive, carbonate-hosted copper deposits of Kennecott, Alaska, show similarities to Tsumeb-type mineralization, in that they are closely associated with a sabkha horizon; however, they lack the trace mineral assemblage diagnostic of Tsumeb-type mineralization (Armstrong and MacKevett, 1975; Potter et al., 1977). Uneconomic native copper mineralization is present in the immediately underlying Nikolai Greenstone (Bateman and McLaughlin, 1920). Saxonic vein mineralization, basalt-hosted native copper mineralization, and economically unimportant, strata-bound uranium mineralization occur in Lower to Middle Proterozoic rocks in rift environments on the western margin of the Bear and Slave Provinces, Canada (Kindle, 1972; Badham, 1978; Gandhi, 1978). Pitchblende ages are approximately 1400 m.y. (e.g. Thorpe, 1974), which is comparable to the 1350 m.y. pitchblende age of unconformity-type uranium deposits in the Athabasca basin to the south, where veins similar to Saxonic veins are also known (i.e. at Beaverlodge; Trocki et al., 1984). Stratiform copper mineralization, which is associated with a sabkha sequence, and Saxonic vein mineralization occur farther to the east, in the Lower Proterozoic Cobalt Group of Ontario (Berry, 1971; Chandler, 1984).

The above spatial association between strata-bound uranium mineralization, Saxonic veins and stratiform copper mineralization is not uncommon, and mineralogical and chemical similarities sometimes exist between these deposits. Stratiform copper and strata-bound uranium mineralization occur together in the Colorado Plateau region, U.S.A., where they are closely associated with pipes of probable karst origin which contain uranium and base metal mineralization (Chapter 6.1.6). Another example is the Shinkolobwe-type uranium mineralization of Zaïre, which is associated with diapiric breccia bodies of the Mines Group; this is spatially and temporally related to the Owambo Basin-type association, but it occurs in the same formation as stratiform mineralization of the Mines Group (Kitmut and Kalengwa,

1979).

Many uranium deposits, e.g. roll-front deposits, are mineralogically simple, and contain uranium, vanadium, molybdenum and selenium minerals (Warren, 1972). Uranium deposits of unconformity type and Shinkolobwe type differ mineralogically from roll-front deposits in that they contain nickel arsenide and sulphide minerals, sometimes in economically important quantities (Rimsaite, 1978). A complex mineral assemblage occurs in some ore bodies, and this can include copper-bearing sulphide minerals, cobalt minerals, galena, selenides (e.g. clausthalite), tellurides, native gold, mercury and platinum-group minerals (and abundant monazite at Shinkolobwe). Vein-type mineralization which occurs in basement rocks of unconformity uranium provinces in Canada and Australia (some of which is of Saxonic type) is mineralogically similar to the unconformity-type mineralization in these areas; the vein-type mineralization includes the Beaverlodge veins of Saskatchewan, which contain antimonides and gold-platinum alloy. The Kupferschiefer bed is the only other locality from which gold-platinum alloy has been reported, in an area where the bed contains uranium, mercury and bismuth mineralization. Some stratiform copper deposits of the Zaïrean copperbelt, north of Shinkolobwe, contain uranium, gold and platinum group elements (Ngongo-Kashisha, 1975), and a stratiform copper-uranium-gold association is present in South Australia and elsewhere (e.g. the Olympic Dam ore body, with which hematite, siderite, fluorite, barite and rare earth minerals are associated; Roberts and Hudson, 1983). Therefore, a mineralogical and spatial relationship exists between various types of uranium deposit, basin-related base metal deposit and the Saxonic vein association.

It can be concluded that there is a close spatial and temporal (as well as mineralogical) relationship between base metal ore bodies which occur in epicontinental environments (Fig. 138). These ore bodies include stratiform copper deposits (hosted by either "shale" or sandstone), sedex deposits, sandstone lead deposits, lead-zinc and copper deposits hosted by sedimentary carbonate rocks, and basalt-hosted native copper deposits. This relationship also exists between

stratiform copper deposits and some uranium deposits, and between these two types of deposit and Saxonic vein mineralization (discussed below).

4.6.7 Epigenetic veins in basement rocks and their relationship to basin-hosted ore deposits

The ore deposits discussed in Chapter 4.6.6 include a number of vein-like (or otherwise strongly discordant) types of mineralization. Some of these, such as Mississippi Valley-type and Tsumeb-type mineralization, and the mineralization of Kennecott, Alaska, occur in sedimentary carbonate rocks and show a broadly strata-bound distribution. A genetic relationship between basin fluids and Mississippi Valley-type mineralization is widely accepted, and evidence presented here indicates that Tsumeb-type mineralization has a similar origin. However, this origin has only rarely been proposed for fracture-controlled base metal veins which occur in basement rocks (e.g. Northampton, Western Australia; Michael and Groves, 1977). Evidence for this origin is found in south-eastern France, where the Tsumeb-type mineralization of Daluis gorge is spatially associated with Mississippi Valley-type deposits, sandstone lead deposits, and the germanium-rich zinc veins of Saint Salvy and other lead-zinc veins which occur in basement rocks of the Massif Central (Chapter 4.6.5). Lead isotope studies support a common origin for the veins and the strata-bound mineralization of this area (Chapter 5.3.14). It is suggested here that basin fluids are important in the formation of veins of Saxonic type, and some other base metal veins in basement rocks, consistent with the large scale of lateral migration of basin fluid indicated in this study. This differs greatly from the conclusions of many other workers (e.g. Halls and Stumpfl, 1972; Robinson and Ohmoto, 1973; Badham, 1976).

The Saxonic vein association (Rösler and Baumann, 1970) is difficult to define because, like Tsumeb-type mineralization, it is characterized by compositional and mineralogical diversity. The most characteristic type of vein in the Saxonic association is the Ag-Bi-Co-Ni-As type, which can contain antimony, and which grades into uranium-rich varieties which contain hematite. Important examples are

Cobalt, Ontario (Berry, 1971), North West Territories, Canada (Robinson and Ohmoto, 1973), Kongsberg, Norway (Neumann, 1944), and Freiberg, East Germany (Rösler and Baumann, 1970). These veins grade from varieties with abundant base metal sulphides, to sulphur-deficient varieties which contain arsenide minerals and native metals; claus-thalite, and germanium-rich members of the argyrodite-canfieldite mineral series are present at some localities. Another type of vein in the Saxonic association contains galena and silver minerals; this variety shows identical lead isotopic ratios to associated veins of Ag-Bi-Co-Ni-As type at some localities (Chapter 5.3.15). Gangue minerals include carbonate minerals (siderite is very common), quartz, barite and fluorite, and separate generations of barite and fluorite veins can occur. The mineralogy of the Ag-Bi-Co-Ni-As member of the association is transitional to the Rücken (veins) of the Kupferschie-fer, which occur in the Zechstein basin to the north-west of the type locality (Chapter 4.6.5), and to the Kupferschiefer itself. The mineralogy of uranium-rich varieties of this mineralization is trans-itional to that of unconformity-type uranium ore bodies and the Beaver-lodge veins (Chapter 4.6.6). The mineralogy of some members of each of these types of mineralization is identical and unlike that of any other type of mineralization, and closely related geneses are therefore indi-cated. This is further supported by lead isotope, stable isotope and fluid inclusion data from the Echo Bay district, Canada and the Saxonic association of north-western Europe (Chapters 5.3.15, 6.2.5, 6.3.5).

The ages of Saxonic veins are often poorly known, because they are commonly confined to basement rocks. Saxonic veins of the type area in north-western Europe provide the best example of a mineral province for which the age is known. The Saxonic veins of Saxony, Thuringia, and the Schwarzwald, (in Germany and Czechoslovakia) and Kongsberg (Norway) occur in basement highs, on the margin of the area formed by the Permian Oslo rift, and the Zechstein salt basin and Kupferschiefer basin of Permian age. Similar veins are represented by the Kupferschiefer Rücken (some of which extend downwards into basement rocks), and by veins in the Harz Mountains (e.g. the Clausthal veins), an inlier within the Kupferschiefer basin. The mineralization of the Kupferschiefer bed itself, and native copper mineralization in the

underlying Rotliegende, and in Permian basalt of the Oslo rift, occur within this area (Chapter 4.6.6). Lead isotope data are consistent with a genetic relationship between mineralization of the Kupferschiefer bed and some of the Saxonic veins (Chapter 5.3.15). The Saxonic veins are late- or post-Hercynian (i.e. not older than Carboniferous), and there is no unequivocal evidence that any of the veins are younger than Permian. Some veins are cut by dolerite dykes of Permian age (Bugge, 1978), Permian K/Ar isotopic ages have been obtained from clay minerals in alteration zones associated with the veins (Ineson et al., 1975), and the sulphur in the veins appears to have been derived from Permian sea-water sulphate (Chapter 6.2.5). It is therefore suggested that the Saxonic veins form part of a Permian mineral province of north-western Europe, which contains different types of genetically-related mineral deposit.

Lead isotope evidence for lateral migration of ore fluids on a regional scale along unconformities is presented in Chapter 5.3, and has been advanced elsewhere. Basin fluids can move downwards into underlying basement rock under suitable hydrodynamic conditions (Magara, 1973), and can also move laterally up-dip, into rocks which form adjacent basement highs (Chapter 6.3.1). Evidence for this is the presence of important petroleum reservoirs in basement rock (including granite), which contain petroleum that is compositionally similar to that in overlying sedimentary rocks (P'an, 1982). Petroleum traps of this type commonly occur where basement rock has developed secondary porosity along fissures, below an unconformity surface, and Saxonic veins may form in a similar manner. It is shown in subsequent chapters that strata-bound, base metal mineralization of sedimentary basins, discordant bodies (e.g. Tsumeb), and some veins in basement rocks adjacent to sedimentary basins (e.g. Saxonic veins and the germanium-rich veins of Saint Salvy) may have a common origin in connate fluids of sedimentary basins.

CHAPTER FIVE

ISOTOPE STUDIES

5.1 SULPHUR ISOTOPES

Sulphur isotope studies were undertaken to determine the source of sulphur in sulphide ore, and to interpret some of the physico-chemical conditions during ore deposition (Chapter 6.2). Sulphur isotope ratios were determined in sedimentary sulphate minerals and native sulphur, and in sulphide minerals from ore bodies of the Otavi Mountain Land and central Africa. Galena was commonly chosen for analysis because it can form over a wide range of pH and oxygen fugacity conditions. A total of 43 samples were analysed; details of the method used, and all data, are given in Appendix 2.1. The principles of stable isotope geochemistry, and its applications to ore deposit studies, are discussed in Ohmoto (1972) and Ohmoto and Rye (1979).

Studies elsewhere in the world have shown that gross zoning of sulphur isotope ratios within ore bodies is preserved to high metamorphic grades, although the relative isotopic enrichment factor obtained from mineral pairs can reflect the temperature of metamorphism in rocks metamorphosed to greenschist facies (i.e. 320°C) or higher grades (Rye and Ohmoto, 1974). Ore bodies of the Otavi Mountain Land have mostly been metamorphosed to below greenschist facies, and the Tsumeb ore body has only undergone advanced diagenesis or very low grade metamorphism (Chapter 3.7.11). There is uncertainty about the grade of metamorphism undergone by ore bodies discussed from outside the Otavi Mountain Land, but none have been metamorphosed to higher than lower greenschist facies.

5.1.1 Anhydrite, gypsum and native sulphur, Tsumeb Subgroup

Gypsum and nodular anhydrite from zone T7 in the Tsumeb area,

and anhydrite from Kombat, show a restricted range of $\delta^{34}S$ ratios (from +31 to +33 ‰; Fig. 124D). The sulphur isotope ratios of marine evaporites, and therefore of sea water, have varied with geological age (Schidlowski et al., 1977). Extremely positive ratios of the type seen at Tsumeb and Kombat are rare in the geological record, and have only been recorded from Phanerozoic evaporites of Cambrian to Ordovician, and Upper Devonian, age. Few published data are available from Precambrian evaporites, and the ages of these rocks are poorly known; however, most data are from Late Proterozoic rocks and these indicate lighter values than those obtained from the Otavi Mountain Land. Evaporites from the Shaler Group, Canada, have $\delta^{34}S$ ratios of +15 ‰, and evaporites from the Bitter Springs Group, Australia, show a large spread of values, with a mean of +18 ‰ and a maximum of +25‰. The ages of these rocks are thought to be in the intervals 635-800 m.y., and 800-1000 m.y., respectively. Anhydrite (including nodular anhydrite) from the Lower and Upper Roan Supergroups of central Africa, which pre-date Kundelungu Supergroup rocks and their contained Tsumeb-type mineralization, shows a restricted range of +16 to +21 ‰ (Fig. 124K). The isotopically heavier data from the Tsumeb Subgroup are therefore consistent with the latest Proterozoic age interpreted for rocks of this subgroup (Chapter 4.6.4).

Native sulphur and pyrite from zone T7 of the Tsumeb mine area have $\delta^{34}S$ values of +16 to +17 ‰, and the pyrite is attached to gypsum, which it appears to have replaced. These values, and the textural relationship, indicate that sulphur was derived from an isotopically heavy sulphate source of crustal origin, such as the sulphate minerals of zone T7. This is because native sulphur and sulphide minerals, precipitated from solution under equilibrium or non-equilibrium conditions, can have significantly lighter, but only slightly heavier, sulphur isotopic ratios than the solution. The range of heavier values is restricted except at very high pH values, or during sulphate reduction in systems closed to sulphate ion. It was previously thought to be limited to a few per mil in the first instance (Ohmoto and Rye, 1979), but recent studies by Meyer et al. (1983) indicate that it may be limited to a maximum of one per mil under all pH conditions found in geological environments. Strata-bound

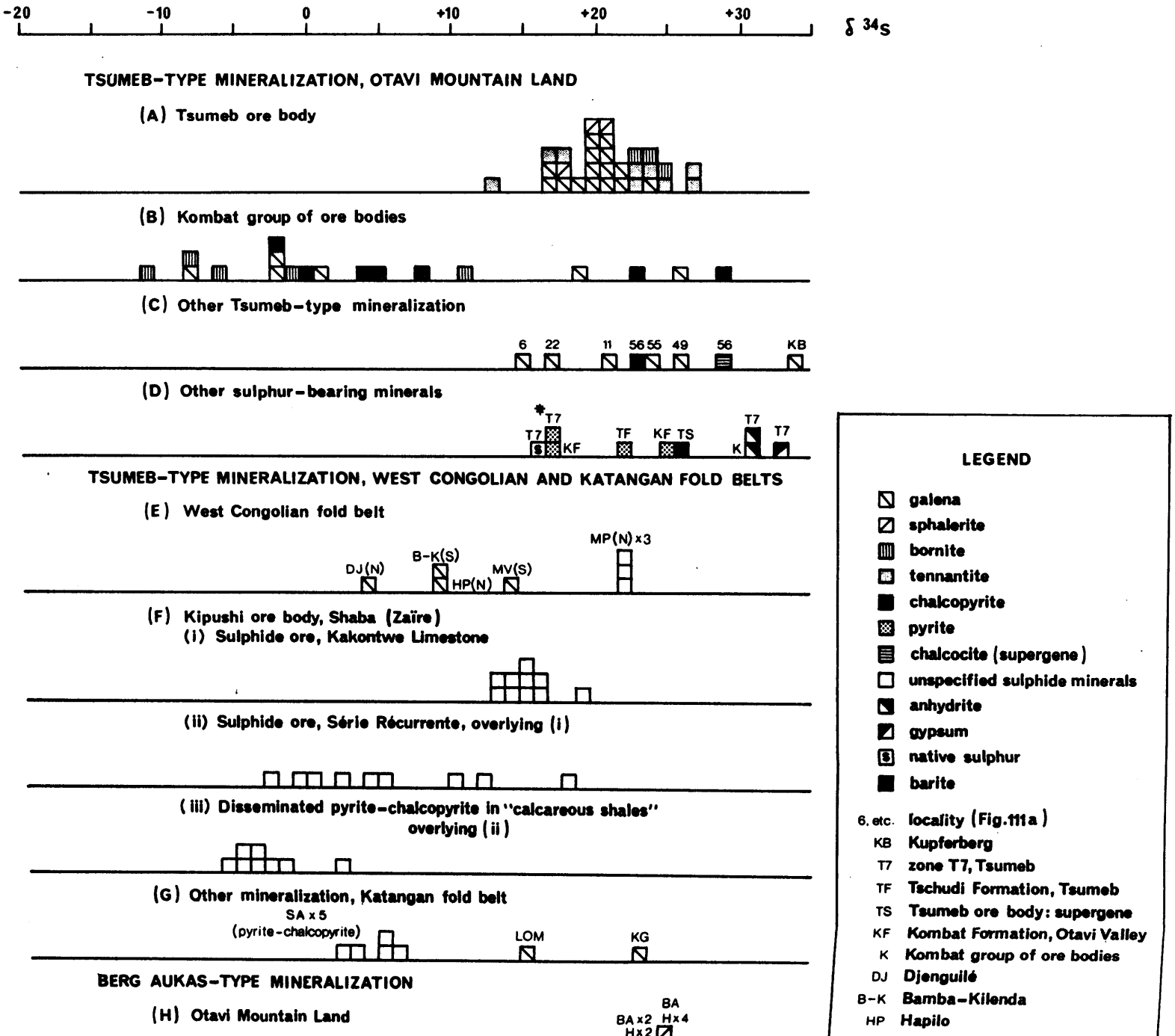
-20
-10
0
+10
+20
+30
δ 34S
TSUMEB-TYPE MINERALIZATION, OTAVI MOUNTAIN LAND
(A) Tsumeb ore body
(B) Kombat group of ore bodies
(C) Other Tsumeb-type mineralization
6 22 11 56 55 49 56 KB
(D) Other sulphur-bearing minerals
T7 T7 KF TF KF TS T7 K T7
TSUMEB-TYPE MINERALIZATION, WEST CONGOLIAN AND KATANGAN FOLD BELTS
(E) West Congolian fold belt
DJ(N) B-K(S) HP(N) MV(S) MP(N)x3
(F) Kipushi ore body, Shaba (Zaïre)
(i) Sulphide ore, Kakontwe Limestone
(ii) Sulphide ore, Série Récurrente, overlying (i)
(iii) Disseminated pyrite-chalcopyrite in "calcareous shales" overlying (ii)
(G) Other mineralization, Katangan fold belt
SA x 5
(pyrite-chalcopyrite)
LOM
KG
BERG AUKAS-TYPE MINERALIZATION
(H) Otavi Mountain Land
BA
BA x2 H x4
H x2
BA
H x2 x2
LEGEND
galena
sphalerite
bornite
tennantite
chalcopyrite
pyrite
chalcocite (supergene)
unspecified sulphide minerals
anhydrite
gypsum
native sulphur
barite
6. etc. locality (Fig.111a)
KB Kupferberg
T7 zone T7, Tsumeb
TF Tschudi Formation, Tsumeb
TS Tsumeb ore body: supergene
KF Kombat Formation, Otavi Valley
K Kombat group of ore bodies
DJ Djenguilé
B-K Bamba-Kilenda
HP Hapilo
MV Mavoio
MP M'Passa

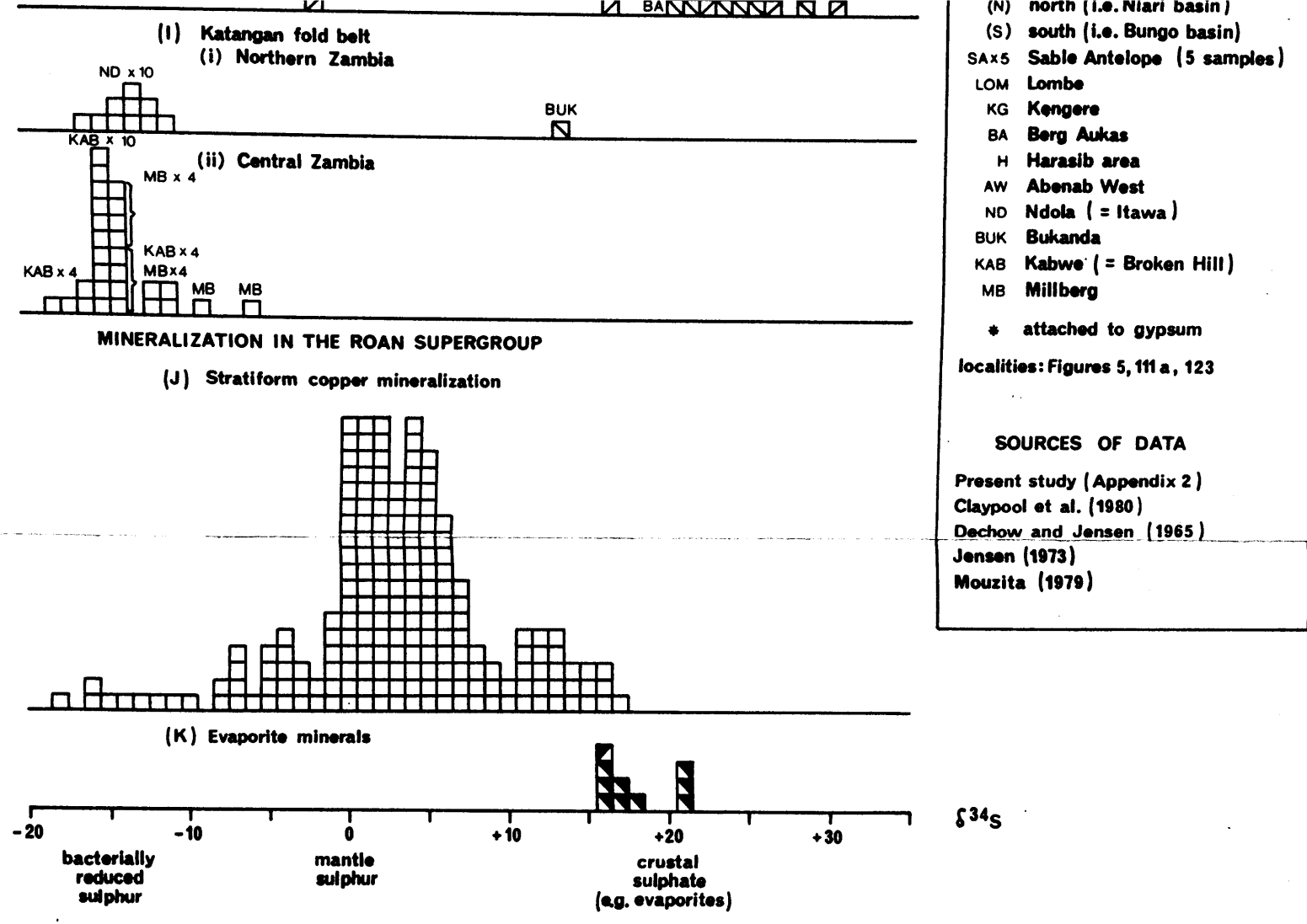

Fig. 124

Sulphur isotopic compositions of ore minerals and related sulphur-bearing minerals from central Africa. Crustal sources of isotopically heavy sulphate ion are interpreted to have given the observed ratios by: (1) reduction at elevated temperatures (e.g. Tsumeb), (2) reduction under conditions of variable oxygen fugacity (e.g. Kombat), and (3) bacterial reduction (e.g. central Zambia).

pyrite from the Tschudi Formation and Kombat Formation has $\delta^{34}S$ ratios of +17 ‰ to +25 ‰. Pyrite in the base of the Tschudi Formation overlies the sulphate- bearing horizon of zone T7, which was therefore a probable source of the reduced sulphur which formed the pyrite. A similar origin can be invoked for pyrite in the Kombat Formation.

The lead isotope study indicates that strata-bound pyrite in the base of the Tschudi Formation did not form during the ore-forming event at Tsumeb, but data from pyrite of the Kombat Formation is inconclusive (Chapter 5.3.7). Textural evidence (i.e. replacement of pyrite by ore minerals) indicates that the pyrite of the Tschudi Formation pre-dated the ore-forming event. The native sulphur and pyrite which are confined to the sulphate-rich rocks of zone T7 do not show any spatial relationship to ore minerals. The $\delta^{34}S$ ratios of these minerals, and of strata-bound pyrite from the Kombat Formation, are slightly more negative than the sulphate minerals which are the most probable source of their sulphur. These ratios are consistent with non-equilibrium reduction of sulphate, which can only occur above 80°C (Krouse, 1977; Sakai and Dickson, 1978), rather than with bacterial reduction at low temperatures (Ohmoto and Rye, 1979; see following discussion). A late diagenetic or hydrothermal origin, during deep burial, is therefore indicated.

Undeformed barite crystals of probable supergene origin which occur in the upper part of the Tsumeb ore body have $\delta^{34}S$ values of +26‰, consistent with derivation of their sulphur from either sulphate minerals in zone T7, or from sulphide minerals within the ore.

5.1.2 Tsumeb-type mineralization, Otavi Mountain Land

The $\delta^{34}S$ ratios of most ore minerals from the Tsumeb ore body show a range in values of only 9 ‰, from +18 ‰ to +27 ‰ (Fig. 124A). The range of values for individual sulphide minerals is even more restricted. Most bornite and tennantite values are within a range of 4 ‰, and most galena values are within a range of 5 ‰ (with a median of +21 ‰). Galena values show no systematic variation with

depth in the Tsumeb pipe (Fig. 135), and sphalerite shows a similar range of isotopic values to galena. It proved impossible to sample pure sphalerite from coexisting, more abundant galena, and no consistent isotopic temperatures can be obtained from the data of Jensen (1973), possibly also for this reason.

Sulphide minerals from the Kombat ore body show a completely different range of $\delta^{34}S$ values to those shown by the Tsumeb ore body, from -11 ‰ to +26 ‰. At least 34 ‰ of this range is shown by galena alone (Fig. 124B). Hypogene barite intergrown with ore minerals has a value of +29 ‰. Ore minerals and barite from Tsumeb-type ore bodies west of Tsumeb, and from west of Kombat but some distance below the base of the Kombat Formation, show a similar range of values to sulphide minerals from Tsumeb (but extend to slightly more positive values, i.e. +15 to +34 ‰; Fig. 124C).

A temperature of 250°C is indicated for ore deposition in the Otavi Mountain Land (Appendix 3). It can therefore be assumed that sulphur isotopic equilibrium between aqueous sulphate and sulphur species was approached, because this should theoretically be reached rapidly at this temperature under the low pH conditions interpreted for the Tsumeb ore body (Chapter 6.2). For example, equilibrium will be reached in ten years at pH 5,5 and a total sulphur concentration of 0,01 m; this will reduce to a few hours at pH 4,5 and 0,1 m total sulphur (Sakai and Dickson, 1978). The mineralogy of Tsumeb-type ore bodies in the Otavi Mountain Land indicates that some minerals precipitated under low oxygen fugacity (as well as low pH) conditions (Chapter 6.2). The most positive $\delta^{34}S$ ratios shown by hypogene sulphide minerals should therefore approximate to the ratios of the ore solutions from which they precipitated (they could otherwise give estimates as much as 27 ‰ too negative at 250°C, but not significantly more positive than the ratios of the ore solutions). The most positive values are +27 ‰, +26 ‰ and +34 ‰ for the Tsumeb ore body, Kombat ore bodies, and other Tsumeb-type ore bodies of the Otavi Mountain Land, respectively (Figs. 124A, B, C). These values indicate an extremely heavy sulphur source, such as the evaporite minerals of zone T7 (average +32 ‰).

The restricted range of $\delta^{34}S$ values shown by individual minerals in the Tsumeb ore body, and the lack of variation of these values with depth, indicates that the source (or sources) of reduced sulphur involved in ore deposition had a unique value under a restricted range of physico-chemical conditions. This does not prove that complete equilibrium existed between aqueous sulphate and reduced sulphur in solution, and such equilibrium might only be approximated, e.g. as the result of rapid mixing of a reduced, metal-bearing fluid and an oxidized, sulphur-bearing fluid. All sulphide minerals sampled have lighter $\delta^{34}S$ values than the most obvious sulphate source. This difference, and the different isotopic ratios shown by individual minerals, can possibly be explained by variations in physico-chemical variables (e.g. pH, temperature, oxygen fugacity) during precipitation of different minerals, i.e. the minerals did not all precipitate under conditions in which reduced sulphur species were the major sulphur species in solution. However, the restricted range of values shown by individual minerals is remarkable, because these values are very sensitive to small changes in the physico-chemical state of the ore fluid within the fields in which sulphur isotopic variation can occur (Ohmoto, 1972). It is more probable that the ratios of these minerals reflect slight, but systematic, disequilibrium (i.e. kinetic fractionation) between oxidized and reduced sulphur species in solution, and that the sulphide minerals were precipitated in the field in which reduced sulphur species are dominant. This is below the field of $\delta^{34}S$ variation shown in Fig. 132. The $\delta^{34}S$ values of the minerals would be too negative if they precipitated in the sulphate-dominant field, and some of the minerals could not form in this field (Chapter 6.2). Kinetic fractionation of this type will produce reduced sulphur species with lighter $\delta^{34}S$ ratios than the equilibrium ratios. Alternatively, the isotopic ratios of the few anhydrite and gypsum samples analysed may not be typical of these minerals in zone T7, but may be anomalously heavy. The limited range of values shown does not support the model of Hopwood (1975), who proposed that the ore fluid became more oxidizing with time, until it oxidized earlier sulphide minerals (Chapter 3.2).

The large range of $\delta^{34}S$ values shown by sulphide minerals from the Kombat ore body have previously been explained in a number of ways, all of which involve mixing of multiple sources of sulphur. The sources proposed include: (1) isotopically heterogeneous basement

rocks (Jensen, 1973), (2) sedimentary anhydrite, and pyrite from the base of the Kombat Formation (Hopwood, 1975), and (3) reduced sea water sulphate and magmatic sulphur (Innes and Chaplin, in press, 1985). These proposals were based on the original isotope data of Jensen (1973), which showed a range in $\delta^{34}S$ values from -11 ‰ to +11 ‰. Additional data from the present study confirm these values, and increase the range to +26 ‰. This supports crustal sulphur as one, or the only, sulphur source.

Pyrite from the Kombat Formation is isotopically too heavy to have provided a second source of sulphur (Chapter 5.1.1), and there is no independent evidence for an isotopically light component of sulphur (the argument for "magmatic" sulphur was based on the mean of zero per mil obtained from the data of Jensen, 1973). Isotopically light values can be obtained by bacterial reduction of isotopically heavy crustal sulphate alone, but this is inconsistent with the large range, and lack of clustering, of isotopic ratios (Ohmoto and Rye, 1979). The observed range in values could be obtained by mixing of bacterially reduced sulphur with the isotopically heavy sulphur source, or by precipitation of sulphide minerals outside the field in which reduced sulphur species are the dominant sulphur species. The presence of iron oxide minerals and barite in the Kombat ore supports the latter conclusion (Chapter 4.4.3). Innes and Chaplin (1985) suggested that these minerals existed prior to deposition of the sulphide minerals, to which they are genetically unrelated, but the restriction of these minerals to the isotopically lightest ore bodies in the Otavi Mountain Land is unlikely to be coincidental. One possible explanation is that pre-existing iron oxide bodies affected the sulphur isotopic ratios of the sulphide minerals by buffering the oxygen fugacity of the ore solutions at high values. However, the small size of the iron oxide bodies, relative to the size of sulphide ore bodies which contain isotopically light sulphide minerals, and the presence of both magnetite and isotopically heavy sulphide minerals in single polished sections, do not support this. The oxide and sulphide minerals are therefore considered to have formed during a single mineralizing event, during which the oxygen fugacity or pH of the ore solutions varied.

Sulphide minerals which show a variation of 27 ‰ can be produced by variations in these parameters alone at 250°C (39 ‰ at 150°C) The isotopically lightest sulphide mineral analysed from the Kombat ore. bodies has a ratio of -11 ‰, 43 ‰ lighter than the assumed source of sulphate; the lightest mineral of definite hypogene origin has a ratio of -8‰. Therefore, the observed ratios could be produced by oxygen fugacity or pH variations during a temperature drop of approximately 100°C. Alternatively, if non-equilibrium reduction of sulphate occurred, as proposed for Tsumeb, the sulphur isotopic variation observed in the Kombat ore bodies might have been produced by variations in oxygen fugacity or pH alone, at temperatures above 200°C (consistent with temperatures indicated by the fluid inclusion data; Appendix 3). Another alternative is that the average isotopic ratio of the sulphur source was slightly lighter than the average ratio of the few gypsum and anhydrite samples analysed, as noted for the Tsumeb ore body.

The isotopically heavy values of hypogene barite from Kombat and locality 56 are similar to the values of sulphide minerals from Tsumeb, and to the proposed evaporitic sulphur source in the Hüttenberg Formation, and could have been produced directly from that source under conditions of high oxygen fugacity.

5.1.3 Tsumeb-type mineralization elsewhere in central Africa

The sulphur isotopic ratios of sulphide minerals from Tsumeb-type ore bodies of the West Congolian and Katangan fold belts (Fig. 123) indicate that the source of sulphur in these ore bodies was isotopically heavy, crustal sulphate, as in similar ore bodies of the Otavi Mountain Land. The most positive sulphur isotopic ratio recorded from ore bodies in the Schisto-calcaire Group of the West Congolian fold belt is +22 ‰, (M'Passa ore body, Congo Republic; Mouzita, 1979). The most positive values recorded from Tsumeb-type ore bodies of the Kundelungu Supergroup of the Katangan fold belt are +19 ‰ and +23 ‰, the former from Kipushi, Zaïre, (Dechow and Jensen, 1965) and the latter from Kengere deposit (which lead isotope data indicate is genetically related to the Kipushi deposit; Figs. 124F, G). An evaporite horizon occurs in the Série Récurrente of Southern Zaïre (including in the Kipushi area), and this was a probable source of sulphur in the Kipushi, Lombe and Kengere ore bodies. An evaporite horizon is also known near the Djenguilé occurrence, in the West

Congolian fold belt, and this was a probable source of sulphur for the Djenguilé, Hapilo and M'Passa ore bodies (Chapter 4.6). The Bamba Kilenda ore body, with isotopically light galena (+9‰), contains barite (Fig. 124E); this, together with a paucity of very light values typical of bacterial reduction in these ore bodies, is consistent with high oxygen fugacity (and possibly pH) conditions as the cause of the lighter isotopic values.

Sulphur isotopic ratios vary with stratigraphic position in the Kipushi ore body, consistent with either mixing of two sulphur sources, or variations in oxygen fugacity or pH during ore deposition (Fig. 124F). Ore in the Kakontwe Limestone shows constant, isotopically heavy $\delta^{34}S$ ratios, and chalcopyrite is the dominant copper mineral. Ore in the overlying Série Récurrente shows variable ratios, extending to lighter values, and bornite plus pyrite is the dominant copper-bearing assemblage. The bornite plus pyrite assemblage forms under conditions of higher oxygen fugacity than chalcopyrite (at constant temperature and total sulphur concentration), and this supports oxygen fugacity variation as the cause of the observed isotopic variation.

5.1.4 Berg Aukas-type mineralization

Galena and sphalerite from Berg Aukas-type mineralization of the Otavi Mountain Land shows very positive values, mostly between +20 and +30 ‰ (Fig. 124H). These samples include minerals from the Berg Aukas and Abenab West ore bodies, and from the Harasib Main occurrence and localities 29 and 34 (Fig. 111a). These values indicate that, as in the Tsumeb-type occurrences, the sulphur was derived from isotopically heavy, crustal sulphate. This is consistent with textural evidence for former anhydrite nodules in the sequences which host the Berg Aukas and Abenab West ore bodies (Chapter 2.3.5). Sphalerite from the Berg Aukas ore body, which occurs at the base of the Otavi Group, shows values up to +29 ‰, and it is probable that the entire Otavi Group contained evaporites which were isotopically heavier, and therefore of different age (i.e. younger) than evaporites which occur in the Roan Supergroup (Fig. 124K). However, the Otavi Group evaporites were possibly isotopically similar to evaporites in the

overlying Kundelungu Supergroup, which hosts Tsumeb-type mineralization (c.f. Kengere galena, Fig. 124G), although no data are available from sulphate minerals of the Kundelungu Supergroup evaporites.

Data from Berg Aukas-type deposits of Zambia can be divided into two groups, consisting of occurrences from northern and central Zambia (Fig. 124I). The northern group consists of the Ndola (Itawa) and Bukanda occurrences, which lead isotope data indicate contain lead which is genetically related, despite the large geographic separation of these occurrences (Chapter 5.3.10). These occurrences show very different $\delta^{34}S$ values, the ten Ndola samples clustering at -13 $\pm$3 ‰ (2σ), and the Bukanda sample having a value of +13 ‰. The tight clustering of the very negative values, which are 30 to 45 ‰ lighter than the average value of contemporaneous crustal sulphate, is typical of reduced sulphur formed by bacterial reduction. Similar clustering of isotopically light values is observed in sulphide minerals from the Kabwe mine and Millberg occurrence, of central Zambia (Fig. 124I).

The Kabwe ore body of central Zambia contains lead which is isotopically distinct from that of the northern Zambian occurrences (Chapter 5.3.10). However, the very similar, and isotopically light, $\delta^{34}S$ ratios of the central Zambian mineralization and the Ndola occurrence of northern Zambia are distinct from those of all other occurrences studied throughout central Africa. This indicates that both groups of deposits utilized bacterially-reduced sulphur, derived from sulphur sources which were isotopically similar. Bacterial reduction of sulphur is confined to temperatures below 50°C, and therefore occurs at shallow depths (Ohmoto and Rye, 1979). The ore fluids which formed the occurrences with different lead isotope ratios may have existed at different times, and have derived their sulphur from earlier pyrite formed from bacterially reduced sulphur species. Alternatively, the two groups of occurrences may have formed at a similar time from fluids which contained isotopically different lead, but which utilized shallow, broadly contemporaneous sulphur sources (Chapter 5.3.8).

5.1.5 Summary

Sulphide ore of both Tsumeb type and Berg Aukas type, which occurs in the Otavi Mountain Land, derived its sulphur from sedimentary sulphate minerals of latest Proterozoic age. The sulphate minerals have an average $\delta^{34}S$ value of +32 ‰, and are found in the vicinity of the ore bodies. Pyrite in the base of the Mulden Group, and probably also pyrite and native sulphur in evaporite-bearing rocks of the Tsumeb mine area, formed subsequent to deep burial but prior to mineralization. These minerals formed from a similar sulphur source to that which provided sulphur to the later ore minerals.

Isotopically heavy, crustal sulphate was also the source of sulphur in ore bodies of Tsumeb and Berg Aukas type in the West Congolian and Katangan fold belts. Evaporite horizons, which were a probable source of this sulphate, occur in the vicinity of ore bodies in both fold belts. Isotopically light values in these areas, and the Otavi Mountain Land, were mostly produced by variations in oxygen fugacity or pH during ore deposition, although bacterially reduced sulphur was important in some Berg Aukas-type occurrences of Zambia.

5.2 CARBON AND OXYGEN ISOTOPES

Carbon and oxygen isotope studies were made (1) to confirm the presence of different generations of gangue minerals in the Tsumeb pipe (as interpreted from paragenetic studies), (2) to determine the isotopic composition (and source) of these elements in the ore solutions, and (3) to obtain data on physico-chemical conditions during the ore-forming process (Chapter 6.2). Carbon and oxygen isotope ratios were determined in 45 samples of sedimentary carbonate rock, hydrothermally altered (i.e. calcitized) rock, and vein- and vug-filling gangue minerals.

Details of the analytical method used, and all data, are given in Appendix 2.2. Carbon isotope ratios are expressed relative to the PDB standard and oxygen isotope ratios are expressed relative to the SMOW standard.

5.2.1 Sedimentary carbonate rocks of the Otavi Group

Carbon and oxygen isotope ratios were determined in the carbonate fraction of eight sedimentary carbonate rocks, and these data are plotted in Figure 125a, together with previous determinations by Schidlowski et al. (1975). Eichmann and Schidlowski (1975) reported $\delta^{13}C$ ratios of -20 to -23 ‰ for organic carbon from some of the rocks analysed by Schidlowski et al. (1975).

The data of Figure 125a are divided into two fields, representing rocks from stratigraphically below (A), and above (B), the contact between zones T4 and T5 of the Tsumeb Subgroup. Field A may not adequately represent the lower sequence because some formations are only represented by a single point, and the Gauss Formation is not represented.

The $\delta^{13}C$ ratios of most normal marine carbonate rocks are within a relatively narrow range of -4 to +4 ‰ (Hudson, 1977). Field A is within this range, but a number of samples of field B are in the range +4 to +8 ‰, with one value of +10 ‰ recorded by Schidlowski et al. (1975). Various workers have noted that carbonate rocks which form in semi-restricted, commonly hypersaline, environments are characterized by heavy $\delta^{13}C$ values (Veizer et al., 1980). Carbon isotope ratios of +3 to +4 ‰ occur in sedimentary carbonate rocks and carbonate cements of modern sabkhas and shallow, hypersaline lakes and seas (Shinn, 1969; Aharon et al., 1977; McKenzie, 1980; Botz and Borch, 1984). However, ratios of +4 to +6 ‰ occur in rocks associated with some former, major salt basins, e.g. the pinnacle reefs of the Niagara Group of Michigan (Sears and Lucia, 1980), reefs of the Canadian Arctic (Davies, 1977), the Zechstein of north-western Europe (M. Coleman, pers. comm., 1984), and the Castile Formation, San Andres Formation and Smackover Formation of the southern U.S.A. (Dean et al., 1975; Moore and Druckman, 1981; Bein and Land, 1982). Precambrian dolostone, at least partly evaporite-bearing, of the Lomagundi Group and Deweras Group of Zimbabwe has an average $\delta^{13}C$ value of +8,2 ‰ (range +2,6 to +13,6 ‰) over a strike length of 300 km (Schidlowski et al., 1976).

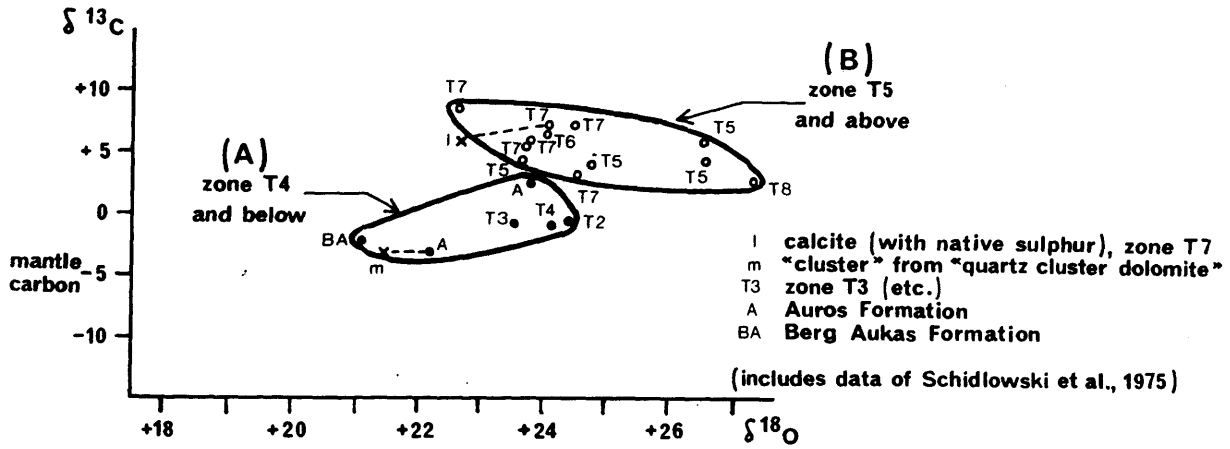

(a) Sedimentary carbonate rocks

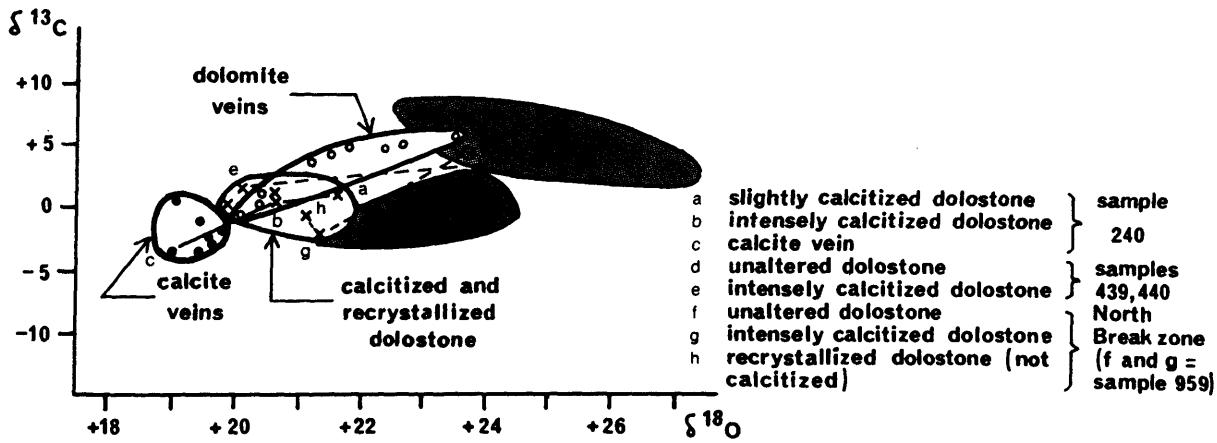

(b) Carbonate veins and hydrothermally altered dolostone

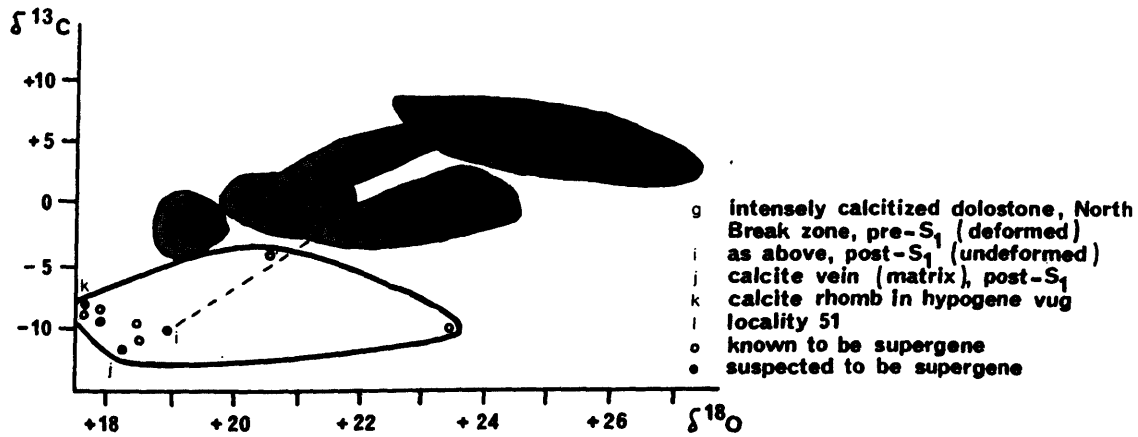

(c) Calcite of supergene origin

Fig. 125
Carbon and oxygen isotopic compositions of host rocks, gangue minerals and supergene minerals of the Tsumeb ore body. Important features are: (1) the positive $\delta^{13}C$ ratios of dolostone from the upper part of the Tsumeb Subgroup, (2) the restricted carbon and oxygen isotopic ratios of calcitized dolostone formed from dolostone which is more variable isotopically, and (3) the negative $\delta^{13}C$ ratios of supergene calcite relative to hydrothermal calcite.

A number of explanations have been proposed for the heavy $\delta^{13}C$ ratios in the above sedimentary carbonate rocks. The first is that the rocks were deposited in closed bodies of water, which were enriched in ^{13}C as the result of preferential removal of ^{12}C by the formation of large volumes of isotopically-light organic matter (Schidlowski et al., 1976; Aharon et al., 1977). Another explanation is that carbonate minerals were precipitated from oxidized carbon species that were in equilibrium with methane in natural gas. Alternatively, isotopically heavy, oxidized carbon species might remain after non-equilibrium, bacterial production of methane (Hudson, 1977). A methane-related origin is obvious for small volumes of dolostone which show extreme isotopic variations in samples taken from adjacent localities, e.g. -64 to +21 ‰ (Deuser, 1970). However, this origin has also been proposed for large volumes of dolostone, considered to have formed during reflux of hypersaline brines associated with evaporites, which show only a small, positive range of $\delta^{13}C$ ratios (Sears and Lucia, 1980). The other explanation for heavy $\delta^{13}C$ ratios in carbonate rocks is that the solubility of carbon dioxide was low because of the high temperature of the water (e.g. up to 57°C; Aharon et al., 1977). The carbon dioxide was lost to the atmosphere, and remaining bicarbonate ion was enriched in ^{13}C. This explanation is consistent with the close association of large volumes of isotopically heavy carbonate rocks with evaporite minerals. However, the other explanations are also possible (e.g. there can be an association between evaporites and closed bodies of water).

Regardless of the origin of positive $\delta^{13}C$ ratios in rocks of the upper Tsumeb Subgroup, these rocks are spatially closely related to evaporite minerals in zone T7. Five of the isotopically heavy samples of Figure 125a contain, or are thought to replace, evaporite minerals, and a sixth sample comes from the same part of the sequence. Isotopically heavy samples from zones T5 and T6 may also reflect former evaporitic conditions, because these rocks formed in shallow water. The isotopically light values of zone T4 and below do not preclude the possibility that similar environments existed lower in the sequence; the samples are widely spaced, and some rocks associated with evaporite

horizons elsewhere in the world do not have heavy $\delta^{13}C$ ratios.

The $\delta^{18}O$ ratios of the rocks of Figure 122a are isotopically light, but range up to values close to those of marine carbonate rocks of late Phanerozoic age (Hudson, 1977). The range in values probably results from early and late diagenetic effects, which will shift $\delta^{18}O$ ratios to lighter values (Veizer and Hoefs, 1976).

5.2.2 Alteration zone and gangue minerals

The $\delta^{13}C$ and $\delta^{18}O$ ratios of dolomite and calcite veins associated with the Tsumeb ore body, and of hydrothermally recrystallized and calcitized dolostone, are shown in Figure 125b. The field of "calcite veins" includes veins and other open-space fillings of calcite spar from between 17 and 33 levels. Some of the analysed vein calcite post-dates sulphide mineralization (e.g. Fig. 50), while other analysed calcite bodies are thought to be replaced by galena (Chapter 3.6.14). The range in $\delta^{18}O$ values of the calcite field is 0,9‰, and the range in $\delta^{13}C$ is 4 ‰.

The field of "dolomite veins" includes veins and other open-space fillings of dolomite spar from between 10 and 38 levels. The analysed samples include dolomite veins which cut massive sulphide ore. Some of these veins contain later sulphide minerals in vugs. Some dolomite pre-dates sulphide veinlets, both at 15 level and at depth in the silicified zone (Fig. 53; Chapter 3.6.14). The range in $\delta^{18}O$ values of the dolomite field is 3,4‰, and the range in $\delta^{13}C$ is 6,3‰.

The field of "calcitized and recrystallized dolostone" includes altered rock from throughout the calcitized zone of the pipe, from 29 to 33 levels. The Tsumeb pipe is extensively calcitized over this depth interval, and this alteration is thought to both pre-date, and to be synchronous with, sulphide mineralization. Also shown are a calcitized dolostone from the strata-bound North Break zone, and a pink dolostone which is not calcitized but is thought to be hydrothermally recrystallized, from the same locality outside the Tsumeb pipe (points g and h). The range in $\delta^{18}O$ ratios of the field of "calcitized and

recrystallized dolostone" is 1,8‰, and the range in $\delta^{13}C$ is 4‰ (1,6‰ if the samples from the North Break zone are excluded).

The total range in $\delta^{18}O$ and $\delta^{13}C$ ratios for the three fields defined by calcite veins, dolomite veins, and calcitized and recrystallized dolostone are 4,5‰ and 9,2‰, respectively. Part of the range in oxygen and carbon isotopic ratios shown by the Tsumeb samples must be the relative isotopic enrichment factor between dolomite and calcite. This fractionation would be 1,4‰ for $\delta^{18}O$, and 0,9‰ for $\delta^{13}C$ at approximately 250°-200°C, the temperature at which mineralization is thought to have occurred (Appendix 3). The variation in $\delta^{18}O$, of approximately 3‰ after correction, is therefore very small. A very small range for $\delta^{18}O$ is also known in carbonate minerals from other hydrothermal ore deposits, and has been reported from Mississippi Valley-type ore deposits of south-east Missouri (Hannah and Stein, 1984).

5.2.3. Controls on oxygen isotopic ratios

The fields of calcite veins and dolomite veins each include carbonate minerals which both pre-date and post-date some sulphide mineralization; if the interpretation of the large, open-space filling calcite bodies as pre-dating some massive sulphide ore is accepted (Chapter 3.6.14), then the minerals sampled span a large part of the mineralizing event. The $\delta^{18}O$ range for the two fields must be caused dominantly by a temperature variation, or a variation in $\delta^{18}O_{\Sigma O}$ (the oxygen isotopic ratio of the ore fluid). The observed range for calcite veins could be produced by a temperature drop of 20°C from 250°C (or 15°C from 200°C); the range for dolomite veins corresponds to a 65°C drop from 250°C (40°C from 200°C). A larger temperature variation could be represented if the $\delta^{18}O$ of the ore fluid decreased as the temperature decreased (e.g. during mixing of connate water and meteoric water). However, a 10% decrease in $\delta^{18}O$ would have to be balanced by a temperature decrease in excess of 100°C, from an initial temperature in the range 250°-200°C. Fluid inclusion data does not indicate a temperature decrease of this magnitude (Appendix 3), and limited variations in the $\delta^{18}O$ ratio of

the fluids are therefore indicated.

The range in $\delta^{18}O$ ratios shown by calcitized and recrystallized dolostone shows only a very small overlap with the range shown by calcite veins, and is isotopically heavier. Reasons that have been proposed for this type of isotopic relationship in alteration zones which occur distant from associated major veins and mineralization are: (1) decreased temperature in the alteration zones relative to the veins, and as a result, a larger isotopic fractionation between calcite and the ore fluids (Hall and Friedman, 1969), (2) incomplete isotopic exchange between the rock and ore fluid (Pinckney and Rye, 1972), or (3) a lower water-rock ratio (Pinckney and Rye, 1972; Sverjensky, 1981). The relationship between (1) weakly calcitized, but unrecrystallized dolostone, (2) intensely calcitized and recrystallized dolostone and (3) an immediately adjacent calcite vein, all from a single sample (points a, b and c), is shown in Fig. 125b. The relationship between calcitized dolostone and immediately adjacent unaltered dolostone (points d-g), is also shown. The tight clustering of data from calcitized dolostone at different elevations in the ore body, and at differing distances from veins, and the large difference between samples b and c, is not consistent with the former presence of a temperature gradient adjacent to veins. Incomplete isotopic exchange could not explain the difference between intensely calcitized dolostone and calcite veins, because the former has commonly reacted completely to form new calcite spar. The difference in $\delta^{18}O$ between the two fields is best explained by a lower water-rock ratio within the calcitized breccia. The results also indicate that significant isotopic re-equilibration is confined to bleached (i.e. weakly calcitized) or recrystallized rocks, and does not extend into adjacent dolostone in which alteration cannot be identified megascopically (samples d and e were taken a few centimetres apart).

The $\delta^{18}O$ ratio of the fluid in equilibrium with calcite at 250°-200°C was +10 to +12‰; the $\delta^{18}O$ ratio determined from dolomite is +9 to +15‰ (the lighter values corresponding to lower temperatures in each case). Calcite is volumetrically far more abundant than dolomite, so an average value of +11‰ is indicated, which

possibly increased a few per mil during dolomite deposition.

5.2.4 Carbon source, and controls on carbon isotopic ratios

The carbon isotopic compositions of hydrothermal carbonate minerals from Tsumeb are heavy (-3,5 to +5,7‰). The ratios can be compared with ratios in thirteen ore deposits reviewed by Ohmoto and Rye (1979). Samples from ten of these deposits show some values close to -10‰, only two deposits show any ratios more positive than 0‰, and only one, Pine Point, shows values more positive than +5‰.

The $\delta^{13}C$ ratio of a mineral which is precipitated from a hydrothermal fluid will differ from the $\delta^{13}C_{\Sigma C}$ value of the fluid, as a function of the temperature, oxygen fugacity, pH, and to a much lesser extent, ionic strength (which is ignored here). The temperature of ore deposition is taken as 250°C for the following discussion (Appendix 3), but the qualitative conclusions would not change for higher or lower temperature conditions.

Calcitized dolostone and calcite veins are considered initially, because calcite is volumetrically the most important hypogene carbonate mineral in the Tsumeb pipe, and is thought to have formed throughout much of the ore-forming episode. A change in pH or oxygen fugacity of the ore solution could produce a maximum variation of 29‰ in the $\delta^{13}C$ ratio of a carbonate mineral precipitated from an ore fluid of constant carbon isotopic composition. The magnitude of this isotopic change would be very sensitive to even slight variations in oxygen fugacity within the field shown in Figure 132, near the boundary between the fields in which H_2CO_3 and CH_4 are dominant (Ohmoto, 1972). However, the variation in $\delta^{13}C$ ratios of calcite within the Tsumeb ore body is only 5‰ (4‰ for calcitized dolostone or calcite veins individually), so conditions during calcite precipitation correspond to those outside the field shown. This is consistent with the apparent instability of reduced carbon within the calcitized zone of the pipe (because graphite is only stable in the vicinity of the above field in which large changes in carbon isotopic composition occur). An upper limit for oxygen fugacity variation has already been

established from the sulphur isotope data (Chapter 5.1.2, Fig. 132).

The two fields defined for calcite precipitation correspond to the regions within which calcite has a $\delta^{13}C$ value between 1,5‰ more negative and 3,5‰ more positive, and more than 13‰ more positive than the ore fluid, respectively. The calcite veins have an average $\delta^{13}C$ ratio of -1,5‰, which corresponds to a $\delta^{13}C$ ratio in the ore fluid in the range 0‰ to -5‰, or more negative than -14,5‰, depending on the field chosen. Values lighter than -14,5‰ require that a major component of organic carbon was present in the ore fluid. It is not possible to identify a unique source of carbon which has the heavier range of isotopic compositions (e.g. mantle carbon and some dolostone = -5‰), but the predicted range is consistent with a carbon source in dolostone of the Otavi Group. This could be dolostone from zone T4 and below or, if a small component of oxidized organic carbon was present in the ore fluid, dolostone from higher in the sequence. A dolostone source is more consistent with the oxygen fugacity conditions predicted from the sulphide mineralogy, which are consistent with the precipitation of calcite above, rather than below, the field in which carbon isotopic variation can occur in Figure 132 (Chapter 6.2).

The dolomite veins, which are volumetrically far less important than hydrothermal calcite at Tsumeb, display $\delta^{13}C$ values which range from ratios equivalent to dolomite in isotopic equilibrium with calcite veins, to dolomite nearly 6‰ more positive. This can be explained by precipitation of dolomite from a fluid with a variable and slightly lower oxygen fugacity (and possibly also temperature) than that which precipitated calcite, consistent with the chemical stability of reduced carbon in the upper zone of the pipe where dolostone is stable.

5.2.5 Calcite of supergene origin

Calcite of supergene origin was identified by its crustiform nature, its crystallized form, the absence of deformation textures, and the presence of interlayered (or paragenetically earlier) supergene

minerals, such as dioptase and duftite. Carbon and oxygen isotope ratios of calcite known, or suspected, to be of supergene origin, are plotted on Figure 125c. These have $\delta^{13}C$ ratios which are, on average, more than 8‰ lighter than those of calcite veins of hypogene origin. The $\delta^{18}O$ values of eight out of ten supergene samples cluster at a value which is approximately 1‰ lighter than the veins of hypogene calcite.

The $\delta^{18}O$ ratios of the samples of supergene calcite are considered to have a completely different origin to the ratios in samples of hypogene calcite, and to result from precipitation at low temperatures from isotopically light, meteoric water. The isotopically light $\delta^{13}C$ values result from the low ratios of the supergene fluids, which probably oxidized isotopically light carbon of the Tsumeb pipe. A sample of supergene calcite from light to medium grey dolostone at locality 51, with which vanadate minerals are associated, contains isotopically heavy carbon (Fig. 111a).

Hopwood (1975) proposed that sulphide ore at Tsumeb was oxidized by the hypogene ore fluid, which became cooler, sulphur-deficient and oxidizing with time. However, the resulting oxidized mineral assemblage was deposited synchronously with the calcite described here as supergene. There is no supporting evidence for the proposal of Hopwood (1975), such as continuity between the isotopic ratios of hypogene calcite and calcite described here as supergene, or more positive $\delta^{18}O$ ratios in the supergene calcite samples than in the hypogene calcite (as a result of decreasing temperature).

Three samples of uncertain origin fall within the field of supergene calcite. The first, i, is a sample of brown, coarsely crystalline, pyrolusite-bearing calcite spar from the North Break zone. Textural evidence indicates that it post-dates both the hypogene calcite, and the S_1 cleavage (Chapter 3.4.4). The second sample, j, is calcite from veins within the fourth type of breccia described in Chapter 3.3.2, which also post-dates the S_1 cleavage. This calcite lacks deformation textures, and displays fibrous, radial forms and concentric growth layering. The third sample, k, is a calcite rhomb,

found on vug-filling dolomite crystals of hypogene origin; calcite crystals are common within such vugs, where they post-date crystals of dolomite and sulphide minerals. Calcite of this type was thought to be of hypogene origin, and it was hoped that approximate relative isotopic enrichment factors (and therefore isotopic temperatures) might be estimated from adjacent dolomite and calcite crystals within vugs. However, this calcite, and the other two types of calcite, are clearly of supergene origin.

5.2.6 Other carbonate minerals

Two other types of carbonate minerals which fill open spaces are plotted in Figure 125a. The first consists of calcite veins with an infill of native sulphur (point 1), which occur in unaltered, zone T7 dolostone (see tie-line). Native sulphur and associated calcite which are produced at shallow depths in the cap-rock of salt domes are products of bacterial reduction of gypsum (Nielsen, 1979). The metabolic reaction utilized by the bacteria results in the following reaction, where C-H represents unspecified hydrocarbon compounds:

$$Ca^{2+} + SO_4^{2-} + C\text{-}H \longrightarrow H_2S + CaCO_3$$

The H_2S is then oxidized to native sulphur. The resulting calcite has a light $\delta^{13}C$ ratio (e.g. Dean et al., 1975); this is not true of the calcite analysed, which must have formed by some other mechanism. The positive $\delta^{34}S$ value of the native sulphur is also more consistent with a non-bacterial origin (Fig. 124D).

The other type of carbonate mineral analysed (point m) consists of dolomite spar from the "clusters" of the "quartz cluster dolomite" (Chapter 2.3.5, Fig. 12). The "clusters" have the same carbon isotopic ratio as the host dolostone; the dolostone itself consists of abundant, fine-grained dolomite spar, and it is therefore probable that its $\delta^{13}C$ and $\delta^{18}O$ ratios are not representative of the original rock.

5.3 LEAD ISOTOPES

Variations in lead isotope ratios can provide information about the origin and time of formation of ore bodies, as well as solving petrogenetic problems. The isotope ratios retain a time-integrated record of the U/Pb and Th/Pb ratios of the sources in which the lead developed, and therefore provide information about time-dependent geochemical behaviour of these elements within the lithosphere. The major application of lead isotope studies in ore genesis, other than in estimating the age of the mineralization, is in defining the source material for the lead in the ore. A second application, illustrated in this study, is in determining possible genetic links between ore bodies which, on geological evidence alone, do not obviously have a closely related (or even similar) origin. This can be used in the economic evaluation of ore prospects; the lead of a prospect can be "finger-printed" for comparison with lead from producing ore deposits in the same district, because different producing deposits within a district often have similar lead isotopic compositions (Doe and Stacey, 1974; Köppel and Grünenfelder, 1979).

The lead isotope study, unlike the carbon, sulphur and oxygen isotope studies, is not the sole work of the author. Instead, it was a co-operative project with Dr. H.J. Welke and Prof. H.L. Allsopp of the Bernard Price Institute of Geophysics, who performed the major part of the analytical work. A total of 70 galena samples, 17 rock and pyrite samples, and 2 zircon samples were analysed. The analytical techniques used, and all data, are summarized in Appendix 2.3.

5.3.1 Inherent error in lead isotope measurements

There are a number of sources of error inherent in lead isotope measurements. These include the random uncertainty which results from variations in the procedure used to load samples on the filament, and from the mass spectrometer run itself. Loading and running procedures were standardized to minimize variations in isotopic fractionation from these sources. The NBS standard 981 was run at regular intervals for the purpose of normalising data (the composition assumed for this

standard was: $^{206}Pb/^{204}Pb$ = 16,9371, $^{207}Pb/^{204}Pb$ = 15,4913, $^{208}Pb/^{204}Pb$ = 38,7213). Within-run precisions on both the samples and the standard were found to be approximately $\pm$ 0,005 ($1\bar{\sigma}$, standard error of the mean), for the quoted $^{206}Pb/^{204}Pb$ and $^{207}Pb/^{204}Pb$ values, and $\pm$0,011 for $^{208}Pb/^{204}Pb$ values. The standard runs were compared with the NBS values, and a mean fractionation correction was calculated at regular intervals. This correction, which averaged between 0,1 and 0,2 % per atomic mass unit, was applied to all sample data.

The between-run uncertainties determined from repeated analysis of the NBS standard were found to equal the uncertainties obtained from replicate runs of galena samples, and to be $\pm$0,008 (1σ) for $^{206}Pb/^{204}Pb$ values, $\pm$0,010 for $^{207}Pb/^{204}Pb$ values, and $\pm$0,025 for $^{208}Pb/^{204}Pb$ values. These uncertainties are much larger than the within-run precision because of the ^{204}Pb error, and a larger error which results from a variable (i.e. between run) degree of mass-dependent isotopic discrimination (produced mainly during the process of ionization at the filament). The larger values of these between-run uncertainties were therefore used as blanket errors during regression analysis.

Ludwig (1980) calculated a correlation coefficient of 0,94 between $^{206}Pb/^{204}Pb$ and $^{207}Pb/^{204}Pb$ ratios as the result of these sources of error, and this factor was used in the least-squares fitting of straight lines to galena data on common lead plots, using the method of York (1969). The same method was used for rock lead data, but these were assumed not to contain correlated errors (Brooks et al., 1972). The 1σ errors in the lead isotope ratios, the $^{235}U/^{204}Pb$ and $^{238}U/^{204}Pb$ ratios, and the $^{232}Th/^{204}Pb$ ratios were found to be $\pm$0,1, $\pm$2, and $\pm$5 percent, respectively (the error in the $^{232}Th/^{204}Pb$ ratio is not accurately known: Appendix 2.3). All linear arrays defined by galena data have MSUM values larger than 2,5, and are therefore errorchrons (i.e. "geological error" is present). The method of York (1966) was used in the calculation of parameters for errorchrons, although all MSUM values quoted have been calculated using the method of York (1969).

The decay constants used for ^{238}U, ^{235}U, and ^{232}Th are 0,155125 x 10^{-9} yr^{-1}, 0,98485 x 10^{-9} yr^{-1}, and 0,049475 x 10^{-9} yr^{-1}, respectively.

5.3.2 Galena from the Otavi Mountain Land

Figures 126a, b and c are uranogenic and uranothorogenic lead plots of data from galena of the Otavi Mountain Land. The data on these figures have been classified according to the mineralogical subdivisions of Figure 111b, and the two-stage growth curves of Stacey and Kramers (1975) have been plotted for reference (the uranogenic growth curve is almost identical to the orogenic curve of Doe and Zartman, 1979).

Mines and mineral prospects studied include occurrences of the Berg Aukas mineralogical type at localities 1, 23 (Abenab West), 26, 27, 31 (Harasib Main), 34, 41, 44 (Berg Aukas), and 45 (Figs. 111a, b). Galena samples of this type from strata-bound breccia horizons within zone T4 are from (1) near the Harasib Main prospect, in the central Otavi Mountain Land, (2) from locality 48, in the southern Otavi Mountain Land, and (3) from the Karuchas zone, between locality 24 and the Abenab West ore body. Galena occurrences of Tsumeb type include localities 2 (Tsumeb pipe, the adjacent E2200 breccia pipe, and the North Break zone), 6, 11, 53 (Kupferberg) and 57 (the Kombat group of mines). A mineral prospect with significant chalcopyrite and bornite, and another in which copper is the element of economic interest, are represented by galena samples from localities 55 and 21, respectively; these were suspected to be of Tsumeb mineralogical type prior to the lead isotope study. Galena samples from mineralogically unclassified occurrences at localities 49 and 64 in the Otavi Valley area, and locality 22 in the Tsumeb area, were also analysed. The Tschudi type of mineralization is represented by galena from locality 14, in the northern Otavi Mountain Land. An oxidation zone mineral from the Tsumeb ore body, wulfenite, was analysed to compare the isotopic ratios of hypogene and supergene (i.e. oxidation zone) minerals.

Regression analysis was carried out where linear, or apparently

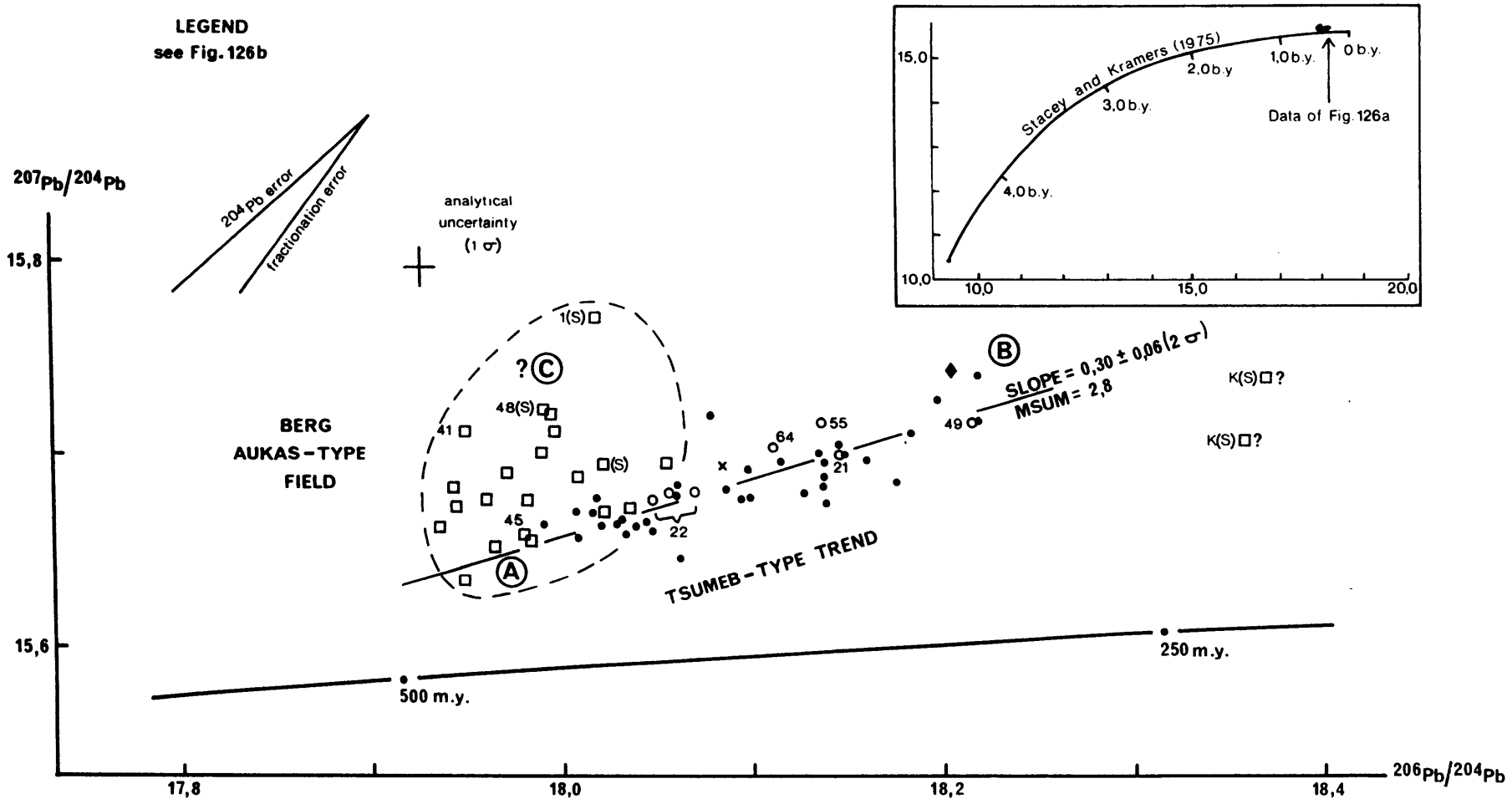

Fig. 126a

Uranogenic lead data from galena of the Otavi Mountain Land. Samples from the mineralogically-distinct Tsumeb and Berg Aukas types of mineralization are also isotopically distinct. A sample of Tschudi type plots with data of Tsumeb type.

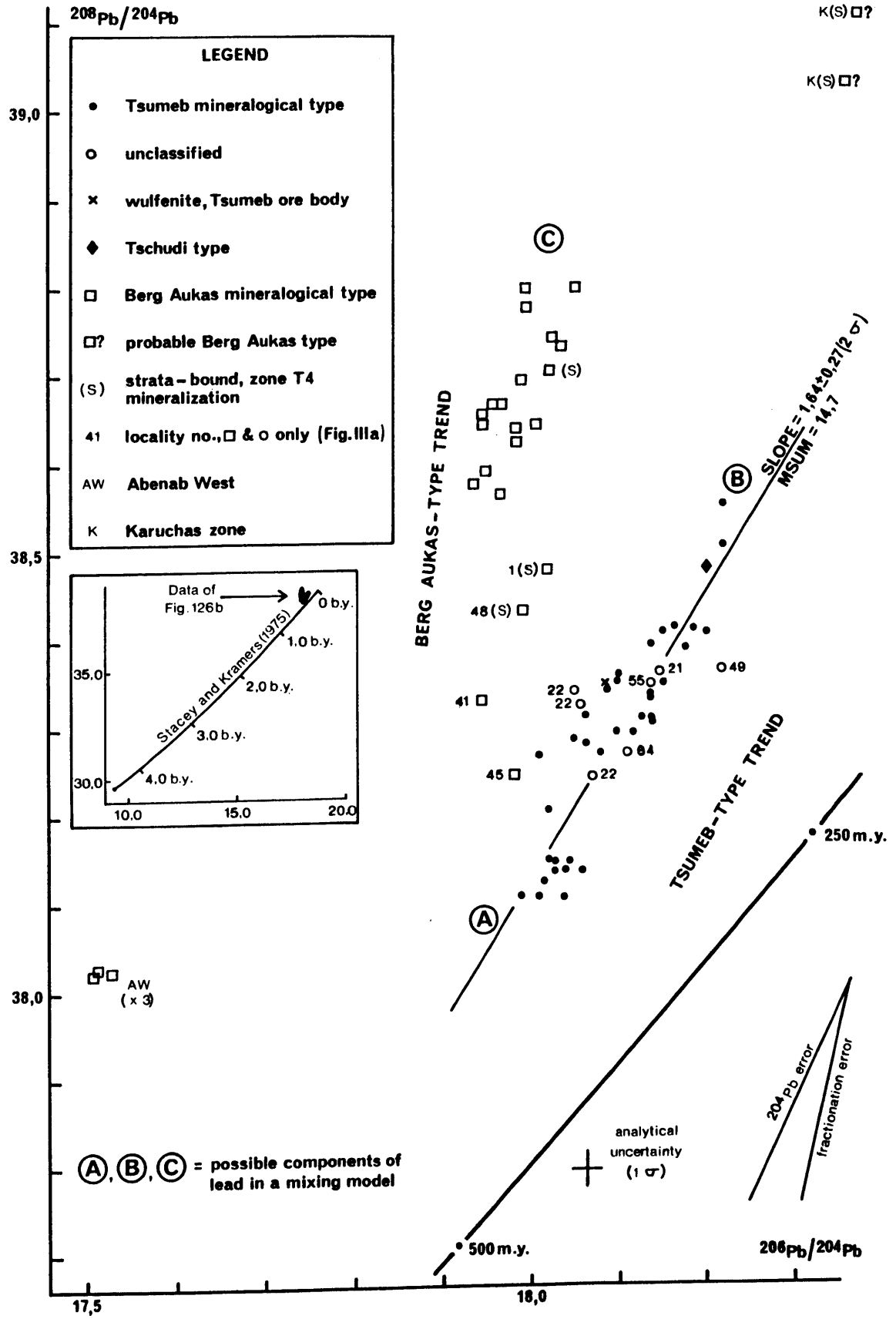

Fig. 126b
Uranothorogenic lead data from galena of the Otavi Mountain Land. Data from the mineralogically-distinct Tsumeb and Berg Aukas types of mineralization are isotopically different. A sample of Tschudi type plots with data of Tsumeb type.

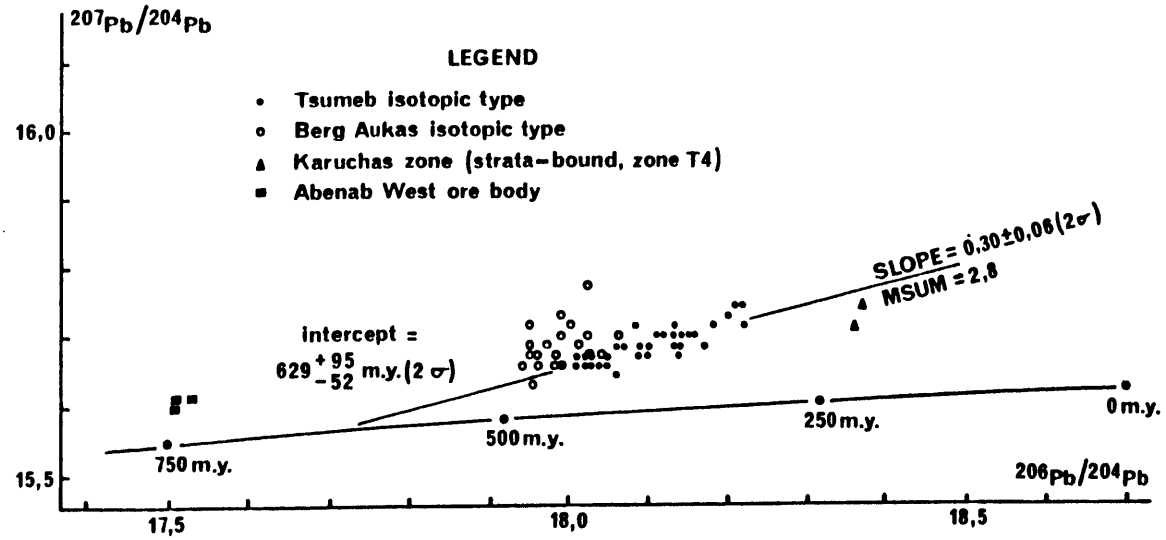

Fig. 126c
Uranogenic lead data from galena of the Otavi Mountain Land, showing that a regression line through data of Tsumeb type does not project through data of the Abenab West ore body or the Karuchas zone.

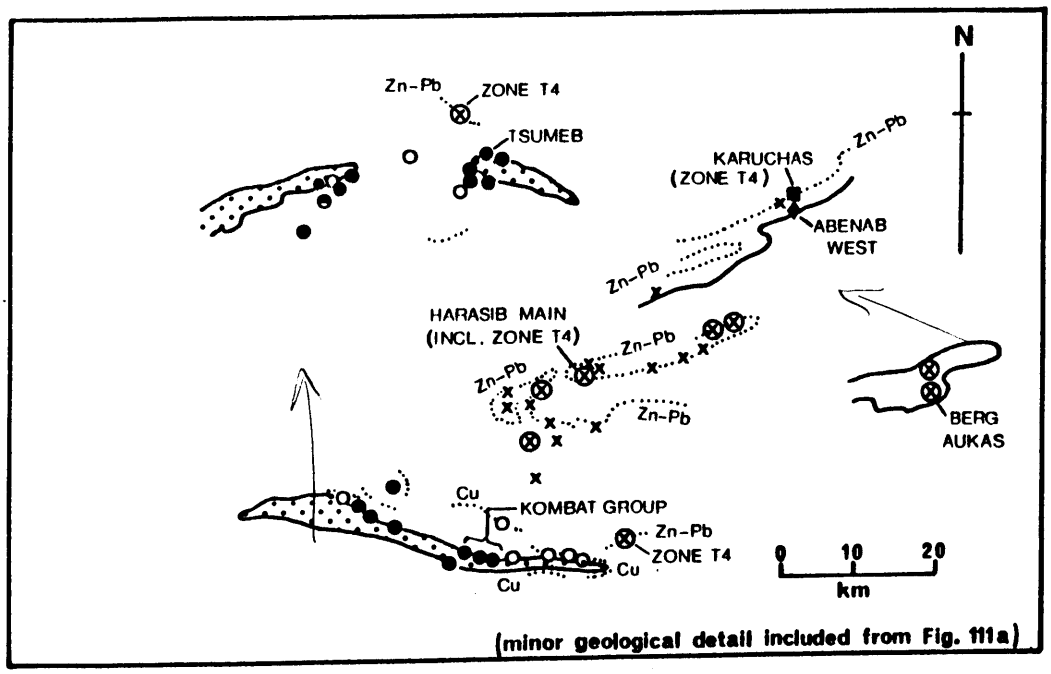

FIG.127 Mineralogical and lead isotopic classification of mineralization in the Otavi Mountain Land

(i) Tsumeb type
- Tsumeb type (isotopic and/or mineralogical)
- Cu major
- Cu significant
- Cu in strata-bound breccia, zone T4
- } probable Tsumeb mineralogical type
- Tschudi mineralogical type (Tsumeb isotopic type)

(ii) Berg Aukas type
- Berg Aukas isotopic type
- Discordant bodies
- Zn-Pb in strata-bound breccia, zone T4
- } Berg Aukas mineralogical type

(iii) Other
- Abenab West isotopic type
- Karuchas isotopic type

linear, arrays of data points were observed on the uranogenic and uranothorogenic lead plots. The regression lines are indicated on the appropriate figures, and the significance of these trends is discussed in the light of calculated uncertainties in slope and intercept values. A computer programme was written to calculate the intercepts between these trends and the second stage of the growth curves of Stacey and Kramers (1975), which have μ and W values of 9,74 and 36,84, respectively. The errors of these intercepts, and therefore of the model lead ages, were calculated in a similar manner to the mean values. Lines which represent the error limits on the regression data (i.e. lines with the maximum and minimum slopes and intercepts) were projected through the centroid of the regression data. The error limits on the model lead ages were obtained from the intercepts of these lines with the growth curves of Stacey and Kramers (1975).

The data from Tsumeb-type mineralization, including Tsumeb and the Kombat group of ore bodies, show a linear trend (or elongated field) on the uranogenic lead plot of Figure 126a. This trend also includes all samples from prospects suspected to be of Tsumeb type, prospects of unknown type, and Tschudi-type mineralization from locality 14. Samples of Berg Aukas type mostly cluster as a field which overlaps the trend defined by Tsumeb-type mineralization. Exceptions are samples of Berg Aukas type from the Karuchas zone, and samples from Abenab West mine, both of which plot outside the trend of Tsumeb-type mineralization and the field of Berg Aukas-type mineralization (Figs. 126a, c).

Data from the Tsumeb and Berg Aukas types of mineralization define two separate, but intersecting, linear trends on the uranothorogenic plot of Figure 126b. The trend for Tsumeb-type mineralization includes the same prospects as does the equivalent trend on the uranogenic plot. The linear trend shown on the uranothorogenic plot by data from mines and prospects of Berg Aukas type (with the exception of samples from the Karuchas zone and Abenab West mine) shows negligible overlap with the trend for Tsumeb-type mineralization. The trend defined by data of Berg Aukas type is sub-parallel to the trend that could be produced by isotopic fractionation within the mass spectro-

meter. However, the trend is too large to result from instrument fractionation (as indicated by good agreement on replicate runs over a period of years).

The following genetic conclusions can be drawn from the above relationships:

1) Data from the Tsumeb and Kombat ore bodies, and from other mineralization of Tsumeb type throughout the Otavi Mountain Land, lie on a single isotopic trend and have a common evolutionary history. There is good agreement between regression lines drawn on independent sets of uranogenic data from (1) the Tsumeb ore body (slope = 0,33 $\pm$ 0,12, 2σ; $^{207}Pb/^{204}Pb$ intercept = 9,7 $\pm$ 2,1), (2) the northern Otavi Mountain Land, exclusive of the Tsumeb ore body (slope = 0,35 $\pm$ 0,09; $^{207}Pb/^{204}Pb$ intercept = 9,4 $\pm$ 1,7), and (3) the southern Otavi Mountain Land (slope = 0,34 $\pm$ 0,12; $^{207}Pb/^{204}Pb$ intercept 9,5 $\pm$ 2,2). These slopes and intercepts do not differ significantly at the 95% level of confidence. The equivalent regression lines on the uranothorogenic plot also show good agreement. The parameters for the Tsumeb ore body (slope = 1,28 $\pm$ 0,39,2σ; $^{208}Pb/^{204}Pb$ intercept = 15,2 $\pm$ 7,1), northern Otavi Mountain Land (slope = 0,89 $\pm$ 0,50; $^{208}Pb/^{204}Pb$ intercept = 12,7 $\pm$ 6,5), and southern Otavi Mountain Land (slope = 1,41 $\pm$ 0,36; $^{208}Pb/^{204}Pb$ intercept = 12,7 $\pm$ 6,5) do not differ significantly at the 95% level. This good agreement indicates that the ore bodies represented by these three groups are related by a single process, regardless of whether this is a mixing trend or an isochron. It follows that they are broadly contemporaneous.

2) Other occurrences which were suspected to be of the Tsumeb mineralogical type (localities 55 and 21), and occurrences of unknown type (localities 22, 49 and 64), also plot on this trend, and are probably also of Tsumeb type (Fig. 111a).

3) The Tschudi type of mineralization of the northern Otavi Mountain Land (represented by only one sample) might also have formed during this event, consistent with geological evidence that both Tsumeb-type

and Tschudi-type mineralization formed subsequent to deposition of the Tschudi Formation (Chapter 4.5).

4) Most mineral occurrences of the Berg Aukas mineralogical type were related to a mineralizing event that differed in the source of its lead, its timing, or both, from the event which formed the occurrences of Tsumeb type. A specimen of galena from strata-bound breccia in zone T4 of the Harasib area has an almost identical isotopic ratio to galena from locality 31 (Harasib Main) and locality 34, both of which are discordant breccia bodies which terminate downwards in the strata-bound breccia of the central Otavi Mountain Land. A close genetic relationship between mineralization in the two types of breccia is indicated (Chapter 4.4.7).

5) Strata-bound mineralization which occurs in stratigraphic zone T4 differs isotopically in different areas of the Otavi Mountain Land. Mineralization from the southern and central Otavi Mountain Land and from locality 1, north of Tsumeb, is isotopically similar to most other occurrences of the Berg Aukas mineralogical type. However, mineralization of the Karuchas zone, which occurs in zone T4 near Abenab West, is isotopically different (Fig. 111a).

6) The Abenab West ore body (of Berg Aukas mineralogical type) and mineralization of the Karuchas zone (thought to be of Berg Aukas type) are not obviously related to each other, to the main field of Berg Aukas type lead, or to the isotopic trends of Tsumeb type. These occurrences may have formed during one or two additional, and separate events, or from different lead sources. Data from the Karuchas zone plot close to the projection of the uranogenic trend defined by Tsumeb-type occurrences. The slope and $^{207}Pb/^{204}Pb$ intercept of the regression line ($2\sigma^-$) on the Tsumeb trend are 0,30 $\pm$ 0,06 and 10,2 $\pm$ 1,2, respectively, (MSUM = 2,8). These variables are 0,23 $\pm$ 0,05 and 11,5 $\pm$ 1,0 (MSUM = 3,1) if the points from the Karuchas zone are added, and these populations do not differ significantly at the 95% level of confidence. However, this is not an adequate test for agreement between these populations because the two sets of data compared are not independent. Any possible relationship between the Tsumeb-type and

Karuchas zone data is less obvious on the uranothorogenic lead plot. The slope and $^{208}Pb/^{204}Pb$ intercept of the regression line (2σ) on the Tsumeb uranothorogenic trend are 1,64 $\pm$ 0,27 and 8,6 $\pm$ 4,9, respectively, (MSUM = 14,7), or 2,28 $\pm$ 0,30 and -3,0 $\pm$ 5,4 (MSUM = 50,3) if the Karuchas zone points are added; these slopes differ significantly at the 95% level of confidence, despite the large amount of data common to both data sets. The Karuchas zone points do not therefore appear to belong to the Tsumeb trend, although it is argued later that a strong genetic relationship may exist between these different types of mineralization. Data from the Abenab West ore body lie close to a uranogenic lead trend that includes data from the Tsumeb trend and the Karuchas zone. However, the slope and $^{207}Pb/^{204}Pb$ intercept (2σ) of the regression line on the uranogenic trend which includes the Abenab West and Karuchas zone points (0,14 $\pm$ 0,03 and 13,2 $\pm$ 0,5, respectively) differ significantly from the slope and intercept of the Tsumeb trend at the 95% level of confidence. Data from the Abenab West ore body do not lie near the equivalent trend on the uranothorogenic lead plot, nor near the projection of the Tsumeb trend alone.

A further possibility is that data from the Karuchas zone, the main Berg Aukas field, and the Abenab West ore body, form a single trend (although the MSUM values would be 9,3 and 58,4 for the uranogenic and uranothorogenic trends, respectively). This would only be possible if extreme instrument fractionation had caused the trend present in the Berg Aukas uranothorogenic field, a conclusion rejected here. The remaining possibility is that the Abenab West and Karuchas data lie on a single trend which is different to the Berg Aukas or Tsumeb trends. However, it would appear anomalous that the greatest difference in lead isotope ratios from the entire Otavi Mountain Land should occur between two occurrences in the immediate proximity of each other, which are isotopically related in some simple manner. A model is favoured in which the Abenab West ore body formed at a different time, or from a different source of lead, despite its close geographic and stratigraphic proximity to the Karuchas zone.

Figure 127 is a revised version of Figure 111b, in which all

occurrences of unknown mineralogical type that lie on the isotopic trend for Tsumeb-type mineralization have been grouped with occurrences known to be of Tsumeb mineralogical type. Occurrences of Berg Aukas mineralogical type have been subdivided into Berg Aukas, Abenab West and Karuchas zone isotopic types.

Two conclusions which can be drawn from the above (both of which have been noted by previous workers in other areas, e.g. Doe and Stacey, 1974) have economic significance to mineral exploration in the Otavi Mountain Land, and are independent of any genetic interpretation. The first is that lead isotope ratios of single galena samples could, in many instances, be used to distinguish if a mineral prospect was of Berg Aukas type, or of the economically more important Tsumeb type. The second is that the sample of wulfenite from the Tsumeb mine plots, as could be expected, on the Tsumeb trend, and that secondary ore minerals might therefore be used in the classification of mineral prospects for exploration purposes.

5.3.3 Geographic and stratigraphic variations in lead isotope ratios

Figures 128a and b are uranogenic lead and uranothorogenic lead plots of all points on the Tsumeb isotopic trend. A distinction has been made on these plots between the occurrences of the Otavi Valley and Tsumeb areas. Occurrences in the Tsumeb area can be seen, on average, to be distinctly more radiogenic on both plots. Figures 128c and d are plots of data from the Otavi Valley area alone. Data from the more productive members of the Kombat group of ore bodies (Asis West to Kombat East), which occur immediately below the base of the Mulden Group, plot in a very restricted field. Data from most of the smaller mines to the east (E900 and Asis Ost), and prospects to the west are more radiogenic, but exceptions occur, and geographic zoning is not pronounced. Locality 49 is the only analysed occurrence from some distance north of the Otavi Valley, and it contains the most radiogenic lead. Figures 128e and f are plots of data from the Tsumeb area alone; the Tsumeb ore body is excluded for reasons discussed below. Samples from locality 22, the prospect farthest to the south and west (strata-bound breccia at the contact between stratigraphic

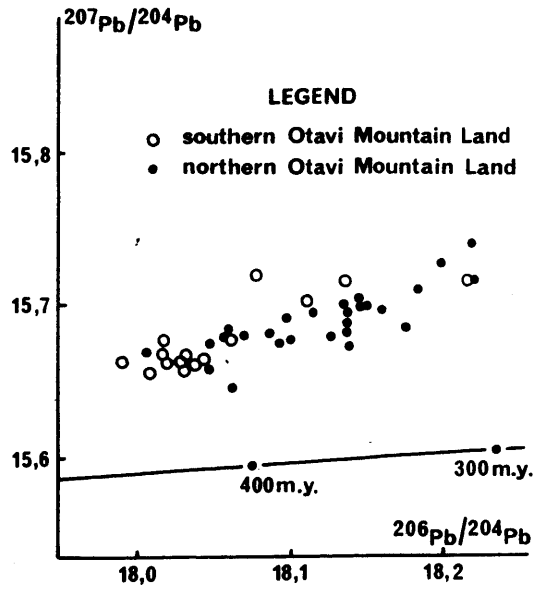

FIG. 128a

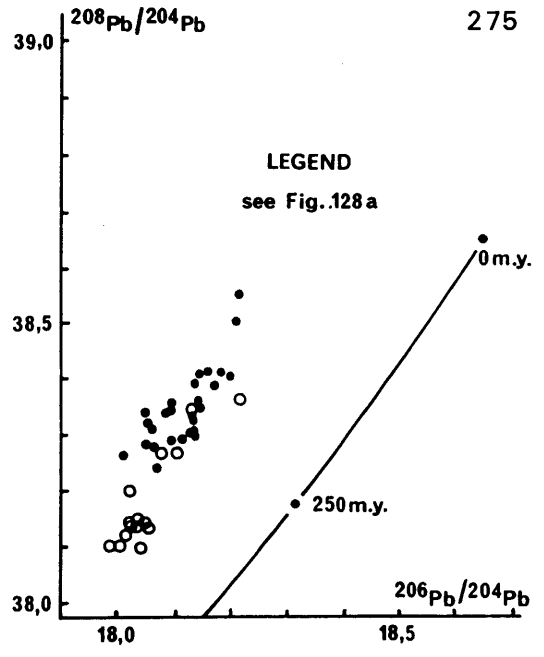

FIG. 128b

Figs. 128a,b
Uranogenic and uranothorogenic lead data of Tsumeb type, showing the more radiogenic composition of lead in galena from the northern Otavi Mountain Land (Tsumeb area), relative to galena from the southern Otavi Mountain Land.

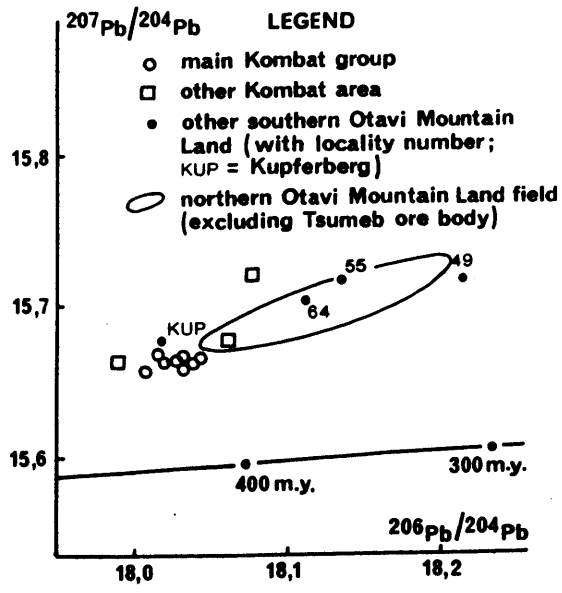

FIG. 128c

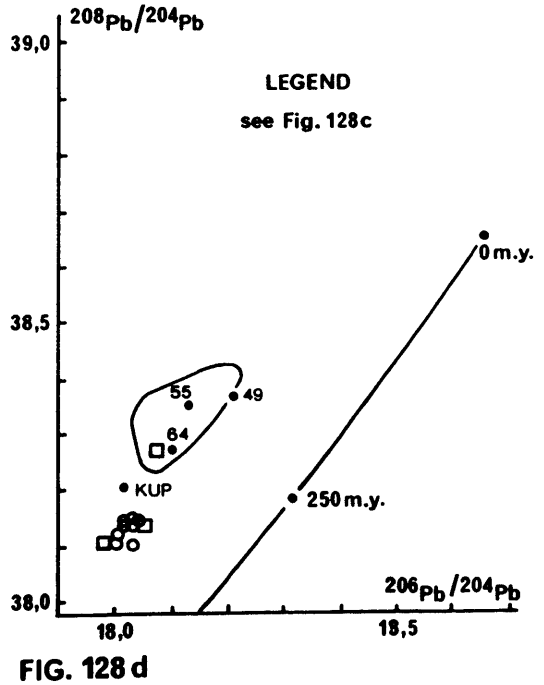

FIG. 128d

Figs. 128c,d
Uranogenic and uranothorogenic lead data of Tsumeb type from galena of the southern Otavi Mountain Land. The least radiogenic samples are from the Kombat group of ore bodies, which occur on the contact between the Otavi Group and Mulden Group. Locality 49 is north of the other occurrences, and its galena contains the most radiogenic lead.

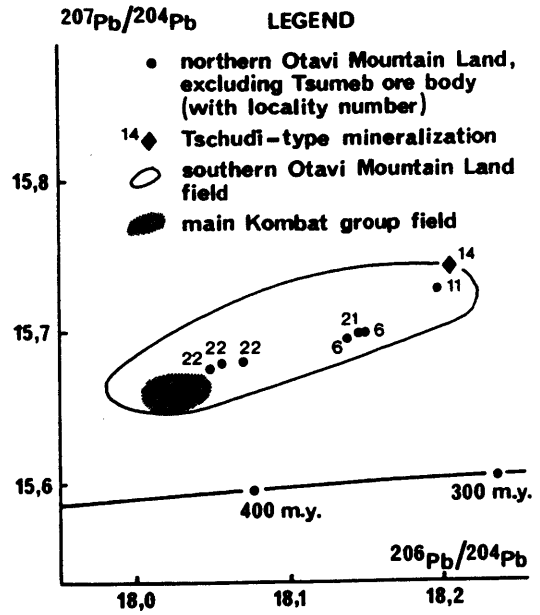

FIG. 128 e

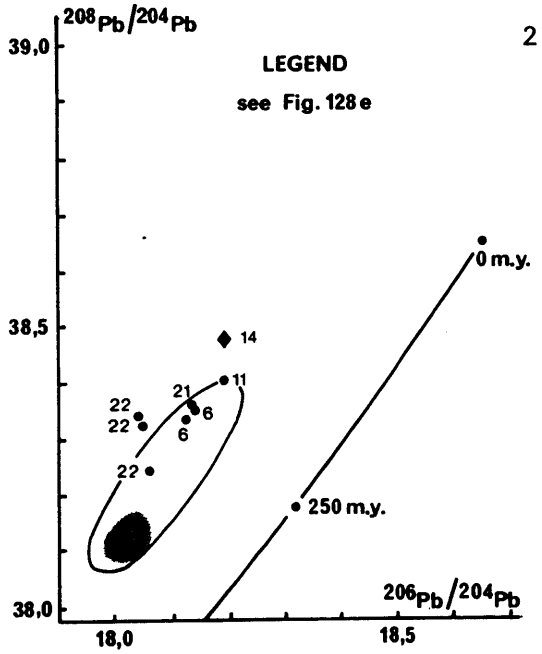

FIG. 128 f

Figs. 128e,f
Uranogenic and uranothorogenic lead data of Tsumeb type from galena of the northern Otavi Mountain Land, excluding the Tsumeb ore body. Locality 22 is south of the other occurrences, and its galena contains the least radiogenic lead. The most radiogenic lead occurs in Tschudi-type mineralization of the Mulden Group.

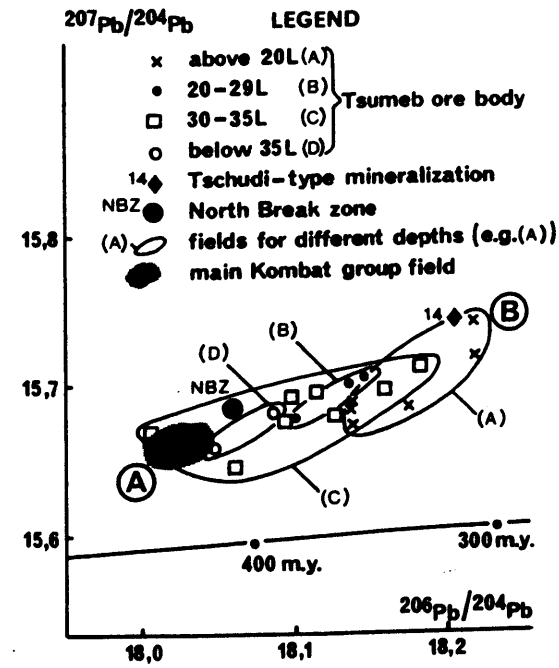

FIG. 128 g

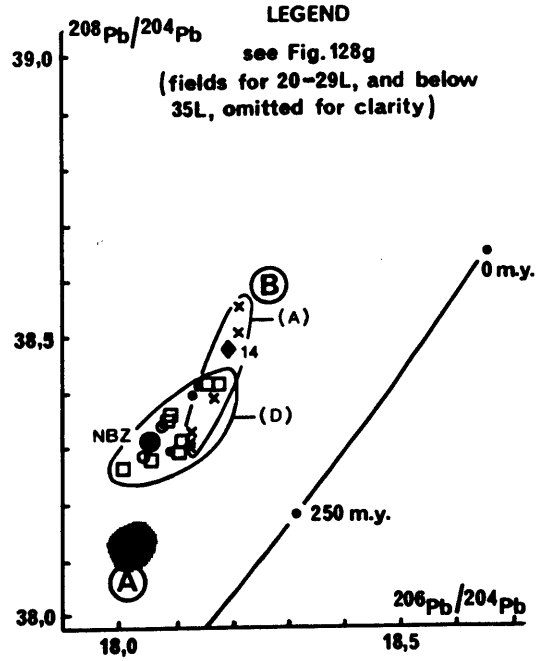

FIG. 128 h

Figs. 128g,h
Uranogenic and uranothorogenic lead data from galena of the Tsumeb ore body. The data are increasingly radiogenic with decreasing stratigraphic elevation. The composition of galena samples from the North Break zone and the Mulden Group (i.e. Tschudi type) are consistent with a model in which isotopically distinct components of lead, A and B, were introduced to the Tsumeb pipe from these probable paleoaquifers.

zones T7 and T8), are significantly less radiogenic than the other samples on each plot. All of the occurrences occur in the uppermost two zones of the Tsumeb Subgroup, and one of the two most radiogenic samples occurs within the basal Mulden Group, the reverse of the pattern in the Otavi Valley area.

No stratigraphic zonation, and only a poorly-defined geographic zonation, is evident within the linear trend defined by data of Berg Aukas type on the uranothorogenic lead plot (Fig. 126b). Three of the four least radiogenic samples are from the south-central Otavi Mountain Land (localities 41, 45 and 48), but the other sample is from north of Tsumeb (locality 1). The more radiogenic samples are from the central Otavi Mountain Land, farther to the north (i.e. the Harasib area), and from the Berg Aukas ore body. Data from single ore bodies or prospects, e.g. Berg Aukas and Harasib Main, or restricted geographic areas, e.g. central Otavi Mountain Land, show only very limited isotopic variation.

The variation of lead isotope ratios of galena which is observed on a regional scale is also present on a local scale in the Tsumeb pipe, where there is a marked decrease in lead isotope ratios with increasing depth below the base of the Mulden Group. Figures 128g and h are uranogenic and uranothorogenic lead plots of data from the Tsumeb ore body alone. Data on the uranogenic plot span the entire range of isotopic ratios observed in Tsumeb-type lead throughout the Otavi Mountain Land. The uranothorogenic data span the entire range except for the least radiogenic points represented by the Kombat group of mines. The data have been divided into four fields, according to the depth at which galena was sampled within the mine. Two of these fields (20 to 29 level, and below 35 level) only contain three and two samples respectively, but the other fields contain six and seven samples (above 20 level, and 30 to 35 levels, respectively). Samples from deeper levels in the Tsumeb mine are distinctly less radiogenic than samples from higher levels, on both plots (this definitely cannot be ascribed to mass-dependent fractionation on the uranogenic plot, because of both the known precision of the data and the large angle between the Tsumeb trend and the isotope fractionation line; Fig. 126a). These observa-

tions support the argument advanced in Chapter 5.3.2, that Tsumeb-type mineral occurrences of the southern and northern Otavi Mountain Land are related by a single process and are therefore broadly contemporaneous. An important implication of the data is that two fluids were involved in the mixing process, because the volume of the pipe is insufficient for a lead component to have been derived from its sedimentary infill.

It can be concluded that lead isotope ratios from galena of Tsumeb isotopic type in the Tsumeb area (excluding Tsumeb) are, on average, more radiogenic than lead isotope ratios in the Otavi Valley area. Two samples indicate that lead isotope ratios with intermediate values might be expected in the intervening area, but this could not be tested because of a lack of galena samples from the few copper prospects that occur in this area. Stratigraphic controls on lead isotope ratios are also present. The least radiogenic galena samples from the Otavi Mountain Land occur immediately below the base of pelite of the Kombat Formation in the Otavi Valley area, and these show a very restricted range of isotopic compositions. The most radiogenic samples are from immediately below and within the Tschudi Formation of the Tsumeb area. Evidence that this variation is stratigraphic as well as geographic is found in the Tsumeb mine, where the radiogenic nature of the lead decreases with increasing depth below the base of the Mülden Group. A continuum of lead isotope ratios is therefore indicated for lead of Tsumeb isotopic type throughout the Otavi Mountain Land. Data of Berg Aukas type show a poorly-defined geographic variation, with the least radiogenic samples in the southern Otavi Mountain Land.

5.3.4 The linear lead isotope trends as isochrons

Two alternative origins are considered for the linear trends shown on the lead-lead plots by data of Tsumeb and Berg Aukas types. These alternatives are that the trends approximate to isochrons, with time significance, or that they represent mixing lines. Only a simple isochron model is considered, involving one stage of lead evolution subsequent to continuous, or two-stage, growth of the type modelled by

Cumming and Richards (1975), Stacey and Kramers (1975) and Doe and Zartman (1979). However, the Tsumeb uranogenic trend, and the Tsumeb and Berg Aukas uranothorogenic trends, are errorchrons with MSUM values of 2,8, 14,7 and 14,8, respectively. Either of the alternatives considered is therefore an over-simplification, because other "geological error" is present.

The uranogenic trend of galena from Tsumeb-type occurrences intersects the two-stage growth curve of Stacey and Kramers (1975) at $629\ ^{+95}_{-52}$ m.y. (2σ). This is a realistic age for mineralization (Chapter 3.7.12), consistent with the assumption that the linear trend approximates to an isochron, the slope of which is a function of the age of the source of the lead and the time of mineralization:

$$\text{slope} = \frac{^{207}Pb}{^{206}Pb} = \frac{1}{137,88} \cdot \frac{e^{\lambda_5 t_1} - e^{\lambda_5 t_2}}{e^{\lambda_8 t_1} - e^{\lambda_8 t_2}} \qquad .....(1)$$

The estimated age of the lead source, calculated from the second intercept on the two-stage growth curve, is $3276\ ^{+331}_{-445}$ m.y. (2σ). The nearest rocks recorded to be of this age form part of the central Congo craton in north-eastern Angola and Zaïre (Kröner, 1977a, b). Rocks of this age may exist in the poorly studied region farther to the south, but their lead isotopic systems have probably been re-set in later tectono-thermal events.

The average $^{238}U/^{204}Pb$ ratio, μ_2, of the system in which the Tsumeb-type lead evolved can be calculated from the mean $^{206}Pb/^{204}Pb$ value, using equation (2):

$$\left(\frac{^{206}Pb}{^{204}Pb}\right)_{t_2} = \left(\frac{^{206}Pb}{^{204}Pb}\right)_{t_1} + (e^{\lambda_8 t_1} - e^{\lambda_8 t_2}) \qquad .....(2)$$

This value is $10,5 \pm 1,6$, compared with a value of 9,7 for the second stage of the Stacey-Kramer curve. This value would not necessarily represent the μ value of the whole rock from which the lead was extracted, because the ore lead could have been selectively leached

from sites within the lead source, e.g. from radiogenic cement between the grains of a feldspathic sandstone. It is possible that the above source of lead evolved in a system with a different average μ value than that adopted for the second stage of the two-stage growth curve of Stacey and Kramers (1975), e.g. larger, and closer to the upper crustal growth curve of Doe and Zartman (1979). However, this would not greatly alter the above conclusion.

The $^{232}Th/^{238}U$ ratio of the system in which the Tsumeb-type lead evolved can also be estimated. The slope of an isochron on the uranothorogenic lead plot is not only a function of the age of the lead source and the time of mineralization, but also of the $^{232}Th/^{238}U$ ratio of the system, and therefore of μ and W:

$$\text{slope} = \frac{^{208}Pb}{^{206}Pb} = \frac{^{232}Th}{^{238}U} \cdot \frac{e^{\lambda_2 t_1} - e^{\lambda_2 t_2}}{e^{\lambda_8 t_1} - e^{\lambda_8 t_2}} \quad \ldots\ldots (3)$$

The isochron will intersect the uranothorogenic growth curve at t_1, but will only intersect the curve at t_2 in the special case where lead developed between t_1 and t_2 in a system with the same $^{232}Th/^{238}U$ ratio as that of the uranothorogenic growth curve prior to t_1 (Appendix 2.3.2). The computed value of $^{232}Th/^{238}U$ is $6,4 \pm 1,2$, which is a large value, typical of lower crustal environments (Doe and Zartman, 1979). This value is inconsistent with the moderately large value indicated for μ, which is typical of orogenic and upper crustal environments. The $^{232}Th/^{238}U$ ratio must have been relatively constant between t_1 and t_2 to give the linear trend shown by galena of Tsumeb type on the uranothorogenic lead plot. This requires special conditions because uranium, thorium and lead have geochemically different behaviour, and the $^{232}Th/^{204}Pb$ and $^{238}U/^{204}Pb$ ratios must have been variable in the lead source. The larger MSUM value of the uranothorogenic Tsumeb trend (14,7), relative to the uranogenic trend (2,8) is consistent with the greater scatter to be expected in the former.

The $^{232}Th/^{204}Pb$ ratio, W_{2_i}, of a system within which the lead isotope ratio of an individual sample formed can be computed from:

$$W_{2_i} = \frac{^{232}Th}{^{238}U} \cdot \mu_{2_i} \quad \ldots\ldots (4)$$

The average ratio for all such systems within which Tsumeb-type lead developed can be calculated from the average value of μ_2, computed above. This average value, W_2, is 66,9 $\pm$ 16,1, which is a very large value, even for upper crustal environments (Doe and Zartman, 1979).

The trend for Tsumeb-type lead intersects the uranothorogenic growth curve at $729 \pm^{342}_{118}$ m.y., rather than at $3276 \pm^{331}_{445}$ m.y. (t_2). This age could be greater if the W_1 value for the preceding stage of growth was smaller than estimated, i.e. smaller than the value of 36,8 used by Stacey and Kramers (1975); however, it would not approach the age estimated from the uranogenic lead plot. This lack of agreement between the two lead-lead plots indicates that the values of t_1 and t_2 calculated from the uranogenic plot, and the slope of the Tsumeb-type trend on the uranothorogenic plot, are not consistent with each other, or with the interpretation of these trends as isochrons.

Lead isotope ratios from samples of Berg Aukas type occur in a confined field on the uranogenic lead plot, indicating that μ_2 was not significantly larger than the value adopted by Stacey and Kramers (1975). However, the slope of the linear trend on the uranothorogenic lead plot is very large (incalculable using York, 1966), and the values of $^{232}Th/^{238}U$ and $^{232}Th/^{204}Pb$ must also be very large. Also, the intercept of the uranothorogenic lead trend with the growth curve at approximately 470 m.y. (which should correspond to t_2), is equal to, or younger than, the age of mineralization predicted from geological evidence (Chapter 3.7.12). The linear trend on the uranothorogenic lead plot does not, therefore, approximate to a geologically reasonable isochron.

It is shown above that the values of the variables computed from either the Tsumeb-type or Berg Aukas-type lead isotope data show no agreement when determined independently from the uranogenic and uranothorogenic lead plots. Therefore, the errorchrons obtained do not approximate to geologically reasonable isochrons. Unfortunately the computations require that the error limits on the variables are accurately known, and this cannot be assumed for any errorchron (Brooks et al., 1972). The magnitudes of the MSUM values are direct indicators of the magnitudes of the "geological errors" involved, and these are moderately large for these trends. The trends contain 42 and 21 samples, respectively, and the MSUM value required to discriminate between isochrons and errorchrons is close to 2,0, rather than the commonly adopted value of 2,5, but no trends have values smaller than 2,8. The validity of conclusions made from Berg Aukas-type samples is quite insensitive to large increases in the error limits, but the argument based on the Tsumeb-type data would be invalidated by a moderate increase in the error limits (which cannot be predicted). However, it is shown below that other evidence indicates that the linear arrays defined by the Tsumeb-type data approximate to two-component mixing lines, rather than isochrons.

5.3.5 A mixing origin for lead of the Otavi Mountain Land

The most convincing evidence for a mixing model is the geographic and stratigraphic variations shown by lead isotope ratios in the Otavi Mountain Land. The only isochron model that can explain the systematic variation of lead isotope ratios with depth in the Tsumeb ore body requires that the depth at which galena precipitated within the pipe, as well as the lead isotope ratios in the ore solutions, varied with time, although all lead was derived from sources which were temporally and isotopically related to each other. It is also necessary to invoke additional special conditions to explain the more radiogenic nature of lead in general throughout the northern Otavi Mountain Land. Doe and Delevaux (1972) suggested this type of model to explain systematic variations in lead isotope ratios with stratigraphic elevation in Mississippi Valley-type ore of south-eastern Missouri. However, later studies indicated that isotopic variations in ore of

south-eastern Missouri resulted from mixing of different lead components (Chapter 5.3.12). The model suggested by Doe and Delevaux (1972) would be possible where lateral flow of ore fluid is indicated to have occurred in sub-horizontal sedimentary rocks, so that fluid flow could be deflected into stratigraphically higher beds with time. However, this explanation is highly improbable in an ore body such as Tsumeb, where the ore fluids were mostly confined to a vertical pipe less than 100 m in diameter, in which any isotopic zoning could be expected to be parallel to the walls of the pipe.

A mixing trend, in its simplest form, could result from incomplete mixing of two components, A and B, to give the linear lead isotope trends displayed by data of Tsumeb type (Figs. 126a, b). One component of lead of Berg Aukas type could also be provided by component A, but another component, C is also required to explain these data points. This is a simplified model, because the scatter of points along the trends (i.e. the "geological error" in the data) indicates that some of the components must have had a variable isotopic composition, or that small amounts of additional components were involved in the mixing process. It is important to establish that lead components of the correct isotopic composition could have existed in the area at the time of mineralization, and that spatial variations in the isotopic ratios of galena are consistent with the spatial distribution of these lead components, and with the pattern of flow of the ore fluids interpreted from geological evidence. An important implication of this model is that the intersection of isotopic trends with the "primary" (e.g. single-stage, two-stage, or continuously evolving) growth curve need not have any age significance. However, these intercepts could approximate to t_2 in the case where the evolution of one mixing component approximated to "primary" growth. This may be the case for the uranogenic and uranothorogenic evolution of both Tsumeb-type lead ($629 \pm \frac{95}{32}$ m.y. and $729 \pm \frac{342}{118}$ m.y., respectively) and Berg Aukas-type lead (approximately 470 m.y. on both plots).

The following constraints on lead sources and ore fluid migration paths in the Otavi Mountain Land can be inferred from geological data and lead isotope analyses of galena:

1) The distribution of mineralization and rock alteration in the Tsumeb ore body indicates that the flow of ore fluid was mostly confined to the pipe, and therefore vertical, except where the pipe is intersected by strata-bound zones of rock alteration. The least radiogenic lead is present in galena from the greatest depth in the pipe, and vice-versa, and it follows that ore solutions which contained the least radiogenic lead component, A, entered the pipe at depth. This model was tested by analysing galena from a probable paleo-aquifer at depth in the Tsumeb area, the North Break zone (Chapter 3.4.4); this strata-bound zone was altered and mineralized by the ore fluid and might therefore have introduced ore fluid to the Tsumeb pipe. Galena from this paleoaquifer was found to be one of the least radiogenic in the Tsumeb pipe or the northern Otavi Mountain Land, consistent with the above interpretation (Figs. 128g, h). This paleoaquifer was not necessarily the only source of component A for the Tsumeb pipe, because: (1) lead isotope ratios at greater depth than this in the pipe are distinctly less radiogenic than those above, (2) the chemistry of rock alteration is different at greater depth (consistent with introduction of fluid to the pipe below the level of the North Break zone; Fig. 135), and (3) there is geological evidence elsewhere in the Otavi Mountain Land for a strata-bound paleoaquifer in zone T4 which contains lead of different isotopic types (Chapter 5.3.2). One of these lead types plots near to component A on both isotope plots (i.e. locality 48, immediately north of the Otavi Valley). The other lead type plots close to component B on both plots (i.e. in the Karuchas zone). Copper mineralization in zone T4, north of the Otavi Valley, is probably of Tsumeb type, but no samples could be obtained to verify this. Mineralization elsewhere is of Berg Aukas isotopic type (Chapter 5.3.2). This strata-bound horizon is therefore thought to have acted as an aquifer for Tsumeb-type and Berg Aukas-type ore fluids at different localities.

2) The more radiogenic lead component, B, must have been introduced to the Tsumeb pipe at a higher stratigraphic level. A number of possible paleoaquifers exist from zone T7 upwards (e.g. leached evaporite horizons, oolitic chert which contains disseminated mineralization, sandstone of the Mulden Group). A single paleoaquifer

is again improbable; however, the greatest influence of this lead component is seen in galena from the Mulden Group and the uppermost Tsumeb Subgroup of the northern Otavi Mountain Land (Figs. 128e, f).

3) The lead isotopic compositions of galena from the North Break zone, and of samples from the lower part of the Tsumeb pipe, are similar to those of the least radiogenic galena samples from Tsumeb-type occurrences of the southern Otavi Mountain Land (i.e. from near the base of the Mulden Group in the Kombat group of ore bodies). There is geological evidence for extensive lateral migration of the ore fluids which precipitated both the Tsumeb and Tschudi types of mineralization, as well as the isotopically distinct Berg Aukas type of mineralization (i.e. strata-bound mineralization and rock alteration occur at various stratigraphic levels throughout the Otavi Group and Mulden Group; Chapter 4.3). The isotopic evidence is therefore consistent with a model in which the least radiogenic component, A, migrated northwards from a source area in the south of the present Otavi Mountain Land, and was mixed with a component B in the northern Otavi Mountain Land (or at various localities in the intervening area).

4) The isotopically distinct Tsumeb and Berg Aukas types of mineralization both formed subsequent to the start of deposition of the Tsumeb Subgroup. The Tsumeb type (if not both types) was deposited subsequent to the karsting of these rocks, which occurred prior to deposition of the Mulden Group. However, both types formed before the Mulden Group was deformed (i.e. prior to the close of F_1 folding; Chapter 4.5). The complete stratigraphic separation of the Tsumeb and Berg Aukas types of mineralization within any particular geographic area (Chapter 4.5) is consistent with a model in which lead component A is common to both types of mineralization, but components B and C were added to separate fractions of the ore fluid which travelled along different pathways.

Lead isotope studies of rocks and minerals were undertaken to investigate sources of lead which might be consistent with the lead sources required by the above mixing model.

5.3.6 Dolostone isochrons, Otavi Group

The U-Pb systematics of data from five dolostone samples, taken from different stratigraphic levels in the Otavi Group, define two isochrons and an errorchron (Figs. 129a, b, c; Appendix 2.3.1). The results are:

	Age(1σ)	Initial ratio(1σ)	MSUM
$^{207}Pb/^{204}Pb$ vs $^{235}U/^{204}Pb$	649±105 m.y.	15,69±0,02	0,1
$^{206}Pb/^{204}Pb$ vs $^{238}U/^{204}Pb$	631± 96 m.y.	18,45±0,16	43,1
$^{207}Pb/^{204}Pb$ vs $^{206}Pb/^{204}Pb$	629±135 m.y.		0,3

The error limits are large because of the small variation in the $^{207}Pb/^{204}Pb$ ratio with age in such young rocks. However, the means of the slope ages and lead-lead age do not differ significantly at the 95 % level of confidence, and the ages fall within the limits indicated by other radiometric data (Chapter 3.7.12). The $^{207}Pb/^{206}Pb$ initial ratio is not significantly different from the ratios of galena samples from the northern or southern Otavi Mountain Land. However, the $^{206}Pb/^{204}Pb$ initial ratio differs considerably from this ratio in galena of the southern Otavi Mountain Land (this galena has a minimum value of approximately 17,99). The dolostone samples come from both areas, and the initial ratios do not therefore reflect contamination by ore lead during the mineralizing event.

The lead-lead isochron age is commonly found to be the best estimate of the age of a rock, because it is not sensitive to recent changes in parent-daughter ratios. However, the $^{207}Pb/^{204}Pb$ versus $^{235}U/^{204}Pb$ data do not show evidence of recent lead loss, and the best estimate of the age is taken as the mean of the two isochron ages, i.e. approximately 640 m.y. The age and initial ratios reflect the last event which homogenized the $^{207}Pb/^{204}Pb$ and $^{206}Pb/^{204}Pb$ ratios in dolostone of the entire Otavi Group. The large error in the age (1σ approximately 100 m.y.) permits a number of alternative interpretations. This event could be (1) sedimentation, (2) early or late dolomitization or diagenesis, (3) a

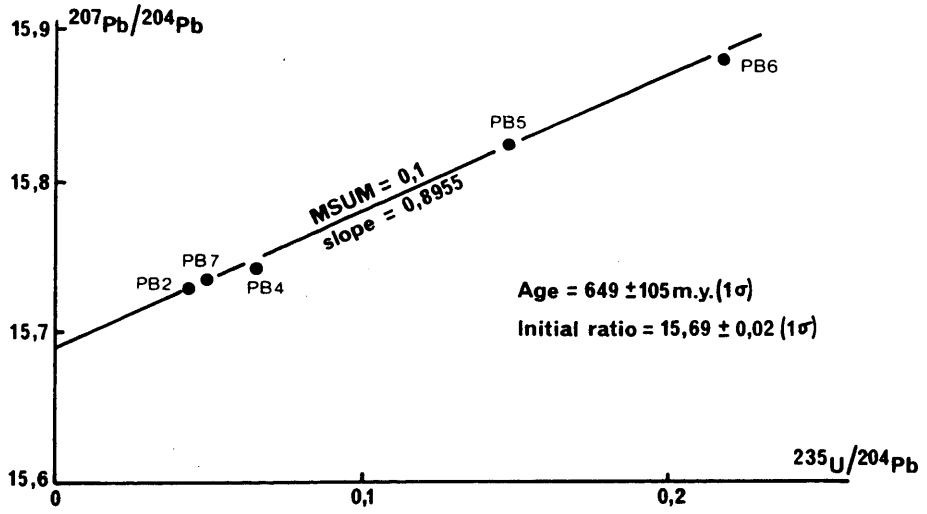

(a) $^{207}Pb/^{204}Pb$ versus $^{235}U/^{204}Pb$ isochron

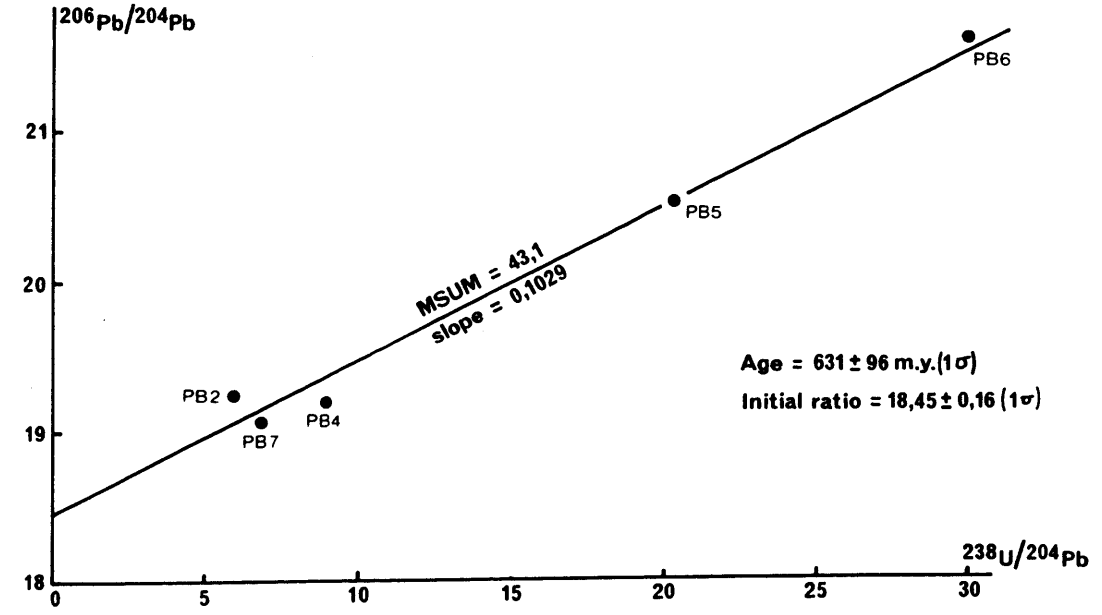

(b) $^{206}Pb/^{204}Pb$ versus $^{238}U/^{204}Pb$ errorchron

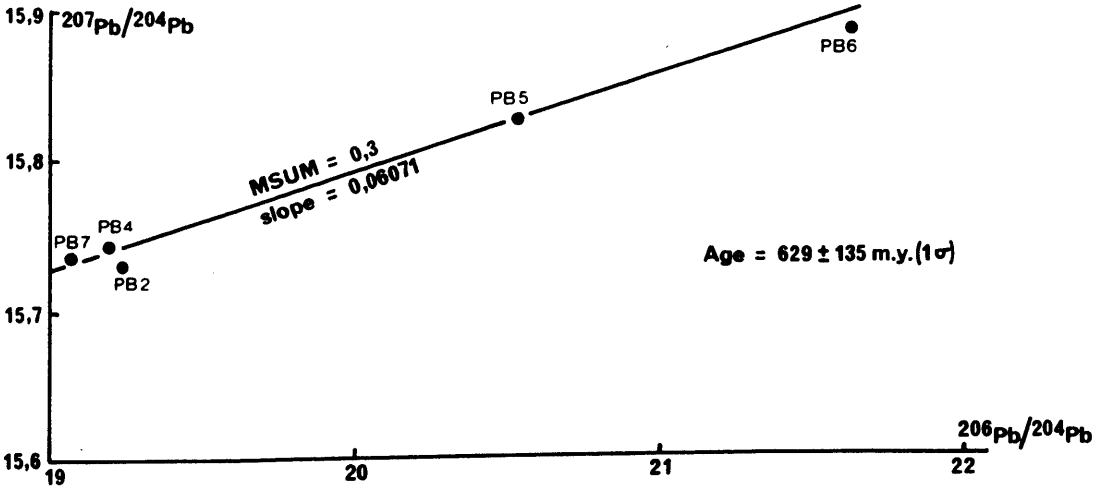

(c) $^{207}Pb/^{204}Pb$ versus $^{206}Pb/^{204}Pb$ isochron

Fig. 129
U-Pb systematics of dolostone from the Otavi Group.

metamorphic event which may have affected the Otavi Group prior to deposition of the Mulden Group (Chapter 3.7.12), or (4) metamorphism subsequent to ore deposition. Although dolostone can form by primary precipitation, most dolostone probably forms by replacement of pre-existing sediment (Land, 1985), and there is evidence that this occurred in the Otavi Mountain Land. It is therefore improbable that the above ages represent a true depositional age. Early dolomitization or diagenesis is probable, because permeability and pervasive fluid circulation (and therefore the capacity for isotopic homogenization) decrease during progressive burial. However, regardless of which of these interpretations is correct, the event establishes a maximum (if not very useful) limit for the age of the Tsumeb-type mineralization. This is because the mineralization post-dates sedimentation of the basal Mulden Group, and therefore post-dates most diagenesis and metamorphism (Chapter 3.7.12). The only exception would be if the event was the post-ore metamorphism, which was of very low metamorphic grade (Chapter 3.7.11); this is rejected for the reason given above.

5.3.7 Source of the ore lead

A requirement for a mixing model is that lead components A, B and C could have existed in the rocks of the Otavi Mountain Land at the time of mineralization (Chapter 5.3.5). Also, the locations of these components should be consistent with the stratigraphic and geographic zoning of lead isotope ratios in the mineralization (Chapter 5.3.3). The most important aspects of this zoning are: (1) the increasingly radiogenic nature of Tsumeb-type lead with decreasing depth in the Tsumeb ore body, (2) the presence of both the least and most radiogenic occurrences of Tsumeb isotopic type in the basal Mulden Group of the southern and northern Otavi Mountain Land, respectively, and (3) the more radiogenic nature of galena of both Tsumeb type and Berg Aukas type from the northern and central Otavi Mountain Land, relative to galena from the southern Otavi Mountain Land.

Possible sources of lead in mineralization of the Otavi Mountain Land include sedimentary carbonate rocks of the Otavi Group, and sandstone and pelite of the Mulden Group (Fig. 2). These rocks

constitute most of the sequence which hosts the mineralization, and within which the observed variations in the isotopic composition of ore lead occur. Other possible sources of lead include sandstone and volcanic rocks of the Nosib Group (which could have acted as paleo-aquifers and metal sources) and basement rocks. Rock lead studies were confined to rocks of the Otavi Group and Mulden Group because these were the only units from which unmineralized and unweathered samples could be obtained (Appendix 2.3.1).

The present lead isotopic composition of rock samples was corrected for lead added by the radioactive decay of uranium and thorium since the time of the mineralizing event. The lead isotopic composition at the time of mineralization was thereby obtained, and the potential of the rock as a source of lead could be evaluated. Eight samples of dolostone from the Otavi Group, three samples of slate from the Kombat Formation, and two samples of sandstone from the Tschudi Formation were analysed (Appendix 2.3.1). The best estimate of the age of the Tsumeb-type mineralization (and probably all the mineralization in the Otavi Group and Mulden Group) is between 730 m.y. and 590 m.y. (Chapter 3.7.12). The lead isotopic composition of these rocks was therefore calculated for ages of 550 m.y., 600 m.y., 650 m.y. and 700 m.y. In the case of the thorogenic lead the resulting isotope ratios are insensitive to the moderately large errors which may exist in the thorium analyses at low thorium concentrations (Appendix 2.3.1).

The lead isotopic compositions of the rock samples at 600 m.y. are shown on the uranogenic lead plot of Figure 130a. Data from two of the slate samples from the Kombat Formation plot in the vicinity of the predicted position of component A. Data from two of the three most lead-rich dolostone samples plot close to component B, but have a slightly lower $^{207}Pb/^{204}Pb$ ratio. These dolostone samples have a lead content of 19-38 ppm lead, compared with an average of 4 ppm lead in other dolostone samples, and contain elevated values of Cu, Zn, Co, Ni, Ag and Mo (Table 1). Data from galena of the Karuchas zone also plot close to the field defined by the dolostone samples, and data from the Abenab West ore body plot near the Tschudi Formation sandstone in the field defined by sandstone and slate of the Mulden Group. The

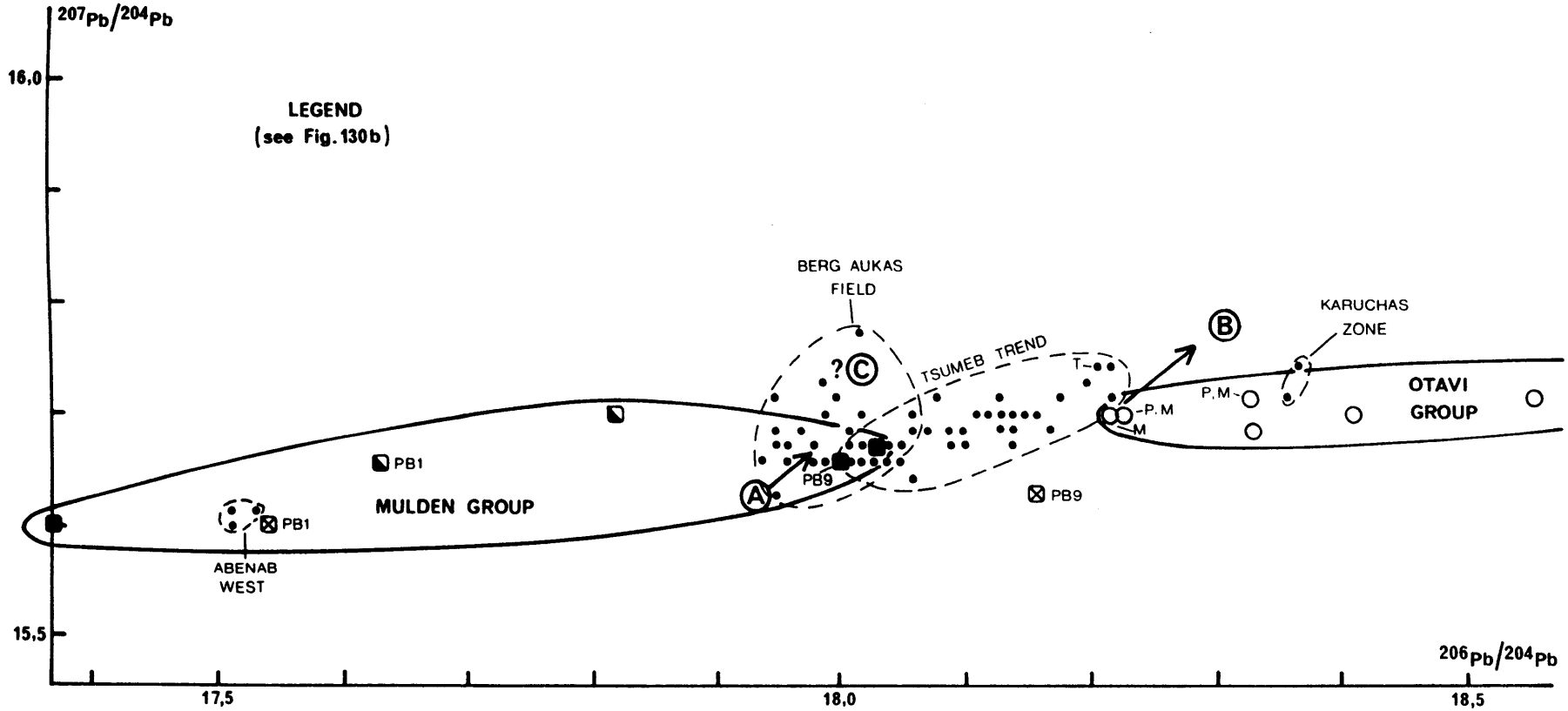

Fig. 130a

Uranogenic lead data from rocks of the Otavi Group and Mulden Group, corrected for lead added by the radioactive decay of uranium since 600 m.y. (the probable time of the mineralizing event). Slate of the Kombat Formation, metal-rich and phosphatic dolostone of zone T8, and sandstone of the Tschudi Formation were possible sources of lead in component A, component B, and the Abenab West ore body, respectively. Pyrite from the Tschudi Formation (PB1) is isotopically similar to its host sandstone but isotopically distinct from Tschudi-type mineralization (T) by which it is replaced.

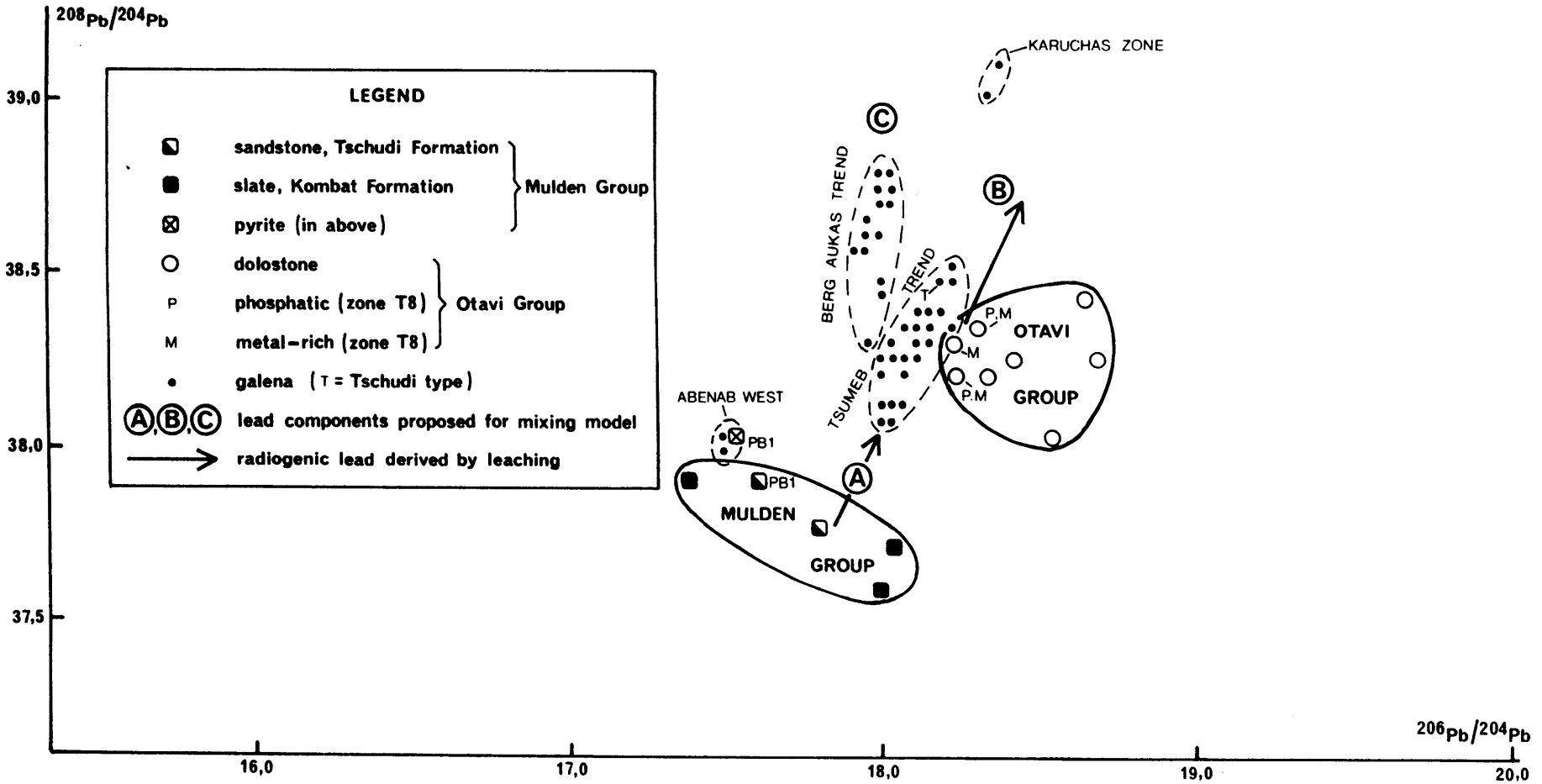

Fig. 130b

Uranothorogenic lead data from rocks of the Otavi Group and Mulden Group, corrected for lead added by the radioactive decay of uranium and thorium since 600 m.y. (the probable time of the mineralizing event). Slate of the Kombat Formation, metal-rich and phosphatic dolostone of zone T8, and sandstone of the Tschudi Formation were possible sources of lead in component A, component B, and the Abenab West ore body, respectively (especially if some selective leaching of radiogenic lead is assumed). Pyrite from the Tschudi Formation (PB1) is isotopically similar to its host sandstone, but isotopically distinct from Tschudi-type mineralization (T), by which it is replaced.

agreement between rock lead ratios and ore lead ratios is not as good at 550 m.y. and 650 m.y. It is very poor at 700 m.y. because no samples plot in the vicinity of component A, although all of the dolostone samples cluster in the vicinity of component B.

Similar relationships are observed on the uranothorogenic plot (Fig. 130b). It should be noted that the slope of the Berg Aukas trend, although steep, is not accurately known on this plot. The slope could not be calculated using York (1966) because the percentage residuals of $^{206}Pb/^{204}Pb$ were zero. The slope calculated by York (1969) was -12,6, but this is obtained by unwarranted correlation of geological error. A simple regression analysis, considering only the position of data points, gives a slope of 1,8; this is also inaccurate because analytical error is ignored, and because of the sensitivity of the data to a few outlying points. Data from the Mulden Group plots close to component A at 550 m.y. and 600 m.y. on this plot, but the agreement is poor at 650 m.y. and 700 m.y. The $^{208}Pb/^{204}Pb$ ratio of the dolostone samples is much smaller than that of component B at all ages. However, the only dolostone samples which plot close to the trend at 550 m.y. and 600 m.y. are the metal-rich samples (all dolostone samples cluster close to this trend at 650 m.y. and 700 m.y.). Data from the Abenab West galena samples plot near the Tschudi Formation sandstone, as on the uranogenic plot, but no rock type plots close to data from the Karuchas zone.

Three assumptions have been made in comparing the above data. The first assumption is that there has been no significant loss or gain of uranium, thorium or lead in the samples subsequent to the time of mineralization. The dolostone isochrons, the ages of which probably date an event prior to mineralization, support this assumption. Four Mulden Group rocks in which the thorium was analysed by a single technique define an isochron on the $^{208}Pb/^{204}Pb$ versus $^{232}Pb/^{204}Pb$ plot, with age 522 ± 37 m.y. (1σ), initial $^{208}Pb/^{204}Pb$ ratio = $38,03\pm0,11$, and MSUM = 0,3. However, the uranium-lead and lead-lead data do not define isochrons, and it is doubtful that rocks as different as feldspathic sandstone and slate would have identical $^{208}Pb/^{204}Pb$ initial ratios. A

possible example of open-system behaviour is shown by pyrite from slate of the Mulden Group (Fig. 130a). The low $^{207}Pb/^{204}Pb$ ratio and high $^{206}Pb/^{204}Pb$ ratio of this pyrite, relative to the lead of either the ore or host rock, may result from uranium loss during a metamorphic event which recrystallized pyrite grains and converted their margins to pyrrhotite (Chapter 4.4.5).

The second assumption which has been made is that the lead isotopic composition of the rock immediately subsequent to leaching by the ore fluid was identical to the lead isotopic composition of the lead which was leached. Leaching experiments by Doe and Delevaux (1972) indicate that this is improbable, and that lead leached from the rock was probably more radiogenic than that which remained. This is because lead produced by radiogenic decay of uranium- and thorium-rich phases is less tightly bound than lead tied up in other rock-forming minerals. The composition of the lead which was leached cannot be predicted accurately because the lead could have been leached preferentially from certain minerals. However, in the simplest case the $^{206}Pb/^{204}Pb$, $^{207}Pb/^{204}Pb$ and $^{208}Pb/^{204}Pb$ ratios would have been similar in both the ore fluid and the remaining rock (indicated on Figures 130a, b). Preferential leaching of minor quantities of lead with more radiogenic $^{206}Pb/^{204}Pb$ and $^{207}Pb/^{204}Pb$ from Mulden Group rocks and metal-rich dolostone would not alter the above conclusions regarding metal sources for components A, B, the Abenab West ore body or the Karuchas zone. However, leaching of more radiogenic $^{208}Pb/^{204}Pb$ in similar proportions would improve the match between component A and the Kombat Formation slate, and between component B and the metal-rich dolostone, on the uranothorogenic lead plot. No other conclusion would be altered, except that the uranothorogenic data does not support an origin for Karuchas zone lead by mixing of Tsumeb-type lead and dolostone lead as indicated on the uranogenic plot; this is only possible if a large degree of preferential leaching of ^{208}Pb is proposed, relative to other lead isotopes. The Tsumeb-type isotopic trend could theoretically be derived by leaching of the Kombat Formation alone. However, this is not consistent with the geographic and stratigraphic distribution of

lead isotope ratios, nor could it explain the origin of the Berg Aukas-type trend.

The third assumption made in the above discussion is that ore lead was not added to the rocks at the time of mineralization. The possibility of contamination of this type can be rejected for two of the three lead-rich, phosphatic dolostone samples which are possible sources of lead component B. This is because these two samples come from the Otavi Valley area, where lead component A occurs in ore bodies almost to the exclusion of component B. However, contamination must be considered a possibility for pyrite-bearing rocks of the Mulden Group. Sandstone PB1, which contains 0,75 percent sulphur and 7 ppm lead, contained 6 ppm lead at 600 m.y. of which only 1 ppm lead was contributed by the pyrite present in the rock. The lead isotopic composition of the pyrite at 600 m.y. was similar to that of the sandstone, but unlike lead component A or B. Pyrite of this type is replaced elsewhere by copper minerals of the Tschudi-type mineralization. The Tschudi-type mineralization contains galena which plots on the Tsumeb-type isotopic trend, close to component B. The data indicate that the pyrite formed in sandstone of the Tschudi Formation during an event which pre-dated the event which formed the Tsumeb-type and Tschudi-type mineralization (Chapter 4.4.1). Sandstone sample PB12 contains 1,4 percent sulphur, but only contains one ppm more lead than sample PB1, and a similar history to sample PB1 is probable. Sample PB8, a slate sample which contains 13 ppm lead, is a good match for lead component A, but contains less than 0,01 percent sulphur and a lead content which is below average for a shale. It has therefore not been contaminated by the ore lead. It is concluded that contamination of Mulden Group rocks by ore lead can be dismissed for most of the samples analysed.

5.3.8 Conclusions from the Otavi Mountain Land data

It can be concluded that former shale of the Kombat Formation, phosphatic and metal-rich dolostone of zone T8, and sandstone of the Tschudi Formation were possible sources of lead at approximately 600 m.y., the most probable time of mineralization in the Otavi Mountain Land. These rocks could have supplied lead for component A, component

B, and the Abenab West ore body, respectively. Component C had a moderately high $^{207}Pb/^{204}Pb$ ratio and a high $^{208}Pb/^{204}Pb$ ratio relative to its $^{206}Pb/^{204}Pb$ ratio, when compared with the growth curves of Stacey and Kramers (1975). Lead of this composition might be found in immature sandstone derived from an Archean or Early Proterozoic rock which had an early residence in the upper crust, followed by a similar period of later residence in the lower crust. The source of component C has not been identified, but one possibility is sandstone of the Nosib Group, which has a suitable stratigraphic position and geographic distribution.

The geographic and stratigraphic positions of each of the above components is consistent with the isotopic zoning of ore lead in the Otavi Mountain Land, and with the northwards migration of ore fluid from a source area to the south of the Otavi Mountain Land. The preferred interpretation is that the ore fluid leached component A from the Kombat Formation and redeposited it in galena of the Otavi Valley area. The fluid then migrated northwards through different aquifers, three of which were of regional significance. It is suggested that the first aquifer was the Nosib Group sandstone, which progressively added component C to the ore fluid to form the Berg Aukas-type lead; this fluid penetrated the lower part of the dolostone sequence of the Otavi Group, reaching progressively higher stratigraphic levels during its northward migration (Chapter 4.3). The second important aquifer was the contact between the Otavi Group and Mulden Group, where metal-rich dolostone of zone T8 progressively added lead component B to the ore fluid as it migrated northwards. The third aquifer was the strata-bound zone of fracturing and brecciation in zone T4, in which fluids from the other two aquifers flowed (within separate geographic areas). Mixing of unmodified lead component A in fluids of this aquifer with overlying fluids in the base of the Otavi Group (which contained a mixed lead component, A + B) produced the isotopic zoning with depth in the Tsumeb pipe (Fig. 135). A model for fluid flow and metal sources is described in more detail in Chapter 6.4.2.

The above model has a number of important implications for ore fluids in sedimentary basins:

(1) Single events of ore fluid migration may occur on a much larger scale than is normally assumed. Tsumeb- and Tschudi-type mineralization has penetrated a stratigraphic thickness of more than 1300 m in the Otavi Mountain Land. Berg Aukas-type mineralization, which is interpreted to have formed during the same mineralizing event, penetrated a similar thickness of the underlying sequence. Mineralization of comparable scale in Phanerozoic rocks could occur in rock types of more than one geological Period, and a number of mineralizing events would commonly be assumed to be represented.

(2) Ore fluids may be able to migrate laterally for great distances through sedimentary sequences (in this case more than 60 km), from the source area of the fluid, or the source of its contained metal, to the site of precipitation.

(3) Ore bodies with different lead isotopic compositions, which occur in a single area, might have formed during the migration of a single ore fluid (e.g. during a single pulse of dewatering of the rocks of a sedimentary basin). The different isotopic compositions may result from the different rocks leached of metal by the fluid (see also the discussion of the Kabwe and northern Zambian occurrences in Chapters 5.1.4 and 5.3.10).

(4) Ore bodies with contrasting chemical compositions may also form in the above manner; different types of ore deposit will be considered to be present if the sulphide minerals are precipitated in different types of ore loci, and genetic relationships between ore deposits will be obscured. The present study indicates that the different members of the Owambo Basin ore association formed in this manner. This association includes carbonate-hosted lead-zinc mineralization (Berg Aukas type, similar to Mississippi Valley type), carbonate-hosted copper-lead-zinc mineralization (Tsumeb type), and stratiform copper mineralization (Tschudi type).

(5) Pyrite has a different lead isotopic composition from later galena in Tschudi-type mineralization. This has important implications for stratiform copper mineralization elsewhere, because it supports a

model in which the ore fluid has replaced an earlier sulphur source, pyrite, which has a late diagenetic or hydrothermal origin related to an underlying sabkha horizon (Chapter 5.1.1).

5.3.9 U-Pb zircon studies

Zircons separated from sandstone ("pseudo-aplite") of the Tsumeb ore body range from rounded, anhedral and metamict grains, to elongated, subhedral and clear grains (the dominant type; Botha, 1960). Zoning is common. Two fractions were analysed, selected to nearly conform to these two extreme types, and a feldspar from the sandstone was also analysed to obtain the correction for common lead. Both fractions yield highly discordant U-Pb ages, and the two results are in disagreement (Fig. 134, Appendix 2.3.1). The ages obtained are:

(1) $^{207}Pb/^{206}Pb$ age = 1407 m.y. $^{207}Pb/^{235}U$ age = 857 m.y.
$^{206}Pb/^{238}U$ age = 661 m.y.

(2) $^{207}Pb/^{206}Pb$ age = 1311 m.y. $^{207}Pb/^{235}U$ age = 933 m.y.
$^{206}Pb/^{238}U$ age = 781 m.y.

No definite age can be deduced from the data, but the patterns are typical of normal lead loss; all ages are considered to be minimum ages, with the $^{207}Pb/^{206}Pb$ ages most closely approximating to the true ages. The ages are 200 to 400 m.y. greater if the data are extrapolated on a concordia diagram, assuming continuous or time-dependent diffusion. Alternatively, if a mixing model is assumed with a lower intercept of 600 m.y. (the minimum possible age if the "pseudo-aplite" is an igneous rock), extrapolation of the discordia through one of the data points gives an age of approximately 2200 m.y., but extrapolation through the other point does not yield an upper intercept on the concordia curve. The data are therefore not consistent with a mixing model (e.g. as the result of incorporation into a magma of zircon xenocrysts derived by the assimilation of country rock).

The experimental errors in the $^{207}Pb/^{206}Pb$ ages are ± 32 m.y. (2σ), and the observed difference between the ages is

therefore real. The two samples do not belong to a single population, irrespective of whether episodic lead loss, a diffusion model, or a mixing model are assumed. The data are most consistent with the zircons being detrital minerals in a sandstone (as strongly indicated by geological evidence; Chapter 3.3), the zircons having been derived from two sources. The age obtained from the diffusion model is only broadly consistent with the zircon U-Pb age of approximately 1800 m.y. obtained from granitoid rock of the Fransfontein Suite (Burger et al., 1976), which was a possible source of zircon in the "pseudo-aplite".

5.3.10 Galena from central Africa

Lead isotope studies have also been made of galena from mineralization of Tsumeb and Berg Aukas types which occurs in the Katangan and West Congolian fold belts (Fig. 123, Chapters 4.6.1 to 4.6.4). These results support or complement some of the conclusions made from Otavi Mountain Land data in Chapter 5.3.8. The preliminary results of this study, which is not yet complete, have been reported in Hughes et al. (1984). Mineral occurrences which show similar, restricted clustering of their lead isotope ratios on both the uranogenic and uranothorogenic lead plots are interpreted to be genetically related. Lead isotope studies of rocks which could have been the sources of lead in the mineralization have not been made. It is therefore not possible, in most cases, to relate mineral occurrences which might have formed from different lead sources during a single mineralizing event.

Lead isotope data from galena of the Kipushi, Lombe and Kengere occurrences of the Katangan fold belt indicate that this mineralization is genetically related. The Kipushi ore body is of Tsumeb mineralogical type and all three occurrences are located in the same stratigraphic unit, the Kakontwe Limestone (Chapter 4.6.3). Galena from the Mazabuka prospect, Zambia, is isotopically similar to galena from these three localities, to which it may be genetically related; however, nothing is known about the Mazabuka prospect except that it occurs in sedimentary carbonate rocks of probable Katangan age. If it is accepted that all ore bodies of Tsumeb mineralogical type throughout

central Africa formed by similar processes (i.e. by lateral migration of fluids which derived their contained lead from the enclosing rocks), then the above isotopic data support the proposal that single events of ore fluid migration of this type can occur on a very large scale. Evidence is advanced in Chapter 5.3.8 that the ore fluids which formed Tsumeb-type mineralization of the Otavi Mountain Land penetrated a stratigraphic thickness in excess of 1300 m, and migrated up-dip for more than 60 km through the enclosing sequence. The Kipushi, Lombe and Kengere occurrences are located up to 200 km apart, measured parallel to the probable depositional strike of their host rocks. This indicates that either the ore fluids migrated parallel to the depositional strike, unlike the ore fluids of the Otavi Mountain Land, or more probably that the ore fluids migrated up-dip from the adjacent sedimentary basin at various points (i.e. not necessarily on a continuous front) over a distance of 200 km (600 km if the Mazabuka prospect is included). Although this distance is large, it should be noted that there are only two major requirements for a model of this type, both of which are geologically reasonable. The first requirement is a source rock for the lead, and this rock must have had a moderately homogeneous lead isotopic composition over this distance. The second requirement is that bodies of fluid capable of extracting the lead from the rock occurred in places over this distance, and that these fluids migrated through the rock at approximately the same time.

Lead isotope data from the Bukanda, Ndola and Kiseba occurrences of the Katangan fold belt indicate that they are genetically related to each other. These lead-zinc occurrences are of unknown mineralogical type, and they were not suspected to be genetically related prior to this study because they occur in widely separated stratigraphic units (the Calcaire rose and Kakontwe Limestone of the Kundelungu Supergroup, and in the basal Roan Supergroup, respectively). The above data are consistent with a mineralizing event which penetrated most of the Katanga Sequence. The Ndola occurrence has a different isotopic composition to the Kabwe ore body, Zambia, which is of Berg Aukas mineralogical type. However they both have distinctive, negative sulphur isotopic ratios, and it is possible that they formed from different lead sources during a single mineralizing event (Chapters

5.1.4, 5.3.10). The Kabwe ore body has a similar lead isotopic composition to the Berg Aukas ore body of the Otavi Mountain Land, but there is no obvious reason to propose a genetic relationship between ore bodies 1200 km apart. Nevertheless, the possibility that source rocks with a similar lead isotopic composition occurred in both areas cannot be excluded.

Mineralization of the West Congolian fold belt occurs in two areas on the northern and southern margins of the M'bridge-Mbanzu Ngungu ridge, in the southern Niari basin and northern Bungo basin respectively (Fig. 123). Mineralization of both areas occurs in the same stratigraphic position and is mineralogically similar, although the rare minerals diagnostic of the Tsumeb type of mineralization have only been recorded from the Niari basin. The lead isotope data show that mineral occurrences confined to either one of the two areas are isotopically related, but that there is a distinct difference in isotopic composition between the areas. Galena samples analysed from the Niari basin are from the M'Passa and Mindouli ore bodies of Tsumeb mineralogical type, and from the adjacent Hapilo, N'Zala-Diangala, Boko-Songho, Djenguilé and Yanga-Koubanza occurrences. Samples analysed from the Bungo basin are from the Bamba-Kilenda, Mangulu (Toni) and Mavungu (Toni) occurrences. The samples from both areas are from mineralization in both the sedimentary carbonate rocks of the Schisto-calcaire Group and the overlying arenites of the Mpioka and Inkisi Groups. The lead isotope data show that mineralization in both stratigraphic groups is isotopically identical in any one area, which indicates that mineralization post-dated deposition of the arenites in both areas, as in the Otavi Mountain Land. The apparent anomaly, that the two mineral districts in the West Congolian fold belt are isotopically distinct but show temporal, spatial, stratigraphic and mineralogical relationships to each other, can be explained using the type of model proposed for mineralization of the Otavi Mountain Land. Mineralization of the two districts occurs in probable paleokarst structures in evaporite-bearing rocks on both margins of a basement high, the M'bridge-Mbanzu Ngungu ridge (Chapters 4.6.2, 5.1.3). It is suggested that ore fluids migrated southwards and northwards through isotopically different rocks of the Niari basin and Bungo basin,

respectively, to form isotopically distinct mineral districts on opposite sides of the basement high at approximately the same time.

It is concluded that the lead isotope study of galena from central Africa (including the Otavi Mountain Land) indicates the existence of mineral districts which individually contain genetically related mineralization, including Tsumeb-type mineralization, over large areas. The data indicate that galena from occurrences of Tsumeb type in the Damaran and West Congolian fold belts significantly post-dates the rocks which host the mineralization. More importantly, the lead isotope data from different areas variously indicate, or are consistent with: (1) migration of large volumes of fluid on a regional scale, and (2) the formation of ore deposits with different chemical and lead isotopic compositions, in different types of ore loci, by genetically related, broadly contemporaneous processes. It is shown below that this may have important implications for basin-hosted ore deposits in general. In particular, the most important requirement for the formation of mineral districts (but not individual ore deposits) in sedimentary basins may be large volumes of fluid capable of leaching metal from the enclosing rocks, rather than the presence of unique metal sources. The isotopic composition and unique chemical composition of individual ore deposits, or groups of ore deposits (e.g. Tsumeb-type deposits) might be determined by the compositions of relatively minor stratigraphic units (e.g. phosphatic dolostone of the Tsumeb Subgroup).

5.3.11 Comparisons with lead isotope data from ore deposits of related type

It has been recognized for many years that lead in ore deposits is not derived from a single, uniform reservoir, such as the mantle. Instead, the lead isotopic compositions of individual ore deposits reflect the isotopic compositions of the geological environments in which the ore deposits occur; these include environments in which igneous activity of appropriate age is negligible, as in the lead-zinc districts of the Mississippi Valley, U.S.A. (Doe and Zartman, 1979). Even ore bodies which show an obvious spatial relationship to bodies of

intrusive igneous rock can contain lead which cannot have been derived solely from the igneous rock itself, but which must contain a minor or major component of lead from the host rocks (Stacey et al., 1968; Hall et al., 1978). Isotopic evidence for a lead source within the local geological environment, as proposed here for ore deposits of the Otavi Mountain Land, has therefore been obtained from very different types of ore deposit. Models advanced to explain linear isotopic trends in galena from these ore bodies have proposed incomplete mixing of lead from multiple sources (including different parts of a single lithological unit), or derivation of lead from a single source of variable isotopic composition.

It is shown in Chapter 4.6 that there are mineralogical and other similarities between a number of different types of ore deposit (including those of the Owambo Basin) which have formed in epicontinental environments in which igneous activity is negligible. Lead isotope studies of Mississippi Valley-type lead-zinc, sedimentary exhalative copper-lead-zinc (sedex), sandstone lead, stratiform copper and Ag-Ni-Bi-Co-U (Saxonic) ore deposits from the literature are discussed below. It is shown that the lead isotope data indicate, or are consistent with, closely related origins for some of these ore deposits, and with lead source(s) within the sedimentary sequences which host the ore deposits.

5.3.12 Mississippi Valley-type ore deposits

Ore deposits of Mississippi Valley type are the best studied of the ore deposits listed above, and are commonly interpreted as the result of circulation of warm brines, unrelated to magmatic activity (Mitchell and Garson, 1981). Mississippi Valley-type deposits are the most relevant to the present study, because they are indistinguishable from Berg Aukas-type mineralization except for a lower average temperature of deposition. Heyl et al. (1966) studied "J-type" galena from Mississippi Valley-type deposits in the central U.S.A., and concluded that their data could not be used to determine if the lead was derived from either a single source or multiple sources. However, they noted a systematic, district-wide progression in lead isotope

ratios in the Upper Mississippi Valley district, indicating a regional gradient that can be explained by progressive mixing in an ore fluid migrating laterally up-dip through the strata. Brown (1967) studied lead isotope ratios in Mississippi Valley-type deposits from south-eastern Missouri, and suggested that these ratios resulted from mixing of lead from the enclosing sedimentary sequence, and a radiogenic component of lead from basement rocks. He also noted that the earliest galena to have been deposited is the least radiogenic, and that lead isotope ratios are spatially zoned within any individual ore deposit.

Doe and Delevaux (1972) tested the model of Brown (1967) by studying lead isotope ratios in sedimentary carbonate rock, shale, sandstone and basement rock of south-eastern Missouri. They concluded that their data excluded all except the Lamotte Sandstone as a major source of lead in the ore, but that the lead could have been derived from the sandstone alone, by leaching of radiogenic cement. This relationship between lead in the Lamotte Sandstone and in the lead ore is less clear if the mineralization is older than was assumed in the above study (Doe and Zartman, 1979), as is indicated by paleomagnetic data (Wu and Beales, 1981). Doe et al. (1983) concluded from a U-Th-Pb isotope study of basement granite in the Upper Mississippi Valley district that granite similar to that studied could have been a radiogenic end member for lead in the Upper Mississippi Valley and south-east Missouri districts. However, this requires that mineralization occurred at least 260 m.y. ago.

Sverjensky et al. (1979) and Hart et al. (1981, 1983) studied galena, including single galena crystals, from the south-east Missouri district. They found that cuboctahedral galena is less radiogenic than later cubic galena, and that these two types of galena show separate, but parallel, lead isotopic trends. Single crystals of cuboctahedral galena were found to have progressively less radiogenic lead isotope ratios from core to margin. This zoning can be correlated between crystals at the scale of a vug, and possibly at the scale of kilometers, and the range in lead isotope ratios of a single crystal can exceed that of the entire district. A direct correlation was

observed between $^{206}Pb/^{204}Pb$ and $\delta^{34}S$ ratios, with the most radiogenic galena containing the lightest sulphur. The authors concluded that the presence of early, less radiogenic galena is not consistent with a single source of lead in the Lamotte Sandstone, and noted that the relationship between lead and sulphur isotope ratios could only be explained by mixing of three or more lead sources. A mixing model has also been proposed for Mississippi Valley-type ore deposits in south-western Virginia, in which early galena is also less radiogenic than later galena (Foley et al., 1981).

It can be concluded that a complex mixing origin involving multiple lead sources, probably located in rocks of the enclosing sequence and immediate basement, is strongly indicated for lead-zinc ore of the Mississippi Valley region.

5.3.13 Sedex deposits

Sediment-hosted, massive, lead-zinc sulphide deposits, commonly termed sedex (sedimentary exhalative) deposits, have also been studied extensively. The currently prevailing model for these deposits involves exhalation of metals on to the sea floor, or replacement of sediments in the vicinity of the sea floor, in epicratonic or intra-cratonic, fault-bounded basins (Large, 1983). Badham (1981) suggested that the ore fluids could be heated formation waters similar to those which may form Mississippi Valley-type deposits, which escaped to the sea floor along growth faults. Important examples are McArthur River (Australia), Sullivan (Canada), Meggen (West Germany), and Silvermines and Tynagh (Ireland).

Sedex deposits typically show a tight clustering of lead isotope data from the galena of any one deposit, or from deposits of the same age within a single basin. The galena of sedex deposits commonly contains the least radiogenic lead of any type of ore deposit within contemporaneous rocks of the surrounding area (Godwin and Sinclair, 1982; Godwin et al., 1982; Walker et al., 1983). Godwin et al. (1982) found that lead isotope ratios of galena from shale-hosted sedex deposits within the Selwyn basin, Canada (e.g. the Cirque deposit),

cluster tightly and are similar to ratios in most of the Mississippi Valley-type deposits of the same area. Some of these Mississippi Valley-type deposits also include more radiogenic lead than that in nearby sedex deposits (e.g. the Robb Lake deposit), and data from the Mississippi Valley-type deposits define a trend which the authors interpreted as an isochron. Godwin et al. (1982) proposed that the ore fluid for both types of ore deposit originally had an isotopic composition similar to that of the sedex deposits. However, the ore fluids which formed some of the Mississippi Valley-type deposits migrated from the shale basin through a great length of source rocks, and were mixed with radiogenic lead generated between t_1 and t_2 (i.e. so points lie on an isochron).

A mixing model which involves shale lead, and lead from a different source, appears to be equally consistent with the above data. Walker et al. (1983) proposed this model for the Coxco deposit, of Mississippi Valley type, and the HYC deposit, of sedex type, at McArthur River, Australia. The two deposits are only 7 km apart, and both are spatially related to a fault zone which forms the margin of a fault-bounded basin. The lead isotope ratios are identical, except that the Coxco data extends to more radiogenic values. Walker et al. (1983) suggested that non-radiogenic, deep, basinal brines which formed the HYC deposit were introduced to the fault zone and mixed with radiogenic lead derived by brine leaching of the enclosing rocks.

Godwin and Sinclair (1982) studied galena from shale-hosted, zinc-lead deposits of sedex type throughout the Canadian Cordillera. Shale sequences of Proterozoic and Phanerozoic age which host these ore deposits were deposited along the western margin of the North American craton, and were derived largely from the upper crustal, crystalline rocks which formed the western part of the Canadian Shield. The age of the ore deposits is well known, and Godwin and Sinclair (1982) were able to fit a growth curve to the data which gave satisfactory model ages. They assumed that growth followed the two-stage growth curve of Stacey and Kramers (1975) until 1,89 b.y., and then evolved to the present day along a growth curve with $\mu = 12,2$, $W = 49,1$. A "primary" lead source for the ore deposits is therefore indicated (i.e. in the

shale). The lead isotopic evolution of ore deposits of different age should reflect the isotopic evolution of the shale sequences (no U-Th-Pb isotope data from the shales were presented to confirm this).

The lead isotope data and geological relationships in the Selwyn basin and McArthur basin strongly indicate a genetic relationship between sedex and Mississippi Valley-type deposits, and also indicate a relatively homogeneous "primary" lead source within the shale basins. The data are consistent with mixing (of uncertain type) between this less radiogenic shale lead, present in both types of ore deposit, and a more radiogenic lead of unknown origin which is present in some Mississippi Valley-type deposits which occur in adjacent sequences of sedimentary carbonate rock. The independent evidence for mixing obtained from Mississippi Valley-type deposits elsewhere indicates that the above model may have general application. Deposits of Mississippi Valley type which occur on the immediate margins of shale basins typically show a tight clustering of data points, which are non-radiogenic for the region concerned, e.g. Pine Point, Canada (Cumming and Robertson, 1969), and Triassic ("Alpine-type") deposits of southern Europe (Köppel, 1983). Mississippi Valley-type deposits (and some other ore deposits) can also display "J-type" trends and other linear arrays; these are less common, and most examples discussed by Doe and Zartman (1979) occur well interior to continental margins (e.g. the Mississippi Valley districts). Even in the Mississippi Valley districts, the least radiogenic lead occurs in ore deposits closest to the continental margin of Upper Pennsylvanian-Lower Permian age (a probable age of mineralization for at least some districts; Wu and Beales, 1981), and therefore closest to probable shale basins at that time. Galena from Pennsylvanian shale is the least radiogenic for the region (Heyl et al., 1974), and the isotopic ratios of this galena indicate that shale cannot be excluded as a possible source of a non-radiogenic lead component in ore of these districts.

5.3.14 Sandstone lead deposits

There is general agreement that sandstone lead deposits form by lateral flow of ore fluids within sedimentary rocks, although there is

controversy about the nature of the fluids or the direction of fluid migration (i.e. up-dip migration of basin brines versus down-dip percolation of meteoric water; Bjorlykke and Sangster, 1981). Sandstone lead deposits commonly overlie granitoid basement rocks, distant from continental margins, and deposits in the Cambrian of Scandinavia contain "J-type" lead. Lead isotope studies of galena and rocks from Scandinavia and the Massif Central, France, indicate that granitoid basement (or sediments derived from it) was a possible source of lead in ore of these areas, but few alternative rock types have been investigated (Rickard et al., 1981; Bjorlykke and Thorpe, 1982; Brevart et al., 1982). Moderately large lead isotopic variations occur at the scale of centimetres in the Laisvall ore body, and Rickard et al. (1981) recorded a weak correlation between the $\delta^{34}S$ and $^{206}Pb/^{204}Pb$ ratios of galena from this ore body, indicating possible mixing of lead from different sources.

Sandstone lead deposits and Mississippi Valley-type deposits occur in close proximity to each other in some areas, e.g. lead ore is present in places in the Lamotte Sandstone, within the classical Mississippi Valley-type district of south-east Missouri (Snyder and Gerdemann, 1968). Sandstone-hosted lead, copper and zinc deposits also occur together within well-defined mineral provinces, indicating a close genetic relationship between these different ore deposits (Caïa, 1976; van Eden, 1978). The Largentière lead sandstone deposit of southern France occurs 90 km from the Mississippi Valley-type deposit of Les Malines (Chapter 4.6.5). The Les Malines deposit occurs in sedimentary carbonate rocks which overlie and underlie Triassic sandstone which hosts the Largentière deposit, and galena from both Largentière and Les Malines shows similar lead isotope ratios. These ore deposits form part of a group of isotopically similar lead-zinc deposits, which include vein deposits in basement rocks and the important germanium-bearing zinc ore body of Saint Salvy. Members of this group have distinctly different lead isotope ratios to many lead-zinc deposits in Cambrian rocks of the same area (Brevart et al, 1982). A similar relationship is indicated farther to the north in the same sandstone basin (the Bunter Sandstone basin), in West Germany. Triassic sandstone lead deposits (e.g. Maubach, Mechernich), lead-zinc

deposits in sedimentary carbonate rocks of Devonian and Carboniferous age, and galena-quartz veins in sedimentary rocks of Paleozoic age, all plot on single uranogenic and uranothorogenic lead trends (Large et al., 1983). These trends are distinct from three isotopic fields defined by deformed lead-zinc veins in Devonian rocks (e.g. Ramsbeck), Saxonic veins in Paleozoic rocks, and lead-zinc veins in Cretaceous to Tertiary karst-fill sediments, all of which occur in the same area.

It can be concluded that the isotopic composition of lead in lead sandstone deposits of Scandinavia reflects the geological environment of the host rock, and that mixing of lead from different sources may have occurred. Lead isotope data from southern France support a genetic relationship between sandstone lead deposits and Mississippi Valley-type deposits. They also support a relationship between these deposits and base metal veins in basement rocks (including the most productive germanium ore body in the world).

5.3.15 Stratiform copper deposits and the Saxonic vein association

It is generally accepted that stratiform copper deposits have derived their metals from rocks within the epicontinental sedimentary (or volcano-sedimentary) sequences in which they are situated, although there is controversy about the nature of their ore fluids (e.g. sea water, subsurface connate fluids; Rickard, 1974). Wedepohl et al. (1978) studied lead isotope ratios of galena from stratiform copper-lead-zinc occurrences of the Kupferschiefer bed in Germany. The data define linear trends on uranogenic and uranothorogenic lead plots, but samples from the Kupferschiefer bed in England, Holland and Poland show completely different lead isotope ratios, indicating different lead sources. Creelman (1983) studied lead isotope ratios of galena and other sulphide minerals, and of host rocks, from stratiform copper deposits in the Cattle Grid area, South Australia. He found that the linear uranogenic and uranothorogenic isotope trends defined by the ore minerals matched more extensive trends of the Tapley Hill Formation, within which the ore occurs. He interpreted the linear arrays shown by the ore data as mixing lines which resulted from mixing of more radiogenic, and less radiogenic, lead components derived from different

parts of the Tapley Hill Formation. Creelman (1983) rejected the possibility that the lead isotope ratios of rocks sampled throughout the district were overprinted by ore lead, although this is true of all rock types within the Cattle Grid area. However, the average of 104 ppm lead in those sedimentary carbonate rocks of the Tapley Hill Formation which are thought to be unmineralized is high. Also, the isotopic trends of data from these rocks, where they occur distant from the Cattle Grid area (but in the vicinity of other mineralization) depend partly on samples of sedimentary carbonate rock which contain up to 310 ppm lead, so the results are not considered conclusive. The alternative is that a mineralizing event introduced isotopically related lead to localities more than 100 km apart.

Many origins have been proposed for the Saxonic (Ag-Ni-Bi-Co-U) vein association. However, it is suggested in Chapters 4.6.7 and 6.3.5 that this mineralization may form from ore solutions genetically related to the fluids which form the stratiform and strata-bound ore types discussed above. In particular, it is suggested that there is a distinct Saxonic mineral province of Permian age in north-western Europe and southern Scandinavia which is genetically related to stratiform copper-lead-zinc mineralization in the Kupferschiefer bed. It is shown below that the small amount of modern lead isotope data that is available from these ore deposits are consistent with this interpretation.

Moorbath and Vokes (1963) showed that occurrences of Saxonic type in southern Norway contain "J-type" lead, and their data indicate a genetic relationship between quartz - base metal (e.g. lead) - barite veins and classical Saxonic-type veins in this area. Lippolt et al. (1983) studied galena from Saxonic-type veins and other base metal veins of the Schwarzwald, West Germany, and obtained linear arrays on uranogenic and uranothorogenic isotope plots. They noted that the Schwarzwald data lies on the radiogenic extension of the Kupferschiefer data of Wedepohl et al. (1978) on both lead-lead plots. Saxonic veins also occur in the Clausthal-Sanct Andreasberg region of the Harz Mountains, and Wedepohl et al. (1978) noted the similarity between lead isotope ratios of galena from the Kupferschiefer, and from the Grund

vein, Clausthal, which is probably genetically related to Saxonic veins in the same area. These observations are consistent with a genetic relationship between the Saxonic veins of the Harz Mountains and Schwarzwald, and the adjacent Kupferschiefer (although this differs greatly from the interpretations of Wedepohl et al., 1978, and Lippolt et al., 1983).

Further evidence for a genetic relationship between lead-rich base metal veins and Saxonic mineralization is found in the Willyama Complex of Australia. Base metal mineralization is present as the stratiform Broken Hill type, which has undergone high grade metamorphism, and crustiform veins of Thackaringa type (galena-siderite-quartz) and Consols type (Saxonic), which post-date this prograde metamorphic event. Data from galena of Broken Hill type plot as a tight cluster of points on both uranogenic and uranothorogenic lead plots. Thackaringa-type and Consols-type data plot together in a confined field that is isotopically distinct from Broken Hill-type lead, and also from another fluorite-bearing mineralization of the same area (Cooper, 1970; Reynolds, 1971). Reynolds (1971) suggested that the Thackaringa-type lead contains a component of Broken Hill-type lead; however, evidence for this is very limited when the Silver King and Yuba occurrences, now thought to be of Broken Hill type, are excluded from his Thackaringa-type data. The isotope data are consistent with an origin in which most, or all, of the lead in the Thackaringa- and Consols-type veins was derived from a source other than the Broken Hill-type mineralization or the basement rocks which host the veins. An alternative source exists in late Proterozoic rocks of the Adelaide "Geosyncline", to the west, which contain various types of basin-related mineralization (Chapters 4.6.5, 4.6.6).

It is concluded that lead isotope data from Norway, Germany and Australia indicate a genetic relationship between veins of Saxonic type, and other base metal (especially lead) veins of similar age in these areas. Lead isotope data from Germany are consistent with a genetic relationship between stratiform copper-lead-zinc mineralization and veins of Saxonic type.

5.3.16 Conclusions

Lead isotope data from the present study indicate a genetic relationship between stratiform copper mineralization in arenite and copper-lead-zinc mineralization in sedimentary carbonate rocks. The data are consistent with a relationship between these and carbonate-hosted lead-zinc mineralization, comparable to Mississippi Valley-type mineralization. Lead isotope data from elsewhere in the world indicate a genetic relationship between: (1) Mississippi Valley-type deposits, lead sandstone deposits, and base metal veins (including germanium-rich veins) in basement rocks, (2) Mississippi Valley-type and sedex deposits, and (3) Saxonic veins and base metal (especially lead-silver) veins. The data are consistent with a genetic relationship between stratiform copper-lead-zinc mineralization and Saxonic veins. These relationships are summarized in Figure 138. It follows from this that ore deposits in each of the above groups formed at broadly similar times, from similar lead sources, consistent with formation during single mineralizing events within each area (e.g. basin dewatering events of limited duration; Chapter 6.3).

The isotopic composition of lead in many of the above deposits is similar to the composition of the enclosing sequence or underlying basement rock at the time of formation of the ore deposits. A homogeneous, "primary" lead source within shale basins is indicated for many sedex deposits, and for some Mississippi Valley-type deposits. Models which involve single lead sources have commonly been invoked for occurrences of sandstone lead type and Mississippi Valley type which show linear arrays of lead isotope data points, but these could also be explained by mixing models involving extensive lateral migration of fluid. A complex mixing origin, involving two or more lead sources, is strongly indicated for some Mississippi Valley-type and Tsumeb-type ore deposits, and less definitely indicated by data from sandstone lead deposits. The spatial distribution of lead isotope ratios in some of these deposits is consistent with the addition of a radiogenic lead component to a "primary" lead component as the fluids migrated out of shale basins into adjacent shelf or platform rocks.

It is suggested in Chapter 6 that all of the ore deposits discussed above, including Tsumeb-type ore deposits, formed during dewatering of fluids from sedimentary basins.

CHAPTER SIX

GENESIS OF THE OWAMBO BASIN-TYPE ORE ASSOCIATION

The variables involved in the formation of hydrothermal ore deposits were discussed in Chapter 1.1. These are summarized below for the Owambo Basin-type ore association, and a genetic model is developed for representatives of this ore association throughout central Africa.

6.1 FORMATION OF THE ORE LOCUS

It was concluded in Chapter 3.3 that the Tsumeb pipe and associated strata-bound cavities formed by karsting and solution collapse, and were subsequently infilled by siltstone and sandstone, foreign to the enclosing sequence. The timing of karsting relative to sedimentation, the source of sedimentary infill of the Tsumeb pipe, and the controls of karsting and syn-sedimentary fracturing are considered in the following discussion. A model is developed for formation of the Tsumeb pipe, and for ore loci elsewhere in the Owambo Basin. Finally, comparisons are made with modern, and ancient, karst and solution collapse structures elsewhere in the world, and with mineralized examples of these structures.

6.1.1 Source of the sedimentary infill of the Tsumeb pipe

The source of the Tsumeb pipe sandstone has been debated by those workers who considered it to be a sedimentary rock. Söhnge (1964) suggested that Nosib Group sandstone which underlies the area was "fluidized" by magmatic activity, because Nosib Group sandstone is compositionally similar to sandstone in the Tsumeb pipe. However, the distribution of sandstone within the Tsumeb pipe is not consistent with the intrusion of Nosib Group sandstone into a more than 2700 m stratigraphic thickness of overlying sedimentary carbonate rocks. Negligible sandstone is present in the lower part of the pipe, which is

approximately 1500 m above the top of the Nosib Group, and the volume of sandstone increases upwards in the pipe. There is no independent evidence to indicate that magmatic activity was involved in the formation of the Tsumeb ore body, or even that magmatism was contemporaneous elsewhere in the Otavi Mountain Land. Igneous intrusive activity was confined to rare and small mafic dykes, and those dykes associated with the Tsumeb ore body post-date sulphide mineralization. Finally, it has not been demonstrated that lithified sandstone can be remobilized, in the manner proposed by Söhnge (1964), to produce a "fluid" composed of the separate grains which formed the original sedimentary rock.

Hopwood (1975) suggested that water-saturated sandstone interbeds within the zone T6 dolostone were syntectonically injected into the Tsumeb pipe to form the pipe sandstone. However, sandstone does not occur as interbeds within the zone T6 dolostone, but fills strata-bound karst cavities in this member (Chapter 3.3.7). Sandstone beds are absent from the entire Tsumeb Subgroup, which is therefore an improbable source of the sandstone, and sandstone beds are very rare and thin in underlying formations of the Otavi Group.

Some workers (e.g. le Roex, 1955; Söhnge, 1976) proposed that sandstone was introduced to the pipe by sedimentation from the overlying Mulden Group. A 700 m stratigraphic thickness of sandstone is still preserved in the Tschudi Formation of the Mulden Group, in the immediate vicinity of Tsumeb, and the original thickness is unknown. This is the only important sandstone that occurs higher than the Nosib Group in the Damara Sequence of the Otavi Mountain Land. It is also the only sandstone which could have been unconsolidated when dolostone of the Tsumeb Subgroup fractured, prior to the emplacement of sandstone in the Tsumeb pipe. The introduction of sediment from the overlying sequence is consistent with the karst origin proposed for both the Tsumeb pipe and associated strata-bound cavities in zone T6, and with the decrease in the volume of sandstone with depth in the pipe (a feature also present in the Tsumeb West pipe and the Kombat ore bodies).

The Tschudi Formation sandstone is texturally, mineralogically and chemically identical to sandstone of the Tsumeb pipe (Chapter 3.3). Botha (1960), who considered the "pseudo-aplite" to be an igneous rock, noted that there were differences in the shape, composition and abundances of heavy minerals in the two rock types. Differences which he observed between the shape and colour of the two tourmaline populations can be ascribed to the presence of ragged, hydrothermal overgrowths on detrital tourmaline within the "pseudo-aplite" (Chapter 3.4.6). Other differences between the heavy mineral populations of the two rock types may result from the very immature nature and local provenance of the pipe sandstone, which would correspond to the earliest sandstone deposited in the Tschudi Formation.

The source of the pipe siltstone is also thought to be the Mulden Group. The only siltstone and shale within the upper part of the Tsumeb Subgroup near Tsumeb occur as thin beds within zone T7. However, the pipe structure and its contained sandstone extends above this stratigraphic level. The probable source of the pipe siltstone is carbonate-rich siltstone and shale of the basal Mulden Group (i.e. stratigraphically below sandstone of the Tschudi Formation). The pipe siltstone and Mulden Group slate are both characterized by a high TiO_2 content (Chapter 3.3.1).

It is concluded that the sandstone and siltstone of the Tsumeb pipe were derived from the Mulden Group, because of: (1) the similarity between rocks from the two locations, (2) the lack of other realistic sources for the rocks of the pipe, (3) the same sequence of depositional events, shale then siltstone, in both the Tsumeb pipe and the Mulden Group, and (4) the decrease in the volume of sandstone with depth in the pipe.

6.1.2 Controls on karsting and syn-sedimentary faulting

It follows from Chapter 6.1.1 that the Tsumeb pipe formed by karsting subsequent to deposition of the Tsumeb Subgroup, but prior to deposition of the Mulden Group. Evidence from elsewhere in the Owambo Basin is consistent with a major interval of karsting and erosion at

this time (Chapters 4, 6.1.4). No controls on the siting of the Tsumeb pipe were recognized during this study, but these could have been subtle structural controls (e.g. the intersections of minor vertical fractures). Joints or fractures are essential to initiate downward percolation of water in carbonate rocks which lack inter-granular permeability (Stringfield et al., 1979).

Karsting can occur in either the vadose or phreatic zone (Ford and Ewers, 1978). The regular form and major, unbroken vertical extent of the original solution pipe at Tsumeb is consistent with an origin in the vadose zone (Herak and Stringfield, 1972). The bottom of the pipe has not been reached in the present mine workings. However, the projected position of the strata-bound zone T4 breccia is close to the deepest point drilled. This may be the lower limit of the pipe, and may mark: (1) the position of a water table which formed during uplift of the Tsumeb Subgroup, (2) the former presence of soluble horizons which were preferentially karsted, or (3) a strata-bound paleokarst that was rejuvenated at this time. The lead isotope study indicates that one component of lead in the ore was introduced near the bottom of the pipe, consistent with the presence of a strata-bound paleoaquifer in this position. Strata-bound karsting in the lower part of zone T6 may have developed during a period of higher water table (e.g. successive levels of cavern formation occurred during uplift of the Austrian Alps; Herak and Stringfield, 1972). Alternatively, the location of this karsting may have been controlled by the high solubility of some beds in this part of the sequence (Chapter 3.4.4). This solution activity and related collapse is also thought to be responsible for the overlying manto fractures.

The karsting which formed the Tsumeb pipe involved both dissolution of the carbonate rocks and collapse of the pipe walls. Some upward stoping by roof collapse is possible, but this would have followed solution activity. This is because, in the absence of strong vertical fracturing, a stable pressure arch would have formed over the cavity unless rock solution had advanced some part of the pipe above the point at which collapse was occurring. The height of such a pressure arch is typically only twice its width (Cummins and Given,

1973).

The fractures which form the margin of the Tsumeb pipe formed subsequent to lithification of the dolostone breccia core of the pipe and its siltstone matrix, but prior to, or synchronous with, deposition of sandstone within the pipe (Chapter 3.7.5). This fracturing occurred during sedimentation of the Mulden Group and prior to deep burial of the top of the pipe, if the conclusions of Chapter 6.1.1 are accepted. The breccia column may have subsided into a cavity produced by solution of rock at depth, and failure was concentrated near the contact between the breccia column and its stronger wall rocks. Collapse, solution activity, or both, formed a pipe within the breccia at this time, and both this and the marginal fractures were filled with sandstone (Chapter 3.3.6). The marginal fractures are not related to solution activity and collapse in the strata-bound North Break zone alone, because major fracturing is present to at least 130 m stratigraphically below the base of this zone, and minor marginal fractures, some of which contain sandstone, continue to much greater depth. Solution activity at the base of the pipe, e.g. in zone T4, is probable. Similar marginal fracturing has been reported from breccia pipes of karst and solution collapse origin which occur in young, unfolded sequences (Chapter 6.1.5).

6.1.3 A model for formation of the Tsumeb pipe

The sequence of events involved in the formation of the Tsumeb ore body were (Fig. 131):

1) The Tsumeb pipe and associated strata-bound cavities in zone T6 formed by subaerial karsting of the Otavi Group dolostone, subsequent to deposition of the shallow-water sediments of zones T7 and T8, but prior to deposition of the Mulden Group. The pipe may have formed between the surface and a strata-bound collapse breccia in zone T4. It was subsequently partly filled by breccia, produced by collapse of its wall rock.

2) The karst topography was submerged, and silt and clay were

1

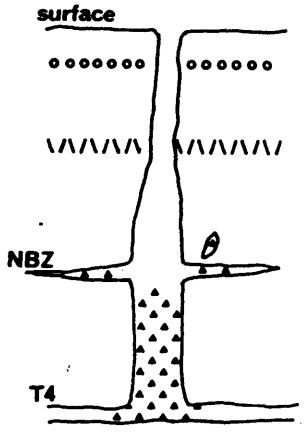

Karsting and solution collapse. Pipe partly filled with collapse breccia

2

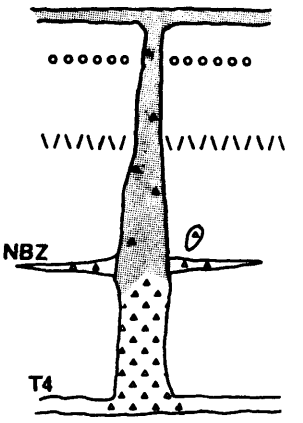

Submergence and continued collapse. Siltstone introduced to pipe

3

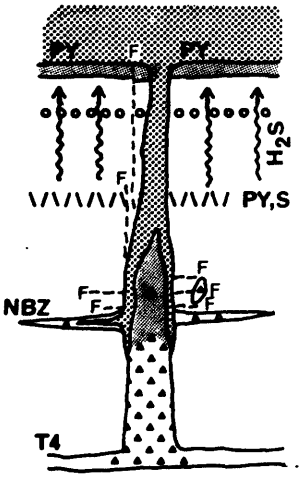

Continued submergence and collapse, with fracturing at pipe boundaries and above the North Break zone. Sandstone introduced to pipe and fractures. Reduced sulphur species, derived from the evaporite horizon, formed pyrite in the basal Mulden Group

4

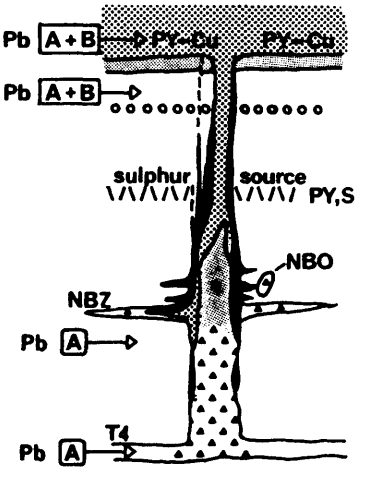

Continued burial. Ore fluids with different lead isotope components, A and B, introduced to pipe through different aquifers; sulphide ore precipitated by interaction between the fluids and an evaporitic source of sulphur

5

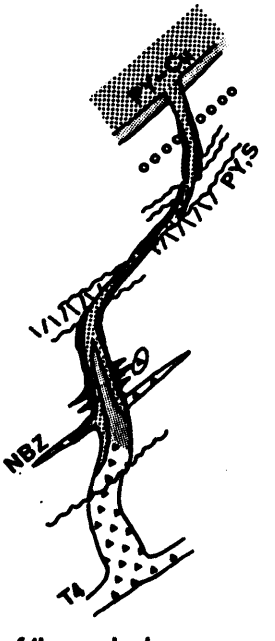

Deformation of the ore body

LEGEND

- sandstone, siltstone — Mulden Group
- dolostone and limestone
- oolite: zone T8
- anhydrite, gypsum: zone T7
- NBZ — North Break zone
- T4 — strata-bound breccia: zone T4

(Otavi Group)

- breccia
- massive ore, including mantos
- NBO — North Break ore body
- PY,S,PY-Cu — pyrite, native sulphur, pyrite-copper mineralization
- F — fracture
- thrust zone
- Pb A — lead isotope component (A, A+B)

Fig. 131
Stages in the development of the Tsumeb ore body.

introduced to the pipe during deposition of the lower formation of the Mulden Group. This sediment penetrated the interstices of the earlier collapse breccia, and further wall rock collapse occurred, to produce dolostone breccia with a siltstone matrix. Clasts which occur near the margins of the breccia body were derived from the adjacent wall rocks (Fig. 31), but clasts within the interior of the pipe are foreign to their immediate surroundings. The dark colour of dolostone clasts interior to the pipe between 26 and 30 levels is consistent with their derivation from higher in the pipe.

3) Concentric fracturing occurred parallel to the walls of the pipe; these fractures were mostly concentrated near the margin of the breccia body, particularly at lower elevations, but also occurred within the breccia body and the dolostone wall rocks. Fractures also developed between the Tsumeb and E2200 breccia pipes. The fractures were initially relatively open, although they contained some dolostone breccia produced by in situ fracturing of the dolostone wall rock.

Different generations of Mulden Group sand filled the upper part of the Tsumeb pipe. The composition of Mulden Group sedimentation changed with time, from silt and sand to clay, and sediments with the composition of sub-greywacke and feldspathic sandstone succeeded siltstone and shale within the pipe. The sand also filled a number of features lower in the pipe; these were: (1) the fractures described above, (2) strata-bound cavities in zone T6, immediately adjacent to the pipe, and (3) a cylindrical cavity within the dolostone breccia, associated with, but immediately interior to, the sandstone-filled marginal fracture zone (Chapter 3.3.6). The sand incorporated fragments of wall rock, and earlier generations of siltstone and sandstone from within the pipe. Some clasts, such as rounded pebbles, may have been introduced from the Mulden Group. The sand penetrated the marginal fractures to a minimum depth of 1300 m below the base of the Mulden Group, but the volume of sand decreased significantly below 500 m depth, and became insignificant below 850 m.

4) The pipe was mineralized, then subjected to D_1 deformation and subsequent reverse faulting (5).

6.1.4 Ore loci elsewhere in the Owambo Basin

The composition, form and distribution of discordant sandstone and dolostone breccia bodies throughout the Otavi Mountain Land is consistent with a karst and solution collapse origin for these bodies, prior to folding of the Tsumeb Subgroup (Chapter 4.5).

Karsting was related to at least one, and possibly more, erosion surfaces. The oldest erosion surface recognized within the Otavi Group of the Owambo Basin is at the top of the Abenab Subgroup; another surface immediately overlies this, at the top of the Chuos Formation. The Abenab West ore locus, at the top of the Abenab Subgroup, immediately underlies the lower of these surfaces and may be genetically related to it. Breccia bodies and cavities of the underlying Gauss Formation may also be related to this surface, although there is no direct evidence for this. The lower surface is an unconformity in the western Otavi Mountain Land and throughout most of the western Owambo Basin; the upper surface is conformable throughout much of the Otavi Mountain Land, but becomes an angular unconformity to the south (Chapter 2).

The most important erosion surface, to which karsting can be directly related, is present at the top of the Tsumeb Subgroup. Paleokarst features associated with this surface, such as the Tsumeb pipe, the Tsumeb West pipe, and pipes in the Kombat mines, contain siltstone and sandstone interpreted as Mulden Group rock, and some extend as deep as zone T4. Pre-existing fracture zones may have been karsted in some areas (e.g. the Tsumeb West fracture zone, and possibly some ore loci in the Kombat mines). The Mulden Group and Tsumeb Subgroup are paraconformable within the Owambo Basin, but to the west of Tsumeb there is evidence of an erosional hiatus. The top of the Tsumeb Subgroup in the Otavi Valley area was eroded to as deep as zone T4, and thick lenses of sedimentary breccia were deposited (Chapter 2.3.2). This erosion surface is a major unconformity along the western and southern boundaries of the Owambo basin. The Tsumeb Subgroup was eroded in places prior to deposition of the Mulden Group at Fransfontein, near the south-western boundary of the basin. Valleys more

than 150 m deep, with nearly vertical walls, were incised into sedimentary carbonate rocks of the Otavi Group and underlying crystalline rocks, and a karst topography developed. At least 3000 m thickness of Mulden Group rocks, possibly including 1000 m of the Owambo Formation, are preserved in a probable intermontane basin (Frets, 1969; Guj, 1974; Hedberg, 1979). Metamorphism and deformation of the Otavi Group occurred prior to Mulden Group deposition at Fransfontein and farther to the south (Chapter 2.1). This surface must have formed between 730 m.y. and 590 m.y. (Chapter 3.7.12). It has been suggested that a major zone of transcurrent movement occurred to the south of the Otavi Valley (Smit, 1958), and the above features indicate that the southern margin of the Owambo basin was an active zone of faulting throughout the Late Proterozoic. This faulting probably determined (1) the northern boundary of a major graben during deposition of the Nosib Group, (2) the southern margin of the Kamanjab-Tsumeb basement ridge (which in turn controlled facies variations and karsting in the Otavi Group and Mulden Group), and (3) the position of minor grabens or oblique-slip basins during deposition of the Mulden Group.

It is concluded that karsting and solution collapse processes were responsible for the majority of ore loci in the Owambo Basin, and that the resulting structures are spatially related to erosion surfaces of regional extent. A similar origin has been proposed for ore loci which host Tsumeb-type mineralization in the Katangan and West Congolian fold belts (Chapter 4.6.2).

6.1.5 Comparisons with modern solution collapse and karst structures

It has been argued that strata-bound bodies of solution collapse breccia underlay at least 2 500 square kilometres of the Otavi Mountain Land during exposure of the Tsumeb Subgroup (Chapter 4.5). Solution pipes may have connected with these over vertical depths of up to at least 1300 m, e.g. the Tsumeb pipe. It is shown below that karst features of similar form are widespread in younger rocks, and that some of these have dimensions comparable to those of the Tsumeb pipe.

Cavities and breccia bodies formed by solution and solution collapse can be divided into two main groups. These result from: (1) solution of sedimentary carbonate rocks, with minor collapse, and (2) solution of evaporites (both halite and sulphate rocks), with large-scale collapse of overlying rocks, and dissolution of these overlying rocks along fractures initiated by collapse. The two groups differ only in the rock types dissolved, and the differing response of those rocks, and the overlying sequences, to dissolution. Solution chimneys occur in both groups, the main requirement probably being the presence of vertical fracturing that is continuous between the surface and a permeable horizon at depth (or between the surface and the water table within a permeable sequence).

Modern karst systems in sedimentary carbonate rocks extend to depths in excess of 800 m, and vertical solution pipes and collapse dolines are common. Modern, unfilled, vertical solution chimneys in dolostone reach depths of 330 m in Trieste and 430 m in Mexico, France and Switzerland; inter-connecting horizontal caves and vertical solution chimneys (shaft caves) have depth extents of up to 850 m (Herak and Stringfield, 1972; Stringfield et al., 1979). Therefore, individual pipes extend for at least one third of the depth proposed for the Tsumeb pipe. Modern solution pipes and dolines extend down to aquifers filled with meteoric water (including rapidly flowing rivers), brackish water, or sea water (Herak and Stringfield, 1972). Cavernous zones in rejuvenated, strata-bound paleokarst horizons have been intersected in drill holes at depths of 400 - 1700 m (Vernon, 1969; Stringfield et al., 1979).

The dissolution of evaporites can produce subtle effects in overlying strata on a regional scale, although spectacular structures develop in localized areas. Subsidence of the overlying sequence can be gradual if lateral flow of evaporites occurs concurrently with evaporite removal, and large cavities do not necessarily develop. The immediately overlying strata collapse and fragment, but the effects of this decrease upwards. Cavern formation and roof collapse are sometimes relatively minor, and strata which occur some distance above the evaporites can be little disrupted (Stanton, 1966). Total removal of

evaporite horizons would appear to be typical, rather than anomalous, in older sedimentary sequences. Evaporite solution advances down-dip from the outcrop, or inwards from the margins, of evaporite horizons (and can also occur within the horizons), and hundreds of metres thickness of evaporites can be completely removed in this way (Bowles and Braddock, 1963; Christiansen, 1967). Thin horizons of breccia and indirect indications of former evaporites, such as length-slow chalcedony and evaporite pseudomorphs, may be all that remain, e.g. in the Cretaceous Edwards Limestone of central Texas, in which a small remnant of gypsum remains to confirm this interpretation (Fisher and Rodda, 1969; Folk and Pittman, 1971; Beales and Hardy, 1977).

Evaporite solution can also produce strata-bound breccia bodies up to hundreds of metres thick in the immediate vicinity of former evaporite horizons (Blount and Moore, 1969), and can produce transgressive breccia bodies and fault blocks of regional extent in overlying rocks. Evaporite solution has removed thicknesses of up to 200 m of halite in the Middle Devonian Prairie Formation, Canada, and the overlying sequence has collapsed along linear fault blocks to form fault troughs up to 160 km long (Bishop, 1956; de Mille et al., 1964; Christiansen, 1967). These follow structural trends in the basement, and permeable reef horizons associated with such structural trends (de Mille et al., 1964; Camfield and Gough, 1977). The rocks overlying evaporite horizons can be extensively fragmented, for example in the Mackinac breccia of the Michigan Basin, which includes both transgressive and strata-bound breccias in sedimentary carbonate rocks. Vertical bodies from a few metres to more than a hundred metres wide, both tabular and pipe-like, are thought to have a depth extent of up to 460 m, and to contain fragments which have dropped up to 230 m vertically at this locality (Landes et al., 1945).

Breccia pipes which extend between the surface and underlying, strata-bound breccia horizons in sedimentary carbonate rocks of Texas, New Mexico, and South Dakota, have been produced by the down-dip dissolution of evaporite horizons (Bowles and Braddock, 1963; Anderson and Kirkland, 1980; Gustavson et al, 1980). Similar features are present in Pennsylvanian to Triassic rocks over a large area of the

western central U.S.A., including the Colorado Plateau, where some pipes host mineralization (Anderson and Kirkland, 1980). Breccia pipes in South Dakota and Texas are up to 335 m and 425 m deep, respectively. Pipes from these two localities have derived their infill from their wall rocks and from sediments introduced to the pipes from above. Some breccia matrices consist of silt and clay (at least some of which has come from above). Successive generations of infill occur; pipes in western Texas are filled by collapse breccia derived from Permian wall rocks, but later cores of Triassic, Tertiary or Quaternary sediments can be present. Some pipes are bounded by concentric fracture zones (Braddock, 1963); the boundaries between competent wall rocks and the pipe cores are zones of strong shearing, with nearly vertical bedding and rare slickensides (Gustavson et al., 1980).

The largest pipes known to be associated with evaporites are located in Saskatchewan, Canada, in the area underlain by the Prairie Formation. The 914 m deep Crater Lake "collapse", an average 107 m in diameter, occurs in sedimentary carbonate rocks, sand and shale, overlying salt. It is bounded by two concentric fault zones at surface, 100 m and 213 m in diameter, which Christiansen (1971) interpreted as outer and inner cylinders of collapse. The outer cylinder formed 19600 years ago, and caused a total downthrow of 90 m; the resulting structure was infilled with lake sediments near surface, and the sequence of sediment infill indicates that the inner cylinder collapsed prior to the outer cylinder. Seismic evidence indicates that a thickness of 38 m of salt has been removed at the base of the structure, and Gendzwill and Hajnal (1971) interpreted the body as a breccia pipe which formed by the collapse of rocks above a solution cavern in the salt. This proposed origin was not described in detail, but the small diameter and great vertical extent of the pipe, comparable in dimensions to the Tsumeb pipe, indicate that solution activity must have operated in addition to upward stoping (i.e. because of the space problem involved in accommodating the increased volume of the broken rock). Another pipe, the Howe Lake Structure contains fragments of Quaternary and Tertiary rocks, mixed with silt, to at least 138 m depth (the greatest depth drilled; Christiansen et al., 1973).

The above discussion illustrates the importance of karsting of evaporites and carbonate rocks to form breccia bodies; these can be vertical, tabular bodies, or pipes, and they can have a vertical extent of many hundreds of metres. Evaporite horizons, hundreds of metres thick, can be completely dissolved on a regional scale, and disruption of the overlying rocks can be confined to the immediate vicinity of the former evaporite horizon. Alternatively, extensive brecciation and regional fault zones can form above areas of evaporite solution. Unfilled, vertical solution pipes in sedimentary carbonate rocks, up to 430 m deep, are known (i.e. one third of the depth of the Tsumeb pipe), and breccia pipes formed above areas of salt solutions reach dimensions comparable to those of the Tsumeb pipe. Breccia fragments within some pipes and vertical, tabular breccia bodies have dropped hundreds of metres, and some breccia bodies have a silt and clay matrix introduced from above; both the fragments and matrix can be derived from surface. Concentric faults occur at the margins of some breccia pipes formed by karsting, and successive periods of both collapse and sedimentation can be recognized in some pipes. A well defined paleo-aquifer, or a soluble lithology, is commonly present at the base of pipes, regardless of their origin.

It is concluded that the form, composition, dimensions and interpreted history of the Tsumeb pipe and other ore loci of the Otavi Mountain Land are comparable with those of modern karst and solution collapse features. The former presence of an evaporite horizon at depth is not required by the model, but is possible at the stratigraphic level of the strata-bound breccia in zone T4.

6.1.6 Mineralized karst and solution collapse features elsewhere in the world

Mineralized karst and solution collapse features are not unique to the Late Proterozoic mineral province of central Africa. Mississippi Valley-type lead-zinc-barite mineralization in some areas of the south-central U.S.A. is hosted by strata-bound breccia bodies and breccia pipes, of probable karst and solution collapse origin. Breccia pipes in eastern Tennessee, which have been interpreted as solution

chimneys, extend at least 245 m below the unconformity to which they are spatially related. Volcanic ash and fossiliferous sedimentary rocks, foreign to the enclosing sequence, occur 183 m below the unconformity in one unmineralized pipe (Hoagland et al., 1965). The stope plans of some zinc mines resemble complex cave networks developed along joint systems (e.g. figure 6, Fulweiler and McDougal, 1971), and domal breccia bodies which are concentrated in specific horizons have been interpreted as solution collapse structures (e.g. figures 5 and 6, McCormick et al., 1971). Mineralized, cave-like bodies and collapse structures of some areas are filled with shale from overlying formations (e.g. Tri-State district).

Mineralized pipes in undeformed Pennsylvanian to Triassic rocks of the Colorado Plateau, U.S.A., are probable karst and solution collapse structures (Chapter 6.1.5). These pipes have been mined for uranium, copper and silver, and to a lesser extent, lead, zinc and gold; it is probable that the Apex germanium-gallium ore body, Utah, is part of this province (Chapter 4.6.5). Some of these pipes penetrate non-carbonate rocks, such as mudstone and siltstone, over at least part of their vertical extent. Breccia pipes commonly have approximately 100 m vertical extent, but the largest example, the Orphan pipe, is 50 - 150 m in diameter, with a depth extent of at least 460 m. Some pipes are bounded by one or more concentric ring faults, with which ore is associated, at the contact between the pipe infill and wall rock (Hilpert and Moench, 1960; Kelley et al., 1968; Gornitz and Kerr, 1970). The pipes can contain fragments of wall rock from higher in the sequence, sedimentary infill from the sequences which overlie the top of the pipe, and rounded pebbles; the Orphan pipe contains sandstone from 207 m higher in the sequence (Gornitz and Kerr, 1970). It has been suggested that the pipes developed as the result of karsting and solution collapse at depth in Mississippian or Permian limestone, or as the result of dissolution of Pennsylvanian halite (Kerr et al., 1957; Gornitz and Kerr, 1970; Bowles, 1977).

The Terlingua mercury ore bodies of western Texas are vertical breccia pipes which bottom in mineralized, gypsiferous cave-fill sediments (Yates and Thompson, 1959). The pipes are up to at least 335

m deep, and contain fragments derived from a minimum of 305 m (possibly 460 m) higher in the sequence. All of the pipes terminate within the upper 15 m of limestone stratigraphically equivalent to the Edwards Limestone, which elsewhere contains evaporite horizons (Chapter 6.1.5; Fisher and Rodda, 1969). Mineralization is mostly confined to the margins of the pipes.

Some ore bodies, such as the copper deposits of Kennecott, Alaska, are hosted by beds which were formerly permeable as the result of the dissolution of evaporite minerals from sedimentary carbonate rocks (Armstrong and MacKevett, 1975). The shapes of other ore bodies in sedimentary carbonate rocks resemble complex systems of caverns and solution pipes, but the origin of the ore loci (i.e. meteoric karsting versus hydrothermal dissolution) has not been demonstrated. Examples occur in the Santa Eulalia lead-zinc-silver district, Mexico, where vertical pipes up to 700 m in vertical extent are known, and in which mineralization is spatially associated with thick beds of anhydrite (Hewitt, 1968).

It is concluded that karst and solution collapse features are important ore loci for a number of types of ore deposit. Mineralized structures of this type, the dimensions of which are of the same order of magnitude as ore loci in the Otavi Mountain Land, are not unique to that area but are of widespread occurrence. Many of these pipes are genetically related to the dissolution of evaporite horizons. Breccia pipes that: (1) contain wall-rock fragments and foreign sediments, (2) are surrounded by concentric, marginal fractures, and (3) which lack closely associated igneous rocks, occur in flat-lying, although commonly block-faulted, rocks of the areas discussed.

6.2 PHYSICO-CHEMICAL CONDITIONS DURING ORE DEPOSITION, AND THE SOURCE OF SULPHUR

Physical and chemical conditions during ore deposition in the Tsumeb ore body are interpreted from fluid inclusion data, stable isotope data, and the mineralogy, compositional zoning and

paragenesis of the sulphide ore and its associated rock alteration. The approach used is similar to that of Ohmoto (1972) and Crerar and Barnes (1976). The reasons for mineralogical zoning and for the characteristic mineralogy of Tsumeb-type mineralization are considered, and evidence is presented for the importance of a separate sulphur source in localizing the Tsumeb ore body. The lead isotope data show that the fluids which formed the Kombat and Tsumeb ore bodies contained lead which was isotopically similar, indicating that the lead was derived from the same lead sources at a similar time. This indicates a genetic relationship between the ore fluids which formed the two ore bodies, despite major differences which exist in their mineralogy and the sulphur isotopic ratios of their sulphide minerals. The lead isotope data also indicate a possible genetic relationship between Tsumeb-type mineralization, Tschudi-type mineralization and much of the Berg Aukas-type mineralization, consistent with their formation from genetically-related ore fluids during a mineralizing event of limited duration.

The similar, intermediate range of temperatures indicated by fluid inclusion studies (approximately 250°C) supports the conclusion that the Tsumeb ore body, the Kombat ore body, and many examples of the Berg Aukas type of mineralization have closely related origins (Appendix 3). The ore fluids were saline waters and brines, dominated by sodium and chloride ions. The presence of a "potassium halide" mineral, presumably sylvite, in the concentrated brine inclusions of the Kombat ore bodies indicates that potassium may also have been an important component. Carbon dioxide and hydrogen sulphide are present in significant concentrations in some fluid inclusions from the upper part of the Tsumeb ore body. Muscovite, albite and probable anhydrite are important daughter minerals in the fluid inclusions. The ore fluids which formed the three groups of ore bodies had minimum salinities of 2-4 per cent NaCl equivalent, and the maximum salinities exceeded 10 per cent (with greater than 20 per cent in the Kombat ore bodies). An ionic strength of 1,0 is therefore used to model conditions during ore deposition at Tsumeb. A low confining pressure, of only 500-700 bar, is indicated for the Tsumeb ore fluid.

Sulphide minerals are among the first minerals to re-equilibrate during metamorphism (Barton, 1970). Mineralization of the Otavi Mountain Land has been deformed, and has probably undergone low grade metamorphism in the south of the area (Chapter 3.7.11). At least some Tsumeb-type and Berg Aukas-type mineralization of central Africa may also have been metamorphosed to low grades (Chapter 4.6.1.). The present mineral assemblages in these occurrences may therefore reflect conditions (1) during ore deposition, (2) during metamorphic re-equilibration of a hydrothermal assemblage, or (3) both (i.e. because only some minerals have re-equilibrated). A further possibility is that ore deposition was broadly synchronous with the major, prograde metamorphic event in some areas, so that (1) and (2) were identical (e.g. in the Kombat ore bodies). Minerals with large stability fields would not be expected to show evidence of metamorphic re-equilibration, but the effects of this could be important for some of the mineral assemblages which are most diagnostic of physico-chemical conditions, e.g. sulphur fugacity. The only mineral assemblages which can be assumed with reasonable confidence to be original hydrothermal assemblages are those of the northern Otavi Mountain Land, where burial conditions may not have exceeded those of advanced diagenesis. This conclusion is supported by the presence, and zoning, in the Tsumeb ore body of assemblages diagnostic of high sulphur fugacity conditions (Chapter 6.2.1.), rather than of the lower sulphur fugacity conditions typical of sulphide minerals which have undergone regional metamorphism (e.g. Ferry, 1981).

6.2.1 Oxygen fugacity, sulphur fugacity, pH and sulphur concentration of the Tsumeb ore fluid

The physico-chemical characteristics of the Tsumeb ore fluid, such as oxygen fugacity and sulphur fugacity, can be estimated directly from the available data. However, pH and the total sulphur concentration cannot be accurately determined because of a lack of appropriate analytical data from fluid inclusions, and because there have been no studies of similar ore deposits with which comparisons can be made with confidence. It is shown below that, if reasonable maximum and minimum concentrations are assumed for potassium, calcium

and carbon, the existing data are consistent with conditions of formation similar to those of other base metal ore deposits. A moderately high sulphur concentration is indicated for the ore fluid if these assumptions are accepted. The compositions of sulphide minerals referred to below are given in Table 6.

(i) Oxygen fugacity

There is no significant variation in either the $\delta^{34}S$ values of sulphide minerals in the Tsumeb ore body, or in the $\delta^{13}C$ values of hydrothermal calcite (Chapter 5). Also, graphite and carbonaceous material are rare within the calcitized zone of the ore body (Chapter 3.4.5). Graphite is theoretically only stable within the field in which major $\delta^{13}C$ variation can occur in carbonate minerals, even when the carbon concentration of the fluid is as high as 10^{-1}m. These observations indicate that the oxygen fugacity and pH of the ore fluid did not correspond to conditions in either of the two fields in which significant variation can occur in the sulphur or carbon isotope ratios. Instead, conditions corresponded to that in one of the three adjacent or intervening fields (Fig. 132). The $\delta^{34}S$ values of the sulphide minerals are too positive for these minerals to have formed at larger values of oxygen fugacity or pH than in the field in which significant sulphur isotopic variation can occur under near-equilibrium conditions. Equilibrium fractionation under these conditions would have produced $\delta^{34}S$ ratios 27‰ lighter that the $\delta^{34}S$ ratio of the ore fluid, which would have had an improbable value of approximately +50‰, inconsistent with the argument presented in Chapter 5.1.2. It is therefore concluded that sulphide minerals precipitated under conditions which correspond to the area below the field of significant sulphur isotopic variation in Figure 132. This is consistent with the absence of hematite, magnetite and barite from the Tsumeb ore body (Figs. 132 and 133). Sulphide minerals could have precipitated above or below the lower field in which carbon isotopic variation can occur. However, abundant ore which contains the bornite plus pyrite assemblage, rather than chalcopyrite, could only have precipitated below this field if the ore fluid which formed much of the ore had an improbably high sulphur concentration (greater than 3,2 wt%). Therefore the Tsumeb ore fluid had an oxygen

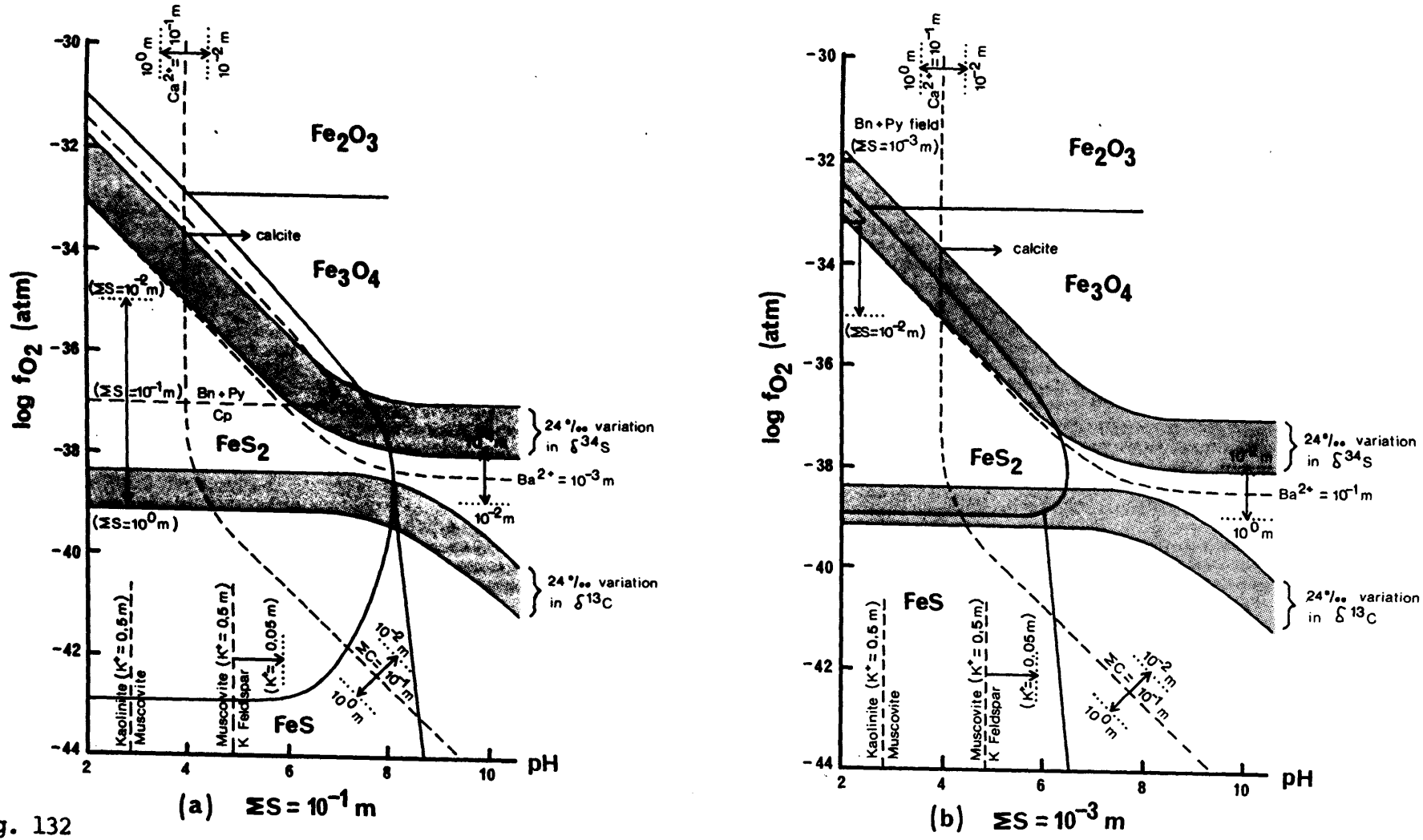

Fig. 132

Oxygen fugacity - pH diagrams showing the stability fields of minerals in the Tsumeb ore body under the following conditions: T = 250°C, I = 1,0, $\Sigma C = 10^{-1}$m, $Ca^{2+} = 10^{-1}$m, $K^+ = 0,5$m, Ba^{2+} = (a) 10^{-3}m, (b) 10^{-1}m. The fields in which significant isotopic variation can occur in sulphur and carbon minerals are also shown. The field of major variation in $\delta^{34}S$ would be at more negative values of fo_2 at pH values larger than 8,5 if the data of Meyer et al. (1983) are accepted. Sources of data: Ohmoto (1972), Crerar and Barnes (1976).

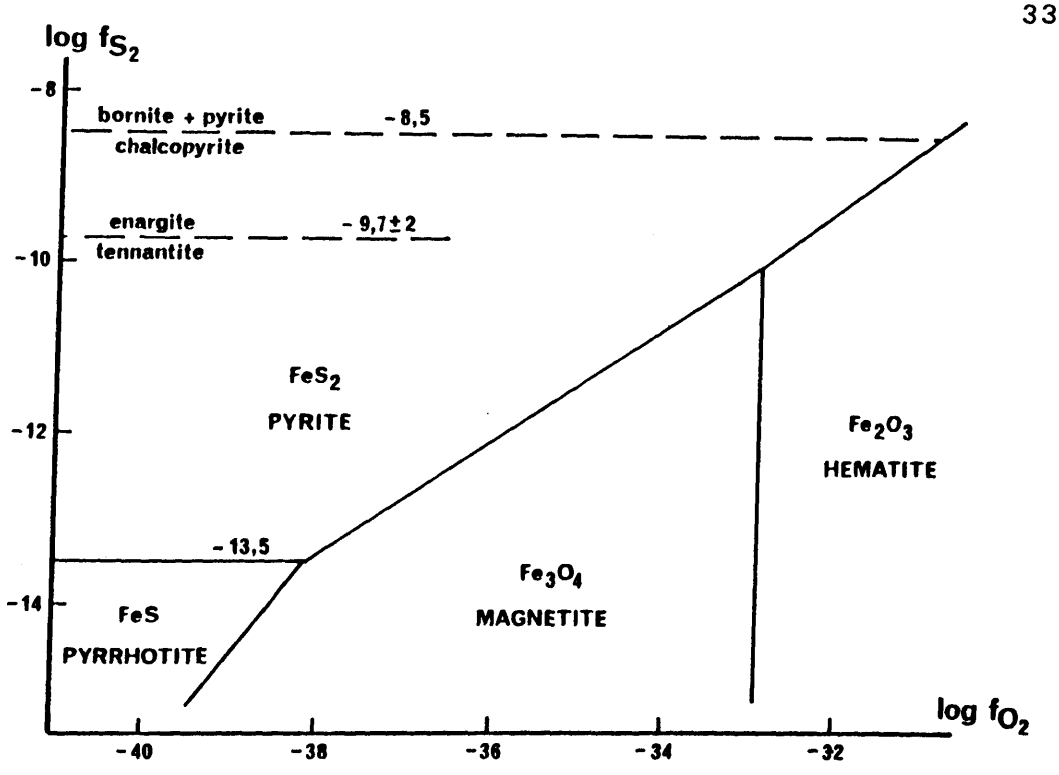

Fig. 133
Sulphur fugacity - oxygen fugacity diagram, showing the stability fields of minerals present in Tsumeb - type mineralization.

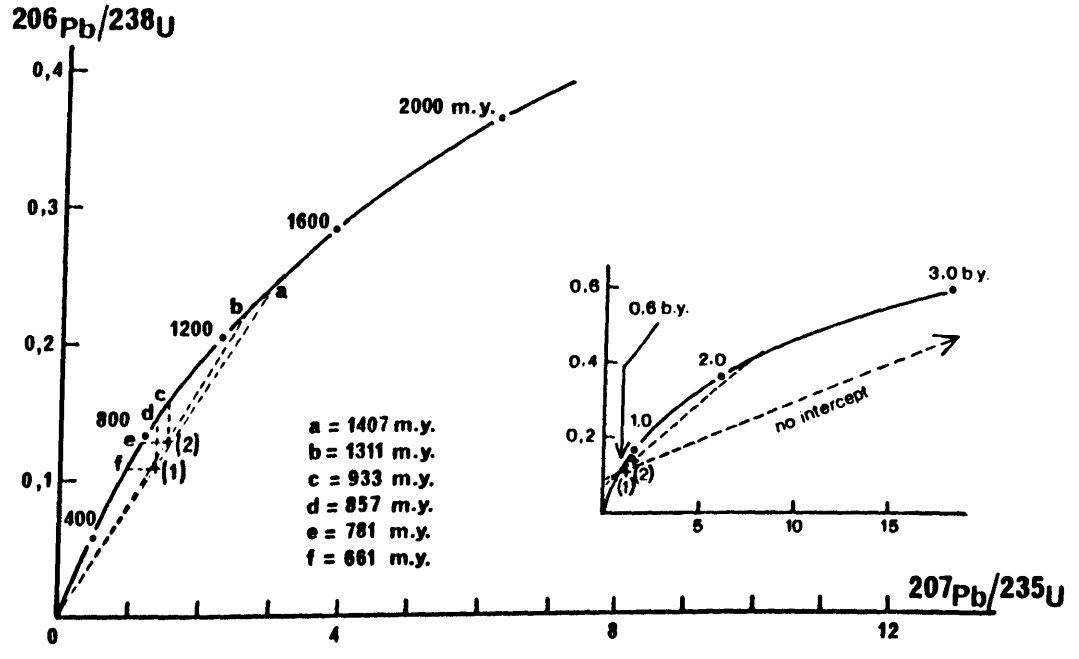

Fig. 134
U-Pb zircon diagram of data from two, morphologically distinct fractions of zircon, (1) and (2), in a single sample of sandstone ("pseudo-aplite") from the Tsumeb pipe. The $^{207}Pb/^{206}Pb$ age (a,b), $^{207}Pb/^{235}U$ age (c,d) and $^{206}Pb/^{238}U$ age (e,f) are shown. The inset shows a mixing model with a lower intercept of 600 m.y.

fugacity smaller than 10^{-33}, and probably greater than 10^{-39}, over the interval pH 2 to pH 10.

(ii) Sulphur fugacity

Pyrite is the only important iron mineral in Tsumeb ore, and other iron minerals such as hematite, magnetite, pyrrhotite or iron-rich carbonate or silicate phases are absent, or present in insignificant quantities. The minimum value of sulphur fugacity during ore deposition is therefore constrained by the stability field of pyrite, as well as by the lack of isotopic variation in sulphide and carbonate minerals (Fig. 132). The stability field of pyrite is defined by sulphidation and oxidation reactions of the form:

$$\underset{\text{pyrite}}{3\ FeS_2} + 2O_2 \rightleftharpoons \underset{\text{magnetite}}{Fe_3O_4} + 3\ S_{2(g)}, \text{ and}$$

$$\underset{\text{pyrrhotite}}{2\ FeS} + S_{2(g)} \rightleftharpoons \underset{\text{pyrite}}{2\ FeS_2}$$

from which the sulphur fugacity can be calculated (Crerar and Barnes, 1976). These are simplified forms of a series of solvation reactions such as:

$$2\ FeS + H^+ + 1{,}5\ H_2S_{(aq)} + 0{,}5\ SO_4^{2-} \rightleftharpoons 2\ FeS_2 + 2\ H_2O$$

The minimum sulphur fugacity was $10^{-13{,}5}$, defined by the absence of pyrrhotite (Figs. 132, 133).

A further constraint on sulphur fugacity is the abundance of the bornite plus pyrite assemblage, relative to chalcopyrite (Crerar and Barnes, 1976). These phases are related by the sulphidation reaction:

$$\underset{\text{chalcopyrite}}{5\ CuFeS_2} + S_{2(g)} \rightleftharpoons \underset{\text{pyrite}}{4\ FeS_2} + \underset{\text{bornite}}{Cu_5FeS_4}$$

which is the simplified form of a series of sulphide solvation reactions, e.g.

$$5\ CuFeS_2 + H^+ + 1{,}5\ H_2S_{(aq)} + 0{,}5\ SO_4^{2-} \rightleftharpoons Cu_5FeS_4 + 4\ FeS_2 + 2\ H_2O$$

The minimum sulphur fugacity at which the bornite plus pyrite assemblage could have formed is $10^{-8,5}$ (Fig. 133), i.e. the area of Figure 132 bounded by the univariant curve for this reaction at any given sulphur concentration.

It should be noted that the presence of bornite without pyrite is not diagnostic of the above sulphur fugacity conditions, but may only reflect the Cu:Fe ratio of the ore solution. For example, bornite plus chalcopyrite rather than bornite plus pyrite can crystallize at high values of this ratio (Gustafson, 1963), i.e.

$$\underset{\text{pyrite}}{FeS_2} + 0{,}5\ H_2O + Cu^+ \rightleftharpoons \underset{\text{chalcopyrite}}{CuFeS_2} + H^+ + 0{,}25\ O_{2(g)}$$

There is a paucity of pyrite in some bornite ore, the average Cu:Fe ratio of the Tsumeb ore body is large (Table 7), the pyrite content is small, and iron-poor varieties of many ore minerals are present (e.g. sphalerite, tennantite, germanite, briartite, gallite). Also, germanite ($Cu_3Fe_{0,5}Ge_{0,5}S_4$) is important, in addition to renierite ($Cu_{2,5}FeGe_{0,5}S_4$). This indicates that the Cu:Fe ratio of the ore fluid was high (note that none of the mineralogical indicators alone is sufficient evidence for this, because the iron content of these minerals can be a function of other variables, such as sulphur fugacity). The insignificant volume of chalcopyrite in the ore body cannot be considered evidence that all ore deposition was at a sulphur fugacity greater than $10^{-8,5}$ for the above reason, and also because tennantite is widespread and can form at lesser values of sulphur fugacity (see below).

Independent evidence exists to support the large sulphur fugacity predicted from the bornite plus pyrite assemblage. This is the presence of enargite and tennantite, which are related by the sulphidation reaction:

$$0{,}67\ \underset{\text{tennantite}}{Cu_{12}As_4S_{13}} + S_{2(g)} \rightleftharpoons 2{,}67\ \underset{\text{enargite}}{Cu_3AsS_4}$$

which is the simplified form of a series of solvation reactions such as:

$$0{,}67\ Cu_{12}As_4S_{13} + H^+ + 1{,}5\ H_2S_{(aq)} + 0{,}5\ SO_4^{2-} \rightleftharpoons 2{,}67\ Cu_3AsS_4 + 2\ H_2O$$

Experimental data from which the sulphur fugacity of the enargite plus tennantite univariant curve can be calculated are not available (Maske and Skinner, 1971). However, a figure of $10^{-9,7}$ is obtained if the approximation of Craig and Barton (1973) is used to calculate the free energies of the sulphosalt minerals. A large value is therefore indicated for the sulphur fugacity, despite a probable uncertainty of ± 2 in the log value. Tennantite, rather than enargite, is the dominant sulphosalt mineral in both chalcopyrite ore and ore which contains the bornite plus pyrite assemblage. This may reflect a sulphur fugacity greater than $10^{-8,5}$ for the tennantite-enargite assemblage under the conditions considered (i.e. this is the value of the chalcopyrite-bornite-pyrite univariant curve). Tennantite ("green enargite") which has incipiently replaced the interiors of enargite grains, and which pseudomorphs enargite crystals, is not considered here (Chapter 3.6.2). This tennantite is texturally distinct from the above tennantite (which shows sharply defined contacts with enargite) and might have formed by desulphidation of enargite during burial (i.e. advanced diagenesis).

The absence of hypogene covellite in the Tsumeb ore body is not used to constrain sulphur fugacity conditions because of the probable ease with which re-equilibration (e.g. desulphidation) of this phase can occur at low temperatures. It is concluded that all ore deposition in the Tsumeb ore body was at a sulphur fugacity greater than $10^{-13,5}$, and that much ore formed at a value greater than $10^{-8,5}$.

(iii) pH

The pH of the Tsumeb ore fluid cannot be accurately determined from the available data, but broad limits can be estimated from the stability fields of kaolinite, muscovite, potassium feldspar and carbonate minerals if certain assumptions are made (Fig. 132). Muscovite was stable during the deposition of all ore types, and potassium feldspar within sandstone was altered to muscovite; kaolinite is rare and might not have been related to the hypogene phase of mineralization (Chapter 3.4). The stability fields of these minerals cannot be shown accurately on Figure 132 because the potassium concentration of the fluid is unknown. Upper and lower limits of 0,5 m and 0,05 m potassium have been chosen, which are the extreme values found in some ore fluids associated with igneous intrusions (e.g. porphyry copper deposits) and Mississippi Valley-type ore deposits, respectively (Crerar and Barnes, 1976). The minimum and maximum pH values obtained using these values are pH 3 and pH 6 (neutral is pH 5,5 at 250°C). The oxygen fugacity is constrained to a value greater than approximately 10^{-42}, consistent with the limit of 10^{-39} indicated by other data, if this pH range is accepted. This is because calcite is unstable within the stability field of muscovite at smaller values of oxygen fugacity (Fig. 132).

The stability fields of calcite and dolomite can provide additional information about the pH of the ore fluid, if assumptions are made about the maximum and minimum calcium and carbon concentrations. Dolostone has been extensively replaced by quartz and sulphide minerals in parts of the Tsumeb ore body, but large volumes of calcite and dolomite occur elsewhere with sulphide minerals (Chapter 3.4). The pH range of the Tsumeb ore fluid must have included a value close to the stability limit of calcite and dolomite. There is no concentration data for calcium, and only a maximum value of $10^{0,55}$m for carbon (i.e. in the upper part of the ore body; Appendix 3). Fluids which form other types of base metal ore deposits have calcium concentrations within the range 10^{0}m to 10^{-2}m. The range of carbon concentrations found in these fluids is more variable, but 10^{-1}m carbon is the usual maximum concentration, and 10^{-2}m is more typical (Hitchon, 1977; Sverjensky, 1981). A total

range of 10^{0}m to 10^{-2}m carbon is shown in Figure 132, to include the Tsumeb data. The lower stability limit of calcite gives a lower pH limit of 3,5. If the lower limit of 10^{-39} is accepted for the oxygen fugacity, the upper stability limit of calcite gives an upper limit of pH 5. These values are consistent with the pH range estimated independently by assuming maximum and minimum potassium concentrations. That is, the total pH range of the ore fluid was not less than 3 or greater than 6, and it included a value within the range 3,5 to 5. This would only be invalid if the Tsumeb ore fluid had concentrations of both potassium and calcium (or carbon) outside the ranges found in ore fluids which form other base metal deposits.

(iv) Total sulphur concentration

The sulphur fugacity, oxygen fugacity and stable isotope data constrain the total sulphur concentration of the ore fluid if the above pH limits are accepted. The stability fields of sulphide minerals in Figure 132 are drawn for sulphur concentrations of 10^{-1}m and 10^{-3}m. The stability field of the bornite plus pyrite assemblage, exclusive of the field in which a $\delta^{34}S$ variation can occur in sulphide minerals, is very small at total sulphur concentrations smaller than 10^{-2}m in the range pH 2 to 10. The field does not exist at pH values larger than 3,5, the probable minimum pH. The bornite plus pyrite field is sufficiently large at a sulphur concentration of 10^{-1}m to permit an oxygen fugacity variation of one log unit, or a pH change of one unit, during formation of this assemblage. This moderately large value is therefore the most realistic estimate of the minimum sulphur fugacity conditions under which most of the ore was deposited.

6.2.2 Zoning of rock alteration

A simple interpretation of the zoning of rock alteration within the Tsumeb pipe is that a single fluid was introduced to the bottom of the pipe, and that the composition of this ore fluid was modified progressively by reaction with the pipe breccia during ascent of the fluid. Rock alteration within the pipe is mostly confined to the pipe structure, rather than the surrounding rocks,

and alteration zoning extends to higher elevations in the marginal fracture zone of the pipe than in the pipe core (Chapter 3.1, Fig. 18). This is consistent with upward flow of fluid, mostly confined to the pipe structure (i.e. it is consistent with a higher water-rock ratio in the permeable fracture zone than in the core, with less rapid modification of fluid composition as a result).

Dolostone was dissolved at the bottom of the pipe and quartz was deposited to form the silicified zone of the pipe. A probable cause of quartz precipitation was a decrease in temperature of the ore fluid, which would also increase the solubility of dolomite (Holland and Malinin, 1979). Alternatively, the pH of the fluid could have been so low that dolostone was dissolved at depth, but the pH of the fluid might have increased upwards in the pipe as a result of this dissolution, until the stability field of carbonate minerals was reached. Dolomite was stable in the "unaltered" zone of the pipe, above the calcitized zone (Fig. 135). This indicates that the ore fluid in the "unaltered" zone had a $m_{Ca^{2+}}/(m_{Ca^{2+}} + m_{Mg^{2+}})$ ratio less than 0,93 at 250°C (Holland and Malinin, 1979). This is consistent with the alteration of dolomite to calcite in the underlying calcitized zone, which would decrease the Ca:Mg ratio of the fluid at higher elevations. A similar explanation cannot be used to explain the change in composition of the carbonate phase on passing from the silicified zone to the calcitized zone. Calcite was the stable carbonate mineral in the calcitized zone, which indicates an extremely high Ca:Mg ratio. However, the presence of minor dolomite (and no calcite) in the underlying silicified zone indicates that this ratio was smaller at depth, and progressive dissolution of dolostone could not increase the ratio in the ascending fluid beyond that in equilibrium with dolomite. This zoning can be explained if fluid mixing is invoked, rather than progressive reaction between rock and a single fluid. The North Break zone intersects the Tsumeb pipe in the vicinity of the calcitized zone and fluid with, for example, a large Ca:Mg ratio might have been introduced to the pipe from this paleoaquifer (Chapter 5.3.5). The lead isotope study indicates that two different components of lead were introduced to the upper and lower parts of the Tsumeb pipe, respectively (Fig. 135). This required the mixing of a minimum of two fluids within the pipe,

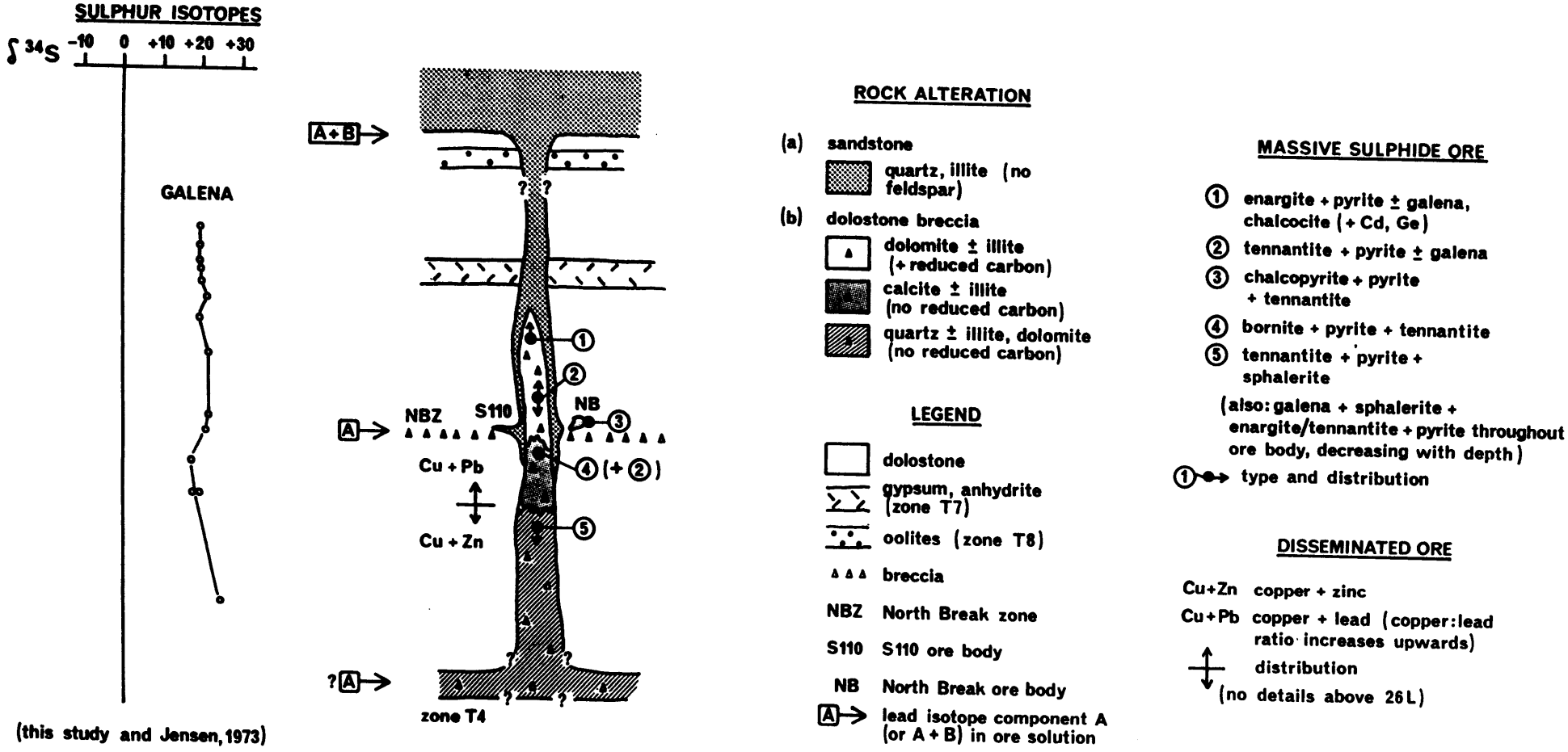

Fig. 135
Alteration zoning, mineralogical zoning and isotopic variation with depth in the Tsumeb pipe.

which may have been chemically, as well as isotopically, distinct. These fluids could have been introduced through steeply dipping faults, as well as through a number of paleoaquifers which intersect the pipe.

It can be concluded that a simple model which involves progressive alteration by a single ore fluid is inadequate to explain the zoning of rock alteration in the Tsumeb pipe. A complex model is indicated, in which compositionally distinct fluids were introduced to the pipe at different elevations, where they mixed and modified their composition by continued reaction with the pipe breccia.

6.2.3. Sulphide mineral zoning and chemical controls of ore deposition.

Mineralogical zoning of sulphide minerals within the Tsumeb pipe is difficult to interpret because of the probable importance of mixing of fluids and metals derived from different sources. Also, it is not known if sulphur was introduced to the pipe in the same fluid as some of the metal (e.g. with one component of the lead). Haynes (1985) proposed a simple model which involved progressive reaction, with systematic changes in the activities of copper, iron, arsenic and hydrogen ion, to explain zoning in the Tsumeb pipe. However, this was based on a different paragenetic sequence and sulphide mineral zonation to that interpreted from the present study (e.g. it assumed some tennantite prior to enargite, some tennantite plus enargite after chalcocite plus bornite, and mostly neglected the effects of early-formed pyrite and sphalerite).

The temporal and spatial relationships observed between enargite and tennantite in the Tsumeb ore body indicate that the sulphur fugacity was highest in the upper part of the ore body where enargite occurs in addition to tennantite (Chapter 6.2.1, Fig. 135). This assumes that there was no major increase in temperature with either time or decreasing depth. The increase in sulphur fugacity could have resulted from an increase in either oxygen fugacity, or total sulphur concentration, of the ore fluid. The negligible variation in the $\delta^{34}S$ values of ore minerals indicates that any

increase in oxygen fugacity was small, although the data do not exclude this as a mechanism. However, enargite-bearing ore only appears in the immediate vicinity of the evaporite horizon in zone T7, and the sulphur isotope data indicate that sulphur in the ore minerals was derived from a sulphur source which had a similar isotopic composition to anhydrite in this horizon. The data are most consistent with an increase in the total sulphur concentration of the ore fluid with increasing elevation within the Tsumeb pipe (i.e. towards the evaporite horizon). The absence of the bornite plus pyrite assemblage from the lower part of the Tsumeb ore body, where tennantite is almost the only copper mineral, is consistent with this conclusion. Tennantite has replaced enargite within the upper part of the ore body, consistent with a decrease in sulphur fugacity with time.

The only important concentration of chalcopyrite observed during the present study is in the North Break ore body, immediately outside the Tsumeb pipe (Fig. 135), and no comparable concentrations are known to have existed in mined-out areas of the Tsumeb ore body (i.e. they are not indicated by polished sections of Tsumeb Corporation Limited, although they might have existed). An equilibrium assemblage of bornite plus pyrite is important within the pipe at the elevation of the North Break ore body. These different mineral assemblages are diagnostic of different fugacities of sulphur, which could have resulted from variations in temperature, oxygen fugacity or total sulphur concentration. Major temperature variation is not indicated by fluid inclusion data, and the magnitude of any oxygen fugacity variation is limited, although not excluded, by the sulphur isotope data. The increase in total sulphur concentration within the Tsumeb pipe, discussed above, is the most probable cause of this zoning of copper-iron sulphide minerals in the vicinity of the North Break ore body. The lead isotope study indicates that the sparsely mineralized North Break zone may have been an aquifer, through which metal-bearing fluid was introduced to the Tsumeb pipe. The above data are consistent with the former presence of a sulphur-deficient ore fluid within this zone: the amount of mineralization increased, and the mineralogy changed, as

the total sulphur concentration of this fluid increased towards the pipe.

Sulphur-deficient fluids with the temperatures and salinities of the Tsumeb and Kombat ore fluids could transport sufficient base metals as chloro-complexes for them to constitute ore fluids. The following computations use the solubility data of Federov et al. (1970) for zinc, and Helgeson (1969) for lead, as discussed in Barrett and Anderson (1982). These data indicate that at 250°C, in 1,0m NaCl solution with pH 4,5 and a total reduced sulphur concentration of 10^{-5}m, 63 ppm lead and 537 ppm zinc are soluble in solution. These values decrease by approximately ninety per cent if the sulphur concentration is 10^{-4}m, the temperature is 50°C lower, or the pH is 5. However, the NaCl concentration chosen is an absolute minimum, and the effect of changing any one of these variables would be largely offset if the NaCl concentration was close to 2,0m (c.f. 1,4m and 3,4m indicated by fluid inclusion studies at Tsumeb and Kombat, respectively). The data of Crerar and Barnes (1976) indicate that hundreds of ppm of copper and iron would be transported by solutions in equilibrium with the chalcopyrite-bornite-pyrite assemblage under the same conditions. These concentrations of greater than 1000 ppm total metal greatly exceed the concentration of 1 to 10 ppm base metals which is the minimum commonly accepted for ore fluids (Crerar and Barnes, 1976). Dilution and an increase in pH would aid the precipitation of sulphide minerals from such a fluid, but the effect of varying parameters other than temperature would be negligible compared with the effect of increasing the concentration of reduced sulphur in the fluid by four orders of magnitude, from 10^{-5}m to 10^{-1}m. An important implication of chloro-complexing is that Tsumeb-type mineralization would not have been copper-rich if the ore fluids had significantly lower temperatures. The copper-deficient nature of Berg Aukas-type mineralization, which also formed at 250°C, indicates that the presence of a suitable source of copper might have been an equally important factor in determining the copper-rich nature of Tsumeb-type mineralization.

It can be concluded from the above that the probable cause of major zoning in the Tsumeb pipe of minerals belonging to the

Cu-Fe-As-S system was an increase in the total sulphur concentration of the ore fluid in the vicinity of the zone T7 evaporite horizon. It follows that, since sulphur was added to the ore fluid from this stratigraphic horizon, the major reason for localization of ore within the Tsumeb pipe was the interaction between this source of sulphur and a metal-rich ore fluid. This conclusion is supported by the close spatial relationship between evaporite horizons and other ore bodies of the Owambo Basin-type ore association (Chapter 4.6.1).

6.2.4 Controls of ore composition in the Owambo basin-type ore association.

Many mineralogical differences between members of the Owambo basin-type ore association can be explained by variations in oxygen fugacity, pH and sulphur fugacity during ore deposition or metamorphic re-equilibration (Chapters 5.1, 6.2.1). For example, chalcopyrite is abundant relative to the bornite plus pyrite assemblage in the Kombat ore bodies, and enargite is rare and very subordinate to tennantite. This indicates a low sulphur fugacity relative to conditions in at least the upper part of the Tsumeb ore body. The presence of minor arsenopyrite in the Kombat ore bodies, and its total absence in the Tsumeb ore body, is consistent with this conclusion (McKinstry, 1963), i.e.:

$$\underset{\text{arsenopyrite}}{4\ FeAsS} + \underset{\text{chalcopyrite}}{12\ CuFeS_2} + 9{,}5\ S_2 \rightleftharpoons \underset{\text{tennantite}}{Cu_{12}As_4S_{13}} + \underset{\text{pyrite}}{16\ FeS_2}$$

The large variations in the $\delta^{34}S$ ratios of sulphide minerals, including chalcopyrite, in the Kombat ore bodies indicate that chalcopyrite was stable in the field within which such variations can occur (Fig. 132). It follows that, since the sulphur fugacity was small, the average sulphur concentration of the ore fluid must also have been small if the pH of the ore fluid was within the range 3-6 estimated for the Tsumeb ore fluid (unless sulphur isotopic or phase re-equilibration occurred during metamorphism). A large variation in oxygen fugacity or pH is indicated by the sulphur isotope data. The presence of minor amounts of the bornite plus pyrite assemblage and traces of enargite indicates that high sulphur fugacity conditions

were also present in parts of the Kombat ore bodies. An unconfirmed report of the MnS_2 mineral, hauerite (Geier, unpub. rept.) would, if correct, indicate an extremely high sulphur fugacity, near that in equilibrium with rhombic sulphur (Vaughan and Craig, 1978). Some of the mineralogical zoning within the Kombat ore bodies probably reflects zoning prior to metamorphism, because phases in different parts of the ore bodies are not in equilibrium. Pyrrhotite plus pyrite (a metamorphic assemblage) is present in slate of the Kombat Formation, but barite occurs with hematite and magnetite on the contact between the Kombat Formation and the underlying Tsumeb Subgroup. These minerals are absent from sulphide mineralization at greater depth in the Tsumeb Subgroup. The significance of iron and manganese silicate minerals which occur on the above contact cannot be evaluated because these mineral assemblages are currently subject to studies by other workers, and have been excluded from this study. Some of these minerals (e.g. tephroite and rhodonite) occur together elsewhere in the world, both in hydrothermal assemblages formed at 300°C and in metamorphic assemblages in very low grade to low grade terrains (Casadevall and Ohmoto, 1977; Peters et al., 1973).

The nearly uniform chemical composition on a regional scale of some types of mineralization (e.g. of Berg Aukas type) indicates that the average metal ratios in these ore deposits were controlled predominantly by the metal ratios in their ore fluids, rather than by variations in other physico-chemical parameters which affected the solubilities of individual elements at the sites of deposition. Major chemical differences between mineralogically distinct types of mineralization, which each show the uniform characteristics noted above, may reflect major differences in the compositions of their ore fluids. An important example is the abundance of copper and characteristic minor elements in Tsumeb-type mineralization, relative to Berg Aukas-type mineralization. Other chemical differences between individual ore bodies of a single mineralogical type are not as well established on a regional scale (e.g. the paucity of arsenic and zinc in the Kombat ore bodies, relative to the Tsumeb ore body). It is not obvious if these differences were caused by different metal ratios in the ore fluids, or by variations in other physico-chemical parameters which controlled the solubilities of individual elements.

Variations in the metal ratios of the ore fluids may also have caused some minor mineralogical differences between ore bodies. For example, the presence of germanite ($Cu_3Fe_{0,5}Ge_{0,5}S_4$) and renierite ($Cu_{2,5}FeGe_{0,5}S_4$) in the Tsumeb ore body, but only renierite in the Kombat and Kipushi ore bodies, may reflect a higher Cu:Fe ratio in the Tsumeb ore fluid (Viaene and Moreau, 1968; Chapter 6.2.1).

The chemical composition of Tsumeb-type mineralization is gradational to that of other types of ore deposit which occur in sedimentary rocks of epicontinental, non-magmatic environments elsewhere in the world (Chapter 4.6.5). For example, the average content of germanium (and possibly gallium) in some extremely copper-deficient zinc ore bodies, in which germanium and gallium occur in sphalerite, is greater than in the Tsumeb ore body (Geldron, 1983). The diagnostic feature of Tsumeb-type mineralization is not its concentration of minor elements, but its mineralogy (i.e. the presence of copper-bearing germanium, gallium and vanadium minerals in an arsenical, base metal sulphide mineralization). Therefore, it was probably the copper-rich nature of the ore fluids which formed Tsumeb-type mineralization, in addition to the minor and trace element content of the fluid, which has made this mineralization unique.

6.2.5 The importance of sedimentary sources of sulphur

Ore deposits which are spatially associated with each other in epicontinental, sedimentary sequences (referred to here as basin-related ore deposits) show mineralogical, chemical and geological similarities to each other, and to the Owambo basin-type ore association. Lead isotope data variously indicate, or are consistent with, genetic relationships between these deposits (Chapters 4.6, 5.3). The sulphur and lead isotope studies of mineralization in the Otavi Mountain Land indicate that evaporite minerals and stratiform pyrite were important sources of sulphur in base metal mineralization, and were also probable causes of ore deposition (e.g. at Tsumeb and locality 14). Spatial relationships and sulphur isotope data indicate that an evaporite horizon in the Tsumeb area may have been the ultimate source of sulphur in

stratiform pyrite, which was itself a source of sulphur for later mineralization (Chapter 5.1.1). It is shown below that this is another important similarity between different types of ore deposit in epicontinental rocks, i.e. there is a close spatial relationship between ore bodies and sedimentary, or diagenetic, sources of sulphur, and there is evidence that some of these sulphur sources have influenced ore deposition.

Sulphur isotope ratios of sulphide minerals in basin-related ore deposits typically have moderately large, positive or negative values, which rarely cluster close to zero per mil. The most positive ratios present in ore deposits which do not show extremely negative values are commonly similar to the ratios of barite in the same deposits. These ratios approximate to the average value of sedimentary sulphate minerals of similar age to the rocks which host the ore deposits. This is true of most Mississippi Valley-type deposits of the U.S.A. ($\delta^{34}S$ typically +10 to +25‰), the Laisvall sandstone lead deposit of Sweden ($\delta^{34}S$ = +18 to +28‰), the Owambo basin-type association, and sedex deposits (Ohmoto and Rye, 1979; Rickard et al., 1981; Large, 1983; Akande and Zentilli; 1984). Sulphur isotope ratios of this type are most consistent with the reduction of crustal sulphate at elevated temperatures.

Sulphide minerals in some basin-related ore deposits show extremely negative sulphur isotope ratios, which are most consistent with near-surface, bacterial reduction of sea water sulphate to form isotopically light hydrogen sulphide. Examples include the Permian stratiform copper deposits of Creta, Oklahoma, and the Kupferschiefer bed, with $\delta^{34}S$ values of -19 to -35‰ and -30 to -50‰, respectively (Lockwood, 1976; Ohmoto and Rye, 1979). Isotopic ratios as light as -36‰ in the sedex deposit at Silvermines, Ireland, have probably been produced in this way, although most sedex deposits fall in the range +10 to +20‰ (Large, 1983). Sulphide minerals from Mississippi Valley-type deposits in Triassic rocks of southern and western Europe (from France to Czechoslovakia) show a range in $\delta^{34}S$ values of +2 to -31‰, with most major deposits averaging -10 to -20‰ (compared with +10 to +15‰ in Triassic evaporite minerals; Schroll and Pak, 1983). Base metal sulphide mineralization in salt

domes of the Gulf Coast, U.S.A. is associated with gypsum and native sulphur in the cap rocks (Chapter 6.3.4). Lead-zinc mineralization also occurs in the cap rocks of salt diapirs in north-western Africa (Rouvier et al., 1985). The $\delta^{34}S$ values of sulphide minerals from one potentially economic occurrence are consistent with a source of bacterially-reduced sulphur (Price and Kyle, 1983).

Other basin-related ore deposits have clearly formed from crustal sulphur, but the origin of their isotope ratios is less certain. Sulphide minerals in the stratiform copper deposits of Zambia and Zaire have $\delta^{34}S$ ratios of up to +16‰, a value similar to that of sedimentary anhydrite within the ore deposits (Fig. 109I). The ratios in sulphide minerals average +10 to 0‰, ranging down to -10‰, and are therefore not very light (Dechow and Jensen, 1965). Similarly, sulphur isotope ratios of sulphide minerals from the stratiform copper deposit at White Pine, Michigan, average +20 to -10‰, isotopically light values being most frequent (Burnie et al., 1972). Schwarcz and Burnie (1973) suggested that sulphur isotope values of this type might reflect bacterial reduction in systems in which the rate of sulphate reduction exceeded the rate of sulphur supply. However, these ratios are equally consistent with the reduction of sulphate ion at elevated temperatures, followed by precipitation of sulphide minerals under conditions of high oxygen fugacity and variable oxygen fugacity or pH (Chapter 5.1).

Sulphide minerals in vein-type mineralization of basement rocks adjacent to sedimentary basins can also contain crustal sulphur. Barite from all important Saxonic occurrences in Germany has a $\delta^{34}S$ ratio of +9 to +13‰, indicating a common source of sulphur in these deposits; this approximates to the value of sea water sulphate of Permian age, which is the probable source (Rösler and Baumann, 1970). Other sources of crustal sulphur are unlikely because Permian sea water sulphate was lighter than sea water sulphate of other ages. Sulphide minerals show a large range of negative $\delta^{34}S$ values at all localities, with a total range of 0 to -33‰, indicating either bacterially-produced H_2S or a high oxygen fugacity of the ore fluids. The common presence of uraninite, hematite and carbonate gangue minerals in these veins is consistent with high oxygen fugacity

conditions. The Saxonic veins of Echo Bay, Canada contain sulphur derived from a heavy source, which Robinson and Ohmoto (1973) suggested was sea water sulphate with a $\delta^{34}S$ ratio of +25‰.

Sulphur isotope data from basin-related ore deposits therefore indicate that a major part of the sulphur in almost all of these deposits is of crustal derivation, and that it has been produced by bacterial reduction, or as the result of reduction at elevated temperatures (although the above suggestion of Schwarcz and Burnie, 1973, is also possible for some occurrences). In addition, it has long been recognized that many basin-related ore deposits are closely associated with evaporite horizons, or with diagenetic pyrite (Davidson, 1965). These deposits include the Owambo basin-type association (in which late diagenetic pyrite is itself interpreted to be localized by an evaporite horizon) and the carbonate-hosted copper deposits of Kennecott, Alaska. Other examples are: (1) Mississippi Valley-type deposits of Triassic age in Europe, and Pine Point, Canada, (2) the sandstone lead and copper deposits at Largèntiere, France, and in Lower Cretaceous rocks of western Africa, and (3) stratiform copper deposits of central Africa, Michigan, the south-western U.S.A., and the Kupferschiefer (in which stratiform pyrite is immediately overlain by evaporites). Base metal deposits which occur in the vicinity of salt basins are also invariably associated with sulphate-bearing sequences (Chapter 6.3.6). It is possible to invoke permeability, produced by evaporite dissolution, as the cause of the above spatial association in only a minority of cases. It is therefore probable that the sulphur minerals have exerted a direct, chemical control on sulphide deposition at many localities, and textural evidence indicates that ore minerals have directly replaced pyrite or anhydrite in some of these deposits (Brown, 1978). However, it is probable that the sulphur was not only supplied directly by the sulphur-bearing minerals, but also by fluids in their vicinity which contained oxidized or reduced sulphur species.

A relationship between sedimentary sources of sulphur and ore bodies is not obvious in all cases, and is not indicated for some sedex deposits, although the relationship exists in some Irish

deposits of this type, and in the Mount Isa and McArthur River deposits of Australia (Wells, 1980). Also, there is evidence that basin-related ore deposits can precipitate by a variety of mechanisms that do not require mixing of separate metal- and sulphur-bearing solutions, e.g. lead-zinc deposits of the Upper Mississippi Valley district and Virginia, U.S.A. (McLimans et al., 1980; Foley et al., 1981). This has also been suggested for the large Mississippi Valley-type ore deposits of the south-east Missouri lead belt, (Hart et al., 1981), although this evidence is equivocal (Hughes et al., 1984). Nevertheless, sulphur in the ore deposits of the south-east Missouri district was locally derived because sulphur isotope ratios of galena in the Old Lead Belt are heavy and range up to +28‰, consistent with a Cambrian to Ordovician source of sulphate (the age of the host rocks; Sverjensky, 1981). However, Wu and Beales (1981) proposed an early Permian age for the mineralization from paleomagnetic data. Permian sulphate minerals have $\delta^{34}S$ ratios close to +10‰, inconsistent with the ratios of the galena. If the Permian age is accepted, the sulphur must have remained in the sequence which hosts the ore body for at least 250 m.y. (i.e. it could not have been introduced from rocks of a different age). The sulphate-bearing rocks which Beales and Hardy (1980) interpret to have existed, or sulphur-bearing fluids or gases associated with these rocks, are a probable source of sulphur in the ore. Locally derived sulphur (in addition to a source of suitable fluid) can therefore be an important factor in localizing mineral districts.

The relationship between basin-related ore deposits and sedimentary sources of sulphur is too common to be coincidental. The data obtained from the present study indicate that sedimentary sources of sulphur, especially evaporite horizons, can be important in localizing ore deposits in their vicinity. It can be concluded that many large ore deposits were probably localized in this manner, that spatial relationships between ore bodies (or mineral districts) and sulphur sources of this type have genetic significance, and that evidence for former sulphur sources can be an important guide to ore during mineral exploration.

6.3 FLUID SOURCE

The lead isotope and sulphur isotope studies indicate that the source of sulphur, and at least a major part of the metal, in ore deposits of the Owambo basin-type association was the sedimentary sequence that hosts the ore bodies. There is no evidence that igneous activity was contemporaneous with mineralization within the mineralized areas. Geological and lead isotope data indicate extensive, lateral migration of large volumes of ore fluid throughout the south-eastern Owambo basin and part of the Katanga Sequence. It is therefore probable that the source of the fluid was also the sedimentary sequence of the area, and it is shown below that this is consistent with constraints imposed by the temperature, composition, and $\delta^{18}O$ ratio of the ore fluid.

6.3.1 Fluid flow and temperatures in sedimentary basins.

Fluid flow within the strata of sedimentary basins can be dominantly of steady-state type, in which the rate of fluid recharge to the basin rocks equals the rate of discharge, or transient type, in which the volumes of both recharge and discharge are insignificant relative to the volume of the rock reservoir. Topographic head in the recharge area is the major driving potential for steady-state flow, and meteoric water is the dominant fluid. Transient flow involves the release of fluids from storage within the basin rocks, e.g. during dewatering of connate fluid from a sedimentary sequence; sediment compaction during burial provides the driving potential (Cousteau et al., 1975; Hitchon, 1976; Hanor, 1979). Fluid flow can also be induced by convection about localized heat sources in some basins (e.g. rift or oblique-slip basins).

It is shown in subsequent discussions that basins dominated by transient flow are probable sources of many basin-related ore fluids. Geopressured fluids in such basins can have pressures equivalent to 50 - 80 per cent of lithostatic load (Jones and Wallace, 1974; Carstens and Dypvik, 1981). Growth faulting facilitates geopressuring to depths of greater than 5000 m by creating closed,

anticlinal, fluid traps, and by sealing aquifers up-dip (Jones and Wallace, 1974). Hot, geopressured fluids can subsequently be released by later faulting, and migrate rapidly out of the basin. Price (1980) argued that petroleum can migrate laterally, up-dip, for at least 600 km (and possibly for thousands of kilometres in some areas). This has important implications for ore fluids, in that mineralized stratal fluids may be able to penetrate thick sedimentary sequences on a regional scale, yet the source of the fluid might be laterally distant from the resulting mineral districts. Sharp (1978) modelled sedimentation in the Ouachita flysch and concluded that migration of overpressured fluids from the flysch basin, northwards to the Mississippi Valley mineral districts, was a feasible process. Cathles and Smith (1983) concluded, on the basis of thermal constraints, that this fluid release would need to be rapid and episodic for such fluids to retain deep basin temperatures at the site of ore deposition. The lateral migration of at least 60 km proposed here for ore fluids in the Owambo basin is therefore consistent with these studies.

The temperature of 250°C indicated for ore fluids in the Otavi Mountain Land provides constraints on the type of basin which could have generated the fluids. Carbonate platform margins can exhibit geothermal gradients as low as 5,5°C/km (Fig. 136). Geothermal gradients in most older basins are in the range of 18° - 30°C/km, and parts of younger basins range up to 45°C/km. Shallow, simple interior basins typically have low gradients, although anomalous gradients in some atypical basins of this type reach in excess of 50°C/km. Back-arc basins commonly have gradients of 50° - 80°C/km, and many rift and oblique-slip basins possess steep gradients, up to 300°C/km in restricted volumes of rock, particularly in their early stages of development (Bailey and Snelson, 1981; Reading, 1981; Fig. 136). The extremely steep geothermal gradient in the Salton trough (curve 1 of Fig. 136) is probably the result of a local thermal high related to magmatism (Crowell, 1981). Steep gradients of this type could be expected in other oblique-slip and rift basins.

Ore bodies which form at 100°C could be produced from fluids derived from most types of basin at depths of 2 to 3,5 km (Fig. 136).

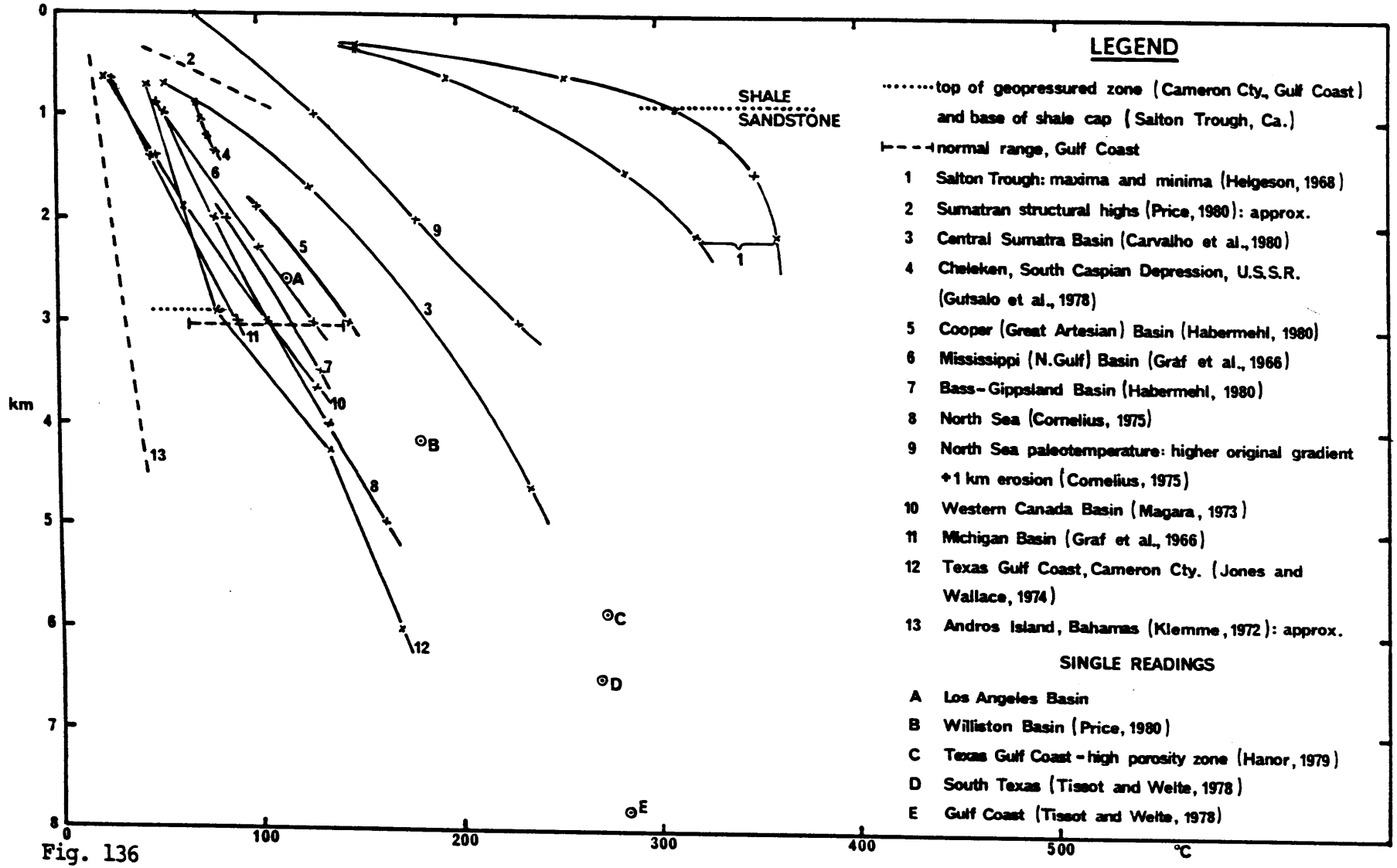

Fig. 136

Temperature variations with depth in sedimentary basins. Extremely low and extremely high temperature gradients occur in carbonate shelf (13) and oblique-slip environments (1), respectively. Higher temperature gradients occur during early stages of basin development (e.g. 9 versus 8), and temperatures of almost 300°C can occur at a depth of only 6km (e.g. C,D).

Depths of less than 5 km would be involved if the fluid temperature was 150°C. However, ore bodies which form at 200°C could not involve fluids from shallow depths in most older basins. These fluids could be produced in young basins at depths of 4 to 6 km. Simple interior basins with anomalously high geothermal gradients (e.g. the Cooper basin) would be too shallow to supply these fluids. Only rift, oblique-slip and back-arc basins are potential sources of ore fluids with temperatures of 300°C at shallow depths. Atypical sediment thicknesses would be required to achieve this temperature in most rift basins unless exceptionally high geothermal gradients, related to shallow magmatic activity, were involved. Ore fluids of the Otavi Mountain Land could therefore have been produced at shallow depths in one of these three types of basin, or at depths greater than 5 km in other basins.

6.3.2 The origin of brines in sedimentary basins

There is a lack of consensus as to the origin of mineralized brines in sedimentary basins. The origin which is probably the most widely accepted is that of membrane filtration, described below, although some workers have emphasized the importance of evaporite-related brines. It is argued here that the latter fluids, particularly connate bitterns and their diluted and diagenetically-modified equivalents, form most mineralized brines of this type. It is shown during later discussion that this is important to the timing of ore deposits during tectonic development of a region, to the spatial distribution of ore deposits, and to the time-dependence of certain types of ore deposit (including Tsumeb-type deposits) throughout geological time.

Many workers have emphasized the importance of membrane filtration in producing saline waters and brines from sea water (White, 1965; Billings et al., 1969a, b; Hitchon and Friedman, 1969; Hitchon et al., 1971; Barnes and Hem, 1973; Hanor, 1979). Chemico-osmosis results from the difference in anionic concentration between two aqueous solutions, subjected to equal pressures and temperatures and separated by a semi-permeable (e.g. shale) membrane. This difference results in the movement of water but not solute

across the membrane, from the more dilute to the more concentrated solution (van Everdingen, 1968). If a sufficient pressure gradient exists to drive water upwards against a chemico-osmotic gradient, membrane filtration of charged species will occur. The water on the input side will then become progressively more saline (Hanor, 1979).

Some workers have questioned the ability of membrane filtration to produce saline fluids, and have emphasized the importance of evaporites as sources of brine (Carpenter et al., 1974; Carpenter and Trout, 1978; Hobson, 1980). The evidence advanced for membrane filtration is: (1) the theoretical efficiency of the membrane filtration process, (2) the presence of brines, but apparent lack of evaporites, in some basins, and (3) geochemical evidence. The first argument is questioned by the above authors, the second proved difficult to substantiate during this study, and evidence advanced for the third argument is equivocal. Hanor (1979) quoted the observation of White (1965) that saline waters are known from evaporite-free basins. White (1965) referred to Chave (1960), and data in White et al. (1963), in support of this statement. Chave (1960) cited the Illinois basin and the Tertiary coastal basins of California as examples of evaporite-free basins. The most saline water sample which Chave (1960) listed from the Illinois basin is from the St. Genevieve Limestone. Evaporites do occur in the Illinois basin (de Witt et al., 1979) and are best developed in the St. Louis Limestone, which immediately underlies the St. Genevieve Limestone. Evaporites are also known from the Tertiary of California, in the Salton trough (Dibbler, 1955). Oblique-slip basins adjacent to the San Andreas fault contain marine, lacustrine and fluvial sediments, and conditions suitable for evaporite development can occur during the initial stages of formation of basins of this type, while the basins are enclosed or subjected to intermittent marine incursions. The above examples of evaporites now consist of gypsum and anhydrite, but halite may formerly have been present.

The data referred to in the second reference, White et al. (1963), are analyses of two brines from the Michigan basin which are "not known to be associated with crystalline salt deposits".

However, Hanor (1979) noted the Michigan basin to be "characterized by the presence of evaporites", which include halite. Evidence for the origin of the brines from the Michigan basin can be obtained by use of the Cl versus Br plot of Carpenter (1978; Fig. 137). Bromine is a useful tracer element because: (1) it is commonly abundant in brines, (2) it does not participate in diagenetic reactions, and (3) it concentrates in residual brine solutions. Figure 137a illustrates the evolutionary trend of evaporating sea water with respect to Cl and Br. The Cl:Br ratio remains constant until the halite saturation point is reached at the inflexion of the curve. Compositions on the curve to the right of this point represent brines which would coexist firstly with precipitated halite, and then with magnesium and potassium salts. The effect of mixing sea water and a halite-saturated brine (e.g. A), which is no longer in contact with halite, is also shown. Mixtures would lie along the curve A-B-sea water. The mixing of brine A with fresh water would result in a trend A-E parallel to the sea water evaporation trend. The dissolution of halite by sea water would result in the curve sea water-D. A brine such as B could also be produced by a more complicated path, such as the mixing of brine C and fluid D in the correct proportions. The data of White et al. (1963) for brines from the Michigan basin reveal no evidence of halite dissolution (as noted by these authors), but clearly indicate connate evaporitic brines (Fig. 137b). White et al. (1963) noted the low Cl:Br ratios of Na-Ca-Cl brines in general.

Carpenter (1978) presented evidence for a connate evaporitic origin of mineralized Na-Ca-Cl brines from Mississippi, using Cl:Br ratios (Figs. 137d-e, 140). These ratios indicate that most of these brines have not mixed significantly with meteoric or connate sea water. They have also not been derived by dissolution of salt deposits, although such brines are known elsewhere (McClure, 1973; Anderson and Kirkland, 1980; and the Tertiary of Louisiana in Figure 137f). The evidence indicates that the Mississippi brines are connate fluids, probably derived from the underlying Louann Salt, and the δD and $\delta^{18}O$ ratios of brines from this area are consistent with this origin (a meteoric origin is also possible because of the isotopic similarity of meteoric water and sea water at this latitude;

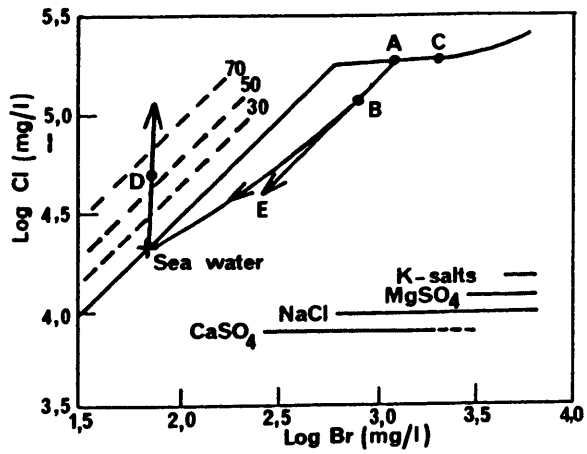

(a) EXPLANATORY DIAGRAM
(see text for details)

50 30 % of Cl in brine contributed by dissolved halite

Carpenter (1978)

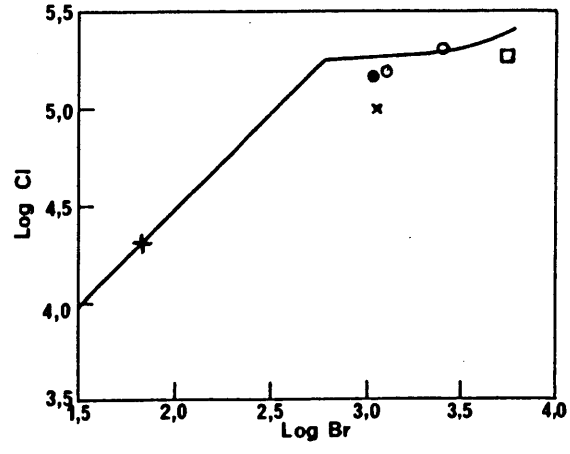

(b)

- o Michigan-basin brine (White et al., 1963)
- ● Michigan-native copper (White, 1965)
- □ Saskatchewan-unconformity uranium (Pagel et al., 1980)
- × Buick mine, SE Missouri-MVT (Panno et al., 1983)

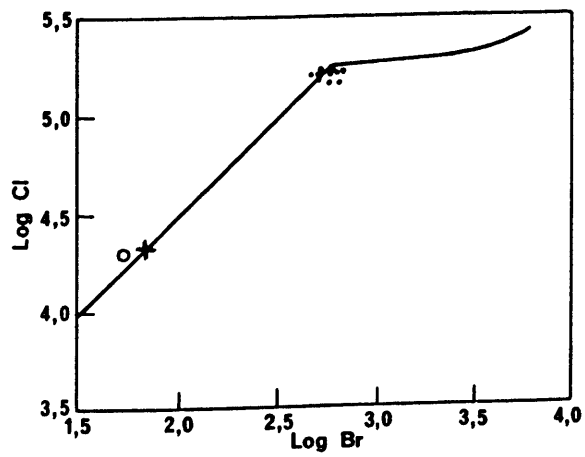

(c) CHELEKEN

- • Na-Ca-Cl brine (mineralized)
- o HCO_3-SO_4 water

Lebedev (1972)

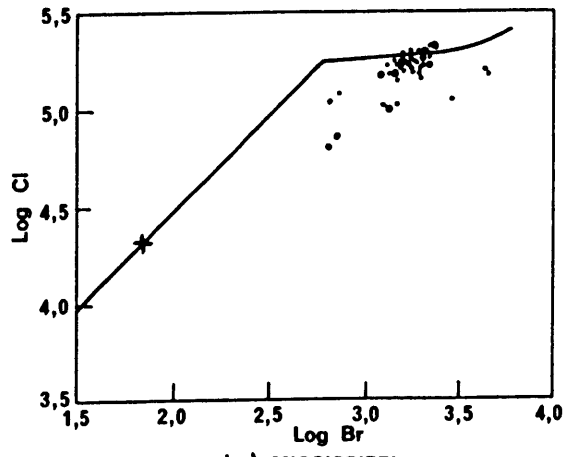

(d) MISSISSIPPI

- • Smackover Formation
- • Cotton Valley Formation

} Jurassic

Carpenter (1978)

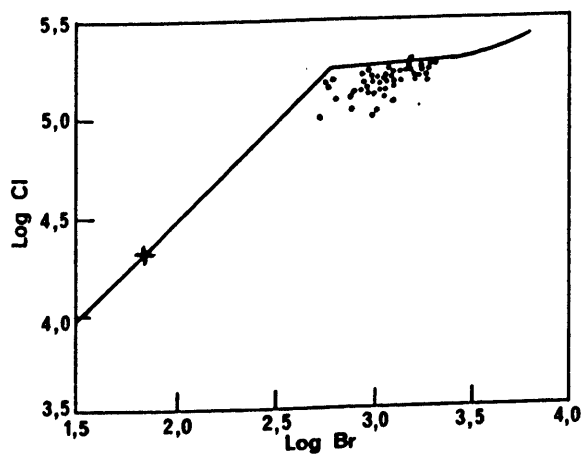

(e) MISSISSIPPI

Hosston Formation (L.Cretaceous) - mineralized (Carpenter, 1979)

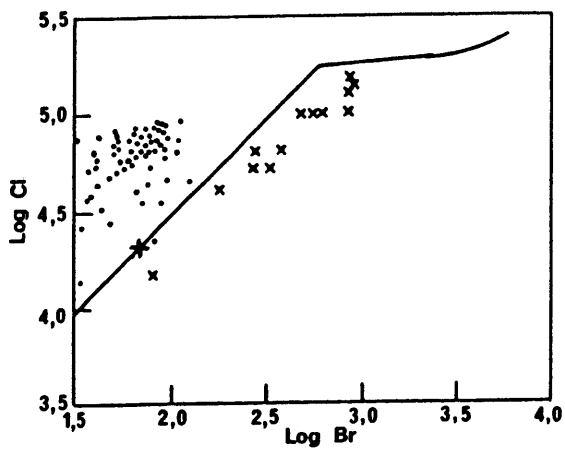

(f)

- • Tertiary, Louisiana (Collins, 1975)
- × Edwards Group (L.Cretaceous), Texas - mineralized (Land and Prezbindowski, 1981)

Fig. 137

Chlorine-bromine plots of stratal fluids in sedimentary basins. (a) Curve "sea water - A - C" shows the variation in sea water composition during evaporation, and therefore possible compositions of stratal fluids formed in this manner. Curves "A - B - E" and "A - B - sea water" show the compositions of fluids formed by mixing with fresh water and sea water, respectively. Sea water which dissolves halite evolves along curve "sea water - D". (b) - (f) Compositions of present-day stratal fluids and fluid inclusions from ore deposits.

Clayton et al., 1966). The Cl:Br ratios of mineralized brine from Cheleken, U.S.S.R., indicate that this fluid also had a connate evaporitic origin (Fig. 137c); this origin is supported by the $\delta^{18}O$ and δD ratios (Gutsalo et al., 1978).

The third type of evidence advanced in support of membrane filtration is geochemical. Billings et al. (1969a) found positive linear correlations between the total dissolved solid (T.D.S.) content and the K:Na, K:Li and Rb:Li ratios of saline waters and brines of the Western Canada basin. They considered this to be evidence for membrane filtration. However, they also noted a positive, linear relationship between the K:Na ratio and temperature. These results could alternatively be explained by diagenetic reactions, such as the sympathetic dissolution of potassium minerals and the formation of sodium minerals (e.g. feldspars), or by the mixing of fluids with different compositions and temperatures. Billings et al. (1969b) presented plots of T.D.S. versus Br for fluids from the Western Canada basin which indicate that the brines studied were less saline than those from Mississippi. They may therefore be connate fluids which have not quite reached the point of halite saturation, or more saline connate fluids which have mixed with a component of sea water or meteoric water. These fluids were studied isotopically by Hitchon and Friedman (1969) and were found to have a large component of meteoric water, confirming the latter interpretation (most of the basin is undergoing steady-state flow).

It has been argued that the Cl:Br ratio may not be an unambiguous indication of the ultimate origin of a brine. The argument presented above assumes that brine derived from the dissolution of halite has the same Cl:Br ratio as the halite, and this requires that the halite is totally dissolved. This is a geologically reasonable assumption because halite beds have an extremely low porosity and permeability subsequent to burial, and dissolution can be expected to concentrate at an interface between halite and a fluid. However, Land and Prezbindowski (1981) argued that, if partitioning of bromine between halite and a fluid was a reversible, equilibrium process, then a solution formed by dissolution of halite precipitated from sea water should have a Cl:Br

ratio exactly that of sea water, not halite. They therefore considered that some brines with a low Cl:Br ratio may have formed by dissolution of halite. There are two objections to this argument, other than the impermeability of halite. The first is that the Cl:Br ratio of sea water is considerably smaller than that of many brines, including the metal-bearing Na-Ca-Cl brines of the Edwards Group of Lower Cretaceous age which Land and Prezbindowski (1981) studied from the South Texas basin (i.e. up-dip from the Louann Salt). They suggested that this could be explained if the partition coefficient between halite and fluid varied significally with temperature. The second objection is that brines of this type would need to extract their bromine from a volume of undissolved halite very much larger in volume than the brine. For example, a brine which contains 25% NaCl and 800 mg/l Br would need to extract its bromine from a more than twenty times greater volume of undissolved halite (i.e. with a bromine content of 130 ppm; Kaup and Hite, 1978). The chlorine and bromine contents of basin fluids are therefore thought to provide a powerful tool for evaluating the origins of such fluids. The data from the Edwards Group, discussed by Land and Prezbindowski (1981), plot close to the evolution trend for evaporating sea water, and indicate a brine evaporated slightly past the point of halite precipitation which has mixed with meteoric water or connate water (Fig. 137f).

Salt basins commonly contain large bodies of evaporite minerals (e.g. 500-4000 km long, 100-600 km wide, 1-7 km thick; Fig. 140), and they form over relatively short periods of time (e.g. less than 10 m.y.; Kinsman, 1975). Large volumes of brine will be associated with salt basins, and the rapid sedimentation in these basins will increase the probability that brine will be preserved at depth. Salt has a very low permeability subsequent to burial, and the presence of brines in aquifers immediately below some salt horizons (Cousteau et al., 1975) indicates that salt may be able to trap its own connate fluids. Therefore brine might not be trapped in pore spaces within salt but could be retained in formations which underlie, overlie, are interbedded with, or occur adjacent to the salt. For example, consider a basin which contains 1000 x 200 x 2,5 km of halite deposited from a brine which precipitated 50 per cent of

its contained salt. If only one per cent of this fluid was buried and became an ore fluid with a total content of only 200 mg/l metal, the ore fluid could form 900 ore bodies of comparable size to either Tsumeb or a stratiform copper ore body (i.e. 25 million tonnes of 25 per cent metal, or 200 million tonnes of 3 per cent metal). A small basin with only 300 x 50 x 1 km of halite could produce 27 ore bodies. However, the volume of halite deposited in a salt basin is no indication of the maximum amount of brine originally present if the brine formed by evaporation to slightly less than the point of halite precipitation. A brine of this type could have a salinity in excess of 25 per cent.

It is concluded that there is little evidence that brines can be produced by membrane filtration, and sea water concentrated by evaporation to form brine or halite is the source of most major dissolved components in basin brines. In particular, mineralized brines found in some basins are connate fluids expelled from evaporites, and large bodies of halite in major salt basins indicate that these basins had the potential to produce huge volumes of potential ore fluid. It is shown below that this model also has important implications for the tectonic setting and timing of basin-hosted ore deposits.

6.3.3 The compositions of contemporary, mineralized basin fluids

The highest concentrations of base metals found in basin fluids occur in very concentrated Na-Ca-Cl and Ca-Mg-Cl brines (Krejci-Graf, 1978; Carpenter and Grethen, 1979; Hobson, 1980). These are mostly low temperature brines which occur in petroleum traps in basins which are no longer actively dewatering, and larger metal concentrations could be expected in hotter brines within geologically young basins. Mineralized brines of Cheleken (U.S.S.R.), central Mississippi, the Western Canada basin, and the Salton Sea are considered in detail in Chapter 6.3.4. However, numerous other mineralized brines have been reported from the south-eastern Russian platform, the Baku Archipelago (near Cheleken), the Irkutsk basin, the Angara-Lena basin (all in the U.S.S.R.), Germany (in Permian salt), Algeria, Kansas, and from brines in Texas

and Alabama which are probably genetically related to the brines of central Mississippi (McClure, 1973; Krejci-Graf, 1978; Lur'ye, 1978; Carpenter and Grethen, 1979; Hobson, 1980; Land and Prezbindowski, 1981).

The range of metal concentrations found in these mineralized brines is: iron 10-2000 ppm, manganese 1-100 ppm, zinc 5-500 ppm, lead 1-100 ppm, and copper 1-10 ppm (rarely 100 ppm). There is an unconfirmed report of 1000 ppm copper in oilfield brine from Algeria (Ranoux, 1962). Other elements of interest to this study are rarely analysed in basin fluids. Arsenic is only known to exceed 10 ppm in a few fluids (both brine and dilute bicarbonate water), but a concentration of 243 ppm arsenic has been reported from brine in a modern playa (White et al., 1963; Krejci-Graf, 1978; Hobson, 1980). Many brines contain 1-6 ppm lithium, but concentrations of 200-300 ppm are known (Carpenter and Trout, 1978). The barium and boron concentrations of brines are commonly 10-100 ppm (exceptionally 1000's of ppm), and beryllium and chromium are concentrated in some brines (White et al., 1963; White, 1965; Schmidt, 1973; Krejci-Graf 1978; Carpenter and Grethen, 1979; Hobson, 1980). Petroleum can contain large concentrations of the same elements which are concentrated in organic and phosphatic sediments (Hunt, 1979). Nickel and vanadium concentrations of 100 ppm and 1000 ppm, respectively, are common and the following maximum concentrations of other elements have been recorded (in ppm): Co (15), Mo (345), Hg (23), Ge (0,7), Ga (0,3).

The sulphur concentration is small in many basin brines, including some mineralized brines, the sulphur being lost at an early stage by precipitation of anhydrite or pyrite, or loss of hydrogen sulphide (Table 11; Carpenter, 1978; Carpenter and Grethen 1979; Hanor, 1979). This is consistent with the model discussed in Chapter 6.2.5, in which sulphur is added to the ore fluid close to the site of ore deposition. Also, many mineralized brines have a small total concentration of reduced sulphur species (e.g. less than 10^{-5}m). This is consistent with chloro-complexing of the contained metals, since large concentrations of base metals can be transported in this manner in such brines (Barnes, 1979).

TABLE 11

CONTEMPORARY MINERALIZED FLUIDS

	UNIT	Fe	Mn	Cu	Pb	Zn	Cd	Ag	As	H_2S	SO_4	S	pH (25°C)	Eh	Total dissolved solids	T°C	Major elements	References
Cheleken,* U.S.S.R.	mg/l		45	2-8 (15)	15 (77)	4	2 (6)		0,4	7	150-470		5,9	+100-+185mV	27%	75°	Na-Ca-Cl	Lebedev (1972) Gutsalo et al (1978)
Western Canada Basin	mg/l	0,5 (3)	6	0,1 (0,3)		19 (290)				2					9-31%	76° (119°)	Na-Ca-Cl	Billings et al (1969c) Carpenter (1979)
Central Mississippi	mg/l	(400)	(150)	1	10-80 (110)	180 (360)				2			4,3 (at 130°C and 390 bar)			100°-150°	Na-Ca-Cl	Carpenter et al (1974) Carpenter (1979) Hobson (1980)
Salton # Trough, California	ppm	3000	1000	20	100	500	2	2	12			16-30 (probably SO_4)	5,2 (minimum 4,7)		26%	330°	Na-Ca-Cl	White (1968) Hitchon (1977) White (1981)

* B(20), Li(8), Mo "anomalous
# B(500), Li(320), Ba(200), Ni(2), Be/As/Sb (trace)
Maximum values given in brackets

The pH of basin brines, both mineralized and unmineralized, is normally in the range which has been predicted for brines which form base metal ore deposits, including ore bodies of the Otavi Mountain Land. Also, this range includes pH values at which brines can transport large amounts of metal as chloro-complexes. Basin brines have a normal pH range of 4,5 to 9,5 (at 25° C), but few brines exceed pH 7,5 and values as low as pH 3,0 have been measured (White et al., 1963; Hitchon, 1977; Krejci-Graf, 1978; Hobson, 1980). The pH values of mineralized brines in Mississippi and Texas have been modelled under reservoir conditions, and estimates of pH 4,3 (at 130° C and 390 bar) and pH 5,7 (at 138° C and 787 bar) obtained, respectively (Sverjensky, 1984). Positive Eh values are confined to shallow depths, and brine values can be as negative as -450 mV to -600 mV at pH values less than neutral (Boulegue, 1978; Hobson, 1980).

It is concluded that elements which occur in the ores and alteration zones of the Owambo basin-type ore association can occur in significant concentrations, mostly x to xooo ppm, in basin fluids. These elements include Fe, Mn, Cu, Pb, Zn, As, Ag, Ba, Li, B and Be. The highest concentrations of most of these elements are found in brines, particularly concentrated Na-Ca-Cl brines, which contain only a small concentration of reduced sulphur, and which have similar pH and Eh values to those predicted for the Tsumeb ore fluid. The minimum total concentration of base metals which an ore fluid (as distinct from a mineralizing fluid) must contain is commonly accepted as 1-10 ppm (Barnes, 1979). The above basin brines are therefore potential ore fluids. Molybdenum, Ge, Ga and Hg, elements also anomalous in Tsumeb type ore, can occur in significant concentrations in petroleum.

6.3.4 The tectonic setting and origin of contemporary, mineralized brine

Well documented examples of metal-bearing basin fluids range in composition from low to high temperature, marine connate to meteoric, brines (e.g. Table 11). The brines occur in sequences of

red-beds and sedimentary carbonate rocks, in tectonic environments which range from platforms to rift basins and oblique-slip basins. It is shown below that many of these brines are spatially associated with petroleum and genetically related to salt basins.

(a) Cheleken, U.S.S.R.

The mineralized geothermal brine, and associated petroleum, of Cheleken occurs at depths of 200-1500 m on the north-eastern margin of the South Caspian basin (Table 11). The Cheleken brine, metal-bearing brine farther to the west, and economically important petroleum and natural gas, are associated with structural highs along the northern margin of the basin (Dvorov and Pavlov, 1978; Lur'ye, 1978). The basin contains evaporites and a thick shale and red-bed sequence of Tertiary age, and the presence of "volcanoes" of gas, petroleum and mud along the northern margin of the basin indicate that the sediments are actively dewatering (Gorin, 1964; Davidson, 1967; Lebedev, 1972; Degens and Paluska, 1979).

The δD and $\delta^{18}O$ ratios, and bromine and chlorine concentrations, of petroleum-associated water (e.g. bicarbonate-sulphate water) from the area indicate that it consists of evolved, connate sea water (Fig. 137c). Data from the mineralized brine plot close to the point of halite precipitation on a Cl:Br plot (i.e. it is a connate bittern). The stable isotope data indicate that the mineralized brine is an evolved mixture of sea water and meteoric water, with no component of magmatic water required by the data (Gutsalo et al., 1978). Sulphide minerals in the reservoir rocks have $\delta^{34}S$ ratios of +11 to +15‰. It can be concluded that the metal-bearing fluid is a connate brine expelled from salt beds in an actively dewatering basin, and that sulphide minerals which precipitated from the brine contain sulphur derived from evaporitic sulphate minerals (possibly from anhydrite beds which occur at Cheleken).

(b) Central Gulf Coast, U.S.A.

Rifting commenced in the Gulf of Mexico during the Triassic to Early Jurassic, and rift basins with salt up to 1500 m thick, the Louann Salt, formed in the Middle Jurassic (Fig. 140, 141c). This was followed by sea-floor spreading, subsidence and the formation of major basins and carbonate banks (Buffler et al., 1980; Moore and Druckman, 1981). Metal-rich brine from the Mississippi salt basin has been described in detail, and there are brief references to metal-bearing brines in Texas and Alabama. The former presence of mineralized fluids is indicated by the presence of mineralization in the Northern Gulf basin, the North Louisiana salt basin, the South Texas basin, and the upper Gulf Coast, Texas. Tertiary (but not Mesozoic) sediments of the region are still actively dewatering (Carpenter et al., 1974; Carpenter, 1979; Carpenter and Grethen, 1979; Land and Prezbindowski, 1981; Moore and Druckman, 1981; Figs. 137d-f).

The mineralized brine of the Mississippi salt basin occurs in Lower Cretaceous rocks at depths of 2,5 to 4 km over an area of at least 5000 sq. km (Table 11). The bromine and chlorine concentrations of unmineralized brines in underlying Jurassic rocks indicate that these fluids formed as interstitial fluids at the time of precipitation of the Louann Salt (Carpenter, 1979; Fig. 137d). The metal-bearing brine in Lower Cretaceous rocks of the Hosston Formation occurs 1200 m above the Smackover Formation of Jurassic age; the Cl:Br ratio of this fluid indicates that it has a similar composition to the Jurassic brine, but that it has been diluted slightly with fresher water (Fig. 137e). The Louann Salt does not appear to be the source of the lead and zinc in the brine, because brine in the rocks closest to the salt is uniformly low in these metals and there is an upward increase in metals with distance above the salt. Carpenter et al. (1974) suggested that the metals were derived from shale of the Cotton Valley Group during cross-formational movement of brine, although Carpenter (1979) favoured derivation from red-beds in this group.

Minor lead and zinc sulphide mineralization occurs in ooid grainstone of the Smackover Formation in the North Louisiana salt basin (Moore and Druckman, 1981), and in the sulphur-rich cap rocks of at least fourteen salt domes in the northern Gulf basin, Louisiana, and the upper Gulf Coast, Texas (Siebenthal, 1915; Hanna and Wolf, 1941; Price and Kyle, 1983; Chapter 6.2.5). The salt domes have trapped fluids, including petroleum and brine, adjacent to their margins, and the brine has probably been derived from the underlying Louann Salt. Potentially economic mineralization at the Hockley salt dome, Texas, with which minor uranium mineralization is associated, was deposited from highly saline brine at 120°-140° C, equal to the present temperature of the Louann Salt at depth (Price and Kyle, 1983). The lead isotopic composition of galena from this salt dome is identical to that of lead in metal-bearing brine elsewhere in Texas. Mineralization in some salt domes, including Hockley dome, is at least as young as Cenozoic, and in one case is Oligocene or younger (e.g. Siebenthal, 1915; Price and Kyle, 1983). This mineralization must have formed more than 100 m.y. after deposition of the salt, possibly because the highly impermeable salt was an ideal aquiclude which could trap connate fluid (consistent with the presence of mineralized, connate brines more than 150 m.y. old elsewhere in the basin). A close spatial relationship between Mississippi Valley-type mineralization, sedex mineralization and Triassic salt diapirs has also been reported from north-western Africa (Rouvier et al., 1985). Some of this mineralization occurs in Oligocene rocks, at least 150 m.y. younger than the salt with which it is intimately associated.

(c) Western Canada basin.

Metal-bearing brine occurs in petroleum reservoirs in carbonate rocks of Middle Devonian age in the Western Canada basin (Table 11; Billings et al., 1969c). Most fluid in this basin is undergoing steady-state flow, and the basin is being flushed with meteoric water (van Everdingen, 1968; Hitchon, 1969a, b). However, evolved connate fluids remain in parts of the basin (Magara, 1973), and most brines probably contain a major component of connate fluid (Chapter 6.3.2). The metal-bearing brine may have leached its metals

from shale of the Mackenzie basin, to the north (Billings et al., 1969c). Concentrations of up to 3216 ppm zinc and 82 ppm lead occur in the basal shale (Smith et al., 1983), although these large values probably reflect enrichment by the brine. The source of the brine may be salt deposits which are known to underlie the shale. Billings et al. (1969c) suggested that the brine was expelled from the Mackenzie basin to its present location through a conduit provided by the Presqu'ile reef.

(d) Salton trough, California

The Salton trough is a pull-apart basin of Tertiary age beneath which a spreading centre may exist. It is located between the San Andreas fault and two adjacent faults (Crowell, 1981). Playa evaporites within the trough are overlain by more than 6000 m of sedimentary rocks of Tertiary age, which have mainly been derived from the Colorado River, and these are overlain by gypsiferous shale of Plio-Pleistocene age. The rocks which contain the mineralized fluid have been converted to low grade metamorphic rocks by the Salton Sea geothermal system, the volume of which is at least 116 km^3 to a depth of 3000 m (White, 1981; Table 11). Fluid flow is probably caused by convection in the vicinity of a local thermal high related to magmatism (Chapter 6.3.1).

The δD and $\delta^{18}O$ ratios of the metal-bearing brine indicate that its water has a dominantly meteoric origin; a small component of magmatic water could be present, but is not required by the data. The brine has a very large Cl:Br ratio (i.e. larger than sea water), consistent with an origin by solution of playa evaporites (White, 1968, 1981), although a connate playa origin is also possible. The isotopic compositions of strontium and lead in the brine indicate that these metals could have been derived from the Tertiary rocks (e.g. from feldspar and mica) by high-temperature interaction with the brine; a component of magmatic lead could be present, but is not required by the data. Sulphide minerals in the brine reservoir have $\delta^{34}S$ values of -1,5 to +3 ‰, and White (1981) interpreted this as evidence for magmatic sulphur. However, the sulphur isotopic ratios of sulphide minerals would be 20 ‰ lighter than that of the fluid

under the conditions which Helgeson (1968) modelled for the brine, and evaporitic sulphate minerals are a probable source of the sulphur.

The Salton trough may be representative of smaller rift and oblique-slip basins which contain small hydrothermal systems driven by magmatic heat energy, in which heat is possibly the only significant form of magmatic input. Compaction dewatering and hydrodynamic flushing could be expected to dominate in larger rift and oblique-slip basins with less intense, and less localized, heat sources.

(e) Conclusions

It is concluded that many mineralized brines in sedimentary basins are connate bitterns associated with the dewatering of evaporitic rift basins and major salt basins, or with thermal convection within such basins. A spatial relationship exists between these fluids and petroleum. The metal contained in the brines may have been derived from the aquifer rocks during migration of the fluids, and not from the source areas of the brines. Sulphide minerals present in reservoir rocks which host the brines contain crustal sulphur, which is probably derived from evaporite sequences similar in age to the sources of the brines. Potential ore fluids of this type can be retained within sedimentary sequences for in excess of 150 m.y.

6.3.5 Comparison with ore fluids which form basin-related ore deposits

It is shown above that some stratal fluids in sedimentary basins, particularly connate fluids expelled from evaporites, are potential ore fluids. The pH, Eh, chemical composition, and to a lesser extent temperature, of such brines are similar to those predicted for ore fluids in the Otavi Mountain Land. Also, the range of calcium concentrations of 10^{0}m to 10^{-2}m shown in Figure 132 is the entire range in brines which occur in sedimentary basins. The range of total carbon concentrations found in these fluids is more

variable; 10^{-1}m is the maximum normal concentration, and 10^{-2}m is more typical. The Ca:Mg ratios required to cause calcitization of dolomite at 250°C are also similar to those found in some Na-Ca-Cl brines (Hitchon, 1977; Sverjensky, 1981). The characteristics of the fluids which form many other types of basin-hosted ore deposit are discussed below, and are found to be consistent with an origin as basin brines.

Fluid inclusion data indicate that a number of types of basin-related ore deposit formed from brines with the low to intermediate temperatures characteristic of stratal fluids at depth in basins, i.e. mostly 100°-250°C. These include stratiform copper deposits, native copper deposits, sandstone lead deposits, sedex deposits, Mississippi Valley-type deposits (including Berg Aukas-type mineralization), unconformity uranium deposits (the Shinkolobwe - type mineralization also contains brine inclusions), and Saxonic veins and associated lead-rich veins in basement rocks (Fig. 138). There have been few fluid inclusion studies of stratiform copper, sandstone lead, or sedex deposits, partly because of the small grain-size and lack of gangue minerals in these ore deposits, so the examples given in Figure 138 are not necessarily typical of these deposits. However, although workers who favour a syn-sedimentary origin for stratiform copper deposits have commonly implied a low temperature origin for these deposits (e.g. the sabkha-diagenetic model, Smith, 1974), it has not been demonstrated that low temperature origins are true of all (or any) of these deposits. The temperature of 145°C from the Kamoto stratiform copper deposit, Zaire, is supported by relationships in the Michigan copper district, U.S.A., where native copper deposits in conglomerate, sandstone and lava are closely associated with stratiform chalcocite mineralization in overlying shale. The temperature shown in Figure 138 is estimated from the prehnite-pumpellyite grade metamorphic event with which the native copper deposits are thought to be genetically related (i.e. 250° - 300°C). Jolly (1974) proposed that the ore fluids were produced by dehydration reactions within the volcanic sequence, but the data are more consistent with the circulation of brines which originated outside the sequence.

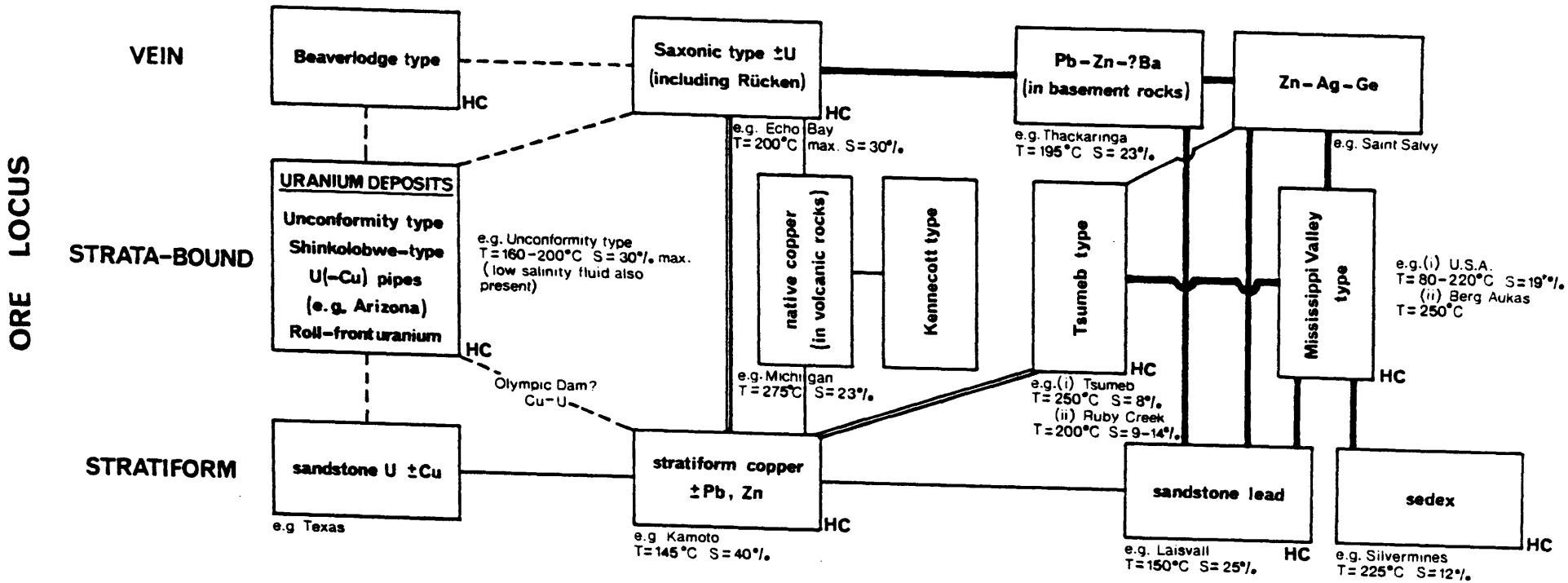

Fig. 138

Relationships between ore deposits in sedimentary rocks of epicontinental environments (unrelated to igneous intrusive activity).

There are similarities between the chemical composition of stratal fluids and the compositions of saline waters and brines which form basin-related ore deposits, in addition to the similar temperatures of these deposits (Fig. 138). Only minor differences exist between the compositions of fluid inclusions from Mississippi Valley-type ore deposits and the Mississippi brines discussed in Chapter 6.3.4. (Carpenter, 1978; table 11). The main differences are the higher salinity and lower potassium and sulphate contents of the Mississippi brines relative to the fluid inclusions, i.e. 713 c.f. 2800 ppm and 15 c.f. 2000 ppm, respectively (also see Sawkins, 1968). A large variation in potassium concentrations (700-8000 mg/l) occurs in the Jurassic to Cretaceous brines of Mississippi discussed above, probably because of diagenetic reactions between the brines and the aquifer rocks, and this difference may not have genetic significance (Carpenter, 1978). A brine with the composition of the fluid inclusion brine could otherwise be derived from the Mississippi brine by simple mixing with more dilute, sulphate-rich fluid. Panno et al. (1983) used Cl:Br ratios of whole rock samples from the Buick ore body to show that connate evaporitic brines might have been important in forming the Mississippi Valley-type deposits of the south-east Missouri district. Also, the small Cl:Br ratio of Ca-Na-Cl brine from a "drip" within amygdaloidal lava of the native copper mines of Michigan, U.S.A. (White, 1965) indicates that it has a connate evaporitic origin (Figs. 137b, 138). Fluid inclusions from copper-bearing calcite veins at this locality also consist of Ca-Na-Cl brine (Kelly and Nishioka, 1985). The δD ratios of fluid inclusions from the Mississippi Valley region are 0 to -25 ‰ (Taylor, 1979), consistent with formation from a fluid of largely connate origin (but not diagnostic of this origin, because of the latitude dependence of δD values). The above evidence is consistent with the highly saline nature of connate evaporitic brines, which makes them ideal ore fluids because of their ability to transport base metals as chloro-complexes (Barnes, 1979).

Some Saxonic veins and other types of uranium mineralization have formed from fluids similar to those which formed strata-bound base metal deposits. Fluid inclusion and mineral studies show that Saxonic veins at Echo Bay, N.W.T., and Cobalt, Ontario, formed from

highly saline fluids with a low total sulphur content, i.e. less than 10^{-2}m (Scott and O'Connor, 1971; Robinson and Ohmoto, 1973). The $\delta^{18}O$ value of the Echo Bay ore fluid, calculated from mineral studies, was very constant at +1‰ SMOW during the mineralizing event, consistent with an ore fluid derived from connate or sea water (note, however, that the oxygen isotopic composition of Proterozoic sea water may have differed from that of Phanerozoic sea water). Robinson & Ohmoto (1973) favoured an origin by boiling of sea water at shallow burial depths, but noted other possibilities, including the heating of connate, evaporitic brine. Both unconformity-type and Shinkolobwe-type uranium deposits contain fluid inclusions of very concentrated Na-Ca-Cl brine, and those from the unconformity uranium deposits indicate moderately high temperatures (Fig. 138). Fluid inclusions in an unconformity-type uranium deposit in which this ratio was determined have a small Cl:Br ratio, consistent with a connate, evaporitic origin (Derriks and Vaes, 1956; Pagel and Jaffrezic, 1977). There is also evidence for mixing between brines and dilute fluids with a high carbon dioxide content in unconformity deposits, and it is not known which fluid contained uranium. For example, Dunsmore (1977) noted that uranium might become concentrated in connate, evaporitic brines, consistent with the Cl:Br data of Figure 137b, without the need for a separate source of uranium. However, Ypma and Fuzikawa (1980) recorded that hematite daughter minerals were present in inclusions of dilute fluid at one locality, and suggested that the brine acted as a reductant for uranium in the dilute fluid. A large variation in oxygen fugacity is interpreted to have occurred during deposition of Saxonic veins and unconformity-type uranium deposits (e.g. Robinson and Ohmoto, 1973). Shallow depths of ore formation, but not necessarily of brine generation, are indicated for these ore deposits, by analogy with oxygenated stratal fluids.

The association of hydrocarbon compounds, particularly liquid petroleum and pyrobitumen, with the ore fluids which formed some basin-related ore deposits provides a further link between different types of basin-hosted ore deposit. It also supports a possible relationship between the ore fluids and stratal brines associated with petroleum deposits (Dozy, 1970). Fluid inclusions which

contain liquid petroleum occur in a number of Mississippi Valley-type deposits, as do concentrations of hydrocarbon compounds (Spooner, 1981; Rouvier et al., 1985). The composition of n-alkanes in inclusions within sphalerite from the sandstone lead deposit of Laisvall, Sweden, indicates a complicated history, consistent with that undergone by petroleum in sedimentary basins (Rickard et al., 1979). The significance of hydrocarbon compounds (and "graphite" alteration) in other ore deposits, particularly higher temperature and metamorphosed ore deposits, cannot be interpreted without a detailed study of their composition and thermal history. This is because hydrocarbon compounds could also be generated from the host rocks of the ore, near the site of ore deposition (Macqueen and Powell, 1983). Bitumen, or pyrobitumen, is associated with other sandstone lead deposits, and with Tsumeb-type mineralization of the Otavi Mountain Land, Zaire, and Ruby Creek, Alaska (Caia, 1976; Hitzman, 1983), with Saxonic veins (e.g. Thunder Bay, Canada; Kongsberg, Norway), and with sedex mineralization of Ireland (Morrissey et al., 1971). Petroleum occurs in fluid inclusions within calcite veins which contain copper minerals, and which intersect a cupriferous shale deposit at White Pine, Michigan (Kelly and Nishioka, 1985). "Graphite" alteration, transgressive to the stratigraphy, shows a close spatial relationship to stratiform copper mineralization in the Mufulira ore body, Zambia (Annels, 1979). Bitumen is closely associated with strata-bound uranium deposits of the south-western U.S.A. (Dunsmore, 1977), and pyrobitumens are present in both unconformity uranium deposits and the Beaverlodge uranium veins (Dahlkamp, 1978; Rimsaite, 1978). Petroleum has been reported from fluid inclusions in an unconformity uranium deposit in Canada (Pagel and Jaffrezic, 1977).

It can be concluded that the fluids which form many types of basin-hosted ore deposit, including members of the Owambo basin-type association, show temperatures, chemical compositions and an association with hydrocarbons which is also common to stratal fluids in sedimentary basins. In particular, brine inclusions in ore bodies as different as Mississippi Valley-type deposits, native copper deposits, and unconformity uranium deposits have large salinities and Cl:Br ratios which indicate a connate, evaporite origin, consistent

with the model proposed originally by Davidson (1965). Basin-hosted ore deposits of different type may therefore have closely related origins (Fig. 139a), consistent with the chemical, mineralogical and spatial relationships between these ore deposits, the ubiquitous presence of crustal sulphur in their ores, and lead isotopic evidence for their common origin. An important implication is that the presence of one type of ore deposit may indicate the potential for different types of ore deposit in different rock types (e.g. economically unimportant Saxonic veins might indicate the potential of an adjacent basin for strata-bound and stratiform ores).

6.3.6 The importance of major salt basins

Davidson (1965) noted that a close spatial relationship commonly exists between salt basins (i.e. basins which contain significant thicknesses of halite) and mineral districts in geologically young terrains, and suggested that the salt was the source of the brines which formed the ore bodies. Examples of such districts and provinces have already been described, such as the Triassic province of southern and western Europe and north-western Africa (Fig. 141b), the Permian mineral province and associated Rotliegende-Zechstein salt basin of northern Europe (Fig. 141a), and the Lower Cretaceous sandstone lead and copper province of western and north-western Africa and Brazil (Fig. 141d). Another example is the stratiform copper mineralization of Bolivia, which overlies Cretaceous salt deposits (Davidson, 1965). The stratiform copper deposits of Kazakhstan (which includes Djezkazgan), U.S.S.R. are associated with important salt deposits of Permian age, as is similar mineralization in the western Ural Mountains (Popov, 1962; Davidson, 1965; Fig. 141a). The stratiform copper province of Texas, Kansas and Oklahoma, the carbonate-hosted base metal deposits of the Gilman-Leadville district, Colorado, and the Mississippi Valley-type and sandstone lead deposits of eastern Canada occur on the margins of Permian and Carboniferous salt basins (Johnson, 1976; De Voto, 1983; Waugh, 1985; Fig. 141a). Mississippi Valley-type deposits of Pine Point and the northern Rocky Mountains, Canada, are adjacent to Devonian salt deposits of the Elk Point Basin and Mackenzie Basin (Smith et al., 1983; Rhodes et al., 1984; Fig.

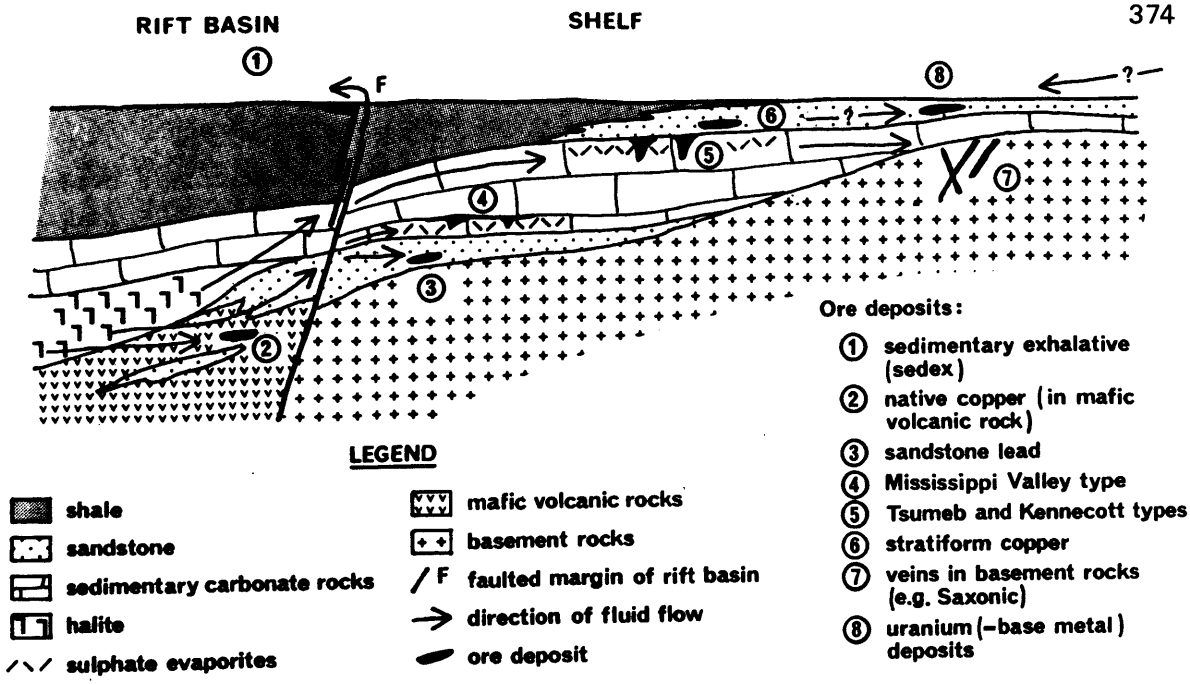

Fig. 139a
A model for the genesis of ore deposits in epicontinental environments which lack igneous intrusive activity. Buried halite expels connate brine, which migrates up fault zones and through permeable rock types (which contribute various metals to the brine). Sulphide ore is deposited in different ore loci, in rocks which contain sulphur sources of crustal origin.

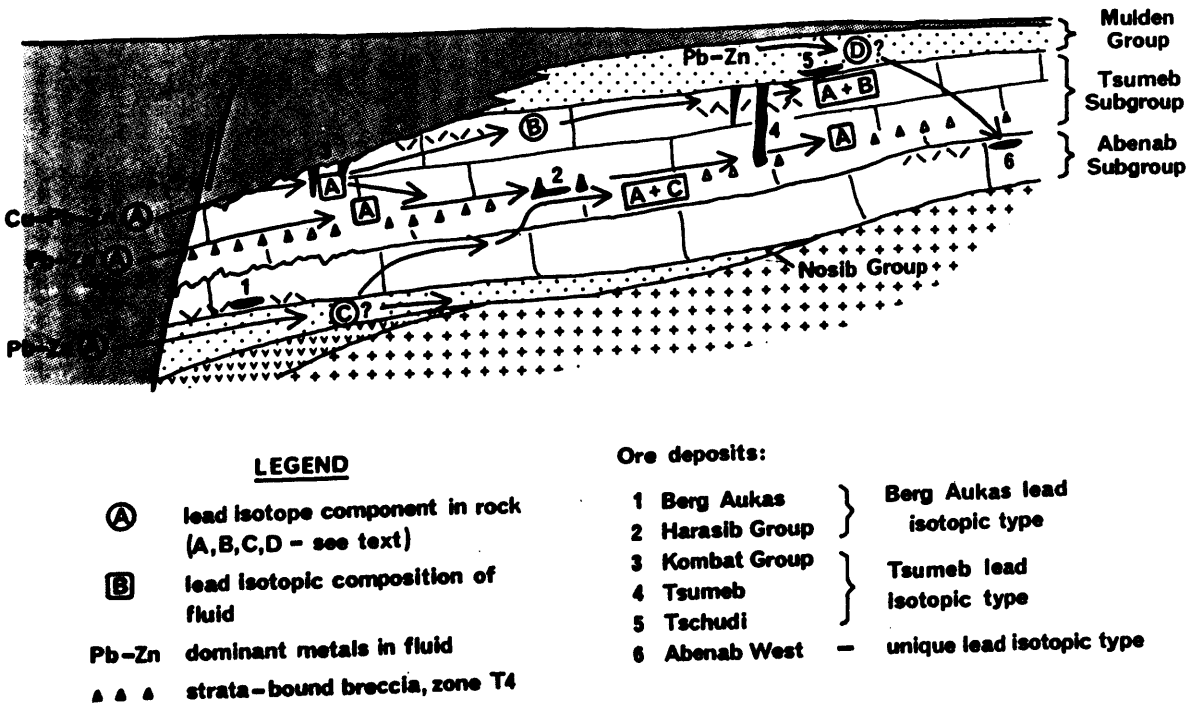

Fig. 139b
A model for ore genesis in the Owambo basin, showing fluid channelways, fluid compositions, sources of lead, and the locations of ore deposits (see Fig. 139a for explanation and additional legend). Fluid flow is three-dimensional and cannot be represented adequately in section (e.g. the fluid which formed the Abenab West ore body did not necessarily migrate downwards).

14la). Stratiform copper and carbonate-hosted lead-zinc mineralization of the Lena River area, U.S.S.R., is closely associated with large Cambrian salt deposits (Davidson, 1965). Strata-bound uranium deposits occur in the vicinity of salt basins, in areas which also contain stratiform copper mineralization, as noted by Dunsmore (1977). Examples include mineralization adjacent to Permian salt of the Paradox basin, U.S.A., and Mississippian salt of Nova Scotia (Fig. 14la).

The relationship between salt basins and ore deposits is not obvious in Precambrian rocks because known salt basins of this age are very rare, probably because of salt dissolution (Chapter 6.1.5). However, many basin-related ore deposits in Precambrian rocks occur in rifts and aulacogens in which salt deposits might have been present, and there is some indirect evidence of this. Diapiric breccia bodies of Proterozoic age occur in the important stratiform copper province of the Adelaide Geosyncline of South Australia, and base metal mineralization is common in association with the margins or cores of these bodies (Chapters 4.6, 5.3.15). The cores of the diapirs consist typically of the Callana Beds, from the base of the sedimentary sequence (Dalgarno and Johnson, 1968). The origin of these diapirs is controversial, but Mount (1983) and Lemon (1985) concluded from petrographic and structural studies that the mobility of the diapirs, which were active during sedimentation, was caused by the former presence of evaporite minerals. Diapiric bodies of similar age occur in the Amadeus basin and Officer basin, farther to the north-west, and some of these bodies contain beds of gypsum (Wells, 1980). There is also evidence that evaporitic conditions were extensive in the Roan Supergroup, which hosts the important stratiform copper deposits of central Africa. Nodular anhydrite and albitized, anhydritic breccia occur, and scapolite is widespread (Garrard, 1974; Ramsay and Ridgeway, 1977). Magnesite, talc, palygorskite and iron-poor chlorite (after palygorskite) are also common, and occur in stratiform copper deposits, Shinkolobwe-type uranium deposits and Tsumeb-type mineralization, in the "R.A.T." horizon, and in diapiric breccia bodies similar to those of South Australia, which contain a core of "R.A.T." rocks. The "R.A.T." horizon, which occurs at the base of the Mines Group, immediately

below the copper ore bodies, was an important horizon in which thrusting and diapirism was concentrated (Bartholome, 1974; Cahen, 1974; Intiomale, 1982). Sodium- and magnesium-rich assemblages of the above type in younger rocks elsewhere in the world are commonly associated with evaporites, including the margins of salt diapirs, and with magnesium-rich brines (Dings and Whitebread, 1965; Moine et al., 1981; Laufer and Mossman, 1982, Rouvier et al., 1985). It has been proposed that evaporitic conditions were widespread in the Roan Supergroup (Moine et al., 1981), and it is suggested here that major salt deposits were present, particularly in the immediate vicinity of the "R.A.T." horizon. Some ore bodies, such as Kipushi and possibly the Shinkolobwe-type uranium deposits, may have been deposited in solution structures on the margins of original salt diapirs (or other bodies related to salt tectonism).

Sedex (sedimentary exhalative) ore deposits can also show an obvious spatial relationship to both salt basins and individual salt diapirs, e.g. in north-western Africa (Rouvier et al., 1985). Evaporitic sulphate minerals are known in the Carboniferous rocks which host the sedex deposits of Ireland, and evaporite pseudomorphs and scapolite are volumetrically important in the Middle Precambrian sequences which host the Mount Isa and McArthur River deposits of Australia (MacDermot and Sevastopulo, 1972; Wells, 1980; Andrew and Ashton, 1985), and salt basins may have been present in these areas. The Mississippi Valley-type deposits of western Canada (discussed above) are spatially related to salt basins, and lead isotope data indicate a possible genetic relationship between these and sedex deposits elsewhere in the same area, and at McArthur River (Chapter 5.3.13). A relationship between sedex deposits and salt basins may therefore be more important than has commonly been recognized.

The relationship between salt basins and some types of ore deposit may not be obvious, for example Saxonic veins which occur in basement rocks adjacent to the Permian salt basins of northern Europe. The spatial association, age, lead isotope and sulphur isotope data, and fluid inclusion data (discussed above) are all consistent with formation of these veins in Permian times from brines related to those which formed the stratiform mineralization of the

Kupferschiefer bed. The main objection to this origin is that the veins are mostly confined to basement rocks, but it is suggested here that this objection is not valid (Chapter 4.6.7). Calcium chloride brines have been found at depths of greater than one kilometre (up to eleven kilometres) in crystalline rocks of the Eastern-European platform and the Canadian Shield. The Canadian brines occur within some of the mineral provinces which have been discussed earlier, e.g. in Michigan (Fig. 137b) and in the Yellowknife and Sudbury areas of Canada, in provinces which contain stratiform copper mineralization, unconformity uranium deposits, and the Saxonic veins of Echo Bay, Cobalt and Thunder Bay (Frape and Fritz, 1982; Frape et al., 1984; McNutt et al., 1984). The brines are unlike any other brines known in that the most concentrated brines have $\delta^{18}O$ ratios 10‰ lighter than Phanerozoic sea water, which might result from low temperature re-equilibration, but the brines probably contain a component with a δD ratio similar to that of sea water (the isotopic composition of the Michigan brine is unknown). The chemical compositions of the most concentrated brines, including the Cl:Br ratios, are similar to that of sea water evaporated well past the point of halite saturation, except that the magnesium and potassium concentrations are very low. The slope of the trend defined by the Cl:Br ratios is consistent with a connate evaporite brine which has mixed with meteoric water (fig. 10, Frape et al., 1984). Brines with similarly low magnesium (but not potassium) contents have been recorded from sedimentary rocks (e.g. in dolostone from Michigan; Krejci-Graf, 1978). The low potassium content may result from the modification of brine compositions by reaction with basement rocks. Chemical and isotopic data from brines of the Eastern-European platform indicate that these brines may also contain modified sea water (Vovk, 1985). The Canadian and Eastern-European brines may be the residues of huge volumes of fluid which penetrated the basement rocks adjacent to former salt basins, on a far greater scale than has commonly been assumed, and this has important implications for the origin of vein-type mineralization in these rocks.

It can be concluded that many basin-related ore deposits are closely associated with salt basins, and that the association is probably genetic and related to the source of ore-forming brine. The

presence of sources of sulphur at shallow depth, such as sabkha sequences adjacent to the salt basins, will be an additional important factor in localizing mineral districts. A similar origin must therefore be suspected for ore fluids in the Owambo basin.

6.3.7 Source of the Owambo basin-type ore fluids

The chemical composition, temperature, timing and migration paths of the fluids which formed the mineralization of the Otavi Mountain Land provide some constraints on the nature and source of the fluids. The fluids which formed mineralization of Tsumeb-type and Berg Aukas type varied in composition from brine, with a salinity greater than 20 % NaCl equivalent, to saline water, and had temperatures of approximately 250°C. The lead isotope data are consistent with fluid migration from south to north, and indicate that the probable source of the fluids which formed all members of the Owambo basin-type ore association was no farther north than the southern Otavi Mountain Land. This migration occurred at approximately 600 m.y., subsequent to initial deposition of the Mulden Group, but prior to its deformation (or the close of deformation). The oxygen isotopic composition of the Tsumeb fluid does not provide conclusive evidence of its origin, partly because of uncertainty about the oxygen isotopic composition of natural fluids of Precambrian and Paleozoic age. The $\delta^{18}O$ ratio of the Tsumeb ore fluid was approximately +11‰, compared with +5,5 to +10‰ for magmatic water, and +5 to +25‰ for metamorphic water. The maximum ratio measured in present day, low-temperature stratal fluids is +9‰, but values of +10 to +12‰ have been recorded from fluids which equilibrated with rock minerals at intermediate temperatures (Knauth et al., 1980). The mean $^{87}Sr/^{86}Sr$ ratio of 0,712 obtained from carbonate minerals of the Tsumeb pipe, combined with the small lanthanum and cerium concentrations of the samples, does not support a carbonatitic origin for these minerals (Allsopp and Ferguson, 1970). The strontium isotope ratios are similar to those of the enclosing sedimentary carbonate rocks, but the possibility cannot be excluded that a radiogenic component of strontium was added from outside this sequence (e.g. data from the host rocks might be found to define an errochron if the precision of the analytical method was increased).

A magmatic origin for the water in the ore fluids is not favoured. This is because there is no evidence of major magmatism within the Otavi Mountain Land, and because of: (1) the large volume of fluid involved,(2) the association of pyrobitumen with mineralized sites (and therefore the probable association of hydrocarbons with the fluids), and (3) the lead isotopic evidence that a major proportion of at least one metal (i.e. lead) in the ore fluid could have been derived from the sedimentary sequence, so that it is not necessary to invoke an exotic metal (or fluid) source. Localized magmatism is an improbable cause of fluid migration (e.g. by thermal convection), or of the intermediate temperature of the fluids, because of the scale of fluid migration and the fairly constant temperature of the ore fluids throughout an entire mineral district.

It is shown above that data from modern mineralized fluids and from fluid inclusion studies of ore bodies, together with the distribution of mineral districts relative to salt basins, indicate that former salt basins may be the source of most fluids which formed ore deposits genetically related to sedimentary basins. The temperatures of the ore fluids which formed the ore deposits of the Otavi Mountain Land were moderately high compared with mineralized stratal fluids, but such temperatures could be produced at considerable depth, or in a basin with an anomalously high geothermal gradient, such as a rift or oblique-slip basin. The Damara Sequence of the intra-continental branch of the Damaran fold belt was deposited initially in a rift environment, in at least four parallel grabens, and conditions suitable for the formation of salt deposits may have existed in the basal Nosib Group. Evidence has recently been found for formerly extensive deposits of both playa-lake and marine evaporites in cyclical dolomitic-pelitic sedimentary sequences in the Nosib Group of the southern graben. Some evidence of former evaporites has also been found in the northern graben, the northern boundary of which extends at least from the southern margin of the Kamanjab inlier to south of the Otavi Valley (Behr et al., 1981; Behr and Horn, 1982; Behr et al., 1983a, b; Figs. 1,3). The evidence consists of pseudomorphs after sodium carbonate and sodium sulphate minerals; these are associated with albitolite horizons,

talc, and chlorine-rich scapolite. Fluid inclusions from these rocks are concentrated Na-Ca-Cl brines which commonly contain abundant potassium and carbon dioxide, and some inclusions contain hydrocarbon compounds. Behr et al. (1981) interpreted unusual rocks that occur along thrust planes of nappes in the Naukluft Nappe Complex as the metasomatic products of hot, saline intrusions, which formed when metaevaporites were squeezed into the thrust planes from farther north in the southern graben. Behr and Horn (1982) and Behr et al. (1983a) commented on the close association of stratiform copper mineralization and former evaporites in the northern and southern grabens of the Damaran fold belt, and noted that a similar spatial relationship exists in Late Proterozoic rocks of Zambia, Zaire and the Adelaide Geosyncline. Behr et al. (1983a) suggested that the ore solutions which formed both the stratiform copper mineralization of these areas, and also the Tsumeb and Kombat ore bodies, had a playa source.

Two objections could be raised to the proposal that evaporites of the Nosib Group were the source of the fluids which formed the ore deposits of the Otavi Mountain Land. The first is that these evaporites have an age of at least 730 m.y., but ore deposition occurred at approximately 600 m.y. The brine would need to have been trapped for at least 100 m.y.; however, there is evidence that this occurred in the central Gulf Coast, U.S.A., and in north-western Africa (Chapter 6.3.4). The second objection is that Nosib Group and Otavi Group rocks underwent deformation and metamorphism prior to deposition of the Mulden Group, at least to the south of the Kamanjab inlier (Frets, 1969), and it is commonly assumed that connate fluids are expelled from sedimentary sequences during, or prior to, conditions of low grade metamorphism. However, brine was associated with thrusting and alteration at 530 m.y. or later in the Naukluft Nappe Complex, described above, despite evidence for earlier deformation and metamorphism in the area thought to be the source of the evaporites and brine (Behr et al., 1983b). Behr and Horn (1982) suggested that large volumes of brine were trapped as fluid inclusions in dolomite spar during burial. However, this volume would be potentially small. An alternative possibility is that the extreme impermeability of salt permits fluid to be retained for long

periods, possibly in permeable reservoir rocks within or adjacent to the salt, even under conditions of low grade metamorphism (Chapter 6.3.2).

An alternative to a fluid source in evaporites of the Nosib Group is that salt, of which no evidence has yet been reported, was deposited within the Mulden Group of the northern graben. The northern graben appears to have been reactivated subsequent to deposition of the Tsumeb Subgroup, and considerable relief was developed along the northern boundary of the graben, between the southern margin of the Kamanjab inlier and the southern Otavi Mountain Land (Chapter 6.1.4). Salt might have been deposited in the graben prior to its being filled with Mulden Group sediments, or during deposition of the Owambo Formation, which includes dolostone and evidence of evaporites in its upper member within the central Owambo basin (Hedberg, 1979).

Evaporites of the Nosib Group are favoured here as the source of the ore fluids, with some reservations because of uncertainty about the metamorphic history of these rocks, and about the ability of salt deposits to retain connate fluid under low grade metamorphic conditions. This origin (i.e. late release of fluids from salt deposits) receives some support from the close association of base metal mineralization with the cores and margins of probable former salt diapirs in Late Proterozoic rocks of the Adelaide Geosyncline and the Katangan fold belt (the possible continuation of the intra-continental branch of the Damaran fold belt; Chapter 6.3.6). The horizon involved in diapirism in both these areas occurs at the base of a probable rift sequence, but mineralization associated with the diapiric bodies post-dates rocks of much younger age. This conclusion as to the source of the fluids, if accepted, has two important implications. The first is that salt basins which form during early rifting might provide ore fluid for different types of mineralization, over extended periods of time. For example, stratiform copper mineralization in Zaire occurs towards the base of the Roan Supergroup, and Tsumeb-type mineralization occurs in the Kundelungu Supergroup, adjacent to a diapiric body with its source at the base of the Roan Supergroup. The second important implication is

TABLE 12 AVERAGE TRACE ELEMENT CONTENTS OF VARIOUS ROCK TYPES (ppm)

ROCK TYPE		Mn	Li	Be	B	Ba	Sr	U	Th	F	P	As
SANDSTONE	"Sandstone"	10-250	2-18	< 1-1	19-39	1-250	4-85		12	10-80 (-210)	100-560	1 (-12)
	Arkose											
	Greywacke											
SEDIMENTARY CARBONATE ROCK	Limestone	105-650	12	< 1-1	< 20 (-200+)	3-42	400-1400	2-3		31-90 (-350)	180-550 (-1100)	< 1-2 (-15)
	Dolostone	80-220 (-4500)	1-10	< 1	16	9-50 (-180)	90-220			50-125 (-265)	95-330 (-1300)	1-2 (-6)
EVAPORITES	"Evaporites"		Anom		Anom (-1000's)		Anom					
	Halite											
	Anhydrite											
SHALE	Shale	270	46 (-70)	3	100	460	171	1,2	11	510	200-600	13 (-53)
	Black shale	150 (-700)		1 (-3)	70 (-100)	400 (-600)	200 (-700)	6-74 (-100)				
	Phosphatic sediments	30	7 (-11)	4 (-1%)		100	1000	50-200	7-26	%'s	%'s	11-61 (-188)
	Bauxite											
	Coal	25	5 (-Anom)	1,6 (-Anom)	55 (-Anom)	25	22			45	215	4 (-Anom)
IGNEOUS ROCKS	Felsic	300	3	2	15	550	75			380	275	2
	Mafic		10			300	500					1,5

LEGEND

Anom	=	Anomalous (i.e. significantly higher than the crustal average)
X	=	Average value
X - Y	=	Usual range
(-Z)	=	Maxima for regional units
C (org.)	=	Organic (reduced) carbon

SOURCES OF DATA

Larsen & Chilingar (1979)
Connor & Ebens (1980)
Hitchon (1977)
Vine & Tourtelot (1970)
Cubitt (1979)
Wedepohl (1974)
Thiede & Cameron (1978)
Kraynov (1967)
Leventhal & Kepferle (1981)

	F	P	As	Sb	Se	V	Mo	Bi	Ga	Ge	Co	Ni	Hg	Ag	Zn
12	10-80 (-210)	100-560	1 (-12)	< 1	0,15	12-80			6 (-15)	1	2-5 (-12)	4-11 (-30)	< 0,01 -0,02		30 (-75)
						43-210			8-20 (-36)	0,9-3,5					70-120
	31-90 (-350)	180-550 (-1100)	< 1-2 (-15)	0,3	0,2-0,3	6-13 (-80)			2,5	0,3-1,3	2-4	2-4	0,02 -0,03		20 (-30)
	50-125 (-265)	95-330 (-1300)	1-2 (-6)		0,2-0,3 (-6)	6-12 (-45)					2-5	4-6	0,02 -0,04		20 (-55)
															0-3
															2-10
1	510	200-600	13 (-53)	1 (-3)	0,6 (-45)	90-260	2,6* (-54)	1,5	8-17 (-22)	1,5 (-6)	8-18	24-42	0,3	0,05* (-44)	100 (-197)
						150-650	10 (-70)		25 (-50)	1,8	10 (-15)	60 (-100)		0,8 (-4)	200 (-700)
5	%'s	%'s	11-61 (-188)	0,2-1,3 (-7)	10 (-1000)	200-600 (-1000)	30 (-1000)		3-10 (-Anom)			1000 (-1000+)	10 (-1000)	4 (-300+)	300 (-1000+)
				2											
	45	215	4 (-Anom)		2	13 (-Anom)	Anom	Anom	86 (-110+) Anom	1-50 (-1000)	3 (-Anom)	20 (-Anom)	0,1		23
	380	275	2		0,1	5				1	5	6	0,02		50
			1,5			250			20	1	40	75			

r (1979)
(1980)
(1977)
(1970)
(1979)
(1974)
(1978)
(1967)
rle (1981)

* Hitchon (1977) quotes higher values for the Western Canada Basin.

Ga	Ge	Co	Ni	Hg	Ag	Zn	Cd	Pb	Cu	Cr	Ti	Sn	C (org.)
6 (-15)	1	2-5 (-12)	4-11 (-30)	< 0,01 -0,02		30 (-75)	< 0,1	11-25 (-82)	< 1-2 (-9)				
8-20 (-36)	0,9-3,5					70-120			7-33 (-60)				
2,5	0,3-1,3	2-4 2-5	2-4 4-6	0,02 -0,03 0,02 -0,04		20 (-30) 20 (-55)	3 (-10) Marl	5 (-80)	1,5-5 (-33)				
						0-3		0,6	0,4				
						2-10		10	2				
-17 -22)	1,5 (-6)	8-18	24-42	0,3	0,05* (-44)	100 (-197)	0,3 (-13)	22 (-55)	23-88 (-300)	154	3500	6 (-11)	1,6%
25 -50)	1,8	10 (-15)	60 (-100)		0,8 (-4)	200 (-700)		25 (-70)	80 (-110)	100 (-250)	3500		5% (-7)
-10 nom)			1000 (-1000+)	10 (-1000)	4 (-300+)	300 (-1000+)	5-90 (-200)	0-100	1-400	7-1600	100- 3000	Anom	
86 110+) nom	1-50 (-1000)	3 (-Anom)	20 (-Anom)	0,1		23		48	22				
	1	5	6	0,02		50		19	2				
20	1	40	75						100	150			

that this provides a mechanism by which the temperature range at which some basin-related ore deposits form could exceed the generally accepted maximum of 250°C by more than 100°C. This is consistent with the high temperatures indicated by brine inclusions that occur both in meta-evaporite horizons of the Damaran fold belt, and in thrust planes within the Naukluft Nappe Complex (Behr and Horn, 1982).

6.4 METAL SOURCE AND FLUID CHANNELWAYS

Major chemical differences between the Tsumeb and Berg Aukas types of mineralization probably reflect major differences in the concentrations of different metals in their ore fluids (Chapter 6.2.4). The lead isotopic composition of galena is consistent with a source of lead in rocks of the Kombat Formation, with additional components of lead being added during lateral migration of the ore fluids through sedimentary rocks of the south-eastern Owambo basin. These rocks, particularly the aquifer rocks through which the ore fluids migrated, were therefore the probable sources of metals in the ore fluids. It is shown below that rocks in sedimentary basins are potential sources of the elements present in metal-bearing stratal fluids, a conclusion supported by the brine leaching experiments of Long and Angino (1982). Rocks which might have supplied metals to ore fluids in the Otavi Mountain Land are identified.

6.4.1 Minor elements in rocks of sedimentary basins

Typical concentrations of minor elements in various lithologies are listed in Table 12. The maxima shown are averages for entire rock units, rather than for individual samples. The fraction of these elements which can be leached will be a function of mineralogy (e.g. barium in feldspar c.f. mica), fluid chemistry and other physical conditions (e.g. permeability). The present values in these rocks will differ from those that existed prior to diagenesis and deep burial. However, concentrations of certain elements vary greatly in different rock types, and reflect original differences in sediment chemistry, and therefore the varying

potentials of these rocks as sources of different elements in fluids of sedimentary basins.

Lithium, Be, B, Ba, Sr, F, P, U, As, Sb, Se, V, Mo, Co, Ni, Ti, Cr, Hg, Ag, Zn, Cd, Pb and Cu concentrate in shale (particularly carbonaceous shale) and phosphorite relative to other rocks (Table 12). These rocks are also thought to be important source rocks for petroleum. Many of these elements are closely associated with organic matter in shale and phosphorite and, together with germanium, gallium and rhenium, in coal. Gallium substitutes for aluminium and has a low, constant concentration in most rock types. However, it is enriched in coal, bauxite, and possibly in wavellite-bearing phosphorite (McKelvey et al., 1953). No data is available on germanium and gallium in phosphorite, but ash from coal can average up to 1,4% Ge and 1,5% Ga (Buckland, 1959). Arsenic, Pb, Sr, U and V also substitute for phosphorus and calcium in the apatite lattice within phosphorite. The ratios of metals such as copper, lead and zinc can vary greatly between different shale units, although the zinc content is usually high. Boron, strontium and to a lesser extent, fluorine, concentrate in sedimentary carbonate rocks, as well as in shale and phosphorite.

A number of elements occur in exceptionally high concentrations in phosphorite relative to other rock types. These include Be, Ag, Cd, Hg, Re, Zn and Mo. Some alumino-phosphate minerals present in phosphorite (e.g. wavellite) contain up to 5 000-10 000 ppm Be (Vlasov, 1966). Average concentrations of silver and cadmium in phosphorite of the Phosphoria Formation are 3 and 90 ppm, respectively. Mercury and rhenium are enriched to more than five times their Clarke values. Values as high as 10 000 ppm Zn, 1000 ppm Mo and 200 ppm Cd occur in some parts of the Phosphoria Formation, and mercury averages 10-1 000 ppm in phosphorite of some other regions (Gulbrandsen, 1966, 1977). Some shale (e.g. the Kupferschiefer) also shows exceptional enrichment of metal, but it is probable that this reflects hypogene mineralization on a regional scale. The Sb:As ratios of both shale and phosphorite are consistently low (averaging 1:50 and 1:7 respectively) in all areas. Phosphorite of the Phosphoria Formation has an average Zn:Cd ratio of

3:1, compared with 300:1 for average shale. These ratios could influence the ratios of these elements in base metal ores, although they will also be a function of the relative solubilities of the elements in the ore fluids.

It is concluded from the above and Table 12 that shale, phosphatic sediment, and rocks rich in organic matter are potential sources of all the elements present in basin-related ore bodies. Igneous rocks and sandstones, excluding orthoquartzite, are possible sources of some elements (e.g. Cu, Pb, Zn and Ba). Elements such as Cd, Mo, Hg, Be and Ag have rarely, or never, been reported in anomalous concentrations in basin fluids. However, these elements have been determined in few basin fluids, and their high concentrations in some basin rocks indicates that such fluids may occur. It is probable that a source rock which is anomalously enriched in base metals, relative to the same lithology elsewhere, is not essential for the formation of ore fluids (Skinner, 1979), although a geochemically specialized source rock may be required to provide certain minor elements characteristic of some mineral districts. The only essential requirement may be a fluid of suitable physical and chemical composition (e.g. a hot, concentrated brine), which is in prolonged contact with a large volume of rock with a metal content that is large relative to that of other lithologies (e.g. shale, rather than limestone; Chapter 5.3.10). It is noted above that many basin-related ore deposits are spatially associated with salt basins, which were probable sources of ore-forming brine. The formation of mineral districts of this type may therefore be primarily a function of process-dependent factors (i.e. the migration of suitable fluids), rather than of the existence of long-lived geochemical anomalies in the crust (Chapter 1.1).

6.4.2 Metal sources and fluid channelways in the Otavi Mountain Land

It is concluded from the lead isotope data that the Tsumeb and Tschudi types of mineralization of the Otavi Mountain Land formed at the same time, from an ore fluid which had a variable composition. This fluid migrated laterally from south to north, through different aquifer systems in the upper Tsumeb Subgroup and lower Mulden Group,

to be deposited in different host rocks. Most examples of the Berg Aukas type of mineralization formed from an ore fluid that was broadly coeval with the ore fluid that formed the Tsumeb and Tschudi types of mineralization. The preferred model is that the Berg Aukas-type fluid migrated at the same time as the other ore fluid, through stratigraphically lower aquifers, although it is possible that this event was separated in time.

The lead isotope study indicates that one component of lead, A, in the ore fluids which produced the Owambo Basin-type ore association could have been derived from pelitic rocks of the Kombat Formation (Fig. 139b). Metal-rich dolostone of zone T8, and sandstone of the Tschudi Formation, were possible sources of lead component B, and lead component D in the Abenab West ore body, respectively. A possible source of lead component C has not been identified, but one possibility is sandstone of the Nosib Group, which has a stratigraphic and geographic distribution consistent with this lead isotope model. The different chemical and mineralogical compositions of the Tsumeb and Berg Aukas types of mineralization, the trace element compositions expected in lithologies of the type found in the Otavi Mountain Land, and the lead isotope data, are consistent with derivation of lead from different aquifer rocks along the different routes taken by the ore fluids. Sandstone of the Nosib Group, and phosphatic dolostone of the upper Tsumeb Subgroup were possible sources of lead.

The phosphatic dolostone (or equivalent, deeper-water facies which are not seen) might also have supplied other metals, such as Cd, Hg, Be and Ga which are enriched in the Tsumeb type of mineralization. Phosphatic rocks are moderately widespread and may also be important sources of metals in other mineral districts (e.g. the Mississippi Valley districts, the germanium-rich deposits of Saint Salvy, France, and the Apex ore body, Utah). However, many of the elements characteristic of the Tsumeb ore type could have been supplied by former shale of the Kombat Formation, and it is impossible to distinguish between metal sources in shale and phosphatic rock without quantitative geochemical data from the entire area, because both rock types contain (or could be expected to have

contained) a similar suite of elements. Some elements, such as copper, may have been supplied by rocks outside the Otavi Mountain Land (e.g. volcanic rocks of the Nosib Group), although the Kombat Formation was also a potential source of copper. Some minor elements present in the Kombat ore bodies are characteristic of brines in sedimentary basins, and elements such as lithium and boron might have been introduced to the brines in their source area. However, elements such as boron and beryllium can probably be introduced to brines as the result of diagenetic reactions (e.g. these elements occur enriched in shale and phosphatic rocks, respectively).

The present trace element content of rocks in the Otavi Mountain Land is considered to be of limited use in predicting the former potential of the rocks as sources of metal in ore bodies of the area. For example, lead isotope data strongly support rock of the Kombat Formation as a source of some lead in the ore bodies. However, slate of this formation has a much smaller lead content than average shale, and contains only average concentrations of zinc and copper (Tables 2, 12). This rock may therefore have been leached of metal by the ore fluid. Nevertheless, the data confirm that former shale of the Kombat Formation and sedimentary carbonate rocks of zone T8 (particularly phosphatic rocks) were the most metal-rich sources available in the sedimentary sequence of the south-eastern Owambo basin (Tables 1, 2). The germanium concentration of slate and one sample of sandstone from the Mulden Group is large (Tables 2, 12). This, the common association of germanium, gallium, molybdenum and other elements enriched in Tsumeb-type mineralization with organic material, and the close spatial association between pelitic rocks, hydrocarbon compounds (e.g. pyrobitumen) and mineralization in some ore bodies of Tsumeb type (e.g. Kombat, Kipushi) is consistent with a source of germanium in organic-rich pelitic rocks. The only evidence in favour of a source in the phosphatic rocks is the small germanium content of sphalerite in the Berg Aukas type of mineralization (Emslie, 1979), which is considered here to have also derived its lead from shale of the Kombat Formation. All of the metals present in ore bodies of the Otavi Mountain Land could have been supplied from rocks within the known mineralized area, although much of the metal may have been added to the ore fluids farther to the south.

For example, all of the lead in the Tsumeb ore body could be obtained by leaching 50 ppm of lead from a rock unit 200m thick over an area of 100 km^2.

It is concluded in Chapter 6.3.5 that basin-related ore deposits of different types may have closely related origins (Fig. 139a). The requirements of such a model are: (1) a source of hot brine, (2) aquifer rocks of suitable chemical composition, and (3) a supply of reduced sulphur, usually at shallow depths. These requirements would be met in rift or oblique-slip basins in which early-formed salt deposits have become deeply buried, adjacent to shelf or platform environments in arid climates. This model can be applied to ore deposits of the Owambo basin (Fig. 139b). Paleo-isopach data of Hedberg (1979) indicate that the Tsumeb ore body is located close to the area of minimum thickness of each of the Abenab Subgroup, Chuos Formation, Maieberg Formation, Elandshoek Formation and Huttenberg Formation, on the eastern extension of the Kamanjab-Tsumeb basement ridge. The Tsumeb ore body was probably emplaced near the top of this ridge during (or soon after) deposition of the Mulden Group. Other ore bodies of the Otavi Mountain Land were confined to the southern flank of this high, consistent with the south to north migration of ore fluid required by the model.

6.5 THE TIME DEPENDENCE OF TSUMEB-TYPE ORE DEPOSITS

Salt basins are probable sources of ore-forming brine, and may therefore be the dominant factor in localizing adjacent mineral districts (Chapter 6.3.6). Many basin-related ore deposits are spatially associated with rift zones, and it is shown below that this relationship may be genetic, because salt basins commonly form during rifting. Rifting events can occur on the scale of continents, or even supercontinents (Piper, 1976), and extensive rifting events can occur during a short period of time, subsequent to long periods during which there is no rifting (Windley, 1977). This provides an explanation for the time-dependence of many ore deposits, including the Owambo basin-type ore association, within the framework of the present model (Chapter 1.1). Mineral provinces which contain

basin-related ore deposits would form during periods of rifting, when such rifting occurred at latitudes suitable for the formation of salt basins. This temporal, as well as spatial, relationship between ore deposits and salt basins indicates that the spatial relationship is dependent upon a source of brine, not just sulphur. This is because sulphur sources such as sabkha sequences, but not major salt basins, have formed throughout geological time.

Major periods during which basin-related ore deposits formed are the Lower Cretaceous (western Africa and Brazil; Fig. 14ld), Triassic (Mediterranean region; Fig. 14lb), and Carboniferous-Permian (1. Kazakhstan, U.S.S.R.; 2. Western Europe, including the Kupferschiefer and the sedex deposits of Ireland; 3. eastern Canada, and 4. the U.S.A., including stratiform copper deposits of the south-western U.S.A. and possibly the Mississippi Valley districts; Fig. 14la). Earlier periods of mineralization occurred in the Devonian (Pine Point, the northern Rocky Mountains and Arctic Canada; Godwin et al., 1982), and Cambrian (1. Swedish Caledonides, 2. the Owambo Basin-type ore association, and 3. the southern Rocky Mountains and Selwyn Basin, Canada; Andrew et al., 1982). Age relationships are less well known in Precambrian rocks. A well-defined period of formation of stratiform copper deposits occurred at approximately 1000 m.y.; this includes deposits in Zambia and Zaire, the Adelaide Geosyncline, the Michigan district, and the Belt basin (north-western U.S.A.). An important mineralizing period is represented in Canada at approximately 1400 m.y.; this includes the sedex ore bodies at Sullivan (British Columbia) and elsewhere, the unconformity uranium deposits of Saskatchewan, and Saxonic veins of the North West Territories. Lastly, an important period of formation of sedex deposits occurred at 1700 m.y. in Australia (e.g. McArthur River, Mount Isa, and Broken Hill). The majority of these ore bodies are associated with rifts and aulacogens. Major Precambrian examples associated with rifting include McArthur River and Mount Isa, Sullivan, the Belt basin, Michigan, and probably the Adelaide Geosyncline. Rift environments have also been proposed for the sedimentary sequence in the copperbelt of Zaire and Zambia (Annels, 1984), and for the younger rocks which host the Owambo basin-type ore association.

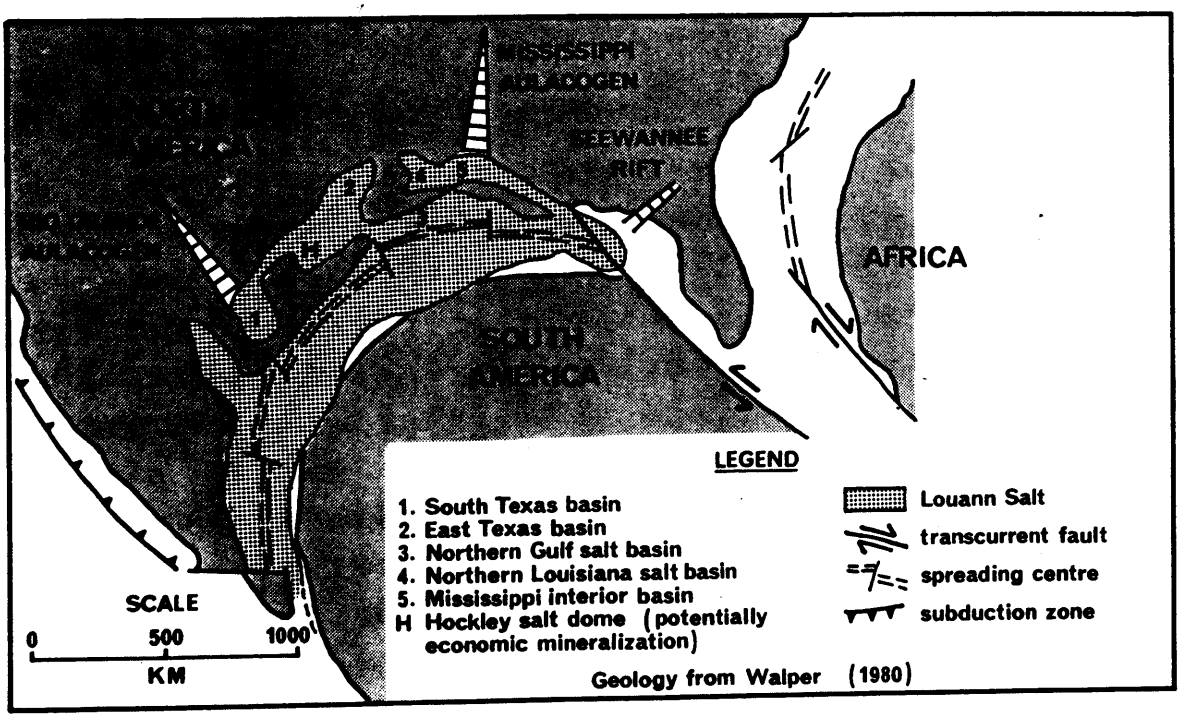

Fig. 140
Distribution of the Louann Salt during continental separation in the Jurassic. The Louann Salt was the probable source of metal-bearing brines and minor base metal mineralization present in each of the identified basins.

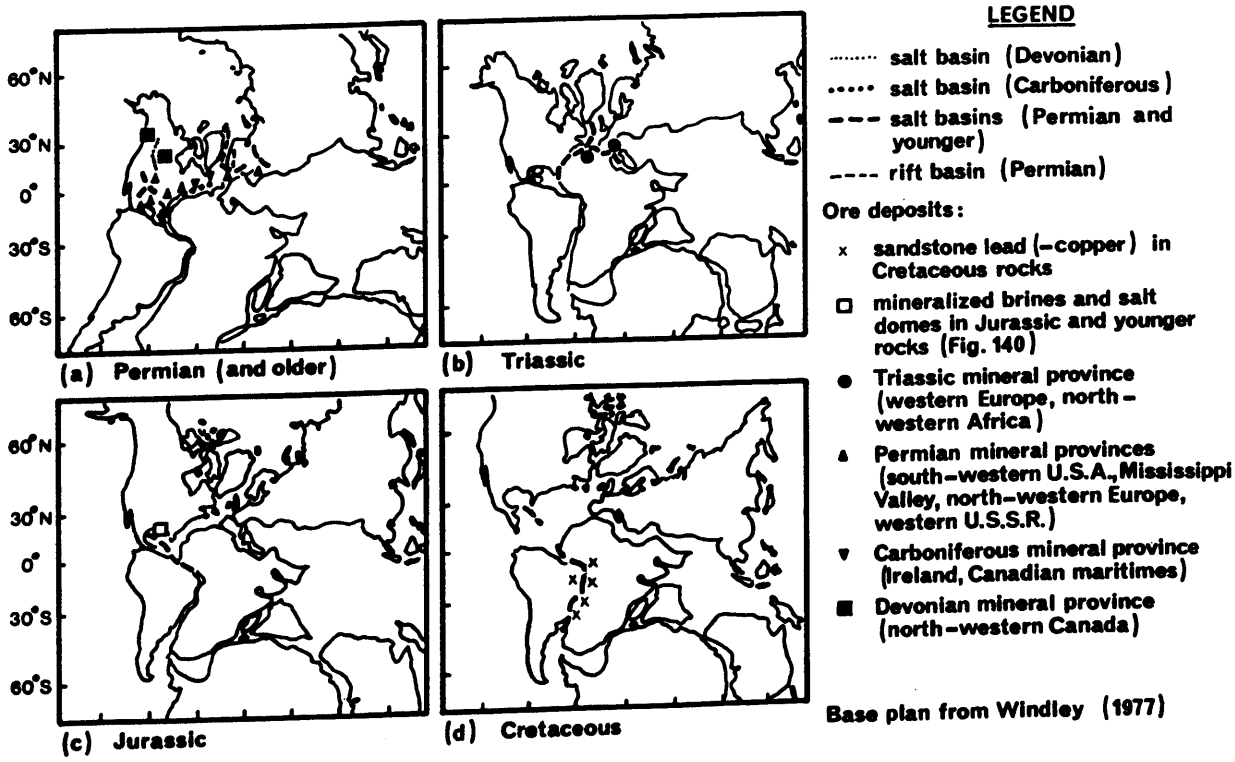

Fig. 141
Relationship between salt basins, basin-related ore deposits and the break-up of Pangaea. Salt basins formed during rifting at intermediate latitudes, and most ore deposits formed adjacent to the basins in sedimentary rocks of similar age to the halite.

Many of the major periods of formation of basin-related ore deposits correspond to periods of rifting on a continental scale. Ore deposits 1000 to 600 m.y. in age may have formed during the Late Proterozoic break-up of a supercontinent composed of all of the major continents, proposed by Piper (1976). The continents of Gondwanaland and Euramerica united to form another supercontinent in the Silurian, and Asia combined with this in the Permo-Triassic to form the supercontinent of Pangaea (Windley, 1977). Rifting was initiated in northern Europe in the Carboniferous and Permian, prior to the break-up of Pangaea, with the formation of the Oslo graben and major salt basins in the North Sea, Zechstein basin and western U.S.S.R. (Fig. 141a). There is some evidence for minor rifting in the northern part of the North Atlantic region at this time, (e.g. between Greenland and Scandinavia, and east of Newfoundland and Maine) and rift-bounded salt basins formed in the south-western U.S.A. (e.g. near the lead-zinc district of Gilman-Leadville, Colorado; Behre, 1953). Rift-bounded salt basins of Carboniferous age occur in eastern Canada, but salt basins of Carboniferous or Permian age (the probable age of mineralization) are unknown in the southern Appalachian region, in the vicinity of the Mississippi Valley lead-zinc district. However, evidence for such basins might be concealed by the continent-directed thrust belt which formed during the Alleghanian orogeny of Permo-Carboniferous age. The main separation of Pangaea started in the Triassic with the formation of Triassic salt basins in the North Atlantic and Tethys regions, with which the Triassic mineral provinces of southern Europe and north-western Africa are spatially associated (Fig. 141b). This was followed by opening of the Gulf of Mexico in the Jurassic, and the formation of a salt basin which contains mineralized salt domes and brines (Chapter 6.3.4; Figs. 140, 141c). Finally, the South Atlantic region between South America and Africa opened in the Lower Cretaceous, and major salt basins formed (Burke, 1975; Fig. 141d). Mineralization is spatially associated with these basins in Africa and Brazil.

Some of the important periods during which major salt basins, rift zones, and ore deposits formed coincide with major variations in

the sulphur isotopic ratios of evaporite minerals (and therefore of contemporaneous sea water sulphate). The secular trend for sea water sulphate shows excursions to lighter values during the late Proterozoic, Devonian, Permo-Triassic and Lower Cretaceous (Claypool et al., 1980). The important rifting and mineralizing event during the Permian and Triassic is characterized by the lightest sea water sulphate ratios at any time subsequent to the late Proterozoic. The light values characteristic of the late Proterozoic might themselves represent an event, rather than a continuous trend to lighter values in older rocks, if the heavy values which Robinson and Ohmoto (1973) suggest for Middle Proterozoic sea water are correct (Chapter 6.2.5). The secular variation of the sulphur isotopic composition of sea water sulphate is a function of various sulphur fluxes which act on the ocean, and the reasons for these variations are not well understood (e.g. precipitation of gypsum should cause only a slight depletion in the $\delta^{34}S$ ratio of sea water sulphate). Possibly they occur because the $\delta^{34}S$ ratio of sulphate ion in solution is very sensitive to change when its concentration is low, during periods in which major salt basins form (Faure, 1977). Nevertheless, the above relationships show that some important periods during which basin-related ore deposits have formed coincide with light sulphur isotopic ratios of sea water sulphate. This may reflect the formation of major salt basins (and therefore huge volumes of potential ore fluid) at these times.

This model has a number of important implications. Not all salt basins within a particular tectonic province are exactly contemporaneous, and single basins probably dewater during episodic events. Therefore ore deposits which are spatially and temporally related, and which show identical chemical and isotopic characteristics, have not necessarily formed during a single pass of ore fluid, although they might have formed during a single, protracted and episodic dewatering event. Conversely, ore deposits formed from fluids which migrated through different pathways during a single pass of ore fluid (or during a protracted dewatering event) could show different chemical or isotopic characteristics (Chapter 5.3.8). Most ore deposits will be broadly contemporaneous with salt deposition within basins to which the ore deposits are genetically

related. However, ore fluids of this type could penetrate large stratigraphic thicknesses, and major exceptions will occur in which ore deposits form in rocks older than the salt basin to which they are genetically related (e.g. Saint Salvy, and the Saxonic vein association; Chapters 5.3.14, 5.3.15). It is not obvious why some salt basins lack spatially associated ore deposits (e.g. the Miocene of the Mediterranean region) but this may be related to the subsequent burial history of the salt, which can determine if heated brines are produced. Alternatively, the lack of ore deposits may be related to the absence of fluid channelways adjacent to the salt basins, such as inter-connected aulacogens and continental rifts, or permeable shelf or platform sequences.

It is concluded that there is a close temporal and spatial relationship between rifting, formation of salt basins and the existence of many mineral districts and provinces. The time dependence of the ore deposits can be explained as a response to both deep-seated processes (i.e. rifting, which results in salt basins and high geothermal gradients), and shallow processes (i.e. circulation of heated, connate, evaporitic brines). This model can explain the occurrence of mineralization of one type, such as Tsumeb-type mineralization, which is distributed over large regions but restricted in time. The time dependence is determined by the time of continental rifting at latitudes suitable for the formation of salt basins. The type of mineralization is primarily a function of the chemical composition of the rocks traversed by the resulting brines, and the form and composition of the permeable sites available for mineralization.

CHAPTER SEVEN

CONCLUSIONS

The following conclusions result from this study:

1. The Tsumeb pipe and associated strata-bound cavities formed by karsting and solution collapse during subaerial exposure of the top of the Tsumeb Subgroup. These structures were subsequently filled with silt (previously unrecognized) and sand during deposition of the overlying Mulden Group. Fractures which formed at the margins of the pipe at this time were also filled with sand. Similar, mineralized structures elsewhere in the Otavi Mountain Land and central Africa also formed during this, and earlier, periods of karsting.

2. The Tsumeb pipe and other ore-bearing structures of the Otavi Mountain Land were mineralized at approximately 600m.y., prior to major deformation of the Mulden Group, or during the early stages of such deformation.

3. Previous workers concluded that the Tsumeb ore body, and the isotopically-related Kombat ore body, formed from saline waters and brines in which sodium and chloride were the dominant ions (I=1,4-3,4). It is calculated here that the Tsumeb ore fluid had an oxygen fugacity smaller than 10^{-33} (and probably greater than 10^{-39}), and a sulphur fugacity greater than $10^{-13,5}$. Much ore deposition occurred at a large sulphur fugacity, greater than $10^{-8,5}$, from a fluid with a large Cu:Fe ratio. Unless the fluid had significantly different concentrations of both potassium and calcium (or carbon) relative to the ore fluids which have formed other base metal ore bodies, two further conclusions can be made. These are: (1) the pH of the fluid was between 3 and 6, and (2) much ore deposition occurred at a high total concentration of sulphur (approximately 10^{-1}m).

4. The dominant cause of vertical zoning of rock alteration in the Tsumeb pipe was the mixing of at least two fluids of different chemical compositions, as indicated by lead isotope evidence. The

zoning of minerals which belong to the Cu-Fe-As-S system was controlled mostly by variations in the total sulphur concentration of the ore fluid (which in turn controlled the sulphur fugacity of the fluid).

5. The unique mineralogical and chemical composition of Tsumeb-type ore, both in the Otavi Mountain Land and throughout central Africa, resulted from the unique compositions of the fluids which formed these ore bodies. The unique feature of these fluids was the combination of their copper-rich composition (a function of the availability of copper and the temperatures of the fluids) and their content of unusual trace elements.

6. The Tsumeb ore body and other members of the Owambo basin-type ore association throughout central Africa (i.e. the Tsumeb, Berg Aukas and Tschudi types of mineralization) contain sulphur of crustal, probably evaporitic, origin. There is geochemical and sulphur isotopic evidence that an evaporite horizon in the upper part of the Tsumeb Subgroup was the dominant cause of ore deposition in the Tsumeb ore body. Lead isotope data indicate that stratiform copper mineralization of Tschudi type replaced pre-existing strata-bound pyrite.

7. Geological and lead isotope data from members of the Owambo basin-type ore association, and constraints imposed by the temperature, composition and $\delta^{18}O$ ratio of the Tsumeb ore fluid, are most consistent with an evolved connate origin for the ore fluids which formed these ore deposits. The probable source of the fluids which formed ore deposits in the Otavi Mountain Land were former evaporite deposits within the Nosib Group (or younger units) in a graben farther to the south. The preferred model, based on lead isotope data, is that the ore fluids which formed each of the members of the Owambo basin-type ore association migrated through separate aquifers at the same time, although it is possible that the events were slightly separated in time. The data are consistent with the formation of very different types of mineralization on a regional scale during a single dewatering event. These different types of mineralization include karst-filling copper-lead (-zinc)

mineralization (Tsumeb type), karst-filling lead-zinc mineralization (Berg Aukas type), and stratiform copper mineralization in sandstone (Tschudi type). The ore fluids were derived from large areas of basin and migrated more than 60 km up-dip to form mineral districts at least 5000 sq. km in area, penetrating sedimentary sequences more than 1000 m thick en route.

8. Lead isotopic data from galena of the Tsumeb, Berg Aukas, and Tschudi types of mineralization indicate that rocks of the Kombat Formation were a possible source of lead in the ore bodies. Additional components of lead were added during lateral migration of the ore fluids through sedimentary rocks of the south-eastern Owambo basin, and these rocks were probable sources of other metals in the ore fluids, including elements such as germanium and gallium. The "metal domains" of Routhier (1983) can therefore determine the type of mineralization present in a mineral district, while not necessarily being a major reason for the formation of the mineral district.

9. The time dependence of many mineral districts marginal to sedimentary basins, including the districts which host the Owambo basin-type ore association of central Africa, is primarily related to the periodic release of heated brine from the adjacent basins. The position and timing of such districts is controlled by the localized and time-dependent nature of rifting, continental break-up, and the formation of salt basins. The compositional types of ore deposits formed (e.g. Tsumeb type) depend on the metals transported by the ore fluids. The location of an individual ore deposit (e.g. Tsumeb) is determined by other variables, such as permeability (e.g. paleokarst) and the availability of sulphur.

The above conclusions have significance for mineral exploration. This study reinforces previous evidence for the importance of paleokarst features and evaporites in ore genesis, and emphasizes that both can be guides to individual ore bodies, not just to mineral districts. The model developed above implies that the presence of one type of ore body can indicate potential for other types of ore body in the same area, in different rock types and ore

loci. Finally, lead isotope ratios of single galena samples, or even secondary lead minerals, could be used in many instances to determine if a mineral prospect from one of the central African fold belts considered in this study was of Berg Aukas type, or of the economically more important Tsumeb type.

Aharon, P., Kolodny, Y., and Sass, E., 1977, Recent hot brine dolomitization in the "Solar Lake", Gulf of Elat, isotopic, chemical and mineralogical study: Jour. Geology, v.85, p.27-48.

Akande, S.O., and Zentilli, M., 1984, Geologic, fluid inclusion, and stable isotope studies of the Gays River lead-zinc deposit, Nova Scotia, Canada : Econ. Geol., v.79, p.1187-1211.

Allsopp, H.L., and Ferguson, J., 1970, Measurements relating to the genesis of the Tsumeb pipe, SWA: Earth Planet. Sci. Letters, v.9, p.448-453.

Anderson, R.Y., and Kirkland, D.W., 1980, Dissolution of salt deposits by brine density flow: Geology, v.8, p.66-69.

Andrew, A., Godwin, C.I., and Sinclair, A.J., 1984, Mixing line isochrons : a new interpretation of galena lead isotope data from southeastern British Columbia : Econ. Geol., v.79, p.919-932.

Andrew, C.J., and Ashton, J.H., 1985, Regional setting, geology and metal distribution patterns of Navan orebody, Ireland: Inst. Mining Metallurgy Trans., sec. B., v.94, p.B66-B93.

Annels, A.E., 1974, Some aspects of the stratiform ore deposits of the Zambian copperbelt and their genetic significance, *in* Bartholomé, P., ed., Gisements stratiformes et provinces cuprifères: Centenaire de la Société Géologique de Belgique, Liège, p.235-254.

---------- 1979, Mufulira greywackes and their associated sulphides: Inst. Mining Metallurgy Trans., sec. B., v.88, p.B15-B23.

---------- 1984, The geotectonic environment of Zambian copper-cobalt mineralization: Geol. Soc. London Jour., v.141, p.279-289.

Armstrong, A.K., and McKevett, E.M., Jr., 1975, Relations between Triassic carbonate sabkhas and Kennecott-type copper deposits, Wrangell Mountains, Alaska: Econ. Geol., v.70, p.1316-1317.

Bachtiger, K., 1963, Die Kupfer- und Uranmineralisationen der Mürtschenalp (Kt. Glarus, Schweiz.): Beitr. Geol. Schweiz., Geotech. Ser., v.38, 113p.

Badham, J.P.N., 1976, Orogenesis and metallogenesis with reference to the silver-nickel, cobalt arsenide ore association: Geol. Assoc. Canada, Spec. Paper 14, p.559-571.

---------- 1978, Magnetite-apatite-amphibole-uranium and silver arsenide mineralizations in Lower Proterozoic igneous rocks, East Arm, Great Slave Lake, Canada: Econ. Geol., v.73, p.1474-1491.

---------- 1981, Shale-hosted lead-zinc deposits: products of exhalation of formation waters?: Inst. Mining Metallurgy Trans., sec. B., v.90, p.B70-B76.

Baka, D.M., 1975, Les mineralisations en Cu, Pb, Zn de M'Passa (Congo-Brazzaville). Exemple du role metallogenique des emersions: These, Docteur de Specialite (Geologie Appliquee - Metallogenie), Universite de Nancy 1, 172p.

Bally, A.W., and Snelson, S., 1980, Realms of subsidence: Canadian Soc. Petroleum Geologists, Mem., v.6, p.9-74.

Barnes, H.L., 1979, Solubilities of ore minerals, *in* Barnes, H.L., ed., Geochemistry of hydrothermal ore deposits: New York, John Wiley and Sons, p.404-460.

Barnes, I., and Hem, J.D., 1973, Chemistry of subsurface waters: Ann. Rev. Earth Planet. Sci., v.1, p.157-181.

Barr, M.W.C., Cahen, L., and Ledent, D., 1977, Geochronology of syntectonic granites from central Zambia: Lusaka granite and granite NE of Rufunsa: Ann. Soc. Géol. Belgique, v.100, p.47-54.

Barrett, T.J., and Anderson, G.M., 1982, The solubility of sphalerite and galena in NaCl brines: Econ. Geol., v.77, p.1923-1933.

Bartholomé, P., 1974, On the diagenetic formation of ores in sedimentary beds with special reference to Kamoto, Shaba, Zaïre, *in* Bartholomé, P., ed., Gisements stratiformes et provinces cuprifères: Centenaire de la Société Géologique de Belgique, Liège, p.203-213.

Barton, P.B., 1970, Sulfide petrology: Mineralog. Soc. America, Spec. Paper 3, p.187-198.

Bateman, A.M., and McLaughlin, D.H., 1920, Geology of the ore deposits of Kennecott, Alaska: Econ. Geol., v.15, p.1-80.

Beales, F.W., and Hardy, J.L., 1977, The problem of recognition of occult evaporites with special reference to southeast Missouri: Econ. Geol., v.72, p.487-490.

---------- 1980, Criteria for the recognition of diverse dolomite types with an emphasis on studies on host rocks for Mississippi Valley-type ore deposits: Soc. Econ. Paleontologists Mineralogists Spec. Pub. no. 28, p.197-213.

Beck, R., 1905, The nature of ore deposits: Engineering and Mining Jour., v.1.

Behr, H-J., Ahrendt, H., Martin, H., Porada, H., Röhrs, J., and Weber, K., 1983a, Sedimentology and mineralogy of Upper Proterozoic playa-lake deposits in the Damara Orogen, *in* Martin, H., and Eder, F.W., eds., Intracontinental fold belts : Springer-Verlag, p.577-610.

Behr, H-J., Ahrendt, H., Porada, H., Röhrs, J., and Weber, K., 1983b, Upper Proterozoic playa and sabkha deposits in the Damara Orogen, SWA/Namibia : Geol. Soc. South Africa Spec. Pub., v.11, p.1-20.

Behr, H.J., Ahrendt, H., Schmidt, A., and Weber, K., 1981, Saline horizons acting as thrust planes along the southern margin of the Damaran Orogen (Namibia/SW-Africa): Geol. Soc. London Spec. Pub., v.9, p.167-172.

Behr, H-J., and Horn, E.E., 1982, Fluid inclusion systems in metaplaya deposits and their relationships to mineralization and tectonics : Chem. Geology, v.37, p.173-189.

Behre, C.H., Jr., 1953, Geology and ore deposits of the west slope of the Mosquito Range : U.S. Geol. Survey Prof. Paper 235, 176 p.

Bein, A., and Land, L.S., 1982, San Andres carbonates in the Texas Panhandle : Bur. Econ. Geol., Austin, Texas, Rept. of Investigations no. 121, 48 p.

Berning, J., 1951, Report on the geology immediately west and north-west of Tsumeb West: Unpub. rept. Tsumeb Corporation Ltd., Tsumeb.

Berry, L.G., 1971, ed., The silver-arsenide deposits of the Cobalt-Gowganda region, Ontario: Canadian Mineralogist, v.11, no. 1, 429p.

Bigotte, G., 1959, Contribution à la geologie du bassin du Niari. Étude sédimentologique et metallogénique de la région minière: Bull. Dir. Mines et Géol. A.E.F., Brazzaville, v.9, 186p.

Billings, G.K., Hitchon, B., and Shaw, D.R., 1969a, Geochemistry and origin of formation waters in the Western Canada sedimentary basin, 2. Alkali Metals: Chem. Geology, v.4, p.211-223.

---------- 1969b, Geochemistry and origin of formation water in the Western Canada sedimentary basin - III - Factors controlling chemical composition: Geochim. et Cosmochim. Acta, v.35, p.567-598.

Billings, G.K., Kessler, S.E., and Jackson, S.A., 1969c, Relation of zinc-rich formation waters, Northern Alberta to the Pine Point ore deposit: Econ. Geol., v.64, p.385-391.

Bishop, R.A., 1956, Explanation of the Avonlea fault block, southern Saskatchewan: Jour. Alberta Soc. Petroleum Geologists, v.4, no. 10, p.235-236.

Bjørlykke, A., and Sangster, D.F., 1981, An overview of sandstone lead deposits and their relation to red-bed copper and carbonate-hosted lead-zinc deposits: Econ. Geol., 75th Anniv. Vol., p.179-213.

Bjørlykke, A., and Thorpe, R.I., 1982, The source of lead in the Osen sandstone lead deposit on the Baltic Shield, Norway: Econ. Geol., v.77, p.430-440.

Blount, D.N., and Moore, C.H., Jr., 1969, Depositional and non-depositional carbonate breccias, Chiantla Quadrangle, Guatemala: Geol. Soc. America Bull., v.80, p.429-442.

Both, A., 1978, Remobilization of mineralization during retrograde metamorphism, Broken Hill, New South Wales, Australia, *in* Verwoerd, W.J., ed., Mineralization in metamorphic terranes: Geol. Soc. South Africa Spec. Pub. no.4, p.481-489.

Botha, B., 1960, The arenaceous rocks and the pseudo-aplite of the Otavi Mountain Land, SWA: D.Sc thesis, Univ. Pretoria, South Africa.

Botz, R.W., and von der Borch, C.C., 1984, Stable isotope study of carbonate sediments from the Coorong area, South Australia: Sedimentology, v.31, p.837-849.

Boulegue, J., 1978, Metastable sulfur species and trace metals (Mn, Fe, Cu, Zn, Cd, Pb) in hot brines from the French Dogger: Am. Jour. Sci., v.278, p.1394-1411.

Bowles, C.G., 1977, Economic implications of a new hypothesis of origin of uranium- and copper-bearing breccia pipes, Grand Canyon, Arizona: U.S. Geol. Survey Circ. 753, p.25-27.

Bowles, C.G., and Braddock, W., 1963, Solution breccias of the Minnelusa Formation in the Black Hills of South Dakota and Wyoming: U.S. Geol. Survey Prof. Paper 475-C, p.91-95.

Braddock, W.A., 1963, Geology of the Jewel Cave southwest quadrangle, Custer County, South Dakota: U.S. Geol. Survey Bull. 1063-G.

Brandt, R.T., 1955, The geology and mineral resources of the Big Concession, Mumbwa District: Bull. Geol. Survey N. Rhodesia, v.2, 56p.

Brant, A.A., 1973a, Tsumeb fluid inclusion studies: Unpub. mem., Newmont Exploration Ltd., Danbury, Sept. 24th 1973.

---------- 1973b, Tsumeb fluid inclusion studies: Unpub. mem., Newmont Exploration Ltd., Danbury, 10th Oct 1973.

Brecke, E.A., 1979, A hydrothermal system in the midcontinent region: Econ. Geol., v.74, p.1327-1335.

Brett, R., 1964, Experimental data from the system Cu-Fe-S and their bearing on exsolution textures in ores: Econ. Geol., v.59, p.1241-1269.

Brevart, O., Dupré, B., and Allègre, C.J., 1982, Metallogenic provinces and the remobilization process studied by lead isotopes: lead-zinc ore deposits from the southern Massif Central, France: Econ. Geol., v.77, p.564-575.

Brigo, L., Kostelka, L., Omenetto, P., Schneider, H-J., Schroll, E., Schulz, O., and Štrucl, I., 1977, Comparative reflections on four Alpine Pb-Zn deposits, *in* Klemm, D.D., and Schneider, H-J., eds., Time and strata-bound ore deposits: Springer-Verlag, p.273-293.

Brooks, C., Hart, S.R., and Wendt, I., 1972, Realistic use of two-error regression treatments as applied to rubidium-strontium data : Revs. Geophysics Space Physics, v.10, p.551-577.

Brown, A.C., 1978, Stratiform copper deposits - evidence for their post-sedimentary origin: Minerals Sci. Eng., v.10, p.172-181.

Brown, J.S., 1967, Isotopic zoning of lead and sulfur in southeast Missouri: Econ. Geol. Mon. 3, p.410-426.

Buckland, F.C., 1959, Germanium in British Columbia: Western Miner and Oil Review, v.32, no. 9, p.30-34.

Buffard, R., 1977, Le Bassin de Kakontwe, Shaba Meridional, Republique du Zaïre. Evolution d'un Bassin Carbonate: Ann. de la Société Géologique de Belgique, v.100, p.183-192.

Buffler, R.T., Watkins, J.S., Shaub, F.J., and Worzel, J.L., 1980, Structure and early geologic history of the deep central Gulf of Mexico Basin, *in* Pilger, R.H., Jr., ed., Proc. Symp., The origin of the Gulf of Mexico and the early opening of the central North Atlantic Ocean: Louisana State Univ., Baton Rouge, p.1-16.

Bugge, J.A.W., 1978, Norway, *in* Bowie, S.H.U., Kvalheim, A., and Haslam, H.W., eds., Mineral deposits of Europe: London, Inst. Mining Metallurgy, v.1, p.199-249.

Bührmann, H.T., 1973, The geology of the northern flank of the Otavi Valley syncline between Hermanstal Ost 513 and Gross Otavi 805: Unpub. rept. Tsumeb Corporation Ltd., Tsumeb.

Burger, A.J., Clifford, T.N., and Miller, R.McG., 1976, Zircon U-Pb ages of the Fransfontein granitic suite, northern South West Africa: Precambrian Research, v.3, p.415-431.

Burke, K., 1975, Atlantic evaporites formed by evaporation of water spilled from Pacific, Tethyan and Southern oceans: Geology, v.3, p.613-616.

Burnie, S.W., Schwarcz, H.P., and Crocket, J.H., 1972, A sulfur isotopic study of the White Pine mine, Michigan: Econ. Geol., v.67, p.895-914.

Cahen, L., 1974, Geological background to the copper-bearing strata of southern Shaba (Zaïre), *in* Bartholomé, P., ed., Gisements stratiformes et provinces cuprifères: Centenaire de la Société Géologique de Belgique, Liège, 1974, p.57-77.

---------- 1978, La stratigraphie et la tectonique du Supergroupe Ouest-Congolien dans les zones mediane et externe de l'orogène Ouest -Congolien (Pan Africaine) au Bas-Zaïre et dans les regions voisines: Ann., Musée Royal de l'Afrique Centrale, Tervuren, v.83, 150p.

Caïa, J., 1976, Paleogeographical and sedimentological controls of copper, lead and zinc mineralizations in the Lower Cretaceous sandstones of Africa: Econ. Geol., v.71, p.409-422.

Callahan, W.H., 1971, Evaluation of exploration possibilities in the Otavi Mountain area, South West Africa: Unpub. rept. Tsumeb Corporation Ltd., Tsumeb, April 1971, 40p.

Camfield, P.A., and Gough, D.I., 1977, A possible Proterozoic plate boundary in North America: Canadian Jour. Earth Sci., v.14, p.1229-1238.

Carpenter, A.B., 1978, Origin and chemical evolution of brines in sedimentary basins: Oklahoma Geol. Survey Circ., v.79, p.60-77.

---------- 1979, Interim report on lead and zinc in oil-field brines in the central Gulf Coast and in southern Michigan: Soc. Mining Engineers, Am. Inst. Mining Engineers, Preprint, v.79-95, 1979, p.1-15.

Carpenter, A.B., and Grethen, B.L., 1979, The origin of metal-rich brines in sedimentary basins (abstract): Am. Inst. Mining Engineers, mtg., 108th, New Orleans, Abstracts with Programs, p.18.

Carpenter, A.B., and Trout, M.L., 1978, Geochemistry of bromide-rich brines of the Dead Sea and southern Arkansas: Oklahoma Geol. Survey Circ., v.79, p.78-88.

Carpenter, A.B., Trout, M.L., and Pickett, E.E., 1974, Preliminary report on the origin and chemical evolution of lead- and zinc-rich oil field brines in Central Mississippi: Econ. Geol., v.69, no. 8, p.1191-1206.

Carstens, H., and Dypvik, H., 1981, Abnormal formation pressure and shale porosity: Am. Assoc. Petroleum Geologists Bull., v.65, no. 2, p.344-350.

Carvalho, H.d.S., Purwoko, Siswoyo, Thamrin, M., and Vacquier, V., 1980, Terrestrial heat flow in the Tertiary basin of central Sumatra: Tectonophysics, v.69, p.163-188.

Casadevall, T., and Ohmoto, H., 1977, Sunnyside mine, Eureka mining district, San Juan County, Colorado: geochemistry of gold and base metal ore deposition in a volcanic environment: Econ. Geol., v.72, p.1285-1320.

Cathles, L.M., and Smith, A.T., 1983, Thermal constraints on the formation of Mississippi Valley-type lead-zinc deposits and their implications for episodic basin dewatering and deposit genesis : Econ. Geol., v.78, p.983-1002.

Chandler, F.W., 1984, Sedimentary setting of an Early Proterozoic copper occurrence in the Cobalt Group, Ontario : a preliminary assessment : Canada Geol. Survey Paper 84-1A, p.185-192.

Chatterjee, A.K., 1979, Geology of the Meat Cove zinc deposit, Cape Breton Island, Nova Scotia: Nova Scotia Dept. Mines Paper, v.79-3, 27p.

Chave, K.E., 1960, Evidence on history of sea water from chemistry of deeper subsurface waters of ancient basins: Am. Assoc. Petroleum Geologists Bull., v.44, no. 3, p.357-370.

Christiansen, E.A., 1967, Collapse structures near Saskatoon, Saskatchewan, Canada: Canadian Jour. Earth Sci., v.4, p.757-767.

---------- 1971, Geology of the Crater Lake collapse structure in southeastern Saskatchewan: Canadian Jour. Earth Sci., v.8, no. 12, p.1505-1524.

Christiansen, E.A., Gendzwill, D.J., and Derry, D.R., 1973, Pipe-shaped structures: Econ. Geol., v.68, no. 8, p.1334-1336.

Cikin, M., and Drysdale, A., 1971, The geology of the country north-west of Mumbwa (the Big Concession): Geol. Survey Zambia Rept., v.27, 72p.

Clauer, N., and Kröner, A., 1979, Strontium and argon isotopic homogenization of pelitic sediments during low-grade regional metamorphism: the Pan African Upper Damara sequence of northern Namibia (South West Africa): Earth Planet. Sci. Letters, v.43, p.117-131.

Claypool, G.E., Holser, W.T., Kaplan, I.R., Sakai, H., and Zak, I., 1980, The age curves of sulfur and oxygen isotopes in marine sulfate and their mutual interpretation: Chem. Geology, v.28, p.199-260.

Clayton, R.N., Friedman, I., Graf, D.L., Mayeda, T.K., Meents, W.F., and Shimp, N.F., 1966, The origin of saline formation waters - 1. Isotopic composition: Jour. Geophys. Research, v.71, p. 3869-3882.

Clifford, T.N., 1967, The Damaran episode in the Upper Proterozoic-Lower Paleozoic structural history of southern Africa: Geol. Soc. America Spec. Paper 92, 100 p.

Coleman, M.L., and Moore, M.P., 1978, Direct reduction of sulfates to sulfur dioxide for isotopic analysis: Analytical Chemistry, v.50, p.1594-1595.

Collins, A.G., 1975, Geochemistry of oilfield waters: Elsevier, 496 p.

Connor, J.J., and Ebens, R.J., 1980, Geochemistry of bedrock units in Missouri and parts of adjacent states : U.S. Geol. Survey Prof. Paper 954-F, 55p.

Cooper, J.A., 1970, Lead isotope classification of the A.B.H. Consols and Browne's shaft veins at Broken Hill, N.S.W.: Australian Inst. Mining Metallurgy Proc., no.234, p.67-69.

Cornelius, C-D., 1975, Geothermal aspects of hydrocarbon exploration in the North Sea area: Norges geologiske undersøkelse, v.316, p.29-67.

Cousteau, H., Rumeau, J.L., Sourisse, C., Chiarelly, A., and Tison, J., 1975, Classification hydrodynamique des bassins sédimentaires, utilisation combinée avec d'autres méthodes pour rationaliser l'exploration dans des bassins non-productifs: World Petroleum Cong., 9th, Proc., Tokyo, 1975, Applied Science Pub. (London), v.2, p.105-119.

Cox, S.F., Etheridge, M.A., and Hobbs, B.E., 1981, The experimental ductile deformation of polycrystalline and single crystal pyrite : Econ. Geol., v.76, p.2105-2117.

Craig, J.R., and Barton, P.B., 1973, Thermochemical approximations for sulfosalts : Econ. Geol., v.68, p.493-506.

Creelman, R.A., 1983, A petrological, mineralogical and lead isotope study of copper in sandstones and related sediments: Unpub. Ph.D. thesis, Macquarie University, North Ryde, Australia.

Crerar, D.A., and Barnes, H.L., 1976, Ore solution chemistry V. Solubilities of chalcopyrite and chalcocite assemblages in hydrothermal solution at 200° to 350°C: Econ. Geol., v.71, p.772-794.

Crowell, J.C., 1981, An outline of the tectonic history of southeastern California, *in* Ernst, W.G., ed., The geotectonic development of California: Prentice-Hall, p.583-600.

Cubitt, J., 1979, Geochemistry, mineralogy and petrology of Upper Paleozoic shales of Kansas: Kansas Geol. Survey Bull. 217, 117p.

Cumming, G.L., and Richards, J.R., 1975, Ore lead isotope ratios in a continuously changing earth: Earth Planet. Sci. Letters, v.28, p.155-171.

Cumming, G.L., and Robertson, D.K., 1969, Isotopic composition of lead from the Pine Point deposit: Econ. Geol., v.64, p.731-732.

Cummins, A.B., and Given, I.A., 1973, SME Mining Engineering Handb., v. 1: New York, Soc. Mining Eng., Am. Inst. Mining Metallurgy Petroleum Engineers.

Dahlkamp, F.J., 1978, Geologic appraisal of the Key Lake U-Ni deposits, northern Saskatchewan: Econ. Geol., v.73, p.1430-1449.

Dalgarno, C.R., and Johnson, J.E., 1968, Diapiric structures and late Precambrian - early Cambrian sedimentation in Flinders Ranges, South Australia: Am. Assoc. Petroleum Geologists Mem. 8, p.301-314.

Davidson, C.F., 1965, A possible mode of origin of strata-bound copper ores: Econ. Geol., v.60, p.942-954.

---------- 1967, Discussion of paper by Beales and Jackson, 1967: Inst. Mining Metallurgy Trans., sec. B., v.76, p.B175.

Davies, G.R., 1977, Former magnesian calcite and aragonite submarine cements in upper Paleozoic reefs of the Canadian Arctic: a summary: Geology, v.5, p.11-15.

Dean, W.E., Davies, G.R., and Anderson, R.Y., 1975, Sedimentological significance of nodular and laminated anhydrite: Geology, v.3, p.367-372.

Dechow, E., and Jensen, M.L., 1965, Sulfur isotopes of some Central African sulfide deposits: Econ. Geol., v.60, p.894-941.

Degens, E.T., and Paluska, A., 1979, Hypersaline solutions interact with organic detritus to produce oil: Nature, v.281, p.666-668.

de Mille, G., Shouldice, J.R., and Nelson, H.W., 1964, Collapse structures related to evaporites of the Prairie Formation, Saskatchewan: Geol. Soc. America Bull., v.75, p.307-316.

Derriks, J.J., and Vaes, J.F., 1956, The Shinkolobwe uranium deposit: Current status of our geological and metallogenic knowledge: Internat. Conf., Peaceful uses of Atomic Energy, New York, 1956, v.6, p.94-128.

de Vos, W., Viaene, W., and Moreau, J., 1974, Minéralogie du gisement de Kipushi, Shaba, Zaïre, *in* Bartholomé, P., ed., Gisements stratiformes et provinces cuprifères: Centenaire de la Société Géologique de Belgique, Liège, 1974, p.165-183.

Deuser, W.G., 1970, Extreme $^{13}C/^{12}C$ variations in Quaternary dolomites from the continental shelf: Earth Planet. Sci. Letters, v.8, p.118-124.

de Voto, R.H., 1983, Central Colorado karst-controlled lead-zinc-silver deposits (Leadville, Gilman, Aspen, and others), a late Paleozoic Mississippi Valley-type district: Internat. Conf. on Mississippi Valley-type lead-zinc deposits, Proc., p.459-485.

de Witt, W., Jr., Sable, E.G., and Cohee, G.V., 1979, Evaporite deposits in Mississippian rocks of the eastern United States: U.S. Geol. Survey Prof. Paper 1010-T, p.430-439.

Dibbler, T.W., Jr., 1955, 2. Geology of the Imperial Valley region, California: Californian Div. Mines Geol., Bull., v.170, p.21-28.

Dimanche, F., 1974, Paragenèse des sulfures de cuivre dans les gisements du Shaba (Zaïre): I. Kipushi; II. Kamoto, *in* Bartholomé, P., ed., Gisements stratiformes et provinces cuprifères: Centenaire de la Société Géologique de Belgique, Liège, 1974, p.185-201.

Dings, M., and Whitebread, D.H., 1965, Geology and ore deposits of the Metaline zinc-lead district, Pend Oreille County, Washington: U.S. Geol. Survey Prof. Paper 489, 109 p.

la Direction de la Geologie, 1968, Les minéralisations plombifères de la République Démocratique du Congo, *in* Gisements de Plomb et Zinc en Afrique: Ann. Mines et Geol. Tunisie, v.23, p.357-391.

Doe, B.R., and Delevaux, M.H., 1972, Source of lead in southeast Missouri galena ores: Econ. Geol., v.67, p.409-425.

Doe, B.R., and Stacey, J.S., 1974, The application of lead isotopes to the problems of ore genesis and ore prospect evaluation: a review: Econ. Geol., v.69, p.757-776.

Doe, B.R., Stuckless, J.S., and Delevaux, M.H., 1983, The possible bearing of the granite of the UPH deep drill holes, northern Illinois, on the origin of Mississippi Valley ore deposits: Jour. Geophys. Research, v.88, p.7335-7345.

Doe, B.R., and Zartman, R.E., 1979, Plumbotectonics I, The Phanerozoic, *in* Barnes, H.L., ed., Geochemistry of hydrothermal ore deposits, 2nd ed.: New York, John Wiley and Sons, p.22-70.

Dolanski, J., 1974, Sulvanite from Thorpe Hills, Utah: Am. Mineralogist, v.59, p.307-313.

Dozy, J.J., 1970, A geological model for the genesis of the lead-zinc ores of the Mississippi Valley, U.S.A.: Inst. Mining Metallurgy Trans., sec. B., v.79, p.B163-B170.

Dunsmore, H.E., 1977, A new genetic model for uranium-copper mineralization, Permo-Carboniferous basin, northern Nova Scotia : Canada Geol. Survey Paper 77-1B, p.247-252.

Dvorov, V.I., and Pavlov, D.I., 1978, Near-fault zones of sulfide enrichment and a possible mechanism for formation of metalliferous brines: Internat. Geol. Rev., v.21, no.7, p.806-814.

Eichmann, R., and Schidlowski, M., 1975, Isotopic fractionation between coexisting organic carbon-carbonate pairs in Precambrian sediments: Geochim. et Cosmochim. Acta, v.39, p.585-595.

Emslie, D.P., 1978, A mineralogical study of the copper, lead and zinc sulphides of the Otavi Mountainland: Technical Mem., Mineralogy Division, Natl. Inst. Mineralogy (Johannesburg), 15th May 1978, no. 13136.

---------- 1979, The mineralogy and geochemistry of the copper, lead and zinc sulphides of the Otavi Mountainland, South West Africa : Unpub. Ph.D. thesis, Univ. Orange Free State.

Faure, G., 1977, Principles of isotope geology: Wiley, 464p.

Federov, V.A., Chernikov, G.E., and Mironov, V.E., 1970, Influence of ionic strength and temperature on the formation of chloro-complexes of zinc : Russian Jour. Inorganic Chemistry, v.15, p.1082-1084.

Ferry, J.M., 1981, Petrology of graphitic sulfide-rich schists from south-central Maine : an example of desulfidation during prograde regional metamorphism : Am. Mineralogist, v.66, p.908-930.

Fisher, W.L., and Rodda, P.U., 1969, Edwards Formation (Lower Cretaceous), Texas: dolomitization in a carbonate platform system: Am. Assoc. Petroleum Geologists Bull., v.53, no. 1, p.55-72.

Fogliérini, F., Bernard, A., and Verraes, G., 1980a, Le gisement des Malines (Gard): Internat. Geol. Congr., 26th, 56 p.

Fogliérini, F., Samama, J.C., and Rey, M., 1980b, Le gisement stratiforme de Largentière (Ardèche): Internat. Geol. Congr., 26th, 55 p.

Foley, N.K., Sinha, A.K., and Craig, J.R., 1981, Isotopic composition of lead in the Austinville - Ivanhoe Pb-Zn district, Virginia: Econ. Geol., v.76, p.2012-2017.

Folk, R.L., and Pittman, J.S., 1971, Length-slow chalcedony: a new testament for vanished evaporites: Jour. Sed. Petrology, v.41, no.4, p.1045-1058.

Ford, D.C., and Ewers, R.O., 1978, The development of limestone cave systems in the dimensions of length and depth: Canadian Jour. Earth Sci., v.15, p.1783-1798.

Foss, D.W., Gatten, O.J., and Young, R.S., 1983, Shiloh Church molybdenum deposit, Polk County, Georgia: Soc. Mining Engineers, Am. Inst. Mining Engineers, Ann. Mtg. 1983, Preprint, V.83-86, 9p.

Francotte, J., Moreau, J., Ottenburgs, R., and Levy, C., 1965, La briartite, $Cu_2(FeZn)GeS_4$, une nouvelle espèce minérale: Soc. Française Minéralogie Cristallographie Bull., v.88, p.432-437.

Frape, S.K., and Fritz, P., 1982, The chemistry and isotopic composition of saline groundwaters from the Sudbury basin, Ontario : Canadian Jour. Earth Sci., v.19, p.645-661.

Frape, S.K., Fritz, P., and McNutt, R.H., 1984, Water-rock interaction and chemistry of groundwaters from the Canadian Shield : Geochim. et Cosmochim. Acta, v.48, p.1617-1627.

Frets, D.C., 1969, Geology and structure of the Huab-Welwitschia area, South West Africa: Precambrian Research Unit, Univ. Cape Town, Bull., v.5, 235p.

Fulweiler, R.E., and McDougal, S.E., 1971, Bedded-ore structures, Jefferson City mine, Jefferson City, Tennessee: Econ. Geol., v.66, p.763-769.

Gandhi, S.S., 1978, Geological observations and exploration guides to uranium in the Bear and Slave structural provinces and the Nonacho Basin, District of Mackenzie: Canada Geol. Survey Paper 78-1B, p.141-149.

Geier, B.H., 1952, Early rock alteration and mineralization in the Tsumeb ore body: Mineralogical Rept. no. 119, Tsumeb Corporation Ltd., Tsumeb.

---------- 1953, Mineralization in the Tsumeb ore body between the 1990 ft. and 2390 ft. levels with particular consideration of the spatial distribution of the ore minerals: Unpub. Rept. Tsumeb Corporation Ltd., Tsumeb, 12th June 1953.

---------- 1972, Contention: is the Tsumeb mineralization pre- or post-deformation: Mineralogical Rept. no. 616, Tsumeb Corporation Ltd., Tsumeb, 29th January 1972.

---------- 1974, Mineralogische Studie der Blei-, Zink- und Kupfer-lagerstätte, Tsumeb: S.W.A. Wissenschaftliche Gesellschaft, 1973/4, v.28, p.35-52.

Geier, B.H., and Ottemann, J., 1970a, New primary vanadium-, germanium-, gallium-, and tin-minerals from the Pb-Zn-Cu deposit, Tsumeb, South West Africa: Mineralium Deposita, v.5, p.29-40.

---------- 1970b, New secondary tin-germanium and primary tungsten - (molybdenum-, .vanadium-) germanium minerals from the Tsumeb ore deposit: Neues Jahrb. Mineralogie Abh., v.114, no.1, p.89-107.

---------- 1972, Briartit, das dritte Germanium-sulfid-Mineral aus der Erzlagerstätte Tsumeb: Neues Jahrb. Mineralogie Abh., v.118, no. 1, p.97-109.

---------- 1973, Über Betechtinit von Tsumeb: Neues Jahrb. Mineralogie Monatsh., v.9, p.416-426.

Geiser, P.A., and Sansone, S., 1981, Joints, microfractures, and the formation of solution cleavage in limestone: Geology, v.9, p.280-285.

Geldron, A., 1983, Le germanium: un élément valorisant des gisements hydrothermaux à Zn-Cu-(Pb): Chron. rech. min., no.470, p.25-32.

Gendzwill, D.J., and Hajnal, Z., 1971, Seismic investigation of the Crater Lake collapse structure in southeastern Saskatchewan: Canadian Jour. Earth Sci., v.8, p.1514-1524.

Godwin, C.I., and Sinclair, A.J., 1982, Average lead isotope growth curves for shale-hosted zinc-lead deposits, Canadian Cordillera: Econ. Geol., v.77, p.675-690.

Godwin, C.I., Sinclair, A.J., and Ryan, B.D., 1982, Lead isotope models for the genesis of carbonate-hosted Zn-Pb, shale-hosted Ba-Zn-Pb, and silver-rich deposits in the Northern Canadian Cordillera: Econ. Geol., v.77, p.82-94.

Gorin, V.A., 1964, Trends in the distribution of oil and gas deposits in the South Caspian Depression: Internat. Geol. Rev., v.6, no. 1, p.85-90.

Gornitz, V., and Kerr, P., 1970, Uranium mineralization and alteration, Orphan Mine, Grand Canyon, Arizona: Econ Geol., v.65, no. 7, p.751-768.

Graeser, S., 1965, Die mineralfundstellen im Dolomit des Binnatales: Schweizer. Mineralog. Petrog. Mitt., v.45, p.597-795.

Graf, D.L., Meents, W.F., Friedman, I., and Shrimp, N.F., 1966, The origin of saline formation waters, III. Calcium chloride waters : Illinois Geol. Survey Circ., v.397, 60p.

Griffis, A., 1949a, Memorandum on structural geology, Tsumeb mine: Unpub. rept. Tsumeb Corporation Ltd., Tsumeb.

---------- 1949b, A preliminary report on the geology of the Tsumeb mine: Unpub. rept. Tsumeb Corporation Ltd., Tsumeb.

---------- 1950, Notes on the geology of the Tsumeb mine: Unpub. rept. Tsumeb Corporation Ltd., Tsumeb.

Griffis, A.T., and McCue, J.O., 1950, A statistical study of metal trends at the Tsumeb mine : Unpub. rept. Tsumeb Corporation Ltd., Tsumeb.

Groshong, R.H., Jr., Pfiffner, O.A., and Pringle, L.R., 1984, Strain partitioning in the Helvetic thrust belt of eastern Switzerland from the leading edge to the internal zone: Jour. Structural Geology, v.6, p.5-18.

Guj, P., 1970, The Damara mobile belt in the south-western Kaokoveld, South West Africa: Precambrian Research Unit, Univ. Cape Town, Bull., v.8, 168p.

-------- 1974, A revision of the Damara stratigraphy along the southern margin of the Kamanjab inlier, South West Africa: Precambrian Research Unit, Univ. Cape Town, Bull., v.15, p.167-176.

Gulbrandsen, R.A., 1966, Chemical composition of phosphorites of the Phosphoria Formation: Geochim. et Cosmochim. Acta, v.30, p.769-778.

Günzel, A., 1977, A comment on the memo "Possible relationship of the E2200 and Old Compound breccias" by Martin Hughes: Mem. to Cilliers, A.C., Tsumeb Corporation Ltd., Tsumeb.

Gustafson, L.B., 1963, Phase equilibria in the system Cu-Fe-As-S: Econ. Geol, v.58, p.667-701.

Gustavson, T.C., Finley, R.J., and McGillis, K.A., 1980, Regional dissolution of Permian salt in the Anadarko, Dalhart, and Palo Duro Basins of the Texas Panhandle: Austin, Univ. Texas, Bur. Econ. Geology, Rept. Inv. 106, 40 p.

Gutsalo, L.K., Vetshteyn, V.Ye., and Lebedev, L.M., 1978, Recent metalliferous ore-forming hydrothermal solutions of the Cheleken region characterised by the isotopic compositions of hydrogen and oxygen: Geochemistry Internat., v.15, no. 4, p.116-122.

Haack, U., Gohn, E., and Klein, J.A., 1980, Rb/Sr ages of granitic rocks along the middle reaches of the Omaruru River and the timing of orogenetic events in the Damara Belt (Namibia): Contr. Mineralogy Petrology, v.74, p.349-360.

Habermehl, M.A., 1980, The Great Artesian Basin, Australia: Australia Bur. Mineral Resources Geology Geophysics Jour., v.5, p.9-38.

Hälbich, I.W., 1967, The geology of block B between lines 0 and 24, Teco Mining Area: Unpub. rept. Tsumeb Corporation Ltd., Tsumeb, 1967.

Hall, W.E., and Friedman, I., 1969, Oxygen and carbon isotopic composition of ore and host rock of selected Mississippi Valley deposits: U.S. Geol. Survey Prof. Paper 650-C, p.C140-C148.

Hall, W.E., Rye, R.O., and Doe, B.R., 1978, Wood River mining district, Idaho - intrusion-related lead-silver deposits derived from country rock source: U.S. Geol. Survey Jour. Research, v.6, p.579-592.

Halls, C., and Stumpfl, E.F., 1972, The five-element ore association (Ag-Bi-Co-Ni-As) - a critical appraisal of the geological environments in which it occurs, and theories affecting its origin: Internat. Geol. Cong., 24th, Montreal 1972, Proc. sec. 4, p.540.

Hanna, M.A., and Wolf, A.G., 1941, Gold, silver and other elements in salt-dome cap rocks: Am. Assoc. Petroleum Geologists Bull., v.25, p.750-752.

Hannah, J.L., and Stein, H.J., 1984, Evidence for changing ore fluid composition: stable isotope analyses of secondary carbonates, Bonneterre Formation, Missouri: Econ. Geol., v.79, p.1930-1935.

Handin, J., Hager, R.V., Jr., Friedman, M., and Feather, J.N., 1963, Experimental deformation of sedimentary rocks under confining pressure: pore pressure tests: Am. Assoc. Petroleum Geologists Bull., v.47, p.717-755.

Hanor, J.S., 1979, The sedimentary genesis of hydrothermal fluids, *in* Barnes, H.L., ed., Geochemistry of hydrothermal ore deposits: New York, John Wiley and Sons, p.137-172.

Haranczyk, C., 1972, Ore mineralization of the Lower Zechstein euxinic sediments in the Fore-Sudetic Monocline: Archiwum Mineralogiczne, v.30, p.144-168.

Hart, S.R., Shimizu, N., and Sverjensky, D.A., 1981, Lead isotope zoning in galena: an ion microprobe study of a galena crystal from the Buick mine, Southeast Missouri: Econ. Geol., v.76, p.1873-1878.

---------- 1983, Toward an ore fluid lead isotope "stratigraphy" for galenas from the Viburnum trend, S.E. Missouri, *in* Kisvarsanyi, G., Grant, S.K., Pratt, W.P., and Koenig, J.W., eds., Proc. Internat. Conf. on Mississippi Valley type lead-zinc deposits: Univ. Rolla, Missouri, 1983, p.257-270.

Haynes, F.M., 1985, A geochemical model for sulfide paragenesis and zoning in the Cu-Fe-As-S system (Tsumeb, South West Africa/Namibia): Chem. Geology, v.47, p.183-190.

Hedberg, R.M., 1979, Stratigraphy of the Ovamboland Basin, South West Africa: Precambrian Research Unit, Univ. Cape Town, Bull., v.24, 325p.

Helgeson, H.C., 1968, Geologic and thermodynamic characteristics of the Salton Sea geothermal system: Am. Jour. Sci., v.266, p.129-166.

---------- 1969, Thermodynamics of hydrothermal systems at elevated temperatures and pressures : Am. Jour. Sci., v.267, p.729-804.

Herak, M., and Stringfield, V.T., 1972, Karst: Amsterdam, Elsevier.

Hewitt, W.P., 1968, Geology and mineralization of the main mineral zone of the Santa Eulalia district, Chihuahua, Mexico: Soc. Mining Eng. Trans., v.241, p.228-260.

Heyl, A.V., 1967, Some aspects of genesis of stratiform zinc-lead-barite-fluorite deposits in the United States: Econ. Geol. Mon. 3, p.20-32.

Heyl, A.V., Delevaux, M.H., Zartman, R.E., and Brock, M.R., 1966, Isotopic study of galenas from the Upper Mississippi Valley, the Illinois-Kentucky and some Appalachian mineral districts: Econ. Geol., v.61, p.933-961.

Heyl, A.V., Landis, G.P., and Zartman, R.E., 1974, Isotopic evidence for the origin of Mississippi Valley-type mineral deposits: a review: Econ. Geol., v.69, p.992-1006.

Hilpert, L.S., and Moench, R.H., 1960, Uranium deposits of the southern part of the San Juan Basin, New Mexico: Econ. Geol., v.55, no. 3, p.429-464.

Hitchon, B., 1969a, Fluid flow in the western Canada sedimentary basin. 1. Effect of topography: Water Resources Research, v.5, no. 1, p.186-195.

---------- 1969b, Fluid flow in the western Canada sedimentary basin. 2. Effect of geology: Water Resources Research, v.5, no. 2, p.460-469.

---------- 1976, Hydrogeochemical aspects of mineral deposition in sedimentary rocks, *in* Wolf, K.H., ed., Handbook of strata-bound and stratiform ore deposits: Elsevier, v.2.

---------- 1977, Geochemical links between oil fields and ore deposits in sedimentary rocks, *in* Forum on oil and ore in sediments, Proc.: Imperial College, London, p.1-34.

Hitchon, B., Billings, G.K., and Klovan, J.E., 1971, Geochemistry and origin of formation waters in the western Canada sedimentary basin - III. Factors controlling chemical composition: Geochim. et Cosmochim. Acta, v.35, p.567-598.

Hitchon, B., and Friedman, I., 1969, Geochemistry and origin of formation waters in the western Canada sedimentary basin - 1. Stable isotopes of hydrogen and oxygen: Geochim. et Cosmochim. Acta, v.33, p.1321-1349.

Hitzman, M.W., 1983, Geology of the Cosmos Hills and its relationship to the Ruby Creek copper-cobalt deposit : Unpub. Ph.D. thesis, Stanford Univ., 263 p.

Hoagland, A.D., Hill, W.T., and Fulweiler, R.E., 1965, Genesis of the Ordovician zinc deposits in east Tennessee: Econ. Geol., v.60, p.693-714.

Hobbs, B.E., Means, W.D., and Williams, P.F., 1976, An outline of structural geology: John Wiley, 571p.

Hobson, G.D., 1980, Developments in petroleum geology - 2: United Kingdom, Applied Sci. Pubs., 345p.

Holland, H.D., and Malinin, S.D., 1979, The solubility and occurrence of non-ore minerals, *in* Barnes, H.L., ed., Geochemistry of hydrothermal ore deposits: New York, John Wiley and Sons, p.461-508.

Hopwood, A., 1975, A geological study of ore controls of the Tsumeb metal deposit, South West Africa: Unpub. rept. Tsumeb Corporation Ltd., Tsumeb, 192p.

Hudson, J.D., 1977, Stable isotopes and limestone lithification: Geol. Soc. London Jour., v.133, p.637-660.

Hughes, M.J., 1977, Possible relationship of E2200 and Old Compound breccias: Mem. to Cilliers, A.C., Tsumeb Corporation Ltd., Tsumeb.

---------- 1979, Some aspects of the genesis of the Tsumeb ore body, South West Africa, and of its subsequent deformation, *in* Geokongres 79, Abstracts Pt. 1: Cong. Geol. Soc. South Africa, 18th, Port Elizabeth 1979, p.200-206.

Hughes, M.J., Welke, H.J., and Allsopp, H.L., 1984, Lead isotopic studies of some Late Proterozoic stratabound ores of central Africa : Precambrian Research, v.25, p.137-139 (errata: v.27, 1985, p.403).

Hunt, J.M., 1979, Petroleum geochemistry and geology: San Francisco, W.H. Freeman, 617p.

Hurlbut, S.C., Jr., 1957, The wurtzite-greenockite series: Am. Mineralogist, v.42, p.184-190.

Hüttenlocher, H.F., 1936, Zur Mangan-Zinn-Silber-Lagerstätte aus dem Wasserstollen des Amsteger Kraftwerkers: Schweizer. Mineralog. Petrog. Mitt., v.16, p.406-408.

Ineson, P.R., Mitchell, J.G., and Vokes, F.M., 1975, K-Ar dating of epigenetic mineral deposits: an investigation of the Permian metallogenic province of the Oslo region, southern Norway: Econ. Geol., v.70, p.1426-1436.

Innes, J., and Chaplin, R.C., (in press, 1985), The ore bodies of the Kombat mine, South West Africa/Namibia.

Intiomale, M.M., 1982, Le gisement Zn-Pb-Cu de Kipushi (Shaba-Zaïre): D. Sc. thesis, Louvain, 170p.

Intiomale, M.M., and Oosterbosch, R., 1974, Géologie et géochimie du gisement de Kipushi, Zaïre, *in* Bartholomé, P., ed., Gisements stratiformes et provinces cuprifères: Centenaire de la Société Géologique de Belgique, Liège, 1974, p.123-164.

Jensen, M.L., 1973, Sulphur isotopic study of Newmont Southwest Africa deposits: Unpub. rept. Newmont Exploration Company Ltd., Connecticutt, 8p.

Jensen, M.L., and Dessau, G., 1966, Ore deposits of southwestern Sardinia and their sulfur isotopes: Econ. Geol., v.61, p.917-932.

Johnson, K.S., 1976, Permian copper shales of southwestern Oklahoma: Oklahoma Geol. Survey Circ. 77, p.3-14.

Johnson, W., 1965, Copper and lead ore deposits of South Australia: Australian Inst. Mining Metallurgy, Cong. 8th, v.1, p.285-296.

Jolly, W.T., 1974, Behaviour of Cu, Zn and Ni during prehnite-pumpellyite rank metamorphism of the Keweenawan basalts, northern Michigan: Econ. Geol., v.69, p.1118-1125.

Jones, P.H., and Wallace, R.H., Jr., 1974, Hydrogeologic aspects of structural deformation in the northern Gulf of Mexico Basin: U.S. Geol. Survey Jour. Research, v.2, no.5, p.511-517.

Kantor, J., 1977, Pb-Zn ores of the Westcarpathian Triassic and the distribution of their sulphur isotopes, *in* Klemm, D.D., and Schneider, H-J., eds., Time and strata-bound ore deposits: Springer-Verlag, p.294-304.

Karamjan, K.A., 1959, Germanit und Renierit in den Erzen der Kupfer-Molybdän-Lagerstätte Dastakertsk: Sapiski Armjan. Otdel. Wsesojusn. miner. Obsch., v.1, p.101-108.

Kaup, O.B., and Hite, R.J., 1978, Bromine distribution in marine halite rocks : Soc. Econ. Paleontologists Mineralogists, Short Course no. 4, p.105-123.

Kelley, V.C., Kittel, D.F., and Melancon, P.E., 1968, Uranium deposits of the Grants region, *in* Ridge, J.D., ed., Ore deposits of the United States, v.1: New York, Am. Inst. Mining Engineers, p.747-769.

Kelly, W.C., and Nishioka, G.K., 1985, Precambrian oil inclusions in late veins and the role of hydrocarbons in copper mineralization at White Pine, Michigan : Geology, v.13, p.334-337.

Kerr, P.F., Bodine, M.W., Jr., Kelley, D.R., and Keys, W.S., 1957, Collapse features, Temple Mountain Uranium area, Utah: Geol. Soc. America Bull., v.68, p.933-982.

Kindle, E.D., 1972, Classification and description of copper deposits, Coppermine River area, District of Mackenzie: Canada Geol. Survey Bull., v.214, 109 p.

Kinsman, D.J.J., 1975, Salt floors to geosynclines : Nature, v.255, p.375-378.

Kitmut, D., and Kalengwa, M., 1979, Les gisements d'Uranium du Zaïre, *in* Uranium deposits in Africa: geology and exploration: Vienna, Internat. Atomic Energy Agency, p.149-156.

Klemme, H.D., 1972, Heat influences size of oil giants: Oil and Gas Jour., July 24th, 1972.

Knauth, L.P., Kumar, M.B., and Martinez, J.D., 1980, Isotope geochemistry of water in Gulf Coast salt domes: Jour. Geophys. Research, v.85, no. B9, p.4863-4871.

Köppel, V., 1983, Summary of lead isotope data from ore deposits of the eastern and southern Alps, *in* Schneider, H-.J., ed., Mineral deposits of the Alps and of the Alpine epoch in Europe: Springer-Verlag, p.162-168.

Köppel, V., and Grünenfelder, M., 1979, Isotope geochemistry of lead, *in* Jäger, E., and Hunziker, J.C., eds., Lectures in isotope geology: Springer-Verlag.

Kortman, C.R., 1972, The geology of the Zambia Broken Hill mine, Kabwe: Geologie Mijnb., v.51, no.3, p.347-356.

Kraynov, S.R., 1967, Geochemistry of germanium in the thermal carbonate waters (illustrated by examples from the Pamirs and Greater Caucasus): Geochemistry Internat., v.4, p.309-320.

Krejci-Graf, K., 1978, Data on the geochemistry of oil field waters: Geol. Jahrb., D25, p.3-174.

Kröner, A., 1977a, Precambrian mobile belts of southern and eastern Africa - Ancient sutures or sites of ensialic mobility? A case for crustal evolution towards plate tectonics: Tectonophysics, v.40, p.101-135.

---------- 1977b, The Precambrian geotectonic evolution of Africa - plate accretion versus plate destruction: Precambrian Research, v.4, p.163-213.

---------- 1982, Rb-Sr geochronology and tectonic evolution of the Pan-African Damara belt of Namibia, Southwestern Africa : Am. Jour. Sci., v.282, p.1471-1507.

Kröner, A., Halpern, M., and Jacob, R.E., 1978, Rb-Sr geochronology in favour of polymetamorphism in the Pan African Damara belt of Namibia (South West Africa) : Geol. Rundschau, v.67, p.688-705.

Krouse, H.R., 1977, Sulfur isotope studies and their role in petroleum exploration : Jour. Geochem. Exploration, v.7, p.189-211.

Krusch, P., 1911, Die genetischen Verhältnisse der Kupfererzvorkommen von Otavi: Zeitschr. Dt. Geol. Ges., v.63, p.240-263.

Kucha, H., 1982, Platinum-group metals in the Zechstein copper deposits, Poland: Econ. Geol. v.77, p.1578-1591.

Land, B.N., 1977a, Final report: Tsumeb West Vanadium prospect - Tsumeb West Mining Area: Unpub. rept. Tsumeb Corporation Ltd., Tsumeb.

---------- 1977b, Report on surface mapping: Tsumeb mine and environs 1975-1976: Unpub. rept. Tsumeb Corporation Ltd., Tsumeb.

Land, L.S., 1985, The origin of massive dolomite : Jour. Geol. Education, v.33, p.112-125.

Land, L.S., and Prezbindowski, D.R., 1981, The origin and evolution of saline formation water, Lower Cretaceous carbonates, south-central Texas, U.S.A. : Jour. Hydrology, v.54, p.51-74.

Landes, K., Ehlers, G., and Stanley, G., 1945, Geology of the Mackinac Straits region: Michigan Geol. Survey, Geological Series 37, Pub. 44.

Large, D.E., 1983, Sediment-hosted massive sulphide lead-zinc deposits: an empirical model: Mineralog. Assoc. Canada Short Course Handbook 8, p.1-29.

Large, D., Schaeffer, R., and Höhndorf, A., 1983, Lead isotope data from selected galena occurrences in the north Eifel and north Sauerland, Germany: Mineralium Deposita, v.18, p.235-243.
Larsen, G., and Chilingar, G.V., eds., 1979, Diagenesis in sediments and sedimentary rocks : Elsevier.
Laufer, E.E., and Mossman, D.J., 1982, The identification of sepiolite in the Prairie Evaporite Formation of Saskatchewan: Canadian Mineralogist, v.20, p.151-154.
Lauzac, F., 1965, Découverte de reniérite dans une blende germanifère de Sardaigne: Soc. Française Minéralogie Cristallographie Bull., v.88, p.347-348.
Lebedev, L.M., 1972, Minerals of contemporary hydrotherms of Cheleken: Geochemistry Internat., v.9, no. 3, p.485-504.
Lemon, N.M., 1985, Physical modeling of sedimentation adjacent to diapirs and comparison with Late Precambrian Oratunga breccia body in central Flinders Ranges, South Australia : Am. Assoc. Petroleum Geologists Bull., v.69, p.1327-1338.
Le Roex, H.D., 1951, The geology of a portion of Tsumeb West mining claim, Tsumeb, South West Africa: Unpub. rept. Tsumeb Corporation Ltd., Tsumeb, 1951.
---------- 1955, A study of the pseudo-aplite of the Otavi Mountains and the rock alteration in the adjoining dolomite: D.Sc. thesis, Univ. Pretoria.
Leventhal, J.S., and Kepferle, R.C., 1981, Uranium in Devonian shales of the eastern interior United States, *in* Pryor, W.A., ed., Energy resources of Devonian and Mississippian shales of eastern Kentucky : Kentucky Geol. Survey, 44p.
Lippolt, H.J., Schorn, U., and Pidgeon, R.T., 1983, Genetic implications of new lead isotope measurements on Schwarzwald vein and Upper Triassic sediment galenas: Geol. Rundschau, v.72, p.77-104.
Lockwood, R.P., 1976, Geochemistry and petrology of some Oklahoma red-bed copper occurrences: Oklahoma Geol. Survey Circ. 77, p.61-68.
Lombaard, A.F., 1953, A contribution to the geology of the Tsumeb mine: Unpub. rept. Tsumeb Corporation Ltd., Tsumeb.
---------- 1973, Notes on exploration at Kombat mine: Unpub. rept. Tsumeb Corporation Ltd., Tsumeb.
---------- 1976, A review of surface exploration diamond drilling in the vicinity of Tsumeb mine: Unpub. rept. Tsumeb Corporation Ltd., Tsumeb.
Lombaard, A.F., Günzel, A., Innes, J., and Krüger, T.L., in press 1985, The Tsumeb lead-copper-zinc-silver deposit, South West Africa/ Namibia.
Long, D.T., and Angino, E.E., 1982, The mobilization of selected trace metals from shales by aqueous solutions: effects of temperature and ionic strength: Econ. Geol., v.77, p.646-652.
Lovering, T.G., 1972, Jasperoid in the United States - its characteristics, origin, and economic significance: U.S. Geol. Survey Prof. Paper 710, 164p.
Ludwig, K.R., 1980, Calculation of uncertainties of U-Pb isotope data : Earth Planet. Sci. Letters, v.46, p.212-220.
Lur'ye, A.M., 1978, Copper migration conditions in red-bed associations : Geochemistry Internat., v.15, no. 3, p.174-178.
MacDermot, C.V., and Sevastopulo, G.D., 1972, Upper Devonian and Lower Carboniferous stratigraphical setting of Irish mineralization : Ireland Geol. Survey Bull. 1, p.267-280.

Macqueen, R.W., and Powell, T.G., 1983, Organic geochemistry of the Pine Point lead-zinc ore field and region, Northwest Territories, Canada : Econ. Geol., v.78, p.1-25.
Magara, K., 1973, Compaction and fluid migration in Cretaceous shales of western Canada: Canada Geol. Survey Paper 72-18, 81p.
Markham, N.L., 1959, Occurrence of jordanite in the Otavi Mountains, South West Africa: Am. Mineralogist, v.44, p. 682-685.
Markham, N.L., and Ottemann, J., 1968, Betekhtinite from Mt. Lyell, Tasmania: Mineralium Deposita, v.3, p.171-173.
Martin, H., and Porada, H., 1977a, The intracratonic branch of the Damara orogen in South West Africa I. Discussion of geodynamic models: Precambrian Research, v.5, p.311-338.
---------- 1977b, The intracratonic branch of the Damara orogen in South West Africa II.: Precambrian Research, v.5, p.339-357.
Maske, S., and Skinner, B.J., 1971, Studies of the sulfosalts of copper. 1. Phases and phase relations in the system Cu-As-S : Econ. Geol., v.66, p.901-918.
Matsukuma, T., 1971, Betechtinite from the Kuroko deposits of the Furutobe mine, Akita Prefecture, Japan, *in* Proc. IMA-IAGOD Mtg., 1970, IMA Vol.: Mineralog. Soc. Japan Spec. Paper, v.1, p.191-195.
Maucher, W., 1908, Die Erzlagerstätte von Tsumeb im Otavi-Bezirk im Norden Deutsch-Südwestafrikas: Zeitschr. Prakt. Geol., v.16, p.24-32.
McClay, K.R., 1977, Pressure solution and Coble creep in rocks and minerals: a review: Geol. Soc. London Jour., v.134, p.57-70.
McClay, K.R., and Atkinson, B.K., 1977, Experimentally induced kinking and annealing of single crystals of galena: Tectonophysics, v.39, p.175-189.
McClure, J.W., Jr., 1973, Base metal content of oil field brines in eastern Kansas: Geol. Soc. America, Abstracts with Programs, v.5, p.336.
McCormick, J.E., Evans, L.L., Palmer, R.A., and Rasnick, F.D., 1971, Environment of the zinc deposits of the Mascot-Jefferson City District, Tennessee: Econ. Geol., v.66, p.757-762.
McCrea, J.M., 1950, On the isotopic chemistry of carbonates and a paleotemperature scale: Jour. Chem. Physics, v.18, p.849-857.
McDonald, J.A., 1967, Metamorphism and its effects on sulphide assemblages: Mineralium Deposita, v.2, p.200-220.
McKelvey, V.E., Cathcart, J.B., Altschuler, Z.S., et al., 1953, Domestic phosphate deposits, *in* Pierre, W.H., and Norman, A.G., eds., Soil and fertilizer phosphorous in crop nutrition: Agronomy IV, p.347-356.
McKenzie, J.A., 1980, Holocene dolomitization of calcium carbonate sediments from the coastal sabkhas of Abu Dhabi, U.A.E.: a stable isotope study: Jour. Geology, v.89, p.185-198.
McKinstry, H., 1963, Mineral assemblages in sulfide ores: the system Cu-Fe-As-S: Econ. Geol., v.58, p.483-505.
McKnight, E.T., and Fischer, R.P., 1970, Geology and ore deposits of the Picher Field, Oklahoma and Kansas: U.S. Geol. Survey Prof. Paper 588, 165p.
McLimans, R.K., 1977, Geological, fluid inclusion and stable isotope studies of the upper Mississippi Valley zinc-lead district, southwest Wisconsin: Unpub. Ph.D. thesis, Pennsylvania State Univ., 175 p.

McLimans, R.K., Barnes, H.L., and Ohmoto, H., 1980, Sphalerite stratigraphy of the Upper Mississippi Valley zinc-lead district, Southwest Wisconsin: Econ. Geol., v.75, p.351-361.

McNutt, R.H., Frape, S.K., and Fritz, P., 1984, Strontium isotopic composition of some brines from the Precambrian Shield of Canada : Isotope Geoscience, v.2, p.205-215.

Mendelsohn, F., 1961, The geology of the Northern Rhodesian copperbelt: London, Macdonald, 523 p.

Meyer, B., Ward, K., Koshlap, K., and Peter, L., 1983, Second dissociation constant of hydrogen sulphide: Inorganic Chemistry, v.22, p.2345-2346.

Meyer, C., 1981, Ore-forming processes in geologic history: Econ. Geol., 75th Anniv. Vol., p.6-41.

Michael, S.S., and Groves, D.I., 1977, The origin of the Northampton hydrothermal Pb-Zn deposits, *in* Glover, J.E., and Groves, D.I., eds., Recent geological research relating low-temperature aqueous geochemistry to weathering, ore genesis and exploration: Univ. Western Australia, p.36-46.

Miller, R. McG., 1980, Geology of a portion of central Damaraland, South West Africa/Namibia: South Africa Geol. Survey, South West Africa Ser., no.6, 78p.

Miller, R. McG., and Burger, A.J., 1983a, U-Pb zircon age of the early Damaran Naauwpoort Formation: Geol. Soc. South Africa Spec. Pub. no. 11, p.267-272.

---------- 1983b, U-Pb zircon ages of members of the Salem Granitic Suite along the northern edge of the central Damara granite belt: Geol. Soc. South Africa Spec. Pub. no. 11, p.273-280.

Mills, J.W., 1976, Metamorphism of the zinc-lead sulfide ores of the Yellowhead horizon, Metaline limestone formation, northeastern Washington: Econ. Geol., v.71, p.1601-1609.

Milner, S., 1976, Carbonate petrology and syndepositional facies of the lower San Andres Formation (Middle Permian), Lincoln County, New Mexico: Jour. Sed. Petrology, v.46, no.3, p.463-482.

Mitchell, A.H.G., and Garson, M.S., 1981, Mineral deposits and global tectonic settings: Academic Press.

Moine, B., Sauvan, P., and Jarousse, J., 1981, Geochemistry of evaporite-bearing series: a tentative guide for the identification of metaevaporites: Contr. Mineralogy Petrology, v.76, p.401-412.

Moorbath, S., and Vokes, F.M., 1963, Lead isotope abundance studies on galena occurrences in Norway: Norsk Geologisk Tidsskrift, v.43, p.283-343.

Moore, C.H., and Druckman, Y., 1981, Burial diagenesis and porosity evolution, Upper Jurassic Smackover, Arkansas and Louisiana: Am. Assoc. Petroleum Geologists Bull., v.65, no.4, p.597-628.

Moritz, H., 1933, Die sulfidischen Erze der Tsumeb-Mine vom Ausgehenden bis zur XVI Sohle (-460 m): Neues Jahrb. Mineralogie Abh., A, v.67(B), p.118-153.

Morris, D.F.C., and Short, E.L., 1966, Minerals of rhenium: Mineralog. Mag., v.35, p.871-873.

Morrissey, C.J., Davis, G.R., and Steed, G.M., 1971, Mineralization in the Lower Carboniferous of central Ireland: Inst. Mining Metallurgy Trans., v.80, p.174-185.

Mount, T.J., 1983, Diapirs and diapirism in the Adelaide 'Geosyncline', South Australia: Adelaide Geosyncline Symp., Adelaide, Abstracts vol., p.32-33.

Mouzita, D., 1979, Contribution à l'étude géochimique des formations précambriennes du schisto-calcaire supérieur du bassin minier du Niari et de la mine de M'Passa (Rép. Pop. Congo). Implications métallogéniques: These, Docteur Ingénieur, Universite Scientifique et Medicale de Grenoble, 168p.

Murray-Hughes, R., and Fitch, A.A., 1929, The geology of Sable Antelope and neighbouring mines, north-western Rhodesia: Mineralog. Mag., v.41, p.137-147.

Neumann, H., 1944, Silver deposits at Kongsberg: Norges. Geol. Undersøkelse, no. 162, 133 p.

Ngongo-Kashisha, 1975, Sur la similitude entre les gisements uranifères (type Shinkolobwe) et les gisements cuprifères (type Kamoto) au Shaba, Zaïre: Ann. Soc. Géol. Belgique, v.98, p.449-462.

Nhan, N.V. 1970, New ore minerals of the Lower Silesian Zechstein copper-bearing rocks: Polska Akad. Nauk, Prace Min., v.24, p.49-60.

Nielsen, H., 1979, Sulfur isotopes, *in* Jäger, E., and Hunziker, J.C., eds., Lectures in isotope geology: Springer-Verlag.

Ohmoto, H., 1972, Systematics of sulfur and carbon isotopes in hydrothermal ore deposits: Econ. Geol., v.67, p.551-578.

Ohmoto, H., and Rye, R.O., 1979, Isotopes of sulfur and carbon, *in* Barnes, H.L., ed., Geochemistry of hydrothermal ore deposits, 2nd ed.: New York, John Wiley and Sons, p.509-567.

Oja, R.V., 1966, Geochemical investigations of the Thunder Bay silver area: Canada Geol. Survey Paper 66-54, p.211-221.

Orlandi, P., Merlino, S., Duchi, G., and Giovanna, V., 1981, Colusite: a new occurrence and crystal chemistry: Canadian Mineralogist, v.19, p.423-427.

Ottemann, J., 1978, Rythmisch gebänderter Gelpyrit mit Arsen- und Kupfergehalten aus der Erzlagerstätte Tsumeb, S.W.A.: Neues Jahrb. Mineralogie Monatsh., v.7, p.330-336.

Ottemann, J., Nuber, B., and Geier, B.H., 1977, A germanium and zinc-bearing variety of mawsonite from the Tsumeb deposit: Chem. Erde Bd., v.36, p.110-117.

Pagel, M., and Jaffrezic, H., 1977, Analyses chimiques des saumures des inclusions du quartz et de la dolomite du gisement d'uranium de Rabbit Lake (Canada) : C.R. Acad. Sci. Paris, Series D, v.284, p.113-116.

Pagel, M., Poty, B., and Sheppard, S.M.F., 1980, Contribution to some Saskatchewan uranium deposits mainly from fluid inclusion and isotopic data, *in* Ferguson, J., and Goleby, A.B., eds., Uranium in the Pine Creek geosyncline: Vienna, Internat. Atomic Energy Agency, Internat. Symp., Sydney, 1979, Proc., p.639-654.

P'an, C-H., 1982, Petroleum in basement rocks: Am. Assoc. Petroleum Geologists Bull., v.66, p.1597-1643.

Panno, S.V., Harbottle, G., and Sayre, E.V., 1983, Genetic implications of halide enrichment near a Mississippi Valley-type ore deposit: Econ. Geol., v.78, p.150-156.

Park, W.C., and Schot, E.H., 1968, Stylolites: their nature and origin: Jour. Sed. Petrology, v.38, p.175-191.

Pauly, E., 1966, Kupfererzlagerstätten in Angola, *in* Kupfererzla stätten der Welt, ihre Genese und wirtschaftliche Bedeutung: Schriften der Gesellschaft Deutscher Metallhütten- und Bergleute e.V., v.18, p.36-57.

Pennebaker, E., 1952, Geology and exploration at Tsumeb, S.W.A.: Unpub. rept. Tsumeb Corporation Ltd., Tsumeb.

Pennebaker, E., 1954, Review of geology and exploration at Tsumeb, S.W.A.: Unpub. rept. Tsumeb Corporation Ltd., Tsumeb.

Peters, T., Schwander, H., and Trommsdorff, V., 1973, Assemblages among tephroite, pyroxmangite, rhodochrosite, quartz: experimental data and occurrences in the Rhetic Alps: Contr. Mineralogy Petrology, v.42, p.325-332.

Petruk, W., and staff, 1971, Characteristics of the sulphides, *in* Berry, L.G., ed., The silver arsenide deposit of the Cobalt-Gowganda region, Ontario: Canadian Mineralogist, v.11, pt. 1, p.196-231.

Pettijohn, F.J., 1975, Sedimentary rocks, 3rd ed.: Harper and Row.

Picot, P., 1970, Minéralogie de quelques éléments rares dans les minéraux métalliques: Conf., Orleans Univ., Dec. 1970, 35p.

Picot, P., Scolari, G., and Troly, G., 1963, Nouvelles données sur la paragenése du minerai de la mine de M'Passa (République du Congo) et comparaison avec d'autres gisements de l'Afrique centrale: Soc. Française Minéralogie Cristallographie Bull., v.86, p.355-358.

Pinckney, D.M., and Rye, R.O., 1972, Variation of O^{18}/O^{16}, C^{13}/C^{12}, texture and mineralogy in altered limestone in the Hill mine, Cave-in-Rock district, Illinois: Econ. Geol., v.67, p.1-18.

Piper, J.D.A., 1976, Paleomagnetic evidence for a Proterozoic supercontinent: Royal Soc. London, Phil. Trans., v.A280, p.469-490.

Pirmolin, J., 1970, Inclusions fluides dans la dolomite du gisement stratiforme de Kamoto (Katanga Occidental): Ann. Soc. Géol. Belgique, v.93, p.397-406.

Popov, V.M., 1962, Geologic regularities in the distribution of cupriferous sandstones in central Kazakhstan: Internat. Geol. Rev., v.4, p.393-411.

Porada, H., 1979, The Damara-Ribeira orogen of the Pan-African-Brasiliano cycle in Namibia (Southwest Africa) and Brazil as interpreted in terms of continental collision: Tectonophysics, v.57, p.237-265.

Potter, R.W., II., Silberman, M.L., Nissenbaum, A., and Mathews, A., 1977, Mineralogy and isotope geochemistry of the Kennecott massive copper sulphide deposits, Alaska: Geol. Assoc. Canada - Mineralog. Assoc. Canada, Program with Abstracts, v.2, p.42.

Price, L., 1980, Shelf and shallow basin oil as related to hot-deep origin of petroleum: Jour. Petroleum Geol., v.3, no. 1, p.91-116.

Price, P.E., and Kyle, J.R., 1983, Metallic sulfide deposits in Gulf Coast salt dome cap rocks : Gulf Coast Assoc. Geol. Socs., Trans., v.33, p.189-193.

Pufahl, O., 1922, "Germanit" ein Germanium-Mineral und -Erz von Tsumeb, Süd-West-Afrika: Metall und -Erz, v.19, p.324-325.

Ramdohr, P., 1980, The ore minerals and their intergrowths: Pergamon, 2 Vols., 1205p.

Ramsay, C.R., and Ridgway, J., 1977, Metamorphic patterns in Zambia and their bearing on problems of Zambian tectonic history: Precambrian Research, v.4, p.321-337.

Ranoux, J., 1962, General discussion, *in* Lombard, J., and Nicolini, P., eds., Stratiform copper deposits in Africa, v.1: Congrès Géologique Internat., Copenhagen, 1960, Assoc. African Geol. Surveys, p.202.

Reeve, W.H., 1963, The geology and mineral resources of Northern Rhodesia: Geol. Survey Northern Rhodesia, Bull., v.3.

Rentzsch, J., 1974, The "Kupferschiefer" in comparison with the deposits of the Zambian Copperbelt, *in* Bartholomé, P., ed., Gisements stratiformes et provinces cuprifères: Centenaire de la Société Géologique de Belgique, Liège, p.403-418.

Reynolds, P.H., 1971, A U-Th-Pb lead isotope study of rocks and ores from Broken Hill, Australia: Earth Planet. Sci. Letters, v.12, p.215-223.

Rhodes, D., Lantos, E.A., Lantos, J.A., Webb, R.J., and Owens, D.C., 1984, Pine Point orebodies and their relationship to the stratigraphy, structure, dolomitization and karstification of the Middle Devonian barrier complex: Econ. Geol., v.79, p.991-1055.

Rickard, D., Coleman, M., and Swainbank, I., 1981, Lead and sulfur isotopic compositions of galena from the Laisvall sandstone lead-zinc deposit, Sweden: Econ. Geol., v.76, p.2042-2046.

Rickard, D.T., 1974, Low temperature copper geochemistry: gitological aspects, *in* Bartholomé, P., ed., Gisements stratiformes et provinces cuprifères: Centenaire de la Société Géologique de Belgique, Liège, p.1-34.

Rickard, D.T., Willdén, M.Y., Marinder, N-E., and Donnelly, T.H., 1979, Studies on the genesis of the Laisvall sandstone lead-zinc deposit, Sweden: Econ. Geol., v.74, p.1255-1285.

Rickard, D.T., Willdén, M.Y., Marinder, N.E., Donelly, T.H., 1981, Studies on the genesis of the Laisvall sandstone lead-zinc deposit, Sweden - a reply: Econ. Geol., v.76, p.2052-2060.

Rimsaite, J., 1978, Application of mineralogy to the study of multistage uranium mineralization in remobilized uranium deposits, Saskatchewan: Mineralog. Assoc. Canada Short Course Handbook 3, p.403-430.

Roberts, D.E., and Hudson, G.R.T., 1983, The Olympic Dam copper-uranium-gold deposit, Roxby Downs, South Australia: Econ. Geol., v.78, p.799-822.

Robinson, B.W., and Ohmoto, H., 1973, Mineralogy, fluid inclusions and stable isotopes of the Echo Bay U-Ni-Ag-Cu deposits, Northwest Territories, Canada: Econ. Geol., v.68, p.635-656.

Roseboom, E.H., Jr., 1962, Djurleite, $Cu_{1,96}S$, a new mineral: Am. Mineralogist, v.47, p.1181-1184.

Rösler, H.J., and Baumann, L., 1970, On the different origin of Variscan and Post-Variscan ("Saxonic") mineralizations in central Europe, *in* Pouba, Z., and Štemprok, M., eds., Problems of hydrothermal ore deposition: Schweizerbart, p.72-77.

Routhier, P., 1983, Where are the metals for the future?: Bur. Recherches Géologiques et Minières, CID éditions, Nantes, 400p.

Rouvier, H., Perthuisot, V., and Mansouri, A., 1985, Pb-Zn deposits and salt-bearing diapirs in southern Europe and north Africa: Econ. Geol., v.80, p.666-687.

Runnells, D.D., 1969, The mineralogy and sulfur isotopes of the Ruby Creek copper prospect, Bornite, Alaska: Econ. Geol., v.64, p.75-90.

Russell, M.J., 1983, Major sediment-hosted exhalative zinc + lead deposits: formation from hydrothermal convection cells that deepen during crustal extension: Mineralog. Assoc. Canada Short Course Handbook 8, p.251-282.

Rye, R.O., and Ohmoto, H., 1974, Sulfur and carbon isotopes and ore genesis: a review: Econ. Geol., v.69, p.826-842.

S.A.C.S. (South African Committee for Stratigraphy), 1980, Stratigraphy of South Africa, Part 1 (Comp. L.E. Kent). Lithostratigraphy of the Republic of South Africa, South West Africa/Namibia, and the Republics of Bophuthatswana, Transkei and Venda : South Africa Geol. Survey, Handbook 8, 690p.

Sakai, H., and Dickson, F.W., 1978, Experimental determination of the rate and equilibrium fractionation factors of sulfur isotope exchange between sulfate and sulfide in slightly acid solutions at 300°C and 1000 bars: Earth Planet. Sci. Letters, v.39, p.151-161.

Sass-Gustkiewicz, M., Dzulynski, S., and Ridge, J.D., 1982, The emplacement of zinc-lead sulfide ores in the Upper Silesian District - a contribution to the understanding of Mississippi Valley-type deposits: Econ. Geol., v.77, p.392-412.

Sawkins, F.J., 1968, The significance of Na/K and Cl/SO_4 ratios in fluid inclusions and subsurface waters, with respect to the genesis of Mississippi Valley-type ore deposits: Econ. Geol., v.63, p.935-942.

Schampp, C.A., and Schaller, W.T., 1931, Sulvanite from Utah: Am. Mineralogist, v.16, no. 12, p.557-562.

Schenk, P.E., 1969, Carbonate-sulfate-redbed facies and cyclic sedimentation of the Windsorian Stage (Middle Carboniferous), Maritime Provinces: Canadian Jour. Earth Sci., v.6, p.1037-1066.

Schidlowski, M., Eichmann, R., and Junge, C.E., 1975, Precambrian sedimentary carbonates: carbon and oxygen isotope geochemistry and implications for the terrestrial oxygen budget: Precambrian Research, v.2, p.1-69.

---------- 1976, Carbon isotope geochemistry of the Precambrian Lomagundi carbonate province, Rhodesia: Geochim. et Cosmochim. Acta, v.40, p.449-455.

Schidlowski, M., Junge, C.E., and Pietrek, H., 1977, Sulfur isotope variations in marine sulphate evaporites and the Phanerozoic oxygen budget: Jour. Geophys. Research, v.82, p.2557-2565.

Schmidt, G.W., 1973, Interstitial water composition and geochemistry of deep Gulf Coast shales and sandstones: Am. Assoc. Petroleum Geologists Bull., v.57, no. 2, p.321-337.

Schneiderhöhn, H., 1919a, Mineralogische Beobachtungen in den Kupfer-, Blei-, Zink- und Vanadium-Lagerstätten des Otaviberglandes, Südwestafrika. I: Senckenbergiana, v.1, no. 5, p.152-155.

---------- 1919b, Mineralogische Beobachtungen in den Kupfer-, Blei-, Zink- und Vanadium-Lagerstätten des Otaviberglandes, Südwestafrika. II. Chalmersit, $CuFe_2S_3$ in den sulfidischen Erzen der Tsumeb-Mine: Senckenbergiana, v.1, no. 5, p.156-158.

---------- 1920a, Mineralogische Beobachtungen in den Kupfer-, Blei-, Zink- und Vanadium-Lagerstätten des Otaviberglandes, Südwestafrika. III. Paramorphosen von rhombischen Kupferglanz nach regulärem Cu_2S in den sulfidischen Erzen der Tsumeb-Mine und ihre Bedeutung als geologisches Thermometer: Senckenbergiana, v.2, no. 1, p.1-15.

---------- 1920b, Mineralogische Beobachtungen in den Kupfer-, Blei-, Zink- und Vanadium-Lagerstätten des Otaviberglandes, Deutsch-Südwestafrika. IV. Vergleichende Strukturstudien bei der Verdrängung von Buntkupferkies durch Kupferglanz in den sulfidischen Erzen der Tsumeb-Mine und in amerikanischen Kupfererzen: Senckenbergiana, v.2, no. 1, p.62-70.

Schneiderhöhn, H., 1920c, Die Erzlagerstätten des Otaviberglandes, Deutsch-Südwestafrika. V. Die mikroskopische Beschaffenheit der sulfidischen Erze: Metall und Erz, v.17, p.421-428.

---------- 1921, Beiträge zur Kenntnis der Erzlagerstätten und geologischen Verhältnisse des Otaviberglandes: Abh. Senckenbergiana Naturforsch. Ges., v.37, p.220-231.

---------- 1929, Das Otavi-Bergland und seine Erzlagerstätten: Zeitschr. Prakt. Geol., v.37, p.85-116.

---------- 1958, Zur Erforschungsgeschichte der Erze der Tsumeb-Mine und der geologischen Verhältnisse des Otaviberglands, Südwestafrika: Neues Jahrb. Mineralogie Monatsh. 1958, p.125-136.

Schroll, E., and Pak, E., 1983, Sulfur isotope investigations of ore mineralizations of the eastern Alps, *in* Schneider, H-J., ed., Mineral deposits of the Alps and of the Alpine epoch in Europe: Springer-Verlag.

Schüller, A., 1959, Metallisation und genese des Kupferschiefers von Mansfeld: Abh. Deutschen Akad. Wissenschaften zu Berlin, Klasse für Chemie, Geologie und Biologie, 1958, no. 6.

Schüller, A., and Wohlmann, E., 1955, Betechtinit, ein neues Blei-Kupfer-Sulfid aus den Mansfelder Rücken: Geologie, v.4, no. 6, p.535-555.

Schwarcz, H.P., and Burnie, S.W., 1973, Influence of sedimentary environments on sulfur isotope ratios in clastic rocks: a review: Mineralium Deposita, v.8, p.264-277.

Schwellnus, C.M., le Roex, H.D., Strauss, C.A., Kuschke, G.S.C., and Wiid, S.C., 1944, The geology and vanadium deposits of the Otavi Mountainland, South West Africa, *in* Lead deposits in the Union of South Africa and South West Africa: South Africa Geol. Survey Mem. 39.

Sclar, C.B., and Geier, B.H., 1957, The paragenetic relationships of germanite and renierite from Tsumeb, South West Africa: Econ. Geol., v.52, no. 6, p.612-631.

Scolari, G., 1965, Étude géologique de Bassin du Niari oriental (République du Congo-Brazzaville) et de ses minéralisations Cu-Pb-Zn: Bur. Recherches Géologiques et Minières, Mem., v.35, 219 p.

Scott, S.D., and O'Connor, T.P., 1971, Fluid inclusions in vein quartz, Silverfields mine, Cobalt, Ontario, *in* Berry, L.G., ed., The silver arsenide deposits of the Cobalt-Gowganda region, Ontario: Canadian Mineralogist, v.11, pt.1, p.263-271.

Sears, S.O., and Lucia, F.J., 1980, Dolomitization of northern Michigan Niagara reefs by brine refluxion and freshwater/seawater mixing: Soc. Econ. Paleontologists Mineralogists, Spec. Pub. no. 28, p.215-235.

Sharma, T., and Clayton, R.N., 1965, Measurement of O^{18}/O^{16} ratios of total oxygen of carbonates: Geochim. et Cosmochim. Acta, v.29, p.1347-1353.

Sharp, J.M., Jr., 1978, Energy and momentum transport model of the Ouachita Basin and its possible impact on formation of economic mineral deposits: Econ. Geol., v.73, p.1057-1068.

Shearman, D.J., 1978, Evaporites of coastal sabkhas, *in* Dean, W.E., and Schreiber, B.C., eds., Marine Evaporites: Soc. Econ. Paleontologists Mineralogists, Short Course Notes, v.4, Oklahoma City, p.6-42.

Shinn, E.A., 1969, Submarine lithification of Holocene carbonate sediments in the Persian Gulf: Sedimentology, v.12, p.109-144.

Siebenthal, C.E., 1915, Zinc and lead deposits of the Joplin region: U.S. Geol. Survey Bull. 606, p.208-209.
Sillitoe, R.H., and Clark, A.H., 1969, Copper and copper-iron sulfides as the initial products of supergene oxidation, Copiapó mining district, northern Chile: Am. Mineralogist, v.54, p.1684-1710.
Simpson, W., 1956, Aspects of the geology of the western Teco Mining Area and Tsumeb West with special reference to structure: Unpub. rept. Tsumeb Corporation Ltd., Tsumeb.
Skinner, B.J., 1979, The many origins of hydrothermal mineral deposits, *in* Barnes, H.L., ed., Geochemistry of hydrothermal ore deposits: New York, John Wiley and Sons, p.1-21.
Smit, J.M. v.d. M., 1958, The geology of the southern Otavi Mountainland: Unpub. rept. Tsumeb Corporation Ltd., Tsumeb, Dec. 1958.
Smith, G.E., 1974, Depositional systems, San Angelo Formation (Permian), North Texas - facies control of red-bed copper mineralization: Austin, Univ. Texas, Bur. Econ. Geology, Rept. Inv. no. 80, 73 p.
Smith, N.G., Kyle, J.R., and Magara, K., 1983, Geophysical log documentation of fluid migration from compacting shales: a mineralization model from the Devonian strata of the Pine Point area, Canada: Econ. Geol., v.78, p.1364-1374.
Snyder, F.G., and Gerdemann, P.E., 1968, Geology of the southeast Missouri lead district, *in* Ridge, J.D., ed., Ore deposits of the United States: Am. Inst. Mining Engineers, Graton-Sales volume, v.1, p.326-358.
Söhnge, P.G., 1957, Revision of the geology of the Otavi Mountainland, South West Africa (with 1958 amended stratigraphic table): Unpub. rept. Tsumeb Corporation Ltd., Tsumeb, 116p.
---------- 1963, Genetic problems of pipe deposits in South Africa: Anniv. address by President of Geol. Soc. South Africa, Feb. 1963.
---------- 1964, The geology of the Tsumeb mine: Geol. Soc. South Africa Proc., v.65, no.2, p.367-382.
---------- 1972, Application of basement structure, sedimentation and paleophysiography to exploration in the Tsumeb district: Unpub. rept. Tsumeb Corporation Ltd., Tsumeb.
---------- 1976, Exploration in the environs of Tsumeb, South West Africa: Unpub. rept. Tsumeb Corporation Ltd., Tsumeb, 1976.
South Africa Geol. Survey, 1963, Geological map of South West Africa: Government Printer, Pretoria, 4 sheets, 1:1 000 000.
Spooner, E.T.C., 1981, Fluid inclusion studies of hydrothermal ore deposits: Mineralog. Assoc. Canada Short Course Handbook 6, p.209-240.
Stacey, J.S., and Kramers, J.D., 1975, Approximation of terrestrial lead isotope evolution by a two-stage model: Earth Planet. Sci. Letters, v.26, p.207-221.
Stacey, J.S., Zartman, R.E., and Nkomo, I.T., 1968, A lead isotope study of galenas and selected feldspars from mining districts in Utah: Econ. Geol., v.63, p.796-814.
Stahl, A., 1925, Translation of report dated 12th May, 1925 (by A. Günzel): Unpub. rept. Tsumeb Corporation Ltd., Tsumeb.
---------- 1926, Geologische Grundzüge des nördlichen Südwestafrika und Erzlagerstätten des Otavi-Berglandes: Zeitschr. prakt. Geol., v.34, p.145-169.
Stam, J.C., 1960, Some ore occurrences of the Mississippi Valley type in Equatorial Africa: Econ. Geol., v.55, p.1708-1715.
Stanton, R.J., 1966, The solution brecciation process: Geol. Soc. America Bull., v.77, p.843-848.

Stanton, R.L., 1972, Ore petrology: McGraw-Hill, 713 p.
Stanton, R.L., and Willey, H.G., 1970, Natural work-hardening in galena, and its experimental reduction: Econ. Geol., v.65, p.182-194.
---------- 1972, Experiments on a specimen of galena ore from Couer d'Alene, Idaho: Econ. Geol., v.67, p.776-788.
Steclaci, L., 1961/2, Über das germanit-vorkommen in der erzlagerstätte von Toroiaga-Baia-Borşa: Revue Roumaine de Geology, Geophysique et Geographie, v.5, p.313-316.
Stringfield, V.T., Rapp, J.R., and Anders, R.B., 1979, Effects of karst and geologic structure on the circulation of water and permeability in carbonate aquifers, *in* Back, W., and Stephenson, D.A., eds., Contemporary hydrogeology: Elsevier, 1979, p.313-332.
Strunz, H., 1959, Tsumeb, seine Erze und Sekundärmineralien, inbesondere der neu aufgeschlossen zweiten Oxydationszone: Fortschritte der Mineralogie, v.37, p.87-90.
Strunz, H., Geier, B.H., and Seeliger, E., 1959, Gallit, $CuGaS_2$, das erste selbständige Galliummineral, und seine Verbreitung in den Erzen der Tsumeb- und Kipushi-Mine: Neues Jahrb. Mineralogie Monatsh., v.11/12, p.241-264.
Strunz, H., and Tennyson, Ch., 1967, Schaurteit, ein neues Germanium-Mineral von Tsumeb/SW-Afrika und seine Paragenese: Festschrift Dr. Werner T. Schaurte, p.33-47.
Sverjensky, D.A., 1981, The origin of a Mississippi Valley-type deposit in the Viburnum trend, southeast Missouri: Econ. Geol., v.76, p.1848-1872.
---------- 1984, Oil field brines as ore-forming solutions: Econ. Geol., v.79, p.23-37.
Sverjensky, D.A., Rye, D.M., and Doe, B.R., 1979, The lead and sulphur isotopic composition of galena from a Mississippi Valley-type deposit in the New Lead Belt, Southeast Missouri: Econ. Geol., v.74, p.149-153.
Takeuchi, T., Nambu, M., Suzuki, M., and Okada, K., 1956, Germanium bearing black ores from the Kamikita mine, Aomori Prefecture: Mining Geology (Japan), v.66, no.22, p.231-243.
Tauson, V.L., and Abramovich, M.G., 1980, Hydrothermal study of the ZnS-HgS system: Geochemistry Internat., v.17, no.3, p.117-128.
Taylor, H.P., Jr., 1979, Oxygen and hydrogen isotope relationships in hydrothermal mineral deposits, *in* Barnes, H.L., ed., Geochemistry of hydrothermal ore deposits, 2nd ed.: New York, John Wiley and Sons, p.236-277.
Terziyev, G.I., 1966, The conditions of germanium accumulation in hydrothermal mineralization (as illustrated by a Bulgarian copper-pyrite deposit): Geochemistry Internat., v.3, p.341-346.
Thiede, D.S., and Cameron, E.N., 1978, Concentration of heavy metals in the Elk Point evaporite sequence, Saskatchewan : Econ. Geol., v.73, p.405-415.
Thirion, N.C., 1973a, Paleophysiography as related to the origin of some base mineral deposits: Unpub. rept. Tsumeb Corporation Ltd., Tsumeb, 1973.
---------- 1973b, Final report on Berg Aukas 593: Grootfontein district - Grant M46/3/453: Unpub. rept. Tsumeb Corporation Ltd., Tsumeb.
---------- 1974, Summary of prospects within T.C.L. concessions, Otavi Mountainland: Unpub. rept. Tsumeb Corporation Ltd., Tsumeb.

Thorpe, R., 1974, Lead isotope evidence on the genesis of the silver arsenide vein deposits of the Cobalt and Great Bear Lake areas, Canada: Econ. Geol., v.69, p.777-791.

Tissot, B.P., and Welte, D.H., 1978, Petroleum formation and occurrence : Springer-Verlag, 329p.

Trocki, L.K., Curtis, D.B., Gancarz, A.J., and Banar, J.C., 1984, Ages of major uranium mineralization and lead loss in the Key Lake uranium deposit, Northern Saskatchewan, Canada: Econ. Geol., v.79, p.1378-1386.

Tufar, W., 1982, A new type of sulphosalt mineralization in the Myrthengraben gypsum deposit, Semmering, lower Austria, *in* Amstutz, G.C., El Goresy, A., Frenzel, G., Kluth, C., Moh, G., Wauschkuhn, A., and Zimmerman, R.A., eds., Ore Genesis - the state of the art: Springer-Verlag, p.131-140.

Vaes, J.F., 1948, La reniérite: Ann. Soc. Géol. Belgique, v.72, pt. B., p.19-32.

van Eden, J.G., 1978, Stratiform copper and zinc mineralization in the Cretaceous of Angola: Econ. Geol., v.73, p.1154-1161.

van Everdingen, R.O., 1968, Studies of formation waters in Western Canada: geochemistry and hydrodynamics: Canadian Jour. Earth Sci., v.5, p.523-543.

van Zyl, P.J., 1961a, An evaluation of the geological data of Tsumeb West and its bearing on possible future drilling: Unpub. rept. Tsumeb Corporation Ltd., Tsumeb.

---------- 1961b, Report on Friesenberg prospect: Unpub. rept. Tsumeb Corporation Ltd., Tsumeb.

Vaughan, D.J., and Craig, J.R., 1978, Sulfide equilibria in aqueous systems, *in* Vaughan, D.J., and Craig, J.R., eds., Mineral chemistry of metal sulfides: Cambridge University Press, p.315-349.

Veizer, J., and Hoefs, J., 1976, The nature of O^{18}/O^{16} and C^{13}/C^{12} secular trends in sedimentary carbonate rocks: Geochim. et Cosmochim. Acta, v.40, p.1387-1395.

Veizer, J., Holser, W.T., and Wilgus, C.K., 1980, Correlation of $^{13}C/^{12}C$ and $^{34}S/^{32}S$ secular variations: Geochim. et Cosmochim. Acta, v.44, p.579-587.

Veldsman, J.H., 1979, Geologie van die Tsumeb-Subgroep/Mulden -Groep-kontak wes van Tsumeb, *in* Geokongres 79, Abstracts Pt. 1: Congr. Geol. Soc. South Africa, 18th, Port Elizabeth 1979, p.404-414.

Vellet, V., 1968, Geology and exploration at Tsumeb and other parts of northern S.W.A.: Unpub. rept. Newmont Exploration Ltd., Danbury, U.S.A.

---------- 1969, Exploration in the Otavi Mountains and other parts of South West Africa: Unpub. rept. Newmont Exploration Ltd., Danbury, U.S.A.

Vernon, R.O., 1969, The geology and hydrology associated with a zone of high permeability (Boulder Zone) in Florida: Am. Inst. Mining Engineers, Preprint, v.69-AG-12, 22p.

Verwoerd, W.J., 1957, The mineralogy and genesis of the lead-zinc-vanadium deposit of Abenab West in the Otavi Mountains, S.W.A.: Ann. Univ. Stellenbosch, v.33, pt. A., p.235-329.

Viaene, W., and Moreau, J., 1968, Contribution a l'étude de la germanite, de la renierite et de la briartite: Ann. Soc. Géol. Belgique, v.91, p.127-143.

Vine, J.D., and Tourtelot, E.B., 1970, Geochemistry of black shale deposits - a summary report : Econ. Geol., v.65, p.253-272.

Vovk, I.F., 1985, Brines in the crystalline basement of the East-European platform: Geol. Assoc. Canada - Mineralog. Assoc. Canada, Joint Ann. Mtg., May 1985, Program with Abstracts, v.10, p.A66.

Vlasov, K., ed., 1966, Geochemistry and mineralogy of rare elements and genetic types of their deposits: Israel program for scientific translations, 3 vols.

Vokes, F.M., and Gale, G.H., 1976, Metallogeny relatable to global tectonics in southern Scandinavia: Geol. Assoc. Canada, Spec. Paper 14, p.411-441.

Wagner, P.A., 1916, The geology and mineral industry of S.W.A.: South Africa Geol. Survey Mem., v.7, 234p.

Walker, R.N., Gulson, B., and Smith, J., 1983, The Coxco deposit - a Proterozoic Mississippi Valley-type deposit in the McArthur River district, Northern Territory, Australia: Econ. Geol., v.78, p.214-249.

Walper, J.L., 1980, Tectonic evolution of the Gulf of Mexico, *in* Pilger, R.H., Jr., ed., Proc. Symp., The origin of the Gulf of Mexico and the early opening of the central North Atlantic Ocean: Louisiana State Univ., Baton Rouge, p.87-98.

Wang, K., 1984, Geochemical characteristics of sedimentation and metamorphism of the Dongchuan copper deposit, Yunnan province, China : Precambrian Research, v.25, p.135-136.

Warren, C.G., 1972, Sulfur isotopes as a clue to the genetic geochemistry of a roll-type uranium deposit: Econ. Geol., v.67, p.759-767.

Watters, B.R., 1982, A Sr-isotopic study of a suite of Precambrian shoshonites from the Sinclair Group in southern Namibia: Geol. Soc. South Africa Trans., v.85, p.81-86.

Waugh, D.C.E., 1985, Stratigraphy and paleoenvironment of the Penobsquis and Clover Hill potash deposits in New Brunswick: Geol. Assoc. Canada - Mineralog. Assoc. Canada, Joint Ann. Mtg., 1985, Program with abstracts, V.10, p.A67.

Wedepohl, K.H., ed., 1974, Handbook of geochemistry: Springer-Verlag, 2 vols.

Wedepohl, K.H., Delevaux, M.H., and Doe, B.R., 1978, The potential source of lead in the Permian Kupferschiefer bed of Europe and some selected Paleozoic mineral deposits in the Federal Republic of Germany: Contr. Mineralogy Petrology, v.65, p.273-281.

Wells, A.T., 1980, Evaporites in Australia : Australia Bur. Mineral Resources Geology Geophysics, Bull. 198, 104p.

West, I.M., Brandon, A., and Smith, M., 1968, A tidal flat evaporitic facies in the Viséan of Ireland: Jour. Sed. Petrology, v.38, no.4, p.1079-1093.

White, D.E., 1965, Saline waters of sedimentary rocks: Am. Assoc. Petroleum Geologists Mem. 4, p.342-366.

---------- 1968, Environments of generation of some base metal ore deposits: Econ. Geol., v.63, p.301-335.

---------- 1981, Active geothermal systems and hydrothermal ore deposits: Econ. Geol., 75th Anniv. Vol., p.392-423.

White, D.E., Hem, J.D., and Waring, G.A., 1963, Chemical composition of subsurface waters, *in* Data of Geochemistry: U.S. Geol. Survey Prof. Paper 440-F, 67p.

Wilson, C.J.L., 1973, The prograde microfabric in a deformed quartzite sequence, Mt. Isa, Australia: Tectonophysics, v.19, p.39-81.

Windley, B.F., 1977, The evolving continents: Wiley, 385 p.

Winkler, H.G.F., 1976, Petrogenesis of metamorphic rocks: Springer-Verlag, 329 p.

Wu, Y., and Beales, F., 1981, A reconnaissance study by paleomagnetic methods of the age of mineralization along the Viburnum trend, Southeast Missouri: Econ. Geol., v.76, p.1879-1894.

Yates, R.G., and Thompson, G.A., 1959, Geology and quicksilver deposits of the Terlingua District, Texas: U.S. Geol. Survey Prof. Paper 312.

York, D., 1966, Least-squares fitting of a straight line : Canadian Jour. Physics, v.44, p.1079-1086.

---------- 1969, Least-squares fitting of a straight line with correlated errors : Earth Planet. Sci. Letters, v.5, p.320-324.

Ypma, P.J.M., 1973a, Preliminary report on a fluid inclusion investigation of host rock, gangue and ore minerals of base metal mines of the Tsumeb, S.W.A. mining district: Internal company rept. Newmont Mining Co., U.S.A., p.1-59.

---------- 1973b, General conclusions of a systematic study of Tsumeb samples: Internal company rept. Newmont Mining Co., U.S.A.

---------- 1973c, Systematic fluid inclusion investigation of the Tsumeb deposit in S.W. Africa: Unpub. rept. Newmont Exploration Ltd., Danbury, Oct. 15th 1973.

Ypma, P.J.M., and Fuzikawa, K., 1980, Fluid inclusion and oxygen isotope studies of the Nabarlek and Jabiluka uranium deposits, Northern Territory, Australia, *in* Ferguson, J., and Goleby, A.B., eds., Uranium in the Pine Creek geosyncline: Vienna, Internat. Atomic Energy Agency, Internat. Symp., Sydney, 1979, Proc., p.375-395.

Zeigler, P.A., 1975, Geologic evolution of North Sea and its tectonic framework : Am. Assoc. Petroleum Geologists Bull., v.59, p.1073-1097.

APPENDIX 1: CHEMICAL ANALYSES

1.1 TOTAL ROCK ANALYSES (Table A1)

All samples were analysed in duplicate. The writer determined SiO_2, TiO_2, Al_2O_3, Fe_2O_3, MnO, MgO, CaO, K_2O, Ba and P_2O_5 by XRF analysis of fusion discs, and Na_2O and S were determined in pressed pellets. Samples were dried at 110°C to determine H_2O, and the mass change at 1100°C was also recorded. The mine laboratory of Tsumeb Corporation Limited analysed Cu, Pb, Zn and As by XRF. Uranium, thorium and some lead analyses were determined as part of the lead isotope study (Appendix 2.3.1). Carbon and H_2O^+ were analysed by H.H. Lachmann, using combustion and gas chromatography. Total carbon was determined, carbon present as carbon dioxide was checked by using helium instead of oxygen as a carrier gas, and carbon present as graphite was analysed after acid digestion of the sample. Other trace elements were analysed by A. Geraldis, using AAS. The precision of these techniques (other than those used in the lead isotope study) is approximately 2 percent except in the case of Na_2O, S, Cu, Pb, Zn, As, C, H_2O^+ and trace elements, for which the precision varies from 5-10 percent.

FeS_2 was computed by assigning all sulphur to FeS_2 in rocks which did not contain other sulphide minerals. All iron was assigned to FeS_2 in rocks which contained only minor iron-bearing, non-sulphide iron minerals; this is convenient for comparison but it introduces small errors (e.g. iron in carbonate minerals, and sulphide minerals such as bornite). Iron was assigned to Fe_2O_3 in sample 544; much of the iron probably occurs in the sulphide fraction of this sample but the proportion is unknown.

"Additional mass change" is the difference between the mass change at 1100°C and the sum of As, C, CO_2, S and H_2O^+. It consists of the errors in these determinations, and also the mass of oxygen added to Cu, Pb and Zn sulphides during heating. The figure has been corrected for oxygen added during the oxidation of iron sulphide

APPENDIX 1: CHEMICAL ANALYSES

1.1 TOTAL ROCK ANALYSES (Table A1)

All samples were analysed in duplicate. The writer determined SiO_2, TiO_2, Al_2O_3, Fe_2O_3, MnO, MgO, CaO, K_2O, Ba and P_2O_5 by XRF analysis of fusion discs, and Na_2O and S were determined in pressed pellets. Samples were dried at 110°C to determine H_2O, and the mass change at 1100°C was also recorded. The mine laboratory of Tsumeb Corporation Limited analysed Cu, Pb, Zn and As by XRF. Uranium, thorium and some lead analyses were determined as part of the lead isotope study (Appendix 2.3.1). Carbon and H_2O^+ were analysed by H.H. Lachmann, using combustion and gas chromatography. Total carbon was determined, carbon present as carbon dioxide was checked by using helium instead of oxygen as a carrier gas, and carbon present as graphite was analysed after acid digestion of the sample. Other trace elements were analysed by A. Geraldis, using AAS. The precision of these techniques (other than those used in the lead isotope study) is approximately 2 percent except in the case of Na_2O, S, Cu, Pb, Zn, As, C, H_2O^+ and trace elements, for which the precision varies from 5-10 percent.

FeS_2 was computed by assigning all sulphur to FeS_2 in rocks which did not contain other sulphide minerals. All iron was assigned to FeS_2 in rocks which contained only minor iron-bearing, non-sulphide iron minerals; this is convenient for comparison but it introduces small errors (e.g. iron in carbonate minerals, and sulphide minerals such as bornite). Iron was assigned to Fe_2O_3 in sample 544; much of the iron probably occurs in the sulphide fraction of this sample but the proportion is unknown.

"Additional mass change" is the difference between the mass change at 1100°C and the sum of As, C, CO_2, S and H_2O^+. It consists of the errors in these determinations, and also the mass of oxygen added to Cu, Pb and Zn sulphides during heating. The figure has been corrected for oxygen added during the oxidation of iron sulphide

TABLE A1: TOTAL ROCK ANALYSES

	522	196	PB1	PB8	PB10	858A	530	PB5	PB4	439	440	958	544
	PIPE SANDSTONE		MULDEN SAND-STONE	MULDEN SLATE		SILICIFIED DOLOSTONE		T5	T6 DOLOSTONE	E35/30L	E35/30L CALCI-TIZED DOLO-STONE	NORTH BREAK DOLO-STONE	DARK BRECCIA MATRIX
SiO_2	88,92	78,74	88,37	66,32	57,01	83,99	79,83	n.d.	n.d.	n.d.	n.d.	30,56	41,31
TiO_2	0,23	0,29	0,11	0,90	0,85	0,02	0,00	0,00	0,00	0,00	0,00	0,00	0,81
Al_2O_3	4,97	6,02	6,29	14,61	16,78	1,12	0,53	0,50	0,48	0,37	0,55	0,59	13,35
Fe_2O_3	-	-	0,19	5,53	7,38	-	-	0,16	0,11	0,30	-	0,29	1,92
FeS_2	2,66	0,58	1,40	-	2,73	5,97	0,96	-	0,07	-	0,32	-	-
MnO	0,00	0,01	0,00	0,04	0,16	0,01	0,06	0,02	0,00	0,14	0,45	0,43	0,09
MgO	0,25	0,93	0,31	2,52	3,56	1,93	2,47	22,35	22,20	21,69	6,20	8,29	6,38
CaO	0,32	5,85	0,58	0,98	0,24	2,54	5,00	30,65	28,65	30,41	47,52	29,08	7,38
Na_2O	2,60	0,00	0,93	2,49	0,91	0,08	0,29	0,00	0,00	0,00	0,00	0,00	0,00
K_2O	0,49	1,05	2,79	2,75	3,94	0,18	0,00	0,00	0,00	0,00	0,00	0,00	4,79
P_2O_5	0,09	0,14	0,13	0,22	0,21	0,15	0,12	0,19	0,20	0,18	0,28	0,22	0,24
H_2O^+	n.d.	1,70	n.d.	2,37	3,75	n.d.	n.d.	n.d.	n.d.	n.d.	n.d.	n.d.	1,65
H_2O^-	0,11	0,23	0,09	0,08	0,13	0,02	0,05	0,06	0,09	0,05	0,10	0,07	0,09
CO_2	0,17	4,53	0,75	1,26	2,35	3,47	7,80	47,39	47,13	47,14	44,25	32,07	10,86
C	0,02	0,04	0,05	0,12	0,47	0,05	0,02	0,02	0,02	< 0,01	0,05	0,03	0,70
Cu	0,4	0,85	< 0,05	n.a.	< 0,01	0,9	1,30	n.a.	n.a.	0,1	0,1	0,1	5,0
Pb	0,2	0,65	< 0,01	< 0,01	0,2	0,3	0,30	< 0,01	< 0,01	0,2	0,1	0,3	1,0
Zn	0,1	0,20	< 0,05	n.a.	< 0,01	0,4	2,40	n.a.	n.a.	< 0,05	0,05	0,1	0,3
As	0,35	0,15	0,05	n.a.	0,10	0,50	0,15	n.a.	n.a.	0,10	0,09	0,05	0,75
Other S	0,69	0,05	-	< 0,01	-	2,37	0,28	< 0,01	-	< 0,01	0,07	< 0,01	1,47
Additional mass change	-0,20	0,29	-0,06	0,01	-0,70	-1,94	-0,89	-0,22	-0,10	-0,11	-0,22	-0,16	0,12
TOTAL	102,37	102,30	101,98	100,20	100,07	102,06	100,67	101,12	98,85	100,57	99,91	102,02	98,21
Ba (ppm)	87	166	514	439	589	66	20	< 20	< 20	< 20	< 20	366	618

n.d. = not detected
n.a. = not analyzed

see Tables 1, 2, 4 and 5 for sample locations

minerals, where the FeS_2 content is well known.

1.2 ANALYSES OF SULPHIDE AND SULPHOSALT MINERALS

Microprobe analyses of sulphide and sulphosalt minerals, made by the writer, are listed in Tables A2 to A8. These were made on an ARL SEMQ wave-length dispersive electron microprobe, using elemental standards. Analyses of sulvanite, mawsonite, stannite and briartite from Tsumeb and Kipushi are given in Francotte et al. (1965), Geier and Ottemann (1970a, 1972), and de Vos et al. (1974).

1.3 OTHER CHEMICAL ANALYSES

Analyses of reduced (i.e. non-carbonate) carbon in hand specimens of rock and ore, and in channel samples taken through the pipe at different elevations (Chapter 3.4.5), are shown in Table A9. Details of the technique and analysts are described in Appendix 1.1.

Chemical analyses of ore from the Tsumeb pipe are shown in Table A10; all analyses were made by the Mine Laboratory of Tsumeb Corporation Limited.

APPENDIX 2 : ISOTOPE ANALYSES

2.1 SULPHUR ISOTOPES

Samples of ore minerals were drilled from the surfaces of polished sections, and other minerals were hand-picked from heavy mineral concentrates. The sulphur in the samples was converted to sulphur dioxide, using the Cu_2O oxidation method of Coleman and Moore (1978). The samples were mixed with cuprous oxide and reacted in a furnace, and the resulting sulphur dioxide was purified on a separation line constructed by the writer for the purpose of this study. Water vapour was separated in an acetone-dry ice trap, and carbon dioxide was removed from the sample in a second trap. This was achieved by differential sublimation, during melting of n-pentane cooled to liquid

TABLE A2 TENNANTITE AND ENARGITE ANALYSES, TSUMEB

	Tennantite						Enargite
	(1) no location WC (B.H. Geier)	(2) 20L WC (B.H. Geier)	(3) 24L WC (B.H. Geier)	(4) Crystal E65/22L WC (B.H. Geier)	(5) "Mineral T" 21L WC (B.H. Geier)	(6) "Mineral T"? 776 W136/33L MP (this study)	(7) 975 16L MP (this study)
Cu	43,8	43,3	44,0	43,3	45,7	45,7	47,1
Pb	0,2	0,2	0,3	0,2	2,0	-	0,03
Zn	7,8	8,3	7,3	7,8	2,8	2,0	-
Fe	0,6	0,6	0,7	0,9	1,9	1,4	0,03
S	27,4	27,4	27,3	27,1	27,4	28,2	34,0
As	19,8	19,7	19,9	19,7	20,0	18,3	18,6
Ge	-	n.d.	n.d.	-	-	-	-
Sb	0,2	0,1	0,3	0,5	0,2	n.d.	n.d.
Mo	0,09	0,13	0,06	0,02	0,04	n.d.	-
Cd	0,23	0,23	0,24	0,15	n.d.	n.d.	n.d.
Ag	-	300 ppm	380 ppm	530 ppm	n.d.	n.d.	n.d.
Ga	n.d.	n.d.	n.d.	n.d.	n.d.	n.d.	-
Sn	n.d.	n.d.	n.d.	n.d.	n.d.	-	-
W	n.d.	n.d.	n.d.	n.d.	n.d.	-	-
V	n.d.	n.d.	n.d.	n.d.	n.d.	-	-
TOTAL	100 *	100 *	100 *	99,7	100 *	95,6#	99,8

* normalized n.d. = not determined MP = microprobe WC = wet chemical

NOTE: Tennantite crystals: 20L = 0,9 % Fe, 290 ppm Ag; 24L = 420 ppm Ag
Tennantite concentrate: 28L = 0,8 % Fe
#Analysis 5 also had a low total prior to normalization, and sample 776 repeatedly gave low totals (missing element suspected)

TABLE A3 ANALYSES OF OTHER COPPER MINERALS, TSUMEB

	(1) Chalcocite Tsumeb 1116 W80/30L MP (this study)	(2) Chalcocite Tsumeb 1114 S95 stope, 29/30 sill MP (this study)	(3) Digenite* Tsumeb 1114 S95 stope, 29/30 sill MP (this study)	(4) Bornite Tsumeb 1116 W80/30L MP (this study)	(5) Chalcopyrite Tsumeb 975 15L MP (this study)
Fe	-	-	0,1	12,0	31,2
Cu	78,4	79,7	78,2	63,5	34,8
W	n.d.	-	-	n.d.	-
Mo	n.d.	-	-	n.d.	-
V	n.d.	-	-	n.d.	-
S	20,9	21,8	23,5	26,4	35,2
Pb	n.d.	-	-	n.d.	-
Sn	n.d.	0,02	-	n.d.	0,03
Zn	n.d.	-	-	n.d.	-
Ga	n.d.	-	n.d.	n.d.	0,06
Ge	n.d.	-	-	n.d.	-
As	n.d.	-	-	0,1	-
Ce	0,2	n.d.	-	0,04	n.d.
Ni	-	n.d.	n.d.	-	n.d.
TOTAL	99,5	101,5	101,8	102,0	101,3

n.d. = not determined
MP = microprobe
*intergrown with (2), possibly impure

TABLE A4 PYRITE AND CARROLLITE ANALYSES, TSUMEB AND ELSEWHERE

	Pyrite		Ni-carrollite				Carrollite	
	Tsumeb		Tsumeb				Kipushi, Zaïre (7)	Nkana, Zambia (8)
	(1) 1115 MP (this study)	(2) 776 W136/33L MP (this study)	(3) 1116 W80/30L MP (this study)	(4) 1116 W80/30L MP (this study)	(5) 1116 W80/30L MP (this study)	(6) 1116 W80/30L MP (this study)	MP (a)	Wits. 1093 MP (this study)
Fe	47,7	46,7	0,03	1,6	1,1	1,0	0,2	0,6
Co	n.d.	n.d.*	25,7	26,2	26,3	26,7	37,9	40,6
Ni	n.d.	n.d.	11,7	11,1	12,5	14,2	1,2	0,1
Cu	0,2	0,1	22,5	21,3	22,0	18,5	19,9	17,8
S	53,5	52,5	40,5	39,9	39,9	40,3	41,0	41,2
As	-	-	-	-	-	-	n.d.	-
Zn	-	0,02	n.d.	n.d.	n.d.	n.d.	-	n.d.
Pb	-	-	n.d.	n.d.	n.d.	n.d.	-	n.d.
Ge	-	-	n.d.	n.d.	n.d.	n.d.	-	n.d.
Ag	n.d.	n.d.	n.d.	n.d.	n.d.	n.d.	-	n.d.
W	-	-	n.d.	n.d.	n.d.	n.d.	n.d.	n.d.
Mo	-	n.d.	n.d.	n.d.	n.d.	n.d.	n.d.	n.d.
Sn	-	-	n.d.	n.d.	n.d.	n.d.	n.d.	n.d.
Ga	-	n.d.	n.d.	n.d.	n.d.	n.d.	n.d.	n.d.
V	-	0,07	n.d.	n.d.	n.d.	n.d.	n.d.	n.d.
TOTAL	101,4	99,4	100,4	100,1	101,8	100,7	100,2	100,3

n.d. = not determined
MP = microprobe
(a) Dimanche (1974)
* another pyrite grain contained 0,6% Co

TABLE A5 BETEKHTINITE ANALYSES, TSUMEB

	(1) (var.1) MP (a)	(2) (var.1) MP (a)	(3) (var.2) MP (a)	(4) (var.2) MP (a)	(5) (var.3) MP (a)	(6) (var.3) MP (a)	(7) 1114 (S95 stope, 29/30 sill) MP (this study)
Cu	59,7	59,8	59,9	57,7	59,3	58,7	61.2
Pb	17,6	17,2	16,9	17,6	17,6	18,0	18,2
Fe	2,6	2,6	2,6	3,8	2,6	2,7	2,4
Ag	0,7	0,5	1,3	1,3	0,3	0,7	n.d.
S	19,8	19,8	20,0	20,6	20,4	19,7	20,7
V	n.d.	n.d.	n.d.	n.d.	n.d.	n.d.	-
W	n.d.	n.d.	n.d.	n.d.	n.d.	n.d.	-
Mo	n.d.	n.d.	n.d.	n.d.	n.d.	n.d.	-
Sn	n.d.	n.d.	n.d.	n.d.	n.d.	n.d.	-
Zn	n.d.	n.d.	n.d.	n.d.	n.d.	n.d.	-
Ga	n.d.	n.d.	n.d.	n.d.	n.d.	n.d.	-
Ge	n.d.	n.d.	n.d.	n.d.	n.d.	n.d.	-
As	n.d.	n.d.	n.d.	n.d.	n.d.	n.d.	-
TOTAL	100,4	99,9	100,7	101,0	100,2	99,8	102,5

n.d. = not determined
MP = microprobe
WC = wet chemical
(a) Geier and Ottemann (1973)
See Dimanche (1974) for analyses of betekhtinite from Kipushi, Zaïre

TABLE A6 RENIERITE ANALYSES, TSUMEB

	(1)	(2) *	(3)	(4) 1114 S95 stope, 29/30 sill	(5) 776 W136/33L
	MP (a)	WC (b)	WC (b)	MP (this study)	MP (this study)
Cu	43,6	41,2	43,8	42,8	42,6
Fe	13,9	12,8	13,1	14,3	13,9
Ge	6,8	5,5	6,0	6,6	5,9
Ga	-	0,5	0,6	0,06	n.d.
Zn	1,6	-	n.d.	0,8	0,2
Pb	-	2,2	n.d.	-	-
Sn	n.d.	-	n.d.	0,02	-
As	2,4	5,0	4,7	2,2	3,3
S	33,3	30,5	31,3	32,8	32,9
Ni	n.d.	n.d.	n.d.	n.d.	n.d.
Co	n.d.	n.d.	n.d.	n.d.	n.d.
Ag	n.d.	n.d.	n.d.	n.d.	n.d.
Mo	n.d.	n.d.	0,06	-	n.d.
V	n.d.	n.d.	n.d.	0,2	0,04
W	n.d.	n.d.	n.d.	n.d.	-
Other	n.d.	2,0	n.d.	n.d.	n.d.
TOTAL	101,6	99,7	99,6	99,8	98,8

n.d. = not determined
MP = microprobe
WC = wet chemical
tr = trace
*90% pure (galena present)

(a) Viaene and Moreau (1968)
(b) Sclar and Geier (1957)
(c) B.H. Geier, unpublished

See a, b, Dimanche (1974), de Vos et al (1974) for analyses of renierite from Kipushi, Zaïre, and M'Passa, Congo Republic

TABLE A7 GALLITE ANALYSES, TSUMEB

	(1) Gallite	(2) "Maygreen" (Zn-V - gallite?)	(3) "Carnevallite" (Fe-Zn gallite?)	(4) Gallite 1114* S95 stope, 29/30sill
	MP (a)	MP (a)	MP (a)	MP (this study)
Cu	32,2	40,7	35,9	35,3
Fe	-	0,8	6,8	1,4
Zn	-	3,9	4,2	0,1
Ga	35,3	21,0	20,9	32,4
Ge	-	-	-	-
V	-	3,2	-	-
As	-	-	-	-
Sn	n.d.	n.d.	n.d.	0,04
S	32,5	32,2	32,5	32,9
W	n.d.	n.d.	n.d.	-
Pb	n.d.	n.d.	n.d.	-
Mo	n.d.	n.d.	n.d.	-
TOTAL	100,0	101,8	100,3	102,1

(a) Geier & Ottemann (1970a)
n.d. = not determined
* Other gallite grains contained 1,9%, 2,4% and 3,3% Fe

TABLE A8 GERMANITE ANALYSES, TSUMEB

	GERMANITE							W-GERMANITE				V-GERMANITE	
	(1)	(2)	(3)	(4)	(5)	(6) 1114 S95 stope, 29/30 sill	(7) 1115	(8)	(9)	(10)	(11)	(12)	(13)
	MP (a)	MP (a)	MP (a)	MP (b)	MP (b)	MP (this study)	MP (this study)	MP (a)	MP (a)	MP (a)	MP (a)	MP (c)	MP (c)
Cu	46,6	46,8	45,3	45,1	44,2	45,6	45,1	45,3	46,0	45,6	47,8	50,9	48,1
Fe	7,0	7,8	6,8	7,4	6,7	7,1	6,4	-	-	1,0	0,2	3,2	5,5
Zn	0,7	0,7	1,3	1,3	1,5	1,0	0,2	1,5	0,7	2,4	2,1	-	-
W	-	-	-	n.d.	n.d.	0,6	0,4	7,7	7,7	7,4	10,3	n.d.	n.d.
V	-	-	-	n.d.	n.d.	0,3	0,2	-	-	-	-	2,9	2,0
Ge	9,2	10,2	10,0	9,7	9,7	10,8	9,8	9,8	9,3	10,3	8,0	7,2	11,0
Ga	n.d.	n.d.	n.d.	-	-	0,05	-	n.d.	n.d.	n.d.	n.d.	n.d.	n.d.
S	31,4	28,4	31,6	33,4	34,6	31,9	33,2	33,9	34,1	28,7	27,7	31,6	34,6
As	4,5	3,9	4,3	2,6	3,3	1,3	3,2	2,7	4,0	3,5	2,2	4,9	-
Sn	n.d.	n.d.	n.d.	n.d.	n.d.	-	-	n.d.	n.d.	n.d.	n.d.	n.d.	n.d.
Mo	n.d.	n.d.	n.d.	n.d.	n.d.	-	-	n.d.	n.d.	n.d.	n.d.	n.d.	n.d.
Pb	n.d.	n.d.	n.d.	n.d.	n.d.	-	0,03	n.d.	n.d.	n.d.	n.d.	n.d.	n.d.
TOTAL	99,4	97,8	99,3	99,5	100,0	98,7	98,5	100,9	101,7	98,3	98,9	100,7	101,2

MP = microprobe
n.d. = not determined
(a) Geier and Ottemann (1970b)
(b) Viaene and Moreau (1968)
(c) Geier and Ottemann (1970a)
See De Vos et al (1974) for analyses of germanite from Kipushi, Zaïre.

TABLE A9 REDUCED CARBON ANALYSES, TSUMEB

	SAMPLE NO.	ELEVATION (m)	%C	DETAILS
(i) Rock				
	PB5	surface	0,02	Medium grey dolostone, zone T5
	PB4	surface	0,02	Medium grey dolostone, zone T5
	439	+378	< 0,01	Medium grey dolostone
	440	+378	0,05	Calcitized dolostone (same as 439)
	492	+246	0,01	Calcitized dolostone
	958	DDH 3178/380m	0,03	Calcitized dolostone (North Break Zone)
	530	+164	0,02	Silicified dolostone
	858A	+34	0,05	Silicified dolostone
	865A	+393	0,16	Dark grey dolostone
	190	+493	0,17	Dark grey dolostone
	841B	+393	0,05	Medium-dark grey dolostone clasts
	841A	+393	0,14	Black matrix to 841B
	544	+372	0,70	Dark grey dolomitic siltstone matrix
	PB8	DDH ASW95G/230m	0,12	Mulden Group slate
	PB10	DDH AW68A/181m	0,47	Mulden Group slate
	PB1	DDH AP39/117m	0,05	Mulden Group sandstone
	196	+492	0,04	Pipe sandstone ("pseudo-aplite")
	522	+229	0,02	Pipe sandstone ("pseudo-aplite")
(ii) Ore				
	513	+234	0,06	Dark, well mineralized "pseudo-aplite"
	512	+234	0,12	Massive tennantite
	333	+419	0,24	Bornite-chalcocite
	488B	+422	0,20	Bornite-pyrite
	434	+419	0,26	Bornite-chalcocite
	444	+368	1,43	Sheared galena-chalcocite in shale
(iii) Traverses				
	3726-28	+493	0,16	Dolostone breccia
	3729-31	+493	0,07	Dolostone breccia
	3732-34	+493	0,13	Dolostone breccia
	3735-38	+493	0,14	Dolostone breccia
	3739-41	+493	0,10	Dolostone breccia
	7661-7664	+246	0,02	Calcitized dolostone
	7665-7668	+246	0,03	Calcitized dolostone
	7669-7672	+246	0,01	Calcitized dolostone
	4763E-4778E	+ 30	0,02	Silicified dolostone
	4779E-4792E	+ 30	0,01	Silicified dolostone
	4793E-4800E & 7001Z-7004Z	+ 30	0,01	Silicified dolostone

TABLE A10 CHEMICAL ANALYSES OF HAND SPECIMENS OF TSUMEB SULPHIDE ORE

Sample No.	Elevation	XRF (%)							AAS (ppm)		SPEC. SCAN (%*)												
		Cu	Pb	Zn	As	Fe	Cd	Ge	Ag	Bi	Sb (20)	Ga (3)	Sn (10)	W ∦(20)	Mo (5)	Hg (100)	Co (10)	Ni (5)	V (5)	Ba (5)	Tl (1)	In (1)	U (1)
149	+494	53,1	1,3	0,8	0,50	3,90	0,015	0,010	221	< 5	<0,02	.	.	.	0,02+	.	.	< 0,02	.	< 0,02	.	.	.
147	+493	2,6	49,8	20,8	0,71	2,01	0,420	0,003	38	< 5	<0,02	.	.	.	< 0,02	< 0,02	.	.	.	.	.	.	-
189	+493	1,1	9,7	< 0,1	0,23	0,83	0,004	0,022	11	< 5	.	.	.	.	.	.	.	.	.	.	.	.	-
190	+493	0,4	4,4	< 0,1	0,10	0,50	0,004	0,002	3	< 5	.	.	.	.	.	.	.	.	.	< 0,02	.	.	.
193	+492	14,7	30,2	9,8	2,90	1,30	0,26	0,003	200	< 5	0,02+	.	.	.	0,02+	< 0,02	.	.	.	.	.	.	.
229	+486	48,1	5,0	2,4	5,35	9,82	0,047	0,013	472	< 5	<0,02	.	.	.	.	< 0,02	.	.	.	.	.	.	-
230	+486	18,5	29,9	8,7	1,45	1,31	0,185	0,005	92	< 5	<0,02	.	.	.	< 0,02	< 0,02	.	.	.	.	.	.	-
8	+464	0,9	62,8	7,8	0,30	0,60	0,094	0,004	38	< 5	<0,02	.	.	.	0,02+	.	.	.	.	.	.	.	.
263	+419	57,4	0,4	0,2	1,28	8,00	0,016	0,005	741	< 5	<0,02	.	.	.	< 0,02	< 0,02	.	.	.	.	.	.	-
265	+419	25,8	42,0	0,2	1,01	5,69	0,013	0,011	816	< 5	.	.	.	.	< 0,02	.	.	.	.	.	.	.	-
206	+418	56,8	4,7	0,2	1,40	4,00	0,019	0,013	962	< 5	<0,02	.	.	.	0,02+	< 0,02	< 0,02	< 0,02	.	< 0,02	.	.	.
161	+418	48,8	1,0	3,6	8,68	7,05	0,115	0,113	2433	< 5	<0,02	.	< 0,02	.	< 0,02	< 0,02	.	.	.	.	.	.	-
202	+418	2,4	39,3	23,4	0,74	1,21	0,450	0,009	33	< 5	<0,02	.	< 0,02	.	< 0,02	< 0,02	.	.	.	.	.	.	-
261	+417	1,9	34,5	14,0	0,70	0,58	0,250	0,022	48	< 5	<0,02	.	.	.	< 0,02	< 0,02	.	.	.	.	.	.	-
110	+415	6,8	24,0	31,3	2,40	3,60	0,84	0,002	114	< 5	0,02+	.	.	.	0,02+	< 0,02	.	.	.	.	.	.	.
164	+413	70,3	0,1	< 0,1	0,60	6,40	0,005	0,005	738	< 5	<0,02	.	<0,02	.	0,02+	< 0,02	.	< 0,02	.	.	.	.	.
302	+369	1,8	4,1	<0,1	0,20	0,80	0,004	0,001	25	< 5	.	.	.	.	.	.	.	.	.	<0,02	.	.	.
245	+367	62,4	2,2	0,3	0,53	8,46	0,012	0,018	492	< 5	<0,02	.	.	.	< 0,02	.	.	.	.	.	.	.	-
234	+367	1,5	48,4	23,7	0,65	1,10	0,390	0,004	11	< 5	<0,02	.	.	.	< 0,02	< 0,02	.	.	.	.	.	.	-
216	+331	17,7	10,9	<0,1	0,28	1,41	0,004	0,009	66	< 5	.	.	.	.	< 0,02	.	.	.	.	.	.	.	-
219	+331	4,3	39,0	24,3	1,19	1,16	0,720	0,004	41	< 5	<0,02	.	< 0,02	.	< 0,02	< 0,02	.	.	.	.	.	.	-
130	+330	12,7	0,8	10,6	5,10	0,80	0,115	0,013	147	<5	0,02+	.	< 0,02	.	.	<0,02	.	< 0,02	.	<0,02	.	.	.
176	+327	59,7	0,8	0,2	0,30	14,20	0,004	0,003	831	<5	<0,02	.	< 0,02	.	< 0,02	.	.	<0,02	.	.	.	.	.
172	+327	22,6	10,4	9,8	5,70	2,60	0,078	0,010	102	<5	<0,02	.	< 0,02	.	0,02+	<0,02	.	< 0,02	.	.	.	.	.
272	+324	22,0	8,6	3,3	9,14	7,10	0,050	0,009	99	<5	<0,02	< 0,02	<0,02	.	< 0,02	<0,02	.	<0,02	.	.	.	.	-
268	+324	18,6	0,8	1,8	5,59	15,19	0,052	0,385	142	<5	<0,02	.	<0,02	.	< 0,02	<0,02	.	<0,02	.	.	.	.	-
275	+324	1,4	59,1	1,2	0,68	2,17	0,033	0,002	130	<5	.	.	.	.	< 0,02	.	.	< 0,02	.	.	.	.	-
99	+240	3,9	51,6	2,7	1,69	5,29	0,031	0,077	59	<5	<0,02	.	< 0,02	.	<0,02	.	.	.	.	.	.	.	-
168	+170	20,6	1,0	7,2	6,99	3,17	0,111	0,006	746	<5	<0,02	<0,02	<0,02	.	.	.	.	.	.	.	.	.	-

Analyses by Mine Laboratory of Tsumeb Corporation Limited.

+ Analysis of sulphide concentrate prepared from sample.

0,02+ = 0,02 - 1%
0,02 = 0,02%
. = below detection limit
- = not analysed
∦(20) = detection limit 20ppm
*Re(100), Pt(50), Te(200) not detected in any sample

nitrogen temperature.

The sulphur isotope ratio of the purified sulphur dioxide was measured on a Micromass MM602, dual inlet mass spectrometer. Samples were read against a reference sample, prepared in the same way as the samples and, where possible, using the same batch of cuprous oxide. The data were corrected for variations in the $\delta^{18}O$ ratio of the cuprous oxide, when present. The laboratory references were initially calibrated using the "door-stop" chalcopyrite of M. Coleman (-4,56 ‰) and the OGS standard, and values were checked by Geochron Laboratories and good agreement obtained (these latter values were then accepted). The precision of the method is 0,2 ‰, and accuracy is approximately 0,3 ‰ (1σ). Precision was checked by constant running of the reference gas and duplicate samples, and accuracy was checked by the use of other laboratory references, the "door-stop" chalcopyrite, and the OGS international sea water standard. The values obtained for the DSW, "door-stop" and OGS references were +20,1‰, -4,4‰ and +20,5‰, respectively (compared with accepted values of +20,06‰, -4,56‰ and +20,56‰). Details of the preparation method and mass spectrometry are contained in a laboratory manual, prepared by the writer and kept by the Geology Department of the University of the Witwatersrand.

The sulphur isotope data are listed in Table A11.

2.2 CARBON AND OXYGEN ISOTOPES

Samples of carbonate minerals were hand-picked and carbon dioxide was evolved by the phosphoric acid method of McCrea (1950). The study utilized the existing carbon dioxide extraction line at the Nuclear Physics Research Unit, and the Micromass MM602 mass spectrometer used in the sulphur isotope study was also used to read the carbon dioxide samples. Samples were read by a procedure that is well established in the N.P.R.U. laboratory, which involves calibration against the STH and STLII standards of the Weizmann Institute. Precision was better than $\pm$0,3‰ for $\delta^{13}C$, but only $\pm$0,5‰ for $\delta^{18}O$ (1σ). Accuracy is less well known, because the isotopic ratios of the standards are suspected to have changed slightly during

TABLE A11 SULPHUR ISOTOPE ANALYSES

SAMPLE NO.	MINERAL	$\delta^{34}S_{CD}$ per mil	COMMENTS
(1) Tsumeb ore body			
598	Galena	+20,5	9 sub-level, type 1A ore
608	Galena	+20,2	12L, type 1A ore
625	Galena	+20,5	14L, type 1A ore
644	Galena	+20,3	15L, type 1B ore
646	Galena	+20,4	16L, type 1B ore
709	Galena	+21,2	18L, type 1A ore
734	Galena	+19,9	21L, type 2B ore
759	Galena	+22,2	24L, type 3C ore
430	Galena	+21,0	27L - North Break ore body, type 2B ore (Fig. 70)
AU298	Galena	+23,6	below 44L, disseminated
(2) Kombat group of ore bodies*			
1005	Galena	+26,2	DDH AW 74A, +952,5m, Asis West; gn-sp
1007	Galena	+18,6	E80-11 stope, +1233m, Asis West; sp-gn
1009	Galena	+ 0,9	6-4 stope, +1493m, Kombat West; cp-gn
1010	Galena	- 8,1	E80-11 stope, +1240m, Asis West; gn-cp-bn
1011	Galena	- 2,0	W1000-10 West stope, +1328m, Asis West; cp-gn
1014	Chalcopyrite	+ 5,4	W1150-10, stope, +1316m, Asis West; cp-mt
1021	Chalcopyrite	+22,7	DDH AU9/23, 69,1m, Asis West; cp-py-mt
1102	Barite	+28,6	Asis; cp-py-ba
(3) Otavi Mountain Land : other Tsumeb-type mineralization			
AU	Galena	+25,8	Locality 49
BB2	Galena	+16,6	Locality 22
AB	Galena	+20,6	Locality 11
TW5B	Galena	+15,0	Locality 6
GO	Galena	+24,4	Locality 55
KB	Galena	+34,0	Kupferberg
978A	Barite	+22,6	Locality 56 (J. Innes)
(4) Otavi Mountain Land : Berg Aukas-type mineralization			
AW6	Galena	+23,4	Abenab West
(5) Supergene minerals			
978B	Chalcocite	+ 29,4	Locality 56 (J. Innes)
726	Barite	+ 26,1	Tsumeb (20L)

TABLE A11 SULPHUR ISOTOPE ANALYSES (Contd.)

SAMPLE NO.	MINERAL	$\delta^{34}S_{CD}$ per mil	COMMENTS
(6) Mulden Group and zone T7 (Tsumeb Subgroup)			
1106 (PB1)	Pyrite (68ppm Pb)	+22,4	Tschudi Formation (DDH AP39, Tschudi)
PB9	Pyrite (335 ppm Pb)	+25,3	Kombat Formation (DDH AE 115, Kombat East)
1003	Pyrite	+17,3	Kombat Formation (DDH AU 11/100, Asis West)
1124	Anhydrite nodule in dolostone	+30,8	Zone T7, Tsumeb (DDH S67A, 455m)
979	Gypsum in dolostone	+32,5	Zone T7, Tsumeb
590	Native sulphur (associated with gypsum) in dolostone	+16,4	Zone T7, Tsumeb (DDH 227)
621B	Pyrite (on gypsum) in dolostone	+16,8	Zone T7, Tsumeb (14L)
981	Anhydrite in dolostone	+31,3	Kombat (no details)
(7) Central Africa : Tsumeb-type mineralization			
3615	Galena	+14,4	Mavungu (Toni), Zaïre (Bas-Congo)
5346	Galena	+ 9,0	Bamba-Kilenda, Zaïre (Bas-Congo)
4196	Galena	+22,8	Kengere, Zaïre (Shaba)
LOM	Galena	+14,5	Lombe, Zaïre (Shaba)
DJEN	Galena	+ 3,9	Djenguilé, Congo Republic
2822	Galena	+ 8,8	Hapilo, Congo Republic
(8) Central Africa : unclassified			
BGM 5486	Galena	+13,4	Bukanda, Zambia

*Samples 1005-1021 supplied by J. Innes

Abbreviations: gn = galena sp = sphalerite py = pyrite ba = barite
cp = chalcopyrite bn = bornite mt = magnetite

prolonged storage prior to this study; determinations on the NBS18, NBS19 and HlS standards indicate that accuracy is better than $\pm 1,0‰$. The $\delta^{18}O$ values were corrected for fractionation associated with the sample preparation procedure by using the values of Sharma and Clayton (1965). The fractionation factors, α, between carbon dioxide and the carbonate samples are 1,01008 for calcite and 1,00995 for dolomite at 25°C.

The reaction procedure and nature of the samples studied resulted in slow reaction times (only one day for calcite, but ten days for dolomite). It was therefore necessary to devise reaction vessels in the shape of an inverted "y" which could be sealed under vacuum and detached from the line. Approximately 25 mg of powdered carbonate sample was placed in the side arm of the reaction vessel. Five millilitres of 100 % orthophosphoric acid, saturated with P_2O_5, was placed in the main arm. Orthophosphoric acid is ideal because of its low vapour pressure and its low water content (which prevents oxygen exchange between H_2O and CO_2). The vessel was evacuated, the top sealed and the acid tipped onto the sample. The vessel was stored at 25°C (the laboratory temperature) while carbon dioxide was generated. The gas was then passed into a reaction line where water and non-condensible gas were removed. The carbon dioxide was frozen into a sample vessel for reading on the mass spectrometer.

Carbon and oxygen isotope data are summarized in Table A12.

2.3 LEAD ISOTOPES

2.3.1 Analytical techniques

Galena samples were dissolved in hydrochloric acid, followed by anodic electrodeposition. Sedimentary carbonate rocks were dissolved in hydrochloric acid, and any residues were dissolved in hydrofluoric acid and perchloric acid. Slate and sandstone samples were dissolved in hydrofluoric acid and nitric acid, and pyrite was dissolved in nitric acid. Dissolution of rock samples and pyrite was followed by purification, using anion columns and anodic electrodeposition.

TABLE A12 CARBON AND OXYGEN ISOTOPE DATA

SAMPLE NO.	$\delta^{13}C$ per mil	$\delta^{18}O$ per mil	COMMENTS
(1) Calcite; post-S_1 (supergene)			
1107	-8,7	+17,6	Intergrown with bayldonite
1108	-9,6	+18,5	Sample 2724, Geology Department collection
1109	-11,0	+18,5	R. Myers
1110	-3,7	+20,6	Post-dioptase, pre-duftite (C. Gould)
1111	-8,4	+17,9	Post-mottramite (C. Gould)
1112	-9,4	+17,9	Post-dates green arsenate mineral (C. Gould)
1113	-9,9	+23,5	Post-dates green arsenate mineral (C. Gould)
844B	-11,9	+18,2	Vugs and veins in dark dolostone breccia, W20/29L
495B	-8,0	+17,6	Rhomb on dolomite crystals in vug, W120/33L
(2) Calcite; pre-S_1 (ore stage, open-space fillings)			
678	+0,5	+19,0	Vein with hypogene sulphide minerals, 17L
718	-1,9	+19,8	Vein with hypogene sulphide minerals, 20L
755	-2,7	+19,6	Vein with tennantite, 23L
84	-1,1	+19,4	E49/30L; within massive galena (pre-galena?)
240A	-3,5	+18,9	W40/30L; vein with earlier galena
242	-3,5	+19,4	W40/30L
516	-2,2	+19,5	W96/33L; massive body
(3) Calcitized, recrystallized dolostone			
860	+0,7	+20,6	W20/29L; clast from breccia
440	+1,6	+20,0	E35/30L
240B	+0,4	+20,6	W40/30L; recrystallized
240C	+1,1	+21,6	W40/30L; no textural change
490	+1,0	+20,5	W80/33L
515	0,0	+19,8	W96/33L
(4) Dolomite; pre-S_1 (ore stage, open-space filling)			
601	+4,7	+22,3	10L; vein with sulphide minerals
609	+3,5	+21,1	12L; vein with sulphide minerals
651	+5,7	+23,4	15L; dolomite vein cut by later dolomite-tennantite veins
811	+5,1	+22,6	17L; vein with sulphide minerals
726	+5,0	+21,7	20L; vein with later barite in vugs, early sulphide minerals on walls
253	+0,8	+20,3	E65/20L; vein in bedding
495A	-0,6	+20,0	W120/33L; vug in vein - with tennantite
168	+0,1	+20,3	W150/35L; disseminated in silicified dolostone breccia
857	+4,1	+21,4	W30/38L; vein with tennantite
(5) North Break zone (DDH 3178)			
959B	+3,8	+23,6	Unaltered dolostone
958X	-1,1	+21,1	Pink dolostone (recrystallized)
959A	-2,4	+21,3	Deformed calcite
958Y	-10,3	+18,9	Undeformed calcite
(6) Dolostone and limestone			
439	+3,8	+24,7	Dolostone, zone T5, E35/30L
621	+5,2	+23,6	Dolostone, zone T7, 14L
980	+6,8	+24,4	Dolostone, zone T7
590B	+7,0	+24,0	Dolostone, zone T7, DDH 227
979	+5,4	+23,8	Dolostone, zone T7
957	+8,2	+22,5	"Augen limestone marker", zone T7, DDH 3189
(7) Other			
590	+5,6	+22,7	Calcite vein with native sulphur, DDH 227
810B	-3,3	+22,1	"Quartz cluster dolomite", Auros Formation, Abenab West
810A	-3,2	+21,3	"Clusters" in above
573D	+3,9	+23,9	Supergene calcite, Baltika

The samples were analysed on a Micromass MM30 mass spectrometer. Rhenium single filaments were used for lead, and triple filaments (with tantalum side filaments) were used for uranium. NBS standard 981 was run at regular intervals for the purpose of normalising data, and to determine analytical uncertainty (Chapter 5.3.1). Spikes with greater than 99 percent ^{204}Pb and ^{235}U, respectively, were used for the isotope dilution analysis. Thorium concentrations were determined by two techniques. K.P. Jochum of the Max Planck Institute, analysed thorium using spark source mass spectrometry on an AEI-MS 702R mass spectrometer. The separately determined uranium concentrations permitted the use of uranium as an internal standard. Peter Jackson of Mass-Spec (Pty) Ltd. determined thorium by ICP mass spectrometry (VG Micromass). The relative sensitivity factor of thorium was determined by analysing the U.S.G.S. BRC-1 and W-1 rock standards, and laboratory reference samples. The agreement between the two methods of analysis was generally good and the error in the thorium analyses is estimated to be better than $\pm 5\%$, although the technique is still at a preliminary stage and errors may be larger than this at very low thorium concentrations (e.g. less than one ppm). These errors, if present, result from the running procedure adopted for this particular batch of samples. The analytical errors of other analyses are discussed in Chapter 5.3.1.

Galena data are given in Table A13, and other rock and mineral data are given in Table A14.

2.3.2 Intersection of a secondary isochron with the primary uranothorogenic growth curve

The writer could not find any discussion in the literature of the intersection point(s) between a secondary isochron and the primary growth curve on a uranothorogenic lead plot. It is argued here that:

(a) Any point, x, which lies on the continuation of the primary growth curve beyond t_1, at the intersection with a secondary isochron formed subsequent to t_1, has evolved in a system with the same $^{232}Th/^{238}U$ ratio as the primary growth curve. However, x

TABLE A13 LEAD ISOTOPE DATA: GALENA

SAMPLE NO.	$^{206}Pb/^{204}Pb$	1σ	$^{207}Pb/^{204}Pb$	1σ	$^{208}Pb/^{204}Pb$	1σ	LOCATION
(i) Tsumeb ore body							
G8	18,137	,005	15,688	,005	38,329	,010	4L
608	18,218	,006	15,718	,006	38,505	,016	12L
625	18,174	,004	15,686	,004	38,387	,010	14L
644	18,139	,005	15,674	,005	38,308	,012	15L
646	18,137	,004	15,683	,004	38,304	,012	16L
G10	18,218	,006	15,740	,004	38,549	,011	19L
G11	18,146	,007	15,705	,007	38,405	,016	24L
G3	18,099	,005	15,678	,004	38,292	,010	E49/28L
G12	18,134	,003	15,700	,004	38,392	,009	E49/28L
G13	18,061	,009	15,646	,010	38,276	,020	30L
G4	18,007	,003	15,671	,002	38,262	,006	W136/33L
G1	18,160	,009	15,697	,007	38,409	,016	W50/33L
G6	18,098	,004	15,692	,004	38,355	,010	W50/33L
G2	18,115	,004	15,696	,003	38,289	,010	33L
G5	18,126	,003	15,680	,003	38,307	,006	33L
G7	18,181	,005	15,711	,006	38,409	,014	33L
G9	18,086	,008	15,681	,007	38,340	,017	37L
T44	18,048	,005	15,660	,004	38,283	,011	below 44L
M1	18,083	,005	15,695	,005	38,343	,010	wulfenite (not galena)
(ii) Tsumeb area							
E2200	18,094	,006	15,677	,005	38,350	,012	E2200 breccia, 30L, Tsumeb
1127	18,198	,008	15,728	,007	38,404	,017	locality 11
1128	18,148	,007	15,700	,007	38,358	,018	locality 21
1129	18,205	,012	15,746	,010	38,477	,028	locality 14
1130	18,149	,008	15,700	,006	38,349	,015	locality 6
1131	18,138	,004	15,694	,003	38,334	,007	locality 6
1132	18,047	,004	15,678	,004	38,330	,009	locality 22
1133	18,070	,006	15,681	,005	38,242	,012	locality 22
1134	18,056	,007	15,680	,006	38,321	,017	locality 22
AU295*	18,060	,003	15,683	,003	38,311	,007	North Break zone, Tsumeb

* Sample AU295 not included in regression analysis, etc.

TABLE A13 (CONT.)

SAMPLE NO.	$^{206}Pb/^{204}Pb$	1σ	$^{207}Pb/^{204}Pb$	1σ	$^{208}Pb/^{204}Pb$	1σ	LOCATION
(iii) Kombat ore bodies							
K7	18,034	,006	15,659	,005	38,102	,011	Asis West
K8	18,030	,006	15,665	,006	38,143	,014	Asis West
K1	18,045	,003	15,665	,003	38,142	,007	Kombat West
K5	18,009	,002	15,656	,001	38,104	,006	Kombat West
K3	18,039	,007	15,662	,007	38,136	,015	Kombat Central
K6	18,029	,005	15,666	,004	38,132	,010	Kombat Central
K2	18,015	,005	15,668	,004	38,123	,013	Kombat East
K4	18,020	,006	15,664	,005	38,147	,010	Kombat East
E900	18,079	,003	15,720	,003	38,269	,006	Kombat E900
E900B	17,989	,007	15,664	,006	38,104	,015	Kombat E900
A01	18,059	,006	15,679	,006	38,131	,013	Asis Ost
(iv) Other Otavi Valley area							
1135	18,134	,002	15,718	,002	38,346	,005	locality 55
1136	18,111	,002	15,704	,002	38,268	,005	locality 64
KB	18,019	,003	15,678	,002	38,203	,005	Kupferberg
1137	18,216	,006	15,717	,005	38,366	,013	locality 49
(v) Central Otavi Mountain Land							
HM1	17,946	,004	15,673	,004	38,655	,008	Harasib Main
HM2	17,998	,004	15,721	,004	38,795	,010	Harasib Main
HM3	17,973	,007	15,690	,007	38,663	,018	Harasib Main
HM4	17,990	,006	15,701	,005	38,692	,014	Harasib Main
HM5	17,985	,004	15,655	,004	38,622	,007	Harasib Main
HM6	17,961	,004	15,678	,004	38,662	,008	Harasib Main
506	17,951	,006	15,634	,008	38,593	,012	Harasib Main
HM	17,998	,008	15,712	,007	38,772	,016	Harasib Main
877	18,022	,005	15,695	,004	38,702	,010	Strata-bound breccia, zone T4, near Harasib Main
1138	17,964	,006	15,653	,005	38,564	,012	locality 34
1139	18,009	,006	15,687	,009	38,643	,020	locality 34
1140	17,984	,007	15,676	,006	38,637	,015	locality 34
ML10	17,945	,009	15,683	,007	38,643	,015	locality 26
ML11	17,935	,006	15,663	,005	38,576	,015	locality 27

TABLE A13 (CONT.)

SAMPLE NO.	$^{206}Pb/^{204}Pb$	1σ	$^{207}Pb/^{204}Pb$	1σ	$^{208}Pb/^{204}Pb$	1σ	LOCATION
(vi) Other							
1141	17,992	,005	15,725	,005	38,431	,010	Strata-bound breccia, zone T4, locality 48
BA1	18,055	,006	15,695	,005	38,796	,010	Berg Aukas
BA2	18,035	,004	15,672	,003	38,731	,008	Berg Aukas
BA3	18,024	,006	15,670	,006	38,741	,014	Berg Aukas
572C	17,981	,003	15,659	,003	38,245	,007	locality 45
791	17,949	,007	15,713	,005	38,329	,017	locality 41
793	17,514	,006	15,607	,005	38,026	,009	Abenab West
795	17,509	,003	15,609	,002	38,021	,007	Abenab West
AW6	17,531	,003	15,612	,003	38,023	,006	Abenab West
574B	18,371	,005	15,741	,005	39,107	,009	Strata-bound breccia, zone T4 (Karuchas zone), west of Abenab West
790	18,359	,003	15,708	,003	39,033	,007	Strata-bound breccia, zone T4 (Karuchas zone), west of Abenab West
533	18,019	,009	15,773	,008	38,475	,019	Strata-bound breccia, zone T4, locality 1

See Figure 111a for location plan.

TABLE A14 U-Th-Pb ISOTOPE DATA : ROCKS AND MINERALS

SAMPLE	LITHOLOGY	LOCALITY	TOTAL U (ppm)	TOTAL Pb (ppm)	TOTAL Th (ppm)	$^{206}Pb/^{204}Pb$	$^{207}Pb/^{204}Pb$	$^{208}Pb/^{204}Pb$	$^{238}U/^{204}Pb$	$^{235}U/^{204}Pb$	$^{232}Th/^{204}Pb$	%S
987	Phosphatic dolostone	Zone T8?, Kombat area	0,50	37,52	0,13	18,315	15,702	38,234	0,8361	0,0061	0,2180	-
988	Phosphatic dolostone	Zone T8?, Kombat area	0,83	19,37	0,21	18,590	15,729	38,380	2,718	0,0197	0,7036	-
837	Dolostone (with quartz vugs)	Zone T8, Tsumeb	0,38	32,24	0,30	18,297	15,705	38,338	0,7451	0,0054	0,5931	0,05
PB4	Dolostone	Zone T6, south-east of Tsumeb	0,36	2,61	0,18	19,196	15,743	38,354	8,892	0,0645	4,625	0,04
PB5	Dolostone	Zone T5, south-west of Tsumeb	0,26	0,83	(0,0875)	20,529	15,826	38,492	20,269	0,1470	(7,396)	< 0,01
PB6	Dolostone	Zone T4, Kombat area	1,01	2,23	(0,0832)	21,617	15,883	38,328	29,941	0,2172	(2,460)	-
PB7	Dolostone	Gauss Formation, north of Tsumeb	0,40	3,75	(0,161)	19,071	15,736	38,343	6,801	0,0493	(2,831)	-
PB2	Dolostone	Berg Aukas Formation, east of Kombat	0,78	8,52	0,26	19,245	15,730	38,515	5,868	0,0426	2,023	-
PB8	Slate	Kombat Formation, Asis West	3,62	12,87	12,29	19,839	15,782	39,709	18,560	0,1349	64,992	< 0,01
PB9	Slate	Kombat Formation, Kombat East	3,75	9,81	13,91	20,515	15,810	40,555	25,749	0,1807	98,656	0,52
	Pyrite in above rocks		0,18	334,9	-	18,160	15,625	37,963	0,0340	0,0003	-	-
PB11	Slate	Kombat Formation, Asis West	3,62	7,15	(8,78)	20,704	15,796	40,498	34,094	0,2473	(85,497)	0,20
PB1	Sandstone	Tschudi Formation, Tschudi	1,06	6,72	3,52	18,620	15,709	38,926	10,123	0,0734	34,0968	0,75
	Pyrite in above rocks		5,72	68,30	2,51	18,052	15,635	38,117	5,273	0,0382	2,4480	-
PB12	Sandstone	Tschudi Formation, Tsumeb	2,66	7,59	9,38	20,102	15,833	40,305	23,376	0,1695	84,094	1,38
	Pyrite in above rocks		3,11	-	-	-	-	-	-	-	-	-
-	Feldspar (from "pseudo aplite")	Tsumeb pipe, Tsumeb (W130/34L)	-	-	-	18,894	15,746	38,772	-	-	-	-
W130/34	Zircon : 120# <170#	As above	565,5	70,80	-	649,4	71,86	126,7	-	-	-	-
	230# <300#		630,4	49,68	-	602,0	65,17	117,6	-	-	-	-

NOTE: Th analyses in brackets = spark source mass spectrometry

will only correspond to point t_2 on the primary growth curve when the μ and W values of the system in which x evolved between times t_1 and t_2 are equal to the values of the system in which the growth curve evolved prior to t_1 (i.e. $^{232}Th/^{238}U$ = constant, k = W/μ).

Points on the secondary isochron each developed in systems with a constant $^{232}Th/^{238}U$ ratio, i.e. slope of the isochron =

$$\frac{^{232}Th}{^{238}U} \cdot \frac{e^{\lambda_2 t_1} - e^{\lambda_2 t_2}}{e^{\lambda_8 t_1} - e^{\lambda_8 t_2}}$$

Since x also lies on the secondary isochron, all points on this isochron must have the same $^{232}Th/^{238}U$ values as the primary isochron prior to t_1 (but varying μ and W values). Therefore, the secondary isochron will only intersect the primary growth curve at t_1 in the special case where the $^{232}Th/^{238}U$ ratio of the system in which the secondary isochron developed equalled that of the primary growth curve prior to t_1.

(b) Different secondary isochrons each have different, but constant, $^{232}Th/^{238}U$ ratios. Since $^{232}Th/^{238}U = W/\mu = k$, then $W = k\mu$ for each secondary isochron, i.e. there will be an infinite number of points on each isochron, each of which has a different W and μ value, but the same W/μ value. These points include a point for which W = 0 and μ = 0 on each isochron. This point represents lead to which no additional uranogenic lead or thorogenic lead has been added between t_1 and t_2, i.e. it is at t_1 on the primary growth curve. All secondary isochrons must therefore pass through t_1.

It can be concluded that all secondary isochrons generated between t_1 and t_2 will intersect the primary uranothorogenic growth

curve at t_1. There is a single secondary isochron, for which $^{232}Th/^{238}U$ is equal to that of the primary growth curve prior to t_1, which will intersect the primary growth curve at both t_1 and t_2.

APPENDIX 3: FLUID INCLUSION DATA

3.1 TSUMEB ORE BODY

Most fluid inclusions were destroyed by post-ore deformation; no useable inclusions have been found in sphalerite, but inclusions were studied in a limited number of samples of paragenetically-early quartz and carbonate minerals (Ypma, 1973a, b, c). These studies indicated that the fluids which produced the rock alteration (and presumably also the sulphide minerals) in the Tsumeb ore body were brines and saline waters at temperatures of 230° - 260°C. No evidence was found for a major variation in ore fluid temperatures with depth (homogenization temperatures increased slightly at shallow depths, but this was considered to be a pressure effect). The temperatures have been corrected for a pressure of 500 ± 700 bars (i.e. homogenization temperatures are mostly 170° - 220°C). A group of lower temperature inclusions occurs in quartz that is probably unrelated to the mineralizing event. Salinities of 2-10% were estimated by evaporating the water expelled from inclusions and observing the volume of halite produced. These observations agree with a recent study of 26 fluid inclusions in quartz, in which salinities of up to 12 wt. % NaCl equivalent (I = 2,1), with a mean of 8 wt. % (I = 1,4), were measured using freezing point depression methods (Haynes, 1985). These inclusions showed homogenization temperatures of 170°-200°C, with six inclusions in the range 230° - 250°C, and Haynes (1985) proposed an average temperature of sulphide deposition of 250°C.

Fluid inclusions from above 15 level in the Tsumeb ore body were found to be the most dilute, and are three-phase inclusions which contain significant quantities of hydrogen sulphide and carbon dioxide. The presence of carbon dioxide was determined using the critical phase relations of carbon dioxide near 31°C. The concentration of carbon

dioxide was estimated using the temperature of the phase transition and the vapour-liquid ratios of the inclusions, adjusted for the amount of carbon dioxide dissolved in the aqueous phase. It was necessary to ignore the possible effect of compounds which lower the temperature of the transition (e.g. methane). The inclusions contain an estimated 6-8 mol % of carbon dioxide which, at the temperatures of homogenization of the fluid inclusions, corresponds to a confining pressure of 500 - 700 bars during mineralization (Ypma, 1973a, b). This corresponds to 6 - 7 km of hydrostatic pressure or 2,5 - 3 km of lithostatic pressure (c.f. 500 bars at 2,7 - 5 km depth in the Gulf Coast, U.S.A.; Hanor, 1979). Fluid inclusions from near surface at the Tsumeb mine showed critical phenomena at unusually high temperatures of 35° to 43°C. This behaviour, together with a strong smell of hydrogen sulphide during dry crushing of the sample, was interpreted to result from the presence of between 17 and 33 mol % of hydrogen sulphide in the vapour bubbles of these inclusions (Ypma, 1973a, b). It should be noted that the above three-phase samples cannot be positively identified as ore-stage samples from the existing descriptions, unlike the samples from 15 level and below which contain two fluid phases. However, a strong smell of H_2S was noted when samples of ore-stage carbonate minerals from the upper levels were crushed during the present study.

Calcite, chlorite, opaque minerals, and possible anhydrite were identified optically as daughter minerals in inclusions (Ypma, 1973a, b). SEM studies of inclusions in a single sample of pyrite revealed a daughter mineral assemblage of muscovite, albite, a barium mineral (celsian ?), a manganese- and calcium-bearing (carbonate ?) mineral, apatite, galena, chalcopyrite, quartz, and a copper sulphide mineral. Sodium and strontium were detected in the inclusion fluid (D.K. Hallbauer, pers. comm., 1981).

Ypma (1973a, b) concluded that the variable gas mixtures in the upper levels of the ore body (i.e. varying ratios of carbon dioxide and hydrogen sulphide) indicate that the confining pressure of the brine was not much higher than its vapour pressure. He suggested that the sharp variations in gas content indicated explosive gas release and a lack of equilibrium conditions (i.e. near-boiling conditions).

However, the variation in inclusion compositions can also be explained by mixing of different fluids, and there is no unequivocal evidence that boiling occurred.

3.2 OTHER MINERALIZATION IN THE OTAVI MOUNTAIN LAND

There are less data available from other ore bodies in the Otavi Mountain Land. Average homogenization temperatures of 230°C (maximum 260°C) were obtained from inclusions in quartz and carbonate minerals associated with ore minerals in the Kombat ore bodies (Ypma, 1973a, b, c). A temperature of 250°C is assumed for the ore fluid, although the higher homogenization temperatures in fluid inclusions from the Kombat ore bodies indicate that temperatures could have been slightly higher than in the Tsumeb ore body. Daughter minerals determined optically include "sodium and potassium halide" minerals, in addition to chlorite, calcite, opaque minerals, and a mineral tentatively identified as anhydrite. The salinities of the fluid inclusions were found to exceed 20% NaCl equivalent (I = 3,4).

Homogenization temperatures of 200°-250°C were obtained from inclusions in gangue minerals associated with mineralization of Berg Aukas type, both in the central Otavi Mountain Land and the Berg Aukas ore body (Ypma, 1973a, b). Homogenization temperatures of 230°-250°C were found in inclusions within sphalerite from the Berg Aukas ore body (the only measurements from sphalerite in the Otavi Mountain Land). Daughter minerals were identified optically as opaque minerals and probable anhydrite (Ypma, 1973a, b). SEM studies of inclusions in a single galena sample from the Berg Aukas ore body revealed albite and muscovite as daughter minerals. Sodium and strontium were detected in the inclusion fluid (D.K. Hallbauer, pers. comm., 1981). The salinities of inclusions indicate that the ore fluids within single ore bodies varied from low salinity fluids (e.g. 4 - 7% NaCl equivalent) to brines, which contained hydrogen sulphide and carbon dioxide (Ypma, 1973a, b). The hydrocarbon compounds C_2H_4, CH_4, C_3H_8 and C_2H_4 were identified in inclusions from the central Otavi Mountain Land, using gas chromatography (Ypma, 1979).

It is concluded that the Tsumeb and Berg Aukas types of mineralization formed at approximately 250°C, from fluids which varied in composition (within single ore bodies) from concentrated brine to less saline fluids with carbon dioxide and hydrogen sulphide. An important feature of the fluid inclusion data is that ore bodies of both the Tsumeb and Berg Aukas mineralogical types formed at similar, intermediate temperatures, significantly higher than those typical of Mississippi Valley-type ore deposits. However, these temperatures are only 50°C higher than the upper range of temperatures indicated by fluid inclusion studies in some Mississippi Valley districts (e.g. McLimans, 1977).